THE JOURNAL
OF
CHEMICAL PHYSICS

VOLUME 17, NUMBER 11 NOVEMBER, 1949

The Infra-Red and Raman Spectra and the Thermodynamic Properties of Diborane[1]

ALLEN N. WEBB, JOHN T. NEU, AND KENNETH S. PITZER
Department of Chemistry, University of California, Berkeley, California
(Received January 3, 1949)

Deuterated diborane has been prepared by isotopic exchange and its infra-red absorption spectrum measured. The Teller-Redlich product rule ratios lend support to the assignment based on the protonated double bond or bridge model. Redetermination of the Raman spectrum of normal diborane indicates several changes from previous assignments of Anderson and Burg and Wagner. The resulting vibrational assignment was used to calculate the thermodynamic properties of diborane in the range 100–1500°K. The ΔH_f^0, ΔS_f^0, and ΔF_f^0 are also given. Appendix I shows that a quadratic potential term arises for the puckering of a planar ring if the ring is strained.

INTRODUCTION

THIS study was directed to the double objectives of the vibrational spectrum and the thermodynamic properties of diborane. The former is of particular interest in the picture it gives of the bonding forces in this interesting molecule. The latter is of obvious practical importance in relation to the physical and chemical properties of the substance.

EXPERIMENTAL PART

Preparation of B_2H_6 and B_2D_6

Diborane of normal isotopic composition was prepared by the reaction of boron trifluoride diethyl ether complex with lithium borohydride in an ether medium. The reaction is represented by the equation:

$$3LiBH_4+BF_3\rightarrow 2B_2H_6+3LiF.$$

The diborane was purified by bulb to bulb distillations and the center fraction taken for use.

The deuterated diborane was prepared from the normal diborane by successive exchanges with deuterium gas. The deuterium was prepared from heavy water, 99.9+percent D_2, by electrolysis using anhydrous sodium sulfate as an electrolyte. The gas was dried by passing through a cold trap.

The exchange reaction of deuterium and diborane was followed by observing the infra-red spectrum of diborane. Upon mixing diborane and deuterium, absorption at the several characteristic infra-red frequencies decreases. Within the accuracy of measurements made at 1175 cm^{-1}, 1604 cm^{-1}, and 2522 cm^{-1} the rate of change was the same indicating entry of D_2 equally into all parts of the molecule. At 25°C and with a sixfold excess of D_2 (18 moles D_2 to 1 B_2H_6) the half time for the reaction is approximately 60 hours.

The sample of deuterated diborane used for spectral observation was prepared by six successive exchanges (each with six fold excess of D_2) allowing 200 hours or more for reaction before replacing the deuterium. Assuming that the equilibrium constants for all exchange reactions are unity and that equilibrium is reached in the six successive exchanges the mole fraction of B_2D_6 is 0.91 and that of the next most abundant species, B_2D_5H, is 0.08. All others are present in very much smaller concentrations.

Raman Spectrum of B_2H_6

The Raman spectrum of liquid diborane has been redetermined and some qualitative polarization data obtained. The apparatus is similar to that of Anderson and Burg[2] except that filters have been introduced in order to restrict excitation to the e(22,938.1 cm^{-1}), f(22,995.3 cm^{-1}), and g(23,039.2 cm^{-1}) lines of mercury and polaroid sheets used to give qualitative polarization information.

The Raman tube was 22 mm in diameter with a 10 cm illuminated length. For maintaining the liquid diborane at or below its normal boiling point of −92.5°C

[1] This work was supported by the ONR under Contract N7onr-295, Task Order X as Project No. NR-058-097. This aid is gratefully acknowledged.

[2] T. F. Anderson and A. B. Burg, J. Chem. Phys. 6, 586 (1938).

TABLE I.

Line cm^{-1}	Intensity	Difference cm^{-1} from e(22,938.1)	f(22,995.3)	g(23,039.2)	Assignment
22,331.8	v.w.	606			ν_5(?)
22,320.9(?)	v.v.w.	617(?)			
22,244.8	v.w.			794	ν_4 $B^{11}-B^{11}$
22,228.5	v.w.			811	ν_4 $B^{10}-B^{11}$
22,219.3	v.w.			820	ν_4 $B^{10}-B^{10}$
22,200.2	w.		795		ν_4 $B^{11}-B^{11}$
22,174.0	s.	764	821		ν_{12} and ν_4 $B^{10}-B^{10}$
22,145.8	v.s.	792			ν_4 $B^{11}-B^{11}$
22,130.0	v.s.	808			ν_4 $B^{10}-B^{11}$
22,116.3	s.	821			ν_4 $B^{10}-B^{10}$
21,924.6	s.	1013			ν_7
21,830.2	w.				
21,758.2	s.	1180			ν_3
21,617.0	w.	1321			ν_{15}
21,193.3	w.	1745			ν_6
21,153.9	w.	1784			$\nu_5+\nu_{13}$ or $\nu_{12}+\nu_7$
20,934.6	s.			2105	ν_2
20,893.8	s.		2102		ν_2
20,841.2	v.s.	2097			ν_2
20,516.6	s.			2523	ν_1
20,473.7	v.s.		2522		ν_1
20,415.5	v.v.s.	2523			ν_1
20,349.5	s.	2591			ν_{11}

v. = very w. = weak s. = strong

a bath of *n*-pentane was cooled by liquid nitrogen introduced into a 1.5 cm diameter brass tube immersed in the pentane. This tube also served as a support for the Raman tube. The unsilvered Dewar vessel containing the pentane was placed inside a cylindrical water jacket which removed most of the heat from the exciting lamps. This assembly was mounted inside a ring of 12 mercury lamps and the whole surrounded by a cylindrical chromium plated reflector. A blower provided additional cooling.

When starting a run, the pentane bath was cooled to −100°C as indicated by two copper-constantan thermocouples; then the Raman tube containing solid diborane was introduced and the bath further cooled so that some solid pentane (m.p. −130°C) always remained in the bottom of the Dewar.

A prism directly above the window of the Raman tube reflected the scattered light to a lens which focused the image of the window on the slit of the spectrograph. Masking at the window prevented the walls of the Raman tube from being seen. The optical path from Raman tube to slit was approximately 1.2 meters. A Steinheil, type GH, 3 prism glass spectrograph with $f/10$ collimator and $f/10$ camera was used throughout. This arrangement gives a dispersion of 10–12A per mm in the region used.

A Wratten 2*A*-gelatin filter placed in the annular space between the Dewar and the water jacket eliminates excitation from any but the 4358A (*e*) line and its satellites. The outside of the clear Dewar was coated a plastic containing rhodamine 5GDN Extra.[3] This dye reduces the background in the region of the Raman lines.

A one-hour exposure using a 0.025-mm slit and 12 GE AH2 mercury arcs gave 23 distinguishable Raman lines. The Eastman type 103*a*-J plates were developed in D-19 for 3 min. at 23°C. A similar exposure using 11 AH11 arcs gave a plate with less background showing 17 lines. This plate was used in some of the analysis.

With the aid of a microdensitometer tracing and a 6× enlargement of the Raman spectrum and adjacent iron spectrum the frequencies of Table I were obtained. The assignment to excitation lines is given in detail because of previous controversy[2,4] on this matter.

Polarization data were sought by making two exposures successively illuminating the Raman tube through sheets of polaroid film oriented parallel and tangentially to the Raman tube.[5,6]

The apparatus previously described was used unchanged except for the addition of polaroid cylinders which fitted around the inside of the pentane bath. Twelve AH2 arcs were used and the slit width was 0.037 mm. Between the two 30 minute exposures the polaroid cylinder was changed for one of alternate orientation. Unfortunately it was impossible to change the polaroid without some disturbance of the optical system. Consequently only qualitative results were obtained, as follows:

ν_4	792 cm^{-1} 808	Definitely polarized
ν_7	1013	Not strongly polarized
ν_3	1180	Not strongly polarized
ν_2	2101	Definitely polarized
ν_1	2523	Definitely polarized.

Infra-red Spectrum of B_2D_6

The infra-red absorption spectrum of deuterated diborane was observed with a Perkin-Elmer 12B spectrometer. Glass cells of 10 cm length with sodium chloride and potassium bromide windows were used. For the region above 863 cm^{-1} the cell was that used for preparation by exchange with deuterium and contained the excess deuterium from the last exchange. (This aided in preventing decomposition of the sample during the time of study.) When the sample was transferred to a cell with KBr windows for the remaining observations no deuterium was introduced, however.

The width of frequency band resolved in the various regions is indicated on Fig. 1 which shows the observed spectrum.

The infra-red spectrum is also listed in Table II where the vibrational assignment is listed and the B_2H_6 frequencies given. Certain of the weaker bands listed for

[3] G. Glockler and J. J. Haskin, J. Chem. Phys. **15**, 759 (1947).

[4] J. Wagner, Z. physik. Chem. **B53**, 85 (1943).

[5] J. T. Edsall and E. B. Wilson, Jr., J. Chem. Phys. **6**, 124 (1938).

[6] B. L. Crawford, Jr., and W. Horwitz, J. Chem. Phys. **15**, 268 (1947).

B_2D_6 in Table II may, of course, be strong bands of B_2D_5H. Very weak bands were omitted from Table II for the same reason.

INTERPRETATION AND CALCULATIONS

Infra-red Active Frequencies

Since we now have the spectrum of both B_2H_6 and B_2D_6, the Teller-Redlich product rule can be applied. This is of considerable aid in the assignment. There have been numerous previous attempts[7–10] to assign the vibration frequencies of diborane, mostly upon the now accepted bridge or protonated-double bond model. We shall use the frequency numbering scheme of Bell and Longuet-Higgins and their symmetry class arrangement. The actual frequency values for B_2H_6 are taken from Price except for ν_{10}. Recent work of Dr. E. F. Barker, reported in a private communication, indicates a value of 369 cm^{-1} for this lowest fundamental. The band contours were considered in the assignments.

There seems to be no doubt about the three parallel, B_{3u}, frequencies and it will be noted from Table III that the product ratio checks satisfactorily. Anharmonicity usually makes the observed ratio slightly nearer unity than the calculated ratio.

TABLE II. Infra-red spectra of B_2H_6 and B_2D_6.

B_2H_6	Intensity	B_2D_6	Intensity	Assignment
369 cm^{-1}	s.	(265) calc. cm^{-1}	—	ν_{10}
		707	m.	
974	s.	722	s.	ν_{14}
		794	m.	
1175	v.s.	876	s.	ν_{18}
1283	w.	914	m.	ν_{19}
		1075	w.	
1604	v.s.	1203	v.s.	ν_{17}
1861	s.	1461	s.	ν_{13}
2345 ?	m.	1705	m.	$\nu_3+\nu_{18}$
2522	s.	1850	s.	ν_{16}
2614	s.	1994	s.	ν_8
		2506	w.	
		2596	w.	
3670 ?	s.	2768	s.	
		2902	m.	
		3132	m.	
		3372	m.	

w. = weak m. = medium s. = strong v. = very

In the B_{1u} class, ν_8 is definitely and ν_9 very probably as indicated. In B_2D_6 ν_{10} comes at too long a wavelength to be observed, consequently no product rule check can be made.

At this point we must disagree with Bell[11] who as-

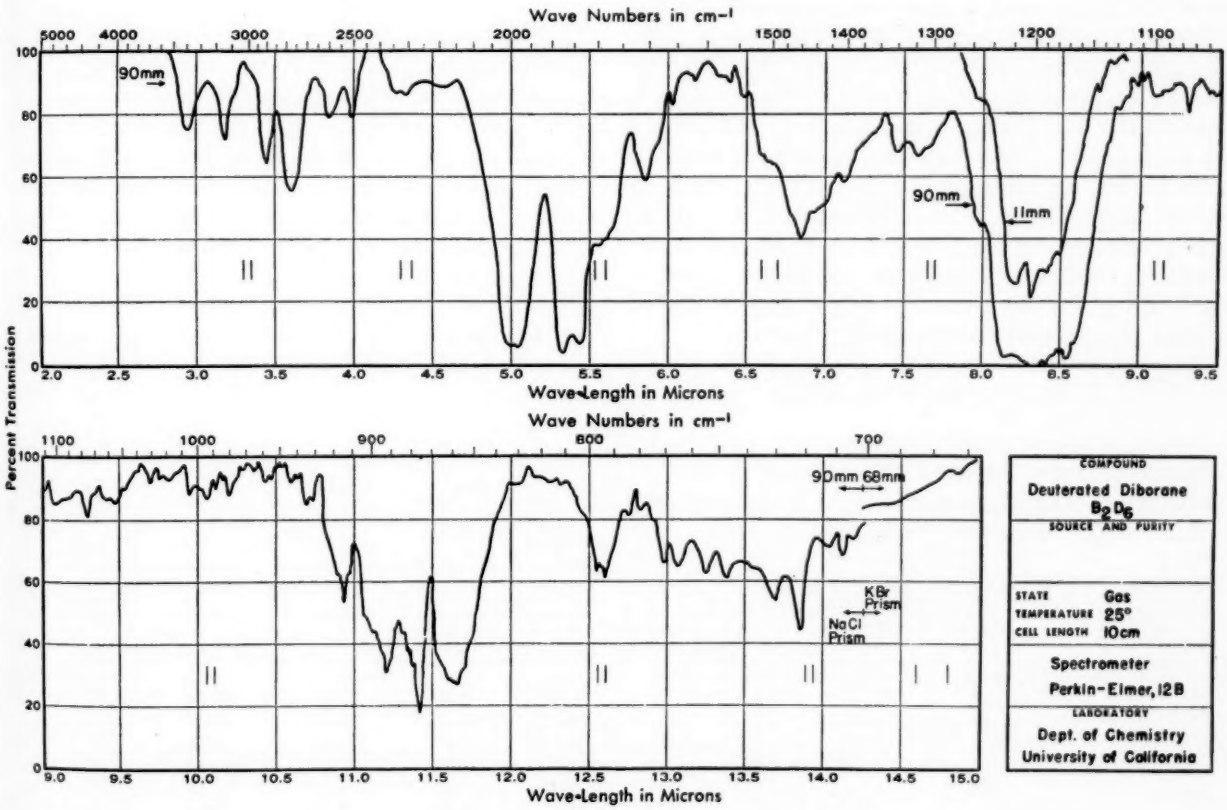

FIG. 1.

[7] F. Stitt, J. Chem. Phys. **9**, 780 (1941).
[8] K. S. Pitzer, J. Am. Chem. Soc. **67**, 1126 (1945).
[9] R. P. Bell and H. C. Longuet-Higgins, Proc. Roy. Soc. **A183**, 357 (1945).
[10] W. C. Price, J. Chem. Phys. **16**, 894 (1948).
[11] R. P. Bell, Proc. Roy. Soc. **A183**, 328 (1944); see also Bell and Longuet-Higgins (reference 9).

TABLE III. Infra-red active frequencies of diborane.

Symmetry	Mode	Frequency B_2H_6	Frequency B_2D_6	Product ratio Theoretical	Product ratio Observed
B_{1u}	ν_8	2614 cm^{-1}	1994 cm^{-1}		
	ν_9	1283	914	0.390	—
	ν_{10}	369	(~265) calc.		
B_{2u}	ν_{13}	1861	1461		
	ν_{14}	974	722	0.552	0.582
B_{3u}	ν_{16}	2522	1850		
	ν_{17}	1604	1203	0.390	0.410
	ν_{18}	1175	876		

sumes that there is no quadratic term in the potential energy for the vibration ν_{10} which destroys the planarity of the central B 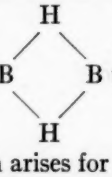 B unit. Appendix I shows that a quadratic term arises for the puckering of a planar ring if the ring is strained. If the bridge structure of diborane is regarded as a ring there is every reason to believe it would be somewhat strained. Likewise the analogy to ethylene suggested by the protonated double bond viewpoint also indicates a normal restoring force for ν_{10}. Thus we believe the frequency 369 cm^{-1} for ν_{10} in B_2H_6 should be regarded as an ordinary harmonic oscillation.

In the B_{2u} class the assignment of 974 cm^{-1} to ν_{14} is clear cut but there is some doubt about ν_{13}. Price assigns the weak band at 1984 cm^{-1} to ν_{13} but states that Dr. R. D. Cowan will report on this in detail. It seems to us doubtful both that ν_{13} can be so weak and that the strong band at 1861 cm^{-1} can be other than a fundamental. Therefore we prefer the assignment given in Table III which has the additional support of better product ratios than appear possible otherwise.

Raman Active Frequencies

Several changes in the previous Raman spectrum assignments[2,4] are indicated. The spectrum here reported is less complex since excitation by mercury lines other than *e*, *f*, and *g* was eliminated.

TABLE IV. Vibration frequencies of B_2H_6 (cm^{-1}).

Sym.	Mode	Frequency	Sym.	Mode	Frequency
A_{1g}	1	2523	B_{2g}	11	2591
	2	2101		12	764
	3	1180			
	4	(792, 808, 821)	B_{2u}	13	1861
A_{1u}	5	613		14	974
			B_{3g}	15	1321
B_{1g}	6	1745			
	7	1013		16	2522
			B_{3u}	17	1604
	8	2614		18	1175
B_{1u}	9	1283			
	10	369			

The relative intensities of the 792-cm^{-1}, 808-cm^{-1}, and 821-cm^{-1} lines, the ν_4 frequencies of $B^{11}-B^{11}$, $B^{11}-B^{10}$, and $B^{10}-B^{10}$, are now in accord with the relative abundance of these isotopic species. The high intensity of the line at 22,116 cm^{-1} (*e*-821) observed by Anderson and Burg is, as they suggested, caused by another frequency, but our data show that it is not an 821-cm^{-1} frequency. However, a new Raman frequency of 2591 cm^{-1} would be nearly coincident when excited by *k*(24,705 cm^{-1}). We find the 2591-cm^{-1} frequency excited by *e* at 20,345 cm^{-1} very close to a strong mercury line at 20,336 cm^{-1} and assign it to ν_{11}. The frequency of 2489 cm^{-1}, previously considered the ν_{11} fundamental, is definitely a mercury line, 20,443 cm^{-1}.

Another Raman line at 2005 cm^{-1} from the *e* mercury line does not appear to arise from a genuine frequency but has the proper position and intensity to be a satellite of ν_2(2097 cm^{-1}) excited by *g*.

Several new lines have been found. The line at 22,174 cm^{-1} is of too great intensity to be explained solely as the satellite of ν_4 of $B^{10}-B^{10}$(821 cm^{-1}) scattered by *f*. The frequency difference from *e* is 764 cm^{-1} and this is tentatively assigned as ν_{12}.

Three other Raman lines have been tentatively assigned, 1321 cm^{-1} as ν_{15}, 1745 cm^{-1} as ν_6 and 1784 cm^{-1} as $\nu_5+\nu_{18}$ or $\nu_{12}+\nu_7$.

It seemed most reasonable to assign one of the two Raman lines at 1745 cm^{-1} and 1784 cm^{-1} to ν_6, a stretching of the central hydrogens, and 764 cm^{-1} and 1321 cm^{-1} to ν_{12} and ν_{15} which are bending motions of the end hydrogens. In these suggestions two choices still remain to be made and a final decision requires more data such as the Raman spectra of deuterated diborane. However the present choice is self consistent and is somewhat substantiated by the assignment of a value to the inactive torsional vibration ν_5.

A combination frequency involving ν_5 may appear in the unassigned spectrum. The most favorable possibility is 1377 cm^{-1} in the infra-red. The appearance of the band is much like that of ν_{14} at 974 cm^{-1} belonging to the B_{2u} class. Since ν_5 is A_{1u} and by analogy with ethylene should lie around 700 cm^{-1}, a Raman active frequency is required and 764 cm^{-1} is a logical choice.

TABLE V. Thermodynamic properties of diborane, calories/degree mole.

T°K	$(H^0-H_0^0)/T$	$-(F^0-H_0^0)/T$	S^0	C_p^0	C_p Stitt
100	8.00	36.73	44.73	8.26	8.34
200	8.57	42.41	50.98	10.28	10.14
298.16	9.64	46.02	55.66	13.48	
300	9.66	46.08	55.74	13.54	13.59
400	11.08	49.05	60.13	17.14	
500	12.64	51.69	64.33	20.56	
600	14.22	54.13	68.35	23.64	
700	15.77	56.44	72.21	26.33	
800	17.24	58.65	75.89	28.65	
900	18.62	60.76	79.38	30.62	
1000	19.90	62.78	82.68	32.29	
1200	22.20	66.58	88.78	34.89	
1500	25.02	71.90	96.92	37.50	

This yields 613 cm^{-1} for ν_5 and indicates that 764 cm^{-1} be assigned to the B_{2g} mode, ν_{12}, and 1321 cm^{-1} to ν_{15}. The very weak Raman line at 606 cm^{-1} may be ν_5 appearing in violation of the gas phase selection rules. Of the Raman frequencies 1745 cm^{-1} and 1784 cm^{-1} the second is most easily explained as a combination of $\nu_5+\nu_{18}$ or $\nu_{12}+\nu_7$ so that 1745 cm^{-1} is assigned as ν_6.

Calculated Thermodynamic Properties

The thermodynamic functions were calculated from the above vibrational assignment, which is summarized in Table IV and other parameters discussed below using the regular formulas. The moments of inertia were taken as 1.08, 4.72, and 5.04 all $\times 10^{-39}$ g cm^2. The two larger moments of inertia were calculated from the bond distances from electron diffraction data.[12] The smallest moment of inertia, which arises entirely from the hydrogen atoms, was calculated from the spectral data of Price[10] and the other moments of inertia. The symmetry number is four.

The heat capacity of gaseous diborane as measured by Stitt[13] was interpolated to even temperatures and is shown in Table V. The agreement is well within the experimental error assigned by Stitt.

In addition the ΔH^0, ΔS^0, and ΔF^0 of formation of diborane at temperatures from 298.16°K to 1500°K have been calculated and are presented in Table VI. Recent data[14, 15] from the National Bureau of Standards furnishes a value for the heat of formation at 298.16°K for the following reaction:

$$2B_{(amorp.)}+3H_{2(g)}\rightarrow B_2H_{6(g)},$$
$$\Delta H_f^0=6.73\pm0.52 \text{ kcal./mole.}$$

For crystalline boron this becomes 7.5 kcal./mole.

Using the tabulated values of heat content and entropy for diborane and hydrogen[16] and the following approximate equation[17] for boron, the ΔH_f^0 and ΔS_f^0 values were calculated.

$$C_{p(B)}=1.54+4.40\cdot10^{-3}T. \quad (273\text{–}1174°K)\ 5 \text{ percent.}$$

A value of 1.7 for S^0 of B_c at 298.16°K was taken from the N. B. S. table.[15]

TABLE VI.

T°K	ΔH_f^0	ΔS_f^0	ΔF_f^0
298.16	7.5 kcal.	−41.4 cal./deg.	19.8 kcal.
300	7.5	−41.5	20.0
400	6.3	−44.8	24.2
500	5.4	−46.9	28.9
600	4.7	−48.1	33.6
700	4.2	−48.9	38.4
800	3.9	−49.3	43.3
900	3.7	−49.6	48.3
1000	3.5	−49.7	53.2
1200	3.3	−50.0	63.3
1500	2.9	−50.2	78.2

APPENDIX I

Bell[11] has stated that the puckering motion or out of plane deformation of planar rings will yield no quadratic term in the potential energy unless there are torsional forces in the ring bonds. The leading potential energy term is then a quartic. This statement is true only if the ring is unstrained. Since most such rings are probably strained, it seems unlikely that the fourth power oscillator will actually arise often in such cases.

Let us consider a symmetrical four membered ring with valence forces as an example. The puckering motion is determined by symmetry—equal plus and minus motions by alternate particles. If this motion has amplitude z and the bond length is d, then the bond angle, α, at a particle is given by

$$\cos\alpha=4z^2/d^2=\sin(\pi/2-\alpha).$$

Furthermore if α remains near $\pi/2$ this becomes

$$(\pi/2-\alpha)=4z^2/d^2.$$

Thus if the equilibrium value of α is $\pi/2$, the potential energy for small displacements is

$$V=(k/2)(\pi/2-\alpha)^2=(8k/d^4)z^4,$$

which is Bell's result of the fourth power potential. However, if the equilibrium value of α is $(\pi/2+\varphi)$ so that the bond angles are strained by an amount, φ, then one has

$$V=(k/2)(\pi/2+\varphi-\alpha)^2=(k/2)(\varphi+4z^2/d^2)^2$$
$$=(k/2)(\varphi^2+8\varphi z^2/d^2+16z^4/d^4),$$

where the first term is the strain energy and the second term is a normal quadratic term in the coordinate z.

Since cyclobutane, an example discussed by Bell, is certainly strained, there will be a normal quadratic potential energy term for its deformation. Thus it can have a strictly planar equilibrium configuration even though there may be single bond torsional forces opposing planarity.

The application of these results to diborane has been considered already.

[12] S. H. Bauer, Chem. Rev. **31**, 43 (1942).
[13] F. Stitt, J. Chem. Phys. **8**, 981 (1940).
[14] Prosen, Johnson, and Yenchius, Special Report to the ONR, "Experimental determination of the heat of formation of diborane. Calculation of the heat of formation of boric oxide." (September 30, 1948.)
[15] Wagman, Evans, and Levine, Special Report to ONR, "Heat, free energy and equilibrium constants of formation, entropy and heat capacity of compounds of boron." (September 30, 1948.)
[16] Wagman, Kilpatrick, Taylor, Pitzer, and Rossini, J. Research NBS **34**, 143 (1945) RP1634.
[17] K. K. Kelley, U. S. Bur. Mines Bull. **371** (1934).

The Infra-Red Absorption Spectra of Propane-D-1 and Propane-D-2*

L. FRIEDMAN AND J. TURKEVICH
Brookhaven National Laboratory, Upton, Long Island, New York
(Received January 10, 1949)

The infra-red absorption spectra of the isomeric mono-deutero propanes have been observed. A difference in the position of the primary and secondary C–C stretching frequencies is reported. This difference places the secondary C–D frequency 45 $cm^{-1} \pm 5$ cm^{-1} lower than the corresponding primary C–D vibration.

INTRODUCTION

AN investigation of the infra-red absorption spectra of propane-D-1 and propane-D-2 was undertaken in an attempt to determine the precise position of the vibrational frequencies of the isolated primary and secondary carbon-deuterium bonds. Interest in these frequencies was based mainly on the need for an analytical method for the determination of the distribution of deuterium in isotopically substituted hydrocarbons.[1]

MATERIALS AND EXPERIMENTAL

The isomeric propane-D-1 and propane-D-2 were prepared in 0.05-mole batches by decomposing normal and isopropyl magnesium bromide with 99.8 percent heavy water. This decomposition was carried out in a vacuum line and initial batches of the gas of the order of 15–20 cc were discarded to minimize any light hydrogen impurity. The propane formed was separated from any contaminating Grignard solvent, which in this case was iso amyl ether, by distillation from dry-ice to liquid-air traps. The infra-red spectra were obtained from 2–15μ with a Baird Associates, NaCl prism, recording spectrophotometer. The gas cell used was a 5-cm long and spectra in the case of propane-D-2 were taken at pressures of 50, 125, and 200 mm. Tank propane and propane-D-1 were measured at pressures of 50, 125, 200, and 400 mm.

TABLE I. Propane.*

Assignment	Infra-Red (Herzberg)	Infra-Red (Observed)
$\gamma_{20}-\gamma_{14}(B_2)$	720 (*M*) *Q*	
$\gamma_{26}(b_2)$	748 (*S*) *Q*	748 (*S*) *Q*
	864 (*W*) *Q*	
$\gamma_8 C-C(a_1)$	870 (*W*)	870 (*W*)
$\gamma_{21} C-C(b_1)$	922 (*M*)	912 (*M*) *Q*
	925 (*M*) *Q*	
$\gamma_{20}(b_1)$	1053 (*M*) *Q*	1060 (*M*) *Q*
$\gamma_7(a_1)\gamma_{19}(b_1)$	1152 (*M*)	1152 (*M*)
$\gamma_{25}(b_2)$	1179 (*M*) *Q*	1172 (*M*) *Q*
$\gamma_{20}+\gamma_{14}(B_2)$	1338 (*M*) *Q*	1338 (*M*) *Q*
$\gamma_6 CH_3(a_1)$	1370 (*M*)	1380 (*M*)
$\gamma L_8 CH_3 b_1$	1375 (*S*)	1390 (*S*)
$\gamma L_7 CH_3(b_1)$	1465 (*S*) *Q*	
$\gamma_4 CH_2(a_1)$	1468 (*S*)	1468 (γS)
$\gamma_{24} CH_3(b_2)$	1470 (γS) *Q*	
$\gamma_8+\gamma_{21}(B_1)$	1730 (*W*)	1730 (*W*)
$\gamma_{20}+\gamma_{21}(A_1)$	1936 (*W*)	1936 (*W*)
$\gamma_6+\gamma L_8(B_1)$	(2640)	2640 (γW)
$\gamma_{16} CH(b_1)$	2885 (*M*) *Q*	
$\gamma_2 CH(a_1)$	2960 (*M*)	2980
$\gamma_{15} CH(b_1)\gamma_{23} CH(b_2)$	2968 (*S*) *Q*	
$\gamma_{22} CH(b_2)$	2980 (*M*)	
	3190 *W*	3120 *W*
		3300 *W*

* All frequencies in Tables I and II are in units of cm^{-1}.

DISCUSSION OF RESULTS

The infra-red absorption spectrum of propane has been investigated by Bartholome[2] and under high resolution by Wu and Barker.[3] The assignment of frequencies presented in Table I is from Herzberg[4] and is essentially that of Wu and Barker with a slight revision due to Pitzer.[5] In addition in Table I our own experimentally observed frequencies for propane are reported. These are in good agreement with the values presented in A.P.I. Research Project 44 serial No. 99.[6] The spectra of propane, propane-D-1 and propane-D-2 are presented in Figs. 1, 2, and 3, and the tabulation of the frequencies of the deuterium compounds in Table II.

The 3.4μ band is due to 4 or 5 unresolved carbon-hydrogen stretching frequencies. The values obtained

TABLE II. Monodeutero propanes.

Propane-D-1	Propane-D-2
	667 (*W*)
702 (*W*)	
744 (*W*)	
870 (*W*) ?	
912 (*S*) *Q*	912 (*S*) *Q*
992 (*W*)	992 (*W*)
1050 (*M*) *Q*	
1140 (*W*)	1150 (*M*)
	1230 (*W*)
1290 (*M*) *Q*	
1335 (*M*)	1325 (*W*)
1350 (*M*)	
1370 (*M*) *Q*	
	1390 (*M*) *Q*
1407 (*M*) *Q*	
1470 (γS)	1470 (γS)
1650 (*W*)	1650 *W*
2164	2125
2980 (γS)	2970 (γS)

* Work presented has been carried out under the auspices of the AEC.

[1] Turkevich, Friedman, Wrightson, and Solomon, J. Am. Chem. Soc. **70**, 2638 (1948).

[2] E. Bartholome, Zeits. f. physik. Chemie **B23**, 152 (1933).

[3] V. L. Wu and E. F. Barker, J. Chem. Phys. **9**, 487 (1941).

[4] G. Herzberg, *Infra-Red and Raman Spectra* (D. Van Nostrand Company, Inc., New York, 1945).

[5] K. S. Pitzer, J. Chem. Phys. **12**, 310 (1944).

[6] A.P.I. Report 44 (National Bureau of Standards, Washington, D. C., 1945).

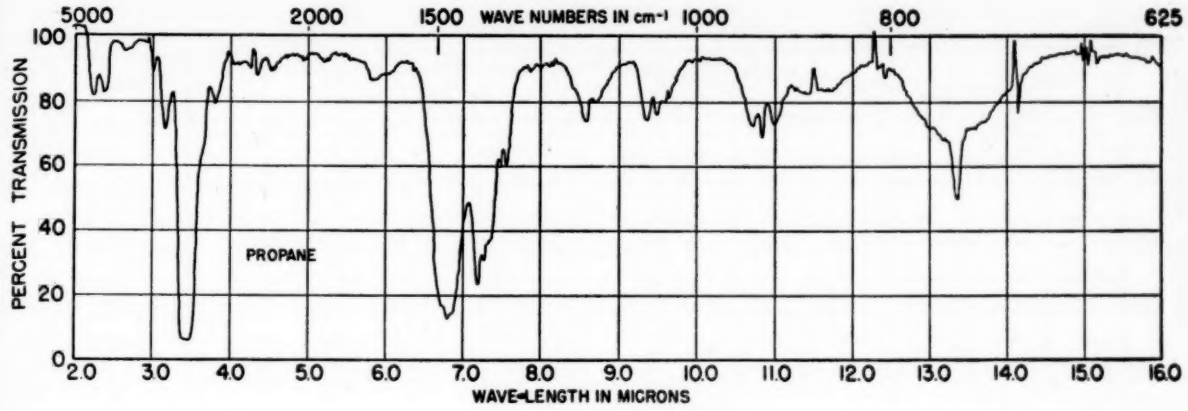

FIG. 1.

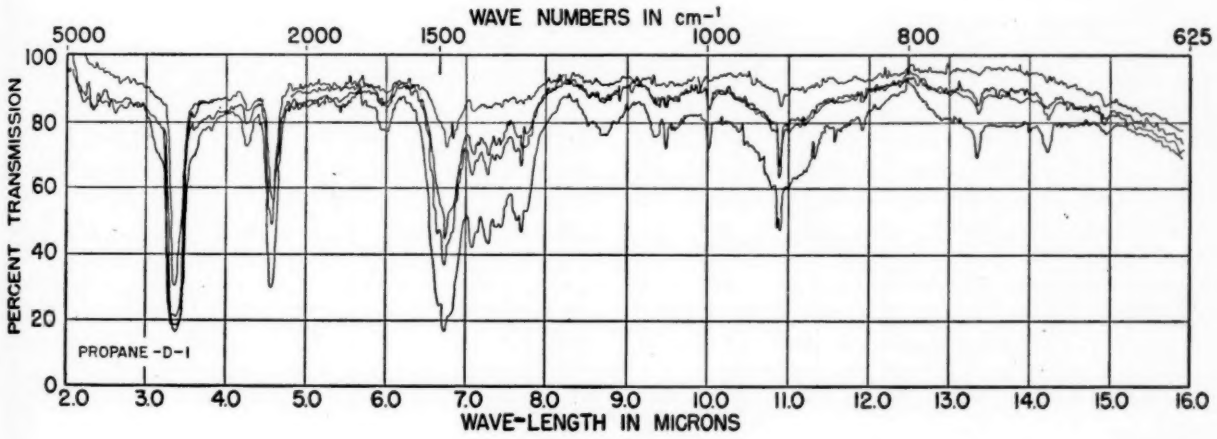

FIG. 2.

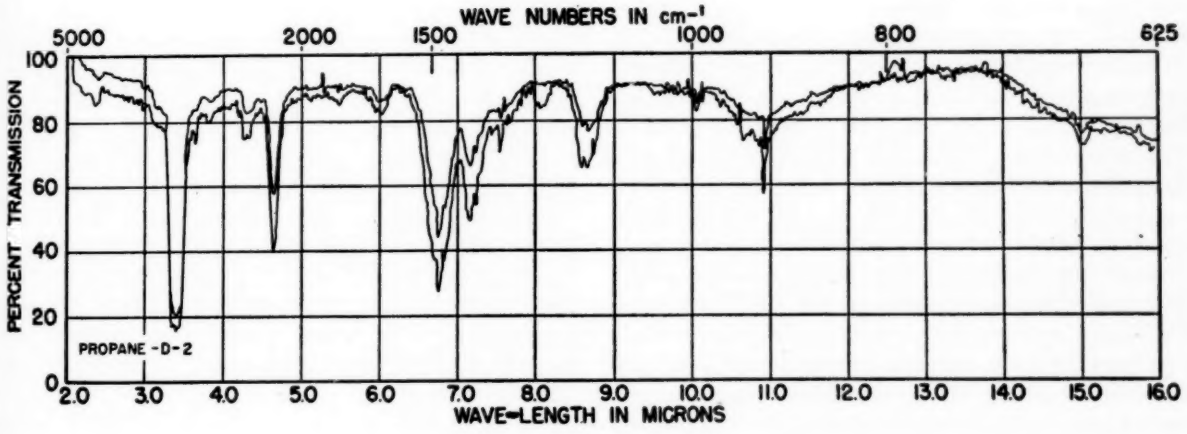

FIG. 3.

for peak of this band are 2980 cm^{-1} and 2970 cm^{-1} for propane-D-1 and propane-D-2 respectively. The difference is not significant in view of an estimated experimental error of 16 cm^{-1} in measurement of frequency in this region of the spectrum. Further discussion of the absorption in this region must await measurements under higher resolution. Fox and Martin[7] have examined, under high resolution, CCl_4 solutions of various hydrocarbons containing CH_3 groups without CH_2 or molecules containing CH_2 groups and no CH_3 groups. They first observed a shift from lower to higher frequency on going from CH_2 to CH_3 stretching vibrations. Two bands were observed in each case and assigned to symmetrical and unsymmetrical vibrations at 2853 cm^{-1} and 2926 cm^{-1} for CH_2 and 2885 cm^{-1} and 2960 cm^{-1} for CH_3 respectively. Thus both frequencies

[7] J. J. Fox and A. E. Martin, Proc. Roy. Soc. London **175**, 208 (1940).

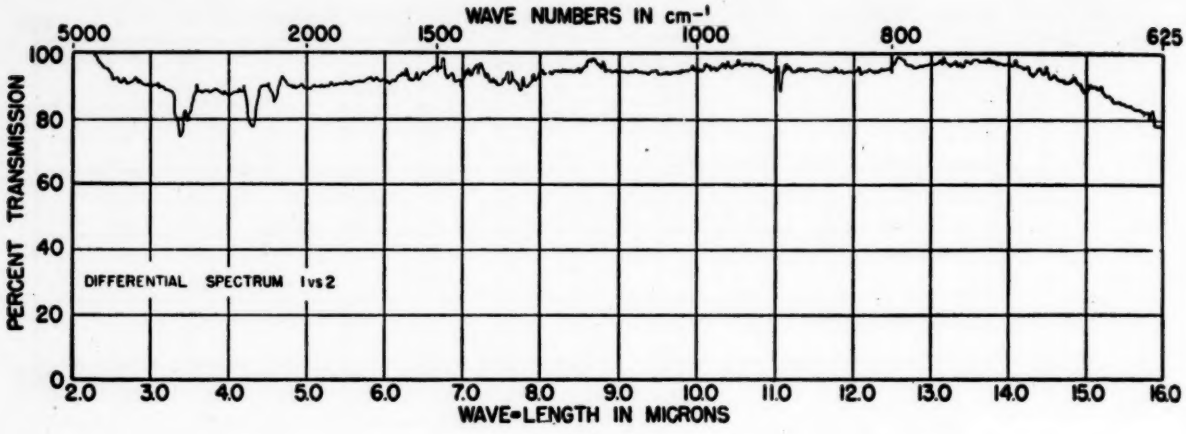

FIG. 4.

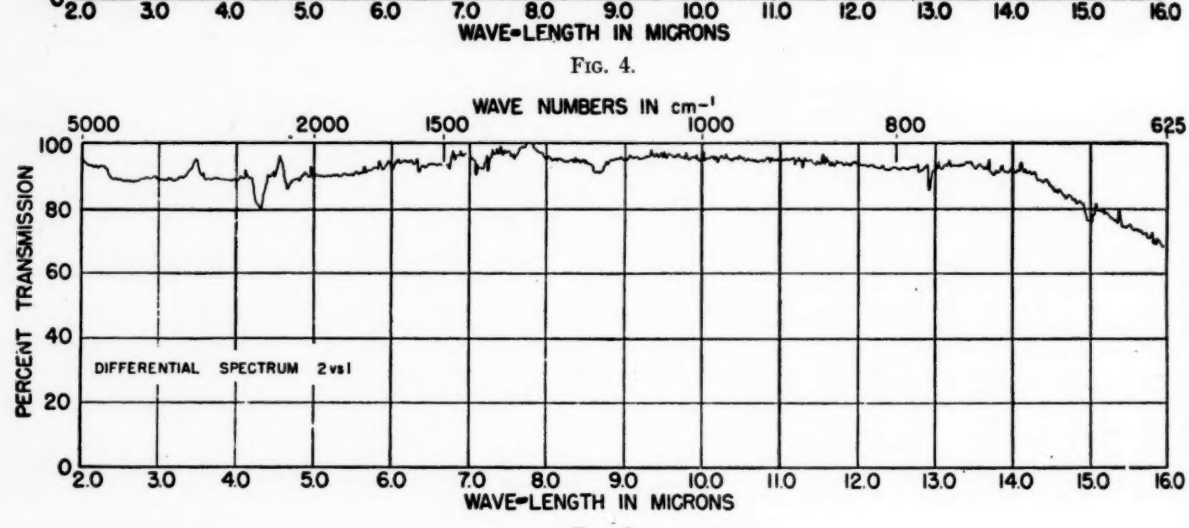

FIG. 5.

shift by approximately 30 cm^{-1} on going from CH_2 to CH_3 groups. In the case of propane which contains CH_2 and CH_3 groups in the same molecule the observed shift is only 12 cm^{-1} (Wu and Barker). The smaller difference between CH_2 and CH_3 in propane must be due to some type of coupling between the CH_2 and CH_3 oscillations. The 4.3μ band is due to absorption by atmospheric carbon dioxide present in the instrument. It is present when a spectrum is taken with no cells in the instrument and is seen in all figures presented.

The 4.6μ band corresponds to the C–D stretching vibration. In propane-D–1, the value is 2164 cm^{-1} and for propane-D–2 the value is 2125 cm^{-1} with an estimated error of 10 cm^{-1}. Since the difference between the observed positions of the C–D bands and the estimated error was rather small, an attempt was made to establish this difference of about 40 cm^{-1} by a more sensitive experimental approach. A difference spectrum was taken by placing a sample of the D–1 compound in one of the two beams of Baird spectrophotometer and the D–2 compound in the other optical path normally reserved for a compensating blank cell. The difference spectra for D–1 *vs.* D–2 and *vice versa* are presented in Figs. 4 and 5. These spectra were taken at 50±5 mm. pressure to minimize the effect of pressure broadening on the position of the band head.

The 4.6μ region of the spectra in Figs. 4 and 5 confirm a difference between the positions of the primary and secondary C–D stretching vibrations giving a separation of 45 $cm^{-1}\pm5$ cm^{-1}, with the secondary C–D vibration coming in at a *lower* frequency. An application of the simple isotope shift rule division of the C–D frequencies by $\sqrt{2}$ to obtain the difference in the C–H frequencies predicts a separation of the order of 60 cm^{-1}. The value is to be compared with the difference observed by Fox and Martin of about 30 cm^{-1} between the CH frequency in CH_3 and CH_2 and is in the proper direction, i.e., CH_2 having lower frequency. Our results and those of Fox and Martin are in disagreement with Wu and Barker who assign the higher frequency, 2980 cm^{-1}, to $\gamma_{22}(CH)(b_2)$ an unsymmetrical CH_2 stretching vibration. Calculation of the C–H frequencies gives 3012 cm^{-1} for C–H secondary and 3075 for the C–H primary stretching vibrations. These values should be compared with the corresponding 2926 cm^{-1} and 2960 cm^{-1} obtained by Fox and Martin from their study of a series of hydrocarbons and 2968 and 2980 of Wu and Barker. Note, however, the reversal of the order reported by the latter workers. We can thus conclude that the coupling in protium propane which decreases the separation of the CH_2 and CH_3 frequencies to 12 cm^{-1} is removed when one goes to the monodeuterated

compounds. Furthermore a reassignment of the 2980 cm^{-1} and 2960 cm^{-1} and 2968 cm^{-1} bands in propane seem in order. The CH_2 stretching vibration $\gamma_{22}CH(b_2)$ cannot be assigned a higher frequency vibration than the unsymmetrical CH_3 stretching $\gamma_2CH(a_1)\gamma_{15}CH(b_1)$ and $\gamma_{23}CH(b_2)$. A better assignment is $\gamma_{22}CH(b_2)$ at 2968 cm^{-1} and $\gamma_{23}CH(b_2)$ at 2980 cm^{-1}.

At 6.8μ there are strong bands of approximately equal intensities in propane, propane-D-1 and propane-D-2. This band has been assigned to methyl and methylene deformation $\gamma_{17}CH_3(b_1)\cdot\gamma_4CH_2(a_1)$ and $\gamma_{24}CH_3(b_2)$ at 1465, 1468, and 1470 cm^{-1} (Tables 1 and 2). No conclusions can be drawn about the validity of the frequency assignment from observations on this band until further isotopic molecules are investigated.

In the 7.0–7.84μ region there is a system of bands which show varying behavior as one goes from propane to the monodeuterated compounds. In propane the frequencies are 1390, 1380, and 1338 cm^{-1}; in propane-D-1 they are 1407, 1370, 1350, 1335, and 1290 cm^{-1}; while in propane-D-2 they are 1390, 1380, 1325 cm^{-1}. The assignments made for these bands in propane is $\gamma_{18}(CH_3)b_1$ to 1390 cm^{-1} and $\gamma_6(CH_3)a_1$ to 1380 cm^{-1} combination band $\gamma_{20}+\gamma_{14}$ to 1338 cm^{-1}. Since the bands at 1338, 1335, and 1325 cm^{-1} are probably this combination, they will not be discussed. The absence of a change in the band structure as one goes from propane to propane-D-2 gives credence to the assignment of the 7.0–7.8-μ band system to methyl deformation frequencies. Furthermore the fact that the 1390–1380 cm^{-1} band in propane and propane-D-2 are replaced by 1407 and 1370 cm^{-1} indicates that these vibrations not only involve the vibrations in methyl groups but also involve some interaction between the methyl groups in the first two compounds which is changed by the introduction of one deuterium into one of the methyl groups.

At 7.6μ there is a band which is present in propane-D-1 (1290 cm^{-1}) and is absent in the other two compounds.

At 8.4μ there are absorption bands in all three compounds at approximately the same frequency 1150 cm^{-1}. This absorption is ascribed to methyl and methylene rocking frequencies.

At approximately 9.5μ there are absorption bands in propane (1053 cm^{-1} and in propane-D-1 at (1050 cm^{-1}) and no band in propane-D-2. The assignment given to this system by Herzberg is $\gamma_{20}(b_1)$ which is methyl rocking. If it is a pure CH_3 rocking frequency it is surprising that it is missing in the propane-D-2 compound where the methyl groups are intact. On the other hand if it is a C–C stretching vibration (Rasmussen,[8] Pitzer,[5] Kohlraush,[9] Kellner,[10] Wu and Barker[3]) its absence in propane-D-2 is even more surprising since these vibrations should be least affected by a particular deuterium substitution.

At 10μ (922 cm^{-1}) there is a weak band in both deuteropropanes which is absent in propane. This is roughly where one might expect an isotope shift on a C–H vibration in the 1400 cm^{-1} region of the spectrum would appear. On the other hand it fits the frequency calculated for C–Cb_1 stretching vibration by Rasmussen (998 cm^{-1}).

At 10.9μ (912 cm^{-1}) there is a strong band in both deuteropropanes which is present as a much weaker band in propane. This band has been assigned by Herzberg as $\gamma_{21}CC(b_1)$ a carbon-carbon stretching variation. However, Rasmussen and Wu and Barker have assigned this as a methyl rocking frequency. The fact that this band persists in all three molecules is strong evidence for the Herzberg assignment.

At 11.5μ (870 cm^{-1}) there is a band with a missing Q branch in propane which is apparently missing in both deuterocompounds. There is a possibility that this band was not detected in the latter compounds because of the increased intensity of the broad band at 10.9μ obscuring it. This band has been assigned as the $\gamma_8(C–C)a_1$ stretching frequency on the basis of Raman data. However, it is possible that this particular carbon-carbon vibration may be coupled with a methyl rocking frequency (see Herzberg,[3] p. 362).

At 13.4μ (748 cm^{-1}) there is a strong band in propane with a sharp central Q band. This band disappears completely in propane-D-2. This has been noted previously in a footnote by Rasmussen. In propane-D-1 there are weak bands at 744 and 702 cm^{-1}. The assignment given by previous workers for this vibration at 748 cm^{-1} is $\gamma_{26}(b_2)$ a methyl rocking. However, Rasmussen prefers to call it a CH_2 rocking frequency. Neither of these assignments explain the spectra and emphasize the fact that the vibrations of the component parts of this molecule are not independent but may be strongly coupled.

In conclusion it should be pointed out that neither a complete assignment of the 22 infra-red-permitted fundamentals of propane nor an unambiguous assignment of all of the 12 or 13 bands observed from 2–15μ can be made from the data available. The two monodeuteropropanes may be readily distinguished from themselves and protium propane. Furthermore by shifting a particular C–H band or set of bands from 3.4μ to the 4.6μ region of the spectrum a means of observing relatively unperturbed carbon-hydrogen vibrations is obtained. The measurements presented indicate a difference of the order of 60 cm^{-1} between primary and secondary C–H frequencies isolated in such a manner. This corresponds to a 4 percent difference in the force constants, in agreement with the results of Fox and Martin.

[8] R. S. Rasmussen, J. Chem. Phys. **16**, 712 (1948).
[9] K. W. F. Kohlraush and F. Koppl, Zeits. f. physik Chemie **B26**, 209 (1934).
[10] L. Kellner, Trans. Faraday Soc. **41**, 217 (1945).

Mass Spectrometer Studies of Thermal Decomposition Products from Hydrocarbons

NORMAN D. COGGESHALL AND NATHAN F. KERR
Gulf Research & Development Company, Pittsburgh, Pennsylvania
(Received January 14, 1949)

A study, by means of a mass spectrometer, has been made of the thermal decomposition products of hydrocarbons. The materials were pyrolyzed in closed ampoules which were subsequently opened to allow the products to be analyzed. A series of runs were made for cetane, *n*-tetradecane and tetradecene-1 in which the pyrolysis time and temperature were independently varied. Data were obtained giving the compositions of the product gases as a function of the pyrolysis parameters. In examining a series of aromatic hydrocarbons it was found that the amount of yield depends primarily upon the number of substituted carbon atoms. A molar yield was defined and found to be a regular function of A/N where A is the number of substituted carbon atoms and N is the total number of carbon atoms per molecule. The pyrolysis residues were washed with iso-octane which was then examined by ultraviolet absorption spectroscopy. It was found that the aromatic skeletons often remained intact throughout the cracking. In addition, it was found that these structures often polymerized or condensed, giving longer wave-length absorption bands.

BY virtue of the range of gaseous products which it can analyze, the minute samples necessary for investigation, its accuracy, and the type of detailed information available, the mass spectrometer is becoming of increasing importance in investigating the thermal decomposition products of organic materials. Brewer[1] and Madorsky and Strauss[2] have studied the decomposition products from polymeric substances. Leifer and Urey[3] have used the instrument to follow the thermal decomposition of dimethyl ether and acetaldehyde. Hipple and Stevenson[4] made a study of the CH_3 radicals produced by thermal decomposition of lead tetramethyl and Eltenton[5] has studied the intermediates occurring during the decomposition of various hydrocarbons ranging from methane to the butylenes. In some of the above investigations specific information in terms of intermediate products and radicals was obtained.

The present report is of some preliminary work wherein no attempt was made to study the intermediate radicals or products. Rather the aim was to obtain information on final decomposition products, obtained under controlled conditions, and to correlate and interpret this in terms of starting materials and decomposition parameters. The method was an empirical one wherein the gaseous products were analyzed after decomposition had ceased. The sample of starting material was in each case charged into a pre-cleaned ampoule. The air was then removed and the ampoule sealed-off. After the pyrolysis a glass tip on the ampoule was broken and the gaseous products removed and analyzed in the mass spectrometer.

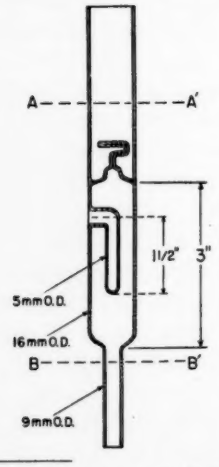

FIG. 1. Schematic view of the decomposition ampoule.

EXPERIMENTAL DETAILS

In Fig. 1 may be seen a cross-sectional view of the type of ampoule used. These were fabricated from Pyrex and with the approximate dimensions shown. In cleaning the ampoule prior to a pyrolysis run the interior of the ampoule was throughly washed with carbon tetrachloride and then with dry acetone. A vacuum line was then attached to the 9-mm O.D. tubing and the vapors removed. At the same time a soft flame was applied to the region between the break-off tip and the section line BB' to bake out the interior surface. Immediately after cleaning the ampoule was charged with the material being investigated. If the sample was liquid and of a sufficiently low viscosity it was introduced by means of a 0.1-ml pipette. If the material was solid or of high viscosity the ampoule was charged by a weight measure. In charging the ampoules it is important that no material cling to the sides near section line BB', as this region gets hot when the ampoule is sealed off and preliminary decomposition may occur in such an event.

With samples of low vapor pressure a vacuum line was attached to the 9-mm O.D. tubing after the charging and the interior pumped down to 10^{-3} mm of Hg or lower. With the vacuum still applied the ampoule was closed off by applying a flame at section line BB'. In the case of volatile materials the ampoule was positioned to the necessary depth in a flask of liquid nitrogen

[1] A. K. Brewer, A. S. T. M. Bulletin, 140 (May, 1946).
[2] S. L. Madorsky and S. Strauss, Ind. Eng. Chem. **40**, 848 (1948).
[3] E. Leifer and H. C. Urey, J. Am. Chem. Soc. **64**, 994 (1942).
[4] J. A. Hipple and D. P. Stevenson, Phys. Rev. **63**, 121 (1943).
[5] G. C. Eltenton, J. Chem. Phys. **15**, 455 (1947).

TABLE I. Composition of decomposition products of refined oil of 375 SUV (210°F)

Compound	Run No. 2	Run No. 13	Run No. 28	Run No. 25
methane	69.9 percent	25.9 percent	23.2 percent	30.5 percent
ethane	25.2 percent	16.1 percent	14.6 percent	22.3 percent
ethylene	1.3 percent	18.8 percent	22.3 percent	7.7 percent
propane	1.7 percent	5.4 percent	4.3 percent	10.5 percent
propylene	0.6 percent	18.8 percent	22.6 percent	13.2 percent
n-butane	—	0.4 percent	0.3 percent	2.0 percent
i-butane	—	1.8 percent	1.7 percent	2.2 percent
butenes	—	8.9 percent	7.6 percent	7.7 percent
C_5's	—	3.6 percent	3.4 percent	3.9 percent
benzene	1.3 percent	0.3 percent	—	—

Run No. 2— 75 minutes at 564°C
Run No. 13— 75 minutes at 473°C
Run No. 28— 45 minutes at 470°C
Run No. 25—120 minutes at 470°C

just prior to the evacuation and during the sealing. The re-entrant 5-mm, O.D. tubing allowed a thermocouple to be inserted to the geometrical center of the ampoule and thus to a position at which the mean temperature would be expected.

The windings of the furnace were of Nichrome wire and the overall length of the heated region was 12 inches. The ampoule was positioned at the center of this for the pyrolysis and the cross-section of the furnace was so designed so that the ampoule and the controlling element of the thermostat were side-by-side. The furnace was controlled with a Partlow Chromalox Thermostat.* The actual temperatures reported in the data were those determined with the thermocouple mentioned above. After pyrolysis the upper tubing of the ampoule was cut along section line AA' and a stopcock and an iron slug for the magnetic break-off were sealed on.

The materials examined were obtained from Phillips Petroleum Company, Eastman, Dupont, Sharples, and Connecticut Hard Rubber Company. In each case they were of the highest purity obtainable. In some cases there was doubt as to the high purity of the material. However, these were not further purified in view of the preliminary nature of the work.

The volume of each ampoule was approximately the same. When the gas was extracted from the ampoule it was expanded into a constant, evacuated volume in each case. The gas in a definite and constant portion of this volume was then further expanded into an expansion reservoir which connected directly with the leak which admitted the gas to the ionization region of the mass spectrometer. Since constant volume relationships existed in each case it was possible to analyze, by well-known methods,[6,7] the mass spectra for the mixtures and to calculate the concentrations of the individual components. These were calculated in terms of convenient arbitrary pressure units which are adequate to allow absolute comparisons between separate samples. Absolute pressure values for individual samples may be obtained by the proper calibration technique. The concentration of molecular hydrogen could not be determined due to a defect in the ion source which would not allow the use of the necessary high accelerating voltages.

In a number of cases the iso-octane soluble components of the residue in the ampoule were examined by ultraviolet absorption spectroscopy. This was done by washing the interior of the ampoule with pure iso-octane which was subsequently examined in a Beckman Quartz Spectrophotometer.

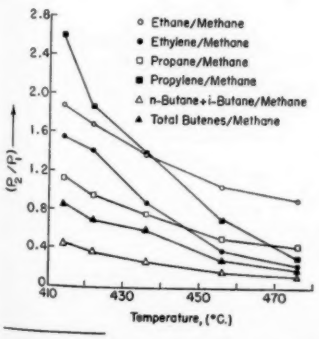

FIG. 2. Plot of (p_2/p_1) ratios for *n*-tetradecane decomposition at various temperatures with a pyrolysis time of 75 minutes.

* Obtainable from Edwin L. Wiegand Co., Pittsburgh, Pa.

DATA AND DISCUSSION

The initial experiments were carried out on a sample of refined oil of 375 Saybolt Universal Viscosity (210°F).

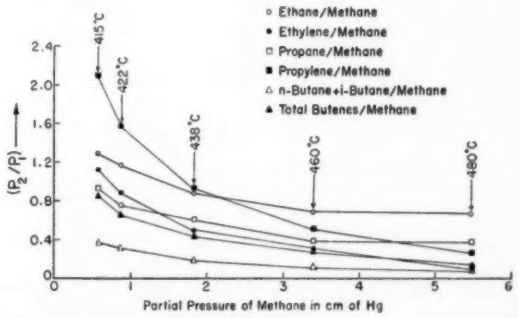

FIG. 3. Plot of (p_2/p_1) ratios versus methane content for tetradecene-1. Constant time of 75 minutes, temperature varied.

[6] Washburn, Wiley, and Rock, Ind. Eng. Chem., Anal. Chem. 15, 541 (1943).

[7] N. D. Coggeshall and J. A. Hipple, Colloid Chemistry, Vol. VI, edited by Jerome Alexander (Reinhold Publishing Corporation, N. Y., 1946), p. 89.

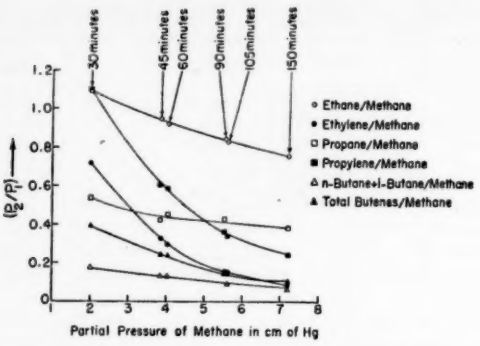

FIG. 4. Plot of (p_2/p_1) ratios versus methane content for cetane. Constant temperature of 475°C, pyrolysis time varied.

This particular oil was of no specific interest but was merely chosen as a convenient material for exploratory work in establishing methods, technique, testing of reproducibility, etc. In Table I may be seen some typical data from the runs made on this material. In each case the concentrations are given as percentages of total gaseous hydrocarbon product. Except as a means of establishing the technique used for later samples the results from these runs were of relatively little value. They did demonstrate that for a constant pyrolysis time an increase of temperature increases the methane and other light material content at the expense of the heavier hydrocarbons. Also they showed that the same thing happened for a series of runs wherein the temperature was maintained constant and the pyrolysis time was increased. In the latter case the rate of change of concentrations was relatively slow. It was found to be difficult to obtain reproducible results for a material of this sort. Part of the trouble was believed to be due to the detailed manner in which the ampoule was charged, i.e., whether the oil was smeared over a sizeable surface or concentrated in a globule.

In order to obtain reproducible data and at the same time to investigate the effects of small differences of molecular structure on the decomposition products a series of runs were made on cetane, *n*-tetradecane, and tetradecene-1. Two sets of data were taken for each compound. In one, the time of pyrolysis was 75 minutes in each case, and the temperature was varied. In the other, the pyrolysis temperature was held constant and the time varied. It was standard practice to charge the ampoule with 0.1 ml of material.

It was found upon scrutinizing the data that the partial pressures of the gaseous products did not always correlate with the pyrolysis parameter, i.e., time or temperature, with the expected consistency. However, the changes of composition were quite regular and it is believed that the inconsistencies are primarily due to an inability to control the degree of thermal cracking by this technique. Therefore, the changes of composition rather than absolute yield values were determined for each pyrolysis. It was found convenient to use the ratios of concentrations of the various products to that of methane as the dependent variables for following the decomposition. This served to demonstrate the composition changes in a manner that allows exact comparisons to be made between samples without determining the absolute yield values. In Fig. 2 may be seen some of the data for *n*-tetradecane. Here may be seen the ratios (p_2/p_1) plotted versus the pyrolysis temperature where p_1 refers to the methane partial pressure in our arbitrary scale of units and p_2 refers to the partial pressure of any of the other components in the same set of units.

We note in Fig. 2 that no data are given for temperatures below 415°C. This is due to the fact that at lower temperatures, using a pyrolysis time of 75 minutes, there is a very small amount of cracking and it becomes difficult to reliably analyze the minute amount of gase-

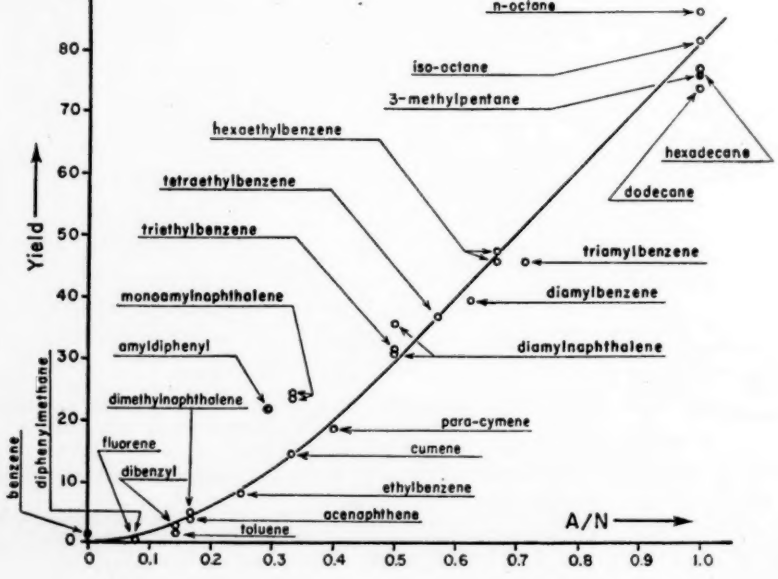

FIG. 5. Molar yield as a function of the A/N ratio for twenty-three hydrocarbons.

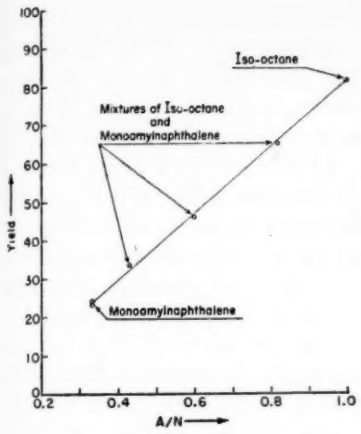

FIG. 6. Molar yield as a function of the A/N ratio for a series of synthetically prepared samples.

ous material formed. This limitation applies to all of the data shown at the low end of the independent variable. In some cases it was found that the composition changes were not regular with changes of cracking temperature or time, but depended rather on the amount of gaseous product formed. This again is due to the inability of the technique to accurately control the degree of cracking. However, if the partial pressure of methane in the product is used as a measure of degree of cracking the data become quite consistent. This may be seen in Fig. 3 where (p_2/p_1) is plotted *versus* the methane concentration for the products from the pyrolysis of tetradecene-1. Here it may be seen that there are regular trends of the composition with increasing methane yield. The cracking time for these runs was 75 minutes. Another set of data, this time for cetane with a constant pyrolysis temperature of 475°C, may be seen in Fig. 4. Here again we have (p_2/p_1) plotted *versus* methane concentration, and it is seen that the data are consistent even though the pyrolysis times are not regularly distributed along the curve.

Complete data, i.e., (p_2/p_1) *versus* temperature, *versus* methane concentration with constant pyrolysis temperature, and *versus* methane concentration with constant pyrolysis time, were obtained and plotted for cetane, *n*-tetredecane, and tetradecene-1. No significant differences in the data which could be correlated with differences in molecular structure were evident. This is really to be expected in view of the close similarities of structure and the fact that after the cracking is well started it is essentially a thermodynamic process. It is significant that in the data shown in Figs. 2, 3, and 4 the concentrations of the olefins changed much more rapidly with temperature and with degree of cracking than did the paraffin concentrations. This shows that the olefins are much more predominant in the early stages of decomposition. Presumably this is because an aliphatic radical may be split off which may, after some re-arrangement and in some cases a loss of a hydrogen atom, become an olefin whereas the formation of a paraffin would require some recombination. As a means of differentiating between compounds which are quite similar in structure this technique appears to hold little promise although the above data demonstrate that consistent data may thereby be obtained for following the change of composition with pyrolysis temperature and with the degree of cracking.

In scrutinizing the data obtained in this manner for a large number of aromatic hydrocarbons it was evident that the amount of product formed depended primarily upon the aliphatic substituents. It is well known that aromatic ring structures are very stable against thermal decomposition and hence this result is not surprising. However, as there appeared to be a regular trend for the amount of product as a function of the number of substituted aliphatic carbons, a procedure for quantitatively evaluating it was tested. In order to do this it was necessary to obtain a total yield figure for each pyrolysis. It was necessary that this

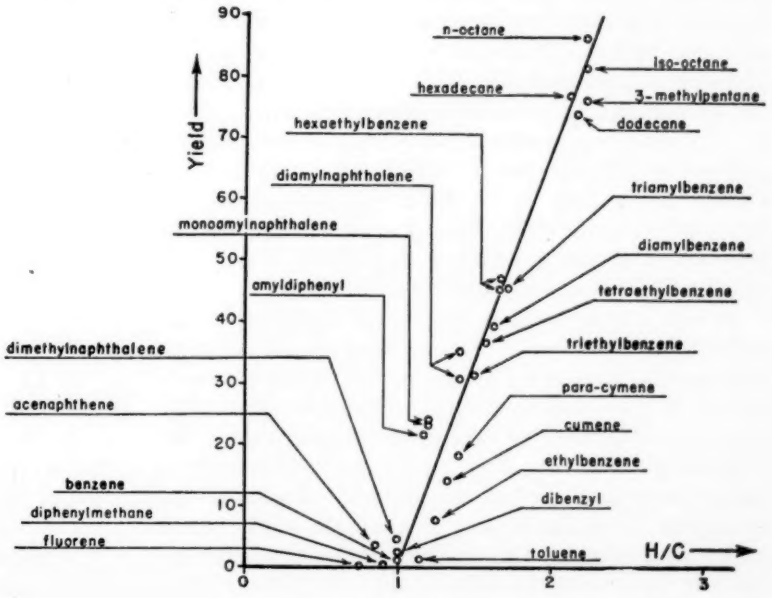

FIG. 7. Molar yield as a function of the H/C ratio for twenty-three hydrocarbons.

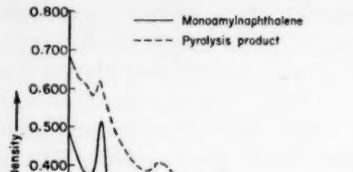

FIG. 8. Ultraviolet absorption spectra of monoamylnaphthalene and of its iso-octane soluble pyrolysis products.

figure account for the total number of carbon atoms in the gaseous products formed by the decomposition. The total yield is defined as:

$$\text{total yield} = \sum n_i p_i,$$

where p_i represents the partial pressure of the ith component and n_i is the number of carbon atoms per molecule of this component. Since the partial pressure values are in arbitrary units, the total yield will be in arbitrary units. However, it will allow absolute comparisons to be made between various compounds and pyrolysis conditions.

Since the densities of the various liquid materials varied and since some of the samples were charged as solids it was necessary to put the results on a common basis which would account for variations in amount of material charged. For this purpose a molar yield was defined. This was defined as the total yield per mole of carbon atoms charged. The moles of carbon atoms charged is merely the fractional mole of material charged multiplied by the total number of carbon atoms per molecule. The molar yield hence gave a value for the pyrolysis products from a sample which could be correlated with the degree of aromaticity. The degree of aromaticity, or conversely of paraffinicity, was defined as the ratio A/N where A is the number of aliphatic carbon atoms and N is the total number of carbon atoms per molecule. With this definition $A/N=0$ for all completely aromatic compounds and $A/N=1$ for all completely paraffin compounds. Aromatic hydrocarbons with unsaturated substituents were not included in the data to be shown as they apparently have different decomposition properties. It was impossible to obtain a sufficient number of these compounds to definitely establish this.

In Fig. 5 may be seen the results when the molar yield is plotted *versus* A/N for twenty-three different compounds. These data are all from 75 minute runs at 520°C. It is to be observed that a definite relationship exists. It is difficult to determine to what extent the scattering of the data depends upon the differences in molecular structure or on the impurity of some of the materials. There was no way in which the purity of the materials exhibiting the greatest deviations from the smooth curve could be reliably assayed. If the experimental data were not quite reproducible it would of course lead to such a scattering. In order to determine the inherent reproducibility of these data repeat runs were made for the three compounds: monoamylnaphthalene, hexaethylbenzene, and diamylnaphthalene. As may be seen from the figure the first two gave quite reproducible values. The data for the latter material did not check so well, although the agreement is still within the scattering exhibited elsewhere along the curve. In view of these results it is believed that the scattering is largely due to impure materials. It is quite significant that the observed correlation exists throughout the various classes of compounds examined. This establishes that the yield of decomposition products depends upon the number of carbon atoms in the substituted groups.

The relationship shown in Fig. 5 immediately suggests the usefulness of such data for assaying the A/N ratio, which may be interpreted in terms of the aromaticity, for a sample of unknown constitution or for a mixture whose proportions are unknown. In order to test such a procedure a series of synthetic samples were made and examined. In one case these samples were made as mixtures of monoamylnaphthalene and iso-octane. The results for them may be seen in Fig. 6. Here it is to be observed that the data for the mixture lie on a straight line drawn between the points for monoamylnaphthalene and iso-octane. Another series of mixtures composed of ethylbenzene and iso-octane were also examined. In this latter case the data also defined a straight line relationship. This is consistent with the data of Fig. 5 as the range of the A/N ratio for the mixtures was over that part of the region wherein the curve of Fig. 5 is essentially a straight line.

The H/C ratio, i.e., ratio of number of hydrogen atoms to the number of carbon atoms per molecule, was calculated for each compound. The molar yield was then plotted versus H/C for the same series of material to test for any correlation. The data for this are shown in Fig. 7. Although a definite trend is demonstrated it is clear that no such definite relationship as seen in Fig. 5 exists. This indirectly confirms the conclusion of above which stated that the molar yield of gaseous products depended primarily upon the number of substituted carbon atoms.

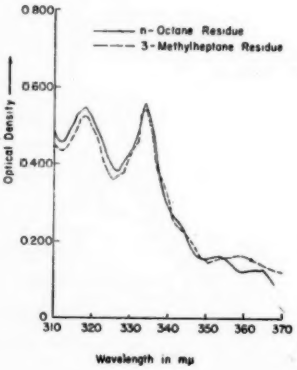

FIG. 9. Ultraviolet absorption spectra of the iso-octane soluble pyrolysis products from *n*-octane and 3-methylheptane.

It is well known that the phenyl ring and other condensed ring aromatic structures are very stable against thermal decomposition. In view of this and of the above results it would be expected that a number of condensation and polymerization products would be found in the pyrolysis residue. As parts of the substituent groups were cracked off it would be expected that there would be considerable condensation taking place among the remaining aromatic radicals. It is fortunate that this may be tested.

It is well known that the absorption in the ultraviolet for aromatic hydrocarbons is due to a resonance phenomenon involving the phenyl rings.[8] It is further known that the conjugation of two such resonating structures or the conjugation of an olefin group with such a resonating structure will give rise to an absorption band occurring at a longer wave-length than the absorption bands possessed by the original components. Hence in comparing the ultraviolet spectra of the pyrolysis residues with the spectra of the original materials we would expect to find two things. One would be the spectra indicative of the original aromatic structure and the other would be absorption bands at longer wave-lengths indicating the conjugation of such structures, either with themselves or with olefin groups which could arise from the cracking of the substituent groups. Such results may be seen in Fig. 8 which shows the spectra between 310 and 380 mμ for monoamylnaphthalene and its pyrolysis product. In this figure the optical density, defined by: optical density$=\log(I_0/I)$, where I_0 is the intensity of the light incident on the sample and I is the intensity of the transmitted light, is plotted versus wave-length. The absorption maximum appearing at about 320 mμ is characteristic of the naphthalene structure. It is to be seen that this same maximum appears in the spectrum of the pyrolysis product. In addition there is another absorption maximum appearing at about 335 mμ which is seen to be absent in the naphthalene spectrum. This longer wave-length band is ascribed to the conjugation of the types described above.

[8] G. N. Lewis and M. Calvin, Chem. Rev. **25**, 273 (1939).

Further results of this type in which conjugation is evidenced by longer wave-length absorption were observed for several other materials. Diamylnaphthalene gave a result essentially the same as seen in Fig. 8. The pyrolysis product from diphenylmethane gave spectra indicative of an olefinic group conjugated with a benzene ring and also of a fluorene type structure. The latter is believed to be due to a partial dehydrogenation of the benzene rings with consequent bridging between them. An interesting result was provided by phenanthrene which possesses no substituted aliphatic groups. The spectrum of its pyrolysis products exhibited the same absorption bands as did the original material. However, the relative intensities were varied with the result that the longer wave-length bands were relatively increased in intensity while the shorter wave-length bands were decreased in intensity. It is not known what this indicates unless it is a polymerization of the structures resulting from partial dehydrogenation. An interesting result of a case wherein the thermal cracking apparently produced some aromatic or other unsaturated material may be seen in Fig. 9. This shows the spectra for the pyrolysis residue for *n*-octane and for 3-methylheptane. Both of these compounds are transparent in this region. The bands exhibited in both cases fall in the region characteristic of naphthalene structures. It is remarkable that the residues from both of these hydrocarbons gave approximately the same spectrum. When the residue from the pyrolysis of dibenzyl (1,2-diphenylethane) was examined it was found to possess a spectrum believed to be due to a higher degree of unsaturation and conjugation. This could result from the partial dehydrogenation of the C_2H_4 group joining the phenyl ring and from bridging between partially dehydrogenated phenyl rings.

Acknowledgment is gratefully made to Dr. C. W. Montgomery for discussions of the subject, to Mr. A. S. Glessner for obtaining some of the ultraviolet absorption data, and to Dr. P. D. Foote, executive Vice-President of Gulf Research and Development Company for permission to publish this work.

Ionic Character and the Dipole Moment of Chemical Bonds. Calculations of the Dipole Moment of HCl*

DAVID Z. ROBINSON†
Mallinckrodt Chemical Laboratory, Harvard University, Cambridge, Massachusetts
(Received March 17, 1949)

The method of assigning the ionic character of chemical bonds by the use of the dipole moment is examined for the case of hydrogen chloride. Using both the atomic orbital and the LCAO molecular orbital approximation, the ionic character of HCl is calculated. Not only do the values so calculated seem unreasonable from energy considerations, but the calculated rate of change of dipole moment with respect to internuclear distance does not agree with the experimentally observed infra-red intensity. This discrepancy is due to the large dipole moment associated with the covalent bond. Although the results for a purely covalent compound are in agreement both with the dipole moment, and the infra-red intensity, if the dipole is assumed to have the orientation Cl^+H^-, this assumption is discredited by the fact that one would have to assume more ionic character for HBr than HCl. If we make the assumption that $s-p$ hybridization occurs, these difficulties are removed. It is shown that the dipole moment of the purely covalent molecule is a very sensitive function of the amount of hybridization, and the covalent molecule can have almost any reasonable dipole moment. Thus it is shown that there are difficulties which must be surmounted before one can use dipole moments to obtain ionic character.

INTRODUCTION

PAULING[1] has given a method for obtaining the ionic character of chemical bonds from electronegativity data. This method is based on the correlation of the electronegativities of the hydrogen halides with their ionic character as obtained from the dipole moments.[2]

The purpose of this paper is to discuss the method of obtaining ionic character from dipole moments, especially the nature of the dipole moment of a covalent molecule.

There have been other attempts to calculate dipole moment of HCl from wave functions.[3,4] Coulson[5] has calculated the dipole moment of the C−H bond in methane using the molecular orbital approximation.

By approximating the wave functions of the electrons in HCl, it is possible to calculate the ionic character from the dipole moment μ. Then by assuming that the ionic character does not vary appreciably with internuclear distance for small displacements, it is possible to calculate $\partial\mu/\partial d$, where d is the internuclear distance. One can compare this with the experimental infra-red intensity.[6] It is thus possible to obtain a check on the ionic character obtained.

The results show that there are difficulties that must be explained before one can use dipole moments to obtain ionic character. The dipole moment of the covalent bond is hard to determine. On the simple picture of a pure p bond it is of the order of -1 debye unit (using the atomic orbital approximation), i.e., the hydrogen negative. When $s-p$ hybridization is taken into effect, values up to $+2$ debye units can be found depending on the amount of hybridization.

ASSUMPTIONS

In the calculation of the dipole moment the following assumptions are made:

1. Polarization of the non-bonding electrons is neglected.
2. The wave functions are assumed to be hydrogen-like functions with screening constants obtained from Pauling and Sherman.[7]
3. The change of ionic character for small changes in interatomic distance can be neglected.

GENERAL FORMULAS

The dipole moment μ is given by Eq. (1) where e is the electronic

$$\mu=ed-e\sum_i \bar{z}_i, \tag{1}$$

charge, d is the internuclear distance, and $\bar{z}_i$ is the average value of z (defined with the chlorine at the origin and the z axis along the bond) for the ith electron and the sum is taken over all the electrons. The first term is due to the proton and the second to the electrons.

If we now assume that all the electrons except the two bonding electrons have their average position at the chlorine nucleus, i.e., no polarization or hybridization of the non-bonding electrons, then Eq. (1) becomes

$$\mu=ed-2e\bar{z}_b, \tag{2}$$

where $\bar{z}_b$ is the average value of z for each bonding electron.

To obtain $\bar{z}_b$ it is necessary to know the wave function for the two bonding electrons, ψ_b (assuming that the complete wave function is a product-type function of all the other electrons).** Then $\bar{z}_b$ is given by Eq. (3).

$$\bar{z}_b=\left[\int|\psi_b|^2 z_1 d\tau_b\right]\Big/\left[\int|\psi_b|^2 d\tau_b\right]. \tag{3}$$

* The research reported in this document received support under Task Order V, Contract N5ori-76, ONR.
† Present address: Baird Associates, University Road, Cambridge, Massachusetts.
[1] Pauling, *Nature of the Chemical Bond* (Cornell University Press, Ithaca, New York), p. 69–75.
[2] See reference 1, p. 46.
[3] Wall, J. Am. Chem. Soc. **62**, 800 (1940).
[4] Mulliken, J. Chem. Phys. **3**, 573 (1935).
[5] Coulson, Trans. Faraday Soc. **38**, 433 (1942).
[6] Bourgin, Phys. Rev. **32**, 237 (1928).
[7] Pauling and Sherman, Zeit. f. Krists. **81**, 1 (1932).
** If the wave function were completely antisymmetrized, then one would have to include small terms involving overlap of non-bonding orbitals with the H orbital.

TABLE I. Table of calculated values of $\bar{z}$ for the bonding electrons, dipole moments, $\partial\bar{z}/\partial d$ and $(1/e)\partial\mu/\partial d$ for the various types of bonds, and comparison with the results quoted by Rollefson.[a]

	$\bar{z}_b$ (Bohr radii)	μ (Debye units)	$\frac{\partial\bar{z}_b}{\partial d}$	$\frac{1}{e}\frac{\partial\mu}{\partial d}$
Atomic orbital pure covalent bond	1.402	−0.98	0.358	0.283
Molecular orbital pure covalent bond	1.541	−1.69		
Atomic orbital mixed ionic covalent	0.989[b]	+1.10	0.150	0.700
Molecular orbital mixed ionic covalent	0.989[b]	+1.10	0.158	0.784
Experimental values		±1.10[a]		±0.197

[a] See refetence 11.
[b] Ionicity chosen so as to fit dipole moment value of +1.10 debye units

It is normally assumed that the chlorine part of the wave function involved in the bonding is a $3p_z$ function (hereafter called p) and that the hydrogen part of the function is a $1s$ function centered around the hydrogen nucleus (hereafter called h). Using the atomic orbital approximation,[8] the wave function for the bonding electrons is given by (4).

$$\psi_b^{\text{cov}}=p(1)h(2)+h(1)p(2). \tag{4}$$

If we make the LCAO molecular orbital approximation, then we obtain[9] (5):

$$\psi_b{}^{1\text{ cov}}(1,2)=[p(1)+h(1)][p(2)+h(2)]. \tag{5}$$

These are wave functions for purely covalent bonds. We must take ionic character into account. In the atomic orbital approximation this means adding a term representing an ionic structure.

$$\psi_b=\psi_b^{\text{cov}}+\lambda p(1)p(2). \tag{6}$$

For the molecular orbital case we put in a factor to show that the electron spends more time around the chlorine nucleus.

$$\psi_b{}^1=[\lambda^1 p(1)+h(1)][\lambda^1 p(2)+h(2)]. \tag{7}$$

It is possible to calculate λ or λ^1 from the observed dipole moment. This type of calculation has been done before, mainly by Pauling,[2] Wall,[3] and Mulliken.[10,4]

Pauling[2] and also Wall[3] assumed that purely covalent HCl would have no dipole moment, in other words, $\bar{z}_b=d/2$. Mulliken[10,4] estimated that the electrons on the average would be at the end of the covalent radius. This would lead to a dipole moment of about −2.5 debye units (the hydrogen end being negative). Neither of these very different assumptions is in accord with the results of the following analysis.

IONIC CHARACTER OF HCl ON THE ASSUMPTION OF *P* BONDS

To obtain $\bar{z}_b$ for a purely covalent bond, it is necessary to substitute Eqs. (4) and (5) into Eq. (3).

$$\bar{z}_1{}^{\text{cov}}=\int[p(1)h(2)+p(2)h(1)]^2 z_1 d\tau_1 d\tau_2 \Big/ \int[p(1)h(2)+p(2)h(1)]^2 d\tau_1 d\tau_2. \tag{8}$$

$$\bar{z}_1{}^{1\text{ cov}}=\int[p(1)+h(1)]^2 z_1 d\tau_1 \Big/ \int[p(1)+h(1)]^2 d\tau_1. \tag{9}$$

On expanding and using the following definitions and equations:

$$\int p(1)^2 z_1 d\tau_1=0; \quad \int h(1)^2 z_1 d\tau_1=d. \tag{10}$$

$$\int p(1)^2 d\tau_1=\int h(1)^2 d\tau_1=1. \tag{11}$$

$$\int p(1)h(1)d\tau_1=S; \quad \int z_1 p(1)h(1)d\tau_1=M. \tag{12}$$

Then

$$\bar{z}_1{}^{\text{cov}}=[d+2MS]/[2+2S^2]. \tag{13}$$

$$\bar{z}_1{}^{1\text{ cov}}=\frac{d+2M}{2+2S}. \tag{14}$$

If we assume ionic character, substituting Eqs. (6) and (7) in Eq. (3), we obtain the following answers for $\bar{z}_b$:

$$\bar{z}_b=\frac{d+2MS+2\lambda M}{2+2S^2+\lambda^2+4\lambda S}, \tag{15}$$

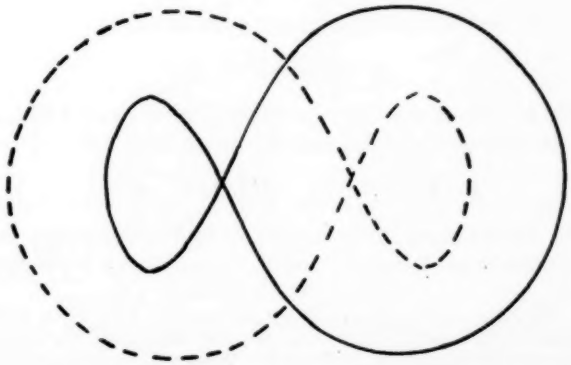

FIG. 1. Schematic representation of bonding (——) and non-bonding (– – –) s-p hybridized orbitals.

[8] See, for example, Pauling and Wilson, *Introduction to Quantum Mechanics* (McGraw-Hill Book Company, Inc., New York, 1935).
[9] For a recent review of the molecular orbital method see Coulson, Quart. Rev. 1, 144 (1947).
[10] Mulliken, ONR Report (1948). Formulas are given here for the dipole moment as a function of ionic charge, overlap moment, etc. We are grateful to Professor Mulliken for an interesting discussion of this report (to be published in J. de Chim. Phys.), and for criticism of this paper.

or

$$\bar{z}_b{}^1=\frac{d+2\lambda^1 M}{1+(\lambda^1)^2+2\lambda^1 S}. \tag{16}$$

Therefore, for all these cases it is only necessary to calculate the overlap integrals

$$S=\int h(1)p(1)d\tau_1, \quad \text{and} \quad M=\int h(1)p(1)z_1 d\tau_1.$$

It is at this point that the present study deviates from those of previous investigators. Both Pauling[2] and Wall[3] implicitly assumed S small so that $\bar{z}_1\rightarrow d/2$. Mulliken[10] overestimated the effect of overlap of the functions and thus obtained a large negative value for μ cov.

S and M were calculated using hydrogen-like wave functions with a screening constant of 6.5.

Numerically:***

$$S=0.4833,$$
$$M=1.078.$$

Substitution of these values into Eqs. (13) and (14) leads to

$$\bar{z}_b{}^{\text{cov}}=1.402 \text{ (Bohr radii)},$$
$$\bar{z}_b{}^{1\text{ cov}}=1.541 \text{ (Bohr radii)}.$$

Substitution of these values into Eq. (2) gives

$$\mu_{\text{cov}}=-0.98\text{D},$$
$$\mu_{\text{cov}}{}^1=-1.69\text{D}.$$

If we assume a value for μ of $+1.10$ debye units,[11] then $\bar{z}_b$ would equal 0.989 Bohr radii. With this assumption we can calculate λ and λ^1 from Eqs. (15) and (16)

$$\lambda=1.14,$$
$$\lambda^1=1.96.$$

These values of λ and λ^1 seem much too high from energy considerations.[2] Furthermore, allowance for polarization of the non-bonding electrons would give an even more negative covalent dipole, and one would have to use even larger λ's to compensate for this.

CHECK WITH $\partial\mu/\partial d$

Differentiating Eq. (2), one obtains

$$\partial\mu/\partial d=e-2e\partial\bar{z}_b/\partial d.$$

We get $\partial\bar{z}/\partial d$ by differentiating Eqs. (15) and (16) so it is necessary to calculate $\partial S/\partial d$ and $\partial M/\partial d$

$$\partial S/\partial d=-0.120, \quad \partial M/\partial d=-0.189.$$

On substituting these values into the formulas, one obtains the following results, assuming λ and λ^1 constant.

$$\partial\bar{z}_{\text{cov}}/\partial d=0.3583,$$
$$\partial\bar{z}/\partial d=0.150,$$
$$\partial\bar{z}^1/\partial d=0.108,$$

and, on further substitution,

$$1/e[\partial\mu_{\text{cov}}]/[\partial d]=+0.2834,$$
$$1/e\partial\mu/\partial d=0.700,$$
$$1/e\partial\mu^1/\partial d=0.784.$$

The experimental value of $1/e[\partial\mu/\partial d]$ is ± 0.197 (as obtained from an effective charge of 0.93×10^{-10} e.s.u.). These results are summarized in Table I. It is important to note that the rather dubious assumption that λ and λ^1 remain constant on stretching has been made.

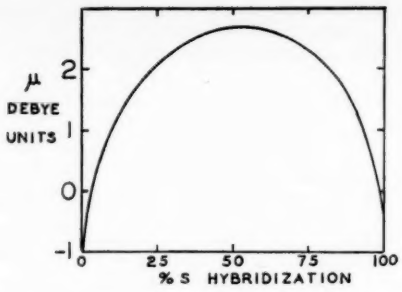

FIG. 2. Dipole moment of covalent HCl as a function of s-hybridization.

From these results one would conclude that highly ionic p bonds are not possible. However, the results are in good agreement with an almost purely covalent compound if we assume that the dipole moment is negative. But if the actual dipole moment were negative one would expect that the calculated value of μ_{cov} for NBr would be smaller than that for HCl since the actual dipole moment of HBr is smaller than that of HCl. This is not the case (as is shown below) so that one would have to assume more ionic character for HBr than HCl, an assumption which seems unreasonable and which, therefore, discredits the idea that the moment is negative.

DIPOLE MOMENT OF COVALENT HBR

Using the same method as used for HCl with a $4P_z$ wave function and a screening constant of 8.90, the values of S and M were found to be 0.492, and 1.362 Bohr radii, respectively. These lead to a dipole moment of -1.40 debye unit, using the atomic orbital approximation.

Since a negative dipole moment is caused by the difference in size of the atoms, this result is not surprising. We, therefore, can eliminate the possibility that HCl has a negative dipole moment.

ASSUMPTION OF $S-P$ HYBRIDIZATION

As pointed out by Mulliken[10] $s-p$ hybridization would improve our results. The atomic orbitals for a hybridized bond are shown schematically in Fig. 1.

*** These two integrals and similar ones for HBr, were calculated by Professor E. B. Wilson, Jr., and checked by the author. The author is grateful to Professor Wilson for lending him his unpublished manuscript.

[11] R. Rollefson and A. N. Rollefson, Phys. Rev. 48, 779 (1935). The sign is not determined experimentally.

We now have to consider dipole moments of the non-bonding s electrons, Qualitatively we can say these are two electrons in the non-bonding orbital while there is one on the average in the bonding orbital. The large negative value of $\bar{z}$ for the non-bonding electrons would lead to a more positive dipole moment. This effect was first discussed by Coulson[5] and is most responsible for his calculated negative value of the C—H dipole moment.†

Now we assume that the chlorine part of the wave function for the bonding electrons is

$$\psi_{cl}=a^{\frac{1}{2}}s+(1-a)^{\frac{1}{2}}p,$$

which leads to the following result for ψ_b on the atomic orbital approximation

$$\psi_b=[a^{\frac{1}{2}}s(1)+(1-a)^{\frac{1}{2}}p(1)]h(2)+h(1)[a^{\frac{1}{2}}s(2)+(1-a)^{\frac{1}{2}}p(2)],$$

where s is a $3s$ function centered at the chlorine nucleus.

The wave function for the non-bonding hybridized electron is

$$\psi_{nb}=[1-a]^{\frac{1}{2}}s-a^{\frac{1}{2}}p.$$

Equation (2) must now be modified

$$\mu=ed-2e\bar{z}_b-2e\bar{z}_{nb}.$$

We now substitute the wave function to obtain the average value of $\bar{z}_{nb}$

$$\bar{z}_{nb}=\int z(\psi_{nb})^2 d\tau=-2[a(1-a)]^{\frac{1}{2}}P,$$

where

$$P=\int spzd\tau=\frac{3[6]^{\frac{1}{2}}}{Z}$$

Bohr radii from atomic wave functions. By the same method as in Eq. (13)

$$\bar{z}_b=\frac{d+2[(a^{\frac{1}{2}}M^1+(1-a)^{\frac{1}{2}}M)(a^{\frac{1}{2}}S^1+(1-a)^{\frac{1}{2}}S)]+2[a(1-a)]^{\frac{1}{2}}P}{2+2(a^{\frac{1}{2}}S^1+(1-a)^{\frac{1}{2}}S)^2},$$

where $S^1=\int shd\tau=0.4744$, and $M^1=\int shzd\tau=0.7395$. The first term is caused by the hydrogen orbital, the second by the overlap, and the third by the chlorine orbital.

The dipole moment of a purely covalent HCl is plotted as a function of the hybridization in Fig. 2. We can see that the moment is a very sensitive function of the amount of hybridization. Therefore, because of this great dependence on hybridization, it is only possible to say that hybridization probably takes place, and that the ionic character is difficult to determine.

SUMMARY OF RESULTS AND CONCLUSIONS

The assumption of pure p bonds for the chlorine wave function of HCl leads to ionic character that is inconsistent both with energy considerations and with the experimental result for $\partial\mu/\partial d$. The main discrepancy is due to the large negative value of the covalent contribution to the dipole moment, arising from the fact that the bonding electrons are closer to the hydrogen nucleus than to the chlorine nucleus. In fact the results for pure p bonds would suggest that the actual value of the dipole moment might well be negative, since the calculated value for $\partial\mu/\partial d$ agrees with the experimental value. However, when the covalent dipole of HBr is calculated, it leads to a more negative value. To fit a negative value of μ it would be necessary for HBr to have greater ionic character than HCl. This does not appear reasonable.

These difficulties are removed if $s-p$ hybridization is considered. Then, although the dipole moment of the bonding electrons is made even more negative, it is more than balanced out by the "atomic" dipole caused by the non-bonding electrons. Now almost any value of dipole moment could be accounted for with purely covalent HCl. A value for the ionic character could be obtained from approximate energy data, and the amount of hybridization could be adjusted so as to fit the dipole moment. However, for the calculation of $\partial\mu/\partial d$, the assumption would have to be made that the amount of hybridization as well as ionicity would stay constant upon stretching. This assumption does not seem reasonable. Consequently, dipole moments do not give a good method for determining ionic character of bonds. The simple picture here presented shows that even in the case of HCl with the very simple assumptions made, the dipole moment is so sensitive to bond hybridization that interpretations are difficult.

However, it is reasonable to assume that the bond in covalent chlorine is not a pure p bond and that some hybridization must occur.[10] This has been suggested by Townes and Dailey[12] who examined the quadrupole coupling constant data for other molecules. A pure p function will probably not represent accurately such properties of the molecule as the dipole moment or quadrupole coupling constant with any great degree of accuracy. Whether the additional complication of $s-p$ hybridization gives a useful picture depends on whether one can predict with it any useful properties of the molecule.

ACKNOWLEDGMENT

The author wishes to thank Professor E. Bright Wilson, Jr., under whom this work was carried out, for his guidance and helpful advice.

† In Coulson's case there is no overbalancing effect from the other electrons since they are involved in other bonds. For HCl the actual moment of the bond is more negative but the moment of the non-bonding electrons balances it out.

[12] Townes and Dailey, J. Chem. Phys. (to be published).

Developments in the Theory of the Secular Equation for Molecular Vibrations

P. TORKINGTON
*The Physical Chemistry Laboratory, Oxford, England**
(Received December 16, 1948)

A general solution for the secular equation is obtained, giving the force constants and normal coordinates, for any molecule, in terms of the fundamental vibration frequencies and molecular constants. The solution is based on the reduction of the secular determinant to Jacobian canonical form; it is shown to have a simple physical interpretation. Methods are developed which enable adjustments to be made to the standard solution as required. The theory is fully illustrated by several worked examples.

I. INTRODUCTION

THE process of calculating the force constants in the potential function for a given molecule from its fundamental vibration frequencies is one determined to some considerable extent by individual preference. One usually carries over as many constants as possible from related molecules and adjusts the whole set to fit the observed frequencies, introducing interaction constants where the adjustment required appears unreasonable. This process involves a series of trial-and-error calculations. As data on various related molecules accumulate, it is in principle possible to adjust the values of the force constants to obtain sets which are mutually consistent, so that any variations from an accepted "normal" value can be taken as having physical significance. In practice, there is usually considerable ambiguity, and values differing by amounts up to 10 percent may be obtained for a given force constant by investigators using different force fields on the same molecule. It would therefore be useful to have available a procedure for obtaining a set of force constants characteristic of each molecule, corresponding to some ideal solution, and for making adjustments to this solution as required. Such a procedure is worked out in the present investigation.

II. THE DERIVATION OF THE SECULAR EQUATION

The secular equation can be expressed in several different forms which, for the sake of completeness, will be derived here from first principles. For a molecule with n vibrational degrees of freedom, in which the motions are assumed to be simple harmonic, the potential energy V can be written as a general quadratic function of n valence-type displacement coordinates Δ_i as follows:

$$2V=\sum_{i=1}^{n}\sum_{j=1}^{n} d_{ij}\Delta_i\Delta_j, \tag{1}$$

where the d_{ij} are force constants, the matrix $\mathrm{d}=[d_{ij}]$ being symmetric. The n internal coordinates can be expressed in terms of $N(N=n+6)$ Cartesian displacement coordinates z_j,

$$\Delta_i=\sum_{j=1}^{N} a_{ij}z_j, \tag{2}$$

where the coefficients a_{ij} are determined by the geometry of the system; they are conveniently written in the form of a matrix $\mathrm{a}=[a_{ij}]$ of order $n\times N$. The equations of motion are

$$(\partial V/\partial z_k)-\lambda m_k z_k=0, \quad (k=1 \text{ to } N), \tag{3}$$

where m_k is the mass corresponding to the displacement coordinate z_k, the latter being assumed to be a sinusoidal function of the time, and λ is related to one of the normal vibrational frequencies ν of the system as,

$$\lambda=4\pi^2\nu^2. \tag{4}$$

The system of N linear and homogeneous Eqs. (3) in z_1 to z_N requires that the determinant of the coefficients shall vanish. This condition leads to the first form of the secular equation, which can be written as

$$|\mathrm{a'da}-\lambda\mathrm{m}|=0, \tag{5}$$

where a' is the transpose of a, and m the diagonal matrix $[m_1m_2\cdots m_N]$. The general element of the matrix $\mathrm{b}=\mathrm{a'da}$ is

$$b_{ij}=\sum_{k=1}^{n}\sum_{m=1}^{n} a_{ki}a_{mj}d_{km}. \tag{6}$$

The determinant in Eq. (5) is symmetric and of order N; the N roots of the equation in λ include the $(N-n)$ zero frequencies of translation and rotation, and the relative displacements $z_1(\nu_k)$ to $z_N(\nu_k)$ in the kth normal mode are given by first minors of any row of the determinant in Eq. (5), with the appropriate root λ_k substituted.

A second form of the equation is obtained by applying the transformation

$$R_p'=\sum_{i=1}^{N}(|{}^N\mathrm{a}|_{pi}/|{}^N\mathrm{a}|)R_i, \tag{7}$$

giving rows R_p' of a new determinant in terms of rows R_i of Eq. (5); the elements $|{}^N\mathrm{a}|_{pi}$ are first minors of the determinant $|{}^N\mathrm{a}|$ formed from the Nth-order square matrix ${}^N\mathrm{a}$ of the coefficients a_{ij} in Eq. (2), in which the last $(N-n)$ rows are from the "null coordinates" expressing the conditions for no translation and

* At present working at the Department of Theoretical Physics, King's College, London, while holding a Research Fellowship granted by Courtauld's Limited.

no rotation (where these are not included in any symmetry properties possessed by the coordinates Δ_i).[a] The secular equation now has the following form:

$$|\mathrm{da}-\lambda({}^{N}\mathrm{a}^{-1})'\mathrm{m}|=0, \tag{8}$$

where $({}^{N}\mathrm{a}^{-1})'$ is the reciprocal of the transpose of ${}^{N}\mathrm{a}$, and the product da is regarded as a square matrix of order $N\times N$ whose last $(N-n)$ rows consist of zero elements. The general element in Eq. (8) is as follows:

$$b_{ij}'=\sum_{k=1}^{n} a_{kj}d_{ik}-(|{}^{N}\mathrm{a}|_{ij}/|{}^{N}\mathrm{a}|)\lambda m_j, \tag{9}$$

the first term being zero in the last $(N-n)$ rows. Eq. (8) is again of order N and, since Eq. (7) involves only the rows of Eq. (5), the relative displacements $z_1(\nu_k)$ to $z_N(\nu_k)$ are again given by first minors of any row.

By means of a further transformation giving columns C_q'' of a new determinant in terms of columns C_j' of Eq. (8), as follows:

$$C_q''=\sum_{j=1}^{N} a_{qj}(M/m_j)C_j', \tag{10}$$

a third form of the secular equation is obtained, which can be written

$$|\mathrm{dA}-\lambda\mathrm{I}|=0, \tag{11}$$

where the elements of the symmetric matrix A are derived from the rows of a in Eq. (2) according to the scheme,

$$A_{ij}=\sum_{k=1}^{N} a_{ik}a_{jk}(M/m_k). \tag{12}$$

I is the unit matrix, and the quantity λ is redefined as

$$\lambda=4\pi^2\sigma^2c^2M, \tag{13}$$

σ being now a normal vibration frequency in cm^{-1} and c the velocity of light in cm sec^{-1}. M is an arbitrary mass (usually chosen to be one of the m_k's), introduced in order that the A_{ij} shall be dimensionless quantities of convenient magnitude. Equation (11) is of order n, the $(N-n)$ null vibrations having been factored out. A is identical with the kinetic energy matrix G of Wilson,[1] apart from the factor M included here for convenience in application; the symbol G is not used in order to avoid confusion. The general element of the matrix B = dA is

$$B_{ij}=\sum_{k=1}^{n} A_{jk}d_{ik}. \tag{14}$$

The transformation in Eq. (10) leads to the expressions for the relative displacements occurring in any normal mode:

$$z_j=\sum_{i=1}^{n} a_{ij}(M/m_j)D_{ki}, \tag{15}$$

$$\Delta_i=\sum_{j=1}^{n} A_{ij}D_{kj}, \tag{16}$$

where the D_{ki} and D_{kj} are first minors of the kth row of the secular determinant in Eq. (11), k having any value from 1 to n.

III. THE SOLUTION OF THE SECULAR EQUATION FOR THE FORCE CONSTANTS

The second-degree equation has been dealt with at some length in a recent investigation.[2] It was found possible to obtain equations giving the complete range of allowed values for the force constants, and to relate these with the forms of vibration and with the potential energy distributions. Formulas were obtained for various singular and related solutions, and it was shown that one of the solutions in which the secular determinant in the form given in Eq. (11) was reduced to the product of its diagonal elements gave reasonable results. No such general treatment is possible with equations of higher degree, but it would be of interest to examine the solution corresponding to the second-degree case, in which the matrix B = dA is reduced to Jacobian canonical form. With the determinant |B| reduced to the product of its diagonal elements, since a given diagonal element B_{kk} is a function of the force constants d_{kj}, $(j=1$ to $n)$, the root $\lambda_k=B_{kk}$ can be regarded as a group frequency characteristic of the coordinate Δ_k, corrected for interaction with the remainder of the molecule. The conditions for the reduction are[2a]

$$\sum_{i=1}^{n} A_{ki}d_{ki}-\lambda_k=0, \quad (k=1, 2, \cdots n), \tag{17}$$

$$\sum_{i=1}^{n} A_{qi}d_{pi}=0, \quad (p>q), \tag{18}$$

where λ_k is derived from the vibration frequency assigned to the normal mode determined primarily by Δ_k. By analogy with the second-degree case,[2] the subscripts are ordered so that $\nu_1>\nu_2\cdots>\nu_n$. The solution of these $\frac{1}{2}n(n+1)$ linear simultaneous equations gives all the elements of d. For convenience, we introduce two subsidiary matrices e and h, with elements as defined:

$$e_{ij}={}^{j}|\mathrm{A}|_{ji}, \quad (=0 \text{ for } i>j), \tag{19}$$

$$h_{ij}=\sum_{k=1}^{j} A_{ik}e_{kj}, \quad (=0 \text{ for } i<j). \tag{20}$$

In the above, ${}^{j}|\mathrm{A}|_{ji}$ is a first minor[b] of the jth row of

[a] If the molecule possesses elements of symmetry, the coordinates Δ_1 to Δ_n are chosen to satisfy the symmetry requirements of the n normal modes in a given symmetry class. Equation (11) is then the symmetry factor of the secular equation for this class of vibration. The total secular equation is the product of all such factors, one from each class.

[1] E. B. Wilson, Jr., J. Chem. Phys. **7**, 1047 (1939); **9**, 76 (1941).

[2] P. Torkington, J. Chem. Phys. **17**, 357 (1949).

[2a] P. Torkington, Nature **162**, 370, 607 (1948).

[b] Throughout, unless otherwise stated, the term "minor" refers to the minor with proper algebraic sign, the first minor being identical with a cofactor; a presuperscript is used to indicate the order of a determinantal element, subscripts referring to derived minors.

the jth-order determinant ${}^{j}|A|$ derived from the first j rows and columns of A; h_{ij} is an unsigned minor of order $(i-j)$ with respect to $i|A|$. The general solution for the force constants is found to be

$$d_{ij}=\sum_{k=i}^{n}(e_{ik}e_{jk}/e_{kk}h_{kk})\lambda_k, \quad (i>j). \tag{21}$$

If, before solving for the constants, the k highest frequencies are factored out by Wilson's method,[1] the same formula applies, the subscripts now referring to elements of the reduced d and A matrices, and λ_1 to λ_n being replaced by λ_{k+1} to λ_n; nothing is gained here, therefore, by making this initial reduction. The nondiagonal elements of d will in general be small compared with the diagonal elements; several obvious approximations arise from Eq. (21). In the next section, methods will be given for eliminating all small interaction constants by adjusting the remainder.

If the λ_k are disregarded, the elements of the series in Eq. (21) are seen to be the terms of a general Schweinsian expansion; because of this fact, the force constants d_{ij}, $(i>j)$, can be expressed in terms of λ_i and of the differences $(\lambda_i-\lambda_k)$, as

$$d_{ij}=({}^{n}|A|_{ij}/{}^{n}|A|)\lambda_i - \sum_{k=i+1}^{n}(e_{ik}e_{jk}/e_{kk}h_{kk})(\lambda_i-\lambda_k). \tag{22}$$

The upper non-diagonal elements of the matrix B=dA follow from Eq. (22):

$$B_{ij}=\sum_{k=i}^{j}(e_{ik}h_{jk}/e_{kk}h_{kk})\lambda_k, \quad (=0 \text{ for } i>j). \tag{23}$$

An alternative form of Eq. (23) is convenient,

$$B_{ij}=-\sum_{k=i+1}^{j}(e_{ik}h_{jk}/e_{kk}h_{kk})(\lambda_i-\lambda_k), \quad (=0 \text{ for } i>j). \tag{24}$$

The normal coordinates corresponding to the solution for the force constants in Eq. (21) can now be found. For the kth normal mode, $(B_{kk}-\lambda_k=0)$, the first k members of the first minors D_{ki} of the kth row of the secular determinant in Eq. (11) are found to be proportional to the corresponding elements e_{ik} of the matrix e defined in Eq. (19); $D_{k,k+1}$ to D_{kn} become zero. Thus,

$$D_{k1}:D_{k2}:\cdots:D_{kk}:D_{k,k+1}\cdots D_{kn}::e_{1k}:e_{2k}:\cdots :e_{kk}:0:\cdots:0. \tag{25}$$

With the above ratios for the minors, the relative atomic displacements describing the geometrical form of a given normal mode are

$$z_j(\nu_k)=(M/m_j)\sum_{i=1}^{k}a_{ij}e_{ik}, \tag{26}$$

and the components in the displacements from the coordinates Δ_1 to Δ_n,

$$\Delta_i(\nu_k)=h_{ik}, \quad (=0 \text{ for } i<k). \tag{27}$$

The quantities defined in Eqs. (26) and (27) are the coefficients in the linear transformations giving the displacements z_j and Δ_i in terms of the (unnormalized) normal coordinate for ν_k.[c] To normalize them, the total potential energy in Eq. (1) is required in terms of the displacements Δ_i as defined in Eq. (27). It is found that

$$2V(\nu_k)=e_{kk}h_{kk}\lambda_k. \tag{28}$$

The potential energy distribution for any given normal mode can now be obtained; the following relations are found to hold:

$$\sum_{i=1}^{n}V_{ki}(\nu_k)=1, \tag{29}$$

$$\sum_{i=1}^{n}V_{mi}(\nu_k)=0, \quad (m\neq k), \tag{30}$$

where $V_{ij}(\nu_k)$ is the fraction of the total potential energy in the term $d_{ij}\Delta_i\Delta_j$, for the kth normal mode, and d_{ij} and d_{ji} are counted separately.

The solution dealt with in this section has a simple physical interpretation. The displacement for ν_k involves only the coordinates Δ_k to Δ_n; thus the reduction of the matrix B=dA to Jacobian canonical form causes the fundamental vibration frequencies to factor out in order of decreasing magnitude, the molecule increasing in rigidity as factorization proceeds. (Compare Taylor and Pitzer.[3]) The force constants d_{ij} are expressed in terms of λ_i to λ_n only (where i is greater than j); they are derived from the rows of the subsidiary matrix e in a manner analogous to that in which the A_{ij} are derived from a. The solution is always real, and it is found that the normal coordinates correspond to the vibrations having idealized geometrical forms; thus, in valence vibrations, the atomic displacement vectors in general lie along the appropriate valence bonds. This last fact is readily seen in the case of ν_1, for which $z_j \propto (a_{ij}/m_j)$.

IV. VARIATIONS FROM THE STANDARD SOLUTION

The standard solution derived in the last section gives all the elements of the matrix d as explicit functions of minors of A and of the vibration frequencies. In practice, many of the nondiagonal elements of d will be found to have small values, this applying to most which would normally be discarded before solving for the constants. To eliminate them, we require the various

[c] The linear transformation giving the (unnormalized) normal coordinates is found to be $\eta_i=\sum_{j=1}^{i}e_{ji}\Delta_j$, where η_i is the normal coordinate for the ith normal mode.

[3] W. J. Taylor and K. S. Pitzer, J. Research Nat. Bur. Stand. 38, 1 (1947).

derivatives $(\partial\lambda_k/\partial d_{ij})$; in this section, these quantities will also be obtained as explicit functions of minors of $|A|$.

Consider the general expanded form of the secular equation of order n,

$$\lambda^n - c_1\lambda^{n-1} + c_2\lambda^{n-2} \ldots + (-1)^{n-1}c_{n-1}\lambda + (-1)^n c_n = 0. \quad (31)$$

The coefficients c_1 to c_n are related to the matrix B of Eq. (14) as

$$c_i = sp_i|B|, \quad (32)$$

where sp_i stands for the sum of all principal minors of order i. c_i is also the ith elementary symmetric function of the n roots λ_1 to λ_n of Eq. (31). For small variations of the coefficients c_i, the corresponding variations in any root λ_k are governed by the relation,

$$(\partial\lambda_k/\partial c_i) = (|\sigma|_{ik}/|\sigma|), \quad (33)$$

where $|\sigma|$ is the Jacobian of c_1 to c_n with regard to λ_1 to λ_n, and $|\sigma|_{ik}$ is the cofactor of the element σ_{ik}; the general element σ_{ij} is the $(i-1)$th symmetric function minus all terms involving λ_j, the first row consisting of unit elements. The minors of the Jacobian are found to have the form

$$|\sigma|_{ik} = (-1)^{i+k}\lambda_k{}^{n-i}\prod_{p,q}(\lambda_p - \lambda_q), \quad (p<q;\ p, q\neq k). \quad (34)$$

The Jacobian itself is the difference-product of λ_1 to λ_n:

$$|\sigma| = \prod_{i,j}(\lambda_i - \lambda_j), \quad (i<j). \quad (35)$$

It follows that

$$(\partial\lambda_k/\partial c_i) = (-1)^{i+1}\lambda_k{}^{n-i}\prod_{p}(\lambda_k - \lambda_p)^{-1}, \quad (p\neq k). \quad (36)$$

The variations in the coefficients c_i may be expressed in terms of variations in the elements B_{ij}, using (32) and the usual rule for differentiating determinants; for diagonal elements,

$$(\partial c_i/\partial B_{jj}) = s_j p_{i-1}|B|, \quad (=1 \text{ for } i=1), \quad (37)$$

where the subscript j denotes the omission of all minors involving B_{jj}. If products of non-diagonal elements are neglected, the expressions for frequency-variation can be shown to be those derived from the following first approximation to the roots of the secular equation,

$$\lambda_k = B_{kk} + \sum_{i=1}^{n}[B_{ki}B_{ik}/(B_{kk} - B_{ii})], \quad (i\neq k). \quad (38)$$

This approximation is suitable when ν_k is a group frequency known to be practically independent of the remainder of the molecule; the series following the summation sign is the first-order perturbation term for the kinetic coupling. Where this is known to be slight,[3a] interaction terms may be neglected and Eq. (38) reduces to

$$\lambda_k = d_{kk}\{A_{kk} + \sum_{i=1}^{n}[A_{ik}^2/(\lambda_k - \lambda_i)]d_{ii}\}, \quad (i\neq k), \quad (39)$$

where approximate values suffice for the d_{ii} and $(\lambda_k - \lambda_i)$. Equation (39) can be used to predict the shifts in a group frequency caused by coupling of the group to different residues, or to estimate variations in a group force constant caused by electronic interaction with different environments.

From Eq. (14),

$$(\partial B_{mk}/\partial d_{ij}) = \begin{cases} A_{kj} & \text{for } m=i, \\ 0 & \text{for } m\neq i, \end{cases} \quad (40)$$

$$(\partial B_{im}/\partial A_{kj}) = \begin{cases} d_{ij} & \text{for } m=k, \\ 0 & \text{for } m\neq k, \end{cases} \quad (41)$$

where d_{ij} and d_{ji} are counted separately. From Eq. (41), possible errors introduced by uncertainties in the molecular dimensions may be estimated and equations for the isotope effect obtained. Thus, for replacement of the mass m_p by an isotope, the increments in the elements A_{ij} are

$$\Delta A_{ij} = -a_{ip}a_{jp}(M/m_p)(\Delta m_p/m_p), \quad (42)$$

and the associated increments in the elements of B as

$$\Delta B_{ij} = -a_{jp}(M/m_p)(\Delta m_p/m_p)\sum_{k=1}^{n}a_{kp}d_{ik}. \quad (43)$$

If we ignore non-diagonal elements of d and B, the following expression is obtained for the frequency-shifts:

$$\Delta\lambda_k = -a_{kp}{}^2 d_{kk}(M/m_p)(\Delta m_p/m_p), \quad (44)$$

and, as a first approximation,

$$(\Delta\lambda_k/\lambda_k) = -(a_{kp}{}^2/A_{kk})(M/m_p)(\Delta m_p/m_p). \quad (45)$$

Where ν_k is a group frequency, Eq. (45) will give a good approximation; where the coordinates Δ_k and Δ_j overlap to any considerable extent (i.e., where (A_{kj}/A_{kk}) and (A_{kj}/A_{jj}) are of the order of unity), the approximation corresponding to Eq. (44) will be obtained by including terms for d_{jj} and d_{kj}, d_{jk} from B_{kk}, B_{jj} and B_{jk}, B_{kj}.

In favorable cases, where the first term of Eq. (21) gives a good approximation for the constant d_{ij}, the errors introduced by uncertainties in the molecular dimensions are readily estimated,

$$d_{ij}{}^0 = (e_{ji}{}^0/h_{ii}{}^0)\lambda_i, \quad (i>j), \quad (46)$$

$$(\Delta d_{ij}/d_{ij}{}^0) = (\Delta e_{ji}/e_{ji}{}^0) - (\Delta h_{ii}/h_{ii}{}^0), \quad (47)$$

where e^0 and h^0 refer to the model with conventional dimensions (e.g., with angles for exact trigonal and tetrahedral hybrid structures), and the variations correspond to possible variations in these dimensions. The errors caused by uncertainties in the vibration frequencies (such as differences between infra-red and Raman

[3a] P. Torkington, Nature **164**, 113 (1949)..

frequencies), may be evaluated directly from the series in Eq. (21); the approximation given in Eq. (46) serves well enough for the main (square term) constants.

For the standard solution obtained in the last section, it is possible to give explicit expressions for the derivatives $(\partial\lambda_k/\partial d_{ij})$. We first require the variations with respect to the B_{ij}. The following relations are found to hold:

$$(\partial\lambda_k/\partial B_{kj})=(e_{jk}/e_{kk}), \quad (=0 \text{ for } j>k) \tag{48}$$

$$(\partial\lambda_k/\partial B_{ik})=(h_{ik}/h_{kk}), \quad (=0 \text{ for } i<k) \tag{49}$$

$$(\partial\lambda_k/\partial B_{ij})=(\partial\lambda_k/\partial B_{ik})(\partial\lambda_k/\partial B_{kj}), \tag{50}$$

where e and h are the matrices which define the force constants and normal coordinates. (See Eqs. (19) and (20)). The general expression for the variation of a given vibration frequency with any particular force constant, counting d_{ij} and d_{ji} separately, is then

$$(\partial\lambda_k/\partial d_{ij})=(h_{ik}h_{jk}/e_{kk}h_{kk}), \quad (=0 \text{ for } k>i \text{ or } j). \tag{51}$$

The derivatives for any particular λ_k therefore form the elements of a symmetric matrix of order $(n-k+1)$, derived from A. The standard d matrix obtained by applying the formula given in Eq. (21) may now be suitably adjusted, or partially diagonalized. The increments

$$\Delta\lambda_k=-\sum_{i,j}(\partial\lambda_k/\partial d_{ij})d_{ij}$$

produced by removing interaction constants d_{ij} are found (remembering that d_{ij} and d_{ji} are counted separately), and the necessary increments $\Delta d_{kk}=-[\Delta\lambda_k/(\partial\lambda_k/\partial d_{kk})]$ required to restore the λ_k to their initial values calculated. In the latter process, use is made of the fact that the $(\partial\lambda_k/\partial d_{ij})$ matrices increase in order from ν_n to ν_1; the balancing increments Δd_{kk} give rise to further variations in λ_1 to λ_{k-1}, which must be estimated and added to the increments already found. The d_{kk} are therefore adjusted in the order $k=n-1$ to 1, proceeding from λ_{n-1} to λ_1. The balancing adjustments need not necessarily be carried out on the diagonal elements d_{kk}; λ_k will usually prove to be most sensitive to d_{kk}, and hence the adjustment required will be a minimum, but in principle it may be performed on any element with a non-zero derivative $(\partial\lambda_k/\partial d_{ij})$.

By means of the above procedure, small non-diagonal elements of d (e.g., these corresponding to zero elements of A), may be removed, and the remainder adjusted to fit data from related molecules. The removal of the larger interaction constants will naturally introduce some degree of approximation; these are often associated with pairs of overlapping coordinates, for which a complete treatment is developed in the following section.

V. TREATMENT OF OVERLAPPING COORDINATES

Where the coordinates Δ_k and Δ_m $(k<m)$, overlap to any considerable extent, and the frequency-difference $(\nu_k-\nu_m)$ is small, the standard solution of Section III will not be satisfactory, since it prohibits Δ_k from taking part in ν_m. This difficulty may be overcome, without introducing any new principle, by replacing Δ_k and Δ_m by two linear combinations of these coordinates, defined as

$$\left.\begin{aligned}\Delta_k'&=p_{kk}\Delta_k+p_{km}\Delta_m\\ \Delta_m'&=p_{mk}\Delta_k+p_{mm}\Delta_m\end{aligned}\right\}, \tag{52}$$

where the ratios (p_{km}/p_{kk}) and (p_{mk}/p_{mm}) are less than unity, to agree with the approximate vibrational assignment. A is then replaced by A′, where the elements of A′ are

$$\left.\begin{aligned}A_{kk}'&=p_{kk}^2A_{kk}+2p_{kk}p_{km}A_{km}+p_{km}^2A_{mm}\\ A_{km}'&=p_{kk}p_{mk}A_{kk}+p_{km}p_{mm}A_{mm}\\ &\quad+(p_{kk}p_{mm}+p_{km}p_{mk})A_{km}\\ A_{mm}'&=p_{mk}^2A_{kk}+2p_{mk}p_{mm}A_{km}+p_{mm}^2A_{mm}\\ A_{ki}'&=p_{kk}A_{ki}+p_{km}A_{mi}, \quad (i\neq k, m).\\ A_{mi}'&=p_{mk}A_{ki}+p_{mm}A_{mi}, \quad (i\neq k, m).\\ A_{ij}'&=A_{ij}, \quad (i, j\neq k, m).\end{aligned}\right\} \tag{53}$$

In the standard solution of $|\mathrm{d}'\mathrm{A}'-\lambda\mathrm{I}|=0$ (d′ being the force constant matrix going with A′), there is no component from Δ_k' in the displacement for ν_m. It follows from Eq. (52) that the initial coordinate Δ_k will take part in ν_m. The treatment can be simplified by taking $p_{kk}=p_{mm}=1$, $p_{mk}=0$, and replacing p_{km} by p, which can be regarded as a parameter which in particular determines the extent to which Δ_k takes part in ν_m. Only the case $m=k+1$ will be considered here; this includes all important examples, and there is no particular difficulty in extending the treatment to the general case.

The matrices e′ and h′ giving the force constants d_{ij}' and the normal coordinates in terms of the coordinates $\Delta_1\cdots\Delta_k'\cdots\Delta_n$ are readily obtained from A′ (see Eqs. (19) and (20)), using Eq. (53). These may now be transformed to e and h, from which are derived the force constants d_{ij} now associated with the initial valence coordinates, and the normal coordinates in terms of these coordinates. The relation between the two sets of force constants is:

$$\left.\begin{aligned}d_{i,k+1}&=d_{i,k+1}'+pd_{ik}', \quad (i\neq k+1)\\ d_{k+1,k+1}&=d_{k+1,k+1}'+2pd_{k,k+1}'+p^2d_{kk}'\\ d_{ij}&=d_{ij}', \quad (i, j\neq k+1)\end{aligned}\right\}, \tag{54}$$

these relations going with the transformations

$$\left.\begin{aligned}e_{k+1,i}&=e_{k+1,i}'+pe_{ki}', \quad (i=1 \text{ to } n)\\ &\quad\ (=0 \text{ for } i<k)\\ e_{mi}&=e_{mi}', \quad (i=1 \text{ to } n,\ m\neq k+1)\\ &\quad\ (=0 \text{ for } i<m)\end{aligned}\right\}. \tag{55}$$

$$\left.\begin{aligned}h_{ki}&=h_{ki}'-ph_{k+1,i}', \quad (i=1 \text{ to } n)\\ &\quad\ (=0 \text{ for } i>k+1)\\ h_{mi}&=h_{mi}', \quad (i=1 \text{ to } n,\ m\neq k)\\ &\quad\ (=0 \text{ for } i>m)\end{aligned}\right\}. \tag{56}$$

It is found that e and h can be written as

$$\left.\begin{aligned} \mathrm{e} &= \mathrm{e}^0 + p\mathrm{e}'' \\ \mathrm{h} &= \mathrm{h}^0 + p\mathrm{h}'' \end{aligned}\right\}, \tag{57}$$

where e^0 and h^0 are the matrices for the standard solution with the initial coordinates, and e'' and h'' have non-zero elements in the kth and $(k+1)$th columns only, as

$$\left.\begin{aligned} e_{ik}'' &= -(e_{k,k+1}{}^0)_{ki}, \quad (i=1 \text{ to } k-1). \\ e_{kk}'' &= 0 \\ e_{k+1,k}'' &= e_{kk}{}^0 \end{aligned}\right\} \tag{58a}$$

$$e_{i,k+1}'' = -(h_{k+1,k+1}{}^0)_{ki}, \quad (i=1 \text{ to } k+1). \tag{58b}$$

$$\left.\begin{aligned} h_{ik}'' &= (h_{i,k+1}{}^0)_{kk}, \quad (i=k+1 \text{ to } n). \\ &\qquad (=0 \text{ for } i<k). \\ h_{kk}'' &= h_{k+1,k}{}^0 \end{aligned}\right\} \tag{59a}$$

$$\left.\begin{aligned} h_{i,k+1}'' &= (h_{i,k+2}{}^0)_{k+2,k}, \\ &\qquad (i=k+2 \text{ to } n). \\ &\qquad (=0 \text{ for } i<k \text{ and } i=k+1). \\ h_{k,k+1}'' &= -h_{k+1,k+1}{}^0 \end{aligned}\right\} \tag{59b}$$

where the subscripts p, q in $(e_{ij}{}^0)_{pq}$ and $(h_{ij}{}^0)_{pq}$ refer to minors derived from the determinantal elements $e_{ij}{}^0$ and $h_{ij}{}^0$; (see Eqs. (19) and (20)). In the series expansions for the force constants, in Eq. (21), ${}^k|\mathrm{A}|$ must be replaced by ${}^k|\mathrm{A}'|$ where it occurs in the denominator of the coefficients of λ_k and λ_{k+1}; ${}^k|\mathrm{A}'|$ can be expressed in terms of p and of minors of $|\mathrm{A}|$ as

$${}^k|\mathrm{A}'| = {}^k|\mathrm{A}| - 2p({}^{k+1}|\mathrm{A}|_{k+1,k}) + p^2({}^{k+1}|\mathrm{A}|_{kk}). \tag{60}$$

${}^k|\mathrm{A}|$ must also be replaced by ${}^k|\mathrm{A}'|$ where it occurs in Eq. (28) from which are obtained the normalization factors for use with e and h.

If desired, the values of p may be chosen to satisfy suitable arbitrary conditions. Two such conditions, with the corresponding solutions for p, are given,

(a) $(\Delta_k/\Delta_{k+1})(\nu_k) = (\Delta_{k+1}/\Delta_k)(\nu_{k+1})$.

$$p^2 + p[(h_{kk}{}^0 + h_{k+1,k}'')/h_{k+1,k}{}^0] + 1 = 0, \tag{61}$$

(b) $V_{k,k+1}(\nu_k) = V_{k,k+1}(\nu_{k+1})$.

$$p^2 + p[(h_{kk}{}^0/h_{k+1,k}{}^0)\{1+(\lambda_k/\lambda_{k+1})\} + (h_{k+1,k}{}^0/h_{k+1,k}'')\{1-(\lambda_k/\lambda_{k+1})\}] + (h_{kk}{}^0/h_{k+1,k}'') = 0, \tag{62}$$

where $(\Delta_i/\Delta_j)(\nu_m)$ is the ratio of the components from the coordinates Δ_i and Δ_j in the displacement for ν_m, and $V_{ij}(\nu_m)$ is the fraction of the potential energy in the term $d_{ij}\Delta_i\Delta_j$ for the mth normal mode. Both Eqs. (61) and (62) always have real roots. Equation (62) also satisfies the conditions $V_{kk}(\nu_k) = V_{k+1,k+1}(\nu_{k+1})$, $V_{kk}(\nu_{k+1}) = V_{k+1,k+1}(\nu_k)$, in the case $k+1=n$; here Δ_k and Δ_{k+1} are the only two coordinates having components in the displacements for ν_k and ν_{k+1}, and there are consequently analogies with the second-degree equation which lead to the existence of related singular solutions.[2] The above conditions relating the potential energy terms are also satisfied by the two values of p

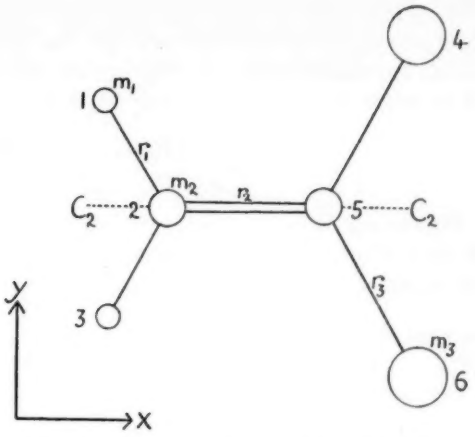

FIG. 1. Coordinates for vinylidene chloride.

which are roots of the equation which is obtained by interchanging the signs of the terms $(\lambda_k/\lambda_{k+1})$ in Eq. (62) if the following additional condition is satisfied:

$$[(\lambda_k - \lambda_{k+1})^2/(\lambda_k\lambda_{k+1})] \geqslant 4[(h_{k+1,k}{}^0)^2/(e_{kk}{}^0 h_{k+1,k+1}{}^0)]. \tag{63}$$

d may be reduced, or adjusted, in the manner already described; the quantities $(\partial\lambda_m/\partial d_{ij}')$ are related to e′ and h′ in the same manner as $(\partial\lambda_m/\partial d_{ij})$ are related to e^0 and h^0 (see Eq. (51)) and $(\partial\lambda_m/\partial d_{ij})$ may be found from $(\partial\lambda_m/\partial d_{ij}')$, using Eq. (54). The introduction of the parameter p allows of an alternative treatment, as follows. For small values of p (where for generality $p_{k,k+1}$ is written for p, as in Eq. (52));

$$(\partial d_{ij}/\partial p_{k,k+1}) = \sum_{m=k}^{k+1} [(e_{im}{}^0 e_{jm}'' + e_{jm}{}^0 e_{im}'')/(e_{mm}{}^0 h_{mm}{}^0)]\lambda_m \tag{64}$$

(where $e_{kk}'' = 0$, and $e_{ik}'' = e_{i,k+1}'' = 0$ for $i > k+1$);

$$[\partial\Delta_i(\nu_j)/\partial p_{k,k+1}] = h_{ij}'',$$

$$\left(=0 \text{ for } j\begin{cases} <k \\ >k+1 \end{cases}, \; i<k, \text{ and } i=j=k+1\right). \tag{65}$$

$$[\partial z_i(\nu_j)/\partial p_{k,k+1}] = (M/m_i)\sum_{q=1}^{k+1} a_{qi}e_{qj}'',$$

$$\left(=0 \text{ for } j\begin{cases} <k \\ >k+1 \end{cases}\right). \tag{66}$$

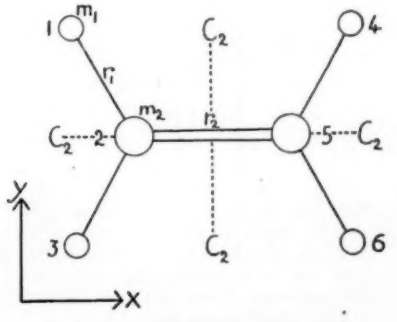

FIG. 2. Coordinates for ethylene.

Equation (64) enables d to be adjusted to correspond to the introduction of one or more small parameters $p_{k,k+1}$; or, conversely, one can estimate the value of $p_{k,k+1}$ required to produce any desired increment in any chosen d_{ij}. Equations (65) and (66) enable the deviations of the displacement vectors from the ideal to be expressed in terms of $p_{k,k+1}$. Equation (65) can also be used to adjust the energy fractions V_{ij}.

VI. EXAMPLES ON THE APPLICATION OF THE METHODS

A. The Class A_1 Vibrations of Vinylidene Chloride

The vinylidene chloride molecule falls into the symmetry point group C_{2v}; the class A_1 normal vibrations arise from a fifth-order factor in the secular equation. The matrix a for a suitable set of coordinates Δ_i of the required symmetry,[d] and the derived matrix A, are given below for the coordinates z_j, see Fig. 1.

a

$z_j=$	x_1, x_3	$y_1, -y_3$	x_2	x_5	x_4, x_6	$y_4, -y_6$	
$\Delta_1=\Delta r_{12}+\Delta r_{23}$	$-(1/2)$	$(\sqrt{3}/2)$	1	·	·	·	$\cdots \nu_{CH_2}{}^s$
$\Delta_2=\Delta r_{25}$	·	·	-1	1	·	·	$\cdots \nu_{CC}$
$\Delta_3=r_1(\Delta\theta_{13}-\Delta\theta_{15}-\Delta\theta_{35})$	$\sqrt{3}$	1	$-2\sqrt{3}$	·	·	·	$\cdots \delta_{CH_2}{}^s$
$\Delta_4=\Delta r_{45}+\Delta r_{56}$	·	·	·	-1	$(1/2)$	$(\sqrt{3}/2)$	$\cdots \nu_{CCl_2}{}^s$
$\Delta_5=r_3(\Delta\theta_{46}-\Delta\theta_{24}-\Delta\theta_{26})$	·	·	·	$2\sqrt{3}$	$-\sqrt{3}$	1	$\cdots \delta_{CCl_2}{}^s$

A ($M=m_2$)

$$\begin{bmatrix} (1+2\mu_1) & -1 & -2\sqrt{3} & 0 & 0 \\ & 2 & 2\sqrt{3} & -1 & 2\sqrt{3} \\ & & 4(3+2\mu_1) & 0 & 0 \\ & & & (1+2\mu_3) & -2\sqrt{3} \\ & & & & 4(3+2\mu_3) \end{bmatrix}$$

$\cdots \nu_{CH_2}{}^s$, $\cdots \nu_{CC}$, $\cdots \delta_{CH_2}{}^s$, $\cdots \nu_{CCl_2}{}^s$, $\cdots \delta_{CCl_2}{}^s$

where $\mu_1=(m_2/m_1)$, $\mu_3=(m_2/m_3)$, and the angles are taken as 120°. With the coordinates chosen, e and h become

e

$$\begin{bmatrix} 1 & 1 & 2\sqrt{3} & A_{33}' & -2\sqrt{3}A_{33}'A_{44}' \\ 0 & A_{11} & -2\sqrt{3}A_{11}' & A_{13}' & -2\sqrt{3}A_{44}'A_{13}' \\ 0 & 0 & A_{11}'' & -2\sqrt{3}A_{11}' & 12A_{11}'A_{44}' \\ 0 & 0 & 0 & D & 2\sqrt{3}A_{11}'A_{33}' \\ 0 & 0 & 0 & 0 & D' \end{bmatrix}$$

h

$$\begin{bmatrix} A_{11} & 0 & 0 & 0 & 0 \\ -1 & A_{11}'' & 0 & 0 & 0 \\ -2\sqrt{3} & 2\sqrt{3}A_{11}' & D & 0 & 0 \\ 0 & -A_{11} & 2\sqrt{3}A_{11}' & D' & 0 \\ 0 & 2\sqrt{3}A_{11} & -12A_{11}' & -2\sqrt{3}A_{11}'A_{33}' & D'' \end{bmatrix}$$

where
$A_{11}'=(A_{11}-1)$, $A_{11}''=(2A_{11}-1)$
$A_{33}'=(A_{33}-12)$
$A_{44}'=(A_{44}-1)$
$A_{13}'=(A_{11}A_{33}-12)$
$D=(A_{33}A_{11}''-12A_{11})$, $D'=(A_{44}D-A_{13}')$, $D''=\{A_{55}D'+12(12A_{11}'+A_{33}'-A_{44}A_{13}')\}$

The fundamental frequencies are[4] 3035, 1620, 1395, 605, and 295 cm^{-1}, assigned to ν_1 to ν_5 in the order given. With these values, the standard d matrix becomes

d

$$\begin{bmatrix} 2.641 & 0.3931 & 0.0088 & 0.0380 & -0.0041 \\ & 10.64 & -0.2551 & 1.057 & -0.1134 \\ & & 0.1368 & -0.0329 & 0.0035 \\ & & & 2.452 & 0.1415 \\ & & & & 0.1016 \end{bmatrix} \times 10^5 \text{ dynes/cm.}$$

[d] It is the usual practice to include a normalizing factor in the symmetry coordinate, so that the constant going with any particular coordinate is identical with the valence force constant. These factors would take the following values here: for Δ_1 and Δ_4, $(1/\sqrt{2})$; for Δ_3 and Δ_5, $(1/\sqrt{3})$; for Δ_2, 1. Since the constants refer only to vibrations in one particular symmetry class, it is considered preferable not to normalize the coordinates, but to obtain the valence force constants by combining components from the different symmetry classes. Thus, the C–H stretching constant will be $(d_{11}+d_{66})$, where d_{66} is the constant going with the coordinate $\Delta_6=\Delta r_{12}-\Delta r_{23}$, of symmetry B_2.

[4] H. W. Thompson and P. Torkington, Proc. Roy. Soc. **A184**, 21 (1945).

The components in the displacements are given below; the elements $\Delta_i(\nu_j)$ are obtained from h by dividing the elements in the jth column by h_{jj}. The elements N_j in the row vector N are the normalizing factors for the appropriate columns of $\Delta_i(\nu_j)$, i.e., $N_j=\Delta_j(\nu_j)$, (in tenths of an angstrom), for the first vibrational level.

	$j=$	1	2	3	4	5	
	N_j	[0.2625	0.1010	0.7816	0.1264	0.4159]	$\times 10^{-9}$ cm
$\Delta_i(\nu_j)$		1	0	0	0	0	
		−0.040	1	0	0	0	
		−0.140	1.696	1	0	0	
		0	−0.5103	0.0168	1	0	
		0	1.768	−0.0581	−1.392	1	

The potential energy distribution is as given below; the elements are percentages of the total potential energy in each mode:

$[[V_{ij}(\nu_k)]]$

i \ k	1				2			
1	100.65	−0.60	−0.05	0	0			
2		0.66	−0.05	0	0	112.39	−4.57	−5.70	−2.12
3			0.10	0	0		4.16	0.30	0.11
4				0	0			6.74	−1.35
5					0				3.35

i \ k	3			4		5
3	100.56	−0.41	−0.15			
4		0.51	−0.10	108.74	−8.74	
5			0.25		8.74	100.00

The $[[V_{ij}(\nu_k)]]$ matrices are symmetric, d_{ij} and d_{ji} being counted separately; the energy term $d_{ij}\Delta_i\Delta_j$ is thus twice the matrix element given.

The relative atomic displacements, derived from e and h, are

$z_j=$	$x_1(=x_3)$	$y_1(=-y_3)$	x_2	x_5	$x_4(=x_6)$	$y_4(=-y_6)$
$\nu_1\cdots$	−1	$\sqrt{3}$	$2\mu_2$	0	0	0
$\nu_2\cdots$	−1	$\sqrt{3}$	−4	$2(2+\mu_2)$	0	0
$\nu_3\cdots$	1	$(1+\mu_2)/\sqrt{3}$	$-\mu_2$	$-\mu_2$	0	0
$\nu_4\cdots$	−1	0	−1	−1	$(1+\mu_2)\mu_3$	$\sqrt{3}(1+\mu_2)\mu_3$
$\nu_5\cdots$	1	0	1	1	$-(1+\mu_2)\mu_3$	$\{1+\mu_3(1+\mu_2)\}/\sqrt{3}$

where $\mu_2=(m_1/m_2)$, $\mu_3=(m_2/m_3)$.

The main features of the standard general solution are well illustrated by the above data. The potential energy distribution agrees with the vibrational assignment; the energy in ν_i is found mainly in the square term $\frac{1}{2}d_{ii}\Delta_i^2$. The simple form of the atomic displacement vectors should be noted; in the stretching vibrations, the displacement vectors of the appropriate atoms lie directly along the valence bonds.

The quantities $(\partial\lambda_k/\partial d_{ij})$ are given below as matrices characteristic of each normal mode.

$[[(\partial\lambda_k/\partial d_{ij})]]$

i \ k	1					2			
1	24.81	−1	$-2\sqrt{3}$	0	0				
2		0.040	0.140	0	0	1.96	3.32	−1	$2\sqrt{3}$
3			0.484	0	0		5.64	−1.70	5.88
4				0	0			0.510	−1.77
5					0				6.12

i \ k	3			4		5
3	101.1	1.70	−5.88			
4		0.028	−0.099	1.15	−1.60	
5			0.341		2.22	6.06

As in the $V_{ij}(\nu_k)$ matrices, d_{ij} and d_{ji} are counted separately; for interaction constants, $(\partial\lambda_k/\partial d_{ij})$ is twice the

appropriate matrix element. Using the above quantities, the small non-diagonal elements d_{13}, d_{14}, d_{15}, d_{34}, and d_{35} may be eliminated from d, the balancing increments having the values:

$$\Delta d_{11}=-0.0024, \quad \Delta d_{22}=+0.081, \quad \Delta d_{33}=-0.0015, \quad \times 10^5 \text{ dynes/cm.}$$

The elimination of the remaining interaction constants will introduce some degree of approximation; d_{23} and d_{45} are larger than the main constants d_{33} and d_{55}, respectively, and experience has shown that in such cases d_{ij} cannot in general be reduced to zero without making ν_i and ν_j complex. The increments required to balance the elimination of d_{12} and d_{24} are

$$\Delta d_{11}=-0.0314, \quad \Delta d_{22}=-1.06, \quad \times 10^5 \text{ dynes/cm,}$$

giving

$$d_{11}=2.607, \quad d_{22}=9.66, \quad \times 10^5 \text{ dynes/cm,}$$

which values agree reasonably well with similar constants in ethylenic molecules where the term in the potential energy corresponding to the interaction $\Delta r_{CH}\cdot\Delta r_{CC}$ is neglected. Application of Eq. (39) to the C—H stretching vibration gives $d_{11}=2.60\times 10^5$ dynes/cm.

B. The Class A_g Vibrations of Ethylene

The ethylene molecule falls into the symmetry point group V_h; the totally symmetric vibrations arise from a cubic factor in the secular equation. The matrices a and A for a suitable set of symmetry coordinates (see Fig. 2), are given:[6,5]

a

$z_j=$	$x_1, x_3, -x_4, -x_6$	$y_1, -y_3, y_4, -y_6$	$x_2, -x_5$	
$\Delta_1=\Delta r_{12}+\Delta r_{23}+\Delta r_{45}+\Delta r_{56}$	$-(1/2)$	$(\sqrt{3}/2)$	1	$\cdots \nu_{CH_2}{}^s$
$\Delta_2=\Delta r_{25}$	0	0	-1	$\cdots \nu_{CC}$
$\Delta_3=r_1(\Delta\theta_{13}+\Delta\theta_{46}-\Delta\theta_{15}-\Delta\theta_{24}-\Delta\theta_{26}-\Delta\theta_{35})$	$\sqrt{3}$	1	$-2\sqrt{3}$	$\cdots \delta_{CH_2}{}^s$

A $(M=m_2)$

$$\begin{bmatrix} 2(1+2\mu) & -2 & -4\sqrt{3} \\ & 2 & 4\sqrt{3} \\ & & 8(3+2\mu) \end{bmatrix} \begin{matrix} \cdots \nu_{CH_2}{}^s \\ \cdots \nu_{CC} \\ \cdots \delta_{CH_2}{}^s \end{matrix}$$

where $\mu=(m_2/m_1)$.

If Δ_2 is replaced by $\Delta_2'=\Delta_2+p\Delta_3$, the matrices e and h, from which are derived the force constants going with the initial set of coordinates in the standard solution for the new set, and the normal coordinates in terms of these initial coordinates, have the form:

e h

$$\begin{bmatrix} 1 & 2(1+2\sqrt{3}p) & -32\mu p \\ 0 & 2(1+2\mu) & -16\mu\{\sqrt{3}+4(2+\mu)p\} \\ 0 & 2(1+2\mu)p & 8\mu(1+2\sqrt{3}p) \end{bmatrix} \begin{bmatrix} 2(1+2\mu) & 0 & 0 \\ -2 & 8\mu(1+2\sqrt{3}p) & -128\mu^2 p \\ -4\sqrt{3} & 16\mu\{\sqrt{3}+4(2+\mu)p\} & 128\mu^2 \end{bmatrix}.$$

The quantity $^2|A'|$, which occurs in the denominator of the coefficients of λ_2 and λ_3 in the series for the d_{ij}, and in the normalization factors for the potential energy, is

$$^2|A'|=8\mu\{1+4\sqrt{3}p+8(2+\mu)p^2\}.$$

The Cartesian components of the atomic displacement vectors are given below as functions of p:

$z_j=$	x_1	y_1	x_2
$\nu_1\cdots$	-1	$\sqrt{3}$	$(2/\mu)$
$\nu_2\cdots$	$(1-4\sqrt{3}\mu p)$	$-\{\sqrt{3}+4(2+\mu)p\}$	$4(1+2\sqrt{3}p)$
$\nu_3\cdots$	$(\sqrt{3}+8p)$	1	$8p$

With $p=0$, the displacements are those for the standard solution. In this case, the displacement vectors of the hydrogen atoms lie along the C—H bonds in both ν_1 and ν_2, and the C=C bond remains rigid in ν_3. It should

[6] Gallaway and Barker (see reference 5) obtained a value 119° 55′ for the angle $\widehat{HCH}$ in ethylene; the round figure of 120° is used here.
[5] W. S. Gallaway and E. F. Barker, J. Chem. Phys. **10**, 88 (1942).

be noted that a small component from Δ_2 in the displacement for ν_3 has here a much greater effect on the potential energy distribution determining the assignment than the same component from Δ_3 in the displacement for ν_2, since the force constants for the square terms involving these two coordinates are of very different orders of magnitude ($d_{22}\sim 150 d_{33}$); the rigidity of the C=C bond in the standard solution for ν_3 is therefore not such a crude approximation as might appear at first sight. The introduction of the parameter p has no effect on the form of the vibration ν_1, but causes the displacement vectors of the hydrogen atoms in ν_2 and ν_3 to shift from their ideal directions. The shift $\Delta\beta_i$ in ν_i is

$$\begin{cases}\Delta\beta_2=[\arctan(|y_1/x_1|)(\nu_2)-(\pi/3)]\\ \Delta\beta_3=[\arctan(|x_1/y_1|)(\nu_3)-(\pi/3)].\end{cases}$$

It is found that these angles can be expressed in terms of p as follows:

$$\begin{cases}\tan\Delta\beta_2=2[(1+2\mu)/(1+2\sqrt{3}p)]p\\ \tan\Delta\beta_3=[2/(1+2\sqrt{3}p)]p.\end{cases}$$

The values of p corresponding to the solution $V_{22}(\nu_2)=V_{33}(\nu_3)$, $V_{22}(\nu_3)=V_{33}(\nu_2)$, $V_{23}(\nu_2)=V_{23}(\nu_3)$, are the roots of the quadratic equation:

$$p^2+\tfrac{1}{2}\{(\lambda'/\sqrt{3})-(\sqrt{3}\lambda'')/[2(2+\mu)]\}p+[8(2+\mu)]^{-1}=0,$$

where $\lambda'=[(\lambda_2/\lambda_3)+1]$, $\lambda''=[(\lambda_2/\lambda_3)-1]$.

The assignment for ethylene is as follows:[6]

$$\nu_1=3019.3,\quad \nu_2=1623.3,\quad \nu_3=1342.4,\ \text{cm}^{-1}.$$

These figures are used, uncorrected for anharmonicity since only an empirical correction is possible,[7] to give the following standard solution ($p=0$):

d

$$\begin{bmatrix}1.314 & 0.3911 & 0\\ & 10.507 & -0.2316\\ & & 0.06686\end{bmatrix}\times 10^5\ \text{dynes/cm}$$

$[[V_{ij}(\nu_k)]]$

i \ k	1	2	3
1	101.214 −1.214 0 1.314 −0.100 0.100	108.267 −8.267 8.267	[100.000]
2			
3			

Solving the equation giving the values of p corresponding to analogous potential energy distributions in ν_2 and ν_3, we obtain $p=-0.01315$ and -0.6833. The solutions for these two values are:

(a) $p=-0.01315$. ($\Delta\beta_2=-34^\circ\,22'$, $\Delta\beta_3=-1^\circ\,35'$).

d

$$\begin{bmatrix}1.314 & 0.3946 & -0.0017\\ & 10.745 & -0.2751\\ & & 0.06744\end{bmatrix}\times 10^5\ \text{dynes/cm}$$

$[[V_{ij}(\nu_k)]]$

i \ k	1	2	3
1	101.207 −1.225 0.018 1.344 −0.119 0.101	108.668 −5.832 2.996	2.996 −5.832 108.668
2			
3			

[6] G. Herzberg, *Infra-red and Raman Spectra of Polyatomic Molecules* (D. van Nostrand Company, Inc., New York, 1945)).
[7] J. E. Kilpatrick and K. S. Pitzer, J. Research Nat. Bur. Stand. **38**, 191 (1947).

(b) $p=-0.6833$. $(\Delta\beta_2=87°\,42',\ \Delta\beta_3=45°\,0')$.

$$\begin{matrix} & & \text{d} \\ \begin{bmatrix} 1.309 & 0.2640 & 0.0024 \\ & 7.503 & -0.2751 \\ & & 0.09658 \end{bmatrix} & \times 10^5 \text{ dynes/cm} \end{matrix}$$

$$[[V_{ij}(\nu_k)]]$$

i \ k	1	2	2
1	$\begin{bmatrix} 100.845 & -0.819 & -0.026 \\ & 0.938 & -0.119 \\ & & 0.145 \end{bmatrix}$	$\begin{bmatrix} 2.996 & -5.832 \\ & 108.668 \end{bmatrix}$	$\begin{bmatrix} 108.668 & -5.832 \\ & 2.996 \end{bmatrix}$
2			
3			

Solution (b) is given for the sake of completeness; it is seen to correspond to a reversed assignment of ν_2 and ν_3. It may be noted that in solution (a) the displacement vectors of the hydrogen atoms are much more sensitive to p in ν_2 than in ν_3. The small interaction constant d_{13} may be eliminated if desired; the balancing increment to d_{11} is negligible. The larger constant d_{12}, which effectively maintains the displacement vectors of the hydrogen atoms along the C−H bonds in ν_1, may also be eliminated here without introducing any appreciable error, since $(\partial\lambda_1/\partial d_{11})\gg(\partial\lambda_1/\partial d_{12})$; the balancing increment is $\Delta d_{11}=-0.03_2\times10^5$ dynes/cm.

THE JOURNAL OF CHEMICAL PHYSICS VOLUME 17, NUMBER 11 NOVEMBER, 1949

Isothermal Compositional Order-Disorder.* I. Superstructure Solid Solutions in a Salt System

ALEXANDER GRENALL
Research Laboratory, Union Oil Company of California, Wilmington, California

(Received January 17, 1949)

Solid solutions in the system, $NH_4Cl-MnCl_2-H_2O$, exhibit properties characteristic of order-disorder in alloys. Disordered solid solutions are indistinguishable in structure from that of ammonium chloride. Order is revealed by superstructure formation. The familiar compositions A_3B and AB appear as end-members of the ordered solid solution series. Crystal symmetry alteration from cubic to tetragonal results from ordering. Tetragonality is intimately related to the state of order. Though increase in "solute" content produces significant lattice distortion, superstructure unit cell volumes are constant.

Despite their unusual properties, the ordered salt solid solutions exhibit a normal Vegard's law relationship.

The salt system's features resemble those of a low temperature isotherm across Shockley's theoretical phase diagram for alloy order-disorder transformation and are regarded as experimental verification of Shockley's qualitative predictions. A concept of isothermal, compositional order-disorder is used in presenting the results.

Demonstration of a two-phase region, wherein ordered and disordered solid solutions coexist in equilibrium, provides a basis for resolving the controversy over whether the phase rule governs order-disorder transformations.

Identity of the order-disorder phenomenon in metal and salt systems was further shown by producing the disordered state of salt solutions from the ordered by thermal and cold-working methods. In both instances, order was spontaneously restored with aging at room temperature.

INTRODUCTION

In essence, the research to be described consists of x-ray diffraction and phase rule studies of a salt system, $NH_4Cl-MnCl_2-H_2O$, equilibrated at 25°C. From the results of this investigation, there is developed evidence that the solid solutions occurring in this system exhibit properties known to characterize the order-disorder phenomenon in alloys.[1] It is one of the purposes of this paper to set forth these properties along with the data therefor.

It is a further purpose to show that the salient features of this salt system resemble those deduced from a low temperature isotherm drawn across Shockley's phase diagram[2] for alloy order-disorder transformation. The resemblances between the experimentally determined salt system phase diagram and the theoretically based diagram of Shockley point up an aspect of perhaps major importance; in that, both reveal a two-phase region wherein ordered and disordered state solid solutions coexist at equilibrium. Thereby is provided a

* Based upon material presented before the joint meeting of the American Society for X-Ray and Electron Diffraction and the Electron Microscope Society of America, the Mellon Institute and the University of Pittsburgh, Pittsburgh, Pennsylvania, December 5–7, 1946.

[1] F. C. Nix and W. Shockley, Rev. Mod. Phys. **10**, 1–71 (1938).

[2] W. Shockley, J. Chem. Phys. **6**, 130 (1938).

basis for deciding the controversy[3] over whether or not order-disorder transformations are governed by the phase rule, since the indisputable criterion sought for a definite decision on this question has been experimental demonstration of such a two-phase region.

Indeed, the search for this two-solid-coexistence region in alloy systems has occupied the attention of quite a number of investigators.[4] None has claimed to have been successful; although some of these workers gave descriptions of x-ray photographs which showed patterns for the simultaneous presence of ordered and disordered phases in alloys annealed near the critical temperature. Always, however, doubt was expressed that equilibrium had been attained.

Superlattice diffraction effects have been shown to exist for some minerals; as for example, stilpnomelane,[5] pyrrhotite,[6] and arsenopyrite.[7] Order-disorder properties have been demonstrated[8] for Cu_2HgI_4 and Ag_2HgI_4. But, up to now, no evidence has appeared in the literature for the formation, in salt solid solutions, of superstructures possessing order-disorder properties.

Since evidence to be presented is partially based upon an earlier investigation[9] of the system $NH_4Cl-MnCl_2-H_2O$ at 25.000°±0.005°C, it might be well to summarize the pertinent points developed there. The phase diagram for this system is reproduced here as Fig. 1 because of the necessity to refer to it frequently. This diagram has been relettered to permit pointing out certain features. This earlier research established the random (disordered) distribution of manganous chloride dihydrate in the cubic ammonium chloride-rich solid solutions formed in the composition range from A to B, Fig. 1. The mechanism of solid solution formation from non-isomorphous ammonium chloride and manganous chloride dihydrate was demonstrated to consist of the substitution of NH_4^+ by H_2O in two neighboring unit cells of ammonium chloride, with the simultaneous insertion of a Mn^{2+} in the interstitial space between the chloride ions on the common face between the cells. The end-members of the "manganous chloride dihydrate-rich"[10] solid solutions series, extending from C to F, of composition corresponding to molecular formulas of $6NH_4Cl\cdot MnCl_2\cdot 2H_2O$ and $2NH_4Cl\cdot MnCl_2\cdot 2H_2O$, were shown to have tetragonal crystal symmetry. Their unit cell dimensions, number of molecules per unit cell, and the crystal structure of the latter composition were given. Significantly, this earlier publication pointed out that the change of symmetry, from cubic to tetragonal, experienced by the solid solutions on passing the phase boundary BC, must be due to the appearance of an ordered arrangement of altered ammonium chloride cubes.

Experimental

The present research covers the "manganous chloride dihydrate-rich" solid solutions formed in the region, D to F, Fig. 1. Thermostated for several months in contact with the mother liquor from which they formed, these solid phases had undergone repeated crushing to permit homogenization to take place and were not removed from the mother liquor until equilibrium had been established.[9]

X-ray diffraction patterns of the samples were obtained by the Debye-Scherrer technique using unfiltered calcium radiation and the results later verified by photographs prepared by means of copper $K\alpha$-radiation. From data supplied by these photographs, the unit cell dimensions were calculated by a least squares analytical method[11] to eliminate systematic errors.

Results

The tetragonal cell dimensions in KX units for samples 8 to 26, inclusive (same sample designations used previously[9]), are given in Table I. Also listed in Table I are the unit cell volumes calculated on a common basis. Data for ammonium chloride[9] are included for comparison.

The mole percentage chemical compositions of these samples, Table I, were computed from weight percentage compositions found by extrapolation to the manganous chloride dihydrate baseline on the ternary plot of this system.

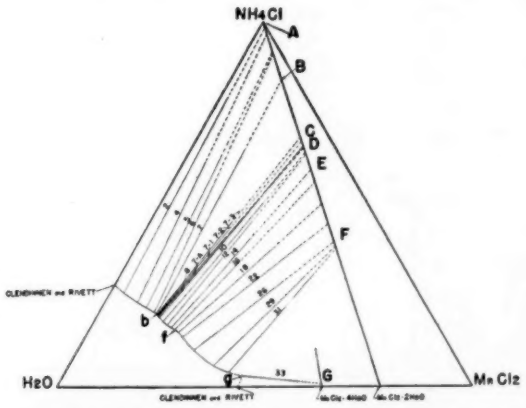

FIG. 1. 25°C isotherm for the system $NH_4Cl-MnCl_2-H_2O$.

[3] W. L. Bragg and E. J. Williams, Proc. Roy. Soc. **A145**, 699 (1934); D. Harker, Trans. A. S. M. E. **32**, 210 (1943); C. S. Barrett, Metals & Alloys **8**, 251 (1937).

[4] (a) R. Hultgren, J. Chem. Phys. **7**, 202 (1939). (b) R. Hultgren and C. A. Zapffe, Zeits. f. Krist. **A99**, 509 (1938). (c) W. S. Gorsky, Zeits. f. Physik **50**, 64 (1928). (d) F. N. Rhines, paper presented before the American Society for X-Ray and Electron Diffraction, Lake George, New York, June 10–14, 1946.

[5] C. O. Hutton and I. Fankuchen, Mineralogical Mag. **25**, 201 (1938).

[6] G. Hägg and I. Sucksdorff, Zeits. f. physik. Chemie **B22**, 444 (1933).

[7] M. J. Buerger, Zeits. f. Krist. **A94**, 425 (1936).

[8] J. A. Ketelaar, Zeits. f. Krist. **87**, 436 (1934); Zeits. f. physik. Chemie **B26**, 327 (1934), *ibid.* **B30**, 53 (1935).

[9] A. L. Greenberg and G. H. Walden, Jr., J. Chem. Phys. **8**, 645 (1940).

[10] This terminology, while not strictly correct, is applied to the second solid solution series of higher manganous chloride dihydrate content as a matter of convenience in reference.

[11] M. U. Cohen, Rev. Sci. Inst. **6**, 68 (1935), Zeits. f. Krist. **A94**, 288 (1936); G. H. Walden, Jr. and M. U. Cohen, J. Am. Chem. Soc. **57**, 259 (1935).

SIGNIFICANCE OF THESE RESULTS

A. Superstructure Formation

It is well known that x-ray photographs of solid solutions exhibit diffraction line position shifts from those of the pure components; the amount of displacement being a function of composition. For a solid solution series whose end-members differ greatly in unit cell dimensions, as in the present investigation, it would be expected that the line positions shift markedly with small composition changes. However, the x-ray photographs of the "manganous chloride dihydrate-rich" solid solutions showed only relatively small line position shifts. Furthermore, it was found that, between the compositions of samples 14 and 16, a transition took place from the large unit cell required by the diffraction effects of one end-member of the series, $6NH_4Cl \cdot MnCl_2 \cdot 2H_2O$, to the smaller one of the other end-member, $2NH_4Cl \cdot MnCl_2 \cdot 2H_2O$.

It is obvious that the unit cell dimensional data would yield unconnected graphs if plotted in the form given in Table I. However, when the data are placed on a common basis, by dividing the dimensions of the larger cells by two, and then plotted as a function of mol percentage composition, the straight line graphs shown by Fig. 2 result.

The linear relationship between cell dimensions and composition has two aspects; it establishes that we are dealing with superstructure formation as well as with the type of unit cell dimensional variation generally encountered in solid solutions. Because, despite possessing a most unusual nature in other respects, the salt solutions exhibit a completely normal Vegard's law[12] relationship.

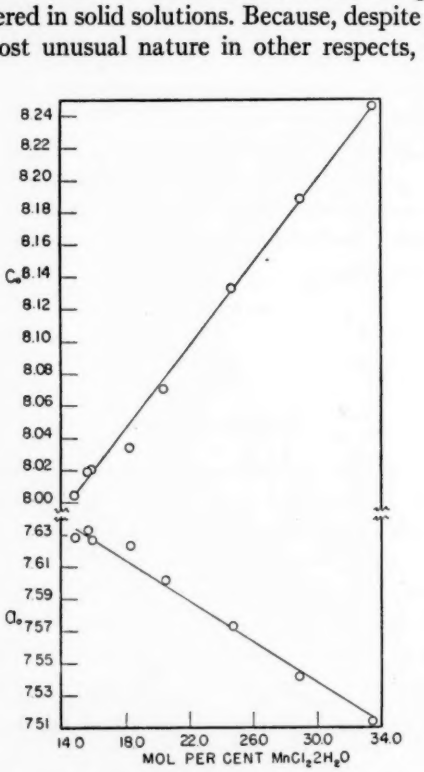

FIG. 2. Variation in unit cell dimensions of ordered solid solutions with solute composition.

TABLE I. Unit cell data for ordered solid solutions.

Sample No.	Tetragonal cell dimensions (Kx Units) a_0	c_0	Unit cell volume[a]	Mole % $MnCl_2 \cdot 2H_2O$
8	15.256±0.002	16.008±0.002	465.7	14.8
10	15.264±0.011	16.038±0.016	467.1	15.6
12	15.252±0.007	16.040±0.010	466.4	15.9
14	15.246±0.011	16.068±0.016	466.9	18.3
16	7.601±0.002	8.071±0.003	466.3	20.4
18	7.573±0.002	8.133±0.003	466.4	24.7
22	7.542±0.002	8.189±0.003	465.8	29.0
26	7.514±0.001	8.247±0.002	465.6	33.5
NH_4Cl[b]	3.8680±0.0003 ×4=15.472	×2= 7.736	463.0	—

[a] Calculated on a comparable basis, the unit cell of $2NH_4Cl \cdot MnCl_2 \cdot 2H_2O$ used as a base.
[b] Included for comparison. Data from reference 9.

B. Development of Tegragonal Symmetry with Ordering

These salt solid solutions are unusual in being formed via a mechanism[9] consisting not only of substitution of one group of atoms by another (NH_4^+ by H_2O) but also of interstitial insertion of atoms (Mn^{2+}) in previously existing "holes" in the basic structure. Even more unusual is the substitution of an electrically neutral molecule, H_2O, for a charged ion, NH_4^+.

Following the terminology[13] of considering substitution to include phenomena wherein "holes" are substituted for certain atoms in a structure, the mechanism can be said to consist of substitution alone. Moreover, since apparently it is a unit that is involved, i.e., $Mn^{2+} \cdot 2H_2O$, the process of solid solution may be regarded as occurring by the simultaneous substitution of a molecular group consisting of a divalent ion and two neutral molecules for another group consisting of a "hole" and two univalent ions.

The orientation of $Mn^{2+} \cdot 2H_2O$ units in the structure[9] of the solid solution corresponding in composition to $2NH_4Cl \cdot MnCl_2 \cdot 2H_2O$ provides a qualitative explanation of whence arise the distortions that transform the originally cubic symmetry properties of the ammonium chloride structure to tetragonal. Disposed regularly throughout the structure in the form of a linear grouping, $H_2O-Mn^{2+}-H_2O$, these units are arranged with their long axis parallel to the c axis. The Mn^{2+} is located, in what was a "hole" in ammonium chloride, between four chloride ions, forming a coplanar group oriented perpendicular to the c axis. With a strong attractive force substituted for repulsive ones, the chloride ions are drawn towards the Mn^{2+}, in a direction perpendicular to the c axis, thus effectively reducing a and b edge dimensions. For the water molecules replacing ammonium ions, repulsive forces take the place of attrac-

[12] L. Vegard, Zeits. f. Physik **5**, 17 (1921).
[13] M. J. Buerger, J. Chem. Phys. **15**, 1 (1947).

tive, in a direction parallel to the c axis, and produce an increase in the c unit cell edge. Since both processes occur simultaneously, it is the resultant distortions from their combined operations that produce a tetragonal structure.

It is clear that, with these $Mn^{2+}\cdot 2H_2O$ units arranged in a random fashion (parallel and perpendicular to the c axis and non-symmetrically disposed), no tetragonal properties will appear. This corresponds to the situation observed[9] in the ammonium chloride-rich solid solutions. Only with an ordered arrangement can the distortions be aligned to produce tetragonality. Tetragonality is, therefore, intimately related to the state of order.

The slopes of the graphs (Fig. 2) show that, experimentally, the degree of tetragonality is a linear function of mol percentage "solute" content of ordered solutions. This relationship may also be described in terms of composition expressed as the number of "solute" groups (atoms, molecules and/or ions) present in each unit cell. Since tegragonality reflects the state of order, we may go the one step further and say that the *degree of tetragonality* is, therefore, dependent upon the number of ordered sites in the unit cell occupied by "solute" groups. Hence, the degree of tetragonality must be a measure of the state of order and may be used to evaluate the latter experimentally. Conversely, the state of order may be *defined* in composition terms, i.e., by the fraction of the total available ordered sites occupied by "solute," and evaluated, for equilibrium solid solutions, on this basis. These aspects of the problem will be treated quantitatively in a future publication.

C. Constancy of Unit Cell Volume

Although ordering leads to significant lattice distortion for these superstructures it introduces no change in unit cell volumes.

Unit cell volume data, Table I, illustrate this feature. The volumes are constant at 466.3 ± 0.4 (percent a.d.$=0.09$), as a mean of the eight determinations.

This situation results as a consequence of the following circumstances: dc_0/dC, the change of c_0 unit cell side with composition, is $+0.0131$ KX units/mol percent and that for da_0/dC, -0.0065. However, for these tetragonal crystals, both a_0 and b_0 change the same amount, so that the total change for a_0+b_0 is equal to -0.0130 KX units/mole percent. The net result, to all practical purposes, is a zero change in total cell dimensions with increased "solute" content of ordered phases.

It may be of interest, to workers employing dilatometric methods in studying order-disorder transformations, to point out that the unit cell volume of ordered salt solid solutions is approximately 0.6 percent greater than that of disordered.

TABLE II. Relationship between diffraction patterns of superstructures and basic pattern of ammonium chloride (copper $K\alpha$-radiation).

$6NH_4Cl\cdot MnCl_2\cdot 2H_2O$			$2NH_4Cl\cdot MnCl_2\cdot 2H_2O$			NH_4Cl		
d/n	Int.	(hkl)	d/n	Int.	(hkl)	d/n	Int.	(hkl)
8.96	$m-$	111						
5.52	$w+$	202	5.58	$ms+$	101			
5.42	f	220	5.31	$w+$	110			
5.05	vvf	103						
4.79	$f-$	113						
4.61	$w-$	131						
4.01	ms	004	4.15	ms	002	3.862	ms	100
3.810	w	400	Missing					
3.557	vf	204						
3.232	vvf	(224*	3.260	f	112			
		(005						
3.125	vf	(422*	3.108	f	211			
		(105						
2.755	vs	(404*	2.782	s	202	2.729	vvs	110
		(225						
2.697	$vs-$	440	2.653	$s-$	220			
2.660	vf	(315						
		(441						
2.576	vf	531						
2.515	f	(206*	2.588	w	103			
		(601						
2.405	vf	(443	2.376	vvf	310			
		(620*						
2.342	vvf	(316						
		(425						
		(533						
2.235	ms	(444*	2.230	m	(222*	2.230	ms	111
		(117			(203*			
2.189	vvf	(406* 632						
		(207 534						
		(515						
2.137	vf	(551 711						
		(336						
2.099	vf	(246*	2.133	f	(302			
		(702			(213*			
		(641						
			2.063	$ms-$	(004*			
					(312			
2.038	f	642						
			2.017	w	321			
1.997	$m-$	008						
		(etc.)						
			1.964	vvf	104	1.929	ms	200
			1.920	vf	(223			
1.902	ms	800			(114			
		(etc.)						
1.872	$f-$	644	1.875	$w+$	(322*			
		(etc.)			(400*			
1.800	vvf	(822*						
		(660*						
		(etc.)						
1.766	vf	(408*	1.811	vvf	204			
		(etc.)						
					(330*	1.724	ms	210
			1.776	vf	(411*			
1.717	m	804	1.707	$f+$	402			
1.698	f	(841 735						
		(607						
1.673	vvf	(319 911						
		(438 508						
1.653	vf	(646*	1.659	f	(323*			
		(etc.)			(005			
1.604	$s-$	448	1.627	$s-$	(224*			
		(etc.)			(332			
			1.584	vvf	115	1.576	vs	211
1.566	s	844						
		(etc.)	1.552	m	(422*			
					(403			
					(314			

* Preferred index.

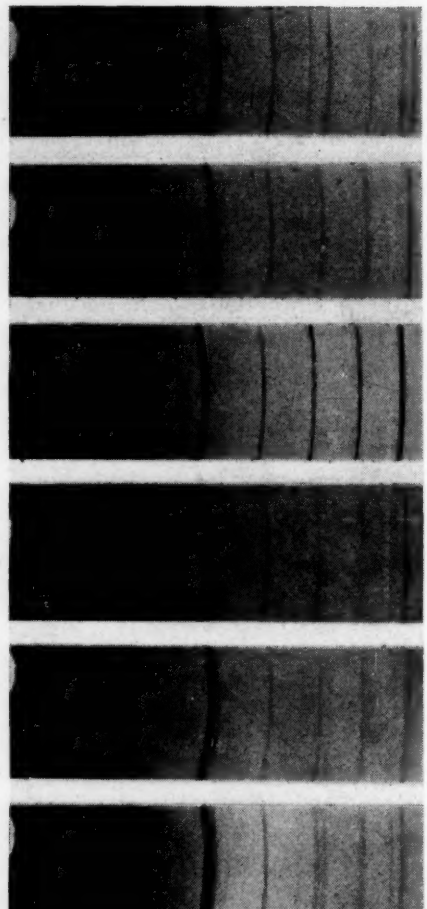

FIG. 3. Transformation of ordered salt solid solution to the disordered state by heating and the restoration of order by aging at room temperature.

A—Ordered state.
Original sample, 3:1 superstructure.
B—Disordered state, A, after heating at 130°C.
C—NH_4Cl (reference).
D—B, After 18 hours at room temperature.
E—B, After 66 hours at room temperature.
F—B, After 162 hours at room temperature.
G—B, After 572 hours at room temperature.

D. Relationship between Diffraction Patterns of the Superstructures and Ammonium Chloride

The relationship between the x-ray patterns of the "end-member" superstructures, $6NH_4Cl \cdot MnCl_2 \cdot 2H_2O$ (sample 8) and $2NH_4Cl \cdot MnCl_2 \cdot 2H_2O$ (sample 26), and that of ammonium chloride is shown by the data in Table II.

The basic reflections and those normally expected to occur because of symmetry alteration from cubic to tetragonal are marked and traced through the pattern sequence by solid lines drawn in Table II. Reflections not so marked are superlattice reflections. It is these reflections that require enlargement of the basic unit cell dimensions of ammonium chloride by a factor of approximately 4 for $6NH_4Cl \cdot MnCl_2 \cdot 2H_2O$ and 2 for $2NH_4Cl \cdot MnCl_2 \cdot 2H_2O$ (compare Table I).

Of the reflections appearing for the $6NH_4Cl \cdot MnCl_2 \cdot 2H_2O$ type structure, those having (*hkl*) divisible by 4 to yield whole number indices are related to the fundamental ammonium chloride pattern. Those, whose division yield fractional indices, are superlattice lines and have no counterparts in the ammonium chloride pattern.

A similar situation prevails for the $2NH_4Cl \cdot MnCl_2 \cdot 2H_2O$ type diffraction pattern. Those reflections are basic whose planar indices are divisible by 2 to produce non-fractional indices, while those not so divisible are superlattice reflections.

Solid solutions of the $6NH_4Cl \cdot MnCl_2 \cdot 2H_2O$ type are related to the $2NH_4Cl \cdot MnCl_2 \cdot 2H_2O$ type as super-superstructures. Reflections, in the former's pattern, with (*hkl*) divisible by 2 to yield whole number indices also appear in the latter's pattern; and those, whose division produces fractional indices (super-superstructure lines) are absent. Pattern relationship between the superstructures is shown by solid and dashed line markings in Table II.

E. Compositional Identity of the Salt Superstructures with Those of Alloys

The superstructure solid solutions of molecular composition ratios, $6NH_4Cl \cdot MnCl_2 \cdot 2H_2O$ and $2NH_4Cl \cdot MnCl_2 \cdot 2H_2O$, are defined by convergence of tie-lines in their respective existence ranges on the triangular phase diagram, Fig. 1, almost as though they were compounds. The reasons for not considering these to be true compounds have been stated previously.[9] Yet, these particular compositions have significance if they are scrutinized with the mechanism of solid solution formation in mind.

On the basis of either substitution of one water molecule for one ammonium ion, or of equivalency for the solution of Mn^{2+}, i.e., $1Mn^{2+}$ for $2NH_4^+$, there is a ratio of 3:1 for "solvent" to "solute" for the first superstructure (above) and 1:1 for the second. Thus is established the compositional identity to the molecular formulas A_3B and AB typically encountered in order-disorder alloy systems.

THE IDENTITY OF THE ORDER-DISORDER PHENOMENON IN SALT AND METAL SYSTEMS

A. Production of the Disordered State from the Ordered by Heat Treatment

A specimen of salt solution (sample 8), 3:1 superstructure, was sealed in a thin-walled glass capillary and and photographed "as is," for a "standard" reference, by the Debye-Scherrer technique. Subsequently, this

specimen was heated at 103°C±2° for four hours, cooled to room temperature and immediately photographed. The capillary was then reheated at 120°C±2° for four hours, cooled and again photographed. Finally, the sample was heated at 130°C±3°C for four hours and photographed.

Visual examination of the x-ray photographs of the sample subjected to temperatures of 103° and 120°C revealed no major alterations in structure. However, a photograph of the specimen subjected to the 130°C heating demonstrated complete transformation of the superstructure pattern to that of ammonium chloride.

As an adjunct to the above experiments, the specimen heat-treated at 130°C was photographed after being held at room temperature for 18, 100 and 300 hours.

The photographs of the aging 130°C heated specimen showed the reappearance and increase in line intensities of the superstructure pattern with passage of time.

To add weight to these results, several other specimens of sample 8 (14.8 mole per cent $MnCl_2 \cdot 2H_2O$), and of samples 7–2 (13.9 mole percent $MnCl_2 \cdot 2H_2O$) and 7–3 (13.4 mole percent $MnCl_2 \cdot 2H_2O$) were similarly heated at 130°C, and photographed. The changes in each heat-treated sample with standing at room temperature were followed by photographing at increasing intervals of elapsed time. In all cases, the observations described above were completely verified.

Some of the x-ray photographs obtained in these experiments are reproduced in Fig. 3. This figure shows the diffraction patterns for: A—the original, "as is," specimen of sample 7–3; B—this specimen heated at 130°C for four hours; C—ammonium chloride; D, E, F and G—the 130° heat-treated specimen after aging at room temperature for 18, 66, 162, and 572 hours, respectively.

The transformation of the ordered state (superstructure pattern, Fig. 3A) to the disordered state (characterized by a body-centered cubic pattern, Fig. 3B) is readily apparent from these diffraction patterns (compare with that for ammonium chloride, Fig. 3C). The gradual reassertion of order is shown in Figs. 3D, E, F, and G.

Significance of These Results

These results demonstrate two features: firstly, that the ordered state of salt solid solutions (3:1 type) may be transformed above a critical temperature to the disordered state and, secondly, that the reverse process, disorder to order, occurs spontaneously with passage of time at a relatively low temperature (it must be noted, however, that room temperature corresponds to 0.7 of the critical temperature in °A). Thus we have evidence that ordered salt solid solutions exhibit the thermal order-disorder phenomenon shown by superstructure alloys.[1]

The order-disorder changes described[8] for Ag_2HgI_4 and Cu_2HgI_4 have been said[14] to resemble those found for the Cu—Au system. The low temperature modifications of these materials have a tetragonal structure while the high temperature forms are cubic; a situation completely analogous to that found in the present investigation.

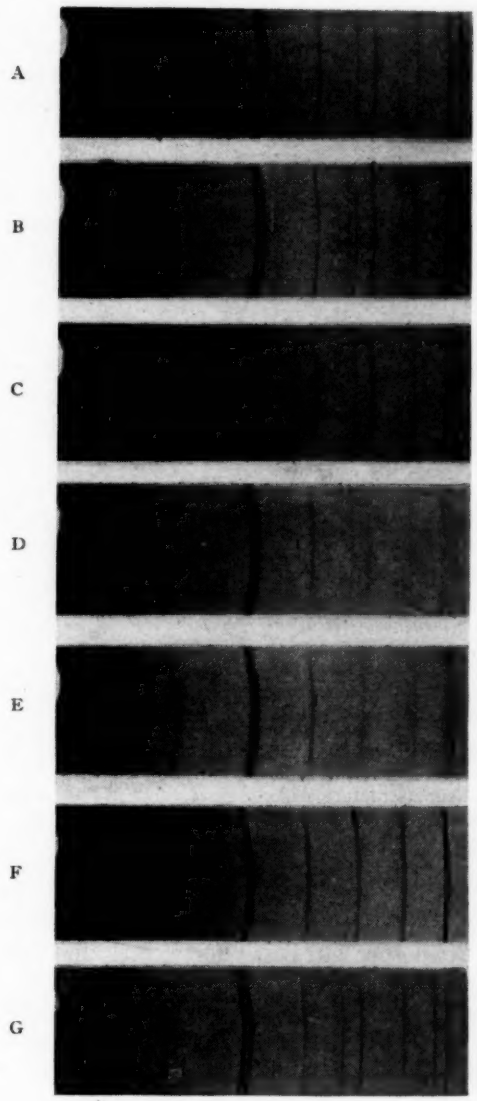

FIG. 4. The disordered state of a salt solid solution produced from the ordered by cold-working.

A—Ordered state.
Original sample, 3:1 superstructure.
B—A, Ground for ¼ hour.
C—A, Ground for ½ hour.
D—A, Ground for 1 hour.
E—A, Ground for 2 hours. Disordered state.
F—NH_4Cl (reference).
G—E, After aging for one month at room temperature.
Order restored.

[14] F. Seitz, *The Modern Theory of Solids* (McGraw-Hill Book Company, Inc., New York, 1940), p. 503.

B. Disorder Introduced by Cold-Work

It has been shown[15] by electrical resistivity measurements that, when an ordered alloy, e.g., Cu_3Au, is drawn or cold worked, the degree of order decreases and that with sufficient working the alloy may be completely disordered.

X-ray diffraction evidence will now be presented to show that cold-working of an ordered salt solid solution results in its conversion to the disordered state.

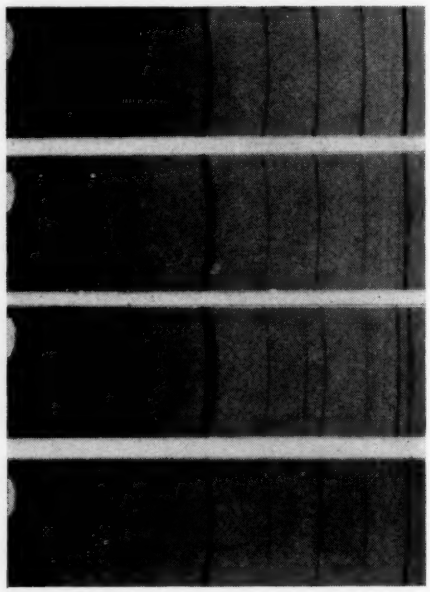

FIG. 5. Diffraction patterns demonstrating the coexistence at equilibrium of ordered and disordered solid solutions.

A—Ammonium chloride. Pattern typifying disordered state.
B—Sample No. 7, two-solid-phase region.
C—3:1 superstructure, ordered state.
D—Sample No. 6, disordered state.

Experimental

Specimens of sample 8 (3:1 type solid solution) were ground by mortar and pestle for $\frac{1}{4}$, $\frac{1}{2}$, 1, and 2 hours, respectively.

Debye-Scherrer photographs were obtained from the crushed crystals immediately after the completion of each grinding period.

Results and Discussion Thereof

The x-ray photographs, prepared in these experiments, are reproduced as Figs. 4B, C, D, and E, respectively, for grinding periods of $\frac{1}{4}$, $\frac{1}{2}$, 1, and 2 hours. For comparison purposes, the diffraction data of the original sample and of ammonium chloride are included as Figs. 4A and 4F, respectively.

The photographs demonstrate an alteration of diffraction line position and intensity with extension of grinding time. These alterations culminate, after 2 hours of cold-working, in practically complete transformation of the superstructure pattern to that of ammonium chloride. These changes in pattern correspond to disarrangement, to the point of randomness, of the orderly distribution of solution components.

Aging of the Worked Sample

The sample disordered by cold-working for 2 hours was photographed after a month's lapse of time during which the sample was at room temperature.

The photograph of this aged sample, Fig. 4G, showed complete restoration of the superstructure pattern.

ISOTHERMAL, COMPOSITIONAL ORDER-DISORDER

The viewpoint has been adopted, in interpreting the results of the present investigation, that order-disorder transformation may be effected by an isothermal, compositional process equally well as by other means, e.g., temperature change. Ample justification for adopting and exploring further this concept will develop from the following sections.

If, with Shockley,[2] we consider the dependence of state of order upon composition at fixed temperature, it is seen from his theoretically derived phase diagram[2] that different phases are stable in different composition ranges. Thus, for a low temperature isotherm, e.g., 25°C, drawn across this diagram, the following equilibrium situations prevail as a result of composition change:

(a) disordered state solid solutions are formed at low "solute" content compositions;
(b) with increasing "solute" content, there appears a two-phase region wherein coexist disordered and ordered solutions;
(c) with still more "solute" added, a region is reached containing a single solid phase, ordered in nature (cubic);
(d) raising the "solute" content higher, a second two-phase region is developed where two types of ordered state solid solutions (cubic and tetragonal) coexist;
(e) finally, a range of compositions is reached where the stable phase is the second type (tetragonal) of ordered solid solution.

These aspects are qualitatively pertinent to the present work. Examining the features of the salt system isotherm at 25°C, we find that they bear a remarkable resemblance to those predicted by Shockley's phase diagram for order-disorder in alloys. There is evidence that:

(a) in the low "solute" composition range, A to B, Fig. 1, there exist disordered type solid solutions;
(b) above a critical composition point, B, a two-phase region, B to C, is formed containing disordered and ordered state (3:1 type) solid solutions in coexistence;
(c) in the region, C to E, the stable phases are solid solutions of 3:1 superstructure type;
(d) there is a transition from 3:1 superstructure to 1:1 at about the composition of sample 16;
(e) composition range, E to F, contains 1:1 superstructure solid solutions.

[15] O. Dahl, Zeits. f. Metallkunde **28**, 133 (1936).

INVARIANT SYSTEMS-COEXISTENCE AT EQUILIBRIUM OF TWO SOLID PHASES

From the phase rule it is known that, in order to produce an invariant system isothermally for the salt system, there would be required the coexistence of four phases: vapor, liquid and two solid phases.

A. The Two Solid Phases Are Ordered and Disordered Solid Solutions

The phase diagram, Fig. 1, very definitely reveals an invariant point on the liquidus curve at *b*. The liquid phase having the composition of this point must therefore be in equilibrium with a vapor and two solid phases. Indeed, a two-solid-phase region extending from B to C is clearly indicated. The two coexisting solid phases in this region are conjugate solid solutions; one an ammonium chloride-rich type having the composition of B, and the other a "manganous chloride-rich" solution with composition corresponding to C.

Previously,[9] solidus sample 7, the product of a mother liquor whose composition corresponded to the invariant point, *b*, was shown to consist of two solids; one isotropic and the other birefringent, when examined under the microscope between crossed Nicols. The x-ray technique employed, at that time, did not succeed in registering the diffraction effects of the birefringent component; only a pattern for ammonium chloride appeared on the photograph.

X-ray photography was repeated on this same sample with present technique and apparatus. The diffraction pattern obtained is reproduced as Fig. 5B. Patterns of ammonium chloride, Fig. 5A, and superstructure type, 3:1, Fig. 5C, are included for ready comparison.

The photographs establish that two solid phases are present: one, disordered cubic; the other, ordered tetragonal of the 3:1 type.

In view of the x-ray evidence and the unmistakable appearance of a two-solid-phase region on the ternary diagram as required by phase rule considerations, it is clear that the phase rule does govern the order-disorder phenomenon.

To eliminate any question of whether the other samples of disordered solid solutions contain any ordered material, an x-ray photograph of the number 6 solidus sample was also prepared by present technique. The composition of this sample lies below that of sample 7 in manganous chloride content. The diffraction lines shown by this photograph, Fig. 5D, were only those expected for random solution in the structure of ammonium chloride.

B. The Two Solid Phases Are the Two Types of Superstructures

The proof for the existence of a two-solid-phase region containing ordered solid solutions of the 3:1 and the 1:1 type is not as clean-cut as the proof of such a region for ordered-disordered phases. It will become obvious that this is caused by the very nature of these solid solutions.

On the triangular diagram, Fig. 1, there appears an inflection, *f*, in the liquidus curve at about the composition of the liquidus phase for sample 16. This must undoubtedly be the invariant point for the coexistence of four phases; vapor, liquid solution and two solid phases. Further indication of this is given by the practically horizontal portion of the phase rule plot, Fig. 5 (previous work[9]), at this sample's composition. The solid phases involved would be two solid solutions; one each respectively of the two types of superstructures. In order to establish this two-solid-phase region beyond doubt, additional sample points must be studied. Samples intermediate in composition between samples 14 and 18 would serve this purpose.

Some evidence for this two-solid-phase region is given by the diffraction data for the transition between the two superstructure types. These data (not given here in order to conserve space) are for the solid solution samples of composition encompassing the range wherein this two-solid region should lie. As evidenced by reflections present on x-ray photographs and relative line intensities, sample 14 is of the 3:1 superstructure type and sample 18 is of the 1:1 type. Now, while the pattern registered for sample 16 is very closely allied to the latter type's, yet, significantly, it contains two reflections that are only found in the former's pattern. The diffraction lines, referred to, are those from (400) and (642).

Because the interplanar spacings of both superstructure types are so closely alike for samples near and in the two-phase region, photographically their reflections will be superimposed. Consequently, only through observance of what reflections are present on photographs of such samples, is it possible to establish the coexistence of these two ordered types by x-ray methods. Ordinarily, the evidence supplied by the appearance on the x-ray photographs of two unexpected reflections would not be relied on too heavily; yet, the registration of these lines is believed to be significant in this instance.

These results, showing the presence in the $NH_4Cl-MnCl_2-H_2O$ system of two-phase changes in order-disorder crystals and two two-phase regions, are regarded as experimental verification of the qualitative predictions made by Shockley[2] on theoretical grounds.

ACKNOWLEDGMENTS

The author acknowledges his indebtedness to Dr. G. H. Walden, Jr., Dr. Alexander Lehrman and the Union Oil Company. Appreciation of the able assistance rendered by Mrs. Juanita M. Cartmel is heartily acknowledged.

The Infra-Red Absorption Spectra of Some Metal Borohydrides*

W. C. PRICE**
Ryerson Physical Laboratory, University of Chicago, Chicago 37, Illinois
(Received March 8, 1949)

The absorption spectra of aluminum, lithium, and sodium borohydride have been obtained in the region from 1–25μ. The aluminum borohydride was investigated as gas and an analysis of the infra-red and Raman bands fits a bridge-type structure of symmetry D_3 (probably D_{3h}). The spectra of lithium and sodium borohydrides were obtained from finely ground slurries of these materials. Their spectra indicate how the bridge structure of the H_2BH_2 metal groups passes over to the tetrahedral structure in a completely ionic lattic.

Using certain bond-distance force-constant relationships in conjunction with data from the diatomic hydrides and accepting electron and x-ray diffraction data for bond distances between the heavier atoms, values for the geometrical parameters are calculated for beryllium, aluminum, and sodium borohydride. These seem more plausible than any so far suggested. Observations on the electronic spectrum of aluminum borohydride have also been made down to 1000A. The diffuseness of the absorption obtained at short wave-lengths prevented any detailed interpretation.

The spectrum of a compound formed between beryllium borohydride and sodium chloride has also been obtained and a consideration of its absorption bands has given information concerning the nature of this material. A spectrum of a slurry of the methyl derivative of lithium borohydride ($LiBH_3CH_3$) indicates considerable change in the structure relative to that of lithium borohydride.

A table of frequencies of related bands in the metal and other borohydrides is given which illustrates the changes referred to above. It includes a number of boron-nitrogen hydrides and shows that the BH frequency, when it is associated with analogous electronic groups, behaves in much the same way as that of CH when it is attached to saturated, olefinic or aromatic groups.

INTRODUCTION

DEFINITE information about the geometrical structure of the metal borohydrides is clearly the preliminary step to the formulation of a satisfactory theory of the nature of their chemical binding. While electron and x-ray diffraction experiments can determine the positions of the heavier atoms in these molecules in a satisfactory manner, the positions of the hydrogen atoms cannot be established with certainty by these methods alone. Now a vibrational analysis of the infra-red and Raman spectra of the molecules, particularly of the bands associated with motion of the hydrogen atoms, might be expected to give a great deal of information about the molecular symmetry and nature of the BH bonds present thus, making it possible to decide between different structures. In this way spectral data can greatly enhance the value of electron diffraction results since, once the form of the molecule is fixed, the scattering curve can then usually be fitted fairly well by a suitable choice of the BH bond distances and angles. Thus information can be obtained which cannot be directly deduced from the spectra. It is also possible, when the vibration bands of a molecule have been satisfactorily assigned, to calculate approximate values for some of the bond distances by using certain force-constant bond-distance relationships. In this way it is possible to check electron-diffraction values for the geometrical parameters in a molecule.

The present work forms part of a program of spectroscopic research being carried out at the University of Chicago on compounds of boron prepared by Professor H. I. Schlesinger's group. The Raman spectrum of aluminum borohydride was obtained by Professor T. F. Young and Dr. B. Rice of the Chemistry Department, and the infra-red results reported here will be described in terms of a normal coordinate analysis which they have made for a model of D_{3h} symmetry with which the experimental evidence is in closest agreement.

EXPERIMENTAL

The aluminum borohydride was a pure sample prepared by Dr. A. Finholt. Owing to its explosive nature care had to be taken to make all gas cells completely leakproof and to cover them with protective wire screen. The cell windows, which were of sodium chloride or potassium bromide, were only lightly attacked by the gas. The hard black wax used for sealing on the windows and the apiezon "L" grease used to grease ground joints were likewise not appreciably affected. An attempt to obtain the spectrum of beryllium borohydride was frustrated by its attack on the rocksalt windows. The spectrum of the fine powder formed on the windows was however recorded and found to give interesting information about its structure. The spectra of lithium and sodium borohydride were obtained by grinding the powders into a fine slurry with liquid paraffin and squeezing this between two rocksalt plates. This procedure had to be carried out immediately on the removal of these substances from the dry box in order to prevent attack by atmospheric moisture.

RESULTS

The spectrum of aluminum borohydride is given in Fig. 1. It shows many features which are clearly analogous to similar ones in diborane.[1] This is because

* Work done under ONR Contract N6ori-20, T.O. IX during the author's leave of absence from Imperial Chemical Industries (Billingham Division) England. For preliminary report, see J. Chem. Phys. 17, 217 (1949).
** Now at King's College, Strand, London.

[1] W. C. Price, J. Chem. Phys. 16, 894 (1947): We wish to call attention to a slight error in Fig. 1 in this article. The band at 1860 cm^{-1} has been plotted 50 cm^{-1} too high due to a misreading of the scale.

most of the bands of frequencies greater than 700 cm^{-1} correspond to vibrations in which the motion is mainly that of the boron and the hydrogen atoms. This general similarlity is considerable evidence for the presence of hydrogen bridges (protonated double bonds) corresponding to those whose existence has been established in diborane. The two bands at 2559 and 2493 cm^{-1} clearly correspond to the infra-red active vibration of terminal BH_2 groupings (2614 and 2522 cm^{-1}) in diborane. This is evidence against the girdle structure originally suggested by Bauer and co-workers.[2,3] In this model, which can be represented by the formula

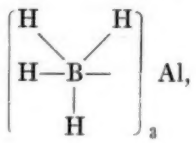

three hydrogen atoms are located between each boron and the aluminum atom, forming a "girdle" round the B–Al bond and there is a single terminal BH which is co-linear with this bond. Such a terminal group would be expected to give rise to only a single band at this frequency, as for example in the spectrum of acetylene. Professor Bauer has kindly informed the author in correspondence that recent calculations involving quite highly unsymmetrical bridge structures now permit of a satisfactory fit with a bridge model. It should also be mentioned that chemical evidence favors a bridge structure as against a girdle structure for diborane.

The bands at 2031 and 1500 cm^{-1} are clearly analogous to the characteristic BH_2B bridge vibrations in diborane (1860 and 1604 cm^{-1}). The shift of one to shorter and the other to longer wave-lengths is to be related to the fact that, as the binding of the boron to the metal becomes more ionic, the higher frequency vibration becomes a stretching vibration of the $(BH_4)^-$ group while the lower one becomes a BH deformation vibration of the same group. This is to be expected from the nature of the vibration assigned to these bridge bands in diborane. The bands at 1114 and 978 cm^{-1} are by analogy associated with in-plane and out-of-plane vibrations of the terminal BH_2 group respectively. The band at 604 cm^{-1} is interpreted naturally as a stretching vibration of the AlB_3 skeleton.

Table I gives the frequencies and assignments of the fundamental bands and includes the Raman frequencies observed by Young and Rice,[4] with whom close cooperation has been maintained. Their assignments have been adopted here. For the detailed normal coordinate treatment and the nature of the normal modes

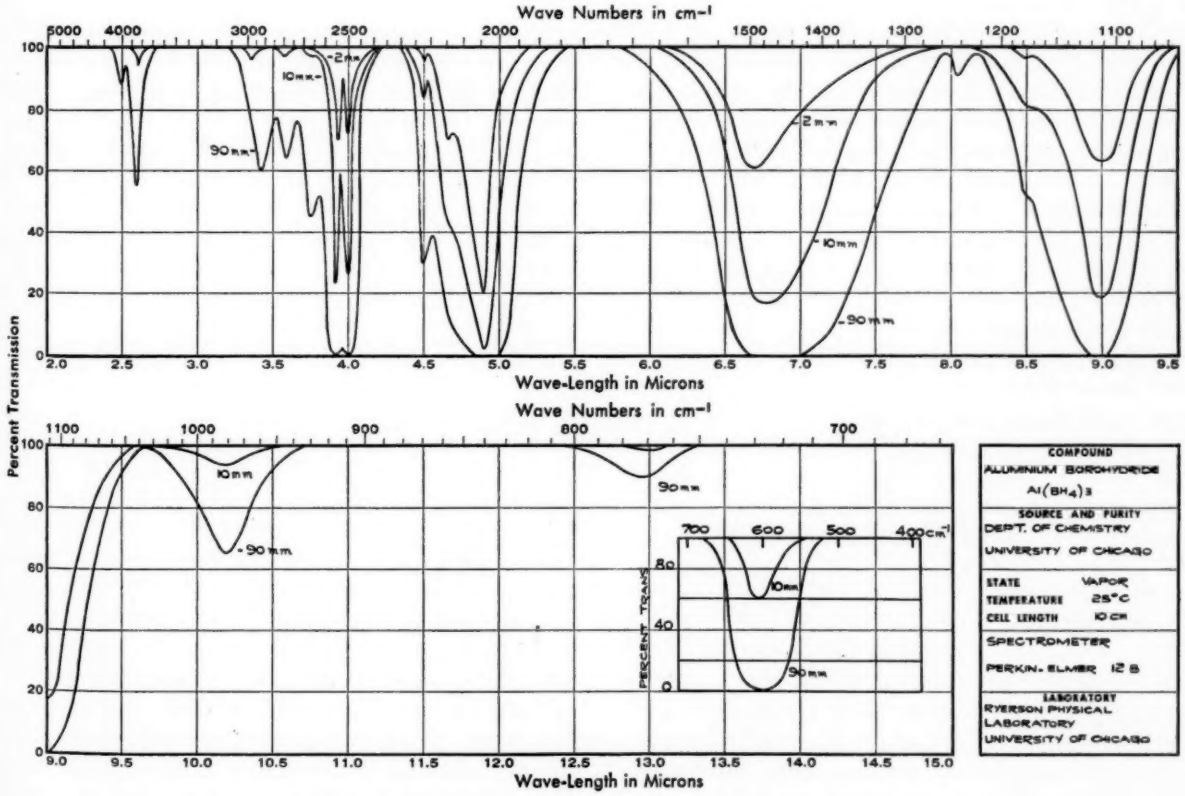

FIG. 1. The infra-red absorption spectrum of aluminum borohydride.

[2] J. Y. Beach and S. H. Bauer, J. Am. Chem. Soc. **62**, 3440 (1940).
[3] G. Silbiger and S. H. Bauer, J. Am. Chem. Soc. **68**, 312 (1946).
[4] T. F. Young and B. Rice, J. Chem. Phys. (in press).

reference should be made to their article. The assignments have been made with respect to a prismatic model of symmetry D_{3h}. This model and the octahedral model (symmetry D_3) have been discussed by Longuet-Higgins.[5] They are illustrated diagrammatically in Figs. 2(a) and 2(b). (To prevent confusion the terminal hydrogens have not been drawn in; but by analogy with diborane each terminal pair would be expected to lie on a line perpendicular to the line joining the pair of bridge hydrogens in the same H_2BH_2Al arm.) The following argument shows that it is difficult to reconcile the most plausible values for bond angles and distances with a regular octahedral model. If the bridge hydrogens are assumed to be equidistant between the boron and the aluminum atom then in a regular octahedral arrangement the angles AlBH and BAlH would have to be 45° and the H−H distance would have to equal the AlB distance. There is no *a priori* reason why this should actually be the case. It is to be expected that the H−H distance will only be slightly larger than its value in diborane (2.13A)[6],† whereas the AlB distance is 2.19A.[2] These happen to be roughly equal but if, as seems likely, the bridge hydrogens are closer to the boron than to the aluminum, then for the bridge hydrogens to lie at the vertices of a regular octahedron there must be a considerable increase in the HH distance. For example if BAlH=45°, AlBH=50° (as in diborane bridge) and AlB=2.19A, then HH=2.39A; if AlBH =55°, then HH=2.58A. The most plausible value for the AlBH angle is probably in the neighborhood of 50°, the value of the BBH angle in diborane. Using this value for the angle AlBH, the value 2.19A for the AlB distance as determined by electron diffraction and a BAlH angle of 45°, the BH bridge bond length works out at 1.56A as compared with 1.39A in diborane. For a 55° AlBH angle the BH bond length works out as 1.69A. These values for HH and BH are not considered plausible; but in order to maintain AlBH at about 50° and HH at about 2.13A the octahedral bonds would have to be considerably distorted (see later), and this would require considerable energy. The octahedral arrangement of the hydrogen atoms about the Al atom thus seems to lose much of its attractiveness. On the other hand, Longuet-Higgins[5] has shown that a prismatic arrangment is compatible with a "protonated" double bond structure in which three 120° coplanar "π" bonds radiate from the Al atom. The "*s*," "*p*" and "*d*" atomic Al orbitals can combine linearly to form such bonds.

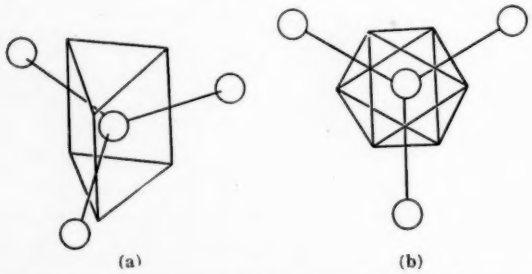

FIG. 2. (a) Prismatic model for aluminum borohydride (symmetry D_{3h})—terminal hydrogens omitted. (b) Octahedral model for aluminum borohydride (symmetry D_3)—terminal hydrogens omitted.

The bearing of the present work on this problem of the structure of aluminum borohydride may be summarized as follows. The vibrational analysis appears to be in good agreement with a molecular symmetry D_{3h}, i.e., the prismatic structure. The normal coordinate analysis of an unsymmetrical octahedral arrangement has not yet been carried out, but this structure is considered improbable on other grounds. The girdle structure is considered to be eliminated by the general resemblace of the spectrum to that of diborane, in particular the existence of two bands corresponding to terminal BH vibrations. Also, as will be shown later, it is difficult to reconcile the frequencies of the observed BH stretching vibrations with the rather large BH distances predicted by the interpretation of the electron diffraction results in terms of a girdle structure.

DISCUSSION OF INDIVIDUAL BANDS

Terminal BH_2 Vibrations

As with diborane it is convenient to discuss the vibrations involving motion of the terminal BH_2 groups in terms of the normal vibrations of this triatomic group and then to consider how the various group vibrations are coupled together. In diborane the symmetrical valence vibrations of the BH_2 group are not much affected by coupling in-phase (2523 cm) or out-of-phase (2522 cm). The same is true of aluminum borohydride where the corresponding frequencies are 2480 and 2493 cm^{-1}. The antisymmetrical valence vibrations are affected more strongly in diborane, being 2614 for the in-phase and 2591†† for the out-of-phase. Assuming the whole of the splitting in diborane is caused by this coupling, then the uncoupled antisymmetrical valence vibration of this group should have a frequency equal the mean of these (2614+2591)/2=2603, i.e., 80 cm^{-1} greater than the symmetrical BH_2 valence frequency. In aluminum borohydride ν_{15} (2556) is the only active normal mode involving the antisymmetric BH_2 valence frequency. This resembles fairly closely, though not exactly, the in-phase combination ν_8 (2614) in diborane and as such should be higher than the antisymmetric BH_2 group valence vibration. A reasonable guess can be made for this difference. In diborane ν_8 is higher than the value deduced for the isolated antisymmetric valence vibration of the BH_2 group by 11 cm^{-1} (2614-2603). Since the coupling is probably not as strong in aluminum borohydride, being exerted across two bonds

[5] H. C. Longuet-Higgins, J. Chem. Soc. **14**, 139 (1946).
[6] S. H. Bauer, Chem. Rev. **31**, 43 (1942).
† It will be shown later that it is probably appreciably smaller.

†† We are indebted to Professor K. S. Pitzer for the information that the Raman line previously reported at 2489 cm^{-1} is spurious and that it should be replaced by a line at 2591 cm^{-1}.

instead of one, it might be expected that in this compound the difference would be considerably lower, say *ca.* 3 cm^{-1}. This gives 2556−3=2553 cm^{-1} for the antisymmetric BH_2 valence vibration which is thus higher than the symmetrical valence vibration of the group (taken as (2480+2493)/2=2487) by 66 cm^{-1}. This compares favorably with the value of 80 cm^{-1} (2603–2523) obtained for diborane and indicates that the terminal groups in the two compounds are essentially the same except that the valence frequencies of the BH_2 group in aluminum borohydride are *ca.* 40 cm^{-1} less than they are in diborane, this being probably accompanied by a corresponding increase in BH distance.‡ The deformation vibrations of the terminal BH_2 groups are also consistently reduced in aluminum borohydride in comparison with those in diborane. The symmetrical in-phase vibration in diborane is 1180 cm^{-1} as compared with 1156 in aluminum borohydride. The corresponding out-of-phase vibrations are 1175 and 1118 respectively. The out-of-phase rocking vibration is hardly changed—974 to 978, i.e., a slight increase in aluminum borohydride.

Bridge Vibrations

A consideration of the data vailable on the infra-red spectra of molecules in general makes it clear that for a molecule such as aluminum borohydride, bands occurring in the region 2100–1400 cm^{-1} can only be due to the stretching of bonds to hydrogen atoms probably tied into some sort of a ring. It will be shown that as the bridge structure gives place to a more ionic structure involving $(BH_4)^-$ the bands gradually move out of this region. Some go up to higher frequencies and become free stretching vibrations and the others go to lower frequencies and become deformation vibrations of the $(BH_4)^-$ ion. This process has clearly started in aluminum borohydride where the bands in the 2050 region correspond to the diborane bands around 1870 cm^{-1}, and the broad band around 1500 cm^{-1} corresponds to the diborane band at 1600 cm^{-1}. As with diborane these bands are the strongest in the spectrum and this is to be associated with the fact that the bridges are the seat of the electron deficiency and displacements of the atoms in this part of the molecule are liable to produce large local dipoles.‡‡ Aluminum borohydride has of course three times as many bridges per molecule as diborane and one and a half times as many terminal BH_2 groups. However, even allowing for this numerical increase, the intensity of the bridge and BH_2 bands (per group) is in general greater than that in diborane. This probably results from the general increase in the ionic character of the molecule.

It was pointed out in the article on diborane that there is still some doubt about the exact nature of the mode of vibration of the bands in the 1870 cm^{-1} region of this molecule as the rotational structure did not agree

TABLE I.† Frequencies and assignments of the fundamental infra-red vibration bands of aluminum borohydride including also the Raman data and assignments of Young and Rice (symmetry D_{3h}).

Character	$A_1'(R)$*	$A_2''(IR)$**	R & $E'(IR)$	$E''(R)$	Assignment
B-H sym. stretching	ν_1				R. 2480
B-H sym. stretching (out-of-phase)			ν_{16}		IR. 2493
B-H antisym. stretching			ν_{15}		R. 2553, IR. 2550
Bridge expansion	ν_2				R. 2082
Bridge expansion (out-of-phase)			ν_{17}		IR. 2031
Bridge stretching (⊥)			ν_{11}		IR. 2154
Bridge stretching (∥)		ν_3			R. 1502
Bridge stretching (∥) antisym.			ν_{18}		IR. 1500 (Broad)
BH_2 deformation	ν_4				R. 1156
BH_2 deformation (out-of-phase)			ν_{19}		R. 1122, IR. 1114
BH_2 rocking (in-plane)			ν_{20}		R. 1407 (?)
BH_2 rocking (out-of-plane)		ν_{13}			IR. 978
BH_2 rocking (out-of-plane) (out-of-phase)				ν_{24}	R. 977
Bridge shearing		ν_{12}			
Bridge shearing (antisym.)				ν_{25}	R. 1407 (?)
BH_2 twisting				ν_{26}	R. 600 (?)
Al-B stretching	ν_5				R. 518
Al-B stretching (antisym.)			ν_{21}		R. 600, IR. 603

† R=Raman, IR.=infra-red. Frequencies in cm^{-1}.

‡ In the light of the new data on the Raman spectrum of diborane it is worth while comparing the values for the stretching frequencies of the CH_2 group in ethylene with those of the BH_2 group in diborane. The values of the uncoupled group frequencies are taken as the mean of the molecular frequencies corresponding to coupling of the group frequencies in-phase and out-of-phase. They are set out in Table A.

TABLE A. Calculation and comparison of XH_2 valence vibrations in ethylene and diborane (frequencies in cm^{-1}).

Ethylene CH_2 antis. vib.	Ethylene CH_2 sym. vib.
3105.5 out-of-phase	2989.5 out-of-phase
3272.3 in-phase	3019.3 in-phase
3188.9 mean (uncoupled)	3004.4 mean (uncoupled)
±83.4 due to coupling	±14.9 due to coupling
Difference (antis.−sym.)=184.5	
Diborane BH_2 antis. vib.	**Diborane BH_2 sym. vib.**
2614 out-of-phase	2523 out-of-phase
2591 in-phase	2522 in-phase
2602.5 mean (uncoupled)	2522.5 mean (uncoupled)
∓11.5 due to coupling	∓0.5
Difference (antis.−sym.)=80.0	

The two sets of data for ethylene and diborane seem to be reasonably consistent in view of the weaker coupling and valence forces in diborane. However, the coupling terms have opposite signs. The explanation of this is thought to be along the following lines. A compression along the C=C bond arising from the motion of one carbon atom in ethylene is reflected from the other carbon atom as a compression, but in diborane the compression from a boron atom through a BH bond is reflected as a rarefaction because of the lightness of the hydrogen atom. It is thought that this change in phase will account for the change in sign of the coupling term.

‡‡ Electron deficiency in the bridges makes itself apparent in the large values obtained for the bridge BH distances when the electron diffraction data are interpreted in terms of a bridge model.

TABLE II. Table giving the frequencies and assignments of the overtone and combination bands of aluminum borohydride.

Frequency	I	Assignment
3995	w	$\nu_2+\nu_{17}=2031+2082=4113$
3924	m to w	$2\times\nu_2=2\times2031=4062$
2938	m to w	$\nu_3+\nu_{18}$ or $2\nu_{18}$– ca. 3000
2790	w	
2695	w	
2222	w	$\nu_4+\nu_{19}=1156+1118=2274$ Or $2\nu_{19}=2236$
1246	w	
770	w	
ca. 400	s	Possibly analogous to diborane band at same frequency

with the vibrational assignment (unless a weaker band at 1993 cm^{-1} was taken as ν_{13}). The exact interpretation of the aluminum borohydride bands around 2000 cm^{-1} must therefore wait until this matter is cleared up.

AlB_3 Vibrations

There is a broad strong band at 603 cm^{-1} which fits in naturally as a vibration of the AlB_3 group. Its strength indicates that there is some ionic character in the AlB bonds as is to be expected.

OVERTONE AND COMBINATION BANDS

Table II gives the frequencies of overtone and combination bands. It is not easy to assign these because of the large number of possibilities. However, the assignments given appear to be the most plausible ones.

ELECTRONIC SPECTRUM

Aluminum borohydride is transparent in the visible and near ultraviolet. An examination of its spectrum in the region 2000–1000A showed diffuse absorption rather similar to that of diborane. The first strong absorption is a broad diffuse band appearing around 1340A at very low pressure equivalent to a thickness of 0.005 cm gas to N.T.P. This is followed by further diffuse absorption of similar strength below 1200A. At higher pressures the absorption spreads to long wavelengths quickly reaching 1500A with a weaker step-out covering the region out to 2000A. The spectrum would be consistent with a first ionization potential of the molecule of about 11 volts but its lack of discrete bands prevents any deductions being made concerning the nature and origin of the electron removed.

THE SPECTRA OF LITHIUM AND SODIUM BOROHYDRIDE

The spectra of these materials obtained as finely ground slurries in liquid paraffin are shown in Fig. 3. The bands of the liquid paraffin used to make the slurries occur mainly in the regions *ca.* 2950, 1450 and 1365 cm^{-1}. As far as could be judged no bands of the borohydrides were overlapped by the paraffin absorption. The bands corresponding to the BH valence vibrations are quite obviously those occurring around 2300 cm^{-1} (slightly higher for the lithium than the sodium compound). Sodium borohydride is considered to be completely ionic both from its ordinary physical proper-

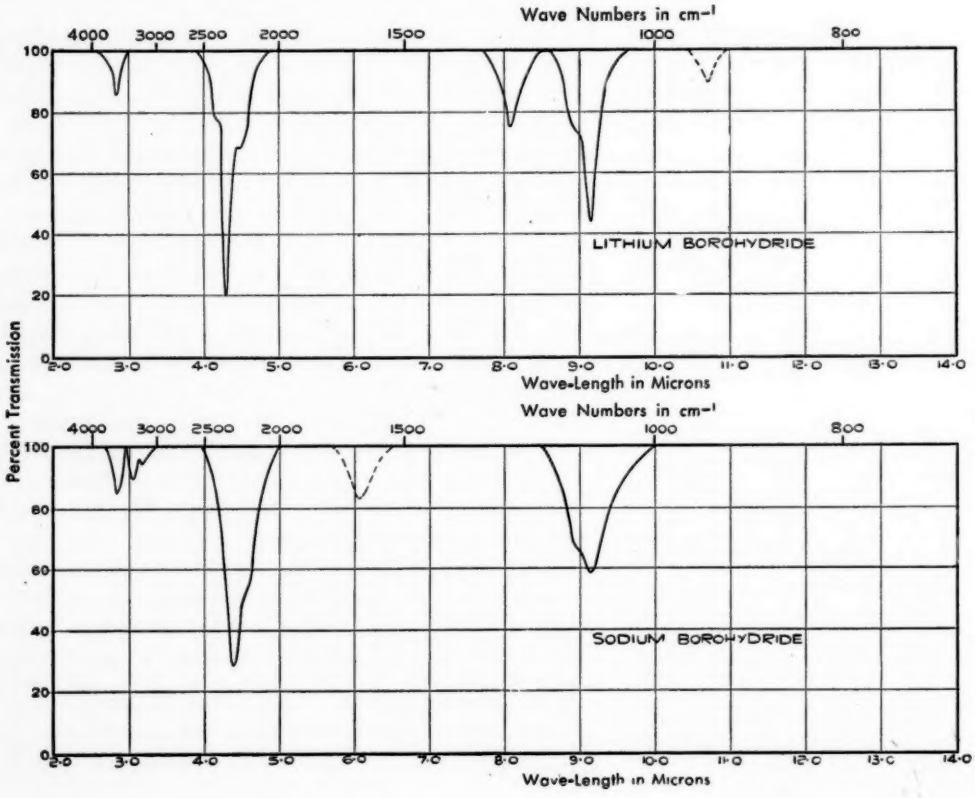

FIG. 3. The infra-red spectra of lithium and sodium borohydride as slurries in liquid paraffin (paraffin bands not shown).

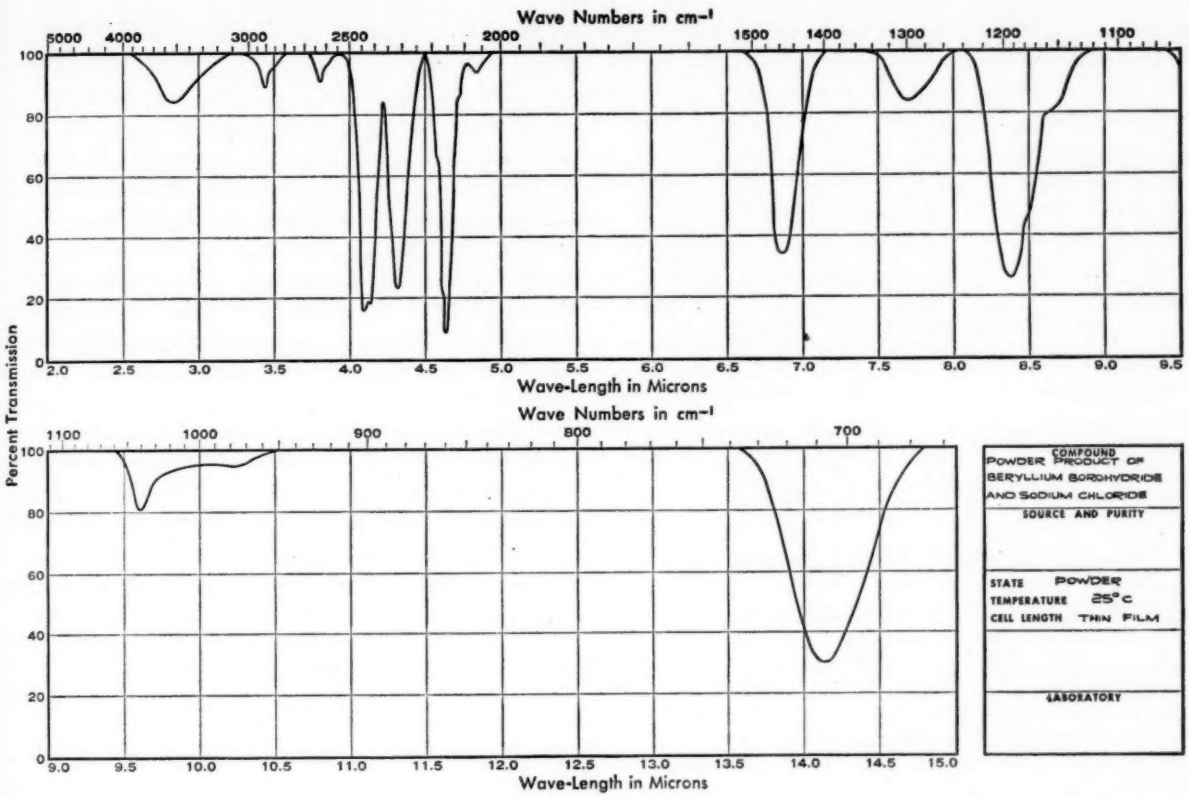

FIG. 4. The infra-red spectrum of a powder product of beryllium borohydride and sodium chloride.

ties and from the x-ray crystal analysis of Soldate.[7] The bands are thus to be associated with the $(BH_4)^-$ ion. Bands at *ca.* 1100 cm^{-1} found for these materials presumably correspond to a deformation vibration of this ion. The binding in lithium borohydride is probably mainly ionic,[7a] but less completely so than that of sodium borohydride in view of the slightly higher BH stretching frequency. It is interesting to note that the spectrum of a slurry of the methyl derivative of lithium borohydride ($LiBH_3CH_3$) showed the BH valence frequency considerably reduced—bands being obtained at 2190 and 2130 cm^{-1}. This may result from a large polarizability effect by the methyl group or possibly from a major rearrangement such as might occur if the methyl group took up a position along the LiB axis. The $(BH_4)^-$ group in the ordinary lithium borohydride may only differ from that of a bridge structure by a slight alteration in the angles of the BH bonds. The configuration of the methyl derivative may be one in which the lithium, boron and carbon atoms are colinear and the three BH bonds may be arranged in a trigonal formation around the B—Li bond forming a "girdle" around it.

Both the lithium and sodium borohydride have a strong combination band in the region 3250–3400 cm^{-1}. This appears to be a combination of BH valence and deformation frequencies and is probably analogous to the corresponding combination band in diborane at slightly higher frequency (3600–3700).

Attempts to obtain the spectra of the $LiAlH_4$ and $NaAlH_4$ have so far been unsuccessful, though some indication that the AlH valence frequency is *ca.* 1700 cm^{-1} has been obtained.

THE SPECTRUM OF A POWDER PRODUCT OF BOROHYDRIDE AND SODIUM CHLORIDE

In an unsuccessful attempt to obtain the spectrum of beryllium borohydride, it was found that this material attacked the sodium chloride windows of the cell, giving a white powder and liberating some diborane. The spectrum of this powder is shown in Fig. 4. It

TABLE III. Table of frequencies of related bands in the metal and other borohydrides.

Substance	Terminal valence BH cm^{-1}		Bridge Class (a)	Bridge Class (b)	Deformation in-plane	Deformation out-of plane
B_2H_6	2614	2522	1990–1850	1600	1175	974
$Be(BH_4)_2$	2630	2515	2165–1985	1530		
$Al(BH_4)_3$	2559	2493	2220–2000	1480	1114	978
$LiBH_4$	2320	(2404–2245)	No strong band		1096	—
$NaBH_4$	2270	(2380–2150)	No strong band		1080	
$B_2H_2(CH_3)_4$			2000–1850	1600	—	—
$B_3N_3H_6$	2535				ca. 1100	920
$B_3N_3H_3(CH_3)_3$	2495				1050–1100	900
$H_2BN(CH_3)_2$	2447 and 2369		No strong band		1156–48	964
$H_2BN(CH_3)_3$	2384	2281	No strong band		1175	
BH	2366					

[7] A. M. Soldate, J. Am. Chem. Soc. **69**, 987 (1947).
[7a] P. M. Harris and E. P. Meeholm, J. Am. Chem. Soc., **69**, 1231 (1947).

has interesting features which throw considerable light on the nature of the material. Bands occurring in the 2450 cm^{-1} region (2465 and 2440 cm^{-1}) are clear evidence of terminal BH_2 groups. The strong band at 2180 cm^{-1} and another at 1450 cm^{-1} are the bands of a BH_2Be bridge which is probably slightly ionic. That at 1196 cm^{-1} corresponds to BH_2 deformation. The new band at 708 probably corresponds to a beryllium-chlorine link, as it did not appear when potassium bromide windows were used. (Admission of air to the cell immediately destroyed the material, the reaction being

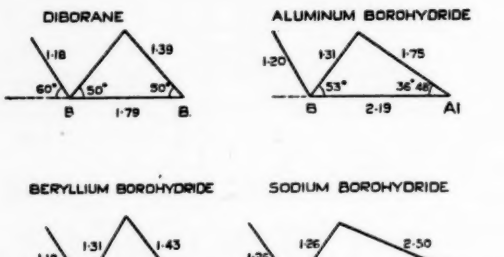

FIG. 5. Structures of metal borohydrides as calculated using electron (or x-ray) diffraction data for bonds between the heavy atoms and assuming certain force constant/bond distance relationships. Diborane data is according to electron diffraction. Terminal BH bonds are shown rotated through 90.

accompanied by the usual green flash.) It is thus clear that the infra-red method can be usefully employed to give information on this peculiar class of compounds which would be very difficult to obtain in any other way.

Frequencies of Related Bands in the Metal and Other Borohydrides

The frequencies of a number of related bands in the metal borohydrides are given in Table III. This shows how the terminal BH_2 frequencies are reduced as the material becomes ionic. The groups of frequencies associated with the hydrogen bridges fall into two classes—(a) a high frequency class occurring at frequencies greater than 1700 cm^{-1} and (b) a low frequency class occurring below this frequency. A correlation of the spectra with the expected ionic character of the molecule indicates that as the bonding to the metal becomes more ionic, the higher bridge frequencies increase and become valence frequencies of the $(BH_4)^-$ ion at *ca.* 2300 cm^{-1}. Those of the lower frequency class are decreased and tend to become deformation frequencies of this ion at *ca.* 1100 cm^{-1}. This is presumably accompanied by a gradual change of the BH bond angles to the tetrahedral value.

The table also contains data on a number of boron-nitrogen hydrides. When these are compared with the corresponding hydrocarbon analogues the interesting point emerges that the BH valence frequency, when it is associated with analogous electronic groups, behaves in much the same way as that of CH. It is well established for instance that the infra-red bands corresponding to the stretching of an aromatic C—H bond lie in the range from 3110 to 3010 cm^{-1}, those of olefinic CH from 3080 to 2980 cm^{-1} and those of saturated CH from 2980 to 2830 cm^{-1},[8,9] i.e., saturated molecules have lower CH frequencies than olefinic or aromatic ones. Similar behavior occurs for the infra-red bands of the BH valence vibration. For borazole the frequency is 2535 cm^{-1} (for N. trimethyl borazole—2495 cm^{-1}), for $H_2B=N(CH_3)_2$ bands at 2447 and 2369 cm^{-1} were obtained, while for $H_3BN(CH_3)_3$ the frequency of the BH valence band is 2384. It should, however, be mentioned that the polarity differences which occur in these compounds but not in the analogous hydrocarbons, are likely to be at least as important a cause of the frequency differences as the differences in hybridization.

Bond Distances and Angles in the Borohydrides

While data by which all the geometrical parameters of the borohydrides can be calculated directly are not available and, with perhaps the exception of beryllium borohydride, may not be available for some time, it seems worth while inquiring whether indirect methods can give any information about them. There is in fact sufficient direct data known which in combination with semi-empirical relationships between force constant and bond distance, etc., can establish beyond reasonable doubt the values of these parameters to a first degree of approximation. The accuracy of the results obtained is adequate for understanding many points in the structure of these molecules. Clearly the policy to be followed in making such calculations is to use as far as possible data which can be reliably determined directly, such as electron diffraction values for BB, BBe, BAl, and BNa (x-ray) distances, also the spectroscopically determined frequencies and distances of the associated diatomic hydrides. The minimum use should be made of empirical relationships or plausible assumptions.

Consider first diborane. The fact that the geometrical parameters obtained by interpreting the electron diffraction data in terms of a bridge model give values of the small moment of inertia which are in agreement with the rotational structure of the perpendicular bands of this molecule is strong, though not absolute, confirmation of the reliability of the electron diffraction results. The BB distance found can certainly be accepted. A value for the terminal BH distance can be calculated from a force-constant bond-distance relationship. We use the Birge-Mecks relationship[10] $-\omega_e r_e^2 = \text{constant}$ in the form $k_e r_e^4 = \text{constant}$ in preference to the other

[8] Barnes, Gore, Stafford, and Williams, Analytical Chem. 20, 402 (1948).
[9] H. W. Thompson, J. Chem. Soc. 328, 1948.
[10] R. T. Birge and R. Mecks, Zeits. f. Physik 32, 823 (1925).

empirical relationships¶ because it appears to be particularly good for hydrides. Now it has been shown in an earlier paragraph that the terminal BH_2 group in diborane behaves as though it had an antisymmetrical valence "group" vibration of 2602 cm^{-1} and a symmetrical one of 2522 cm^{-1}. Assuming the HBH angle of 120°, this gives a force constant for the BH bond which in a diatomic BH molecule would correspond to a frequency of 2550 cm^{-1}. The possible error in this value does not appear to be more than 10 cm^{-1}. Taking the values $\omega_e = 2366$, and $r_e = 1.2326$ for diatomic BH in its ground state[11] and using the $\omega_e r^2 =$ constant relationship we get 1.19A for the terminal BH distance compared with 1.18A by electron diffraction. The same procedure applied to ethylene gives 1.08A for the CH distance as compared with 1.071A obtained spectroscopically.[12] Thus the electron diffraction value for the BH distance is confirmed. A BH distance of 1.27A as is obtained by the interpretation of the electron diffraction results in terms of an ethane-type structure would correspond to BH valence frequencies of about 2200 cm^{-1}. This is a further argument against this model. It can be shown to a fair approximation that for the bridge model the angle between the BB bond and the bridge BH is $= \nu_{13}/\nu_{17}$ which agrees with a value of *ca.* 50° for the bridge. The valence force constants for the bridge BH bonds has also been calculated approximately and shown to be consistent with BH distances of about 1.39A.* As these calculations cannot be made without neglecting certain factors, it is not worth while reproducing them here.

It has already been pointed out that along the series from B_2H_6 to $LiBH_4$ some of the frequencies characteristic of the bridge increase towards the value of the valence frequencies of the $(BH_4)^-$ ion. This process must clearly be accompanied by a decrease in the bridge BH distances. At the same time there is a decrease in the terminal BH_2 valence frequencies and a corresponding increase in their distances as their values approach that of the ion. The next step is thus to calculate a value for the BH distance in the $(BH_4)^-$ ion from the frequencies reported here for sodium borohydride. The magnitude of this distance turns out to be 1.26A (i.e., roughly $(2336/2280)^{\frac{1}{2}} \times 1.233$); the method gives for the CH distance in methane, 1.085A as against the spectroscopic value 1.0936A.[13]

For the calculation of the bond distances in beryllium and aluminum borohydride, the bridge angles have been assigned the values BeBH = 54° and AlBH = 53°. These are unlikely to be more than a degree or so in error since they must be between 50 and 55°. The boron-metal distances are known from electron diffraction[2,3] and the position of the bridge hydrogens appears to be best fixed by placing them so that, for example, in beryllium borohydride the ratio of the BeH and BH distances is equal to the ratio of the internuclear distances in the corresponding diatomic hydrides. This assumption is supported by the fact that the BH bridge distances then appear to be consistent with the values observed for the BH bridge frequencies. Appreciably different values of distance and angles would lead to unacceptable values of the bridge frequencies. The bond distances in the bridges are slightly less than those which might be expected for single electron bonds from hydrogen to the metals, as judged by data available on the spectra of the diatomic hydrides and their ions. The terminal BH distances in beryllium borohydride have been assigned values on the basis of its infra-red spectrum alone.[14] As no Raman data are available, the values for this molecule must be regarded as least certain. The terminal BH_2 angle for the borohydrides cannot be determined with sufficient precision by, for example, a valence force field treatment of the uncoupled BH_2 groups. Such calculations give angles of about 100°.

The dimensions of the bridge structures in beryllium, aluminum, and sodium borohydrides, as calculated according to the above postulates, are shown in Fig. 5. It is believed that they will form a useful guide to further speculation on the structures of these and similar boron compounds. In the case of aluminum borohydride, they indicate that the octahedral structure is improbable, the BAlH angle expected being only 37° as against that of *ca.* 45° which would be necessary to make an octahedral structure stable.

It is stated by Soldate[7] in his paper on the crystal structure of sodium borohydride that "With the assumption of a covalent boronhydrogen bond distance of 1.16A, a van der Waals' radius of 1.00A for hydrogen, and a crystal radius of 0.95A for sodium, it can be seen that the boron-sodium distance of 3.07A and the boron-boron distance of 4.35A are large enough to cause very little steric hindrance to rotational displacements of the BH_4^- tetrahedra." However, it is clear that with the BH distance of 1.26A calculated here, the amount of steric hindrance to be expected in the crystal is considerably increased. Certainly the infra-red spectrum showed no evidence of rotational structure although the resolution employed was more than adequate for its detection.

¶ For a review of the various force-constant bond-distance relationships see G.B.B.M. Sutherland, Ann. Report Chem. Soc. **33**, 53 (1936); Ann. Report Chem. Soc. **35**, 37 (1938).

[11] G. W. King, J. Chem. Phys. **6**, 378 (1936).

[12] W. S. Galloway and E. F. Barker, J. Chem. Phys. **10**, 88 (1942).

* Valence force constants have also been calculated for the bridge model of diborane by Bell and Longuet-Higgins in their original paper (Proc. Roy. Soc. **183**, 357 (1945)) which showed the compatibility of such a model with the observed spectra. The extension here is that values are found for the bond distances by using the force constant bond distance relationship and the diatomic BH distance, which are in agreement with those obtained from the electron diffraction results.

[13] G. Herzberg, *Infra-red and Raman Spectra* (D. Van Nostrand Company, Inc., New York, 1945), p. 439.

[14] Price, Longuet-Higgins, Young, and Rice, J. Chem. Phys. **17**, 217 (1949).

In conclusion, the author wishes to acknowledge the valuable collaboration he has had with Professor T. F. Young and Dr. B. Rice in the work on aluminum borohydride. He is also greatly indebted to Drs. R. D. Cowan and H. C. Longuet-Higgins for much helpful criticism and for permission to quote unpublished data, to members of Professor H. I. Schlesinger's group for providing the materials, and to Professor R. S. Mulliken for his active interest in the spectra of boron compounds, and also to Professor E. Teller. Thanks are due to the ONR for sponsoring the work.

Note added in proof.—It should not be inferred from the comparison of the spectra of *gaseous* beryllium and aluminum borohydride with those of *crystalline* lithium and sodium borohydride that, if the binding in the former were completely ionic, their BH frequencies should approximate those of the latter. The terminal and internal BH frequencies should still fall into two fairly distinct groups in "ionic" beryllium and aluminum borohydrides in the gas phase. These two groups are of course equivalent in sodium borohydride where the $(BH_4)^-$ is surrounded by Na^+ ions.

THE JOURNAL OF CHEMICAL PHYSICS VOLUME 17, NUMBER 11 NOVEMBER, 1949

Internal Motion and Molecular Structure Studies by Electron Diffraction*

ISABELLA LUGOSKI KARLE AND JEROME KARLE
Naval Research Laboratory, Washington, D. C.

(Received January 31, 1949)

A procedure has been developed for the determination of molecular structure by electron diffraction which yields accurate intensity data and obviates the necessity for visual examination of the diffraction photographs. The theory for computing radial distribution curves has been extended to permit accurate curves to be obtained from scattering data covering only a restricted range of angle. From this method, it is possible to obtain not only equilibrium distances but also the probability distributions for the vibrational motion between pairs of atoms in a molecule. The procedure has been applied to CCl_4 and CO_2 and when comparisons may be made with spectroscopic results, satisfactory agreement is obtained.

THE study of molecular structures using electron diffraction by gases has usually involved the visual examination of the diffraction pattern[1] which consists of small oscillations about a steeply falling background. The positions of the apparent maxima and minima are measured, their relative intensities are estimated visually, and some estimate is made of the shape of those features which appear to be neither maxima nor minima. The observed curve is used as the basis for evaluating the equilibrium distances in the molecule being studied. This is accomplished by calculating a radial distribution curve which is used as a guide for selecting various models to represent the structure of the molecule. From these models intensity curves are computed and compared to the visually observed curve. The model chosen to represent the structure of the molecule depends upon the agreement between the computed and observed curves. Some differences are found in the form of the functions used by various investigators to compute the radial distribution and intensity curves.

The uncertainties in the visual examination of the diffraction patterns and in the mathematical analysis, make it very desirable to establish a quantitative procedure which uses an unambiguous theory and eliminates the visual study of the photographs. A procedure to eliminate this visual study has been developed by the Norwegian school and they have used it to study the structures of a large number of molecules.[2] Their procedure involves the use of a rotating sector[3] in order to accentuate the oscillating features of the pattern and the photographs are scanned with a microphotometer. The main difference between their procedure and the one to be outlined concerns the method of analyzing the scattering data. By our method accurate values of the equilibrium distances can be expected and, in addition, it is possible to evaluate the magnitude of the vibrational motion between pairs of atoms in a molecule.

THEORY

When free molecules are struck by a beam of fast electrons, part of the scattering of the primary beam arises from the spacings between the atoms in individual molecules and can be represented by the formula

$$I_m(s)=\sum_{i=1}^{n}\sum_{j=1}^{n} c_{ij}A_{ij}. \quad (i\neq j) \qquad (1)$$

The rest of the scattering does not depend upon the molecular structure and forms a steeply falling background upon which the molecular scattering, Eq. (1), is superimposed. The upper limit n in the summation is

* Presented at the meeting of the American Society for X-Ray and Electron Diffraction, Columbus, Ohio, December 16, 1948.

[1] L. O. Brockway, Rev. Mod. Phys. 8, 231 (1936).

[2] (a) Chr. Finbak, Avhandl. Norske Vid.-Akad. Oslo, I Mat.-Naturv. Kl., No. 7 (1941). (b) Chr. Finbak and O. Hassel, Archiv. f. Mat. o. Naturvid. **B45**, No. 3 (1941). (c) H. Viervoll, Acta Chem. Scand. **1**, 120 (1947). (d) O. Hassel and H. Viervoll, Acta Chem. Scand. **1**, 149 (1947).

[3] (a) C. Finbak, Avhandl. Norske Vid.-Akad. Oslo, Mat.-Naturv. Kl., No. 13 (1937). (b) P. P. Debye, Physik. Zeits. **40**, 66, 404 (1939).

equal to the total number of atoms in the molecule. The coefficients c_{ij} are characteristic of the ith and jth atoms and in the subsequent analysis are assumed to be constant. In practice, this is a good approximation, except for very small scattering angles, if the molecular scattering is obtained by dividing the total scattering by the background scattering. If a molecule is absolutely rigid, then the interference function A_{ij} is equal to $\sin sr_{ij}/sr_{ij}$ where r_{ij} is the distance between the nuclei of the ith and jth atoms and $s=(4\pi \sin\theta/2)/\lambda$ where θ is the scattering angle and λ is the wave-length of the electron beam. Since there is some motion of the nuclei in all molecules, the interference function A_{ij} assumes the form

$$A_{ij}=\int_0^\infty P_{ij}(\rho)(\sin s\rho/s\rho)d\rho, \qquad (2)$$

where $P_{ij}(\rho)d\rho$ is the probability that the distance between the ith and jth atoms has a value between ρ and $\rho+d\rho$.

A Fourier transformation may be made on the molecular scattering function,

$$I_m(s)=\sum_{i=1}^{n}\sum_{j=1}^{n} c_{ij}\int_0^\infty P_{ij}(\rho)(\sin s\rho/s\rho)d\rho, \quad (i\neq j) \qquad (3)$$

by multiplying it by $s\sin sr$ and integrating with respect to s. The result of such a procedure is a function of the variable r which represents the radial distribution curve, $D(r)$;[4]

$$D(r)=\int_0^\infty sI_m(s)\sin sr\,ds \qquad (4)$$

$$=\sum_{i=1}^{n}\sum_{j=1}^{n} c_{ij}\int_0^\infty \sin sr\,ds\int_0^\infty \frac{P_{ij}(\rho)}{\rho}\sin s\rho\,d\rho \qquad (4a)$$

$$=\frac{\pi}{2}\sum_{i=1}^{n}\sum_{j=1}^{n} c_{ij}\frac{P_{ij}(r)}{r}. \qquad (4b)$$

The ordinates of the radial distribution curve essentially represent the probability of the occurrence of the internuclear distances, r, in the molecule. It has been found in our experiments that in the vicinity of an equilibrium distance, r_{ij}, which is not very close in value to other ones in the molecule, the function $D(r)$ can usually be represented by

$$D(r)=c_{ij}(\pi h_{ij})^{\frac{1}{2}}\exp[-h_{ij}(r-r_{ij})^2]/2r_{ij}, \qquad (5)$$

where $(2h_{ij})^{-\frac{1}{2}}$ is a measure of the average deviation from the equilibrium position and is equal to $(\bar{l}_{ij}^2)^{\frac{1}{2}}$ where l_{ij} is the displacement from equilibrium. The quantity r in the denominator in Eq. (4b) may be replaced by r_{ij} when h_{ij} is sufficiently large.

[4] The derivation follow the treatment by P. Debye, J. Chem. Phys. **9**, 55 (1941).

In order to evaluate the integral in Eq. (4), the molecular scattering data must be known to values of s equal to infinity. In practice, only a limited amount of data are available. Nevertheless, this limited data uniquely determines the structure of a molecule. The procedure used is to compute the following modified function,[5]

$$f(r)=\int_0^{s_{\max}} sI_m(s)\exp(-as^2)\sin sr\,ds, \qquad (6)$$

where $s_{\max}$ bounds the range of scattering data and a can be so chosen that the integrand of Eq. (6) makes no essential contribution beyond $s_{\max}$. The computed $f(r)$ curve, therefore, is the same as that which would have been obtained if $s_{\max}$ approached infinity. It is possible then to obtain the desired function, $D(r)$, from $f(r)$ by making use of the relationship[6]

$$f(r)=\frac{1}{2(\pi a)^{\frac{1}{2}}}\int_{-\infty}^{\infty} D(\rho)\exp[-(r-\rho)^2/4a]d\rho, \qquad (7)$$

where a is the same as that used in Eq. (6). The introduction of $D(r)$ as defined in Eq. (5) leads to an evaluation of the integral in Eq. (7), giving for $f(r)$ the expression

$$f(r)=c_{ij}(\pi h_{ij})^{\frac{1}{2}} \times\exp[-h_{ij}(r-r_{ij})^2/(4ah_{ij}+1)]/2r_{ij}(4ah_{ij}+1)^{\frac{1}{2}}. \qquad (8)$$

In practice, the bell-shaped peaks which result from the computation of Eq. (6) are curve fitted by the function, $B_{ij}\exp[-H_{ij}(r-r_{ij})^2]$, where $H_{ij}=h_{ij}/(4ah_{ij}+1)$ (see the exponent in Eq. (8)). Since a is the value used in computing Eq. (6), h_{ij} can be readily obtained. The values of h_{ij} so determined, as pointed out, are the measure of the magnitude of the vibrational motion between pairs of atoms in a molecule.

Equation (8) may be used to illustrate the unique determination of the function, $D(r)$, from a limited amount of data. By this we mean in a mathematical sense that the data may be extended uniquely beyond its experimentally determined range. There is, of course, always some uncertainty in experimental data. In a practical sense, then, it is possible to extend a function on the basis of a uniqueness property in a definite fashion beyond its known experimental range, but the uncertainties in the experiment will introduce some uncertainty into the extension. There is a unique relation between the function in Eq. (8) whose parameters may be determined from experiment and the desired function in Eq. (5). If h_{ij} and r_{ij} are evaluated by applying Eq. (8) to a computed curve, then $D(r)$ is a known numerical function of r. From one rather re-

[5] The damping factor $\exp(-as^2)$ was introduced by Degard in order to improve radial distribution calculations. See C. Degard, Bull. Soc. Roy. Sci. Liege **12**, 383 (1937). The effect of this and other damping factors on radial distribution curves has been studied by J. Waser, Thesis, California Institute of Technology.

[6] E. C. Titchmarsh, *Introduction to the Theory of the Fourier Integral* (Clarendon Press, Oxford, 1937), p. 51.

FIG. 1. Typical microphotometer traces of a light and medium exposure of CCl_4. The vertical scales are not the same.

stricted, but simple, point of view, this uniqueness can be based upon the theoretical result[7] that the computed radial distribution curve can be represented by the sum of Gaussian distributions. From another point of view, the study of the mathematics of positive Fourier integrals shows that the scattering function, $I(s)$, known only in a restricted range of angle is related within narrow bounds to only one positive distribution function. This idea has been used in our laboratory to improve the accuracy of determining electron distributions[8(a)] about atoms. The restrictiveness of positive functions has also been found useful for small angle scattering and in the evaluation of the phases of the Fourier coefficients in the determination of crystal structure.[8(b)]

In the case of gas molecules, though, it is not necessary to resort to powerful mathematical arguments to obtain accurate information from a restricted amount of data. If the experimental curve, $f(r)$, is merely fit well by a function in the vicinity of r_{ij} (though the function may even become negative at some larger distance), a good evaluation of the desired $D(r)$ in the vicinity of r_{ij} can be obtained. This may be seen from Eq. (7) which shows that for values of a usually used (0.005–0.010), the exponential function is practically a delta-function so that $f(r)$ is merely a smeared or broadened version of $D(r)$. The main contribution of the integrand of Eq. (7) is in the vicinity of $\rho=r$.

The radial distribution curve yields three kinds of information; the equilibrium interatomic distances, an evaluation of the vibrational motion between pairs of atoms, and the coefficients for the molecular scattering expression which are related to the areas under the peaks. The structures of many molecules can be completely determined from radial distribution calculations alone. If several interatomic distances in a molecule fall close together, however, the information obtainable from a radial distribution curve is restricted and should be supplemented by additional data which can be obtained from computed intensity curves. The formula to be used is

$$I_m(s)=\sum_{i=1}^{n}\sum_{j=1}^{n} c_{ij}\exp(-s^2/4h_{ij})\,\sin sr_{ij}/sr_{ij} \quad (i\neq j), \quad (9)$$

where the values of c_{ij}, h_{ij}, and r_{ij} for various models are chosen to be consistent with the data available from the radial distribution curve. Equation (9) has been obtained by James[7] by integrating Eq. (3), using a probability distribution function which is derived on the basis of Hooke's law forces.

PROCEDURE

The diffraction photographs were taken with an electron diffraction camera which has been constructed recently in our laboratory. The accelerating voltage usually used is about 40,000 volts and is regulated to about one volt in 10,000. The voltage can be read continuously on a Type K potentiometer. The voltage obtained from the measurement of diffraction rings on a gold photograph agrees to within 0.1 percent with that read on the potentiometer. The electron beam is focused by a focusing grid and two magnetic lenses. The beam passes through a defining aperture of 0.1 mm diameter and is essentially parallel between the aperture and the photographic plate.

A rotating sector is incorporated in the specimen chamber. The sector is attached to a ball-bearing race six inches in diameter which is rotated by a synchronous motor using a friction drive. The motor is in the specimen chamber and its operation does not affect the vacuum nor the electron beam. When the sector reaches a speed of 1300–1400 r.p.m., the motor is turned off and pulled away from the race. The speed decreases to about 800 r.p.m. in five seconds during which time an exposure is made. An s^2 sector which is cut to operate between s values of one and 35 has been used so far. The portion between s values of zero to one acts as a beam stop. In order to facilitate the centering of the sector with respect to the electron beam, a speck of fluorescent material is placed in a 0.1-mm diameter

[7] R. W. James, Physik. Zeits. **33**, 737 (1932).
[8] (a) H. Hauptman and J. Karle, submitted to Phys. Rev. (b) J. Karle and H. Hauptman, submitted to Acta Cryst.

hole bored in the center of the sector. Photographs of the beam using this arrangement show that there is no correction for fogging required for the exposure times ordinarily used.

The diffraction patterns obtained on contrast lantern slides are traced on a Leeds and Northrup microphotometer. During the tracing they are rotated rapidly[9] in order to average out any irregularities caused by graininess. Care is taken to set the zero of the microphotometer on an unexposed portion of the plate. Traces obtained by this procedure are shown in Fig. 1. The microphotometer readings are calibrated to read electron intensities by taking several series of transmission photographs of evaporated gold on Formvar for various exposure times. The results of such a procedure are easily interpreted since the reciprocity law holds for fast elections,[10] that is, the exposure is equal to the product of the intensity and the time. The gold photographs are taken using the rotating sector and are rotated during the tracing in order to duplicate as closely as possible the procedure used with the gas photographs. A typical calibration curve is illustrated in Fig. 2.

The microphotometer readings are converted to intensity readings which are plotted against the variable s and a smooth background is drawn through the oscillations.[11] It usually is easier to draw the background line beyond s values of 5 or 6 if the experimental intensity curve is multiplied by s or s^2 to accentuate the oscillations about the background. In this respect

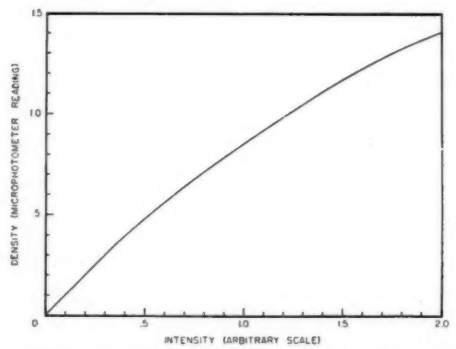

FIG. 2. Typical calibration curve for converting microphotometer readings to electron intensities.

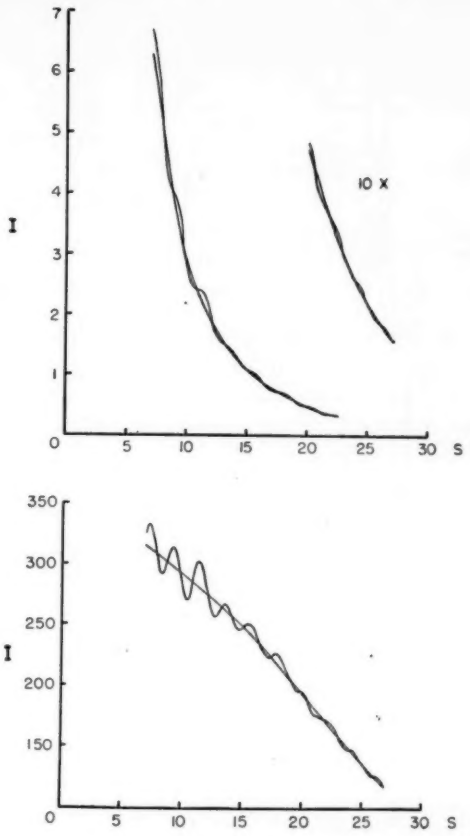

FIG. 3. The upper curve represents the intensity obtained from a fairly dark photograph of CCl_4 taken with an s^2 sector. The lower curve represents the intensity from the upper curve multiplied by s^2. Background curves are drawn through the oscillations.

our experiments would probably have been aided by the use of a sector cut to a power of s higher than 2. Figure 3 illustrates how the background line was drawn for an intensity curve from a photograph of CCl_4 whose useful density range covers values from seven to 27. The molecular scattering is obtained by dividing the experimental intensity by the background curve. This procedure not only eliminates the background scattering but replaces by constants, except at low s values, the variable coefficients in the molecular scattering expression. It is possible to measure the intensity of molecular scattering to much higher accuracy than may be implied by the inaccuracies in determining the absolute intensity. The inaccuracy in absolute measurement may be greater than the magnitude of an oscillation at the larger scattering angles. However, molecular intensity measurements concern the magnitude of an oscillation relative to a background line. The accuracy is therefore determined by the amplitude of an oscillation rather than by the measurement of total photographic intensity. Five photographs ranging from light to heavy exposures were used to obtain the molecular scattering curves. The uppermost curves in Figs. 4 and 5 are the experimental molecular scattering curves for CCl_4 and CO_2. The upper curve in Fig. 5 shows the

[9] Karle, Hoober, and Karle, J. Chem. Phys. **15**, 765 (1947).

[10] (a) A. Becker and E. Kipphan, Ann. d. Physik (5) **10**, 15 (1931). (b) W. Bothe, Zeits. f. Physik **8**, 243 (1922).

[11] Uncertainties in the position of the background line affect mainly the shapes but not the positions of the maxima in the radial distribution curve. Hence, fairly reliable equilibrium distances in a molecule can be obtained from the first computation of a radial distribution curve and an intensity curve based on these distances may be computed. The background line may then be corrected if necessary to correspond to the position of the zero axis in the intensity curve provided that no sudden changes occur in curvature of this line. This procedure may be repeated until it is evident that no additional improvement is possible. The improvement in the position of the background line should ordinarily be accompanied by a decrease in the magnitude of the negative portions of the radial distribution curve. Ideally, the radial distribution curve should be positive.

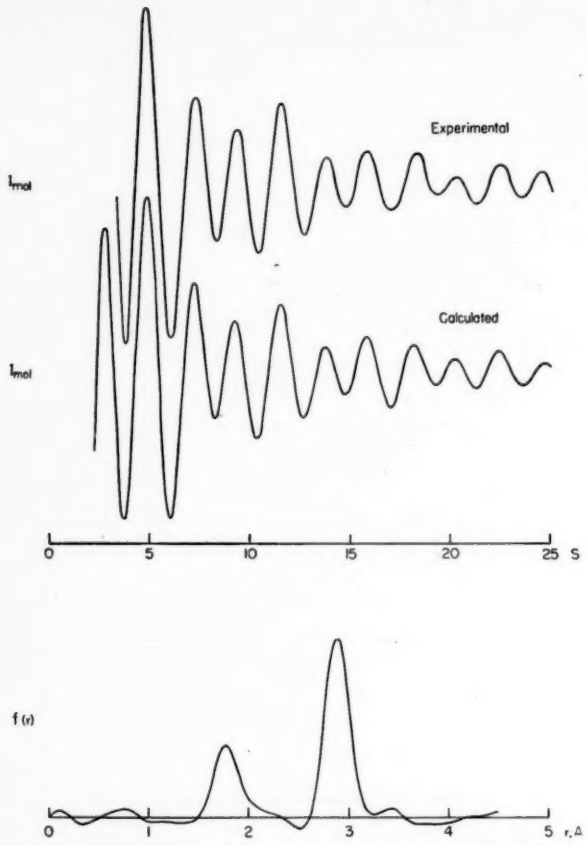

FIG. 4. The three curves represent the experimental molecular scattering, the calculated molecular scattering, and the radial distribution for CCl_4. The vertical scales for the molecular scattering curves are the same.

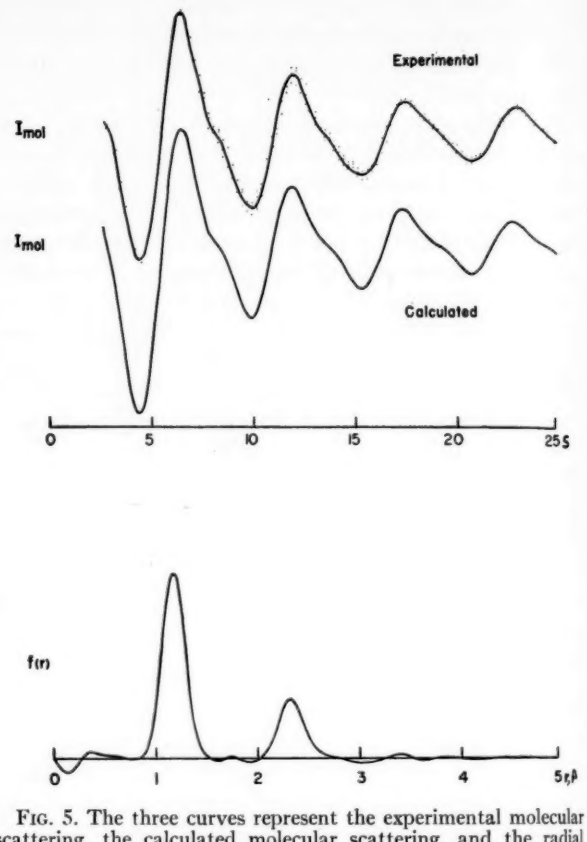

FIG. 5. The three curves represent the experimental molecular scattering, the calculated molecular scattering, and the radial distribution for CO_2. The dots in the upper curve are the experimental points obtained in five independent experiments. Many of the points lie on the curve itself. The vertical scales for the molecular scattering curves are the same.

spread of experimental points for CO_2. The magnitudes of the maxima and minima in this experimental curve are known to within five percent. The characteristic asymmetry in the maxima and minima is well defined.

A radial distribution curve is calculated using the experimental data. The integral in Eq. (6) is replaced by a summation where the s interval is 0.2. For the CCl_4 and CO_2 computations, maximum s was 25 and a was chosen to be 0.0057. The calculations were performed with the aid of punched cards and I.B.M. machines.[12] In the experimental intensity curve there is no useful data below s values of two and the region below s values of three or four does not represent a molecular scattering curve with constant coefficients. Hence, the region between s values of zero to three or four is replaced by an intensity curve computed with constant coefficients from an assumed model. If this model is inconsistent with the results of the radial distribution calculation, the calculated portion of the intensity curve is adjusted and a new radial distribution curve is computed. With this method of successive approximations, relatively few calculations need be made. The radial distribution curve should consist of a series of positive peaks, since the scattering from the electronic shells of the atoms has been eliminated. The radial distribution curves for CCl_4 and CO_2 are illustrated in Figs. 4 and 5.*

Each peak of the radial distribution curve is fitted with the function $B_{ij}\exp[-h_{ij}(r-r_{ij})^2/(4ah_{ij}+1)]$, Eq. (8), to obtain h_{ij} and r_{ij} values. Only the upper two-thirds of a peak is used in order to minimize the effect from small oscillations in the base line. Relative values of the coefficients c_{ij} which are used in the calculated intensity curves can be obtained in two ways; (a) each c_{ij} value is proportional to the area under its corresponding peak multiplied by the equilibrium distance associated with that peak, or (b) the maximum value of the peak, B_{ij}, is proportional to $c_{ij}(h_{ij})^{\frac{1}{2}}/r_{ij}(4ah_{ij}+1)^{\frac{1}{2}}$. Using the experimental h_{ij}, r_{ij}, and c_{ij} values, theoretical intensity curves were computed for CCl_4 and CO_2

[12] Shaffer, Schomaker, and Pauling, J. Chem. Phys. **14**, 659 (1946).

* *Note added in proof.*—Recent investigations in our laboratory on more complicated molecules have demonstrated that extraneous oscillations such as those which appear in the f(r) curves of Figs. 4 and 5 can be considerably reduced by readjusting the background line in the total intensity curves. It has also been found that a peak in the radial distribution curve formed from several interatomic distances may be decomposed into its components which yield directly the detailed structure of the molecule. Computed molecular intensity curves are used mainly to establish the range of uncertainty.

using Eq. (9). As expected, these were found to agree very well with the experimental curves (Figs. 4 and 5). In this instance, the calculated intensity curves merely illustrate the consistency of the procedure. On the other hand, when there are structural features that are not resolved in the radial distribution curve, more emphasis will have to be placed on theoretical intensity curves.

RESULTS

The experimental results are listed in Table I. For CO_2, the C−O distance compares favorably with the spectroscopic result of 1.163A for the equilibrium value. The experimentally determined values for the O−O distance is not exactly double the value for the C−O distance. This deviation, however, falls within the experimental uncertainty. The average amplitude of the vibrations of the C−O bond was calculated from spectroscopic data using the expression[4]

$$l^2=1/2h=(\mu_1+\mu_2)/2\alpha, \tag{10}$$

where α is the force constant between the C and O atoms and μ is the average energy of an oscillator given by Planck's expression, $\mu=h\nu/2+h\nu/(\exp(h\nu/\beta T)-1)$. The expression for the O−O distance is

$$l^2=\mu_1/\alpha. \tag{11}$$

The numerical values used were $\alpha=15.5\times10^5$ dynes cm^{-1}, $\nu_1=4.0\times10^{13}$ sec.$^{-1}$, and $\nu_2=7.0\times10^{13}$ sec.$^{-1}$.[13] The electron diffraction value for $(\bar{l}^2)^{\frac{1}{2}}$ for the C−O distance agrees well with the spectroscopic value. The difference between the electron diffraction and the spectroscopic values of $(\bar{l}^2)^{\frac{1}{2}}$ for the O−O distance may be attributed mainly to the fact that the O−O peak in the radial distribution curve is small which makes the determination less accurate. In addition, it should be noted that the spectroscopic value is computed from a simplified theory (Eq. (11)).

There are no spectroscopic values for the interatomic distances in CCl_4 available for comparison. Our values may be compared with other electron diffraction determinations. Finbak and Hassel[2(b)] obtained 1.770A and 2.876A for the C−Cl and Cl−Cl distances using their sector method. Pauling and Brockway[14] obtained 1.76A and 2.87A for the C−Cl and Cl−Cl distances using the visual method. The spectroscopic values for the vibrational motion between the C−Cl and Cl−Cl pairs listed in Table I have been computed by James[7] using the central force model. Rosenthal[15] has shown that CH_4 is the only tetrahedral molecule to which the central force model is applicable. By applying a general force field to tetrahedral molecules, Rosenthal[16] obtained a value of 3.6×10^5 dynes cm^{-1} for the C−Cl force constant in CCl_4. This is larger than the value 2.0×10^5 dynes cm^{-1} used by James and implies that the amplitude for the vibrational motion obtained by James is too large. Better agreement between the electron diffraction and spectroscopic evaluations of the vibrational motion can be expected therefore from a recalculation of the spectroscopic values based on the more general force model for CCl_4.

TABLE I.

	r_{ij}(A)	$(\bar{l}_{ij}^2)^{\frac{1}{2}}_{\text{elec. diff.}}$	$(\bar{l}_{ij}^2)^{\frac{1}{2}}_{\text{spect.}}$
	CCl_4		
C−Cl	1.770±0.010	0.041±0.005	0.055
Cl−Cl	2.877±0.020	0.054±0.005	0.071
	CO_2		
C−O	1.162±0.010	0.034±0.003	0.034
O−O	2.310±0.020	0.040±0.007	0.029

It should be mentioned that even very small vibrations like those found in CCl_4 and CO_2 damp the intensity of molecular scattering considerably. For CCl_4 the intensity at s equal to 25 is 60 percent less than it would be for a rigid structure while for CO_2 the intensity is 35 percent less.

The c_{ij} values were obtained from the radial distribution peaks using the methods given above. For CO_2 the value found for the ratio c_{C-O}/c_{O-O} is 1.50±0.02. This value may be compared to the ratio $2Z_CZ_O/Z_OZ_O$ which also is equal to 1.50. Z_C and Z_O are the atomic numbers of carbon and oxygen. For CCl_4 the experimental values of the ratio c_{Cl-Cl}/c_{C-Cl} is 4.22±0.04 whereas the ratio $3Z_{Cl}Z_{Cl}/2Z_CZ_{Cl}$ equals 4.25. These figures indicate that the scattering factors of the atoms involved have about the same shape and that their variability with respect to the angle variable s can be eliminated by dividing the total scattering by the background scattering.

An approximation was made in Eq. (5) by replacing the variable r in the denominator by the equilibrium distance r_{ij}. The effect of this approximation on the determination of the equilibrium distances is very small. The correction is equal to $1/2h_{ij}r_{ij}$ and amounts to not more than 0.001A for the CO_2 and CCl_4 molecules. There is a negligible effect on the shape of the peak.

DISCUSSION

The results on CCl_4 and CO_2 indicate that accurate intensity data can be obtained from electron diffraction investigations of gases. This is borne out by the results in Table I and also by the fact that the radial distribution curves are essentially positive. Relatively little error in the experimental intensity can yield large negative fluctuations in the radial distribution curves. By the procedure described above the magnitude and shape of the various features of the diffraction pattern can be reliably determined, thus minimizing considerably the uncertainties which are bound to arise in the visual examination of the diffraction photographs. The

[13] G. Herzberg, *Infra-Red and Raman Spectra of Polyatomic Molecules* (D. Van Nostrand Company, Inc., New York, 1945), p. 173.
[14] L. Pauling and L. O. Brockway, J. Chem. Phys. **2**, 867 (1934).
[15] J. Rosenthal, Phys. Rev. **46**, 730 (1934).
[16] J. Rosenthal, Phys. Rev. **49**, 535 (1936).

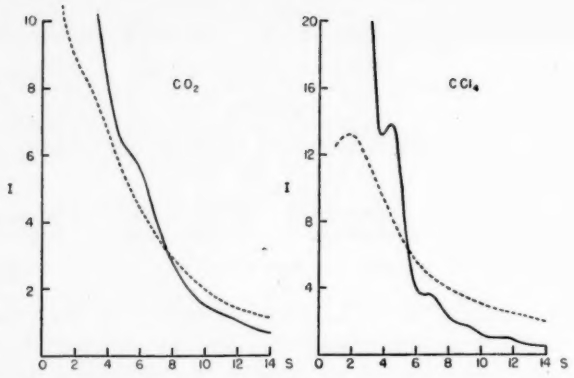

FIG. 6. The solid lines are the experimental scattering curves obtained with an s^2 sector for CCl_4 and CO_2. The dotted lines represent the background scattering calculated from tabulated values and multiplied by s^2.

visual method can be used with confidence to determine the equilibrium distances in a molecule if the diffraction pattern consists of well-defined maxima and minima and if the determination can be based mainly on the positions of these maxima and minima. When the determination of a molecular structure depends upon the relative intensities of the maxima and minima or upon special features such as shelves or asymmetries, the results from the visual method may be considerably less reliable.

There is sufficient difference between the procedure developed by the Norwegian school and the one presented here to merit some comment. In their analysis of the diffraction data, the molecular scattering curve is obtained using the expression[2(c)]

$$I_m(s)=K\left[\frac{P_t(s)}{P_a(s)}-1\right]\left[\frac{\sum_i(Z_i-F_i)^2+\sum_i S_i}{s^4}\right], \quad (12)$$

where $P_t(s)$ is the density reading on a microphotometer trace of a diffraction photograph, $P_a(s)$ is the background curve drawn on this trace to represent the atomic scattering, and $[\sum_i(Z_i-F_i)^2+\sum_i S_i]/s^4$ is the coherent plus incoherent atomic scattering where Z_i is the atomic number, F_i is the atomic scattering factor for x-rays, and S_i is the incoherent scattering function tabulated by Bewilogua.[17] Our procedure differs in that the molecular scattering function with constant coefficients is obtained from the expression

$$I_m(s)=K\left[\frac{I_t(s)}{I_a(s)}-1\right], \quad (13)$$

where the photographic density readings have been converted to intensity readings. In addition, we do not reintroduce the variable scattering factors once they have been eliminated by dividing by the background. The disadvantage of using Eq. (12) for the molecular scattering function is that a proper Fourier inversion cannot be made on an intensity function whose coefficients (corresponding to the c_{ij} in Eq. (4a)) are functions of s. The use of Eq. (12) in a Fourier transform affects the accuracy of determining the equilibrium distances in a molecule very little. However, it is not possible to use such a curve for the evaluation of the vibrational motion in a molecule.

The background scattering merits some discussion. It has always been considered that the background scattering in electron diffraction patterns of gases can be represented by

$$I_a(s)=(K/s^4)[\sum_i(Z_i-F_i)^2+\sum_i S_i]. \quad (14)$$

The results of our experiments are shown in Fig. 6 where the dotted lines represent Eq. (14) calculated from tabulated values and multiplied by s^2, and the solid line is the experimental scattering obtained with an s^2 sector for CCl_4 and CO_2. Theoretically, the solid line should oscillate about the dotted line. The same type of discrepancy is apparent from the examination of published microphotometer traces by the Norwegian school[2] and by Yearian and Barss.[18] Experiments on the scattering from free atoms have been performed and are being continued to establish with certainty that the shape of the background is not a result of some error in the technique of performing the diffraction experiment. The consistency obtained in our experiments to date indicates that the theory of the background scattering may be incorrect. It is obvious, however, from the procedure described in this paper that it is not necessary to have a theoretical expression for the background scattering for the determination of molecular structures.

We wish to thank Professor V. Schomaker of the California Institute of Technology for making available to us a set of punched cards developed in his laboratory for performing electron diffraction computations. We also wish to thank the Naval Ordnance Laboratory for making available their mechanized analysis facilities and the Washington Office of the International Business Machine Corporation for their fine cooperation.

[17] L. Bewilogua, Physik. Zeits. **32**, 740 (1931).

[18] H. J. Yearian and W. M. Barss, J. App. Phys. **19**, 700 (1948).

The Energy of Dissociation $H_2O \rightarrow H+OH$

O. OLDENBERG
Lyman Laboratory of Physics, Harvard University, Cambridge, Massachusetts
(Received January 31, 1949)

The various lines of evidence regarding the energy of dissociation $H_2O \rightarrow H+OH$ are critically discussed. This gives a basis for discussing the energy of activation of the process $OH+OH \rightarrow H_2+O_2$.

I. SURVEY OF MEASUREMENTS

RECENT measurements of the energy of dissociation of the H_2O molecule into H and OH have led to discrepancies. In the present paper we shall examine the various lines of evidence. The dissociation process mentioned was first discussed and its energy measured by Bonhoeffer and Reichardt.[1] They traced the thermal dissociation of water vapor mixed with oxygen at atmospheric pressure and temperatures between 1240 and 1600°C by observing the intensity of the absorption spectrum of free hydroxyl radicals. Later Dwyer and Oldenberg[2] made the test for free hydroxyl more sensitive by observing its absorption spectrum with higher resolving power which permits the observation of the individual rotational lines of the OH radical.

The results for the two energies involved (at 0°K) are as follows: $H+OH=H_2O-118.2\pm0.7$ kcal./mole and $0+H=OH-100.1\pm0.9$ kcal./mole.

An entirely different method was employed by Riechemeier, Senftleben, and Pastorff[3] who dissociated H_2O molecules photo-chemically into H+OH by the energy transferred in impacts of the second kind from excited Hg atoms. Their energy of excitation (4.88 ev) is not quite sufficient for the dissociation process so that a small amount of thermal energy is needed to supply the deficiency. Hence, the transfer becomes increasingly probable with increasing temperature. The authors measured the rate of the photo-chemical decomposition of H_2O as a function of the temperature and thus deduced the energy of dissociation of the H_2O molecule as 117.0 ± 0.9 kcal./mole.

Their method was further examined by Oldenberg[4] who pointed out that it is based upon the tacit assumption that all impacts of the second kind occurring with an energy above the critical value have the same probability of dissociating the H_2O molecule. As a matter of fact, however, an increase of this probability with increasing energy of the collision seems plausible. Therefore, in this method the comparatively rare dissociation processes occurring with barely sufficient energy are not given the proper weight. Hence, the accurate value of the energy to be measured may be lower than this method indicates.

The energy required to dissociate H_2O into H+H+O (218.3 ± 0.2 kcal./mole) is reliably known thermochemically. It may be thought of as supplied in two steps, first producing H+OH and next dissociating OH. Hence, a lower energy value of one of the two steps necessitates the assumption of a higher value for the other step. Thus, Senftleben's measurement leads to the conclusion that the energy of dissociation of OH is 101.3 kcal./mole or higher.

Lewis and von Elbe[5] measured the energy of dissociation of $H_2O \rightarrow H+OH$ by the explosion method and obtained a value of 114 ± 1. The corresponding value for the energy of dissociation of OH is 104 kcal./mole.

We shall not discuss the conclusions drawn from the absorption spectrum of H_2O_2[6] since the recent accurate measurements by Holt[7] failed to confirm the observation on which they are based.

The argument of Rodebush, Keizer, McKee, and Quagliano[8] is more indirect. They analyze the products of the electric discharge through water vapor by condensing the gases flowing out in traps which are cooled by dry ice or liquid air and placed in various distances from the discharge. Among their many interesting results we are concerned with the following observation. When a long glass tube (length 100 cm, diameter 2.5 cm) is inserted between the discharge tube and the trap, and the latter is cooled with liquid air, no H_2O_2 is condensed and practically no H_2O. Hence the discharge practically completely dissociates the water vapor, otherwise the residual H_2O would show up in the trap. Furthermore, the products of the dissociation, when recombining while flowing through the long tube, are non-condensible molecules, that is, H_2 and O_2, instead of the most stable molecule, H_2O, which would be the most plausible product. In other experiments it is ascertained that the recombination of H atoms and OH radicals when occurring in a trap next to the electric discharge produces H_2O_2 and H_2O; hence, in the experiment with the long tube, the absence of these molecules in the trap proves that the atoms and radicals recombine to form H_2 and O_2 while they are flowing through this tube.

The authors interpret the recombination process as follows. They accept the hypothesis first offered by

[1] K. F. Bonhoeffer and H. Reichardt, Zeits. f. physik. Chemie, A139, 75 (1928).
[2] R. J. Dwyer and O. Oldenberg, J. Chem. Phys. **12**, 351 (1943).
[3] Riechemeier, Senftleben, and Pastorff, Ann. d. Physik **19**, 202 (1934).
[4] O. Oldenberg, J. Chem. Phys. **13**, 196 (1945).
[5] B. Lewis and J. von Elbe, J. Chem. Phys. **3**, 63 (1935).
[6] R. S. Sharma, Proc. Ind. Acad. Sci. **4**, 51 (1934).
[7] Holt, McLane, and Oldenberg, J. Chem. Phys. **16**, 225 (1948).
[8] Rodebush, Keizer, McKee, and Quagliano, J. Am. Chem. Soc. **69**, 538 (1947).

Bonhoeffer and Pearson[9] that the electric discharge dissociates H_2O molecules preferentially into H+OH. The authors assume that, although *this dissociation* is nearly complete, the discharge does not further dissociate OH radicals. They assume that H_2 is formed by the recombination of H atoms in the long tube and, finally, come to the inescapable conclusion that the free hydroxyl radicals disappear in the gas phase by the reaction: $OH+OH \rightarrow H_2+O_2$. They assume that this process occurs rapidly during the very short time of travel through the one-meter tube inserted between the discharge and the trap. The authors mention as a difficulty that this reaction is retarded by an energy of activation. In order to attribute to the process just mentioned a sufficient probability they must assume that the energy of dissociation of OH is considerably smaller than the value given in the literature.

II. THE ENERGY OF ACTIVATION OF $OH+OH \rightarrow H_2+O_2$

We are concerned with this energy of activation which, apart from the present argument, has a considerable interest in its own right. Bonhoeffer and Haber[10] argued that this energy is closely connected with the energy of activation which prevents the reaction of hydrogen and oxygen from occurring at and near room temperature. Figure 1 represents the energy levels involved as derived from thermochemical and spectroscopic data.[2] The level OH+OH lies above the level H_2+O_2 by 20 kcal. per mole. The barrier indicated by the broken line which retards the reaction $OH+OH \rightarrow H_2+O_2$ is by this amount lower than the barrier which retards the opposite reaction.

The height of the barrier as it appears from the side H_2+O_2 can be inferred from measurements of the thermal hydrogen-oxygen reaction starting in the volume. For our present problem we want to find the *lowest possible* value of the activation energy of this reaction. This has been reported as 70 kcal. per mole;[11] it applies to the temperature range 490–550°C. At a lower temperature the volume reaction is practically absent, indicating that no volume reaction exists with a still lower activation energy.

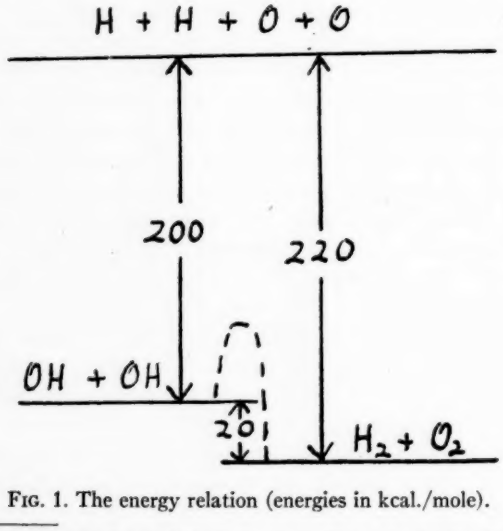

FIG. 1. The energy relation (energies in kcal./mole).

It cannot be claimed, however, that the energy of activation, which is observed for the *over-all reaction* as 70 kcal./mole (or higher) is exclusively due to the *initiating step*. Any link of the chain contributes to the over-all value if it is in competition with another link. Without discussing in detail the chain which was discovered by Lewis and von Elbe[12] and without judging the relative importance of the various steps in the different temperature ranges, we restrict ourselves to the estimate that the step $H+O_2 \rightarrow OH+O$ is conspicuous among the links of the chain by its high activation energy of 17 kcal. per mole. The authors state that this figure is comparatively accurately known (reference 12, p. 382). If we accept the approximation that the activation energy of this step is simply additive to that of the initiation, only 53 kcal./mole are left for the initiating reaction. Considering the possible errors, it is a conservative estimate that no initiating reaction exists with an activation energy of less than 45 kcal./mole. Hence the reaction $H_2+O_2 \rightarrow OH+OH$ cannot have a smaller activation energy. This leads to 25 kcal. per mole or more for the activation energy of the opposite reaction, $OH+OH \rightarrow H_2+O_2$ (see Fig. 1). Semenoff[13] estimates this energy to 45 kcal./mole. A still more prohibitive estimate is based on the rule of Eyring[14] which gives the activation energy as about 28 percent of the two bonds broken when the reaction proceeds in the exothermic direction, that is, in our case, as high as 56 kcal. per mole. Our optimistic estimate of the limiting value of 25 kcal. per mole is still so high that, at room temperature, only one in 10^{19} collisions would be sufficiently energetic. Hence the process suggested cannot be responsible for the complete disappearance of OH during the short time of flow through the long tube

Here it is not claimed that the numerical value of the energy of dissociation found by Dwyer and Oldenberg is absolutely certain. Although no objection is known to their method, the procedure is so highly complicated that a repetition of their measurements seems warranted, as soon as gratings of higher resolving power permit a better measurement of the contours of narrow absorption lines. But the independent method of Senftleben and collaborators, which is based on the near coincidence of the excitation energy of mercury and the dissociation energy of water, seems to exclude a lower

[9] K. F. Bonhoeffer and T. G. Pearson, Zeits. f. physik. Chemie **B14**, 1 (1931).
[10] K. F. Bonhoeffer and F. Haber, Zeits. f. physik. Chemie **A137**, 263 (1938).
[11] O. Oldenberg and A. S. Sommers, Jr., J. Chem. Phys. **9**, 432 (1941).
[12] B. Lewis and B. von Elbe, *Combustion, Flames and Explosions of Gases* (Cambridge University Press, London, 1938), and J. Chem. Phys. **10**, 366 (1942).
[13] N. Semenoff, Acta Physicochimica U.R.S.S. **20**, 291 (1945).
[14] H. Eyring, Sci. Mo. **67**, 183 (1948).

energy of dissociation of OH which would give a lower activation energy. Furthermore, Lewis and von Elbe obtained a higher, not a lower, energy of dissociation. Hence, it does not seem possible to manipulate the figures and so change the conclusion materially.

III. PROCESSES IN THE ELECTRIC DISCHARGE

The hypothesis offered by Rodebush, Keizer, McKee, and Quagliano, assuming a rapid bimolecular reaction $OH+OH \rightarrow H_2+O_2$, leads to another difficulty. It appears to be inconsistent to combine the following two assumptions: firstly, the discharge supplies only H and OH to the tube in which the reaction occurs; secondly, the O_2 is produced by the reaction $OH+OH \rightarrow H_2+O_2$. If this reaction really goes to completion within the tube connecting the discharge and the trap (length 1 m, i.d., 2.5 cm), it must very frequently occur also in the discharge tube itself (length 2 m, i.d., 1 cm). Thus *in the discharge itself* H_2 and O_2 should be formed. It happens that both these molecules are readily dissociated by an electric current, as is evident from the fact that the electric discharge through hydrogen or oxygen is a good source of the respective atoms. In the low current electric discharge through oxygen Wrede[15] found an even higher concentration of atoms than in the discharge through hydrogen. This is well explained by the Franck-Condon rule and the potential curves of the various energy levels of the O_2 molecule which, even in a low energy level, favor dissociation.[16] Hence, even if OH should not be sensitive to direct dissociation by the current, the process postulated by the authors would inevitably produce O atoms in the discharge.[17]

The observed formation of H_2 and O_2 occurring in the long tube between the discharge and the trap may be tentatively explained as follows: Since the water molecules are certainly nearly completely dissociated, we may expect an ample dissociation of the OH radicals, too. The H and O atoms should first form diatomic molecules, H_2, O_2, and OH, either at the wall or, by triple collisions, in the volume. Once we accept triple collisions we may guess that the OH radicals may form H_2O by further triple collisions with H and any third body.[18] However, since hardly any H_2O is observed in the trap, we must explain why the assumption of triple collisions for the formation of the diatomic molecules does not imply that triple collisions are probable as well for the process $H+OH+M \rightarrow H_2O+M$; the latter process should have a much smaller steric factor, since, presumably, most approaches of H+OH lead to a configuration not resembling an H_2O molecule. It is a general rule that reactions, in particular triple collisions, between more complex molecules are handicapped by the requirement of special orientations.[19] Hence the recombination of *two atoms* may be more susceptible to triple collisions than the recombination of *an atom and a radical*. The fate of OH radicals (formed from atoms or directly produced by the dissociation of H_2O) remains to be discussed. Possibly, OH radicals react with O atoms: $O+OH \rightarrow O_2+H$. Another possibility is that they react at the walls. In particular, the reaction $OH+OH \rightarrow H_2+O_2$ *as occurring at the walls* is not excluded by the argument given above. One may question, however, whether in the short time of transit the diffusion to the wall is sufficiently probable. An estimate may be made as follows: Suppose that water vapor is driven through the tube (i.d., 2.5 cm, length 1 m) by the pressure difference between the discharge tube (say 0.1 mm) and a good pump (zero pressure). From Poiseuille's law the time of transit is estimated to be as short as 1/40 sec. On the other hand, the random displacement by diffusion of any water molecule during this time interval is estimated to 4 cm. It may be questioned whether this displacement, taking place in any direction, warrants a strong catalytic activity of the walls. On the other hand, an effect of the walls on the reaction is proven in a similar experiment described by Badin.[20] He observed the processes occurring in a mixture of hydrogen atoms, hydrogen molecules, and oxygen molecules which were flowing through a glass tube under similar conditions as in the experiment under discussion. The pronounced effect of the surface conditions on the reaction observed by Badin proves that the reaction largely occurs on the walls.

The main conclusion is that the processes in the discharge do not force us to the assumption that the reaction $OH+OH \rightarrow H_2+O_2$ is very rapid in the gas phase. The present argument makes it appear unnecessary to assume different values for the energies of dissociation of H_2O and OH than those given by other methods.

---

[15] E. Wrede, Zeits. f. Physik **54**, 53 (1929).

[16] See G. Herzberg, *Molecular Spectra and Molecular Structure I.* (Prentice-Hall, Inc., New York, 1939), p. 474.

[17] Here is an apparent discrepancy in the experimental results. While the paper under discussion demonstrates the preferred formation of O_2 in the gases leaving the discharge, Rodebush and Wahl (J. Chem. Phys. **1**, 696 (1933)) found very little oxygen, either atomic or molecular, present in the discharge. Presumably this discrepancy is due to different types of discharge (d.c. and electrodeless) and different current densities.

[18] The effect of triple collisions as removing OH radicals from the gas has been found by A. A. Frost and O. Oldenberg (J. Chem. Phys. **4**, 781 (1936)) who added up to 7.2 mm helium to the gas.

[19] C. N. Hinshelwood, *The Kinetics of Chemical Change* (Oxford University Press, New York, 1940), p. 142.

[20] E. J. Badin, J. Am. Chem. Soc. **70**, 3651 (1948).

Thermodynamic Functions for Tritium Deuteride. The Dissociation of Tritium Deuteride. Equilibria among the Isotopic Hydrogen Molecules

W. M. JONES
Los Alamos Scientific Laboratory, University of California, Los Alamos, New Mexico
(Received February 14, 1949)

The heat capacity, entropy, internal energy, and free energy are calculated to 2500°K for tritium deuteride. The dissociation of tritium deuteride is considered. Equilibria of the isotopic hydrogens among themselves are calculated.

ACCURATE calculations of the thermodynamic properties of hydrogen have been carried out by Giauque[1] and similar calculations have been made for deuterium and deuterium hydride by Johnston and Long.[2] Recently similar calculations have been made for tritium and tritium hydride.[3] In the present report similar data are given for tritium deuteride. Values refer to one mole of the ideal gas at one atmosphere.

The energy of the tritium deuteride molecule is representable in the form

$$E_{J,\nu}=\omega_e(\nu+\tfrac{1}{2})-X_e\omega_e(\nu+\tfrac{1}{2})^2+[B_e-\alpha_e(\nu+\tfrac{1}{2})+\gamma_e(\nu+\tfrac{1}{2})^2+\delta_e(\nu+\tfrac{1}{2})^3]J(J+1)+[D_e+\beta_e(\nu+\tfrac{1}{2})]J^2(J+1)^2+F_eJ^3(J+1)^3. \quad (1)$$

The constants are listed in Table I. They were computed from the data for ordinary hydrogen, as given by Jeppesen,[4] who expresses the energy in a form slightly different from Eq. (1), through the theory of isotopic diatomic molecules.[5] The partition function and its derivatives were evaluated by direct summation over rotational and vibrational states.

It is felt that in general the calculations are correct to the number of significant figures given, except, perhaps, at the highest temperatures where the large values of ν and, particularly, of J needed for the convergence of the summations lie outside the range employed by Jeppesen in fitting the constants of Eq. (1).

The constants of Table I were calculated taking the atomic weights of deuterium and tritium to be 2.014722 and 3.017050 (physical scale).[6] The physical constants are otherwise those of the International Critical Tables[7] in order that the present calculations may best be utilized with the large body of similar calculations now existing.[8] The spin of the deuterium nucleus is unity and that of the tritium nucleus is one-half unit.[9]

TABLE I.*

Molecular constants for DT.	
ω_e	2853.8 cm^{-1}
$X_e\omega_e$	54.786
B_e	25.380
α_e	0.82641
γ_e	0.011908
$-\delta_e$	0.00073
$-D_e$	0.008093
β_e	0.1142×10^{-3}
F_e	0.37637×10^{-5}

* The similar Table I of reference 3 is incorrectly labeled. The column labeled T_2 should be labeled HT and vice versa. This error was pointed out by Dr. J. Bigeleisen.

Heat Capacity and Entropy

The heat capacity at constant pressure and the entropy for tritium deuteride are given in Table II. The entropy includes the nuclear spin contribution of $R\ln 6$. Figure 1 shows the internal portion of C_v/R at low temperatures for DT, HT, and HD.[2,3]

Internal Energy and Free Energy

The internal energy and the free energy, both given with respect to the state in which $\nu=J=0$, are presented

TABLE II. Heat capacity and entropy (including nuclear spin) of tritium deuteride in cal. deg.$^{-1}$ mole.$^{-1}$.

T, °K	C_p^0	S^0	T, °K	C_p^0	S^0
0	0.000	0.000	250	6.973	39.369
10	5.203	17.551	275	6.975	40.033
15	6.065	19.812	298.1	6.977	40.597
20	6.806	21.669	300	6.977	40.640
25	7.106	23.227	400	6.994	42.649
30	7.147	24.529	500	7.039	44.215
35	7.109	25.628	600	7.124	45.504
40	7.064	26.574	700	7.243	46.611
50	7.010	28.144	800	7.383	47.587
75	6.975	30.977	900	7.533	48.465
100	6.969	32.983	1000	7.682	49.268
125	6.968	34.538	1250	8.021	51.019
150	6.968	35.808	1500	8.296	52.507
175	6.969	36.883	2000	8.685	54.950
200	6.970	37.813	2500	8.943	56.917
225	6.972	38.634			

[1] W. F. Giauque, J. Am. Chem. Soc. **52**, 4826 (1930); see also C. O. Davis and H. L. Johnston, J. Am. Chem. Soc. **56**, 1045 (1934).
[2] H. L. Johnston and E. A. Long, J. Chem. Phys. **2**, 389, 710 (1934).
[3] W. M. Jones, J. Chem. Phys. **16**, 1077 (1948).
[4] C. R. Jeppesen, Phys. Rev. **44**, 165 (1933).
[5] W. Jevons, *Report on Band Spectra of Diatomic Molecules* (The University Press, Cambridge, 1932).
[6] J. Mattauch, Phys. Rev. **57**, 1155 (1940); S. M. Livingston and H. A. Bethe, Rev. Mod. Phys. **9**, 373 (1937).
[7] *International Critical Tables* (McGraw-Hill Book Company, Inc., New York, 1926).
[8] For the corrections to computed thermodynamic functions occasioned by changes in physical constants reference should be made to Wagman, Kilpatrick, Taylor, Pitzer, and Rossini, BS J. Research **34**, 143 (1945).
[9] Bloch, Packard, Graves, and Spence, Phys. Rev. **71**, 373(L), 551(L) (1947).

TABLE III. Internal energy and free energy.

T, °K	$E^0-E_0^0$ cal. mole^{-1}	$-(F^0-E_0^0)/T$ cal. deg.$^{-1}$ mole^{-1}	T, °K	$E^0-E_0^0$ cal. mole^{-1}	$-(F^0-E_0^0)/T$ cal. deg.$^{-1}$ mole^{-1}
10	0.334	12.550	250	475.03	32.502
15	3.54	14.609	275	525.20	33.156
20	11.06	16.149	298.1	571.61	33.712
25	21.16	17.414	300	575.42	33.755
30	32.02	18.494	400	777.10	35.739
35	42.84	19.437	500	981.72	37.284
40	53.43	20.271	600	1192.8	38.549
50	74.09	21.695	700	1414.2	39.624
75	124.59	24.349	800	1648.7	40.559
100	174.70	26.269	900	1897.7	41.390
125	224.72	27.773	1000	2161.8	42.139
150	274.73	29.009	1250	2884.	43.744
175	324.76	30.059	1500	3683.	45.084
200	374.82	30.971	2000	5452.	47.257
225	424.91	31.778	2500	7379.	48.998

in Table III. The internal energy does not include the translational contribution of $\frac{3}{2}RT$. The $-(F^0-E_0^0)/T$ tabulations include the nuclear spin contribution of $R\ln 6$. Less accurate calculations of the free energy function for all the molecular hydrogens have been given by Libby[10] at 25, 100, 200, 300, 400, and 500°C.

The values of S^0 in Table II and the values of $-(F^0-E_0^0)/T$ in Table III must each be decreased numerically by $R\ln 6=3.560$ when they are combined with similar data for other molecules which do not include the nuclear spin contribution. The neglect of spin is, however, a high temperature approximation, and it is not permissible in dealing with equilibria involving a molecular hydrogen below about 175°K.

THE DISSOCIATION OF TRITIUM DEUTERIDE

Values of $-(F^0-E_0^0)/T$ for DT, D, and T may be employed in the calculation of the dissociation constant K for the process DT=D+T through the relationship

$$-R\ln K=\Delta(F^0-E_0^0)/T+\Delta(E_0^0/T). \quad (2)$$

TABLE IV. Dissociation constants for dissociation of isotopic hydrogen molecules in atmospheres.

T, °K	1000	1500	2000	2500
H_2	6.45×10^{-18}	3.60×10^{-10}	2.96×10^{-6}	6.92×10^{-4}
HD	2.48	1.57	1.36	3.28
D_2	3.71	2.70	2.49	6.17
HT	2.26	1.49	1.32	3.21
DT	1.67	1.28	1.21	3.03
T_2	3.01	2.44	2.35	5.94

TABLE V. Percentage dissociation of isotopic hydrogen molecules at a total pressure of one atmosphere.

T, °K	1000	1500	2000	2500
H_2	12.7×10^{-8}	9.5×10^{-4}	8.6×10^{-2}	1.31
HD	7.9	6.3	5.8	0.91
D_2	9.6	8.2	7.8	1.24
HT	7.5	6.1	5.7	0.90
DT	6.5	5.7	5.5	0.87
T_2	8.7	7.8	7.7	1.22

[10] W. F. Libby, J. Chem. Phys. **11**, 101–9 (1943); **15**, 339 (1947).

The values of $-(F^0-E_0^0)/T$ for D and T were taken from references 2 and 3, respectively. The quantity ΔE_0^0 is greater than $D_0(H_2)$ by the difference in the zero point energies of H_2 and DT, and has the value 104,970 ±20 cal. This figure is based on the value 36,116±6 cm^{-1} for $D_0(H_2)$[11] and the I.C.T. physical constants. The equilibrium constants are presented in Table IV along with the constants[1–3] for the dissociation of the other isotopic hydrogens.

The percentage dissociation at a total pressure of one atmosphere may be calculated from the equilibrium constant and is given in Table V along with similar data for the other hydrogens.[1,2,3]

TABLE VI. Equilibrium constants for isotopic equilibria.

T, °K	K_1	K_2	K_3	K_4	K_5	K_6
2500	3.99	4.00	2.00	1.99	2.00	3.97
2000	3.98	4.00	2.00	1.99	2.00	3.97
1500	3.94	4.00	2.00	1.98	2.00	3.96
1250	3.90	4.00	1.99	1.96	2.01	3.94
1000	3.81	3.99	1.98	1.93	2.02	3.90
900	3.76	3.98	1.97	1.91	2.03	3.87
800	3.68	3.98	1.95	1.88	2.04	3.83
700	3.59	3.97	1.94	1.85	2.05	3.78
600	3.45	3.96	1.91	1.80	2.06	3.72
500	3.26	3.93	1.88	1.74	2.09	3.62
400	2.99	3.88	1.82	1.64	2.13	3.48
300	2.58	3.82	1.74	1.48	2.20	3.26
298.1	2.57	3.82	1.74	1.48	2.20	3.26
250	—	3.77	1.67	—	2.26	—
200	1.948	3.69	1.58	1.24	2.34	2.90
150	—	3.57	1.33	—	2.68	—
100	0.945*	3.32	1.18	0.802	2.82	2.26
50	0.242	2.60	0.687	0.353	3.78	1.33
25	—	1.95	0.282	—	6.94	—

* This value differs slightly from the value 0.947 given in reference 3.

EQUILIBRIA AMONG THE ISOTOPIC HYDROGENS

From the tabulations of $-(F^0-E_0^0)/T$ and the zero point energies of the molecules involved, equilibrium constants may be evaluated from a relationship of the form of Eq. (2) for the following equilibria:

$$H_2+T_2=2\,HT, \quad (1)$$

$$D_2+T_2=2\,DT, \quad (2)$$

$$T_2+HD=HT+DT, \quad (3)$$

$$H_2+DT=HD+HT, \quad (4)$$

$$D_2+HT=HD+DT, \quad (5)$$

$$H_2+D_2=2\,HD. \quad (6)$$

The free energy functions for T-containing molecules are from reference 3 and this paper, those of D_2 and HD from reference 2, while those for H_2 at and above room temperature are from reference 1. For values of the free-energy function for H_2 below room temperature the data used is that of Urey and Rittenberg[12] corrected to

[11] Beutler, Zeits. f. Physik. Chemie **B29**, 315 (1935); Beutler and Jünger, Zeits. f. Physik **101**, 304 (1936).

[12] H. C. Urey and D. Rittenberg, J. Chem. Phys. **1**, 137 (1933).

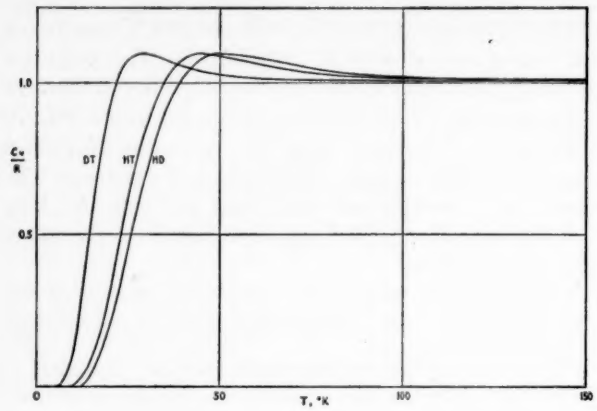

FIG. 1. Internal portion of the low temperature heat capacities at constant volume of HD, HT, and DT.

I.C.T. constants. The constants for (1) are from reference 3. It will be noted that these constants are not all independent and that $K_1=K_3K_4$, $K_6=K_4K_5$, and $K_2=K_3K_5$. Table VI gives the equilibrium constants as a function of temperature. The approach to the classical values of 4 or of 2 may be noted at high T. Constants for these equilibria may be found at 25, 100, 200, 300, 400, and 500°C from the data of reference 9. These constants differ in a random manner by about 3 percent on the average from values obtained by graphical interpolation of the data of Table VI. This agreement is probably within the accuracy of the computations of reference 10, although some of the individual values appear to be more seriously in error.

The writer wishes to express his thanks for the computing assistance given by the following members of Dr. Bengt Carlson's computing group: Josephine Elliott, Bertha Fagan, Max Goldstein, Margaret Johnson and Nell Lane.

This paper is based on work performed at the Los Alamos Laboratory of the University of California under Government Contract W-7405-eng-36, and the information contained therein will appear in Division V of the National Nuclear Energy Series (Manhattan Project Technical Section) as part of the contribution of the Los Alamos Laboratory.

THE JOURNAL OF CHEMICAL PHYSICS VOLUME 17, NUMBER 11 NOVEMBER, 1949

Energy Levels and Thermodynamic Functions for Molecules with Internal Rotation. III. Compound Rotation

JOHN E. KILPATRICK AND KENNETH S. PITZER

The Department of Chemistry, The Rice Institute, Houston, Texas and The Department of Chemistry, University of California, Berkeley, California

(Received March 11, 1949)

A method is given for calculating the elements of the kinetic energy matrix for rotation for any molecule. The treatment includes the effects due to any number of linked rotating groups, balanced or unbalanced. In a simple case these equations reduce to the simpler ones of the two previous papers of this series. This rotational matrix is then converted into the matrix of the internal rotations. The reduced moments of inertia that form the latter are then used with the methods of the previous papers of this series to calculate energy levels and thermodynamic functions.

IN the two previous papers of this series,[1,2] hereafter designated I and II, a treatment was given for all molecules which can be regarded as rigid frames with attached tops, either symmetric or unsymmetric. The discussion was limited to tops directly attached to the basic frame. In the present paper the general case will be considered: rotating groups attached to rotating groups, with no limit upon the symmetry of the groups or upon the number of groups involved in such a sequence. As examples of molecules covered by the present treatment may be mentioned diethyl ether, the normal paraffins after propane, branched paraffins such as 2,2-dimethyl butane, and lead tetraethyl. In none of these examples is there a group (a basic frame) which is attached directly to every rotating top.

In I, tables are given for the contribution of a single internal rotation (strictly of a symmetric top) to the various thermodynamic functions. In II, it was shown that to a lower degree of approximation these tables were applicable to an unsymmetric top internal rotation. In any case the potential energy is assumed to be $V(\varphi)=\frac{1}{2}V_0(1-\cos n\varphi)$.

The parameters involved in these tables for the mth rotation are the height of the restricting potential barriers, V_m, the symmetry number of the top and of the barrier, n_m, the principal moments of inertia of the rigid molecule (I_{xx}, I_{yy}, and I_{zz}), the moment of the top, A_m, and the direction cosines of the top with respect to the principal axes of the molecule (λ_{im}). The aforementioned moments and direction cosines are combined to give a reduced moment for each top. These moments and direction cosines are also the elements of the kinetic

[1] K. S. Pitzer and W. D. Gwinn, J. Chem. Phys. **10**, 428 (1942).
[2] K. S. Pitzer, J. Chem. Phys. **14**, 239 (1946).

energy matrix for rotation of the molecule. For example, if we consider a frame with two attached symmetric tops (whose moments are A_1 and A_2), the rotational kinetic energy matrix is

$$(S)=\begin{vmatrix} I_{xx} & 0 & 0 & \lambda_{x1}A_1 & \lambda_{x2}A_2 \\ 0 & I_{yy} & 0 & \lambda_{y1}A_1 & \lambda_{y2}A_2 \\ 0 & 0 & I_{zz} & \lambda_{z1}A_1 & \lambda_{z2}A_2 \\ \lambda_{x1}A_1 & \lambda_{y1}A_1 & \lambda_{z1}A_1 & A_1 & 0 \\ \lambda_{x2}A_2 & \lambda_{y2}A_2 & \lambda_{z2}A_2 & 0 & A_2 \end{vmatrix}, \quad (1)$$

where λ_{im} is the direction cosine of the mth top with respect to the ith principal axis of the molecule.

The off-diagonal elements are the coefficients in the quadratic expression for the rotational kinetic energy of the cross products of the over-all angular velocities about the principal axes with the angular velocities of the attached tops. This expression is equally valid for an arbitrary orientation of the coordinate axes, so long as the origin remains at the center of gravity of the molecule. For an arbitrary orientation of the coordinate axes, it is necessary to write in the products of inertia (with negative signs, as in the usual "determinant of inertia"). The direction cosines then refer, of course, to the coordinate axes.

When the above matrix is diagonalized about the elements I_{xx}, I_{yy}, and I_{zz}, by means of a congruent transformation, the following expression is the result:

$$\begin{vmatrix} I_{xx} & 0 & 0 & 0 & 0 \\ 0 & I_{yy} & 0 & 0 & 0 \\ 0 & 0 & I_{zz} & 0 & 0 \\ 0 & 0 & 0 & I_1 & -\Lambda_{12} \\ 0 & 0 & 0 & -\Lambda_{12} & I_2 \end{vmatrix},$$

where

$$I_m=A_m-\sum_{i=x,\,y,\,z}\lambda_{im}^2A_m^2/I_{ii}, \quad (2)$$

$$\Lambda_{12}=\sum_{i=x,\,y,\,z}\lambda_{i1}\lambda_{i2}A_1A_2/I_{ii}. \quad (3)$$

Equations (2) and (3) are merely Eqs. (1a) and (1c) of I. The submatrix

$$(D)=\begin{pmatrix} I_1 & -\Lambda_{12} \\ -\Lambda_{12} & I_2 \end{pmatrix} \quad (4)$$

has for elements the reduced moments of inertia corresponding to the two internal rotations. These elements are independent of the orientation of the axes x, y, and z of the molecule. Their physical interpretation is analogous to that of the reduced masses that frequently occur in dynamic problems involving linear motion. The second approximation to the reduced moments given by Eq. (1b)–I consists of an approximate diagonalization of the matrix (D).

These matters have been discussed at some length for the reason that, in the present paper, the matrix (D) will be derived for a much more complicated case, and it is desirable to express the results of the simple case in a form analogous to that which will be employed here.

DEFINITIONS

In order that we may derive an expression for the kinetic energy of internal rotation of a fairly complicated molecule, it is necessary that we define an adequate coordinate system. This system will be capable of describing any deformation of the molecule, but for the present will be used only in connection with over-all translation, over-all rotation, and various internal rotations. That is, it is assumed that the molecule consists of a number of rigid groups which are linked together by single bonds and which may rotate with respect to each other about these connecting bonds. It is assumed that none of these rigid groups are linked so as to form a ring structure but no restrictions are placed on the symmetry of any of the groups, nor on the number of groups which may be joined in sequence.

Let there be a set of Cartesian axes (0) fixed in space. Let there be another set of axes (1) fixed with respect to some one rigid group within the molecule. This group may be chosen arbitrarily although some choices may be more convenient than others. This group is the basic frame to which the rotations of the groups will be referred. The translation and rotation of this basic group will be described by the velocity components of the origin of frame (1) and the angular velocity components of frame (1) about its own axes, all with respect to the fixed frame (0). The instantaneous position of (1) will be given by the coordinates of its origin and by the orientation of its axes, with respect to frame (0).

Let each of the groups that are directly linked to the basic group of frame (1) be fixed, respectively, in the coordinate frames (2*a*), (2*b*), (2*c*), etc. Each of these second-order frames is located with respect to (1) in the same way that (1) is located with respect to (0) except that only rotations are allowed. Similarly, any number of third-order groups, each fixed on its own coordinate frame, may be attached to any of the second-order groups. This branching process may continue indefinitely.

The symbol $\alpha_{mn}{}^{ab}$ will be used for the cosine of the angle between axis a of frame (m) and axis b of frame (n). The components of a general vector with respect to some frame (m) are the elements $\xi_m{}^x$, $\xi_m{}^y$, and $\xi_m{}^z$ of the 1×3 column matrix ξ_m. The relation between ξ_m and ξ_n is the matrix equation

$$\begin{pmatrix} \xi_m{}^x \\ \xi_m{}^y \\ \xi_m{}^z \end{pmatrix}=\begin{pmatrix} \alpha_{mn}{}^{xx} & \alpha_{mn}{}^{xy} & \alpha_{mn}{}^{xz} \\ \alpha_{mn}{}^{yx} & \alpha_{mn}{}^{yy} & \alpha_{mn}{}^{yz} \\ \alpha_{mn}{}^{zx} & \alpha_{mn}{}^{zy} & \alpha_{mn}{}^{zz} \end{pmatrix}\begin{pmatrix} \xi_n{}^x \\ \xi_n{}^y \\ \xi_n{}^z \end{pmatrix}, \quad (5)$$

or by the same equation in a more compact notation,

$$\xi_m = \alpha_{mn}\xi_n. \tag{6}$$

Since all of our coordinate frames are Cartesian frames, this equation represents a rotation and matrix α_{mn} is orthonormal. If we let all of our frames be right-handed, the determinant of α_{mn} is unity and the reciprocal of α_{mn} is equal to its transpose:

$$\alpha_{mn}{}^{-1} = \alpha_{mn}{}'. \tag{7}$$

In addition, presently it will be very useful that any element of α_{mn} is equal to its own cofactor. For example,

$$\alpha_{mn}{}^{xx} = \alpha_{mn}{}^{yy}\alpha_{mn}{}^{zz} - \alpha_{mn}{}^{zy}\alpha_{mn}{}^{yz} \tag{8a}$$

$$\alpha_{mn}{}^{xy} = -\alpha_{mn}{}^{yx}\alpha_{mn}{}^{zz} + \alpha_{mn}{}^{zx}\alpha_{mn}{}^{yz}. \tag{8b}$$

Let the origin of (1) have the coordinates $r_{10}{}^x$, $r_{10}{}^y$, and $r_{10}{}^z$ in frame (0). The components are the elements of the 1×3 column matrix $\mathbf{r}_{10}$. Similarly, the coordinates of the origin of some particular frame (2) with respect to (1) are the elements of $\mathbf{r}_{21}$. There is a different $\mathbf{r}_{2a,1}$, $\mathbf{r}_{2b,1}\cdots$, of course, for each frame (2*a*), (2*b*), etc. The elements of $\mathbf{r}_{32}$ are the coordinates of some particular frame (3) with respect to the frame (2) to which its contained group is attached, and so on.

The various atoms of the molecule may be classified according to the rigid group to which they belong. The coordinates of a typical atom of mass m in a group fixed in a frame (n) are denoted by x_n, y_n, and z_n, the elements of the column matrix $\mathbf{x}_n$. These elements are constant by definition. The (variable) coordinates of this same point mass in the frame ($n-1$) (to which its group is attached) are denoted by $\mathbf{x}_{n-1}$. In this manner, any typical atom fixed in a frame (n) will have $n+1$ sets of coordinates: $\mathbf{x}_0$, $\mathbf{x}_1$, $\mathbf{x}_2$, $\cdots$ $\mathbf{x}_n$.

The angular velocities of any frame (n) about its x, y, and z axes, measured with respect to the ($n-1$) frame to which it is linked, are the elements $\omega_n{}^x$, $\omega_n{}^y$, and $\omega_n{}^z$ of the matrix $\boldsymbol{\omega}_n$.

We shall assume that the matrices $\mathbf{r}_{21}$, $\mathbf{r}_{32}$, $\cdots$, $\mathbf{r}_{n,n-1}$ are all constant and that for frames (2), (3), $\cdots$, (n), rotation occurs only about the z axis of the frame. That is, with the exception of the basic frame (1), the origin of each coordinate frame is fixed with respect to the group to which it is attached and that each of these groups rotates about an axis fixed with respect to the group to which it is attached.

VELOCITY DERIVATION

By the use of Eq. (6) we may write the relation between the coordinates of any typical point in two consecutive frames in the chain between frame (0) and frame (n):

$$\begin{aligned}\mathbf{x}_0 &= \boldsymbol{\alpha}_{10}{}'\mathbf{x}_1 + \mathbf{r}_{10},\\ \mathbf{x}_1 &= \boldsymbol{\alpha}_{21}{}'\mathbf{x}_2 + \mathbf{r}_{21},\\ \mathbf{x}_{n-1} &= \boldsymbol{\alpha}_{n,n-1}{}'\mathbf{x}_n + \mathbf{r}_{n,n-1}.\end{aligned} \tag{9}$$

By definition, the operator $\partial(\ )$ takes the derivative with respect to time of each element of the matrix on which it operates. The following identity has been proved elsewhere:[3]

$$\boldsymbol{\alpha}_{n,n-1}\partial(\boldsymbol{\alpha}_{n,n-1}{}^{-1}) = \partial(\boldsymbol{\alpha}_{n,n-1})\boldsymbol{\alpha}_{n,n-1}{}^{-1}$$

$$= \begin{pmatrix} 0 & -\omega_n{}^z & \omega_n{}^y \\ \omega_n{}^z & 0 & -\omega_n{}^x \\ -\omega_n{}^y & \omega_n{}^x & 0 \end{pmatrix} = \boldsymbol{\Omega}_n. \tag{10}$$

Direct multiplication is sufficient to establish the identity

$$\begin{pmatrix} 0 & -\omega_n{}^z & \omega_n{}^y \\ \omega_n{}^z & 0 & -\omega_n{}^x \\ -\omega_n{}^y & \omega_n{}^x & 0 \end{pmatrix} \begin{pmatrix} x_n \\ y_n \\ z_n \end{pmatrix}$$

$$= -\begin{pmatrix} 0 & -z_n & y_n \\ z_n & 0 & -x_n \\ -y_n & x_n & 0 \end{pmatrix} \begin{pmatrix} \omega_n{}^x \\ \omega_n{}^y \\ \omega_n{}^z \end{pmatrix} \tag{11}$$

for any arbitrary values of x_n, y_n, and z_n. With the aid of the abbreviation

$$\begin{pmatrix} 0 & -z_n & y_n \\ z_n & 0 & -x_n \\ -y_n & x_n & 0 \end{pmatrix} = \mathbf{X}_n \tag{12}$$

Eq. (11) may be written as

$$\boldsymbol{\Omega}_n\mathbf{x}_n = -\mathbf{X}_n\boldsymbol{\omega}_n. \tag{13}$$

The derivatives with respect to time of Eq. (9) are:

$$\begin{aligned}\partial(\mathbf{x}_0) &= \partial(\boldsymbol{\alpha}_{10}{}')\mathbf{x}_1 + \boldsymbol{\alpha}_{10}{}'\partial(\mathbf{x}_1) + \partial(\mathbf{r}_{10})\\ \partial(\mathbf{x}_1) &= \partial(\boldsymbol{\alpha}_{21}{}')\mathbf{x}_2 + \boldsymbol{\alpha}_{21}{}'\partial(\mathbf{x}_2)\\ \partial(\mathbf{x}_{n-1}) &= \partial(\boldsymbol{\alpha}_{n,n-1}{}')\mathbf{x}_n + \boldsymbol{\alpha}_{n,n-1}{}'\partial(\mathbf{x}_n).\end{aligned} \tag{14}$$

From Eq. (10) we have

$$\begin{aligned}\partial(\boldsymbol{\alpha}_{10}{}') &= \boldsymbol{\alpha}_{10}{}'\boldsymbol{\Omega}_1\\ \partial(\boldsymbol{\alpha}_{21}{}') &= \boldsymbol{\alpha}_{21}{}'\boldsymbol{\Omega}_2\\ \partial(\boldsymbol{\alpha}_{n,n-1}{}') &= \boldsymbol{\alpha}_{n,n-1}{}'\boldsymbol{\Omega}_n.\end{aligned} \tag{15}$$

When Eqs. (13), (15) are substituted in Eqs. (14), the following equations are obtained:

$$\mathbf{v} = \mathbf{u} - \boldsymbol{\alpha}_{10}{}'\mathbf{X}_1\boldsymbol{\omega}_1, \tag{16}$$

$$\mathbf{v} = \mathbf{u} - \boldsymbol{\alpha}_{10}{}'\mathbf{X}_1\boldsymbol{\omega}_1 - \boldsymbol{\alpha}_{10}{}'\boldsymbol{\alpha}_{21}{}'\mathbf{X}_2\boldsymbol{\omega}_2, \tag{17}$$

$$\mathbf{v} = \mathbf{u} - \boldsymbol{\alpha}_{10}{}'\mathbf{X}_1\boldsymbol{\omega}_1 - \boldsymbol{\alpha}_{10}{}'\boldsymbol{\alpha}_{21}{}'\mathbf{X}_2\boldsymbol{\omega}_2 \cdots - \boldsymbol{\alpha}_{10}{}'\boldsymbol{\alpha}_{21}{}'\cdots\boldsymbol{\alpha}_{n,n-1}{}'\mathbf{X}_n\boldsymbol{\omega}_n. \tag{18}$$

[3] Frazer, Duncan, and Collar, *Elementary Matrices* (Cambridge University Press, London, 1946), pp. 246–257.

The symbols $\mathbf{v}$ and $\mathbf{u}$ are used for $\partial(\mathbf{x}_0)$ and $\partial(\mathbf{r}_{10})$. They are both column matrices and represent, respectively, the components of the absolute velocity of a typical point mass and the components of the velocity of the origin of frame (1). As has already been emphasized, every atom of the molecule is fixed in some one frame. Equation (16) applies to a mass fixed in frame (1), Eq. (17) to a mass fixed in frame (2), and, in general, Eq. (18) to a mass fixed in frame (n).

KINETIC ENERGY DERIVATION

The kinetic energy of all the atoms in any particular frame is given by

$$2T=\sum m\mathbf{v}'\mathbf{v}, \tag{19}$$

where T is the kinetic energy with respect to the fixed frame (0), $\mathbf{v}$ the velocity of each atom as given by the appropriate Eq. (18), and with the summation taken over all the atoms of the frame.

The expansion of Eq. (19) for some frame (n) obviously contains all the terms found in the expansion for any lower ordered frame. It will be sufficient to treat in detail the expansion for the case of a third-order frame. This is the simplest case that included terms typical of all frames, either of higher or lower order.

The velocity of a typical atom fixed in a frame (3) is given by

$$\mathbf{v}=\mathbf{u}-\boldsymbol{\alpha}_{10}'\mathbf{X}_1\boldsymbol{\omega}_1-\boldsymbol{\alpha}_{10}'\boldsymbol{\alpha}_{21}'\mathbf{X}_2\boldsymbol{\omega}_2-\boldsymbol{\alpha}_{10}'\boldsymbol{\alpha}_{21}'\boldsymbol{\alpha}_{32}'\mathbf{X}_3\boldsymbol{\omega}_3. \tag{20}$$

The total kinetic energy of all the atoms fixed in this frame is given by

$$\begin{aligned}2T=\sum m(&\mathbf{u}'\mathbf{u}-\mathbf{u}'\boldsymbol{\alpha}_{10}'\mathbf{X}_1\boldsymbol{\omega}_1-\mathbf{u}'\boldsymbol{\alpha}_{20}'\mathbf{X}_2\boldsymbol{\omega}_2-\mathbf{u}'\boldsymbol{\alpha}_{30}'\mathbf{X}_3\boldsymbol{\omega}_3-\boldsymbol{\omega}_1'\mathbf{X}_1'\boldsymbol{\alpha}_{10}\mathbf{u}+\boldsymbol{\omega}_1'\mathbf{X}_1'\mathbf{X}_1\boldsymbol{\omega}_1+\boldsymbol{\omega}_1'\mathbf{X}_1'\boldsymbol{\alpha}_{21}'\mathbf{X}_2\boldsymbol{\omega}_2\\&+\boldsymbol{\omega}_1'\mathbf{X}_1'\boldsymbol{\alpha}_{31}'\mathbf{X}_3\boldsymbol{\omega}_3-\boldsymbol{\omega}_2'\mathbf{X}_2'\boldsymbol{\alpha}_{20}\mathbf{u}+\boldsymbol{\omega}_2'\mathbf{X}_2'\boldsymbol{\alpha}_{21}\mathbf{X}_1\boldsymbol{\omega}_1+\boldsymbol{\omega}_2'\mathbf{X}_2'\mathbf{X}_2\boldsymbol{\omega}_2+\boldsymbol{\omega}_2'\mathbf{X}_2'\boldsymbol{\alpha}_{32}'\mathbf{X}_3\boldsymbol{\omega}_3-\boldsymbol{\omega}_3'\mathbf{X}_3'\boldsymbol{\alpha}_{30}\mathbf{u}\\&+\boldsymbol{\omega}_3'\mathbf{X}_3'\boldsymbol{\alpha}_{31}\mathbf{X}_1\boldsymbol{\omega}_1+\boldsymbol{\omega}_3'\mathbf{X}_3'\boldsymbol{\alpha}_{32}\mathbf{X}_2\boldsymbol{\omega}_2+\boldsymbol{\omega}_3'\mathbf{X}_3'\mathbf{X}_3\boldsymbol{\omega}_3).\end{aligned} \tag{21}$$

This equation may be written in the equivalent form

$$2T=(\mathbf{u}',\boldsymbol{\omega}_1',\boldsymbol{\omega}_2',\boldsymbol{\omega}_3')\sum m\begin{bmatrix}\mathbf{E} & -\boldsymbol{\alpha}_{10}'\mathbf{X}_1 & -\boldsymbol{\alpha}_{20}'\mathbf{X}_2 & -\boldsymbol{\alpha}_{30}'\mathbf{X}_3\\ -\mathbf{X}_1'\boldsymbol{\alpha}_{10} & \mathbf{X}_1'\mathbf{X}_1 & \mathbf{X}_1'\boldsymbol{\alpha}_{21}'\mathbf{X}_2 & \mathbf{X}_1'\boldsymbol{\alpha}_{31}'\mathbf{X}_3\\ -\mathbf{X}_2'\boldsymbol{\alpha}_{20} & \mathbf{X}_2'\boldsymbol{\alpha}_{21}\mathbf{X}_1 & \mathbf{X}_2'\mathbf{X}_2 & \mathbf{X}_2'\boldsymbol{\alpha}_{32}'\mathbf{X}_3\\ -\mathbf{X}_3'\boldsymbol{\alpha}_{30} & \mathbf{X}_3'\boldsymbol{\alpha}_{31}\mathbf{X}_1 & \mathbf{X}_3'\boldsymbol{\alpha}_{32}\mathbf{X}_2 & \mathbf{X}_3'\mathbf{X}_3\end{bmatrix}\begin{bmatrix}\mathbf{u}\\ \boldsymbol{\omega}_1\\ \boldsymbol{\omega}_2\\ \boldsymbol{\omega}_3\end{bmatrix}. \tag{22}$$

The indicated summation over the terms of the square matrix in the above expression is the contribution of the third-order group in question to the complete kinetic energy matrix of the molecule. It is important to note that a typical second-order group would yield a similar expression, except that $\boldsymbol{\omega}_3$ and the fourth row and column of the square matrix would be missing. Analogous statements can be made for groups of other orders.

We can readily reduce the submatrices in the square matrix of Eq. (22) to a form much more adapted to numerical calculation. The various elements all prove to be composed of first- and second-order moments of our group (3) about its own z axis, about the z axis of the frame (2) to which (3) is linked, about the x, y, and z axes of frame (1), the total mass of group (3), and the cosines of the angles between the above axes. Since the elements of the kinetic energy matrix of Eq. (22) are typical of a group of any order (the extention to higher order groups is obvious), the following analysis will be sufficient to enable us to write the kinetic energy matrix for any group and by simply adding the corresponding terms from the matrices for all the groups of the molecule, to write the complete kinetic energy matrix.

The kinetic energy matrix of Eq. (22) is actually unnecessarily high in order. Since $\mathbf{u}$, $\boldsymbol{\omega}_1$, and $\boldsymbol{\omega}_2$ and $\boldsymbol{\omega}_3$ have been defined as three-element columns, the kinetic energy matrix as written is 12×12. We have already assumed that $\boldsymbol{\omega}_2$ and $\boldsymbol{\omega}_3$ each have only one non-zero element (ω_2^z and ω_3^z). It is therefore possible to reduce the kinetic energy matrix to a form that is only 8×8: three translational coordinates, three over-all rotational coordinates, the rotation of the group (2) that supports group (3), and the rotation of group (3).

The following abbreviations will be found useful:

M = total mass of the molecule.

I_{ii} = moment of inertia of the whole molecule about axis i of frame (1). Each of the higher order attached groups is assumed fixed in some instantaneous configuration.

I_{ij} = the ij cross moment or product of inertia of the whole molecule, under the above conditions.

A = moment of inertia of some second or higher ordered group about its own z axis. The contribution of all of the higher ordered groups attached to this group (fixed in some particular configuration relative to it) is included. A subscript will frequently be added to distinguish the A's of different groups.

B = the xz cross product of inertia of the above system.

C = the yz cross product of inertia of the above system.

$U^x=\Sigma mx$, the first-order x moment of the above system or its off-balance factor in the x direction.

$U^y=\Sigma my$. Presently we shall assume that each second- or higher ordered group is oriented in its coordinate frame so that $U^y=0$. That is, its center of gravity lies in its xz plane.

The symbols with an asterisk superscript will mean the contribution of the one group under consideration (with no contribution from higher ordered groups). For

example, if a group in some second-ordered frame is being considered, M^* means the mass of this group and A^* the moment of inertia of this group, with no contribution from possible third-order groups which may be attached.

The Diagonal Submatrices

The first block arises from the term in Eq. (22): $\sum mE$. The corresponding block in the kinetic energy matrix is

$$\begin{pmatrix} M^* & 0 & 0 \\ 0 & M^* & 0 \\ 0 & 0 & M^* \end{pmatrix}.$$

The same block in the complete kinetic energy matrix is therefore

$$\begin{pmatrix} M & 0 & 0 \\ 0 & M & 0 \\ 0 & 0 & M \end{pmatrix}.$$

The diagonal block from the three over-all angular velocities is $\sum m\mathbf{X}_1'\mathbf{X}_1$. When this term is multiplied out, we have

$$\sum m \begin{pmatrix} 0 & z & -y \\ -z & 0 & x \\ y & -x & 0 \end{pmatrix} \begin{pmatrix} 0 & -z & y \\ z & 0 & -x \\ -y & x & 0 \end{pmatrix}$$

$$= \begin{pmatrix} \sum m(z^2+y^2) & -\sum mxy & -\sum mxz \\ -\sum mxy & \sum m(z^2+x^2) & -\sum myz \\ -\sum mxz & -\sum myz & \sum m(y^2+x^2) \end{pmatrix}$$

$$= \begin{pmatrix} I_{xx}^* & -I_{xy}^* & -I_{xz}^* \\ -I_{xy}^* & I_{yy}^* & -I_{yz}^* \\ -I_{xz}^* & -I_{yz}^* & I_{zz}^* \end{pmatrix}. \quad (23)$$

The elements of this block are the various moments of inertia of the group in question about the axes of frame (1). The same block in the complete kinetic energy matrix is, of course, the sum of all the matrices of this form, one from each frame, and is therefore

$$\begin{pmatrix} I_{xx} & -I_{xy} & -I_{xz} \\ -I_{xy} & I_{yy} & -I_{yz} \\ -I_{xz} & -I_{yz} & I_{zz} \end{pmatrix}.$$

These moments are computed by summation over all the atoms of the molecule, in some instantaneous configuration, with respect to frame (1). No assumption has been made as yet of any possible relation of the center of gravity of the whole molecule and the origin of frame (1).

The third diagonal block comes from the term $\sum m\boldsymbol{\omega}_2'\mathbf{X}_2'\mathbf{X}_2\boldsymbol{\omega}_2$. This term could be multiplied out exactly as the preceeding term in $\boldsymbol{\omega}_1$ but this would give a 3×3 block as a contribution to the kinetic energy matrix. It is far more satisfactory to drop the formal three-element column matrix $\boldsymbol{\omega}_2$ as a variable and use instead its sole non-zero element $\omega_2{}^z$:

$$\sum m(0, 0, \omega_2{}^z)X_2'X_2 \begin{pmatrix} 0 \\ 0 \\ \omega_2{}^z \end{pmatrix}$$

$$= \omega_2{}^z \sum m(x^2+y^2)\omega_2{}^z = \omega_2{}^z A_2{}^* \omega_2{}^z. \quad (24)$$

$A_2{}^*$ is therefore the contribution of the rotation of a frame (2) to the kinetic energy matrix. A term of this form will arise not only from the kinetic energy expression for a frame (2) but also from the corresponding expressions for all attached groups, be they third-, fourth-, or higher order frames. Each is summed over its own atoms but all are summed with respect to the frame (2). The total contribution of the rotation $\omega_2{}^z$ is therefore A_2: the moment of inertia about the axis of rotation of the group of the frame (2) and all connected, higher order groups, all considered as one rigid body.

The same analysis holds for the contribution of a rotation $\boldsymbol{\omega}_3{}^z$ or of the rotation of any higher order group. The group and all attached higher ordered groups are considered a rigid body. The matrix element is the moment of the structure about its axis of rotation.

The Non-Diagonal or Interaction Submatrices

It is necessary to treat explicitly only the submatrices that lie below the main diagonal since, from the form of Eq. (22), the kinetic energy matrix is symmetric. The blocks that lie above the main diagonal are merely the transposes of the corresponding blocks below the main diagonal.

The interaction term between $\mathbf{u}$ and $\boldsymbol{\omega}_1$ is $-(\sum m\mathbf{X}_1')\boldsymbol{\alpha}_{10}$. As in the preceding cases, this expression is summed over all the atoms of the molecule, for some instantaneous configuration, in order to get the contribution to the complete kinetic energy matrix. The elements of $\sum m\mathbf{X}_1'$ are, of course, zeros and the appropriate off-balance factors for the whole molecule with respect to the axes of frame (1).

Similarly, the interaction block between $\mathbf{u}$ and $\boldsymbol{\omega}_2$ is $-(\sum m\mathbf{X}_2')\boldsymbol{\alpha}_{20}$. Here however, we immediately reduce this 3×3 square matrix to a 3×1 row, so as to take advantage of the fact that $\boldsymbol{\omega}_2$ has only one non-zero element. From Eq. (21), the kinetic energy of the $\mathbf{u}$, $\boldsymbol{\omega}_2$ interaction is

$$-(0, 0, \omega_2{}^z)\sum m \begin{pmatrix} 0 & z_2 & -y_2 \\ -z_2 & 0 & x_2 \\ y_2 & -x_2 & 0 \end{pmatrix} \boldsymbol{\alpha}_{20}\mathbf{u}$$

$$= -\omega_2{}^z(U_2{}^y, -U_2{}^x, 0)\boldsymbol{\alpha}_{20}\mathbf{u}. \quad (25)$$

The interaction block between $\mathbf{u}$ and ω_2^z is therefore $(-U_2^y, U_2^x, 0)\boldsymbol{\alpha}_{20}$. This interaction between translation of the whole molecule and rotation of a second-order frame is of course zero for a balanced second-order frame. The interaction of $\mathbf{u}$ and $\boldsymbol{\omega}_3$ is of the same form: $(-U_3^y, U_3^x, 0)\boldsymbol{\alpha}_{30}$.

The interaction kinetic energy between $\boldsymbol{\omega}_1$ and $\boldsymbol{\omega}_2$ is $\boldsymbol{\omega}_1'\sum m\mathbf{X}_1'\boldsymbol{\alpha}_{21}'\mathbf{X}_2\boldsymbol{\omega}_2$. This expression can be reduced as follows:

$$\boldsymbol{\omega}_1'\sum m\mathbf{X}_1'\boldsymbol{\alpha}_{21}'\mathbf{X}_2\boldsymbol{\omega}_2=\boldsymbol{\omega}_1'\sum m\begin{bmatrix}0 & z_1 & -y_1\\ -z_1 & 0 & x_1\\ y_1 & -x_1 & 0\end{bmatrix}\begin{bmatrix}\alpha_{21}^{xx} & \alpha_{21}^{yx} & \alpha_{21}^{zx}\\ \alpha_{21}^{xy} & \alpha_{21}^{yy} & \alpha_{21}^{zy}\\ \alpha_{21}^{xz} & \alpha_{21}^{yz} & \alpha_{21}^{zz}\end{bmatrix}\begin{bmatrix}0 & -z_2 & y_2\\ z_2 & 0 & -x_2\\ -y_2 & x_2 & 0\end{bmatrix}\begin{bmatrix}0\\ 0\\ \omega_2^z\end{bmatrix}$$

$$=\boldsymbol{\omega}_1'\sum m\begin{bmatrix}z_1(y_2\alpha^{xy}-x_2\alpha^{yy})-y_1(y_2\alpha^{xz}-x_2\alpha^{yz})\\ x_1(y_2\alpha^{xz}-x_2\alpha^{yz})-z_1(y_2\alpha^{xx}-x_2\alpha^{yx})\\ y_1(y_2\alpha^{xz}-x_2\alpha^{yx})-x_1(y_2\alpha^{xy}-x_2\alpha^{yy})\end{bmatrix}\omega_2^z. \quad (26)$$

The coordinates x_1, y_1, and z_1 can be removed by the substitutions:

$$\begin{aligned}x_1&=\alpha_{21}^{xx}x_2+\alpha_{21}^{yx}y_2+\alpha_{21}^{zx}z_2+r_{21}^x\\ y_1&=\alpha_{21}^{xy}x_2+\alpha_{21}^{yy}y_2+\alpha_{21}^{zy}z_2+r_{21}^y\\ z_1&=\alpha_{21}^{xz}x_2+\alpha_{21}^{yz}y_2+\alpha_{21}^{zz}z_2+r_{21}^z\end{aligned} \quad (27)$$

and the use of the property of $\boldsymbol{\alpha}_{21}$ that any element is equal to its cofactor. The following abbreviations will be useful in expressing these and subsequent results:

$$\begin{aligned}\beta_{21}^x&=\alpha_{21}^{zx}A_2-\alpha_{21}^{xx}B_2-\alpha_{21}^{yx}C_2\\ &\quad+(\alpha_{21}^{yz}r_{21}^y-\alpha_{21}^{yy}r_{21}^z)U_2^x\\ &\quad+(\alpha_{21}^{xy}r_{21}^z-\alpha_{21}^{xz}r_{21}^y)U_2^y\\ \beta_{21}^y&=\alpha_{21}^{zy}A_2-\alpha_{21}^{xy}B_2-\alpha_{21}^{yy}C_2\\ &\quad+(\alpha_{21}^{yz}r_{21}^z-\alpha_{21}^{yz}r_{21}^x)U_2^x\\ &\quad+(\alpha_{21}^{xz}r_{21}^x-\alpha_{21}^{xx}r_{21}^z)U_2^y\\ \beta_{21}^z&=\alpha_{21}^{zz}A_2-\alpha_{21}^{xz}B_2-\alpha_{21}^{yz}C_2\\ &\quad+(\alpha_{21}^{yy}r_{21}^x-\alpha_{21}^{yx}r_{21}^y)U_2^x\\ &\quad+(\alpha_{21}^{xx}r_{21}^y-\alpha_{21}^{xy}r_{21}^x)U_2^y.\end{aligned} \quad (28)$$

Equation (26) then reduces to

$$\boldsymbol{\omega}_1'\begin{bmatrix}\beta_{21}^x\\ \beta_{21}^y\\ \beta_{21}^z\end{bmatrix}\omega_2^z.$$

The interaction element of the complete kinetic energy matrix between ω_1^i and ω_2^z is therefore β_{21}^i. A similar proof shows that the interaction term between ω_1^i and ω_n^z is β_{nl}^i.

The last remaining interaction it is necessary to treat is that between ω_2^z and ω_3^z. We have for the kinetic energy:

$$(0, 0, \omega_2^z)\sum m\mathbf{X}_2'\boldsymbol{\alpha}_{32}'\mathbf{X}_3\begin{bmatrix}0\\ 0\\ \omega_3^z\end{bmatrix}=\omega_2^z\beta_{32}^z\omega_3^z, \quad (29)$$

where

$$\begin{aligned}\beta_{32}^z&=\alpha_{32}^{zz}A_3-\alpha_{32}^{xz}B_3-\alpha_{32}^{yz}C_3\\ &\quad+(\alpha_{32}^{yy}r_{32}^x-\alpha_{32}^{yx}r_{32}^y)U_3^x\\ &\quad+(\alpha_{32}^{xx}r_{32}^y-\alpha_{32}^{xy}r_{32}^x)U_3^y,\end{aligned} \quad (30)$$

in analogy to Eq. (28).

We shall now summarize the preceeding results for a system with the following qualitative description: a basic frame (1), two attached groups (frames (2*a*) and (2*b*), and one final group attached to group (2*b*) (frame (3)). It is obvious that there is no interaction between the rotation of group (3) or group (2*b*) and that of group (2*a*), since no kinetic energy term can occur in $\boldsymbol{\omega}_{2a}\boldsymbol{\omega}_{2b}$ or $\boldsymbol{\omega}_{2a}\boldsymbol{\omega}_3$. This point is briefly summarized by the statement that a rotating group interacts only with the lower groups upon which it is based. Group (3) is based on group (2*b*), which in turn is based on group (1). Group (2*a*) is based on group (1) also but (3) and (2*b*) are not directly connected to (2*a*).

In order to introduce some additional simplifications

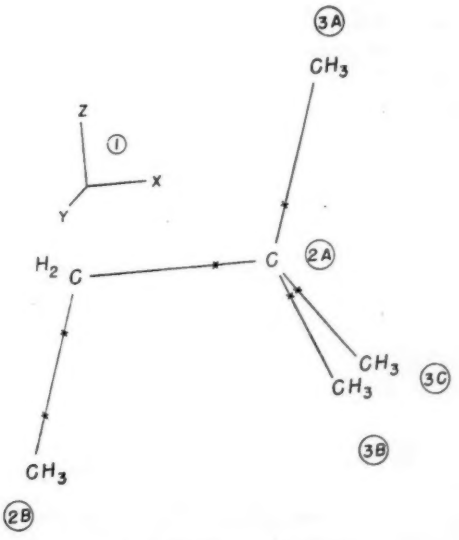

FIG. 1. Neohexane molecule.

into our equation with no loss in generality, we shall assume that the axes of frame (2*a*) are oriented so that the center of gravity of group (2*a*) lies in the *xz* plane of frame (2*a*). Therefore $U_{2a}{}^{y}=0$. We shall further assume that the center of gravity of groups (2*b*) and (3), considered as a unit, lies in the *xz* plane of frame (2*b*), and that of group (2*b*) alone lies in the *xz* plane of frame (3). Therefore, $U_{2b}{}^{y}=0$ and $U_{3}{}^{y}=0$.

The kinetic energy matrix for the above system is then the following expression:

$$\left[\begin{array}{ccc|ccc|ccc}
M & 0 & 0 & 0 & U_1{}^z & -U_1{}^y & \alpha_{2a0}{}^{yx}U_{2a}{}^x & \alpha_{2b0}{}^{yx}U_{2b}{}^x & \alpha_{30}{}^{yx}U_3{}^x \\
0 & M & 0 & -U_1{}^z & 0 & U_1{}^x & \alpha_{2a0}{}^{yy}U_{2a}{}^x & \alpha_{2b0}{}^{yy}U_{2b}{}^x & \alpha_{30}{}^{yy}U_3{}^x \\
0 & 0 & M & U_1{}^y & -U_1{}^x & 0 & \alpha_{2a0}{}^{yz}U_{2a}{}^x & \alpha_{2b0}{}^{yz}U_{2b}{}^x & \alpha_{30}{}^{yz}U_3{}^x \\
\hline
0 & -U_1{}^z & U_1{}^y & I_{xx} & -I_{xy} & -I_{xz} & \beta_{2a1}{}^x & \beta_{2b1}{}^x & \beta_{31}{}^x \\
U_1{}^z & 0 & -U_1{}^x & -I_{xy} & I_{yy} & -I_{yz} & \beta_{2a1}{}^y & \beta_{2b1}{}^y & \beta_{31}{}^y \\
-U_1{}^y & U_1{}^x & 0 & -I_{xz} & -I_{yz} & I_{zz} & \beta_{2a1}{}^z & \beta_{2b1}{}^z & \beta_{31}{}^z \\
\hline
\alpha_{2a0}{}^{yx}U_{2a}{}^x & \alpha_{2a0}{}^{yy}U_{2a}{}^x & \alpha_{2a0}{}^{yz}U_{2a}{}^x & \beta_{2a1}{}^x & \beta_{2a1}{}^y & \beta_{2a1}{}^z & A_{2a} & 0 & 0 \\
\alpha_{2b0}{}^{yx}U_{2b}{}^x & \alpha_{2b0}{}^{yy}U_{2b}{}^x & \alpha_{2b0}{}^{yz}U_{2b}{}^x & \beta_{2b1}{}^y & \beta_{2b1}{}^y & \beta_{2b1}{}^z & 0 & A_{2b} & \beta_{3,2b}{}^z \\
\alpha_{30}{}^{yx}U_3{}^x & \alpha_{30}{}^{yy}U_3{}^x & \alpha_{30}{}^{yz}U_3{}^x & \beta_{31}{}^x & \beta_{31}{}^y & \beta_{31}{}^z & 0 & \beta_{3,2b}{}^z & A_3
\end{array}\right]$$

Our next step is to remove the three rows and columns that refer to translation from kinetic energy matrix of Eq. (31). That is, we want to introduce three new components of translation referred to the center of gravity of the whole molecule. No interaction terms will then be present between **u** and any of the **ω**'s. This end is simply achieved by the process of diagonalization by a congruent transformation about the three **u** elements: *M*, *M*, and *M*. It is easy to show that this process changes the *I*'s, *U*'s, and *β*'s that appear in the three rows and columns that correspond to $\omega_1{}^x$, $\omega_1{}^y$, and $\omega_1{}^z$ to just the values they would have had if we had originally placed the origin of frame (1) at the instantaneous center of gravity of the molecule. There will be a considerable simplification of our subsequent equations if we make that choice now. It is to be noted that though $U_1{}^x$, $U_1{}^y$, and $U_1{}^z$ are now zero, the other *U*'s, referring to the off balance of the higher groups, are not changed and are not necessarily zero. We must still diagonalize about the three *M*'s.

Briefly stated, the process of diagonalization about a block *A* is as follows:

$$\begin{bmatrix} A & B \\ B' & C \end{bmatrix} \rightarrow \begin{bmatrix} A & 0 \\ 0 & C^* \end{bmatrix},$$

where $C^*=C-B'A^{-1}B$. Diagonalization may be carried out about a square block *A* or about a single diagonal element A_{ii}. In the latter case we have the following simple equation for the elements of C^*.

$$C_{jk}{}^*=C_{jk}-B_{ji}B_{ik}/A_{ii}. \tag{32}$$

This procedure is most appropriate if the diagonalization is to be carried out numerically. It may, of course, be repeated as often as desired about a new diagonal element. It is important to remember that a congruent transformation such as this does not change the value of the determinant of a matrix.

If we set the origin of frame (1) at the center of gravity of the molecule and then remove the **u**, **ω**-interaction terms by diagonalization, we have left for the kinetic energy matrix of rotation, including over-all rotation,

$$\left[\begin{array}{c|cccccc}
 & \omega_1{}^x & \omega_1{}^y & \omega_1{}^z & \omega_{2a}{}^z & \omega_{2b}{}^z & \omega_3{}^z \\
\hline
\omega_1{}^x & I_{xx} & I_{xy} & I_{xz} & \beta_{2a,1}{}^x & \beta_{2b,1}{}^x & \beta_{3,1}{}^x \\
\omega_1{}^y & I_{xy} & I_{yy} & I_{yz} & \beta_{2a,1}{}^y & \beta_{2b,1}{}^y & \beta_{3,1}{}^y \\
\omega_1{}^z & I_{xz} & I_{yz} & I_{zz} & \beta_{2a,1}{}^z & \beta_{2b,1}{}^z & \beta_{3,1}{}^z \\
\omega_{2a}{}^z & \beta_{2a,1}{}^x & \beta_{2a,1}{}^y & \beta_{2a,1}{}^z & J_{2a} & -\psi_{2b,2a} & -\psi_{3,2a} \\
\omega_{2b}{}^z & \beta_{2b,1}{}^x & \beta_{2b,1}{}^y & \beta_{2b,1}{}^z & -\psi_{2b,2a} & J_{2b} & \beta_{3,2b}{}^z-\psi_{3,2b}{}^z \\
\omega_3{}^z & \beta_{3,1}{}^x & \beta_{3,1}{}^y & \beta_{3,1}{}^z & -\psi_{3,2a} & \beta_{3,2b}{}^z-\psi_{3,2b} & J_3
\end{array}\right] = (S), \tag{33}$$

where

$$J_n = A_n - (U_n{}^x)^2 M^{-1}, \tag{34}$$

$$\psi_{mn} = U_m{}^x U_n{}^x (\alpha_{m1}{}^{yz}\alpha_{n1}{}^{yz} + \alpha_{m1}{}^{yy}\alpha_{n1}{}^{yy} + \alpha_{m1}{}^{yz}\alpha_{n1}{}^{yz}) M^{-1}. \tag{35}$$

This matrix, (S), is fundamental in any discussion of the mechanical or thermodynamic properties of a molecule with internal rotation. In general, the elements of (S) are not necessarily constants. If any of the rotating groups are not symmetric tops, some or all of the elements of (S) may vary with the internal rotation.

The handling of these varying inertial quantities in thermodynamic calculations was discussed in II. It was shown that the variation of the moments of inertia is effectively compensated by a corresponding variation in the mass factor for vibrations. This compensation strictly is effective only if the vibrations are of low enough frequency to be classical. However, it was also shown that for practically all likely applications the important compensating vibrations are low skeletal bending frequencies which are effectively classical at and above room temperature. Thus it was concluded that one should take the (S) matrix for the equilibrium configuration because the vibration frequencies will be for that configuration.

This matrix, (S), is also fundamental to the calculation of the quantum-mechanical energy levels for internal rotation. While the calculation of the complete energy level pattern seems hardly feasible in a complex case, a calculation to the harmonic oscillator approximation of the lowest levels is practical. Since the torsional oscillation in a low energy level will have only a small amplitude, the (S) matrix for the equilibrium position is again appropriate.

Having established the importance of the constant S matrix for the equilibrium configuration, we proceed to the final step in the calculation, which consists of diagonalizing Eq. (33) about the elements I_{xx}, I_{yy}, and I_{zz}. For the simpler cases I and II give the result. However, in a complex case this process is probably best carried out numerically by means of Eq. (32), taking three successive steps. Let us designate the resulting matrix with the omission of I_{xx}, I_{yy}, and I_{zz} with the symbol (D), corresponding to Eqs. (31) and (32) of I. (D) is the matrix of the internal rotation kinetic energy.

ENERGY LEVELS AND THERMODYNAMIC FUNCTIONS

If the off-diagonal elements in (D) are small compared to the diagonal elements, it is a good approximation to take the diagonal elements as the reduced moments of inertia and treat each rotation separately by the methods of the tables and earlier sections of I. An example of this procedure will be given.

If the off-diagonal elements in (D) are not small, the calculation of the lower energy levels to the harmonic oscillator approximation and of thermodynamic functions may follow the procedures of the last section of I. Because of the now increased generality, the equations will be given again, but the reader should refer to the discussion in I.

For the energy levels to the harmonic oscillator approximation, the complete potential is expanded in power series about the equilibrium configuration.

Including only quadratic terms one has

$$2V = \sum_m \sum_{m'} b_{mm'} \varphi_m \varphi_{m'}, \tag{36}$$

$$b_{mm'} = (\partial^2 V / \partial\varphi_m \partial\varphi_{m'})_e. \tag{37}$$

Then the frequencies are given by the usual secular equation:

$$\begin{bmatrix} b_{11}-4\pi^2\nu^2 D_{11} & b_{12}-4\pi^2\nu^2 D_{12} & b_{1N}-4\pi^2\nu^2 D_{1N} \\ b_{21}-4\pi^2\nu^2 D_{21} & b_{22}-4\pi^2\nu^2 D_{22} \cdots & b_{2N}-4\pi^2\nu^2 D_{2N} \\ \cdots & \cdots & \cdots \\ b_{N1}-4\pi^2\nu^2 D_{N1} & b_{N2}-4\pi^2\nu^2 D_{N2} & b_{NN}-4\pi^2\nu^2 D_{NN} \end{bmatrix} = 0, \tag{38}$$

and the energy levels by

$$W = \sum_{l=1}^{N} (v_l + \tfrac{1}{2}) h\nu_l, \tag{39}$$

where the N roots of the secular equations give the N values of ν_l and the quantum numbers v_l have the usual integral values 0, 1, etc.

The complete classical partition function (not containing the harmonic oscillation approximations) is calculated with the theorem of Edinoff and Aston.[4]

$$Q_{\text{class}} = (2\pi kT/h^2)^{N/2} [D]^{\frac{1}{2}} \int_0^{2\pi/n_1} \cdots \int_0^{2\pi/n_N} \exp(-V/kT) d\varphi_1 \cdots d\varphi_N. \tag{40}$$

[4] M. L. Edinoff and J. G. Aston, J. Chem. Phys. 3, 379 (1935).

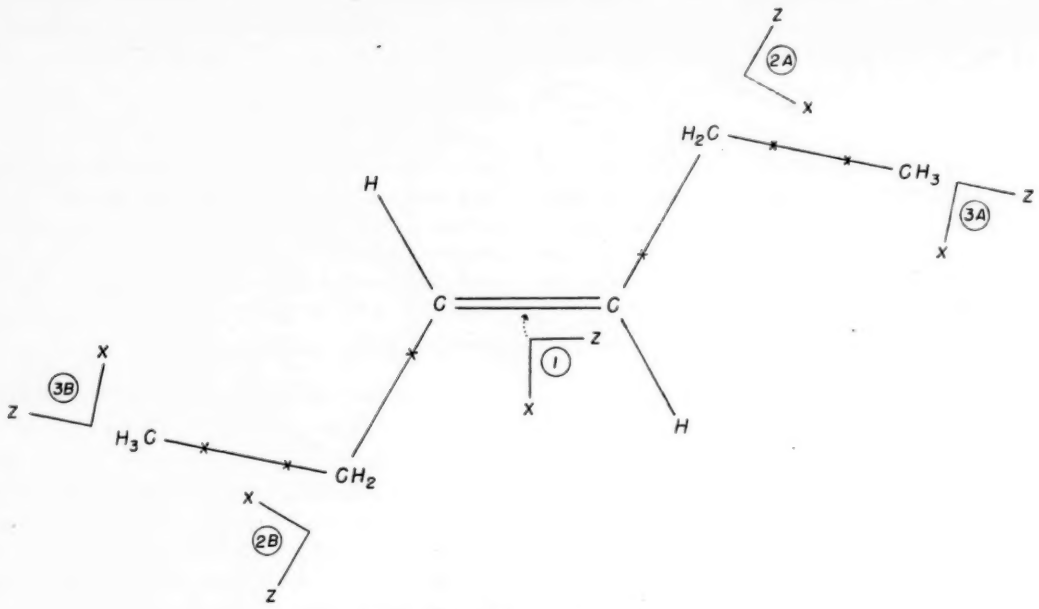

FIG. 2. *Trans*-hexene-3 molecule.

The determinant $[D]$ is removed from the integral even if it is formally dependent on the φ's for the reasons already given and is evaluated for the equilibrium configuration. V is the complete potential energy, a function of the φ's, and the n's are symmetry numbers of the rotations of tops which have symmetry (otherwise $n=1$).

Following the approximation suggested in I, the partition function is taken as

$$Q=Q_{\text{class}}(Q_{\text{H. O. quant}}/Q_{\text{H. O. class}}). \tag{41}$$

In most cases the frequencies of torsional oscillations will be low so that $(h\nu/kT)$ is less than or approximately one. The final formulas recommended for thermodynamic functions follow.

Let $h\nu_l/kT=a_l$: (42)

$$-F/T=R[\ln Q_{\text{class}} + \sum_{l=1}^{N}(a_l/2-a_l^2/24+a_l^4/2880+\cdots)] \tag{43}$$

$$H/T=R[N/2+P'/P + \sum_{l=1}^{N}(-a_l/2+a_l^2/12-a_l^2/720+\cdots)] \tag{44}$$

$$S=R[\ln Q_{\text{class}}+N/2+P'/P + \sum_{l=1}^{N}(a_l^2/24-a_l^4/960+\cdots)] \tag{45}$$

$$C=R[N/2+P''/P-(P'/P)^2 + \sum_{l=1}^{N}(-a_l^2/12+a_l^4/240+\cdots)] \tag{46}$$

$$Q_{\text{class}}=P(2\pi kT/h^2)^{N/2}[D]^{\frac{1}{2}} \tag{47}$$

$$P=\int_0^{2\pi/n_1}\cdots\int_0^{2\pi/n_N}\exp(-V/kT)d\varphi_1\cdots d\varphi_N \tag{48}$$

$$P'=\int_0^{2\pi/n_1}\cdots\int_0^{2\pi/n_N}(V/kT) \times\exp(-V/kT)d\varphi_1\cdots d\varphi_N \tag{49}$$

$$P''=\int_0^{2\pi/n_1}\cdots\int_0^{2\pi/n_N}(V/kT)^2 \times\exp(-V/kT)d\varphi_1\cdots d\varphi_N. \tag{50}$$

EXAMPLE A: 2,2 DIMETHYLBUTANE

As our first example we take neohexane (2,2 dimethylbutane) which in principle falls in the present complex class but actually reduces in good approximation to the simple class treated in I.[5]

We shall use atomic weight—Angstrom units. To convert the resulting moments of inertia to c.g.s. units one multiplies by $10^{-16}/N_0$ or 0.166035×10^{-39}.

In calculating inertial quantities for hydrocarbons the following short-cut method has proven useful. Tetrahedral structures such as CH_4 and $(CH_3)_4C$ are spherical tops and as such have the same moment of inertia about any axis through the center of gravity. In molecules where CH_3, CH_2, and even occasionally CH units appear, one may include terms for a CH_4 located at these carbon atoms and then subtract terms for the hydrogen atoms assumed but not actually present. These missing

[5] J. E. Kilpatrick and K. S. Pitzer, J. Am. Chem. Soc. **68**, 1066 (1946).

hydrogens are along the C−C bonds and hence are easier to locate than the hydrogens actually present. This method will be illustrated in our examples here.

For neohexane we take the C−H distance to be 1.09A, C−C to be 1.54A, and tetrahedral angles throughout. We first choose the CH_2 carbon atom as our coordinate origin (frame (1)) with the x axis directed toward the $C(CH_3)_3$ group and the remaining methyl carbon in the xz plane as shown in Fig. 1. The $C(CH_3)_3$ group is numbered (2*a*) and its methyl groups (3*a*), (3*b*), and (3*c*) as shown in Fig. 1. The other methyl group connected directly to the CH_2 group is (2*b*).

Since all rotating groups are symmetrical, their angular orientation is immaterial; for convenience a specific orientation is desired. The orientation will be assumed which staggers the groups at opposite ends of each C−C bond.

The direction cosines are as follows:

$$\begin{bmatrix}\alpha_{3a,1}{}^{zx}\\ \alpha_{3a,1}{}^{zy}\\ \alpha_{3a,1}{}^{zz}\end{bmatrix}=\begin{bmatrix}1/3\\ 0\\ (8/9)^{\frac{1}{2}}\end{bmatrix};\quad \begin{bmatrix}\alpha_{2a,1}{}^{zx}\\ \alpha_{2a,1}{}^{zy}\\ \alpha_{2a,1}{}^{zz}\end{bmatrix}=\begin{bmatrix}1\\ 0\\ 0\end{bmatrix}$$

$$\begin{bmatrix}\alpha_{3b,1}{}^{zx}\\ \alpha_{3b,1}{}^{zy}\\ \alpha_{3b,1}{}^{zz}\end{bmatrix}=\begin{bmatrix}1 & 0 & 0\\ 0 & -1/2 & (3/4)^{\frac{1}{2}}\\ 0 & -(3/4)^{\frac{1}{2}} & -1/2\end{bmatrix}\begin{bmatrix}1/3\\ 0\\ (8/9)^{\frac{1}{2}}\end{bmatrix}=\begin{bmatrix}1/3\\ (2/3)^{\frac{1}{2}}\\ -(2/9)^{\frac{1}{2}}\end{bmatrix}$$

$$\begin{bmatrix}\alpha_{3c,1}{}^{zx}\\ \alpha_{3c,1}{}^{zy}\\ \alpha_{3c,1}{}^{zz}\end{bmatrix}=\begin{bmatrix}1 & 0 & 0\\ 0 & -1/2 & (3/4)^{\frac{1}{2}}\\ 0 & -(3/4)^{\frac{1}{2}} & -1/2\end{bmatrix}\begin{bmatrix}1/3\\ (2/3)^{\frac{1}{2}}\\ -(2/9)^{\frac{1}{2}}\end{bmatrix}=\begin{bmatrix}1/3\\ -(2/3)^{\frac{1}{2}}\\ -(2/9)^{\frac{1}{2}}\end{bmatrix}$$

$$\begin{bmatrix}\alpha_{2b,1}{}^{zx}\\ \alpha_{2b,1}{}^{zy}\\ \alpha_{2b,1}{}^{zz}\end{bmatrix}=\begin{bmatrix}-1/3\\ 0\\ -(8/9)^{\frac{1}{2}}\end{bmatrix}$$

$$\alpha_{3a,\,2a}{}^{zz}=\alpha_{3b,\,2a}{}^{zz}=\alpha_{3c,\,2a}{}^{zz}=1/3.$$

The coordinates of the center of gravity of the neohexane molecule, referred to coordinate frame (1), are:

$$x_{cg}=[(1.54)(72.146)-(1/3)(1.54)(16.042)+(1/3)(1.09)(1.008)+(1/3)(0.45)(1.008)]/86.172=1.9978$$

$$y_{cg}=0$$

$$z_{cg}=[-(8/9)^{\frac{1}{2}}(1.54)(16.042)+(8/9)^{\frac{1}{2}}(1.09)(1.998)+(8/9)^{\frac{1}{2}}(0.45)(1.008)]/86.172=-0.25331.$$

The last two terms in each of the above equations are for the hydrogens assumed in CH_4 and $(CH_3)_4C$ groups but not actually present.

The over-all moments of inertia are first calculated about the axes of frame (1). These moments are then corrected to a parallel frame (1) with its origin at the center of gravity of the molecule:

$$I_{CH_4}=(8/3)(1.09)^2(1.008)=3.1936$$

$$I_{(CH_3)_4C}=4I_{CH_4}+(8/3)(1.54)^2(16.042)-(8/3)(0.45)^2(1.008)=113.684.$$

Then for neohexane (center of gravity as origin),

$$I_{xx}=113.684+3.1936+(8/9)(1.54)^2(16.042)-(8/9)(1.09)^2(1.008)-(8/9)(0.45)^2(1.008)-(z_{cg})^2(86.172)=143.920$$

$$I_{yy}=113.684+3.1936+(1.54)^2(16.042)+(1.54)^2(72.146)-(1.09)^2(1.008)-(0.45)^2(1.008)-(x_{cg}{}^2+z_{cg}{}^2)(86.172)=192.656$$

$$I_{zz}=113.684+3.1936+(1/9)(1.54)^2(16.042)+(1.54)^2(72.146)-(1/9)(1.09)^2(1.008)-(1/9)(0.45)^2(1.008)-(x_{cg})^2(86.172)=165.613$$

$$I_{xz}=(1/3)(8/9)^{\frac{1}{2}}(0.45)^2(16.042)-(1/3)(8/9)^{\frac{1}{2}}(1.09)^2(1.008)-(1/3)(8/9)^{\frac{1}{2}}(0.45)^2(1.008)-(x_{cg})(z_{cg})(86.172)=37.705.$$

The complete (S) matrix may now be written using the formulas (33), (34), (35), and (28). Because of the symmetry of the tops, the B, C, and U quantities are all zero which greatly simplifies the work. The coupling term between two directly connected rotations ($\beta_{mn}{}^{i}$) reduces to $\alpha_{mn}{}^{zi}A_m$, i.e., the cosine of the angle between the two axes multiplied by the moment of the higher ordered group.

$$(S)=\begin{array}{c}\\ (x)\\ (y)\\ (z)\\ (2a)\\ (3a)\\ (3b)\\ (3c)\\ (2b)\end{array}\begin{array}{c}\begin{array}{cccccccc}(x) & (y) & (z) & (2a) & (3a) & (3b) & (3c) & (2b)\end{array}\\ \begin{bmatrix}143.92 & 0 & -37.71 & 110.490 & 1.0645 & 1.0645 & 1.0645 & -1.0645\\ 0 & 192.66 & 0 & 0 & 0 & 2.6076 & -2.6076 & 0\\ -37.71 & 0 & 165.61 & 0 & 3.0110 & -1.5055 & -1.5055 & -3.0110\\ 110.490 & 0 & 0 & 110.490 & 1.0645 & 1.0645 & 1.0645 & 0\\ 1.0645 & 0 & 3.0110 & 1.0645 & 3.1936 & 0 & 0 & 0\\ 1.0645 & 2.6076 & -1.5055 & 1.0645 & 0 & 3.1936 & 0 & 0\\ 1.0645 & -2.6076 & -1.5055 & 1.0645 & 0 & 0 & 3.1936 & 0\\ -1.0645 & 0 & -3.0110 & 0 & 0 & 0 & 0 & 3.1936\end{bmatrix}\end{array}.$$

We now diagonalize about I_{xx}, I_{yy}, and I_{zz} by three successive applications of Eq. (32) obtaining the (D) matrix.

$$(D)=\begin{array}{c} \\ (2a) \\ (3a) \\ (3b) \\ (3c) \\ (2b) \end{array}\begin{array}{c}\begin{array}{ccccc}(2a) & (3a) & (3b) & (3c) & (2b)\end{array}\\ \begin{bmatrix} 20.283 & -0.3643 & 0.4753 & 0.4753 & 1.4288 \\ -0.3643 & 3.1162 & 0.0180 & 0.0180 & 0.0774 \\ 0.4753 & 0.0180 & 3.1407 & 0.0180 & -0.0180 \\ 0.4753 & 0.0180 & 0.0180 & 3.1407 & -0.0180 \\ 1.4288 & 0.0774 & -0.0180 & -0.0180 & 3.1162 \end{bmatrix}\end{array}.$$

We now have the kinetic energy matrix for internal rotation. In this case it is seen that the off-diagonal terms are relatively small. Since the determinant of D is the significant quantity, one compares the square of an off-diagonal element with the product of the corresponding diagonal elements. Dropping all of the off-diagonal elements affects the value of $[D]$ by about 3 percent or its square root by 1.5 percent. It is the square root which appears in the thermodynamic formulas. Considering the other errors inherent in this type of work the 1.5 percent is not serious and the present authors made this assumption in treating neohexane.[5] One can now take the diagonal elements as reduced moments of inertia for the various rotations and use the tables of I. This procedure also assumes that the potential energy contains no significant cross terms between the various rotations.

EXAMPLE B: *TRANS*-HEXENE-3

As our second example we shall use *trans*-hexene-3. This molecule contains two methyl rotations and two ethyl rotations. The latter are far from being symmetric tops and couple strongly through their large off-balance factors and parallel axes of rotation.

We shall calculate the reduced kinetic energy matrix for internal rotation for the configuration shown in Fig. 2, with the six carbon atoms all in the same plane. The origin of frame (1) is at the center of the C=C bond, with its z axis along the double bond, its x axis in the plane of the paper, and its y axis perpendicular to the plane of the paper, oriented upward. Frames $(2a)$ and $(2b)$ are located at the carbon atoms of the right and left CH_2, respectively. Frames $(3a)$ and $(3b)$ are located at the carbon atoms of the corresponding methyl groups.

The angles around the olefinic carbons are assumed to be 120°; the other (paraffinic) angles tetrahedral. For the C=C bond length we take 1.35A, for the C−C bonds 1.54A, and for the C−H bonds, 1.09A.

The necessary direction cosine are:

$$\alpha_{2a,1}=\begin{bmatrix} 1/2 & 0 & (3/4)^{\frac{1}{2}} \\ 0 & 1 & 0 \\ -(3/4)^{\frac{1}{2}} & 0 & 1/2 \end{bmatrix}=\begin{bmatrix} 0.500000 & 0 & 0.866025 \\ 0 & 1 & 0 \\ -0.866025 & 0 & 0.500000 \end{bmatrix}$$

$$\alpha_{3a,2a}=\begin{bmatrix} 1/3 & 0 & -(8/9)^{\frac{1}{2}} \\ 0 & 1 & 0 \\ (8/9)^{\frac{1}{2}} & 0 & 1/3 \end{bmatrix}=\begin{bmatrix} 0.333333 & 0 & -0.942809 \\ 0 & 1 & 0 \\ 0.942809 & 0 & 0.333333 \end{bmatrix}$$

$$\alpha_{3a,1}=\alpha_{3a,2a}\alpha_{2a,1}=\begin{bmatrix} 0.983163 & 0 & -0.182729 \\ 0 & 1 & 0 \\ 0.182729 & 0 & 0.983163 \end{bmatrix}$$

$$\alpha_{2b,1}=-\alpha_{2a,1}$$

$$\alpha_{3b,1}=-\alpha_{3a,1}$$

$$\alpha_{3b,2b}=\alpha_{3a,2a}.$$

The coordinates of the origins of frames $(2a)$ and $(2b)$ are

$$r_{2a,1}{}^{x}=-r_{2b,1}{}^{x}=-(3/4)^{\frac{1}{2}}(1.54)=-1.333679$$

$$r_{2a,1}{}^{y}=\quad r_{2a,1}{}^{y}=0$$

$$r_{2a,1}{}^{z}=-r_{2b,1}{}^{z}=(1/2)(1.54)+(1/2)(1.35)=1.445.$$

The moment of inertia of CH_4 (equal to the moment of CH_3 about its z axis) is given in the preceding example: 3.1936. The various moments of an ethyl group (frames $(2a)$ and $(2b)$) are calculated as follows:

$$A_2=2(3.1936)+(8/9)(1.54)^2(16.042)$$
$$-(8/9)(1.09)^2(1.008)-(8/9)(0.45)^2(1.008)=38.959$$

$$B_2=(1/3)(8/9)^{\frac{1}{2}}[(1.54)^2(16.042)$$
$$-(1.09)^2(1.008)-(0.45)^2(1.008)]=11.516$$

$$C_2=0$$

$$U_2{}^{x}=(8/9)^{\frac{1}{2}}[(1.54)(16.042)$$
$$-(1.09)(1.008)-(0.45)(1.008)]=21.828.$$

The rotation-rotation coupling terms are:

$$\beta_{2a,1}{}^{x}=-0.866025(38.959)-0.5(11.516)$$
$$-1.445(21.828)=-71.040$$

$\beta_{2a,1}{}^{y}=0$

$\beta_{2a,1}{}^{z}=0.5(38.959)-0.866025(11.516)$
$-1.333679(21.828)=-19.605$

$\beta_{3a,1}{}^{x}=0.182729(3.1936)=0.5836$

$\beta_{3a,1}{}^{y}=0$

$\beta_{3a,1}{}^{z}=0.983163(3.1936)=3.1398$

$\beta_{3a,2a}{}^{z}=0.333333(3.1936)=1.0645$

$\beta_{2b,1}{}^{i}=-\beta_{2a,1}{}^{i}$; $\beta_{3b,1}{}^{i}=-\beta_{3a,1}{}^{i}$

$\beta_{3b,2b}{}^{z}=\beta_{3a,2a}{}^{z}$.

The over-all moments of inertia can readily be calculated by the method explained in Example A. For example, I_{zz} is given by the following expression:

$I_{zz}=2(3/4)(1.09)^2(1.008)-2(3/4)(0.45)^2(1.008)$
$+2(3/4)(1.54)^2(16.042)-2[0.866025(1.54)$
$-0.182729(0.45)]^2(1.008)-2[0.866025(1.54)$
$-0.182729(1.09)]^2(1.008)+2[0.866025(1.54)$
$-0.182729(1.54)]^2(16.042)+4(3.1936)=101.106.$

The other moments are:

$$I_{xx}=353.059,\quad I_{yy}=441.391,\quad I_{xy}=-148.186,$$
$$I_{xz}=I_{yz}=0.$$

We have now calculated all of the terms that appear in the rotational submatrix of the complete kinetic energy matrix. It is not necessary to write the complete matrix down in order to calculate (S), the reduced matrix for over-all and internal rotation. From Eqs. (34) and (35) we see that the only terms that are modified are the diagonal elements for unbalanced internal rotation and the coupling terms between unbalanced rotations:

$J_{2a}=J_{2b}=A_2-(U_2{}^{x})^2/M=38.959$
$-(21.828)^2/156.216=35.909$

$\psi_{2a,2b}=(21.828)^2/156.216=3.050.$

The reduced rotational matrix is

$$(S)=\begin{array}{c}(x)\\(y)\\(z)\\(2a)\\(3a)\\(2b)\\(3b)\end{array}\begin{bmatrix} 353.059 & 0 & 148.186 & -71.040 & 0.583 & 71.040 & -0.583 \\ 0 & 441.391 & 0 & 0 & 0 & 0 & 0 \\ 148.186 & 0 & 101.106 & -19.605 & 3.140 & 10.605 & -3.140 \\ -71.040 & 0 & -19.605 & 35.909 & 1.0645 & -3.0501 & 0 \\ 0.583 & 0 & 3.140 & 1.0645 & 3.1936 & 0 & 0 \\ 71.040 & 0 & 19.605 & -3.0501 & 0 & 35.909 & 1.0645 \\ -0.583 & 0 & -3.140 & 0 & 0 & 1.0645 & 3.1936 \end{bmatrix}.$$

When (S) is reduced about I_{xx}, I_{yy}, and I_{zz} we have for the reduced internal rotational matrix:

$$(D)=\begin{array}{c}(2a)\\(3a)\\(2b)\\(3b)\end{array}\begin{bmatrix} 18.9348 & 0.4219 & 13.9242 & 0.6426 \\ 0.4219 & 2.9772 & 0.6426 & 0.2184 \\ 13.9242 & 0.6426 & 18.9348 & 0.4219 \\ 0.6426 & 0.2184 & 0.4219 & 2.9772 \end{bmatrix}.$$

One can now proceed to use these kinetic terms with an appropriate potential expression to calculate energy levels and thermodynamic function by the methods previously explained.

ACKNOWLEDGMENT

We wish to thank Mrs. Myra Kilpatrick and Mr. William Weltner for checking some of these calculations.

The Theory of Flame Propagation*

J. O. HIRSCHFELDER AND C. F. CURTISS
Naval Research Laboratory, Department of Chemistry, University of Wisconsin, Madison, Wisconsin
(Received March 16, 1949)

The characteristics of steady-state one-dimensional flames are expressed in terms of a set of first-order ordinary differential equations suitable for solution by differential analyzers or high speed digital computing devices. Arbitrary systems of chemical kinetics and reaction rates can be investigated. The effect of ambient temperature, pressure, heat transfer from the flame to the flame holder, diffusion of free radicals, thermal conductivity, etc., are easily estimated. The equations which we use are the ordinary hydrodynamic equations of change generalized to include the effect of the chemical reactions. In these the usual expressions for reaction rates are introduced, that is, the rate at which the composition would change in a closed vessel under the local conditions of temperature and density. Equations expressing the diffusion velocities in terms of the composition gradients are given. The flame holder has been idealized in the form of a porous plug through which the fuel can pass freely from left to right, but a semipermeable membrane prevents the product gases moving in the opposite direction. It is found that heat transfer to this flame holder is required to stabilize the position of the flame. The conditions obtained at the hot boundary are expressed parametrically in terms of the roots of a secular equation.

THE hydrodynamic equations are generalized to include diffusion and chemical kinetics. These equations must govern all flame phenomena including steady-state flames, ignition, and detonation. In this paper, we give detailed consideration to the equations describing the steady-state propagation of one-dimensional flames. These equations are reduced to a form suitable for solution by high speed digital computing devices. Because of diffusion, heat transfer, and the finite rate of chemical reactions, it is difficult to define the initial conditions of a flame. On this account it is necessary to introduce a mathematical idealization of a flame holder. The amount of heat absorbed by the flame holder determines the quenching distance and probably affects the stability. At the hot boundary there is a mathematical indeterminancy which can be removed by the use of L'Hospital's rule. The flame velocity is a characteristic of the equations solved in conjunction with the specified boundary conditions.

The following relations must be solved simultaneously: (1) Equation of state, (2) equation of motion, (3) equation for the conservation of energy, (4) one equation of continuity for each chemical component. The chemical kinetics appear only in the equations of continuity. In the general case, except for the equation of state, these relations are partial differential equations involving three space coordinates and time. The general equations are given in the Appendix A.

In this paper we consider the simpler case of a steady-state one-dimensional flame. Under these conditions all time derivatives vanish and since only one space coordinate is important, the equations become ordinary differential equations. The velocity of the gas on the cold side of the flame is the flame velocity. The physical conditions at the hot and cold boundaries can be satisfied only with a single flame velocity or a single mass rate flow. By imposing these requirements on the solution of the set of equations, one obtains a theoretical value of the flame velocity. Because the flame velocities are always small compared to the velocity of sound, the pressure drop across a flame is negligibly small.[1] For this reason we can assume that the pressure remains constant, ignore the equation of motion and simplify the remaining equations.

1. THE EQUATIONS OF CONTINUITY

The velocity with which component i is flowing is $v+V_i$, where v is the mass average rate of flow and V_i is diffusion velocity of i. From the definition of v it is clear that

$$\sum_i n_i m_i V_i = 0, \tag{1}$$

where n_i is the concentration of component i (moles per cm^3) and m_i is the molecular weight. We let K_i be the rate of production by chemical reaction of molecules of i (moles/cm^3 sec.). This is the same rate of the chemical reaction which would apply in a static reaction vessel under the local conditions of temperature and composition. The form of the dependence of K_i on temperature and composition depends upon the assumed kinetics of the reactions involved. This point will be discussed further in Section 4. In terms of these quantities the equations of continuity can be written

$$(d/dx)[n_i(v+V_i)]=K_i. \tag{2}$$

One rather simple result can be obtained immediately. Since mass is neither created nor destroyed by the chemical reactions, the K_i satisfy the relation

$$\sum_i m_i K_i = 0. \tag{3}$$

Multiplying each Eq. (2) by m_i, adding, and making use of Eqs. (1) and (3), we find

$$(d/dx)(\rho v)=0, \tag{4}$$

* This work was carried out under Navy Bureau of Ordnance Contract NOrd 9938.

[1] See Appendix B.

where ρ is the gas density defined by

$$\rho=\sum_i n_i m_i. \tag{5}$$

This is the over-all equation of continuity and integrates immediately to give

$$\rho v=M \text{ (a constant)}. \tag{6}$$

The constant of integration, M, is the mass rate of flow (g/cm² sec.). The solution of the set of flame equations will satisfy the physically required boundary conditions for only one value of M.

2. THE ENERGY BALANCE EQUATION

Let H_i be the enthalpy (internal energy plus RT) per mole of component i; let q be the total heat flux due to both thermal conductivity and to the transport of energy by diffusion; and let p be the pressure. The energy balance equation can then be written,[2]

$$\frac{d}{dx}[(\sum_i n_i v H_i)-pv]+\frac{dq}{dx}+p\frac{dv}{dx}=0. \tag{7}$$

Since we assume that the pressure variation is negligible, this equation is integrable. The constant of integration is evaluated from the conditions at the hot boundary of flame ($x=+\infty$), where q is zero. Letting the subscript m refer to conditions at the hot boundary, and replacing v by M/ρ, we obtain

$$\frac{q}{M}=\left[\sum_i \frac{n_i H_i}{\rho}\right]_m-\left[\sum_i \frac{n_i H_i}{\rho}\right]. \tag{8}$$

But q can also be expressed in terms of the heat flux due to thermal conductivity and that due to the energy transport by diffusion.

$$q=-\lambda\frac{dT}{dx}+\sum_i n_i H_i V_i. \tag{9}$$

Eliminating q from Eq. (8) we have the energy balance equation,

$$\frac{\lambda}{M}\frac{dT}{dx}=\sum_i \frac{n_i H_i}{\rho}\left(1-\rho\frac{V_i}{M}\right)-\left[\sum_i \frac{n_i H_i}{\rho}\right]_m. \tag{10}$$

3. THE DIFFUSION VELOCITIES

The problem is not completely formulated until an expression for the diffusion velocities is given. In a previous paper,[3] we obtained an expression for the diffusion velocities,

$$V_i=\frac{n^2}{\rho n_i}\sum_j m_j D_{ij}\frac{d}{dx}\left(\frac{n_j}{n}\right), \tag{11}$$

where (assuming the equation of state for a perfect gas)

$$n=\sum_i n_i=p/RT \tag{12}$$

is the total number of moles per cm.[3] The D_{ij} are not the usual diffusion constants for binary mixtures, $\mathfrak{D}_{ij}$, but they can be written in terms of the $\mathfrak{D}_{ij}$ and the composition.

The expression (11) for the diffusion velocities is too complicated for the present application. Instead we use the approximate form[3]

$$V_i=-\frac{n}{n_i}D_i\frac{d}{dx}\left(\frac{n_i}{n}\right), \tag{13}$$

where the D_i are given by

$$D_i=\left(1-\frac{n_i m_i}{\rho}\right)\Big/\sum_{j\neq i}\frac{n_j}{n\mathfrak{D}_{ij}}. \tag{14}$$

Equation (13) is exact in the case of binary mixtures and gives the correct diffusion velocity of any component of a general mixture which is present as a trace. In other cases it is still a good approximation. Inasmuch as it is the diffusion of active particles, such as atoms and free radicals, which are present in small quantities, that is important in the mechanism of flame propagation it seems reasonable to use the approximate form of the diffusion equation.[4]

4. THE WORKING EQUATIONS

At this point we have derived all of the basic relations: a set of continuity equations, the energy balance equation, and a set of diffusion velocity equations. From these equations one obtains the composition, temperature, and rate of diffusion of each component as a function of distance throughout the flame. These equations can be written in a somewhat simpler form by the introduction of new variables. As the composition variables we use the mole fraction of each component

$$y_i=n_i/n. \tag{15}$$

It is convenient to express the diffusion velocities in terms of a quantity I_i which is the rate of flow of component i in moles divided by the total mass rate of flow,

$$I_i=n_i(v+V_i)/M. \tag{16}$$

This gives

$$V_i=(MI_i/ny_i)-v. \tag{17}$$

In terms of the new variables the equations of coninuity, Eqs. 2, become

$$M(d/dx)I_i=K_i. \tag{18}$$

[2] Here we ignore a small viscosity term which remains even in the one-dimensional case. See Appendix A.

[3] C. F. Curtiss and J. O. Hirschfelder, J. Chem. Phys. **17**, 550 (1949).

[4] Because of the conditions imposed upon the V_i by Eq. (1) one should be careful not to use the entire possible set of D_i, i.e., the last one is left as undetermined so that Eq. (1) may be satisfied automatically. This does not cause any difficulties in the subsequent development.

The diffusion velocity equations, Eqs. (13), become

$$\frac{dy_i}{dx}=\frac{M}{nD_i}\left[\frac{ny_i}{\rho}-I_i\right]. \tag{19}$$

The energy balance equation, Eq. (10), becomes

$$\frac{\lambda}{M}\frac{dT}{dx}=\sum_i H_iI_i-\left[\sum_i \frac{n}{\rho}H_iy_i\right]_m. \tag{20}$$

The function K_i appearing in Eq. (18) is the rate of production of molecules of component i due to chemical reaction. The mechanism of the reactions occuring in the flame can be described in terms of a set of chemical reactions describing the actual processes. Each of these can be written in the form

$$\beta_{1j}[1]+\beta_{2j}[2]+\cdots\rightarrow\eta_{1j}[1]+\eta_{2j}[2]+\cdots, \tag{21}$$

the β_{ij} and η_{ij} being integers and the $[i]$ indicating species i. In general, a particular species will occur only on one side of the equation so that many of the β_{ij} and η_{ij} are zero. The rate of such a reaction can be written in the form

$$k_j(T)n_1^{\beta_{1j}}n_2^{\beta_{2j}}\cdots. \tag{22}$$

But since $n=p/RT$ is a function only of T we can also write the rate in the form

$$f_j(T)y_1^{\beta_{1j}}y_2^{\beta_{2j}}, \tag{23}$$

where

$$f_j(T)=k_j(T)n^{\Sigma\beta_{ij}}. \tag{24}$$

The rate at which species i is produced (or reacts) due to this particular reaction is

$$(\eta_{ij}-\beta_{ij})f_j(T)y_1^{\beta_{1j}}y_2^{\beta_{2j}}\cdots, \tag{25}$$

and consequently the total rate of production of component i by chemical reaction is

$$K_i=\sum_j(\eta_{ij}-\beta_{ij})f_j(T)y_1^{\beta_{1j}}y_2^{\beta_{2j}}\cdots. \tag{26}$$

If the system consists of g different atomic species then there are g linear relations among the K_i which lead to g linear relations among I_i. These relations are due to the fact that the total amount of each element present is conserved in a chemical reaction. Let ν_{ik} be the number of atoms of species k in a molecule of i. Then from Eq. (21) and the conservation of atomic species, k, we have for the reaction, j,

$$\sum_i \nu_{ik}\beta_{ij}=\sum_i \nu_{ik}\eta_{ij}. \tag{27}$$

Thus multiplying each of Eqs. (26) by ν_{ik} and summing over i, one finds[5]

$$\sum_i \nu_{ik}K_i=0. \tag{28}$$

Then if we multiply Eq. (18) by ν_{ik}, sum over i, and integrate, we obtain the g relations

$$\sum_i \nu_{ik}I_i=\alpha_k, \quad k=1, 2, \cdots g, \tag{29}$$

where the α_k are integration constants to be fixed by the initial composition of the gas. These relations may be used to reduce the number of I_i variables appearing in any specific problem.

The quantities, f_j, H_i, D_i, λ, and $n=p/RT$, are taken to be known functions of T. Then since ρ is given by Eq. (5) as

$$\rho=n\sum_i m_iy_i, \tag{30}$$

the Eqs. (18), (19), and (20) are sufficient (except for boundary conditions, to be discussed in Section 5) to determine all the y_i, I_i, and T as functions of x. However, it is convenient to reduce the number of equations by one by taking T rather than x as the independent variable. In this way we obtain the working equation:

$$\frac{d}{dT}I_i=\frac{\lambda K_i}{M^2\left[\sum_j H_jI_j-\left(\sum_i \frac{n}{\rho}H_jy_j\right)_m\right]}, \tag{31}$$

and

$$\frac{dy_i}{dT}=\frac{\lambda\left(\frac{n}{\rho}y_i-I_i\right)}{nD_i\left[\sum_j H_jI_j-\left(\sum_i \frac{n}{\rho}H_jy_j\right)_m\right]}. \tag{32}$$

The characteristics of one-dimensional steady-state flames are determined by the integration of Eqs. (31) and (32) simultaneously. The integrations are started at the hot boundary. The initial conditions are discussed in the following section. The value of M is obtained by requiring that the solution satisfy the physical conditions imposed at the cold boundary. In numerical solutions, one obtains M by a successive trial and error procedure.

5. THE BOUNDARY CONDITIONS

We first discuss the boundary conditions in terms of the original problem, i.e., taking x to be the independent variable. From these conditions we obtain the boundary conditions on the equations in which T is the independent variable. At the hot boundary, indicated by a subscript m, all of the fuel has burned and an equilibrium has been established between the fuel and its combustion products. As x approaches infinity, T, y_i, and I_i approach the finite values T_m, $(y_i)_m$, and $(I_i)_m$ asymptotically. Hence,

$$(dT/dx)_m=0, \tag{33}$$

$$(dy_i/dx)_m=0, \tag{34}$$

and

$$(dI_i/dx)_m=0, \tag{35}$$

[5] The relation (3) is of course contained in this set.

and since the diffusion velocity is zero,

$$I_{i_m}=\left(\frac{n}{\rho}y_i\right)_m. \tag{36}$$

These conditions are sufficient to describe a solution to the set of equations. However, one further condition (at the cold boundary) is physically specified. It is this condition which leads to the fact that a satisfactory solution is obtained for only one value of the parameter M.

Conditions at the cold boundary are somewhat more difficult to describe since it is not physically reasonable to separate the flame from the "flame holder" from which it originates. However, the existence of a flame holder is certainly not compatible with a one-dimensional treatment. Thus it is necessary to introduce a somewhat artificial concept to replace the physical flame holder. We first notice two important properties of the flame equations: first, since the reaction rate expressions give a finite rate at the initial temperature, it is necessary to start the solution at a finite value of x; and secondly, since the reaction rate is finite, the concentration gradients are finite and molecules of the product tend to diffuse back past this initial point. These two properties are physically rather unimportant, yet they introduce a mathematical problem which must be considered in describing the cold boundary condition. We picture the flame holder as consisting of a semipermeable membrane; a membrane permeable to the molecules of the fuel gas and inert constituents, but completely impermeable to the product molecules. In this way product molecules are prevented from diffusing back past the initial point. Let the subscript "0" refer to conditions within the mixing chamber or immediately before the membrane, and the subscript "c" to indicate conditions just outside the plug where the flame front really begins. The rate of flow of each component, $n_i(v+V_i)$, is the same on both sides of the membrane. But before the membrane the composition is constant so that the diffusion velocities are zero. Hence,

$$[n_i(v+V_i)]_c=(n_iv)_0, \tag{37}$$

or from the definitions, Eqs. (15) and (16),

$$(I_i)_c=\left(\frac{n}{\rho}y_i\right)_0. \tag{38}$$

It should be noticed from Eq. (16) that

$$\left(\frac{n}{\rho}y^i\right)_c=\left(\frac{n}{\rho}y^i\right)_o\Big/\left[1-\frac{V_i\rho}{M}\right]_c, \tag{39}$$

so that the gas on the flame side of the membrane does not have the exact composition of the fuel mixture. The slight jump in the composition variables is due to the semipermeable nature of the membrane. However, the diffusion velocities near the membrane are small compared to the gas velocity so that $V_i\rho/M\ll 1$ and the jumps in the y_i are extremely small.

The flame holder has one further property. It acts as a heat sink. From Eq. (9) we see that the heat flux through the initial point $(-q_0)$ is

$$-q_0=[\lambda(dT/dx)]_0. \tag{40}$$

The value of $(-q_0)$ is taken to be a property of the flame holder. The maximum flame temperature, T_m, is then determined from the conservation of energy equation, Eq. (20), where T is set equal to T_0.

$$-q_0=\left(\lambda\frac{dT}{dx}\right)_0$$

$$=M\left[\left(\sum_i\frac{n}{\rho}H_iy_i\right)_0-\left(\sum_i\frac{n}{\rho}H_iy_i\right)_m\right]. \tag{41}$$

The composition variables, $(y_i)_0$, and the temperature T_0 are the initial conditions specified by the nature of the problem. The composition at the hot boundary is that characteristic of chemical equilibrium at the temperature T_m. Hence Eq. (41) is an equation for T_m in terms of the $(y_i)_0$, T_0, and the heat lost to the flame holder $(-q_0)$.

Let us consider Eqs. (31) and (32) in which T is the independent variable. The cold boundary condition, Eq. (38), remains unchanged in form. But for the hot boundary conditions in place of Eqs. (33), (34), and (35) we must obtain expressions for all of the dy_i/dT and all of the dI_i/dT. We notice that at T_m all of the K_i are zero since chemical equilibrium has been established. It is then clear that the left sides of both Eqs. (31) and (32) are indeterminant. Thus we must apply L'Hospital's rule, and find that at $T=T_m$,

$$\frac{d}{dT}(I_i)=\frac{1}{M^2z}\left[A_i+\sum_k J_{ik}\frac{dy_k}{dT}\right], \tag{42}$$

where

$$A_i=\lambda\sum_j(\eta_{ij}-\beta_{ij})\frac{df_j}{dT}y_1^{\beta_{1j}}y_2^{\beta_{2j}}\cdots, \tag{43}$$

$$J_{ik}=\lambda\sum_j(\eta_{ij}-\beta_{ij})f_j\frac{\beta_{kj}}{y_k}y_1^{\beta_{1j}}y_2^{\beta_{2j}}\cdots, \tag{44}$$

and

$$z=\frac{d}{dT}\left[\sum_i H_iI_i-\left(\sum_i\frac{n}{\rho}H_iy_i\right)_m\right], \tag{45}$$

or

$$z=\sum_i\left[I_i\frac{dH_i}{dT}+H_i\frac{d}{dT}(I_i)\right]. \tag{46}$$

It is convenient to consider z to be another variable and to consider the differential equation, Eq. (46), to be an additional equation. We thus obtain a parametric solution. Applying L'Hospital's rule to Eq. (32) we find that

at the hot boundary,

$$\frac{dy_i}{dT}=\frac{\lambda RT}{pD_iz}\left[\frac{d}{dT}\left(\frac{n}{\rho}y_i\right)-\frac{d}{dT}(I_i)\right]. \tag{47}$$

The derivative of I_i can be eliminated between Eqs. (42) and (47). The resulting equation is linear in the dy_j/dT,

$$\sum_j\left[\left(\frac{n}{\rho}-zb_i\right)M^2z\delta_{ij}-J_{ij}-\left(\frac{n}{\rho}\right)^2m_jy_iM^2z\right]\frac{dy_j}{dT}=A_i, \tag{48}$$

where

$$b_i=\frac{p}{RT}\frac{D_i}{\lambda}. \tag{49}$$

In a similar way we find from Eqs. (42) and (46)

$$\sum_j L_j\frac{dy_j}{dT}=M^2z^2-N_0M^2z-Q_0, \tag{50}$$

where

$$L_j=\sum_i H_iJ_{ij}, \tag{51}$$

$$N_0=\sum_i (n/\rho)y_i(dH_i/dT), \tag{52}$$

and

$$Q_0=\sum_i A_iH_i. \tag{53}$$

Equations (48) and (50) form a set which is just sufficient to determine all of the dy_j/dT and z. However, from the definition of the y_j we know that

$$\sum_j (dy_j/dT)=0. \tag{54}$$

Equation (48) is consistent with Eq. (54).[6] It is convenient to eliminate one dy_j/dT from Eq. (48) and consider one less equation in the set. A solution may then be made for the remaining dy_j/dT. Let us eliminate dy_1/dT from the set through the relation

$$dy_1/dT=-\sum_{j>1}(dy_j/dT). \tag{54'}$$

Thus, from Eq. (48),

$$\sum_{j>1}\left[\left(\frac{n}{\rho}-zb_i\right)M^2z(\delta_{ij}-\delta_{i1})-J_{ij}+J_{i1}-\left(\frac{n}{\rho}\right)^2(m_j-m_1)y_iM^2z\right]\frac{dy_j}{dT}=A_i. \tag{55}$$

Similarly, from Eq. (50) we obtain

$$\sum_{j>1}(L_j-L_1)dy_j/dT=M^2z^2-N_0M^2z-Q_0. \tag{56}$$

[6] Provided the D_i form a consistant set. See reference 3.

We use all but one of the set of Eqs. (55) (ignoring $i=1$) and Eq. (56) to determine the dy_j/dT ($j\neq1$) and z. The equations are linear in the dy_j/dT and hence z can be obtained as the solution of the secular equation

$$|S_{ij}|=0, \tag{57}$$

where

$$S_{11}=Q_0+N_0zM^2-z^2M^2, \tag{58}$$

$$S_{1j}=L_j-L_1, \qquad j=2,3,4\cdots, \tag{59}$$

$$S_{i1}=A_i, \qquad i=2,3,4\cdots, \tag{60}$$

and

$$S_{ij}=(J_{ij}-J_{i1})+\frac{n}{\rho}\left[\frac{n}{\rho}(m_j-m_1)y_i-\delta_{ij}\right]M^2z+b_i\delta_{ij}z^2M^2, \quad i=2,3,4\cdots, \quad j=2,3,4\cdots. \tag{61}$$

Having obtained z, we can obtain the $dy_j/dT(j\neq1)$ from Eq. (55) (using $i=2,3,4\cdots$). Then dy_1/dT is obtained from Eq. (54) and all of the dI_i/dT from Eq. (42). In this way we obtain the boundary conditions to be applied in solving the flame equations, Eqs. (31) and (32).

The authors wish to thank W. P. Spaulding, M. L. Henkel and Harry Hummel for help in developing the present theory. At the present time W. P. Spaulding, M. L. Henkel, R. Vandervort, and P. Knaplund are trying to obtain numerical solutions for a few specific examples.

APPENDIX A

In this appendix we give the general hydrodynamic equations of change. The set of flame equations discussed in this paper is a special case of the more general case corresponding to one-dimensional steady-state flow. The equations are:

1. The equations of continuity,

$$(\partial n_i/\partial t)+\nabla\cdot[n_i(v+V_i)]=K_i.$$

2. The equation of conservation of energy,

$$\frac{\partial}{\partial t}\sum_i n_iE_i+\nabla\cdot\left[\sum_i n_iH_i(v+V_i)-\lambda\nabla T\right]=v\cdot\nabla p-\tfrac{2}{3}\eta(\nabla\cdot v)^2+2\eta\Phi:\nabla v.$$

Here E_i is the internal energy per mole of component i, η is the coefficient of viscosity, Φ is the symmetric tensor,

$$(\phi_{ij})=\frac{1}{2}\frac{\partial v_i}{\partial x_j}+\frac{1}{2}\frac{\partial v_j}{\partial x_i},$$

and the : indicates the product of two tensors defined by

$$w:y=\sum_{ij}W_{ij}Y_{ij}.$$

3. The equation of motion,

$$\rho\frac{\partial v}{\partial t}+\rho v\cdot\nabla v=-\nabla\cdot p-\tfrac{2}{3}\nabla(\eta\nabla\cdot v)+2\nabla\cdot\eta\Phi.$$

APPENDIX B

In the one-dimensional steady-state case, ignoring viscosity, the equation of continuity becomes

$$\rho v dv/dx=-dp/dx.$$

In this case $\rho v = M$ is a constant and we have, after integration,

$$\rho v^2 = -p + \text{constant}.$$

Indicating the cold side of the flame by subscript "0" and hot side by "m" we have

$$\rho_m v_m^2 - \rho_0 v_0^2 = p_0 - p_m.$$

The velocity of sound in a gas is

$$c = (\gamma p/\rho)^{\frac{1}{2}}.$$

Using this to eliminate the ρ_0 and ρ_m we find

$$\frac{p_m}{p_0} = \frac{1+\gamma(v_0^2/c_0^2)}{1+\gamma(v_m^2/c_m^2)}.$$

The ratio of specific heats, γ, is only slightly larger than unity and in the case of ordinary flames the ratio v/c is small. Hence, p_m/p_0 never varies much from unity and we can ignore variations in the pressure throughout the flame.

To amplify this point, let us consider a typical case. A flame velocity of the order of 30 cm/sec. is usual. This is the velocity of the cold gas relative to the flame front. Since the temperature rises by a factor of about 10, the velocity of the hot gases relative to the flame front is about 300 cm/sec. The velocity of sound in gases at ordinary temperatures is about 3×10^4 cm/sec. The velocity of sound goes up as the square root of T and thus in the hot gases c is about 9×10^4 cm/sec. Taking $\gamma=1.3$ these figures result in

$$p_m/p_0 = 1+1.69\times10^{-6}-1.88\times10^{-5} = 1-1.71\times10^{-5}.$$

Thus the pressure drop through a flame at 1 atmos. pressure is about 0.01 mm of mercury.

It should be pointed out that although variations in the pressure are unimportant in this problem, in the case of a real three-dimensional flame the small variations may be important in determining the geometrical shape of the flame front.

THE JOURNAL OF CHEMICAL PHYSICS VOLUME 17, NUMBER 11 NOVEMBER, 1949

Self-Diffusion in Argon*

FRANKLIN HUTCHINSON
*Sloane Physics Laboratory, Yale University,** New Haven, Connecticut*

(Received March 9, 1949)

The self-diffusion coefficient of argon was measured at five different temperatures between −183°C and 53.5°C by observing the diffusion of radioactive A^{41} into normal argon. The decrease in the observed diffusion coefficient caused by the larger mass of A^{41} was deduced and found to be 0.6 percent. The experimental values are compared with several theoretical calculations. In particular, it is shown that use for argon of an inverse power model ($V \propto r^{-\nu}$), with different values of ν ascribed to different temperature ranges, is not permissible since widely different values of ν at the same temperature can be obtained from different experimental data. The experimental figures agree very well with numerical calculations by Hirschfelder, Bird, and Spotz based on an interaction potential of the form $4E[-(r_0/r)^6+(r_0/r)^{12}]$.

THE rate at which different gases intermingle is usually described by a diffusion coefficient which in general depends on the intermolecular force fields of the diffusing molecules. Enskog and Chapman have derived expressions which relate the value of the diffusion coefficient to these interaction potentials. A knowledge of the values of the coefficients thus enables something to be said about the forces between the diffusing molecules. For this purpose the case of self-diffusion—i.e., all molecules involved being the same—is much the most satisfactory to consider. Only a single type of interaction has to be considered; there is no variation of the coefficient with relative concentration; and the potential function involved, that between like molecules; is usually of greater interest, being also involved in the equation of state and in the coefficients of viscosity and thermal conductivity.

Of course, there is really no such thing as a self-diffusion coefficient for a gas. By definition a self-diffusion coefficient describes the interdiffusion of identical molecules; but since the molecules are identical there is no way of following the course of the diffusion, and therefore no process actually takes place. Now suppose that the molecules of one of the gases differ only very slightly from those of the other gas—a good example would be molecules having the nucleus of one atom in a metastable state only a little above the ground state. The progress of these molecules through normal molecules could be followed, and if the mass of the molecule containing the metastable nucleus were increased only a very small amount, the diffusion coefficient thus measured could be identified with the self-diffusion coefficient calculated classically on the assumption that the origin of each molecule could be determined at any time.

This paper describes measurements at several temperatures of the diffusion of radioactive A^{41} through ordinary argon, which is more than 99 percent A^{40}. The difference in mass between these two molecules is of course quite appreciable, but the next section shows how the "true" self-diffusion coefficient of either isotope may be deduced from results in a case where the diffusing molecules differ only in mass.

* Part of a dissertation presented to the faculty of the Graduate School of Yale University in candidacy for the degree of Doctor of Philosophy.

** Assisted in part by the ONR under Contract N6ori-44.

DEPENDENCE OF DIFFUSION ON MASS OF DIFFUSING MOLECULES

Chapman and Cowling[1] give a first approximation for the coefficient of diffusion D of gas 1 into gas 2

$$D=\frac{3}{16}\frac{kT}{\mu n\Omega^{(1)}(1)}, \tag{1}$$

where

$$\Omega^{(l)}(q)=(kT)^{-q-1}\left(\frac{\pi}{\mu kT}\right)^{\frac{1}{2}}\int_0^\infty e^{-(w^2/kT)}w^{2q+3}dw \times\int_0^\infty(1-\cos^l\chi)bdb, \tag{2}$$

$$w=(\mu/2)^{\frac{1}{2}}g.$$

μ = reduced mass of the system (molecule 1 + molecule 2), $=m_1m_2/(m_1+m_2)$,
g = relative speed of the colliding molecules before impact,
n = total number of molecules per unit volume.

χ is the angle through which the relative velocity of the two colliding molecules is rotated by the collision for a given impact parameter b, and is given by the expression

$$\chi=\pi-2b\int_{r_0}^\infty\frac{dr}{r\left(\left(1-\frac{V(r)}{w^2}\right)r^2-b^2\right)^{\frac{1}{2}}}, \tag{3}$$

where r_0 is the largest real solution of

$$\left(1-\frac{V(r_0)}{w^2}\right)r_0^2=b^2, \tag{4}$$

and $V(r)$ is the potential function describing the interaction of molecules 1 and 2. It is to be noticed from Eqs. (2), (3), and (4) that for a given $V(r)$ the integral in $\Omega^{(l)}(q)$ depends only on the temperature, so that we can write

$$D=f(T)/n\mu^{\frac{1}{2}}, \tag{5}$$

$f(T)$ depending on $V(r)$. Thus from information on the diffusion of one isotope of a gas into another, $V(r)$ being the same no matter which isotope, we can calculate the correction to be applied to get the classical self-diffusion constant describing the process taking place with negligible difference in the molecular weights. Since Chapman and Cowling's first approximations to the transport coefficients are remarkably close[2] any corrections calculated from (5) will be almost exact.

Experimental data on the diffusion of hydrogen and deuterium can be used to check Eq. (5). Heath *et al.*[3] found that the diffusion constant for deuterium into hydrogen $D_{HD}=1.24$ cm²/sec. at 15°C and one atmosphere. From the data of Harteck and Schmidt[4] we can find that the constant describing the diffusion of parahydrogen into orthohydrogen is $D_{HH}=1.40$ cm²/sec. at the same temperature and pressure. This gives the experimental ratio $D_{HH}/D_{HD}=1.40/1.24=1.13$. From Eq. (5) the calculated ratio is

$$D_{HH}/D_{HD}=(\tfrac{2}{3}/\tfrac{1}{2})^{\frac{1}{2}}=1.15,$$

agreeing with the experimental value to within the experimental error.

Inserting the appropriate figures in (5) we find that the "true" self-diffusion coefficient for A^{40} can be obtained by multiplying the observed diffusion coefficient for the diffusion of A^{41} into A^{40} by 1.006.

THE EXPERIMENTAL MEASUREMENTS

Measurement of D at Room Temperature

The measurement of D at room temperature has already been reported.[5] A recalculation of the data leads to a slightly higher value for the diffusion constant of A^{41} into A^{40}, 0.425 ± 0.003 cm²/sec. at 32 cm Hg, 22°C. Using the well-established fact that D is proportional to n^{-1} and the isotope correction factor (1.006) we find

$$D=0.180\pm0.001 \text{ cm}^2/\text{sec.}$$

at 76.0 cm Hg, 22°C, for A^{40}. The error given is the probable error calculated from the scatter of the data.

Measurement of D at Other Temperatures

The apparatus used to measure D at other than room temperature is shown in Fig. 1 and was suggested by the apparatus used by Ney and Armistead.[6] Two chambers each of about 100 cc volume were connected by a straight tube 0.475 cm diameter and 2.85 cm long drilled through a steel block containing a valve which could close off the connecting tube. The entire apparatus was set in a well-stirred bath held at the appropriate temperature, the valve being operated from outside the bath through a metal bellows. In use, with the valve closed one chamber was filled with tank argon, the other with argon containing A^{41}, each at about one atmosphere pressure. The filling was done through capillaries with a total volume less than 1/20 percent of either chamber, making diffusion in and out of the filling tubes a negligible effect. Opening the valve allowed the gases to intermingle, the relative amount of A^{41} in either chamber at any time being determined by the ion current drawn to an insulated electrode inserted into each chamber. Radioactive material in one chamber did not cause an appreciable amount of ionization in the other because the steel block stopped all the 1.18 Mev β-rays from A^{41}, the 1.37 γ-ray causing only a very small fraction of the ionization. A negligible amount of radiation

[1] S. Chapman and T. G. Cowling, *The Mathematical Theory of Non-uniform Gases* (Cambridge University Press, London, 1939), p. 165.
[2] See reference 1, p. 196. See also the last section of this paper.
[3] Heath, Ibbs, and Wild, Proc. Roy. Soc. **A178**, 380 (1941).
[4] P. Harteck and H. W. Schmidt, Zeits. f. physik. Chemie **B21**, 447 (1933).
[5] F. Hutchinson, Phys. Rev. **72**, 1256 (1947).
[6] E. P. Ney and F. C. Armistead, Phys. Rev. **71**, 14 (1947).

could pass through the connecting tube. The collecting voltage was 90 volts, well above the voltage necessary to collect essentially all the ions formed. The currents were in the range 10^{-11}–10^{-12} amperes and were measured by the voltage drop across a 10^{11} ohm resistor. A null method was employed, a vacuum tube electrometer using a Western Electric D-96475 indicating when the variable reference voltage equaled the potential drop across the high resistance.

The voltage V due to the ion current from each electrode passing through the 10^{11} ohms was directly proportional to the average concentration $\bar{c}$ of A^{41} in the corresponding chamber. Denoting the chamber to which a quantity refers by the subscripts 1 and 2

$$V_1=\alpha_1\bar{c}_1, \quad V_2=\alpha_2\bar{c}_2, \tag{6}$$

where α_1 and α_2 are constants. Now

$$\frac{d}{dt}(\bar{c}_1\tau_1)=-\lambda\bar{c}_1\tau_1-AD(\partial c/\partial x), \tag{7}$$

where τ_1 is the volume of chamber 1, λ the radioactive decay constant, A the area of the connecting tube, and $\partial c/\partial x$ the concentration gradient along the axis of the connecting tube at the midpoint. A similar equation can be written for the other chamber and combining gives

$$\frac{d}{dt}(\bar{c}_1-\bar{c}_2)=-\lambda(\bar{c}_1-\bar{c}_2)-\left(\frac{A}{\tau_1}+\frac{A}{\tau_2}\right)D\frac{\partial c}{\partial x}. \tag{8}$$

A plausible assumption is that after the initial very steep gradients have passed away

$$\partial c/\partial x=\theta(\bar{c}_1-\bar{c}_2), \tag{9}$$

where θ is a constant; for a very long thin tube θ would equal the reciprocal of the length of the tube. Substituting this in (8)

$$d/dt(\bar{c}_1-\bar{c}_2)=-(\lambda+\beta)(\bar{c}_1-\bar{c}_2)$$
$$\beta\equiv(A/\tau_1+A/\tau_2)\theta D=KD, \tag{10}$$

or using (6) and integrating,

$$\ln\left(V_1-\frac{\alpha_2}{\alpha_1}V_2\right)=-(\lambda+\beta)t+\text{const.} \tag{11}$$

The ratio α_2/α_1 was determined to be 0.983 by filling both chambers with the same sample of radioactive argon (i.e., making $\bar{c}_1=\bar{c}_2$), measuring the voltages corresponding to each chamber, and using Eq. (6). In a diffusion experiment V_1 and V_2 were measured as a function of time. Plotting $\log[V_1-(\alpha_2/\alpha_1)V_2]$ against time as in Fig. 2, a straight line was obtained, from the slope of which the value of β could be found. λ was set equal to 1.041×10^{-4} sec.$^{-1}$, corresponding to a half-life of 110.8 minutes as determined by a special experiment.

To get D from the experimental values of β four runs were made at room temperature as listed in Table I. The values of β were corrected to 76.0 cm Hg pressure and 22°C by assuming that D, and hence β, varied inversely as the density and as $T^{1.8}$. This last correction was deduced from measurements of the variation of viscosity with temperature,[7] and from the experimental data later obtained was found to be quite accurate enough for the small corrections involved. Each value of β thus obtained was divided by the value for D at room temperature, 0.180 cm^2/sec., giving the values of K listed in Table I. If θ is assumed equal to (tube length)$^{-1}$, K becomes 1.31×10^{-3} cm^{-2}, showing that this assumption is not too bad an approximation.

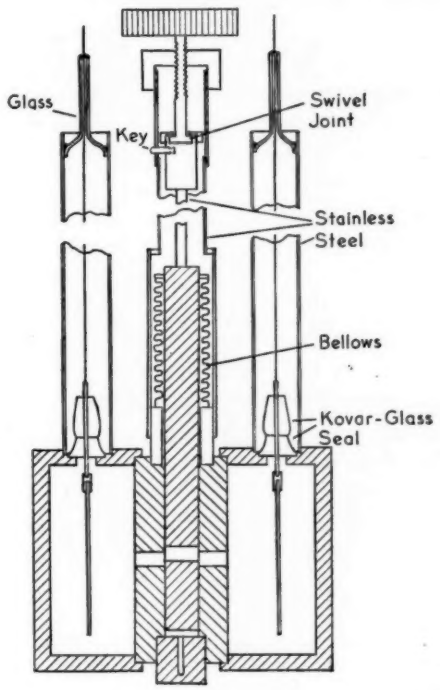

FIG. 1. Apparatus used to measure temperature variation of self-diffusion coefficient D.

If K were strictly a constant the diffusion coefficient at any temperature could be obtained by dividing the observed value of β by K. Actually, K might vary with temperature because (a) θ might involve D, which certainly varies with temperature, and (b) it depends on the dimensions of the apparatus, which also change with temperature.

Considering the second point first, it is easy to show, using the approximation given above for θ and the handbook values of the thermal expansion coefficients of the materials involved in the tube length, τ, and A, that K should be multiplied by the factor $[1-42\times10^{-6}(t-22)]$, where t is the temperature in °C. This correction was made for each point, although at no temperature used did it exceed one percent.

We can show that θ does not depend on D in the following way. The fundamental equation obeyed by c,

[7] See reference 1, p. 223.

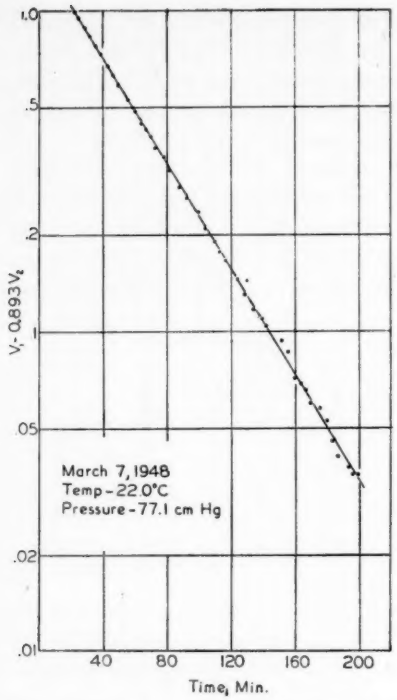

FIG. 2. Typical plot of experimental data for one run. The ordinate, proportional to the difference in A^{41} concentration in the two chambers, is plotted on a logarithmic scale. The scatter in the data is about that usually observed.

the concentration of A^{41}, is

$$\partial c/\partial t = D\nabla^2 c - \lambda c, \tag{12}$$

or writing $c \equiv ge^{-\lambda t}$, $u \equiv Dt$,

$$\partial g/\partial u = \nabla^2 g. \tag{13}$$

Inserting the appropriate boundary conditions, the solution to this equation is

$$c = g(u)e^{-\lambda t}. \tag{14}$$

It is obvious that any dependence of θ on D must be through the parameter u. But the experimental data as exemplified by Fig. 2 show that β, and therefore θ, does not depend on time. θ, then, cannot depend on u, and so does not involve D.

The experimental results at different temperatures are given in Table II. The values of D given are corrected to 76.0 cm Hg in the same way as explained above. The point to be looked on with the greatest suspicion is of course the one at −183°C. Measurement here is more difficult than at the higher temperatures because D is so small that β is only a fraction of λ, and since it is the sum $\lambda+\beta$ which is directly measured, the percent error in D is high. In addition, chilling the valve to this temperature caused it to jam; it was ruined in the process of freeing it, and thus additional measurements were prevented. The error attached to it is that which might be expected in view of the scatter from run to run observed at other temperatures.

The errors listed for the mean values of D at the other temperatures are the probable errors calculated by taking into account the spread in the data and the probable errors in the various parameters used in the calculations, including the value of D at room temperature. There was no way to estimate any systematic errors, the most important possibly being the effects of a small amount (believed less than 0.4 percent) of contaminating gases in the argon. The biggest part of the systematic error is probably in the value of D at room temperature, and since the relative changes in D with temperature are independent of this quantity, these relative changes are more accurate than the absolute values.

COMPARISON WITH THEORY

A quantity of much interest in the kinetic theory of gases is the dimensionless ratio $\epsilon \equiv \rho D/\eta$, where ρ is the density and η the viscosity of the gas. Table III gives the experimental values of ϵ taking the figures for ρ and η from the literature. The first approximation for this quantity given by kinetic theory is[8]

$$\epsilon = \tfrac{3}{5}\Omega^{(2)}(2)/\Omega^{(1)}(1), \tag{15}$$

where $\Omega^{(l)}(q)$ is given by (2).

If the interaction potential $V(r)$ of two colliding molecules is known, then D and ϵ can be calculated by using Eqs. (1), (2), (3), (4), and (15). $V(r)$ is not known exactly; however, by substituting various types of $V(r)$ into these equations and comparing the calculated with the experimental values of D and ϵ some idea can be obtained of the suitability of the assumed type of interaction potential.

Interaction Potential $V(r) = A/r^{\nu}$

A repulsive potential of this type has been much used in kinetic theory because it leads to expressions for the transport coefficients which can be handled analytically. Thus it can be shown[9] that for this model at constant pressure $D \propto T^{s+1}$, $s = \frac{1}{2} + 2/(\nu-1)$, and that ϵ lies between 1.2 and 1.551, depending on the value of ν, with no dependence on temperature. From the first relation it follows that a plot of log$D$ against log$T$ should yield a straight line. Figure 3 shows that this is not so, even in the high temperature region. Also, it is probable that the variation in ϵ with temperature for the first four

TABLE I. Experimental values of K.

Temperature °C	Pressure cm Hg	K cm^{-2}
22.0	76.4	1.212×10^{-3}
23.2	76.9	1.183
22.0	77.1	1.197
21.6	77.7	1.213
	mean	$(1.201\pm0.005)\times10^{-3}$

[8] See reference 1, p. 198.
[9] See reference 1, pp. 172, 248.

TABLE II. Experimental values of D.

Temperature °C	Pressure cm Hg		D (corrected) cm²/sec.
53.5	77.9		0.2144
	77.5		0.2082
	77.2		0.2125
		mean	0.212±0.002
0	78.1		0.1568
	76.5		0.1590
		mean	0.158±0.002
−78.5	69.6		0.0835
	72.3		0.0844
	76.7		0.0820
		mean	0.0833±0.0009
−183	77.1		0.0277±0.0010

TABLE III. Experimental values of ϵ.

Temp. °C	D cm²/sec.	ρ[a] g/cm³	η[b] g/cm-sec.	ϵ
53.5	0.212	1.490×10^{-3}	0.2435×10^{-3}	1.30
22	0.180	1.650	0.2240	1.32
0	0.158	1.783	0.2104	1.34
−78.5	0.0833	2.508	0.1555	1.34
−183	0.028	5.75	0.0765	2.1

[a] Calculated from the density at STP given by the International Critical Tables (1933) and the compressibility data given by L. Holborn and J. Otto, Zeits. f. Physik **30**, 320 (1924). Density at −183° from data by Mathias, Onnes, and Crommelin, Com. Phys. Lab. Leiden, No. 131a (1912) and C. A. Crommelin, Com. Phys. Lab. Leiden, No. 138c (1913).
[b] H. L. Johnston and E. R. Grilly, J. Phys. Chem. **46**, 948 (1942). Viscosity at 53.5°C from A. O. Rankine, Proc. Roy. Soc. **84**, 181 (1910).

points as given in Table III is real. Thus this assumed interaction potential does not agree well with experiment.

Because this form of interaction potential leads to comparatively simple analytical expressions for the transport coefficients, attempts to extend its use are often made by assuming that equations based on it are valid over small temperature ranges, an "effective ν" being used as an index of the manner in which the molecular interaction varies with separation. For example, from the variation of D or η[7] with temperature in the vicinity of 15°C it can be readily calculated that either variation corresponds to a ν of about 8. Thus argon would be regarded as a "soft" molecule whose interaction field at room temperature could be approximated by a potential varying as r^{-8}. But the effective value of ν could just as well be calculated from the value found for $\epsilon(=1.33)$, which gives ν equal to 16! $\nu=8$ corresponds to $\epsilon=1.45$, which differs from the experimental value by much more than the margin of error. We conclude that the common method of retaining this simple molecular model and defining an "effective ν" which varies with the temperature is not a valid procedure and can sometimes lead to incorrect results.

The Sutherland Model

Sutherland used as his model of two colliding gas molecules a system consisting of two elastic spheres with a weak attractive field varying as $r^{-\nu'}$ between them. With this assumption it is found that[10] $D \propto T^{5/2}/(T+S_D)$, where S_D is a constant depending on the fields, and $\epsilon=1.2(1+[S_\eta-S_D]/T)$, S_η being another constant obtained from the variation of viscosity with temperature. Taking[11] $S_\eta=142$, Table IV compares the experimental and calculated values of D and ϵ with $S_D=115$.

The good fit between experimental and calculated values (except at −183°C) does not mean that the simple Sutherland model can be taken as a literal picture of an argon molecule. From the derivation of the Sutherland equations it can be seen that S_D and S_η are each equal to the potential energy of two argon molecules in contact multiplied respectively by functions $i_1(\nu')$, $i_2(\nu')$ tabulated by Chapman and Cowling.[10] From the values of S_D and S_η, as well as their difference as determined by the values of ϵ, it can be determined that the attractive potential field falls off more rapidly than r^{-10}, perhaps as r^{-16}, which is much more rapid than can be understood on physical grounds. Furthermore, the calculated attractive potential energy of two molecules in contact is greater than the mean thermal energy of a molecule at 500°C, which would lead one to expect aggregation of molecules at temperatures where none is observed. The Sutherland equation is perhaps best regarded as a simple interpolation formula.

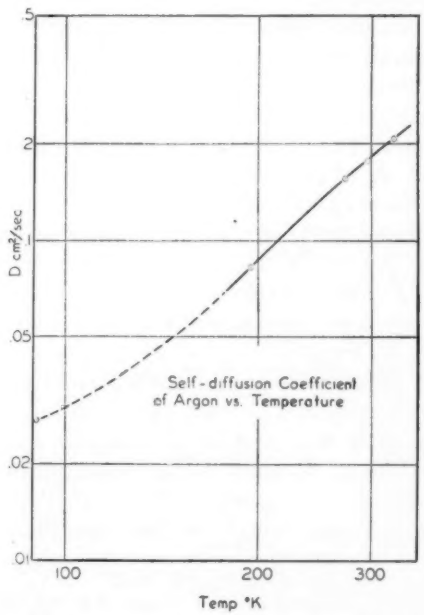

FIG. 3. Log-log plot of D against temperature.

[10] See reference 1, p. 184.
[11] M. Trautz and H. E. Binkele, Ann. d. Physik **5**, 561 (1930); A. O. Rankine, Proc. Roy. Soc. **84**, 181 (1910).

TABLE IV. Calculation of D and ϵ on Sutherland model.

Temperature °C	D, cm²/sec. calc.	expt.	ϵ calc.	expt.
53.5	0.214	0.212	1.30	1.30
22	0.179	0.180	1.31	1.32
0	0.156	0.158	1.32	1.34
−78.5	0.0837	0.0833	1.37	1.34
−183	0.018	0.028	1.6	2.1

TABLE V. Amdur's calculated values for D.

Temperature °C	D, cm²/sec. calc.	expt.
17	0.133	0.175
−3	0.118	0.155
−83	0.0650	0.0794

TABLE VI. Hirschfelder's calculated values of D.

Temperature °C	D, cm²/sec. calc.	expt.	Δ
53.5	0.213	0.212	0.0029
22.0	0.178	0.180	0.0024
0.0	0.154	0.158	0.0018
−78.5	0.0820	0.0833	0.0007
−183.0	0.0178	0.028	0.0001

Interaction Potential $V=Ae^{-ar}-Cr^{-6}-Dr^{-8}-Er^{-10}$

Amdur[12] has recently calculated the transport coefficients for various gases, including argon, using the more realistic potential given above. The parameters a, A, C, D, E, were derived from theoretical calculations of the polarizability of atoms and from the equation of state of argon. This potential is much too complicated to yield analytic expressions for the transport coefficients, and Amdur uses approximation methods to obtain his numerical results. The calculated values of D are compared with experiment in Table V. The computed values are about twenty percent low, which is a somewhat larger difference between theory and experiment than is found for the coefficients of viscosity and thermal conductivity. The reason for these discrepancies could lie either in the values chosen for the parameters describing the interaction potential or in the approximations made in solving for the transport coefficients.

Interaction Potential $V=4E[-(r_0/r)^6+(r_0/r)^{12}]$

Hirschfelder, Bird, and Spotz[13] have selected a potential of this form, the term in r^{-6} being the Van der Waals attraction, that in r^{-12} being a good empirical fit to calculated repulsions due to overlapping electron clouds. This potential was used as the basis for a complete numerical integration to obtain values of the integrals $\Omega^{(l)}(q)$, said to be accurate to one part in 300. For argon, the most accurate values for E and r_0, $E=124.0k$, and $r_0=3.418$A, can be obtained from the variation of viscosity with temperature, and agree excellently with values deduced from the equation of state of argon. The calculated D's in Table VI, obtained by using these values of E and r_0, agree very well with experiment. Thus this form of potential is consistent with this diffusion data. It is significant that no arbitrary constants have been adjusted to fit this particular set of figures.

Since Hirschfelder *et al.* have calculated a number of the $\Omega^{(l)}(q)$ it is also possible to compute the second approximation to D, equal to the first approximation given by Eq. (1) multiplied by $1/(1-\Delta)$. For the case under consideration, where the two molecular species have almost the same molecular weight, the expression for Δ given by Chapman and Cowling[1] can be simplified to

$$\Delta=\frac{5(C-1)^2}{11-4B+8A}, \tag{16}$$

where A, B, and C are functions of the $\Omega^{(l)}(q)$ as given by Chapman and Cowling. The column labelled Δ in Table VI gives the calculated value of this correction. A point of interest is the smallness of Δ, the correction added in the second approximation; the implication is that the first approximation is a very good one.

The calculated values of D at −183°C deviate in every case much more from experiment than do calculated values of the viscosity[14] at the same temperature. Thus it is not too easy to ascribe the discrepancy in D at low temperatures to quantum effects, etc. Indeed, it throws definite suspicion on this measurement at −183°C; nevertheless, there is no indication in the data taken at this point that there was anything wrong, and no reason for taking this run any less seriously than the others except for the somewhat higher percentage error due to the smallness of β compared with λ.

ACKNOWLEDGMENTS

It is with the greatest pleasure that I acknowledge my debt to Prof. E. C. Pollard, who suggested the problem originally, and who has been a constant source of encouragement and help during the work. I would also like to thank the General Electric Educational Fund for the award of a Charles A. Coffin Fellowship for the period in which this work was done.

[12] I. Amdur, J. Chem. Phys. **16**, 190 (1948).
[13] Hirschfelder, Bird, and Spotz, J. Chem. Phys. **16**, 968 (1948).
[14] See, for example, reference 1, p. 228; H. L. Johnston and E. R. Grilly, J. Phys. Chem. **46**, 948 (1942); W. Licht, Jr. and D. G. Stechert, J. Phys. Chem. **48**, 23 (1944).

Heats of Dissociation of Carbon-Hydrogen Bonds in Methane and Its Radicals

K. J. LAIDLER AND E. J. CASEY*
Department of Chemistry, The Catholic University of America, Washington, D. C.
(Received March 14, 1949)

The evidence pertaining to the heat of sublimation of graphite is summarized, with the conclusion that the value of 170.6 kcal. per mole is the most probable. This figure is consistent with a value of 393 kcal. for the heat of removing the four hydrogen atoms from methane, the assignment of the heats of the successive dissociations being as follows:

$CH_4 = CH_3 + H - 101$ kcal.
$CH_3 = CH_2 + H - < 87$ kcal.
$CH_2 = CH + H - > 125$ kcal.
$CH = C(^3P) + H - 80$ kcal.

The limits to the values for the second and third processes are determined on the basis of the kinetics of the reaction between sodium and methylene chloride. The methylene appearing above is in its lowest state, a singlet state in which the bonding to the hydrogen atoms is through p-orbitals of atomic carbon, the bond containing a certain amount of ionic character. It is suggested that the formation of CH_2 in a triplet excited state, in which the bonding to the hydrogen atoms is through sp hybrid orbitals of atomic carbon, corresponds to the following thermochemical values:

$CH_3 = CH_2^* + H - 106$ kcal.
$CH_2^* = CH + H - 106$ kcal.

From this suggestion it follows that the energy of excitation of the methylene "molecule," the lowest state (singlet), to the methylene "diradical," the triplet excited state, is at least 19 kcal. The evidence for the existence of the two states is discussed.

INTRODUCTION

THERE has now accumulated a considerable amount of evidence which points to the following mutually consistent thermochemical values:

$$C_{graphite} = C_{gas}(^3P) - 170.6 \text{ kcal.} \quad (1)$$

$$CO(^1\Sigma^+) = C_{gas}(^3P) + O(^3P) - 256 \text{ kcal.} \quad (2)$$

$$C_{gas}(^3P) + 4H(^2S) = CH_4 + 393 \text{ kcal.} \quad (3)$$

In support of these figures are the following facts:

(1) The most reliable direct determinations of the heat of sublimation of graphite, involving both static and dynamic methods, give a value in the neighborhood of 170 kcal.; some of the results are summarized in Table I. It may be mentioned that in 1924 Kohn and Gückel[1] obtained a value of 147 kcal., but that this is inconsistent with other direct measurements and with the spectroscopic data, to be considered later. The first reliable value is that of Marshall and Norton,[2] while the recent value of Brewer, Gilles, and Jenkins[3] appears to be very accurate.[4]

(2) The spectrum of carbon monoxide leaves a choice between the values of 256.1, 210.8, and 159.7 kcal. for the heat of dissociation, D(CO), of carbon monoxide into $C(^3P)$ and $O(^3P)$.[5] This heat of dissociation can be related to the heat of sublimation of graphite by the following well-established thermochemical relations:[6]

$$C(\text{graphite}) + \tfrac{1}{2}O_2 = CO + 27.2 \text{ kcal.}, \quad (4)$$

$$\tfrac{1}{2}O_2 = O - 58.6 \text{ kcal.}, \quad (5)$$

and the heats of sublimation so calculated on the basis of the three spectroscopic values for D(CO) are given in Table II. The heat of reaction (3) can be calculated from the heat of sublimation using the following values:[6]

$$C(\text{graphite}) + 2H_2 = CH_4 - 16.0 \text{ kcal.}, \quad (6)$$

$$H_2 = 2H - 103.2 \text{ kcal.} \quad (7)$$

The possible values for reaction (3) consistent with the possible spectroscopic values for D(CO) are included in Table II. Of the three spectroscopic values for D(CO), the second, 210.8 kcal., was favored by G. Herzberg,[5] but A. G. Gaydon and W. G. Penney[7] have pointed out

TABLE I. Heats of sublimation of graphite.

Authors	Type of method	Heat of sublimation
Marshall and Norton*	dynamic	177 kcal.
Brewer, Gilles, and Jenkins**	static	170.4 kcal.

* See reference 2.
** See reference 3.

TABLE II. Equivalent thermochemical values.

D(CO) per mole	Heat of sublimation of graphite per mole	Heat of formation of CH_4 from $C(^3P)$ and $4H(^2S)$
256.1 kcal. (11.11 ev)	−170.6 kcal.	+393.1 kcal.
210.8 kcal. (9.14 ev)	−125.0 kcal.	+347.5 kcal.
157.9 kcal. (6.92 ev)	−72.1 kcal.	+294.6 kcal.

* Now a Postdoctoral Fellow of the National Research Council of Canada, Ottawa, Ontario.

[1] Kohn and Gückel, Zeits. f. Physik **27**, 305 (1924).

[2] A. L. Marshall and F. J. Norton, J. Am. Chem. Soc. **55**, 431 (1924).

[3] Brewer, Gilles, and Jenkins, J. Chem. Phys. **16**, 797 (1948).

[4] This value has been criticized by L. H. Long, J. Chem. Phys. **16**, 1078 (1948), whose arguments have been answered by L. Brewer, J. Chem. Phys. **16**, 1165 (1948).

[5] G. Herzberg, Chem. Rev. **20**, 145 (1947).

[6] All thermochemical values are referred to 0°K, and are taken from *Selected Values of Chemical Thermodynamic Properties*, National Bureau of Standards publication.

[7] A. G. Gaydon and W. G. Penney, Proc. Roy. Soc. **A183**, 347 (1945); A. G. Gaydon, *Dissociation Energies* (Chapman and Hall, Ltd., London, 1947).

that if the non-crossing rule for potential-energy curves of the same multiplicity holds, the value 256.1 kcal. must be accepted. This is a compeling argument, as the non-crossing rule has a sound theoretical basis,[8] and does not appear to be violated by any other molecule.

(3) N. V. Sidgwick and H. D. Springall[9] have shown that the strengths of the C-Hg links in $Hg(CH_3)_2$, $Hg(C_2H_5)_2$, and $Hg(C_6H_5)_2$, together with thermochemical data, provide evidence for the set of highest values.

(4) Calculations by G. J. Kynch and W. G. Penney[10] of the excitation energies of benzene, butadiene, and hexatriene lead to the same set of highest values.

On the other hand, some objections to this set of highest values have been suggested. Herzberg, Herzfeld, and Teller[11] suggested that the activation energy for the sublimation of carbon may be about 1.5 times the energy of dissociation; this could lead to the value of 125 kcal. for the heat of sublimation. However, this argument cannot apply to the equilibrium measurements of Brewer *et al.* Another objection relates to the possibility that the carbon in the above equations should be in the tetravalent (^5S) state: these arguments will now be considered.

THE TETRAVALENT (^5S) CARBON ATOM

In discussing this problem a number of authors[12, 13] have concluded that since tetravalent carbon compounds may be regarded as being related to the carbon in an excited (^5S) state, in which a $2s$ electron has been promoted to the $2p$ orbital to give the configuration $(1s)^2(2s)(2p)^3$, the carbon atom occurring in Eqs. (1), (2), and (3) must be regarded as being in the ^5S state. In particular, Long and Norrish[13] have postulated that the ^5S state is 65 kcal. higher than the lowest state, (^3P), and taking the heat of sublimation of carbon to be 190 kcal., obtain 190−65=125 kcal. for the heat of sublimation to the ^3P state. By the same argument the energy of dissociation of carbon monoxide to C(^3P) and O(^3P) is reduced to about 210 kcal., which has been seen to correspond to one of the values suggested by spectroscopic data. However, there are serious difficulties associated with this interpretation: (1) this argument of Long and Norrish was originally advanced to explain Marshall and Norton's value for the heat of sublimation, which, involving a rate measurement, in reality is the energy of activation of the sublimation process: this value might, therefore, refer to the formation of carbon in an intermediate ^5S state, which subsequently falls to the ground state with emission of radiation. The argument is not applicable to equilibrium experiments, in which it can hardly be supposed that ^5S carbon is involved. (2) Even if the equilibrium measurements were discounted, there remains a serious objection to the supposition that carbon sublimes to the ^5S state. The energy of excitation of C(^3P) to the (^5S) state is now known to be 95.9 kcal.;[14] the assumption that graphite sublimes to the ^5S state with heat of 170 kcal./mole reduces the heat of sublimation to the ^3P state to 74 kcal., which would require a much higher vapor pressure than has ever been recorded. (3) The fact that carbon when tetravalent can be regarded as in a ^5S state does not imply that when dissociation occurs the carbon remains in this state; in fact, such an assumption is contrary to what is known about the mechanisms of non-adiabatic reactions.[15] This can be seen most easily for the diatomic molecule CO, the electronic states of which have been discussed by Gaydon and Penney.[7] Although the carbon atom is in the tetravalent state, the lowest state of the molecule CO is ($^1\Sigma^+$), and this dissociates into C(^3P). This argument applies equally well to the more complicated situation existing when solid carbon is sublimed; the lowest potential energy surface for solid carbon, although correlating with C(^5S), will actually give rise to C(^3P) when dissociation of the bonds in solid carbon occurs.

DISSOCIATION ENERGIES OF METHANE AND ITS RADICALS

On the basis of the conclusion, which has been seen to be very highly probable, that the value of 393 kcal. refers to the complete dissociation of methane into C(^3P) and 4H(^2S), it remains to consider how this figure should be divided among the individual steps. Of the four processes corresponding to the successive removal of hydrogen atoms, the heats of two, the first and last, are known with some certainty. The values are as follows:

$$CH_4 = CH_3 + H - 101 \text{ kcal.}, \quad (8)$$

$$CH(^2\Sigma) = C(^3P) + H(^2S) - 80 \text{ kcal.} \quad (9)$$

The first of these figures was obtained by G. B. Kistiakowsky *et al.*[16] using a kinetic procedure involving the bromination of methane. Support for this value is rendered by the work of Polanyi *et al.* on the pyrolysis of methyl iodide[17] and by Stevenson's electron impact

[8] J. von Neumann and E. P. Wigner, Physik. Zeits. **30**, 467 (1927).
[9] N. V. Sidgwick and H. D. Springall, Nature **156**, 599 (1945).
[10] K. G. Kynch and W. G. Penney, Proc. Roy. Soc. **A179**, 214 (1941).
[11] Herzberg, Herzfeld, and Teller, J. Phys. Chem. **41**, 325 (1937).
[12] R. Schmid and L. Gero, Zeits. f. physik. Chemie **B36**, 105 (1937).
[13] L. H. Long and R. G. W. Norrish, Nature **157**, 468 (1946); Proc. Roy. Soc. **A187**, 337 (1946).
[14] A. G. Shenstone, Phys. Rev. **72**, 411 (1947); cf., B. Edlen, Zeits. f. Physik **84**, 746 (1933); Nature **159**, 129 (1947); R. F. Backer and S. Goudsmit, Phys. Rev. **46**, 948 (1934).
[15] Glasstone, Laidler, and Eyring, *The Theory of Rate Processes* (McGraw-Hill Book Company, Inc., New York, 1941), Chapter VI.
[16] Andersen, Kistiakowsky, and Van Artsdalen, J. Chem. Phys. **10**, 305 (1942); E. R. Van Artsdalen, J. Chem. Phys. **10**, 653 (1942); H. G. Andersen and G. B. Kistiakowsky, J. Chem. Phys. **11**, 6 (1943); G. B. Kistiakowsky and E. R. Van Artsdalen, J. Chem. Phys. **12**, 469 (1944).
[17] E. T. Butler and M. Polanyi, Nature **146**, 129 (1940); Trans. Faraday Soc. **39**, 19 (1943); E. C. Baughan and M. Polanyi,

data.[18] The second value, 80.0 kcal., for the heat of dissociation of CH in its lowest state ($^2\Sigma$) was obtained by G. Herzberg[19] from spectroscopic data. These two values, together with the value 393 kcal. for the complete dissociation of methane, lead to

$$CH_3=CH+2H-212 \text{ kcal.} \quad (10)$$

It now remains to consider how the value 212 kcal. is to be divided between the processes $CH_3=CH_2+H$ and $CH_2=CH+H$.

The Methylene Radical

The only positive experimental information that we have been able to discover regarding the energy of the lowest state of CH_2 is found in the work of C. E. H. Bawn and W. J. Dunning,[20] and this gives only a lower limit to the energy of dissociation of the CH_2 molecule. These workers found that the reaction between sodium vapor and methylene chloride is strongly chemiluminescent, emitting the sodium D line. By analogy with many other reactions of this type,[21] the mechanism is most probably

$$Na+CH_2Cl_2=NaCl+CH_2Cl \quad (11)$$

$$Na+CH_2Cl=NaCl^*+CH_2 \quad (12)$$

$$NaCl^*+Na=NaCl+Na^* \quad (13)$$

in which scheme the sodium chloride molecule NaCl* is vibrationally excited and the sodium atom Na* is electronically excited. Since electronic excitation of sodium requires 48.3 kcal., it follows that reactions (11) and (12), with the formation of normal NaCl, must jointly be exothermic by at least this amount; that is,

$$2Na+CH_2Cl_2=2NaCl+CH_2+>48.3 \text{ kcal.}$$

This equation, together with

$$CH_4+2Cl=CH_2Cl_2+2H-40.4 \text{ kcal.} \quad (14)$$

and

$$NaCl=Na+Cl-97.7 \text{ kcal.}, \quad (15)$$

gives rise to

$$CH_4=CH_2+2H-<188 \text{ kcal.} \quad (16)$$

With Eq. (8) this gives

$$CH_3=CH_2+H-<87 \text{ kcal.} \quad (17)$$

and

$$CH_2=CH+H->125 \text{ kcal.} \quad (18)$$

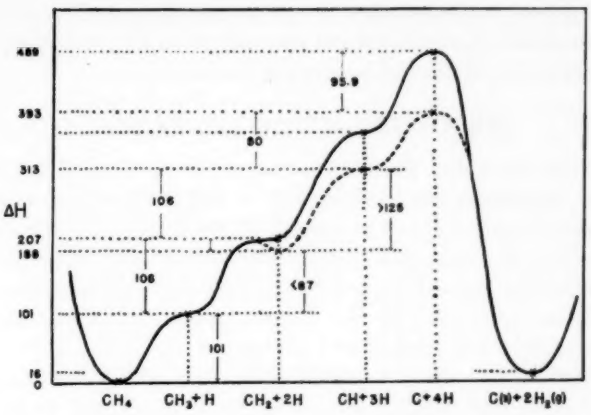

FIG. 1. Schematic representation of the energy levels of CH_4 and its radicals with respect to the gaseous carbon and hydrogen atoms.

Although only a lower limit to the energy of dissociation of methylene has been determined, the results imply that the CH_2 is considerably more stable with respect to removal of a hydrogen atom than is CH_3. This is consistent with our previous conclusion,[22] arrived at on the basis of the shape,[23] that the lowest state of methylene is a singlet state in which the bonds to hydrogen are formed by p-orbitals of carbon, and have considerable ionic character. This means that when an additional hydrogen atom is added to CH_2, promotion of a carbon $2s$ electron to a $2p$ atomic orbital must occur, followed by sp^2 hybridization. The stability due to hybridization is not sufficient to offset the energy required for promotion, so that CH_3 is less stable to dissociation into CH_2+H than is CH_2 to dissociation into $CH+H$. It is to be noted that this point of view differs from that of A. D. Walsh,[24] who has recently discussed the problem: according to him CH_2 is in a triplet state in which each hydrogen atom is held to the carbon through a carbon sp hybrid atomic orbital. This interpretation necessitates that promotion occur during the reaction $CH+H=CH_2$ rather than during the reaction $CH_2+H=CH_3$. It appears that our interpretation is preferable in view of the fact that it is consistent not only with the shape of CH_2 but also with the results of Bawn and Dunning.

The energy levels of CH_3, CH_2, CH, and C with respect to methane are represented schematically in Fig.

TABLE III. Heats of dissociation.

Reaction	Values proposed above ($L=170$)	Voge's values ($L=170$)	Values using ($L=125$)	Voge's values ($L=125$)
$CH_4=CH_3+H$	101	109	101	101
$CH_3=CH_2+H$	<87	124	<87	87
$CH_2=CH+H$	>125	80	>80	80
$CH=C+H$	80	80	80	80

Nature **146**, 685 (1940); Trans. Faraday Soc. **37**, 648 (1941); E. C. Baughan, Nature **147**, 542 (1941); Baughan, Evans, and Polanyi, Trans. Faraday Soc. **137**, 377 (1941).

[18] D. P. Stevenson, J. Chem. Phys. **10**, 291 (1942); J. Am. Chem. Soc. **65**, 209 (1943); D. P. Stevenson and J. A. Hipple, J. Am. Chem. Soc. **64**, 1588, 2766 (1942); J. A. Hipple and D. P. Stevenson, Phys. Rev. **63**, 121 (1943).

[19] G. Herzberg, *Molecular Spectra and Molecular Structure I, Diatomic Molecules* (Prentice-Hall, Inc., New York, 1939).

[20] C. E. H. Bawn and W. J. Dunning, Trans. Faraday Soc. **35**, 185 (1939).

[21] See M. Polanyi, *Atomic Reactions* (Williams and Norgate, London, 1932).

[22] K. J. Laidler and E. J. Casey, J. Chem. Phys. **17**, 213 (1949).

[23] G. Herzberg, Rev. Mod. Phys. **14**, 195 (1942).

[24] A. D. Walsh, Faraday Soc. Discussion **2**, 18 (1947).

1, some of the features of which are suggested by the electronic configurations of the radicals and of analogous molecules; these will be discussed later.

THE EXCITED METHYLENE RADICAL

On surveying the literature concerning the reactions of the methylene radical, one is struck by the inconsistencies in behavior depending upon the manner in which the radical is produced. In our opinion these differences are due to the fact that methylene is produced sometimes in the singlet ground state, and is relatively unreactive, and sometimes in the triplet excited state, and is highly reactive. Thus Pearson, Purcell, and Saigh,[25] producing methylene from diazomethane at 450°C, found that the radical has a comparatively long life, and concluded from this that it is in a singlet state. Belchetz and Rideal[26] found CH_2 at a distance less than the mean free path from a hot carbon filament in methane, and F. O. Rice and A. L. Glasebrook[27] found no CH_2 at greater distances; the CH_2 so formed is apparently more reactive than that in the work of Pearson *et al.*, and is probably in the excited triplet state, a diradical. Recent work of R. G. W. Norrish[28] has indicated high reactivity, presumably because the CH_2 was produced in the excited state.

The high reactivity of methylene in the excited state indicates that reactions such as

$$CH_2^* + CH_4 = 2CH_3,$$

must have little activation energy and hence be not endothermic; together with Eq. (8) this implies that the reaction $CH_3 = CH_2^* + H$ must be endothermic by at least 102 kcal.

A further indication as to the energy level of the excited methylene diradical may be obtained on the basis of the analogy between the C—H bond in the methyl radical and the C—H bond in ethylene, in both of which structures the carbon atom has sp^2 hybridization. This means that the removal of a hydrogen atom from CH_3 to give CH_2 in the triplet state might be expected to require approximately the same energy as is necessary to remove a hydrogen atom from C_2H_4 to give the excited ethylidine radical, in which the C=C—H angle is 180°.

The force constant of the C—H bond in a molecule is derived from the curvature of the potential-energy surface near its position of minimum energy. The lowest stable state of C_2H_4 is known to contain carbon atoms which are in a hybridized ^5S state; in such a molecule the C—H bond vibrational energy levels in the vicinity of minimum energy are such as to be related to dissociation products in which the unsaturated carbon atom is still in the ^5S state. Hence, the C—H force constant in ethylene is related to excited ethylidine $CH_2=C-H$, in which the unsaturated carbon atom forms two sp hybrid orbitals, diametrically opposed, a structure clearly analogous to that of CH_2^*, the methylene diradical. On the basis of the C—H force constant and interatomic distance in ethylene, a value of ~106 kcal. for the dissociation energy of the bond has been deduced; this then very probably refers to the dissociation to give C_2H_3 in the triplet excited state. By this analogy, then, we tentatively assume that this value also applies to the dissociation of the methyl radical to give methylene in the triplet excited state, viz.

$$CH_3 = CH_2^* + H - 106 \text{ kcal.} \qquad (19)$$

This value leads to the relation

$$CH_2^* = CH + H - 106 \text{ kcal.} \qquad (20)$$

From this it follows that the energy of excitation of the methylene molecule to the triplet excited state, the diradical, is at least 19 kcal.

POTENTIAL ENERGY SURFACE FOR THE COMPLETE DISSOCIATION OF METHANE

These values for the successive heats of dissociation of methane and its radicals may be used to construct a schematic potential-energy surface for the complete dissociation of methane; this is shown in Fig. 1. In this diagram, surfaces related to carbon in the ^5S state are represented by full lines, and those for carbon in the ^3P state by broken lines. It is to be noted that carbon in methane and in methyl is necessarily in the ^5S state, but that when a hydrogen is removed from CH_3 the lowest state of CH_2 is reached by a crossing over to the singlet state, in which the carbon is in the ^3P state; this will probably involve a potential energy maximum between CH_3 and CH_2. It follows from this that there will be an activation energy associated with the addition of a hydrogen atom to CH_2 in the ground state. The addition of hydrogen to $C(^3P)$, CH, CH_3, and to CH_2 in the excited state will, however, probably not require any activation energy.

The scheme proposed here differs from previous ones in various respects. It differs from those of Gero,[12] Long and Norrish,[13] and Walsh,[24,29] in accepting the value of 170 kcal. as applying to the heat of sublimation of graphite to give ^3P carbon. It further differs from that of Walsh[24] in that the lowest state of CH_2 is taken to be the singlet state, containing ^3P carbon; according to Walsh, the transition $C(^5S) \rightarrow C(^3P)$ occurs at $CH_2 \rightarrow CH$. Reference may also be made to the recent papers of Gero and Valatin,[30] who assume the energy of the C—H bond in CH_2 to be the same as that of the secondary

[25] Pearson, Purcell, and Saigh, J. Chem. Soc. 409 (1938).
[26] Belchetz, Trans. Faraday Soc. **30**, 170 (1934); Belchetz and Rideal, J. Am. Chem. Soc. **56**, 1168 (1935); *ibid.*, p. 2466.
[27] F. O. Rice and A. L. Glasebrook, J. Am. Chem. Soc. **56**, 2381 (1934).
[28] R. G. W. Norrish and G. Porter, Faraday Soc. Discussions **2**, 96 (1947).
[29] A. D. Walsh, Trans. Faraday Soc. **43**, 60 (1947).
[30] L. Gero, J. Chem. Phys. **16**, 1011 (1948); L. Gero and J. G. Valatin, *ibid.* **16**, 1014 (1948); J. G. Valatin, *ibid.* **16**, 1018 (1948).

bonds of hydrocarbons; since the carbon atoms in the latter have sp^3 hybridization while the carbon in CH_2 binds hydrogens through p atomic orbitals, there is clearly no justification for this view.

Voge[31] has made quantum-mechanical calculations of the C—H bond strengths, obtaining values which are not consistent with the present values. Such calculations can be expected to give only orders of magnitude when it is remembered the assumptions which have to be made. The present conclusions, being based on a theoretical interpretation of reliable experimental data, seem to us to have a firmer basis than conclusions arrived at on the basis of purely theoretical computations. However, it must be mentioned that the acceptance of 125 kcal. for the heat of sublimation of carbon would have led us to a set of values which are quite consistent with those favored by Voge. This might be regarded as an argument in favor of the lower value, but in view of the points raised earlier we prefer the higher one. Our results and those of Voge are listed for comparison in Table III.

[31] H. H. Voge, J. Chem. Phys. **4**, 581 (1936); **16**, 984 (1948).

THE JOURNAL OF CHEMICAL PHYSICS VOLUME 17, NUMBER 11 NOVEMBER, 1949

Role of Hydrogen Peroxide in the Thermal Combination of Hydrogen and Oxygen

R. B. Holt and O. Oldenberg
Lyman Physical Laboratory, Harvard University, Cambridge, Massachusetts

(Received March 21, 1949)

Hydrogen peroxide was identified as an intermediate product in the steady thermal combination of hydrogen and oxygen near 540°C by an examination of the absorption spectrum of the reacting mixture. The absorption at a particular wave-length (2537A) was then used in a quantitative study of the variation of hydrogen peroxide concentration in the reacting mixture as a function of conditions. The results obtained were compared with those obtained by chemical analysis of the gas mixture. The commonly accepted mechanism of the reaction proposed by Lewis and von Elbe is applied to the interpretation of the results obtained.

I. PROBLEM

THE reaction mechanism of the thermal combination of hydrogen and oxygen to form water has been the subject of a very considerable amount of work in recent years. An important part of this work has been the investigation of the intermediate products of the reaction, since an accurate knowledge of what these products are and the relative role and importance of each of them is necessary to an adequate reaction theory. Previous work indicated two definite facts concerning the thermal combination of hydrogen and oxygen at a total pressure of about one atmosphere and at temperatures in the vicinity of 540°C; first, that free hydroxyl (which might logically have been expected as an important intermediate product) does not accumulate in the reaction mixture to an appreciable extent,[1] and second, that hydrogen peroxide is present in fairly large amounts in the exit gases when a mixture of hydrogen and oxygen is passed through a hot reaction vessel under proper conditions.[2]

At the time the present investigation was undertaken, there was no very reliable basis for deciding whether or not the hydrogen peroxide found in the exit gases was present as such in the reacting mixture. Early studies of the thermal decomposition of hydrogen peroxide vapor[3] had indicated an appreciable decomposition even at temperatures below 100°C, although more recent studies[4] showed that, under proper conditions, the molecule is relatively stable to much higher temperatures in the presence of oxygen or nitrogen, but undergoes a reaction with hydrogen at elevated temperatures. Furthermore, it had been noted that the hydrogen peroxide observed as a result of pumping out the products of an electrical discharge through water vapor[5] is undoubtedly formed as a result of the combination of active radicals *in the trap* used to collect the products. As we have reported previously,[6] however, hydrogen peroxide has been identified with virtual certainty in the reacting mixture by observing the absorption spectrum while the reaction was proceeding. In addition hydrogen peroxide has been identified by means of its absorption spectrum as an intermediate product in the

[1] Oldenberg, Morris, Morrow, Schneider, and Sommers, Jr., J. Chem. Phys. **14**, 66 (1946).
[2] R. N. Pease, J. Am. Chem. Soc. **52**, 5106 (1930) and **53**, 3188 (1931).
[3] L. W. Elder and E. K. Rideal, Trans. Faraday Soc. **23**, 545 (1927); C. N. Hinshelwood and C. R. Prichard, J. Am. Chem. Soc. **123**, 2725 (1923); G. B. Kistiakowsky and S. L. Rosenberg, J. Am. Chem. Soc. **59**, 422 (1937); and E. Kondrat'eva and V. N. Kondrat'ev, J. Phys. Chem. USSR **19**, 178 (1945).
[4] E. J. Harris, Trans. Faraday Soc. **44**, 764 (1948); see also a forthcoming article by C. K. McLane in this journal.
[5] W. H. Rodebush and R. W. Campbell, J. Chem. Phys. **4**, 293 (1936) and K. H. Geib, J. Chem. Phys. **4**, 391 (1936); Rodebush, Keizer, McKee, and Quagliano, J. Am. Chem. Soc. **69**, 538 (1947).
[6] R. B. Holt and O. Oldenberg, Phys. Rev. **71**, 479 (1947).

thermal combination of hydrogen and oxygen at low pressures.[7]

The present paper is concerned with a more complete discussion of the identification of hydrogen peroxide in the reacting mixture than we have given previously[6] and with the use of the absorption spectrum as a quantitative measure of the amount of hydrogen peroxide present in the mixture at a pressure of about one atmosphere. For the purpose of the present experiment we re-determined the absorption coefficient of H_2O_2 at 2537A.[8]

II. METHOD

Hydrogen and oxygen were taken from ordinary commercial cylinders, passed through flow meters, mixed, and then allowed to react continuously (using a constant flow of reacting mixture through the system) in a long reaction tube equipped with quartz windows. The reaction vessel was a Pyrex tube with uncoated walls 5.5 cm in diameter and 130 cm long. The reaction tube was placed inside an oven the temperature of which could be controlled to within 0.5°C. The temperature was held uniform within 1°C along the tube. There was also provided a cylinder of nitrogen for sweeping the reaction mixture out of the oven at the end of an experiment. The products of the reaction were caught in a trap placed at the end of the reaction tube and analyzed chemically by titration with potassium permanganate. The mixture in the reaction tube was also "analyzed" for hydrogen peroxide during the course of the reaction by passing ultraviolet light through the mixture and noting the absorption. The presence of hydrogen peroxide was first qualitatively established by a measurement of the absorption spectrum of the mixture over a wide wave-length range and comparing the observed absorption with the known absorption spectrum of all of the stable molecules likely to be present as intermediates in the reaction mixture. We have previously described[8] the apparatus used for the determination of the absorption spectrum. Essentially, for the identification of hydrogen peroxide, a hydrogen discharge tube was used to produce a continuous spectrum in the wave-length range 1850–2600A; the light from this source was rendered parallel, passed through the reaction vessel, and focused on the slit of a small quartz spectrograph; the desired absorption *vs.* wave-length curve for the mixture was determined by conventional microphotometric reading of the plates obtained. The amount of hydrogen peroxide present under any particular set of conditions was measured by determination of the transmission of the mixture at a single conveniently produced wave-length (2537A) for which the absorption coefficient of the vapor was known. The light source employed was an a.c. operated mercury arc (furnishing the line 2537A) and the detector was an ultraviolet-sensitive photo-cell. In order to increase the sensitivity of the test, the light path was increased in some of the experiments to three times the length of the reaction tube by use of a mirror system.

III. EXPERIMENTAL RESULTS

The absorption of the reacting mixture was found to increase steadily from about 2500A to shorter wave-lengths. If an attempt is made to superpose the absorption coefficient *vs.* wave-length curve for hydrogen peroxide vapor[8] and the observed curve for the reacting mixture, perfect agreement is not obtained (see Fig. 1). In constructing Fig. 1, the "absorption coefficient" for the reacting mixture was based on the calculation of the concentration of the absorbing material in the mixture from the chemical analysis of the exit gases for hydrogen peroxide and the assumption that the material was uniformly distributed along the length of the tube. The fact that the absorption coefficient for the mixture increases more rapidly at shorter wave-lengths than that for hydrogen peroxide might be influenced by two factors. In the first place, the absorption coefficient *vs.* wave-length curve should, by analogy with the halogen spectra,[9] have a maximum somewhere in the extreme ultraviolet (below 1850A). The position of the maximum is not known. This maximum might be expected to become broader and flatter at higher temperatures because vibrating and rotating H_2O_2 molecules come into play. The position of the maximum might also depend on temperature. This expected temperature dependence might give a behavior like that noted for the mixture, but since the position of the maximum is not known, it is not possible to be very certain of the magnitude or even of the direction of this effect. In the second place, the high temperature continuous or closely spaced band absorption of oxygen may begin to be large in the wave-length range in which the steep increase for the mixture occurs. This would not be unexpected from a theoretical viewpoint.[10] These two factors may very well both be operative in this case. It does not seem that an easy way of determining just how the absorption curve should be modified by the temperature is available.

At any rate, the agreement with the room temperature curve for hydrogen peroxide is good enough to leave practically no doubt that hydrogen peroxide is

[7] A. C. Egerton and G. J. Minkoff, Proc. Roy. Soc. **A191**, 145 (1947). It should be pointed out that, since at low pressures the surface plays a greater part, the controlling intermediate steps in the thermal combination reaction are almost certainly very different at high and low pressures. The work referred to in this footnote concerns the region below the pressure corresponding to the first explosion limit of the reaction, while the work described in this paper concerns the region between the second and third explosion limits of the reaction. For a description of the general characteristics of the reaction under various temperature and pressure conditions, see O. Oldenberg and H. S. Sommers, Jr., J. Chem. Phys. **9**, 114 (1941) and G. v. Elbe, and B. Lewis, J. Chem. Phys. **10**, 336 (1942).

[8] Holt, McLane, and Oldenberg, J. Chem. Phys. **16**, 225 (1948).

[9] See the discussion in G. Herzberg, *Molecular Spectra and Molecular Structure: I. Diatomic Molecules* (Prentice-Hall, Inc., New York, 1939), p. 409.

[10] *Ibid.*, p. 415.

present in the mixture. The spectra agree well in that firstly both are continuous, secondly the absorption in both cases increases steadily toward shorter wave-lengths, and thirdly even the absolute magnitude of the absorption for the mixture is in good agreement with that expected. The absorption spectra of all other even remotely probable substances except the HO_2 radical are known to be quite different; O_2, H_2, and OH do not absorb over the wave-length range used to any appreciable extent, and O_3 has an opposite type of absorption (strong at 2500A, weak at 2000A). The absorption spectrum of HO_2 is completely unknown, but it is certainly more plausible to conclude that the substance with which we are concerned is hydrogen peroxide, rather than that the absorption spectrum of HO_2 is precisely of the form which our measurements for the reacting mixture revealed.

Table I summarizes the quantitative results obtained in a number of experiments on the thermal combination of hydrogen and oxygen under various conditions. In many cases, values for the concentration are given as determined chemically by analysis of the exit gases and as determined by the absorption of the line 2537A by the reacting mixture. Both of the concentration values given are calculated on the assumption that the concentration is uniform over the length of the tube, which is probably not true. The ratio of the concentrations obtained in the two ways is given for all cases in which both determinations were made in order to facilitate the comparison of the data.

Several facts concerning the data should be pointed out. In the first place, the amount of hydrogen peroxide present for a given set of reaction conditions seemed to be a function of the surface conditions in the tube to such an extent that the amount varied with the age of the tube and its previous history. This conclusion can be checked by comparing the results of experiments 2, 8, 17, and 20*b*, for which all external conditions were the same. Further evidence along this line was obtained by supplementary experiments (not listed in the table) with another reaction tube whose walls had been roughened by running a great many thermal combination reactions. This tube was found to give practically no hydrogen peroxide under conditions otherwise favorable for the production of large amounts.

Sets of experiments run in succession to check the dependence of the hydrogen peroxide concentration on a single variable with other variables held constant did, however, show definite and repeatable trends. For example, experiments 5, 6, 7, and 8 show that the concentration of hydrogen peroxide for a given reaction mixture increases sharply and uniformly with temperature.

It will be seen from an examination of the results of experiments 19 and 17 (and also 9*a* and 8) that a longer

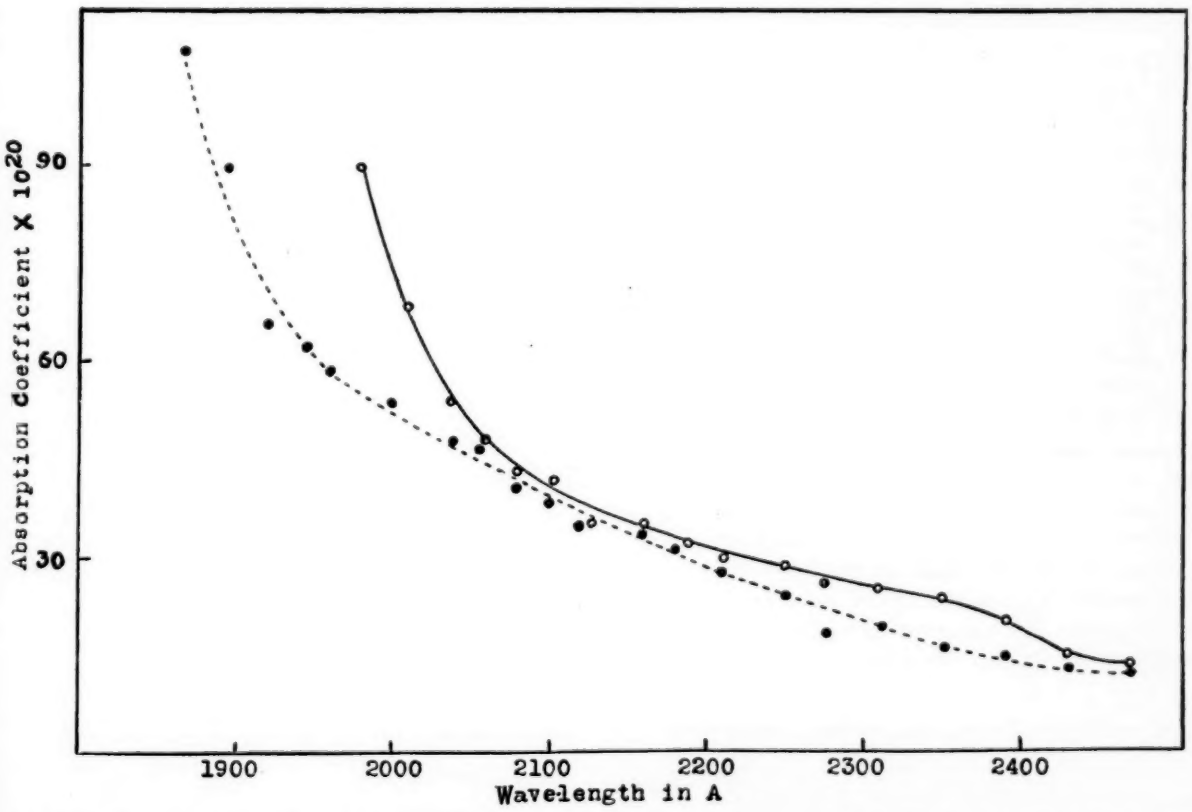

FIG. 1. Comparison of the absorption of a reacting mixture of hydrogen and oxygen at 540°C with the absorption of hydrogen peroxide at room temperature. The solid curve is for the mixture; the broken curve is for H_2O_2 vapor.

TABLE I. Concentration of hydrogen peroxide in reacting mixtures of hydrogen and oxygen.

Experiment No.	Temp. °C	Reactants (liters/min.) H_2	Reactants (liters/min.) O_2	Concentration H_2O_2 (molecules/cc $\times 10^{-15}$, based on:) *A* Analysis of exit gases	*B* Absorption data	Ratio *A*/*B*
1	535	3	1	0.78	0.64	1.2
2	540	3	1	1.0	0.64	1.5
3	545	3	1	—	1.9	—
4	544	3	1	0.92	0.64	1.4
5	530	3	1	2.2	1.3	1.7
6	535	3	1	3.1	1.9	1.6
7	541	3	1	6.5	4.5	1.4
8	540	3	1	6.4	5.2	1.2
9*a*	540	1.5	0.5	13.0	9.9	1.3
b	541	1.5	0.5	—	9.5	—
10	540	2	2	3.5	—	—
11	541	2	2	explosion	7.7	—
12	536	2	2	0.93	—	—
13	540	2	2	2.1	—	—
14	537	3	1	—	1.9	—
15	536	3	1	2.5	1.6	1.5
16	538	2	2	2.4	1.7	1.4
17	540	3	1	2.7	2.1	1.3
18	541	2	2	3.0	2.3	1.3
19	540½	1.5	0.5	10	6.3	1.6
20*a*	540	3	2	—	1.0	—
b	540	3	1	—	1.9	—
c	540	3	0.5	—	2.5	—
d	540	3	0.25	—	2.6	—
e	540	1.5	2.0	—	1.5	—
f	540	1.5	1.0	—	3.1	—
g	540	1.5	0.5	—	4.4	—
h	540	1.5	0.25	—	4.2	—
i	540	1	2	—	1.4	—

heating time for a given ratio of reactants (corresponding to a slower rate of flow through the reaction tube) results in a higher concentration of hydrogen peroxide.

Experiments 8 and 10, together with the various parts of experiment 20, show that, over a considerable range, the formation of hydrogen peroxide is enhanced by a large hydrogen to oxygen ratio in the reacting mixture.

Several other conclusions could be drawn from the data, but the lack of reproducibility of the results makes such conclusions of dubious value. This lack of reproducibility is to be expected—in fact, the results are better than might be anticipated, since the reaction is extremely sensitive to surface conditions and these could not be completely controlled. One of the more surprising features of the results is the good correlation of even the absolute values obtained between spectroscopic and analytical values for the hydrogen peroxide concentration. This would hardly have been expected, since the value of the absorption coefficient in the temperature range studied could have been different from that at room temperature, the concentration of the hydrogen peroxide along the length of the tube is probably not uniform, and the rate of thermal decomposition of hydrogen peroxide probably varies with external and surface conditions.

The generally accepted mechanism for the reaction has been discussed at great length by G. von Elbe and B. Lewis.[11] It is beyond the scope of this paper to reformulate this mechanism in detail. It should be pointed out, however, that the suggested mechanism allows for the formation of appreciable concentrations of hydrogen peroxide in two ways: reaction of HO_2 radicals (formed from H atoms produced in the reaction) with H_2 in the gas phase, and decomposition of HO_2 on the wall:

$$HO_2+H_2\rightarrow H_2O_2+H,$$
$$\text{wall}$$
$$2HO_2\rightarrow H_2O_2+O_2.$$

It is believed by von Elbe and Lewis on the basis of other kinetic data that the gas phase reaction predominates under the conditions present in this series of experiments. Also, there are three reactions in the proposed scheme for the disappearance of hydrogen peroxide: decomposition by collision with some other molecule to form two OH radicals (which immediately react with H_2 to form water and H), surface decomposition into water and oxygen, and gas phase reaction with HO_2 to form water, oxygen, and H.

$$H_2O_2+M\rightarrow 2OH+M \text{ (followed by } OH+H_2\rightarrow H_2O+H),$$
$$\text{wall}$$
$$H_2O_2\rightarrow H_2O+\tfrac{1}{2}O_2,$$
$$H_2O_2+HO_2\rightarrow H_2O+O_2+OH \text{ (followed by } OH+H_2\rightarrow H_2O+H).$$

The latter reaction is thought by von Elbe and Lewis to be the predominating one under the conditions existing in the series of experiments discussed here. If the predominating reactions for the formation and decomposition of hydrogen peroxide are the ones chosen above, then the hydrogen peroxide concentration should be proportional to the mole fraction of hydrogen present. Our data is in fair agreement with this prediction. None of our results, in fact, contradicts this postulated mechanism in any way.

R. B. Holt wishes to express appreciation for a National Research Council Predoctoral Fellowship which made this investigation possible. The authors are grateful for financial support by the Rumford Fund of the American Academy of Arts and Sciences.

[11] G. von Elbe and B. Lewis, J. Chem. Phys. **10**, 336 (1942).

THE JOURNAL OF CHEMICAL PHYSICS VOLUME 17, NUMBER 11 NOVEMBER, 1949

The Born-Mayer Model for Ionic Solids and the Heats of Formation and Lattice Spacings of Alkali Halide Solid Solutions*

W. E. WALLACE
Department of Chemistry, University of Pittsburgh, Pittsburgh, Pennsylvania
(Received March 28, 1949)

Previous attempts to calculate the heats accompanying formation of alkali halide solid solutions from the component salts have met with only limited success. The difficulties may have originated either in the use of Vegard's law to obtain lattice spacings of the solutions or in the general inadequacy of the model employed in computing the energies of the lattices concerned. Since earlier studies were based on the old Born concept of ionic solids, it was of interest to examine the subject again using as a basis the more refined treatment due to Born and Mayer. An expression for the potential energy of a crystalline solution has been developed in terms of the known interaction parameters of the pure constituents and has been used to compute the equilibrium spacings and heats of formation of three chosen systems. The calculated results are compared with experiment. The comparison suggests that further refinement in the model is perhaps necessary before the small changes in lattice spacings and heat contents which accompany solid solution formation can be completely accounted for.

INTRODUCTION

THE ability of certain pairs of the alkali halides to form solid solutions has long been recognized.[1] In some instances, e.g., KCl-KBr,[2] the components are miscible in all proportions at ordinary temperatures. With others, e.g., NaCl-KCl,[3] the components have only a limited solubility in each other and over a portion of the composition range the stable state is a mixture of the two saturated solid solutions. Where direct observation has been possible, it has been noted that the mutual solid solubility of a pair of partially miscible alkali halides increases with temperature, indicating the existence of a heat effect accompanying the formation of a solid solution from its components. For the purpose of the present discussion this heat effect will be referred to as the heat of formation of the solid solution, ΔH_f.

The heat of formation of a solid solution can be readily ascertained if the lattice energies of the pure components and the solid solution are known. Grimm and Herzfeld[4] and, more recently, Tobolsky[5] have applied the Born method for computing lattice energies of ionic crystals to crystalline solutions and have obtained expressions for estimating ΔH_f for alkali halide solid solutions from the observed lattice spacings and assumed interaction potentials of the pure salts. Instead of calculating heats of formation directly Grimm and Herzfeld chose to regard the constant m (appearing in the repulsion potential, B/r^m) as an adjustable parameter to be determined from the calorimetrically observed heats. Values of m ranging between 3 and 8 were required to account for the data. Although these values tended to be smaller than the quantities obtained from compressibilities, the discrepancies could be attributed to the large uncertainties in the heats of formation determined prior to 1923.

Tobolsky obtained an expression for the heat of formation of an equimolal solid solution containing two moles of ion pairs

$$\Delta H_f \cong 9\delta^2, \qquad (1)$$

where δ is the percentage deviation between the lattice constants a_1 and a_2 of the component salts, and the heat is expressed in calories. Equation (1) was developed under the assumption that the solid solution obeyed Vegard's Law and the energies of the lattices concerned were about 180 kcal. per mole. In comparing the heats computed from Eq. (1) with experiment, Tobolsky observed that the agreement was fairly good considering the approximate nature of the treatment.

Tobolsky's calculated heats were compared with experimental data taken from a compilation by Bruni.[6] Bruni apparently failed to recognize that the early experimenters were not of a uniform practice in reporting heats of formation of an equimolal solid solution, some expressing the heat on the basis of one mole of each component and others on the basis of one mole total. Hence, some of the values reported by Bruni referred

TABLE I. Heats of formation of alkali halide solid solutions.

System	δ	ΔH_f (cal./mole of ion pairs) Calc.-Tobolsky	Observed
KCl-RbCl	4.5	83	203[a]
KBr-KCl	4.8	94	232[a]
NaCl-NaBr	5.5	118	335[b]
KBr-KI	7.1	195	390[c]
NaI-KI	9.1	326	625[d]
NaBr-KBr	10.8	480	700[d]
NaCl-KCl	11.5	594	1050[d]

[a] N. Fontell, Soc. Sci. Fenn. Comm. Phys.-Math., **X**, 12, 1 (1939).
[b] M. A. Fineman and W. E. Wallace, reference 7.
[c] G. Bruni and M. Amadori, Atti ist. Veneto **71**, II, 51 (1911).
[d] N. S. Kurnakov and S. F. Zemczuznj, Zeits. f. anorg. allgem. Chemie **52**, 186 (1907).

* Part of a basic research program sponsored by the ONR, Contract No. N6-ori-43, No. 2.

[1] W. C. Blasdale, *Equilibria in Saturated Salt Solutions* (Chemical Catalog Company, New York, 1927), p. 88.
[2] W. E. Wallace and M. A. Fineman, Soc. Sci. Fenn. Comm. Phys.-Math. **XIV**, 6, 1 (1948).
[3] R. Nacken, Sitz. kgl. preuss. Akad. Wiss. **192** (1918).
[4] H. G. Grimm and K. F. Herzfeld, *Zeits. f. Physik.* **16**, 77 (1923).
[5] A. V. Tobolsky, J. Chem. Phys. **10**, 187 (1942).
[6] G. Bruni, Chem. Rev. **1**, 345 (1925).

to one mole of ion pairs, whereas others referred to two moles of ion pairs. Expressing all results on a uniform basis (heat effect for a solution containing one mole of ion pairs) and using more recently determined values, where possible, the data presented in Table I are obtained.

TABLE II. van der Waals and repulsion potential constants.

	$C\times10^{60}$ ergs cm^6/ion pr.	$\beta_1\times10^{12}$ ergs/ion pr.	$\beta_2\times10^{12}$ ergs/ion pr.
mole fraction NaCl		NaCl-NaBr	
1.00	180	5498	24880
0.75	201	6081	30170
0.50	223	6664	35990
0.25	247	7247	42340
0.00	271	7830	49230
mole fraction KCl		KCl-KBr	
1.00	451	13380	30480
0.75	488	14840	35840
0.50	525	16300	41730
0.25	564	17760	48210
0.00	604	19220	55240
mole fraction KCl		KCl-RbCl	
1.00	451	13380	30480
0.50	570	16590	34360
0.00	692	19790	39060

It has been pointed out elsewhere[7] that attempts to calculate heats of formation from lattice energies impose severe demands upon the model used since ΔH_f appears as the difference in lattice energy of the solid solution and a mechanical mixture of the same total mass and composition. These differences are only 0.6 percent to 0.1 percent of the total energy of the lattice so that the calculated heats are extremely sensitive to imperfections in the model. The treatments offered by Grimm and Herzfeld and by Tobolsky were both based on the earlier Born model where van der Waals forces were neglected and the repulsion potential assumed was of the form B/r^m. Since the van der Waals energies of alkali halide crystals are from ten to twenty times larger than the energy changes associated with solid solution formation, and in view of the approximate nature of the B/r^m repulsion potential, it was of interest to investigate the energetics of crystalline solutions using the more refined treatment of ionic lattices due to Born and Mayer[8] and Mayer.[9] Employing interaction parameters characteristic of the pure compounds, equilibrium spacings of the solid solutions can be determined merely by invoking the minimum potential energy principle. Thereby Tobolsky's assumption of the validity of Vegard's Law[10] for the systems concerned is avoided. In the present paper the equations developed have been used (1) to evaluate the equilibrium spacings of the solid solutions at various compositions and to compare these quantities with experiment and with Vegard's Law and (2) to calculate the heats of formation and compare them with experiment for three chosen binary systems for which reliable data are available.

LATTICE ENERGY OF ALKALI HALIDE SOLID SOLUTIONS

Let us consider a binary solid solution containing four ion species, two cationic components, 1 and 3, and two anionic components, 2 and 4.[11] The lattice energy U is given by

$$-U=\Phi_0=-\alpha e^2/r_0-C/r_0^6-D/r_0^8+B(r_0)+1/2h\nu_0. \quad (2)$$

For the present purpose the $1/r_0^8$ term is assumed to make a negligible contribution to the heats of formation and in the remainder of this paper it has been neglected. Undoubtedly, D/r_0^8 is not negligible compared to the heat of solid solution but it seems unlikely that changes in this term could make an appreciable contribution.

The first term is the Coulombic potential which of

TABLE III. Lattice spacings of alkali halide solid solutions.

	298°K $r_0\times10^8$ cm			0°K $r_0\times10^8$ cm		
	Obs.	Calc.-Vegard's Law	Dev.	Calc.-Eq. (8)	Calc.-Vegard's Law	Dev.
			NaCl-NaBr			
Mole Fraction KCl						
1.00	2.8144	—	—	2.790	—	—
0.75	2.8588	2.8560	0.0028	2.837	2.831	0.006
0.50	2.9017	2.8977	0.0040	2.880	2.872	0.008
0.25	2.9411	2.9393	0.0038	2.919	2.913	0.006
0.00	2.9809	—	—	2.954	—	—
			KCl-KBr			
Mole Fraction KCl						
1.00	3.1362	—	—	3.105	—	—
0.75	3.176	3.176	0.000	3.151	3.145	0.006
0.50	3.217	3.216	0.001	3.192	3.184	0.008
0.25	3.257	3.256	0.001	3.229	3.224	0.007
0.00	3.2952	—	—	3.263	—	—
			KCl-RbCl			
Mole Fraction KCl						
1.00	3.1362	—	—	3.105	—	—
0.50	3.216	3.211	0.005	3.185	3.178	0.007
0.00	3.286	—	—	3.251	—	—

[7] M. A. Fineman and W. E. Wallace, J. Am. Chem. Soc. **70**, 4165 (1948).

[8] M. Born and J. E. Mayer, Zeits. f. Physik **75**, 1 (1932).

[9] J. E. Mayer, J. Chem. Phys. **1**, 270 (1933); **1**, 327 (1933).

[10] Grimm and Herzfeld have demonstrated that if the energy of a solid solution is at a minimum, Vegard's Law can be obeyed only if m, the exponent in the repulsion potential, is 2. It is well known that for the salts in Table I m varies between 8 and 10.5. Hence, at the spacings obtained from Vegard's Law, the solid solutions are not in the equilibrium state. Lattice energies and ΔH_f's such as reported in Table I, column 3, correspond to the "Vegard's law solid solution" and not to the equilibrium state.

[11] In the treatment presented in this section the nomenclature of Born and Mayer is employed with appropriate modifications as necessary.

course is the same for a solution as for a pure material allowing for the altered r_0.

In evaluating C for the solution it has been assumed that the two cationic species and two anionic species are distributed randomly over the cation and anion sites, respectively.[12] Consider the van der Waals interaction of a single ion of species 1 with all other ions.

$$\varphi_1 = S'(N_2c_{12}+N_4c_{14})/r^6 + S''(N_1c_{11}+N_3c_{13})/r^6, \quad (3)$$

where N_1 and N_3 are the fraction of cation sites occupied by cations 1 and 3 respectively, and N_2 and N_4 are corresponding quantities for anion sites. c_{12} refers to the interaction between ions of types 1 and 2, c_{13} between 1 and 3, etc. The simple form of Eq. (3) is an immediate consequence of the assumed random distribution of the several species over the accessible lattice sites. Of the l anions r_l distant from the central ion, $N_2 l$ are of species 2 and $N_4 l$ are of species 4. The interaction of the central ion with that shell of anions is $(N_2c_{12}+N_4c_{14})l/r_l^6$. Since the various N's are assumed to be independent of position (completely random), summing over all the lattice sites is particularly simple, and Eq. (3) results. To obtain the complete van der Waals potential, one merely needs to find the average energy per ion pair using Eq. (3) and the other three similar expressions for species 2, 3, and 4.

$$C = S'(N_1N_2c_{12}+N_1N_4c_{14}+N_2N_3c_{23}+N_3N_4c_{34}) + (S''/2)(N_1^2c_{11}+N_2^2c_{22}+N_3^2c_{33} + N_4^2c_{44}+2N_1N_3c_{13}+2N_2N_4c_{24}). \quad (4)$$

In evaluating the contribution of the forces of repulsion to the energy of the lattice, $B(r_0)$, Born and Mayer considered the repulsion potential between a pair of ions to be of the form $\alpha e^{-r/\rho}$. Subsequently Huggins and Mayer[13] showed that the behavior of the alkali halides could be accounted for by taking $\rho = 0.345\times10^{-8}$ cm and setting $\alpha = bc_{ij}e^{(r_i+r_j)/\rho}$, where r_i and r_j are parameters characteristic of the particular ions and $b = 10^{-12}$ erg/ion pair. When the ions are of opposite charge, $c_{ij} = c_0 = 1.00$; for two cations, $c_{ij} = c_1 = 1.25$, and for two anions, $c_{ij} = c_2 = 0.75$.

The repulsion potential for the solid solution was evaluated by considering only the interaction between a given central ion and the M nearest neighbors and M' next-nearest neighbors

$$B(r_0) = \beta_1 e^{-r_0/\rho} + \beta_2 e^{-ar_0/\rho}, \quad (5)$$

where

$$\beta_1 = bMc_0(N_1N_2e^{(r_1+r_2)/\rho} + N_1N_4e^{(r_1+r_4)/\rho} + N_2N_3e^{(r_2+r_3)/\rho}), \quad (6)$$

$$\beta_2 = (bM')/2[c_1(N_1^2e^{2r_1/\rho} + 2N_1N_3e^{(r_1+r_2)/\rho} + N_3^2e^{2r_3/\rho}) + c_2(N_2^2e^{2r_2/\rho} + 2N_2N_4e^{(r_2+r_4)/\rho} + N_4^2e^{2r_4/\rho})]. \quad (7)$$

[12] M. Von Laue, Ann. d. Physik **78**, 167 (1925). See also reference 7.

[13] M. L. Huggins and J. E. Mayer, J. Chem. Phys. **1**, 642 (1933).

In Eqs. (5)–(7) r_0 refers to the equilibrium distance between a given ion and its nearest neighbors, whereas r_1, r_2, etc., are the parameters characteristic of the several ion species; and a is the factor by which the distance from the central ion to the next-nearest neighbors exceeds the distance to the nearest neighbors. Of course, $a = 2^{\frac{1}{2}}$ for the sodium chloride type lattice.

In developing Eqs. (4), (6), and (7) the interactions between a given pair of ions in solution are taken to be identical with those in the pure salt for the same distance of separation. Undoubtedly the numerous parameters do vary somewhat with composition, but the effect of this variation on the computed spacings and heats would be difficult to assess.

TABLE IV. Heats of formation of alkali halide solid solutions.

	ΔH_f (cal./mole of ion pairs)				
	Obs.[a]	Calc.-Eq. (9)	Dev.	Calc.-Eq. (1)	Dev.
	NaCl-NaBr				
Mole Fraction NaCl					
0.75	257	440	180		
0.50	335	540	200	118	−117
0.25	241	380	140		
	KCl-KBr				
Mole Fraction KCl					
0.75	186	360	170		
0.50	232	450	220	94	−138
0.25	163	300	140		
	RbCl-KCl				
Mole Fraction					
0.50	203	400	200	83	−120

[a] For sources of data, see Table I.

EQUILIBRIUM SPACINGS AND ΔH_f FOR BINARY SOLUTIONS

Numerical solutions of the expressions derived in the preceding section were carried out for three binary systems: NaCl-NaBr, KCl-KBr, and RbCl-KCl. For the first two systems, reliable data are available over the entire composition range, while for the latter, data are available only for the equimolal solution. The values for C listed in Table II were obtained from Eq. (4) using the van der Waals constants as reported by Mayer[9] and taking $c_{13} = (c_{11}c_{33})^{\frac{1}{2}}$ and $c_{24} = (c_{22}c_{44})^{\frac{1}{2}}$. β_1 and β_2 values also presented in Table II were obtained using $\rho = 0.345\times10^{-8}$ cm and the various repulsion parameters as tabulated by Huggins and Mayer.[13]

The equilibrium spacings of the solid solutions can be determined from the relationship developed by Born and Mayer that:

$$r_0\left[\frac{d\Phi(r_0)}{dr}\right] = \frac{3T}{N\beta}\left(\frac{dV}{dT}\right)_P, \quad (8)$$

where β is the compressibility. In the absence of expansion and compressibility data for the systems concerned, the equilibrium spacings could only be evaluated for 0°K.

The quantities given in column 5, Table III were computed from Eq. (8). For the sake of consistency the spacings listed for the five pure compounds were also computed from Eq. (8) instead of resorting directly to experiment. The observed lattice spacings at 25°C have been reported by Nickels, Fineman, and Wallace[14] for NaCl-NaBr solutions, by Oberlies[15] for KCl-KBr solutions, and by Havighurst, Mack, and Blake[16] for RbCl-KCl solutions.

Because of the difference in temperature, direct comparison between observed and computed lattice spacings is not possible. It is of some interest, however, to note that the observed deviations from Vegard's Law at 25°C (column 4) agree in sign and rather closely in magnitude with the differences (column 7) between the r_0's calculated from Eq. (8) and the spacings expected (column 6) on the basis of Vegard's Law at 0°K.

The extent of departure from Vegard's Law will, of course, be independent of temperature if the coefficient of thermal expansion of the solid solution is a linear function of composition. The decrease in r_0 between 25°C and 0°K is remarkably constant at about 1 percent for the five salts in Table III. It hardly seems possible that the solutions could have expansions differing substantially from the average for the pure constituents. Allowing for a maximum difference of 10 percent, the deviations in column 4 would be changed by only 0.003 angstrom units in correcting to absolute zero. Hence it appears that the Born-Mayer model is adequate in accounting for the observed spacings, at least for the three systems considered, to within 0.005–0.01 angstrom units or better. Furthermore, it seems that, when viewed from the framework of this model, the reasonably close agreement with the requirement of Vegard's Law is more accidental than fundamental.

ΔH_f is related to the lattice energies of the pure salts and the solid solution as follows:

$$\Delta H_f = U_s - (X_1 U_1 + X_2 U_2), \tag{9}$$

where X_1 and X_2 are mole fractions of components 1 and 2 present in the solution. To evaluate ΔH_f the equilibrium spacings given in Table III, together with constants from Table II, are inserted into Eq. (2). In calculating ΔH_f, the last term in Eq. (2), the zero point energy, is neglected under the assumption that the change in this quantity is small compared to ΔH_f. The results obtained from Eq. (9) are summarized in Table IV together with results obtained from Eq. (1). Again, comparison of observed and computed quantities is complicated by the fact that the two refer to different temperatures. If the solid solutions obey the Kopp-Neumann rule (additivity of heat capacities), then ΔH_f is independent of temperature and it is entirely appropriate to compare the ΔH_f's directly without regard to temperature.

Elsewhere attention has been directed[2] to the widespread use of the Kopp-Neumann rule for systems such as listed in Table IV and the dearth of supporting experiments. In what is perhaps the only comprehensive study of the thermal properties of an ionic solid solution, Eastman and Milner[17] observed that a AgCl-AgBr solid solution conformed to the additivity law for heat capacities within 0.1–0.2 percent at temperatures between 100 and 300°K. Below the liquid air range the departure increased somewhat, but down to about 15°K remained less than 1 percent. Eastman and Milner have expressed the opinion that similar behavior would probably be observed with other systems approaching ideal behavior about as closely as the AgCl-AgBr system.[18]

Eastman and Milner's data reveal that ΔH_f for their AgCl-AgBr solution decreases by less than 3 cal./mole between 298 and 0°K. The solid solutions discussed in this paper are probably less ideal than the silver salts, judging from the ΔH_f values (200–300 *versus* 80 cal./mole), but it appears unlikely that a change of more than 20–30 cal./mole would result from correcting the experimental heats of formation to 0°K. If this estimate of the change in ΔH_f with temperature is valid, then the observed heats listed in Table IV are correct for 0°K within about 10 percent and the deviations noted are due primarily to errors in the computed quantities. This suggests that neither the model used in this paper nor the one upon which Eq. (1) is based are adequate in accounting for the small changes in lattice energies which accompany solid solution formation.

When the individual contributions to ΔH_f are examined, it is found that changes in repulsion energy account for approximately two-thirds of the total. Alteration of the Coulombic energy is responsible for most of the remaining heat effect with the van der Waals' forces making a small (2–5 percent) exothermic contribution. Unfortunately it is the energy of repulsion which is least accurately known of the three energy terms involved, so it appears that a better computation of ΔH_f must await a more accurate description of the factors responsible for repulsion in a crystal. In this connection it is of interest to note that the heats of formation of solid solutions may provide a convenient experimental basis for elucidating the detailed characteristics of the repulsion potential since these heat effects can be readily and precisely determined with

[14] Nickels, Fineman, and Wallace, J. Phys. and Colloid Chem. **53**, 625 (1949).
[15] F. Oberlies, Ann. Physik **87**, 238 (1928).
[16] Havighurst, Mack, and Blake, J. Am. Chem. Soc. **47**, 29 (1925).
[17] E. D. Eastman and R. T. Milner, J. Chem. Phys. **1**, 444 (1933).
[18] This opinion is shared by the present author.

calorimeters currently available and since the repulsion energies may comprise a substantial part of the observed heat of formation.

In summary, it may be said that it appears that the best existing model for ionic solids, the Born-Mayer model, does not serve as an adequate basis to account completely for the small changes in lattice spacing and energy associated with the formation of alkali halide solid solutions. In particular, a better representation of the repulsion potential is needed. It seems that experimental and theoretical studies of the energy changes accompanying solid solution might open an attractive avenue for investigating the detailed characteristics of the forces at work in ionic crystals.

THE JOURNAL OF CHEMICAL PHYSICS VOLUME 17, NUMBER 11 NOVEMBER, 1949

Rotation-Vibration Spectra of Diatomic and Simple Polyatomic Molecules with Long Absorbing Paths. II. The Spectrum of Carbon Monoxide below 1.2μ

G. HERZBERG
National Research Council, Ottawa, Canada

AND

K. NARAHARI RAO
Yerkes Observatory of the University of Chicago, Williams Bay, Wisconsin

(Received March 30, 1949)

The third overtone of CO at 1.19μ has been photographed under high dispersion. From this band precise values for the rotational constants of the CO molecule are derived. They agree excellently with the values obtained from the ultraviolet spectra but are considered to be much more accurate. The equilibrium internuclear distance of CO in the ground state is $r_e = 1.1281_9 \times 10^{-8}$ cm. An attempt to obtain also the fourth overtone failed even with path lengths of 3000 m atmos. The second overtone was observed under low resolution with a path length of 30 m.

1. INTRODUCTION

ROTATION–VIBRATION spectra in the photographic infra-red have thus far been observed almost exclusively for molecules containing hydrogen. For these molecules moderate path lengths (between 4 and 100 m) have proved to be sufficient to obtain strong absorption bands below 1.2μ. Much greater path lengths are required for molecules not containing hydrogen, partly because the vibrational frequencies are lower and therefore only higher overtones fall in the photographic region, and partly because the mechanical and electrical anharmonicities which determine the intensities of overtone bands are smaller. With the long optical paths described in paper I of this series[1] it becomes possible to study these spectra with the high resolution of a 21 foot grating. Up to now this has been done for CO, CO_2 and N_2O. The present paper describes the results for CO.

2. APPARATUS; DESCRIPTION OF SPECTRA

The large absorption tube described in I was filled with CO to a pressure of 1 atmos. The gas was obtained from the Matheson Company and is specified by them to be 92 percent pure. It was used without further purification.

Attempts were made to obtain both the 4−0 and 5−0 bands. However in spite of the use of up to 136 traversals corresponding to 3000 m atmos no trace of the 5−0 band was found. To be sure this band is expected in a region (9564A) where strong overlapping by H_2O lines occurs and where therefore a weak band is more difficult to observe. The 4−0 band was obtained with path lengths of 500 to 1000 m atmos.[2] Figure 1 shows one of the spectra obtained.

The lines of the CO band were measured against third order Fe lines. The averages of six measurements of each of three plates were used for the evaluation. In this way any constant shift relative to the comparison spectrum arising for example from slight temperature or pressure changes during the long exposures should be substantially eliminated. For the conversion to vacuum the index of refraction of air from Barrell and Sears[3] as recommended by Birge[4] was used. The wave numbers of unblended and not too weak lines are believed to be accurate to within less than 0.01 cm^{-1} relative to one another and within 0.03 cm^{-1} on an absolute scale.

Compared to similar CO_2 bands the intensity of the 4−0 band appears surprisingly low. However, a similar

[1] H. J. Bernstein and G. Herzberg, J. Chem. Phys. **16**, 30 (1949).

[2] A larger path cannot be used here because of the low sensitivity of the *I–Z* plates at 11900A.

[3] H. Barrell and J. E. Sears, Phil. Trans. Roy. Soc. (London) **238**, 1 (1939).

[4] R. T. Birge, Phys. Rev. **60**, 771 (1941).

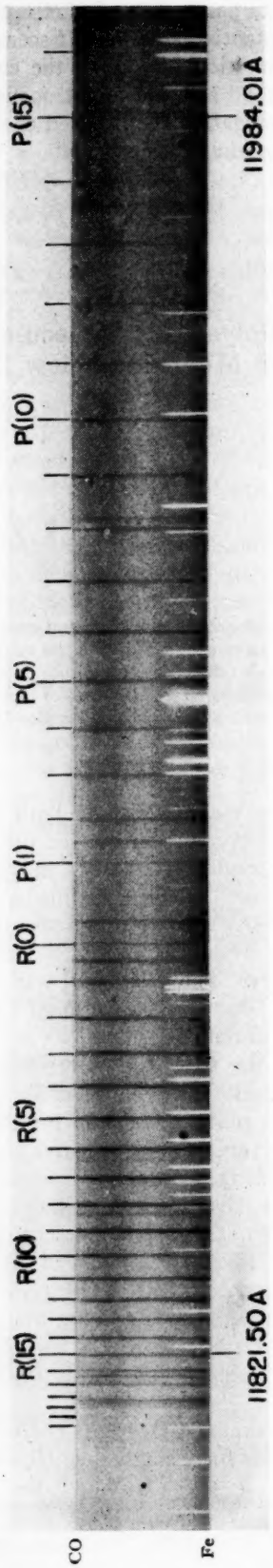

FIG. 1. 4—0 infra-red band of carbon monoxide (absorbing path 800 m at 1 atmos.). Absorption lines that are not marked are due to H_2O vapor.

TABLE I. Wave numbers of the lines in the 4—0 infra-red band of CO; $\nu_0 = 8414.45_8$ cm^{-1}.

	$R(J)$			$P(J)$		
J	ν_{vac}(cm^{-1}) observed	ν_{vac}(cm^{-1}) computed	O-C	ν_{vac}(cm^{-1}) observed	ν_{vac}(cm^{-1}) computed	O-C
0	8418.131	8418.163	−0.032			
1	8421.728	8421.729	−0.001	8410.625	8410.613	+0.012
2	8425.158	8425.154	+0.004	8406.605	8406.628	−0.023
3	8428.440	8428.439	+0.001	8402.509	8402.503	+0.006
4	8431.577	8431.583	−0.006	8398.244	8398.239	+0.005
5	8434.585	8434.587	−0.002	8393.836	8393.836	0.000
6	8437.453	8437.449	+0.004	8389.300	8389.293	+0.007
7	8440.184	8440.171	+0.013	8384.619	8384.612	+0.007
8	8442.761	8442.751	+0.010	8379.765	8379.792	−0.027
9	8445.184	8445.190	−0.006	8374.836	8374.833	+0.003
10	8447.486	8447.487	−0.001	8369.732	8369.735	−0.003
11	8449.644	8449.643	+0.001	8364.528	8364.499	+0.029
12	8451.646	8451.656	−0.010	8359.117	8359.124	−0.007
13	8453.522	8453.527	−0.005	8353.611	8353.611	0.000
14	8455.257	8455.256	+0.001	8347.948	8347.960	−0.012
15	8456.844	8456.842	+0.002	8342.167	8342.171	−0.004
16	8458.281	8458.286	−0.005	8336.268	8336.245	+0.023
17	8459.568	8459.586	−0.018	8330.184	8330.180	+0.004
18	8460.740	8460.743	−0.003			
19	H_2O	8461.756	—			
20	8462.614	8462.626	−0.012			

difference exists for the fundamental of CO which is much weaker (by about a factor 10) than the fundamental ν_3 of CO_2.

One run was taken with Dr. Kuiper's infra-red spectrometer[5] in the region 1.2 to 2.5μ with an absorbing path of 30 m in the small absorption tube at 720 mm pressure. On this record in addition to the 2—0 band at 4259.9 cm^{-1},[6] the 3—0 band appears as a double band with center at 6351.3 cm^{-1}. Apparently this band has not previously been recorded. Its position agrees within the accuracy of this measurement with the value that follows from a study of the ultraviolet Cameron bands[7] that is 6350.4 cm^{-1}. The intensity of this band (20 percent absorption at the peak of the R branch) is

TABLE II. Combination differences $\Delta_2F(J)$.

J	$\Delta_2F'(J)$	$\Delta_2F''(J)$
0		
1	11.109	11.526
2	18.553	19.219
3	25.931	26.914
4	33.333	34.604
5	40.749	42.277
6	48.153	49.966
7	55.565	57.688
8	62.996	65.348
9	70.348	73.029
10	77.754	80.656
11	85.116	88.369
12	92.529	96.033
13	99.911	103.698
14	107.309	111.355
15	114.677	118.989
16	122.013	126.660
17	129.384	

[5] Kuiper, Wilson, and Cashman, Astrophys. J. **106**, 243 (1947).
[6] Lagemann, Nielsen, and Dickey, Phys. Rev. **72**, 284 (1947).
[7] K. N. Rao, to be published.

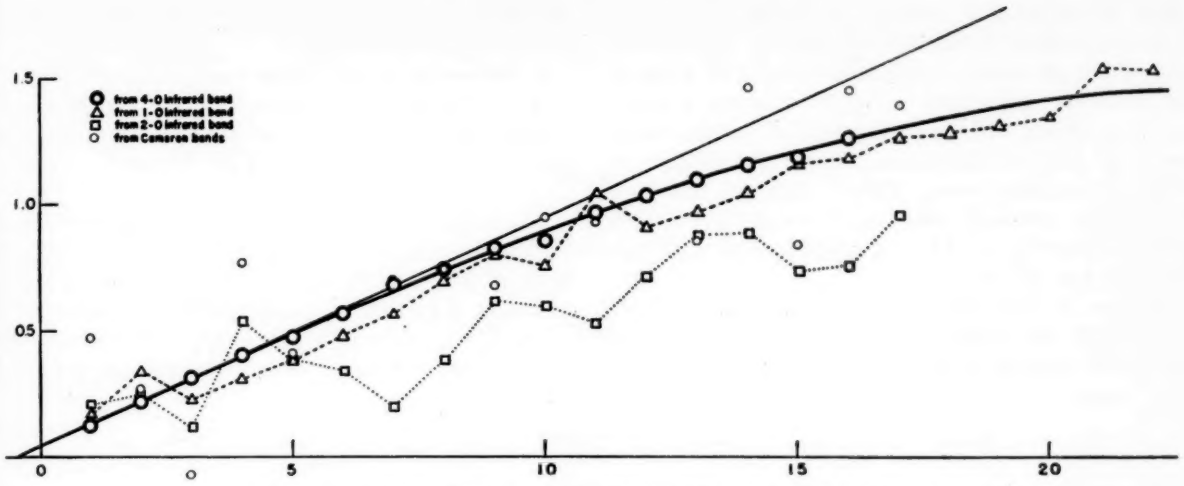

FIG. 2. Combination differences $\Delta_2F''(J)-7.6(J+\frac{1}{2})$ in the $v''=0$ state of CO.

again much smaller than that of the $3\nu_3$ band of CO_2 obtained under comparable conditions.

3. ROTATIONAL ANALYSIS

In the second and fifth column of Table I the wave numbers of the lines of the 4−0 CO band are given as measured in the above described way. From these data the rotational constants were evaluated with the help of the combination differences

$$R(J-1)-P(J+1)=\Delta_2F''(J)$$
$$R(J)-P(J)=\Delta_2F'(J).$$

Table II gives the values of these differences. To illustrate the reliability of the derived constants the deviations of the $\Delta_2F''(J)$ values from the straight line $7.6(J+\frac{1}{2})$ are plotted in Fig. 2 as large circles. It is seen that the points follow very closely a smooth curve whose deviation from a straight line is due to the rotational constant D (representing the effect of centrifugal stretching). For comparison in Fig. 2 the combination differences for $v''=0$ obtained from the 1−0 and 2−0 infra-red bands according to Lagemann, Nielsen, and Dickey[6] and from the Cameron bands in the ultraviolet by Gerö, Herzberg, and Schmid[8] are included and marked by Δ, □ and ○ respectively. It is seen that the scatter in these earlier determinations is much greater. Moreover the values obtained from the 1−0 and 2−0 infra-red bands show systematic deviations from those obtained from the 4−0 band and between themselves. This is probably due to the lack of standards in the infra-red region.[9]

From the usual equation for the rotational term values of a diatomic molecule

$$F_v(J)=B_vJ(J+1)-D_vJ^2(J+1)^2,$$

where

$$B_v=B_e-\alpha(v+\tfrac{1}{2}) \quad \text{and} \quad B_e=\frac{h}{8\pi^2c\mu r_e^2},$$

[8] Gerö, Herzberg, and Schmid, Phys. Rev. **52**, 467 (1937).

[9] It may be noted that if Δ_2F'' were directly plotted against J these small differences would not be noticeable.

TABLE III. Rotational constants in the ground state of CO.

B_0	1.9226_5 cm^{-1}
B_4	1.8527_1 cm^{-1}
D_0	$6.4_5\times10^{-6}$ cm^{-1}
D_4	$6.6_0\times10^{-6}$ cm^{-1}
B_e	1.9313_9 cm^{-1}
α_e	0.01748_5 cm^{-1}
D_e	$6.4_3\times10^{-6}$ cm^{-1}
β_e	$+0.0_4\times10^{-6}$ cm^{-1}
I_0	$14.554_4\times10^{-40}$ g cm^2
I_e	$14.488_5\times10^{-40}$ g cm^2
r_0	$1.1307_5\times10^{-8}$ cm
r_e	$1.1281_9\times10^{-8}$ cm

it follows that

$$\Delta_2F(J)=F(J+1)-F(J-1)$$
$$=(4B_v-6D_v)(J+\tfrac{1}{2})-8D_v(J+\tfrac{1}{2})^3.$$

Using standard graphical methods[10] provisional B_v and D_v values were obtained from the observed $\Delta_2F(J)$ values. A check on these values and at the same time a value for the band origin was obtained by forming $\frac{1}{2}[R(J-1)+P(J)]$ and plotting against J^2. Since

$$\tfrac{1}{2}[R(J-1)+P(J)]$$
$$=\nu_0+(B_v'-B_v'')J^2-(D_v'-D_v'')J^2(J^2+1)$$

and since $D_v'-D_v''$ is very small a straight line is obtained whose intercept with the ordinate axis gives ν_0 and whose slope gives a very precise value of $B_v'-B_v''$. The provisional B_v' and B_v'' values were adjusted to give this $B_v'-B_v''$.

In Table III the final values of all the constants thus obtained are listed. The values for internuclear distance and moment of inertia were derived from the B values with the aid of new conversion factors ($I=27.9830/B$, $r=4.10610/(\mu_AB)^{\frac{1}{2}}$) based on DuMond's[11] fundamental constants.

[10] See for example G. Herzberg, *Molecular Spectra and Molecular Structure I: Diatomic Molecules* (Prentice Hall, Inc., New York, 1939), p. 198f.

[11] J. W. M. DuMond and E. R. Cohen, Rev. Mod. Phys. **20**, 82 (1948).

As a final check the positions of the band lines were calculated from the constants of Table III. These calculated values are given in columns 3 and 6 of Table I. The observed−calculated values in columns 4 and 7 show that almost all lines are represented within the accuracy of the measurements. From the systematic deviations resulting when slightly different constants are used we conclude that the B values are correct within ± 0.00015, α within ± 0.000015 and ν_0 within 0.03 cm^{-1} (see above).

The new B_0 value agrees very well with the value obtained from the Cameron bands,[8] i.e. 1.9228, but poorly with that obtained from the 1−0 and 2−0 infra-red bands,[6] i.e. 1.9150 cm^{-1} (see also Fig. 2 and the accompanying discussion).

A discussion of the vibrational constants of CO in its ground state will be given by one of us (K.N.R.) in a paper on the Cameron bands where the ν_0 value obtained here for the 4−0 band will be used.

Most of the work of this paper was carried out at the Yerkes Observatory of the University of Chicago. The support of this work by the administration of the Observatory is gratefully acknowledged. The junior author (K.N.R.) is holder of a Fellowship of the Government of India for which he wishes to express his sincere thanks.

THE JOURNAL OF CHEMICAL PHYSICS VOLUME 17, NUMBER 11 NOVEMBER, 1949

The Constant Frequency Raman Lines of N-Paraffins

TAKEHIKO SIMANOUTI AND SAN-ICHIRO MIZUSHIMA
Chemical Laboratory, Faculty of Science, Tokyo University, Tokyo, Japan
(Received March 28, 1949)

Assuming the Urey-Bradley field for the intramolecular potential, we have calculated the normal frequencies of long chain molecules in the extended form. Especially the vibration type of the frequencies remaining almost constant throughout the homologous series has been discussed. The result has been applied to the assignment of Raman lines of N-paraffins and of the infra-red absorption lines of polyethylene.

INTRODUCTION

THE Raman frequencies of N-paraffins (C_4 to C_{16}) have been observed in our laboratory by Mizushima, Morino, Okazaki, Nakamura, Takeda, and Simanouti in the solid state as well as in the liquid state. The frequencies observed in the solid state were assigned to the normal vibrations of the extended zigzag chain of N-paraffin molecules (see Table I). Of these frequencies we have already discussed two which are assigned to the chain frequencies corresponding to the Born-Karman condition

$$\lambda' = \pi/N$$

where N is the number of carbon atoms. One of these two frequencies changes from 425 cm^{-1} (C_4) to 150 cm^{-1} (C_{16}) and the other from 837 cm^{-1} (C_4) to 888 cm^{-1} (C_{16}).[1]

There are observed, however, other lines whose frequencies remain almost constant throughout the homologous series. In the case of $C_{16}H_{34}$ these frequencies were found to be 1058, 1135, 1295, 1442, 1471, 2846, 2878, 2934, and 2963 cm^{-1}. We shall discuss, in the following, the nature of these frequencies by calculating the normal modes of an infinite chain.

The calculation of skeletal modes of vibration of long chain molecules was made by Kirkwood,[2] and by Whitcomb, Nielsen, and Thomas,[3] but their method is not convenient for the treatment of molecules with complex potential function. We have, therefore, used Wilson's method for calculating the normal frequencies of the long chain

$$-(CXY-CZU)_n-$$

in the extended form in which all the C-atoms lie along two parallel lines in a plane.

INTERNAL COORDINATES

A part of the extended chain is shown in Fig. 1, from which the meaning of the following internal coordinates will be clear. R_0, r_{10}, r_{20}, $\cdots$ indicated in parentheses denote the equilibrium values.

$R_h(C_h-C'_h=R_0)$	$R'_h(C'_h-C_{h+1}=R_0')$
$r_{1h}(C_h-X_h=r_{10})$	$r'_{1h}(C'_h-Z_h=r'_{10})$
$r_{2h}(C_h-Y_h=r_{20})$	$r'_{2h}(C'_h-U_h=r'_{20})$
$\Theta_h(\angle C'_{h-1}C_hC'_h=\beta)$	$\Theta'_h(\angle C_hC'_hC_{h+1}=\beta')$
$\theta_h(\angle X_hC_hY_h=\alpha)$	$\theta'_h(\angle Z_hC'_hU_h=\alpha')$
$\varphi_{1h}(\angle X_hC_hC'_h=\gamma_1)$	$\varphi'_{1h}(\angle Z_hC'_hC_h=\gamma'_1)$
$\varphi_{2h}(\angle Y_hC_hC'_h=\gamma_2)$	$\varphi'_{2h}(\angle U_hC'_hC_h=\gamma'_2)$
$\varphi_{3h}(\angle X_hC_hC'_{h-1}=\gamma_3)$	$\varphi'_{3h}(\angle Z_hC'_hC_{h+1}=\gamma'_3)$
$\varphi_{4h}(\angle Y_hC_hC'_{h-1}=\gamma_4)$	$\varphi'_{4h}(\angle U_hC'_hC_{h+1}=\gamma'_4)$.

The suffix h of these 18 kinds of coordinates changes from zero to infinity for an infinite chain.

[1] S. Mizushima and T. Simanouti, J. Am. Chem. Soc. **71**, 1320 (1949).
[2] J. G. Kirkwood, J. Chem. Phys. **7**, 506 (1939).
[3] Whitcomb, Nielsen, and Thomas, J. Chem. Phys. **8**, 143 (1940).

TABLE I. Raman spectra of solid N-paraffins.*

C_4H_{10}	C_5H_{12}	C_6H_{14}	C_7H_{16}	C_8H_{18}	C_9H_{20}	$C_{10}H_{22}$	$C_{12}H_{24}$	$C_{16}H_{34}$
								150(3)
							194(2)	
						231(3)		
					249(2)			
				283(3)				
			311(5)					
		373(3)						
	406(3)							
425(4)								
837(6)								
	869(3)							
		898(3)	905(5)	899(2)	888(2)	886(2)	892(1)	888(1)
		1005(0)						
	1031(0)		1028(1)	1045($\frac{1}{2}$)				
1059(5)	1069(3)	1064(3)	1056(3)	1062(2)	1060(1)	1060(3)	1061(2)	1058(2)
			1072(2)					
1151(4)	1145(3)	1143(3)	1139(4)	1138(2)	1136(2)	1136(3)	1136(3)	1135(2)
1300(4)	1303(3)	1300(4)	1296(4)	1297(3)	1297(3)	1295(3)	1297(3)	1295(2)
				1384(1)				
1442(3)	1445(4)	1450(5)	1446(4*b*)	1449(3*b*)	1444(2)	1447(2*b*)	1441(3*b*)	1442(2*b*)
1460(2)	1466(5)	1462(4)	1473(3)	1469(3*b*)	1465(3)	1475(1)	1462(2*b*)	1471(2*b*)
					1486(0)			
	2666(1)				2660(1)	2660(1)		
2703(1)		2696(1)		2699(0)?				
2725(1)	2720(2)	2723(2)	2725(1)	2727(0)	2720(0)	2724(1)	2723(0*b*)?	
				2765(0)?				
2853(8)	2848(2)	2851(5)	2852(3)	2853(3*b*)	2847(2)	2843(2)	2845(4*b*)	2846(3)
	2859(2)							
			2866(2*b*)					
2872(8)		2871(5)	2878(7)		2877(5)	2877(6)	2879(10)	2878(5)
	2885(8)	2885(8)		2882(10)				
2896(10)	2909(4)	2907(5)	2904(2)					
2912(4)								
2931(1)	2934(5)	2934(5)	2930(3)	2937(2)	2934(2)	2935(1)	2933(1)	2934(1)
2950(4)	2956(2)	2953(3)	2950(2)					
2965(9)	2966(6)	2965(6)	2964(7)	2965(5)	2964(4)	2964(3)	2964(3)	2963(2)

*Quite recently N. Sheppard and G. J. Szasz (J. Chem. Phys. **17**, 86 (1949)) observed the Raman lines of solid N-butane, N-pentane, N-hexane, and N-heptane of the frequencies higher than 600 cm^{-1}. Their result agrees fairly well with ours.

THE *G*-MATRICES

By use of these internal coordinates the *G*-matrices related to the kinetic energy can be constructed. There are in all $18\times18=324$ such matrices of ∞th order. We shall only show a part of them.

	$\cdots$	ΔR_{h-1}	ΔR_h	ΔR_{h+1}	$\cdots$	$\cdots$	$\Delta R'_{h-1}$	$\Delta R'_h$	$\Delta R'_{h+1}$	$\cdots$	$\cdots$	$\Delta r_{1,h-1}$	$\Delta r_{1,h}$	$\Delta r_{1,h+1}$	$\cdots$
$\cdots$	$\cdots$	$\cdots$	$\cdots$	$\cdots$	$\cdots$	$\cdots$	$\cdots$	$\cdots$	$\cdots$	$\cdots$	$\cdots$	$\cdots$	$\cdots$	$\cdots$	$\cdots$
$\cdots$	$\cdots$	$\cdots$	$\cdots$	$\cdots$	$\cdots$	$\cdots$	$\cdots$	$\cdots$	$\cdots$	$\cdots$	$\cdots$	$\cdots$	$\cdots$	$\cdots$	$\cdots$
ΔR_{h-1}	$\cdots$	A_0	0	0	$\cdots$	$\cdots$	C'_0	0	0	$\cdots$	$\cdots$	C_{01}	0	0	$\cdots$
ΔR_h	$\cdots$	0	A_0	0	$\cdots$	$\cdots$	C_0	C'_0	0	$\cdots$	$\cdots$	0	C_{01}	0	$\cdots$
ΔR_{h+1}	$\cdots$	0	0	A_0	$\cdots$	$\cdots$	0	C_0	C'_0	$\cdots$	$\cdots$	0	0	C_{01}	$\cdots$
$\cdots$	$\cdots$	$\cdots$	$\cdots$	$\cdots$	$\cdots$	$\cdots$	$\cdots$	$\cdots$	$\cdots$	$\cdots$	$\cdots$	$\cdots$	$\cdots$	$\cdots$	$\cdots$
$\cdots$	$\cdots$	$\cdots$	$\cdots$	$\cdots$	$\cdots$	$\cdots$	$\cdots$	$\cdots$	$\cdots$	$\cdots$	$\cdots$	$\cdots$	$\cdots$	$\cdots$	$\cdots$

Here A_0, C_0, C_{01}, etc., are determined from the molecular configuration and are readily evaluated by Wilson's method:[4]

$$A_0=\mu_0+\mu_0'$$
$$C_0=\mu_0\cos\beta$$
$$C_0'=\mu_0'\cos\beta'$$
$$C_{01}=\mu_0\cos\gamma_1.$$
$$\cdots\quad\cdots$$
$$\cdots\quad\cdots$$

Here μ_0 and μ_0' denote the reciprocal of mass of C_h- and C_h'-atom, respectively.

[4] See J. C. Decius, J. Chem. Phys. **16**, 1025 (1948).

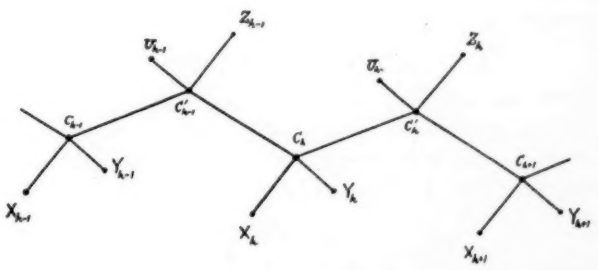

FIG. 1. The extended chain of $-(CXY-CZU)_n-$.

TABLE II. The F- and G-matrices for the infinite chain of $-(CH_2-CH_2)_n-$.

ΔR	a_0															
$\Delta R'$	c_0	a_0														
Δr_1	c_1	c_1	a													
Δr_2	c_1	c_1	c	a												
$\Delta r_1'$	c_1	c_1	0	0	a											
$\Delta r_2'$	c_1	c_1	0	0	c	a										
$\Delta\Theta$	k_0	k_0	l	l	h	h	b_0									
$\Delta\Theta'$	k_0	k_0	h	h	l	l	g	b_0								
$\Delta\theta$	l_0	l_0	k	k	0	0	d_0	u_0	b							
$\Delta\theta'$	l_0	l_0	0	0	k	k	u_0	d_0	0	b						
$\Delta\varphi_1$	k_1	l_1	k_2	l_2	h_1	h_2	e_0	g_0	e	u	b_1					
$\Delta\varphi_2$	k_1	l_1	l_2	k_2	h_2	h_1	e_0	g_0	e	u	e_1	b_1				
$\Delta\varphi_3$	l_1	k_1	k_2	l_2	h_1	h_2	e_0	g_0	e	u	e_2	d_1	b_1			
$\Delta\varphi_4$	l_1	k_1	l_2	k_2	h_2	h_1	e_0	g_0	e	u	d_1	e_2	e_1	b_1		
$\Delta\varphi_1'$	k_1	l_1	h_1	h_2	k_2	l_2	g_0	e_0	u	e	g_1	g_2	u_1	u_2	b_1	
$\Delta\varphi_2'$	k_1	l_1	h_2	h_1	l_2	k_2	g_0	e_0	u	e	g_2	g_1	u_2	u_1	e_1	b_1
$\Delta\varphi_3'$	l_1	k_1	h_1	h_2	k_2	l_2	g_0	e_0	u	e	u_1	u_2	g_1	g_2	e_2	d_1	b_1
$\Delta\varphi_4'$	l_1	k_1	h_2	h_1	l_2	k_2	g_0	e_0	u	e	u_2	u_1	g_2	g_1	d_1	e_2	e_1	b_1

Symmetrical matrix

THE POTENTIAL ENERGY

Assuming the Urey-Bradley field and neglecting the interaction between atoms far apart, we express the potential energy as:

$$\begin{aligned}V_h=&\Sigma_{R,R'}[K'_R R_0(\Delta R_h)+\tfrac{1}{2}K_R(\Delta R_h)^2]\\&+\Sigma_{r1,r2,r'1,r'2}[K'_r r_{10}(\Delta r_{1,h})+\tfrac{1}{2}K_r(\Delta r_{1,h})^2]\\&+\Sigma_{\Theta,\Theta'}[H'_\Theta R_0^2(\Delta\Theta_h)+\tfrac{1}{2}H_\Theta(R_0\Delta\Theta_h)^2]\\&+\Sigma_{\theta,\theta'}[H'_\theta r_{10}r_{20}(\Delta\theta_h)+\tfrac{1}{2}H_\theta r_{10}r_{20}(\Delta\theta_h)^2]\\&+\Sigma_{\varphi1,\varphi2,\varphi3,\varphi4,\varphi'1,\varphi'2,\varphi'3,\varphi'4}[H'_\varphi r_{10}R_0(\Delta\varphi_{1,h})\\&+\tfrac{1}{2}H_\varphi r_{10}R_0(\Delta\varphi_{1,h})^2]+\Sigma_{Q,Q'}[F'_Q Q_0(\Delta Q_h)\\&+\tfrac{1}{2}F_Q(\Delta Q_h)^2]+\Sigma_{q,q'}[F'_q q_0(\Delta q_h)+\tfrac{1}{2}F_q(\Delta q_h)^2]\\&+\Sigma_{p1,p2,p3,p4,p'1,p'2,p'3,p'4}[F'_p p_{10}(\Delta p_{1,h})\\&+\tfrac{1}{2}F_p(\Delta p_{1,h})^2]\end{aligned}$$

where Q_h, Q'_h, q_h, q'_h, $p_{1h}\cdots p'_{4h}$ denote the following interatomic distances not bonded directly with equilibrium values indicated in parentheses.

$$\begin{aligned}&Q_h(C'_{h-1}\cdots C'_h=Q_0) && Q'_h(C_h\cdots C_{h+1}=Q'_0)\\&q_h(X_h\cdots Y_h=q_0) && q'_h(Z_h\cdots U_h=q'_0)\\&p_{1h}(X_h\cdots C'_h=p_{10}) && p'_{1h}(Z_h\cdots C_h=p'_{10})\\&p_{2h}(Y_h\cdots C'_h=p_{20}) && p'_{2h}(U_h\cdots C_h=p'_{20})\\&p_{3h}(X_h\cdots C'_{h-1}=p_{30}) && p'_{3h}(Z_h\cdots C_{h+1}=p'_{30})\\&p_{4h}(Y_h\cdots C'_{h-1}=p_{40}) && p'_{4h}(U_h\cdots C_{h+1}=p'_{40}).\end{aligned}$$

These coordinates can be replaced by the afore-described internal coordinates ΔR_h, $\Delta R'_h$, Δr_{1h}, $\Delta r'_{1h}$, $\cdots\Delta\varphi'_{4h}$ and therefore the potential energy V can also be expressed in a quadratic form containing only these internal coordinates. From this potential energy expression the F matrices can at once be constructed.

ACTIVE FREQUENCIES

For the selection rule for a long chain molecule we have to consider the translational symmetry as well as the rotational symmetry. For the former, so long as the chain is short, a vibration may be active for

$$\lambda'=\pi/N$$

but for a long chain we must have

$$\lambda'=0$$

in other words all the atoms vibrate in phase (totally symmetric vibration).[3] Corresponding to this vibration we have a secular equation of 18th order

$$|\mathbf{GF}-\mathbf{E}\lambda|=0,$$

which is obtained by the reduction of the G- and F-matrices of ∞th order stated above. The elements of matrices of this secular equation can readily be obtained by summing all the elements in a row or a column of the matrices of ∞th order. For example, from the G-matrix shown above we have a new matrix

	ΔR	$\Delta R'$	Δr_1	...	...
ΔR	A_0	C_0+C_0'	C_{01}	...	...
...	...	...	...	...	...

For the molecule of N-paraffin $-(CH_2-CH_2)_n-$ we can set the equilibrium values of interatomic distances and bond angles equal to

$$R_0=R_0'=1.54\text{A},\quad r_{10}=r_{10}'=r_{20}=r_{20}'=r_0=1.09\text{A},$$

$$\alpha=\alpha'=\beta=\beta'=\gamma_1=\gamma_1'=\gamma_2=\gamma_2'=\gamma_3=\gamma_3'=\gamma_4=\gamma_4'=109°28'.$$

We have then the G- and F-matrices of 18th order of the form as shown in Table II.

Expressing the secular equation as

$$|\mathbf{GF}-3M_C\mathbf{E}\lambda|=0$$

(where M_C denotes the mass of a carbon atom), we have for the elements of the G-matrix:

$a_0=6$	$e_0=-8v^2+4v$	$k_0=-8v$
$a=3+w$	$e=4v-4-w$	$k=-4$
	$e_1=-6v^2-2v+5$	$k_1=-4$
$b_0=32v^2$	$e_2=10v^2-2v-3-w$	$k_2=-4v$
$b=16+4w$		
$b_1=12v^2+4v+6+2w$	$g_0=-8v^2+4v$	$l_0=4$
	$g=32v^2$	$l=4v$
$c_0=-2$	$g_1=12v^2+4v$	$l_1=4v+2$
$c=-1$	$g_2=-6v^2-2v$	$l_2=2v+2$
$c_1=-1$		
	$h=4v$	$u_0=-16v$
$d_0=-16v$	$h_1=-4v$	$u=4v$
$d_1=-4(2v^2+2v+1)$	$h_2=2v$	$u_1=10v^2-2v$
		$u_2=-8v^2-8v,$

where $v=r_0/R_0$ and $w=3M_C/M_H$, M_H denoting the mass of a hydrogen atom.

TABLE III. Selection rule for each vibration type.

	C_2	σ	i	
A_{1g}	+	+	+	Raman active
A_{2g}	+	−	+	Raman active
B_{1g}	−	+	+	Raman active
B_{2g}	−	−	+	Raman active
A_{1u}	+	+	−	Infra-red active
A_{2u}	+	−	−	—
B_{1u}	−	+	−	Infra-red active
B_{2u}	−	−	−	Infra-red active

TABLE IV. Force constants in 10^5 dynes/cm.

$K_{CC}=2.8$	$H_{CCC}=0.2$	$F_{CC}'=-0.05$	$F_{CC}=0.3$
$K_{CH}=4.2$	$H_{HCH}=0.4$	$F_{HH}'=0$	$F_{HH}=0.1$
	$H_{CCH}=0.15$	$F_{CH}'=-0.05$	$F_{CH}=0.4$

($\kappa=0.2\times10^{-11}$ dyne·cm)

For the elements of the F-matrix we have:

$$a_0=K_{CC}+\tfrac{2}{3}F'_{CC}+\tfrac{4}{3}F_{CC}+8t_0^2F'_{CH}+4s_0^2F_{CH}$$
$$a=K_{CH}+\tfrac{1}{3}F'_{HH}+\tfrac{2}{3}F_{HH}+4t_1^2F'_{CH}+2s_1^2F_{CH}$$
$$c_0=2(-\tfrac{1}{3}F'_{CC}+\tfrac{2}{3}F_{CC})$$
$$c=-\tfrac{1}{3}F'_{HH}+\tfrac{2}{3}F_{HH}$$
$$c_1=-2t_0t_1F'_{CH}+s_0s_1F_{CH}$$
$$k_0=(\tfrac{1}{3}F'_{CC}+\tfrac{1}{3}F_{CC})/v$$
$$k=\tfrac{1}{3}(F'_{HH}+F_{HH})$$
$$k_1=t_0s_1F'_{CH}+t_1s_0F_{CH}$$
$$k_2=(t_1s_0F'_{CH}+t_0s_1F_{CH})/v$$
$$b_0=\tfrac{1}{2}(H_{CCC}-\tfrac{2}{3}F'_{CC}+\tfrac{1}{3}F_{CC})/v^2+(3\kappa/4\sqrt{2}r_0^2)$$
$$b=\tfrac{1}{2}(H_{HCH}-\tfrac{2}{3}F'_{HH}+\tfrac{1}{3}F_{HH})+(3\kappa/4\sqrt{2}r_0^2)$$
$$b_1=\tfrac{1}{2}(H_{CCH}-s_0s_1F'_{CH}+2t_0t_1F_{CH})/v+(3\kappa/4\sqrt{2}r_0^2)$$
$$e_0=e=e_1=e_2=\kappa/2\sqrt{2}r_0^2$$
$$l_0=l=l_1=l_2=d_0=d_1=g_0=g_1=g_2=g=h=h_1=h_2=u_0=u=u_1=u_2=0,$$

where κ denotes the intramolecular tension[5] and

$$s_0=(R_0+\tfrac{1}{3}r_0)/p_{10},\quad s_1=(r_0+\tfrac{1}{3}R_0)/p_{10},\quad t_0=\tfrac{2}{3}r_0/p_{10},\quad t_1=\tfrac{2}{3}R_0/p_{10}.$$

REDUCTION OF THE SECULAR EQUATION

Taking into account the symmetry of the matrix shown in Table II, we shall use the following symmetry coordinates which are linear combinations of the internal coordinates,*

A_{1g}: $(\Delta R+\Delta R')/\sqrt{2}$
$(\Delta r_1+\Delta r_2+\Delta r_1'+\Delta r_2')/2$
$(\Delta\Theta+\Delta\Theta')/\sqrt{2}$
$(\Delta\theta+\Delta\theta')/\sqrt{2}$
$(\Delta\varphi_1+\Delta\varphi_2+\Delta\varphi_3+\Delta\varphi_4+\Delta\varphi_1'+\Delta\varphi_2'+\Delta\varphi_3'+\Delta\varphi_4')/(8)^{\frac{1}{2}}$

A_{2g}: $(\Delta\varphi_1-\Delta\varphi_2-\Delta\varphi_3+\Delta\varphi_4+\Delta\varphi_1'-\Delta\varphi_2'-\Delta\varphi_3'+\Delta\varphi_4')/(8)^{\frac{1}{2}}$

B_{1g}: $(\Delta R-\Delta R')/\sqrt{2}$
$(\Delta\varphi_1+\Delta\varphi_2-\Delta\varphi_3-\Delta\varphi_4+\Delta\varphi_1'+\Delta\varphi_2'-\Delta\varphi_3'-\Delta\varphi_4')/(8)^{\frac{1}{2}}$

B_{2g}: $(\Delta r_1-\Delta r_2+\Delta r_1'-\Delta r_2')/2$
$(\Delta\varphi_1-\Delta\varphi_2+\Delta\varphi_3-\Delta\varphi_4+\Delta\varphi_1'-\Delta\varphi_2'+\Delta\varphi_3'-\Delta\varphi_4')/(8)^{\frac{1}{2}}$

A_{1u}: $(\Delta r_1+\Delta r_2-\Delta r_1'-\Delta r_2')/2$
$(\Delta\Theta-\Delta\Theta')/\sqrt{2}$
$(\Delta\theta-\Delta\theta')/\sqrt{2}$
$(\Delta\varphi_1+\Delta\varphi_2+\Delta\varphi_3+\Delta\varphi_4-\Delta\varphi_1'-\Delta\varphi_2'-\Delta\varphi_3'-\Delta\varphi_4')/(8)^{\frac{1}{2}}$

A_{2u}: $(\Delta\varphi_1-\Delta\varphi_2-\Delta\varphi_3+\Delta\varphi_4-\Delta\varphi_1'+\Delta\varphi_2'+\Delta\varphi_3'-\Delta\varphi_4')/(8)^{\frac{1}{2}}$

B_{1u}: $(\Delta\varphi_1+\Delta\varphi_2-\Delta\varphi_3-\Delta\varphi_4-\Delta\varphi_1'-\Delta\varphi_2'+\Delta\varphi_3'+\Delta\varphi_4')/(8)^{\frac{1}{2}}$

B_{2u}: $(\Delta r_1-\Delta r_2-\Delta r_1'+\Delta r_2')/2$
$(\Delta\varphi_1-\Delta\varphi_2+\Delta\varphi_3-\Delta\varphi_4-\Delta\varphi_1'+\Delta\varphi_2'-\Delta\varphi_3'+\Delta\varphi_4')/(8)^{\frac{1}{2}}$

where A_{1g}, A_{2g}, etc., designating the type of vibration have the usual meaning. The G- and F-matrices are then reduced, the redundant coordinates disappear, and we have finally:**

$$\mathbf{G}_{A1g}=\begin{pmatrix}2+w, & -4, & 4\\ -4, & 8, & -8\\ 4, & -8, & 8+2w\end{pmatrix}$$

$$\mathbf{F}_{A1g}=\begin{pmatrix}a+c, & 2c_1+2vk_2, & -2k+k_2\\ 2c_1+2vk_2, & \{(a_0+c_0)-8v(2k_0-k_1)+4v^2(4b_0+b_1-6e)\}/2, & k_1+v(b_1-6e)\\ -2k+k_2, & k_1+v(b_1-6e), & (4b+b_1-6e)/2\end{pmatrix}$$

$$\mathbf{G}_{A2g}=(3w)$$
$$\mathbf{F}_{A2g}=(b_1-2e)$$
$$\mathbf{G}_{B1g}=\begin{pmatrix}16, & -8(2v+3)\\ -8(2v+3), & 4(2v+3)^2+6w\end{pmatrix}$$
$$\mathbf{F}_{B1g}=\begin{pmatrix}(a_0-c_0)/2, & k_1\\ k_1, & b_1/2\end{pmatrix}$$
$$\mathbf{G}_{B2g}=\begin{pmatrix}4+w, & -4(6v+1)\\ -4(6v+1), & 4(6v+1)^2+2w\end{pmatrix}$$
$$\mathbf{F}_{B2g}=\begin{pmatrix}a-c, & k_2\\ k_2, & b_1/2\end{pmatrix}$$
$$\mathbf{G}_{A1u}=\begin{pmatrix}2+w, & -4\\ -4, & 8+2w\end{pmatrix}$$
$$\mathbf{F}_{A1u}=\begin{pmatrix}a+c, & 2k-k_2\\ 2k-k_2, & (4b+b_1-6e)/2\end{pmatrix}$$
$$\mathbf{G}_{A2u}=(3w)$$
$$\mathbf{F}_{A2u}=(b_1-2e)$$
$$\mathbf{G}_{B1u}=(18+3w)$$
$$\mathbf{F}_{B1u}=(b_1)$$
$$\mathbf{G}_{B2u}=\begin{pmatrix}4+w, & -4\\ -4, & 4+2w\end{pmatrix}$$
$$\mathbf{F}_{B2u}=\begin{pmatrix}a-c, & k_2\\ k_2, & b_1/2\end{pmatrix}.$$

[5] T. Simanouti, J. Chem. Phys. **17**, 245 (1949).

* The symmetry coordinates of the A_{1g} and the A_{1u} types contain one redundant coordinate each.

** The $\mathbf{G}_{A1g}$-matrix expressed in terms of these symmetry coordinates is of the fourth order. However, through a suitable transformation we have the matrix of the third order shown here. The remaining one root of the secular equation is zero. Similarly we have the $\mathbf{G}_{A1u}$-matrix of the second order which was originally of the third order.

TABLE V. The calculated and the observed frequencies (cm^{-1}).

	Calculated	Observed	
A_{1g}	1073	1135	
	1516	1471	
	2873	2846, 2878	
A_{2g}	978	—	(Raman lines of solid N-cetane)
B_{1g}	1016	1058	
	1435	1442	
B_{2g}	1112	1295?	
	2910	2934, 2963	
A_{1u}	1475	1475	
	2907	2853	
A_{2u}	978	(inactive)	
B_{1u}	1349	1375	(Absorption lines of polyethylene)
B_{2u}	733	728	
	2928	2926	

SELECTION RULE DUE TO THE ROTATIONAL SYMMETRY

As the chain is considered to be infinitely long, the extended zigzag chain has the symmetry C_{2v} and C_{2h}. In the former case the rotation axis C_2 passes through the carbon nucleus and in the latter case it passes through the middle point of a bond connecting two consecutive carbon nuclei. The selection rule is shown in Table III, in which C_2 refers to C_{2v}, σ** to C_{2v} and C_{2h}, and i to C_{2h}. We have, therefore, five infra-red-active frequencies and eight Raman-active frequencies. For the former, one of us[6] derived already the secular equation

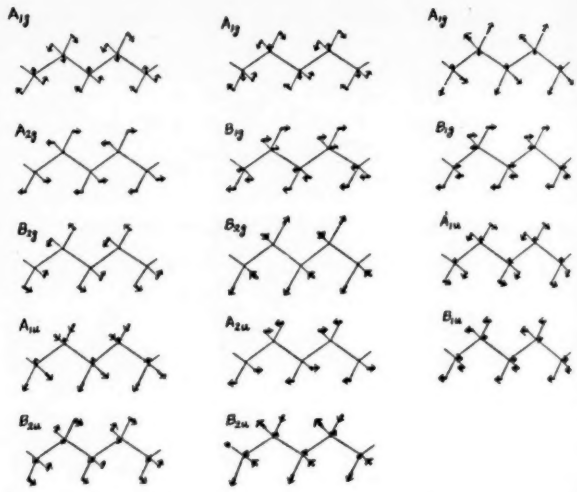

FIG. 2. The nature of the displacements of the atomic nuclei in the vibrations of the chain of $-(CH_2-CH_2)_n-$.

which coincides with the result obtained above. The nature of displacements of the atomic nuclei in these vibrations (Table III) is shown in Fig. 2.

CALCULATION OF FREQUENCIES

For the numerical calculation of frequencies we shall use the values of force constants (shown in Table IV) with which we have hitherto succeeded in calculating the frequencies of the molecules with similar structures.[5,6] In Table V are shown the calculated and observed frequencies, the latter being taken from the Raman spectrum of solid N-cetane and the infra-red absorption spectrum of polyethylene. The agreement between the theoretical and experimental values is good except the line at 1295 cm^{-1}. This line corresponds to that at 1170 cm^{-1} of ethane which is not in good agreement with the theoretical value (E_g) obtainable from a similar secular equation.[6] The discrepancies in these two cases may be due to a common origin.

** σ means the reflection in the plane containing the carbon nuclei.

[6] T. Simanouti, J. Chem. Phys. **17**, 734 (1949).

Thermodynamic Studies of Polyvinyl Acetate Solutions in the Dilute and Moderately Concentrated Range

GEORGE V. BROWNING AND JOHN D. FERRY
Department of Chemistry, University of Wisconsin, Madison, Wisconsin

(Received April 1, 1949)

Osmotic pressure measurements on polyvinyl acetate solutions have provided values of the constant μ in methyl ethyl ketone, 1,2,3-trichloropropane, acetone, dioxane, and dimethyl phthalate. Modifications in techniques have permitted measurements in the first two solvents at different temperatures at concentrations (c) up to 0.07 g/cc. The osmotic pressure can be expressed as a power series in c with three terms; the coefficients of c^2 and c^3 are larger in trichloropropane than in methyl ethyl ketone. The partial molal heats, entropies, and free energies of dilution in these two solvents have been calculated. All are numerically greater for trichloropropane. The heats of dilution are negative; $\Delta\bar{H}_1/v_2^2$ is roughly constant for methyl ethyl ketone but increases somewhat with concentration for trichloropropane. The entropies of dilution are much smaller than those given by the lattice theory.

THE steady flow viscosity and other mechanical properties of polyvinyl acetate solutions show a considerable dependence on the choice of solvent, which may be attributed in part to differences in specific polymer-solvent interaction. The thermodynamic properties also differ, and can provide some information concerning the magnitude of the interactions.

Most thermodynamic data from osmotic pressure measurements on polymer solutions have been limited to the range of very dilute solutions; exceptions are found in the work of Gee and Meyer[1] on rubber and Schick on polystyrene.[2] In the present study, we have extended osmotic pressure measurements on polyvinyl acetate over the concentration range up to about 0.07 g/cc. Data for solutions in methyl ethyl ketone and in 1,2,3-trichloropropane at different temperatures are reported here, together with a few measurements in several other solvents and some comments on experimental techniques. Our systems differ from others which have been investigated in the range of higher concentrations in that both polymer and solvents are polar.

MATERIALS

Polyvinyl acetate AYAX, lot 1232, was obtained through the kindness of Mr. A. K. Doolittle of Carbide and Carbon Chemicals Corporation. The whole polymer was used for some measurements, but it contained material of very low molecular weight which diffused through the osmotic membranes in certain solvents. Accordingly, to obtain samples with a somewhat sharper distribution of molecular weight, a rough fractionation was performed.[3] The solvent was acetone and the precipitant a mixture of equal volumes of water and methyl alcohol. Three fractions were separated; they were dissolved in benzene and dried from frozen solutions. Their relative amounts, number-average molecular weights, and intrinsic viscosities in methyl ethyl ketone at 25° are given in Table I, together with the values of k' in the equation[4] $\eta_{sp}/c=[\eta]+k'[\eta]^2c$. The fractions comprised 85 percent of the initial sample, the remaining 15 percent representing principally material of very low molecular weight.

Density measurements[5] on solutions of the whole polymer over the concentration range up to 10 percent in methyl ethyl ketone and to 5 percent in trichloropropane, at 13° and 40°C, showed that in each case the specific volume of the solution ($\bar{v}$) was a linear function of the weight fraction of polymer (w_2), as represented by the following equations:

in methyl ethyl ketone

$$\text{at } 13°,\ \bar{v}=1.232-0.411w_2;\ \bar{v}_2=0.821$$
$$\text{at } 40°,\ \bar{v}=1.275-0.442w_2;\ \bar{v}_2=0.833,$$

in 1,2,3-trichloropropane

$$\text{at } 13°,\ \bar{v}=0.7161+0.114w_2;\ \bar{v}_2=0.830$$
$$\text{at } 40°,\ \bar{v}=0.7346+0.106w_2;\ \bar{v}_2=0.841.$$

Linear interpolation was used to obtain values at other temperatures. In the case of methyl ethyl ketone, the specific volume and its temperature dependence agreed with the data of Doty and Mishuck.[6] According to the linear dependence on w_2, the partial specific volume of solvent was at all concentrations equal to the specific

TABLE I. Polyvinyl acetate fractions.

No.	Relative amount, percent	$\overline{M}_n$	$[\eta]^a$	k'
Unfractionated	100	140,000	0.96	0.37
I	13	840,000	1.61	0.48
II	56	280,000	0.98	0.46
III	16	62,000	0.34	1.47

[a] $(g/100\ cc)^{-1}$, in methyl ethyl ketone at 25°.

[1] G. Gee, Trans. Faraday Soc. **38**, 48 (1942); G. Gee and W. J. C. Orr, Trans. Faraday Soc. **42**, 507 (1946); Meyer, Wolff, and Boissonas, Helv. Chim. Acta **23**, 430 (1940).
[2] M. Schick, Ph.D. thesis, Polytechnic Institute of Booklyn, 1948; private communication from Professor B. H. Zimm.
[3] In collaboration with Mr. W. M. Sawyer.
[4] M. L. Huggins, J. Am. Chem. Soc. **64**, 2716 (1942).
[5] We are much indebted to Mr. Edward L. Foster for these measurements.
[6] P. M. Doty and E. Mishuck, J. Am. Chem. Soc. **69**, 1631 (1947).

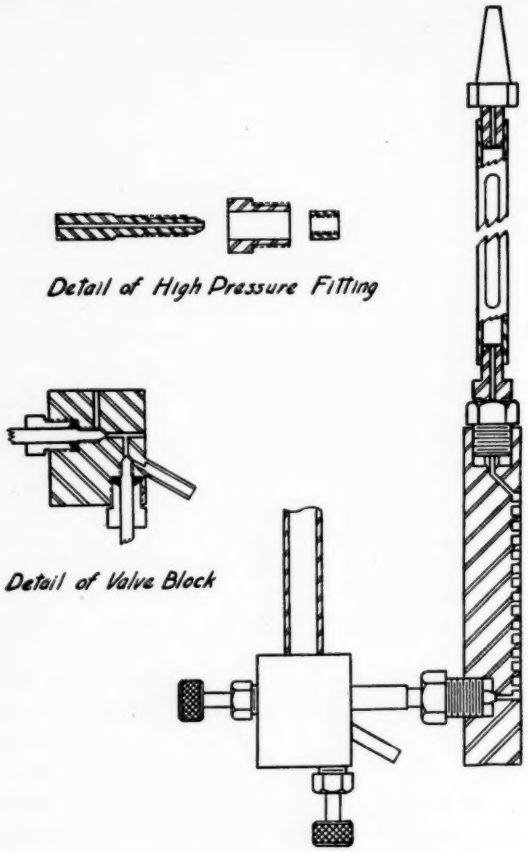

FIG. 1. Stainless steel osmometer.

volume of pure solvent; in subsequent calculations this is assumed to be the case for solutions of Fraction II as well as of the whole polymer. The partial specific volume of polymer, $\bar{v}_2$, is in each case close to the value (0.840) given by the reciprocal of the density of the pure polymer as listed by the manufacturer. Its temperature dependence (expansivity of about 5×10^{-4} per degree) appears to be about twice that of polystyrene in toluene.[7]

Dioxane (Carbide and Carbon Chemicals Corporation) was purified by refluxing with hydrochloric acid, neutralization, and distillation over sodium. Methyl ethyl ketone (Carbide and Carbon Chemicals Corporation) and 1,2,3-trichloropropane (Shell Chemical Corporation[8]) were dried over sodium sulfate and distilled through a 30-plate Oldershaw column. Acetone (C. P. grade) and dimethyl phthalate (Eastman) were used without further purification.

METHOD

Apparatus

An osmometer of the Flory type[9] was constructed of stainless steel, type 316, No. 4Mo. A few modifications were introduced (see Fig. 1). Valves are provided both for filling and for draining the cells, to obtain samples for analysis after equilibration. The conical valve stems are hardened stainless steel (Allegheny 2EZ type 416). Each capillary (0.5 mm), instead of being affixed by a fragile metal-to-glass seal, is enclosed by a stainless steel sleeve and is forced against the osmometer block by pressure from a nut at the top of the sleeve, a lead washer being inserted at each end of the glass tube.[10] Channels are cut in the sleeve to permit observation. The entire osmometer is immersed in a water thermostat regulated to 0.003°C, the capillaries and filling tubes projecting only an inch above the water level. Stainless steel straps attached to the blocks serve for handling. For measurements of osmotic pressures greater than 15 cm of solvent, the solution side of the osmometer can be connected by pressure tubing to a mercury manometer. The manometer is also connected to a 4 l. reservoir of air immersed in the thermostat, to avoid pressure changes due to slight volume changes in the tubing occasioned by fluctuations in room temperature, which would upset attainment of osmotic equilibrium.

Membranes

DuPont Cellophane No. 600 was soaked overnight in 30 percent sodium hydroxide, washed for a few minutes in progressive dilutions of sodium hydroxide and in water, and stored in 50 percent aqueous trimethylene glycol. The progressive dilutions of alkali were essential to avoid wrinkling of the membrane. After being clamped in the osmometer, the membrane was conditioned to the solvent by repeatedly filling and draining both sides of the osmometer.

A measure of the rapidity of approach to equilibrium in various solvents was afforded by noting the rates of hydrostatic adjustment with solvent on both sides of the membrane. Plots of the natural logarithm of the difference in height in the two capillaries against time gave straight lines in every case (except for acetone, where the initial slope is recorded); the slopes in hr^{-1} were as follows: acetone, 3.8; methyl ethyl ketone, 3.8; dioxane, 1.5; 1,2,3-trichloropropane, 0.7; dimethyl phthalate, 0.07; toluene, 0.005. These values reflect, primarily, different porosities of the membrane swollen to equilibrium in the different solvents. Osmotic studies in dimethyl phthalate are feasible, in spite of its high viscosity; but not in toluene with this type of membrane.

The dependence of porosity on solvent was also indicated by the ease of diffusion of low molecular weight components of the unfractionated polymer through the membrane. In acetone and methyl ethyl ketone, as much as 2 percent of the polymer was recovered on the solvent side of the membrane after equilibration, while in dioxane and 1,2,3-trichloropropane no such diffusion occurred.

[7] R. F. Boyer and R. S. Spencer, J. Polymer Sci. 3, 97 (1948).
[8] We are indebted to the Shell Chemical Corporation for a complimentary sample of this solvent.
[9] P. J. Flory, J. Am. Chem. Soc. 65, 372 (1943).
[10] This design was based on discussions with Dr. M. Wales, formerly of the U. S. Rubber Company.

TABLE II. Data from osmotic pressure measurements in dilute solution.

Polymer	Solvent	Temperature	$\bar{M}_n \times 10^{-3}$	μ	A_2 cm³g⁻², ×10⁴
Unfractionated	Acetone	25°	140	0.437	6.0
	Methyl ethyl ketone	25°	150	0.429	5.6
	Dioxane	25°	130	0.407	7.8
	Dioxane+5 percent dimethyl phthalate	25°	130	0.407	7.8
	Dimethyl phthalate	25°	—	0.400	5.0
Fraction I	Methyl ethyl ketone	25°	840	0.44	5
Fraction II	Methyl ethyl ketone	10°	300	0.43	5.3
		45°	300	0.43	5.0
	Trichloropropane	15°	270	0.38	8.0
		50°	270	0.38	8.0
Fraction III	Methyl ethyl ketone	25°	62	0.41	6.8

Equilibration of Impurities of Low Molecular Weight

To determine the effect of solvent impurities, equilibrations were made with pure dioxane against 1 percent solutions of water, dimethyl phthalate, and toluene in dioxane. Before each equilibration, the membrane was conditioned by standing overnight with the corresponding solution in both cells of the osmometer. In each case a difference in height of several centimeters was attained in about one hour, and subsequently fell to zero in about ten hours. The temporary pressure increase appeared on the solution side for the dimethyl phthalate and toluene solutions, but on the solvent side for the water solution, indicating that the water diffused more rapidly than the dioxane. These results emphasize the importance of solvent purity, and of protecting hygroscopic solvents from contact with water vapor.

It is of interest that, although toluene passes very slowly through a membrane immersed in pure toluene, toluene molecules in dilute solution diffuse readily through a membrane swollen in dioxane.

Details of Procedure

The difficulties with air bubbles described by others who have used 0.5 mm capillaries were eliminated by introducing small puffs of air with a rubber bulb at the tops of the capillaries between draining and refilling the cells. After puffing five times at five minute intervals, one fills the cells slowly by opening the filling tube valves, and then the drain valves are opened briefly to allow a few drops of liquid to escape before closing the filling valves.

Air was removed from each solution before loading by warming and briefly reducing the pressure until boiling occurred. The resulting change in concentration was of no consequence, because the final concentration was determined after equilibration. Each cell was drained, rejecting the first cc which represented the dead space between cell and valve; the liquid from the solution side was analyzed by dry weight in vacuum at 100°, and the solvent was also frequently analyzed to determine whether any diffusion across the membrane had occurred.

With unfractionated polymer, about 2 percent of the solute was recovered on the solvent side after twelve hours in methyl ethyl ketone, but none in dioxane. With Fraction II, about 1 percent was recovered after twenty-four hours in methyl ethyl ketone; since equilibrations required only three hours, this was considered negligible. In trichloropropane, equilibrations required about twelve hours, but no diffusion into the solvent side occurred within this period.

RESULTS

The unfractionated polymer and the fractions were studied in dilute solution in several solvents.[11] Fraction II was studied in methyl ethyl ketone at 10°, 25°, and 45°, and in 1,2,3-trichloropropane at 15° and 50° over an extended concentration range. The column heights were converted to pressures in g/cm², using the density

TABLE III. Osmotic pressures of Fraction II in methyl ethyl ketone.

10°		25°		45°	
conc., g/cc	π g/cm²	conc., g/cc	π g/cm²	conc., g/cc	π g/cm²
0.0052	0.77	0.0052	0.80	0.0076	1.50
0.0076	1.39	0.0074	1.40*	0.0078	1.59
0.0129	3.31*	0.0124	3.33	0.0081	1.75
0.0148	4.26	0.0127	3.35	0.0092	2.06
0.0194	7.02*	0.0128	3.45	0.0125	3.50
0.0315	19.0	0.0140	4.12	0.0126	3.52
0.0321	19.8	0.0146	4.28	0.0141	4.30*
0.0479	46.4	0.0165	5.36	0.0192	7.27
0.0572	66.6	0.0190	7.12*	0.0208	8.86
0.0590	73.1	0.0420	35.9	0.0274	15.3
0.0645	87.6	0.0421	35.9	0.0285	16.9
		0.0732	119.1	0.0351	26.1
				0.0453	45.7
				0.0563	73.0
				0.0675	108.0

* Average of duplicate determinations.

TABLE IV. Osmotic pressures of Fraction II in 1,2,3-trichloropropane.

15°		50°	
conc., g/cc	π g/cm²	conc., g/cc	π g/cm²
0.0054	1.23	0.0080	2.39
0.0074	1.96	0.0086	2.70
0.0110	4.06	0.0094	3.14
0.0112	4.12	0.0114	4.74
0.0135	5.67	0.0150	7.88
0.0171	8.95	0.0151	8.00
0.0205	13.85	0.0194	13.25
0.0217	15.00	0.0196	13.66
0.0220	15.11	0.0217	17.00
0.0224	17.10	0.0236	20.6
0.0301	32.5	0.0292	33.1
0.0327	39.4	0.0309	38.2
0.0381	55.8	0.0335	45.6
0.0413	67.1	0.0342	46.9
0.0592	156.5	0.0395	63.8

[11] We are much indebted to Mr. Lester D. Grandine, Jr. and Mr. W. W. Evans for help with these measurements.

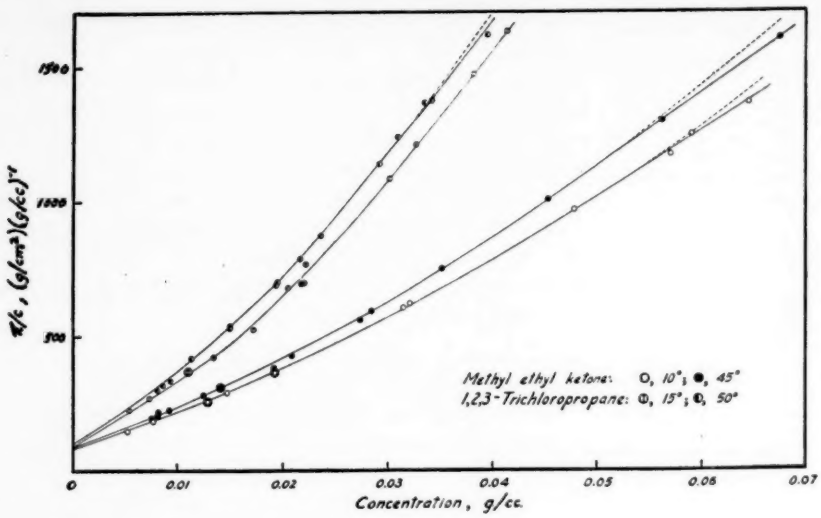

FIG. 2. Osmotic pressures of polyvinyl acetate solutions. Plots of π/c against c in 1,2,3-trichloropropane and methyl ethyl ketone. Dashed lines are calculated from Eq. (1) with the coefficients of Table VII.

TABLE V. Thermodynamic data for Fraction II in methyl ethyl ketone.

			25°C				
w_2	$\Delta\bar{H}_1$ cal./mole, $\times 10^2$	$\Delta\bar{S}_1$ cal./deg. mole, $\times 10^5$	$-\Delta\bar{F}_1$: $\pi\bar{V}_1$ $\times 10^2$	$-\Delta\bar{F}_1$: $-(\Delta\bar{H}_1 - T\Delta\bar{S}_1)$ $\times 10^2$	v_2	$\frac{\Delta\bar{H}_1}{v_2^2}$	$\frac{\Delta\bar{S}_1}{v_2}$
0.005	−0.024	0.29	0.13	0.11	0.0034	−22	0.0009
0.010	−0.11	0.74	0.33	0.33	0.0068	−24	0.0011
0.0175	−0.29	1.88	0.87	0.85	0.0118	−23	0.0016
0.025	−0.72	3.57	1.67	1.78	0.0170	−25	0.0021
0.035	−1.8	5.1	3.34	3.3	0.0238	−33	0.0021
0.045	−2.3	11.7	5.75	5.8	0.0307	−25	0.0038
0.055	−3.0	19.5	8.95	8.8	0.0377	−21	0.0051
0.065	−6.1	22.2	12.9	12.7	0.0447	−30	0.0050
0.075	−7.1	33.0	17.5	16.9	0.0517	−28	0.0064
						avg. −26	

TABLE VI. Thermodynamic data for Fraction II in 1,2,3-trichloropropane.

			30°C				
w_2	ΔH_1 cal./mole, $\times 10^2$	$\Delta\bar{S}_1$ cal./deg. mole, $\times 10^5$	$-\Delta\bar{F}_1$: πV_1 $\times 10^2$	$-\Delta\bar{F}_1$: $-(\Delta\bar{H}_1 - T\Delta S_1)$ $\times 10^2$	v_2	$\frac{\Delta\bar{H}_1}{v_2^2}$	$\frac{\Delta\bar{S}_1}{v_2}$
0.005	−0.23	0.73	0.47	0.45	0.0058	−68	0.0012
0.0075	−0.31	2.08	0.93	0.93	0.0087	−42	0.0024
0.010	−0.51	3.7	1.6	1.6	0.0115	−38	0.0032
0.015	−1.57	7.0	3.6	3.6	0.0173	−52	0.0040
0.020	−3.8	10.6	7.0	7.0	0.0231	−70	0.0046
0.025	−7.3	13.9	11.5	11.4	0.0288	−82	0.0059
0.029	−10.0	20.2	16.0	16.0	0.0335	−89	0.0062

TABLE VII. Coefficients for power series in c.

Solvent	Temperature	A_2 cm^3g^{-2}	A_3 cm^6g^{-3}
Methyl ethyl ketone	10°	5.3×10^{-4}	5.2×10^{-3}
	45°	5.0×10^{-4}	5.4×10^{-3}
1,2,3-trichloropropane	15°	8.0×10^{-4}	17.6×10^{-3}
	50°	8.0×10^{-4}	16.4×10^{-3}

data given above for methyl ethyl ketone and trichloropropane, and, for the other solvents, values calculated on the assumption of additivities of the volumes of polymer and solvent.

Measurements in Dilute Solution

The results for dilute solutions in acetone, methyl ethyl ketone, 1,2,3-trichloropropane, dioxane, dimethyl phthalate, and a 5 percent solution of dimethyl phthalate in dioxane, are summarized in Table II. Plots of π/c against c gave straight lines for the unfractionated polymer and Fraction III; for Fraction II (Fig. 2) and Fraction I there was upward curvature, in the latter case sufficient to make extrapolation somewhat uncertain. The molecular weights were calculated from the intercepts; the slopes are described both by the value of μ as used by Huggins,[12] and by the coefficient A_2 of Zimm.[13] No particular significance is attached to the fact that the values of M_n for different solvents do not appear to be quite identical, the differences being probably within experimental error.

It is clear that trichloropropane is much the best solvent, while the others are all roughly comparable. Our value of μ in acetone agrees well with that obtained by Sirianni, Wise, and McIntosh[14] (0.439), while our value in trichloropropane agrees with theirs in chloroform (0.377), suggesting an interaction characteristic of chlorinated hydrocarbons. A slight decrease in A_2 with increasing molecular weight is observed in methyl ethyl ketone, as predicted by the theories of Zimm[13] and Flory[15] for dilute solutions.

Measurements in Moderately Concentrated Solution

The results for more concentrated solutions of Fraction II in methyl ethyl ketone and trichloropropane are

[12] M. L. Huggins, J. Am. Chem. Soc. **64**, 1712 (1942).
[13] B. H. Zimm, J. Chem. Physics **14**, 164 (1946).
[14] Sirianni, Wise, and McIntosh, Can. J. Research **25B**, 301 (1947).
[15] P. J. Flory, J. Chem. Phys. **13**, 453 (1945).

given in Tables III and IV. The ratio π/c is plotted against c in Fig. 2; even at these moderate concentrations, it attains values enormously greater than the extrapolated, or ideal, value of π/c. It rises far more steeply in trichloropropane than in methyl ethyl ketone.

DISCUSSION

Coefficients for Power Series in c

In a treatment of the statistical mechanics of large molecules, Zimm[13] has expressed the osmotic pressure by the power series

$$\pi = RT(c/M_2 + A_2c^2 + A_3c^3 + \cdots). \quad (1)$$

The curves of Fig. 2 can be fitted by Eq. (1), using three terms; the coefficients are tabulated in Table VII. In Fig. 2, the calculated curves are indistinguishable from the experimental curves except for a slight divergence at the highest concentrations, where they are shown by broken lines. In trichloropropane, A_2 is larger and A_3 is much larger than in methyl ethyl ketone.

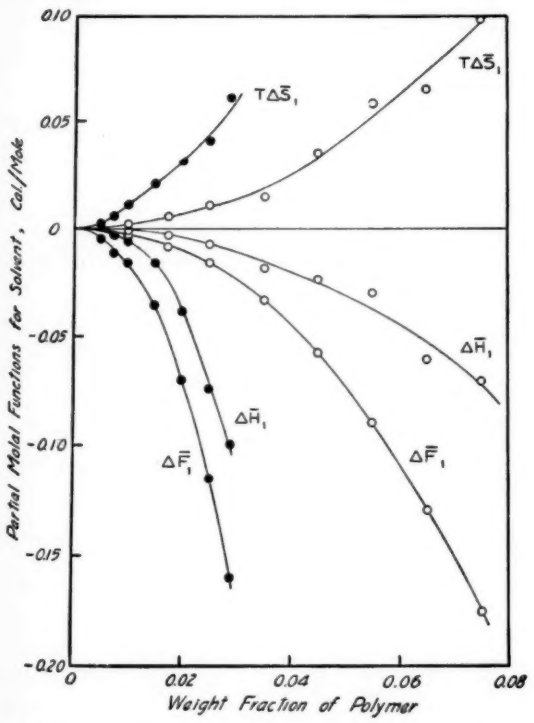

FIG. 3. Derived thermodynamic functions plotted against weight fraction of polymer. ○, methyl ethyl ketone; ●, 1,2,3-trichloropropane.

Derived Thermodynamic Data

The partial molal heat, entropy, and free energy of dilution of the solvent may be calculated by the equations[1]

$$\Delta\bar{H}_1 = \frac{T'(\pi\bar{V}_1)_T - T(\pi\bar{V}_1)_{T'}}{T - T'}, \quad (2)$$

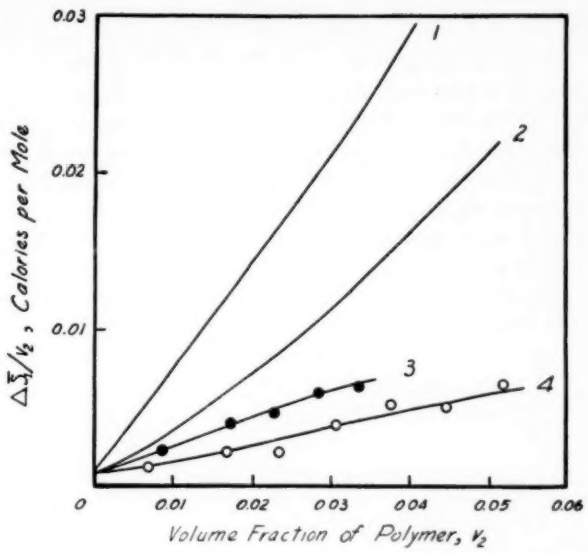

FIG. 4. Plots of $\Delta\bar{S}_1/v_2$ against v_2. 1, lattice theory; 2, rubber in benzene (Gee and Treloar); 3, polyvinyl acetate in 1,2,3-trichloropropane; 4, polyvinyl acetate in methyl ethyl ketone.

$$\Delta\bar{S}_1 = \frac{(\pi\bar{V}_1)_T - (\pi\bar{V}_1)_{T'}}{T - T'}, \quad (3)$$

$$\Delta\bar{F}_1 = -\pi\bar{V}_1, \quad (4)$$

where T and T' refer to two absolute temperatures, and the osmotic pressures are taken at constant weight fraction (w_2). These quantities have been derived from values of π interpolated from the experimental curves in Fig. 2 at concentrations corresponding to selected values of the weight fraction, and they are tabulated in Tables V and VI. The values of $\Delta\bar{F}_1$ refer to an intermediate temperature in each case; the agreement between $-\pi\bar{V}_1$ and $\Delta\bar{H}_1 - T\Delta\bar{S}_1$ indicates the precision of the differencing operations, which is quite satisfactory. Values of $\Delta\bar{H}_1/v_2^2$ and $\Delta\bar{S}_1/v_2$, where v_2 is the volume fraction of polymer, are also included. In Fig. 3, the thermodynamic functions are plotted against w_2.

Heat of Dilution

The heats of dilution are all negative. In the case of methyl ethyl ketone $\Delta\bar{H}_1$ is proportional to v_2^2 over the range studied. This relationship cannot be explained by the usual treatment of cohesive energy densities, of course, which holds only for positive heats of mixing. In trichloropropane $\Delta\bar{H}_1/v_2^2$ is at least twice as great as in the ketone, and increases somewhat with increasing concentration. This greater interaction with the chlorinated compound recalls the negative deviations from ideality in the system acetone-chloroform,[16] and the negative heat of dilution of cellulose acetate-tetrachloroethane.[17]

[16] S. Glasstone, Trans. Faraday Soc. **33**, 200 (1936).
[17] O. Hagger and A. J. A. van der Wyck, Helv. Chim. Acta **23**, 484 (1940).

Entropy of Dilution

In Fig. 4, our values of $\Delta\bar{S}_1/v_2$ are plotted against v_2, together with the data of Gee for rubber in benzene and the theoretical curve given by the lattice theory.[18] The experimental values are all considerably smaller than the theoretical, as Flory[15] points out is generally the case in dilute solutions. The entropies of dilution in the case of polyvinyl acetate are even smaller than those for rubber.

It is of interest to compare the initial slopes in Fig. 4 with those calculated from the theory of Flory in which the entropy of dilution is related to the volume of a coiled molecule as estimated from intrinsic viscosity.[15] The intrinsic viscosities[3] of Fraction II are 0.98 in methyl ethyl ketone and 1.35 in trichloropropane; the corresponding initial slopes from the theory are 29 and 43 cal./deg.-mole, respectively, while the observed values are 26 and 52. The agreement indicates that the higher entropy of dilution in trichloropropane may be due primarily to a more extended configuration of the polymer molecule, at least in very dilute solution.

[18] Reference 15, Eq. (4″) (assuming $z=6$).

In more concentrated solution, it might have been anticipated that the larger negative heat of dilution in trichloropropane would be accompanied by an ordering of the solvent by interaction with the polymer so that the entropy of dilution would be smaller than in methyl ethyl ketone. Nevertheless, $\Delta\bar{S}_1$ is higher in trichloropropane over the whole concentration range studied.

A more detailed interpretation may be facilitated by accumulation of similar thermodynamic data for concentrated solutions of other polymer systems. Correlations with mechanical properties will be given subsequently.

ACKNOWLEDGMENT

This work was supported in part by the Research Committee of the Graduate School of the University of Wisconsin from funds supplied by the Wisconsin Alumni Research Foundation, and in part by a grant from Research Corporation. We wish to thank Professor J. W. Williams for the use of a high precision cathetometer. We are especially indebted to Professor Bruno H. Zimm, University of California, for helpful suggestions in interpretation of the data.

THE JOURNAL OF CHEMICAL PHYSICS VOLUME 17, NUMBER 11 NOVEMBER, 1949

A Theory of Vapor Pressures of Liquids Based on van der Waals' Equation of State. II. Binary Mixtures †

FREDERICK T. WALL AND GUNTHER S. STENT*
Noyes Chemical Laboratory, University of Illinois, Urbana, Illinois
(Received April 4, 1949)

An expression for vapor pressures of binary liquid systems obeying van der Waals' equation of state is developed by generalizing a recent theory of vapor pressures of pure liquids. The resulting partial vapor pressure equations involve composition and temperature, and contain no empirical quantities other than van der Waals' constants including an inter-species interaction term.

The conditions under which Raoult's law holds for these systems are formulated, together with the conditions for which positive or negative deviations occur. The compositions at which azeotropes form are predicted, and the partial miscibility of binary liquid systems is discussed. A number of examples are calculated to illustrate the theory.

INTRODUCTION

In a previous paper[1] an expression was derived for the vapor pressure of a liquid, assuming the validity of van der Waals' equation of state and involving the use of an appropriate mathematical expression for the volume of a van der Waals' liquid. It was also shown that certain empirical laws, such as those of Trouton and Guldberg-Guye, could be deduced qualitatively. It is the purpose of the present paper to extend the vapor pressure treatment to binary mixtures of liquids and to compare the resulting vapor pressure equations with certain well-known rules, such as Raoult's and Henry's laws.

A theory of vapor pressures of binary mixtures obeying van der Waals' equation of state has already been developed by van Laar,[2] who employed methods similar to those of the present treatment but did not make use of a theory of vapor pressures of pure liquids. It is in this connection that the present development offers certain advantages, for vapor pressure relationships are derived involving no empirical quantities other than van der Waals' constants. Recently Wang[3] also discussed the behavior of van der Waals' fluids with some reference to mixtures.

Let us consider a mixture of two fluids and assume that a continuous transition from the gaseous to the

* Present address: Kerchhoff Laboratories of Biology, California Institute of Technology, Pasadena 4, California.
[1] F. T. Wall, J. Chem. Phys. **16**, 508 (1948).
[2] J. J. van Laar, Zeits. f. physik. Chemie **72**, 723 (1910); **83**, 599 (1913).
[3] J. S. Wang, Chinese J. Phys. **6**, 27 (1945).

liquid phase can occur according to van der Waals' equation of state for n moles:

$$(p+n^2a/V^2)(V-nb)=nRT. \quad (1)$$

We can then calculate the free energy change attending a compression of such a fluid from a low pressure (ideal) gaseous state to the liquid state by following a continuous van der Waals' path. We thus arrive at an expression for the total free energy of the liquid mixture, from which it becomes possible to calculate the chemical potential (partial molar free energy) of each constituent in the liquid phase. If the vapor in equilibrium with the solution is assumed to behave ideally, we can readily calculate the partial pressures from the chemical potentials in the liquid, since at equilibrium the chemical potential of each given constituent is the same in both phases.

BASIC THEORY

If a mixture of n_1 and n_2 moles of two fluids obeying Eq. (1) is compressed from the gas at a total pressure p^*, sufficiently low to insure ideal behavior, to the liquid state of fugacity f, then the change in free energy $F-F^*$ attending this compression is

$$F-F^*=(n_1+n_2)RT(\ln f-\ln p^*).\dagger \quad (2)$$

Since Dalton's law holds for the ideal gas,

$$F^*=n_1RT\ln x_1+n_2RT\ln x_2 +(n_1+n_2)RT\ln p^*+n_1\mu_1{}^0+n_2\mu_2{}^0, \quad (3)$$

where $\mu_1{}^0$ and $\mu_2{}^0$ are the standard chemical potentials, which are functions of temperature only, and $x_1=n_1/(n_1+n_2)$ and $x_2=n_2/(n_1+n_2)$. Therefore, the total free energy will be given by

$$F=n_1RT\ln x_1+n_2RT\ln x_2 +(n_1+n_2)RT\ln f+n_1\mu_1{}^0+n_2\mu_2{}^0. \quad (4)$$

The chemical potential, μ_1, of one of the constituents of the liquid then follows:

$$\partial F/\partial n_1=\mu_1=RT\ln f+RT\ln x_1 +(1-x_1)RT(\partial\ln f/\partial x_1)+\mu_1{}^0. \quad (5)$$

If the temperature is sufficiently low so that the partial vapor pressure, p_1, is small, then the chemical potential of this constituent in the vapor phase can be written as

$$\mu_1=RT\ln p_1+\mu_1{}^0. \quad (6)$$

Since the chemical potentials in each of the phases must be equal at equilibrium, we can equate (5) and (6) and thus obtain the vapor pressure equation

$$\ln p_1=\ln f+\ln x_1+(1-x_1)(\partial\ln f/\partial x_1). \quad (7)$$

† Equation (2) can be considered a definition of the fugacity, f, of a fluid mixture. It must not be assumed, however, that f is necessarily equal to the sum of the partial pressures, even if the vapors are ideal.

Similarly,

$$\ln p_2=\ln f+\ln x_2+(1-x_2)(\partial\ln f/\partial x_2). \quad (8)$$

In general, the vapor in equilibrium with the liquid will not have the same composition as the gas from which the liquid was generated by the continuous compression.

Assuming that van der Waals' "constants" a and b are defined for a binary mixture, we can now use the relationship previously derived for the fugacity of a van der Waals' liquid,

$$\ln f=\ln(a/b^2)-a/bRT, \quad (9)$$

and substitute the same in Eqs. (7) and (8). Van der Waals[4] himself suggested a form for a and b applicable to binary mixtures, namely,

$$a=x_1^2a_1+2x_1x_2a_{12}+x_2^2a_2, \quad (10)$$

and

$$b=x_1b_1+x_2b_2, \quad (11)$$

where a_1, a_2, b_1, and b_2 are the constants for the pure constituents and a_{12} a new constant characteristic of inter-species interaction. Equations (10) and (11) seem plausible when it is realized that in the original equation of state, (1), the coefficient of a is quadratic in n, suggesting some sort of bimolecular interaction, whereas the coefficient of b is only linear.

Making use of Eqs. (10) and (11), Eqs. (7) and (8) become

$$\ln p_1=\ln x_1+\ln(a/b^2)+2\left\{\frac{x_1a_1+x_2a_{12}}{a}-\frac{b_1}{b}\right\} +(1/RT)\left\{\frac{ab_1}{b^2}-\frac{2x_1a_1+2x_2a_{12}}{b}\right\}, \quad (12)$$

$$\ln p_2=\ln x_2+\ln(a/b^2)+2\left\{\frac{x_2a_2+x_1a_{12}}{a}-\frac{b_2}{b}\right\} +(1/RT)\left\{\frac{ab_2}{b^2}-\frac{2x_2a_2+2x_1a_{12}}{b}\right\}. \quad (13)$$

Thus we have derived general expressions for the vapor pressures of the two components in a binary solution in terms of the composition, temperature and the van der Waals' constants.

It is evident from (9), (10), and (11) that for a pure component, i.e., when $x_1=1$, the vapor pressure equation reduces to

$$\ln p_1{}^0=\ln(a_1/b_1^2)-a_1/b_1RT, \quad (14)$$

the equation previously derived.[1]

An important restriction implicit in the derivation of (9)[1] is that the heat of vaporization, which was

[4] J. D. van der Waals, *Die Continuität des gasförmigen und flüssigen Zustandes* (Johann Ambrosius Barth, Leipzig, 1899).

TABLE I.

Fig.		$b_1^2a_2/b_2^2a_1$	b_2/b_1	x_1^*
1	0.1	1	1.0694	0.321
2	−0.1	1	1.0694	0.689
3	0	2	0.5346	0.449
4	−0.15	1	1.0694	0.649
5	0	2.72	0.4044	0.403

shown to equal a/b for a single substance, be large compared to RT. For binary systems this requires that

$$\frac{x_1^2a_1+2x_1x_2a_{12}+x_2^2a_2}{x_1b_1+x_2b_2} \gg RT, \tag{15}$$

for all x's. Accordingly, the present treatment is valid only for cases where the inequality (15) is satisfied.

IDEAL AND DILUTE SOLUTION BEHAVIOR

If Eq. (12) is expanded for small values of x_2, one obtains the relationship

$$\ln p_1=\ln x_1+\ln(a_1/b_1^2)-a_1/b_1RT + 2\left(1-\frac{a_{12}}{a_1}\right)\left(\frac{b_2}{b_1}-\frac{a_{12}}{a_1}\right)x_2^2+\cdots. \tag{16}$$

Combining (14) and (16), it is seen that

$$p_1=x_1p_1^0\exp\left[2\left(1-\frac{a_{12}}{a_1}\right)\left(\frac{b_2}{b_1}-\frac{a_{12}}{a_1}\right)x_2^2\cdots\right]. \tag{17}$$

Since the exponential function contains no terms in x_2 lower than degree two, Eq. (17) approaches Raoult's law, $p_1=x_1p_1^0$, asymptotically as $x_2\to 0$.

From the Duhem-Margules equation, with which the vapor pressure equations derived above are, of course, fully compatible, it follows that if one constituent obeys Raoult's law, the other must at least obey Henry's law, i.e., $p_2=K_2x_2$. Furthermore, it can be shown by analogous reasoning that when $x_1\to 0$, $p_2\to x_2p_2^0$ and $p_1\to K_1x_1$. Thus we find that each constituent of a binary liquid mixture of van der Waals' fluids obeys Raoult's law in its concentrated and Henry's law in its dilute solutions.

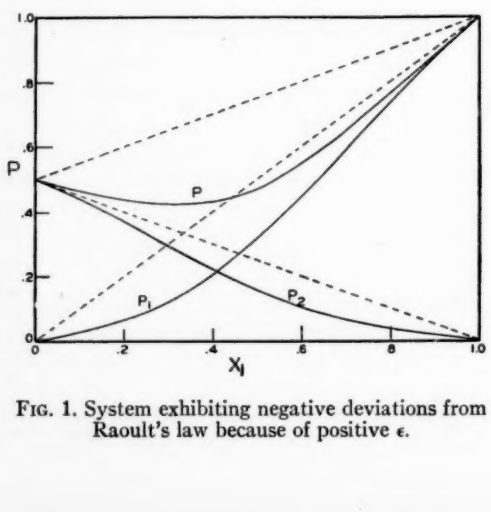

FIG. 1. System exhibiting negative deviations from Raoult's law because of positive ϵ.

The Henry's law constants for the infinitely dilute solutions can be readily evaluated from the limit

$$K_i=\lim_{x_i\to 0}\left\{f\exp\left[(1-x_i)\frac{\partial \ln f}{\partial x_i}\right]\right\}, \tag{18}$$

which, upon proper substitution from (9), (10), and (11), are found to be

$$K_1=\frac{a_2}{b_2^2}\exp\left[2\left(\frac{a_{12}}{a_2}-\frac{b_1}{b_2}\right)+\frac{1}{RT}\left(\frac{a_2b_1}{b_2^2}-\frac{2a_{12}}{b_2}\right)\right], \tag{19}$$

and

$$K_2=\frac{a_1}{b_1^2}\exp\left[2\left(\frac{a_{12}}{a_1}-\frac{b_2}{b_1}\right)+\frac{1}{RT}\left(\frac{a_1b_2}{b_1^2}-\frac{2a_{12}}{b_1}\right)\right]. \tag{20}$$

Van der Waals found[3] for a binary *gaseous* mixture that if

$$a_{12}=(a_1a_2)^{\frac{1}{2}}, \tag{21}$$

and

$$b_1^2/a_1=b_2^2/a_2, \tag{22}$$

then a description of the behavior of the mixture was much simplified. If (21) and (22) are substituted into (12) and (13), we obtain the expressions

$$\ln p_1=\ln x_1+\ln(a_1/b_1^2)-a_1/b_1RT=\ln x_1p_1^0,$$
$$\ln p_2=\ln x_2+\ln(a_2/b_2^2)-a_2/b_2RT=\ln x_2p_2^0,$$

which are, again, statements of Raoult's law, valid now for all compositions. Thus according to the present theory, relationships (21) and (22) are sufficient conditions for ideal behavior, i.e., compliance with Raoult's law; the same conditions can also be shown to be necessary. It is of interest to note that (21) means that the inter-species interaction is the geometric mean of the intra-species interaction, whereas (22) implies the equality of the critical pressures of the two components. Van Laar also found[2,5] that (21) and (22) are sufficient conditions for ideality in the vapor pressure equations derived by him.

NON-IDEAL BEHAVIOR[6]

When Eqs. (21) and (22) do not hold, the binary system will not obey Raoult's law but will exhibit positive or negative deviations therefrom depending upon the numerical relationships between the van der Waals' constants. First let us suppose that Eq. (22) applies, but that in place of (21) we have

$$a_{12}=(a_1a_2)^{\frac{1}{2}}(1+\epsilon), \tag{21a}$$

where ϵ can be either positive or negative. Substituting

[5] J. J. van Laar, *Die Zustandsgleichung von Gasen und Flüssigkeiten* (Leopold Voss, Leipzig, 1924).

[6] See J. H. Hildebrand, *Solubility of Non-Electrolytes* (Reinhold Publishing Corporation, New York, 1936), for a general treatment of non-ideal systems and partial miscibility.

(21a) and (22) into Eqs. (19) and (20), it is readily shown that

$$\ln\left(\frac{K_1}{p_1^0}\right)=2\epsilon\frac{b_1}{b_2}(1-a_2/b_2RT), \tag{23}$$

and

$$\ln\left(\frac{K_2}{p_2^0}\right)=2\epsilon\frac{b_2}{b_1}(1-a_1/b_1RT). \tag{24}$$

Since a_1/b_1 and a_2/b_2 are both large compared to RT, it follows that if ϵ is positive, the system will exhibit negative deviations from Raoult's law and vice versa. This conclusion is a reasonable one, since a positive ϵ implies a larger attraction between unlike molecules than would exist for ideal systems. Although the above deduction was made with respect to the Henry's law constants only, the same conclusions can be shown to

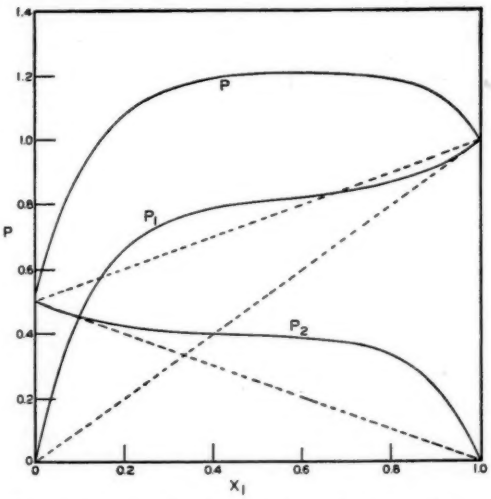

FIG. 2. System exhibiting positive deviations from Raoult's law because of negative ϵ.

be valid at intermediate compositions where Henry's laws would not hold.

If Eq. (21) is obeyed but (22) is not true, then the analysis of the problem is somewhat more complicated. Mathematical manipulations of a somewhat involved nature show that under these circumstances the binary system will generally, but not always, exhibit positive deviations from Raoult's law. Small negative deviations are realized under some circumstances but only if (22) is almost correct or if the vapor pressures of the pure liquids are extremely different. It is evident, therefore, that an actual system exhibiting marked negative deviations from Raoult's law must have a significantly positive ϵ. In this connection it is interesting to note further that a necessary but not sufficient condition for a negative heat of mixing of liquids is that ϵ be positive.[2]

It is also possible to find values for the van der Waals' constants which would enable one to predict negative deviations at one end of the composition scale and positive deviations at the other. Since the ranges of values giving rise to such phenomena are extremely

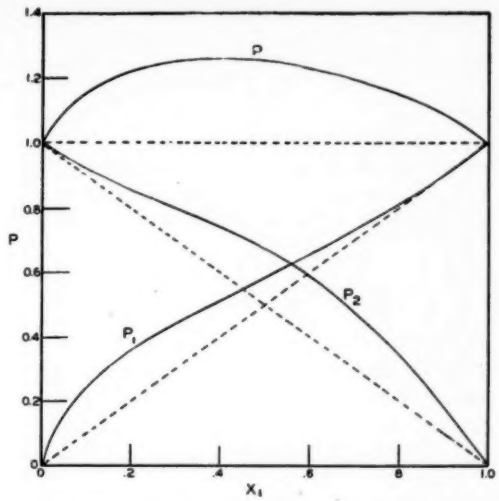

FIG. 3. System exhibiting positive deviations from Raoult's law because of departures from Eq. (22).

limited, it would be expected that such a behavior would be rarely encountered, which is in accordance with observation.

CONSTANT BOILING MIXTURES

If the total vapor pressure of a binary mixture exhibits a maximum or minimum at some composition, the system will form a constant boiling mixture for which the composition of the vapor is the same as that of the liquid. Most systems which show substantial deviations from Raoult's law will form such constant boiling mixtures if the vapor pressures of the pure liquids are near each other. The condition for this behavior is simple for ideal vapors obeying Dalton's law, *viz.*,

$$\ln x_1-\ln p_1=\ln x_2-\ln p_2. \tag{25}$$

Combining the above equation with (7) and (8) it follows that

$$\partial \ln f/\partial x_1=0, \tag{26}$$

which is also the condition for a maximum or minimum of the total vapor pressure. But from (9) it is seen that

$$\frac{\partial \ln f}{\partial x_1}=\frac{d\ln(a/b^2)}{dx_1}-\frac{1}{RT}\frac{d(a/b)}{dx_1}=0, \tag{27}$$

which can be written as

$$a^2\frac{db}{dx_1}-ab\frac{da}{dx_1}-2abRT\frac{db}{dx_1}+b^2RT\frac{da}{dx_1}=0. \tag{28}$$

From (10) and (11) it will be seen that Eq. (28) is a fourth degree equation in the composition. If a constant boiling mixture exists, one of the four roots of Eq. (28) will correspond to the composition of such a mixture; otherwise, all four roots will be physically meaningless.

To avoid solution of a fourth degree equation, it is

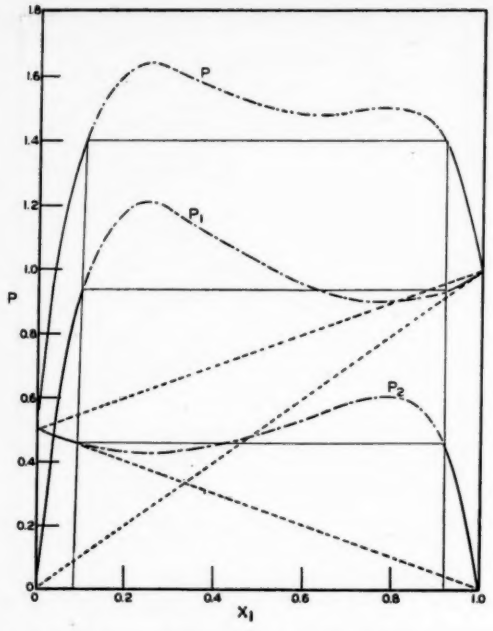

FIG. 4. System exhibiting partial miscibility because of large negative ϵ.

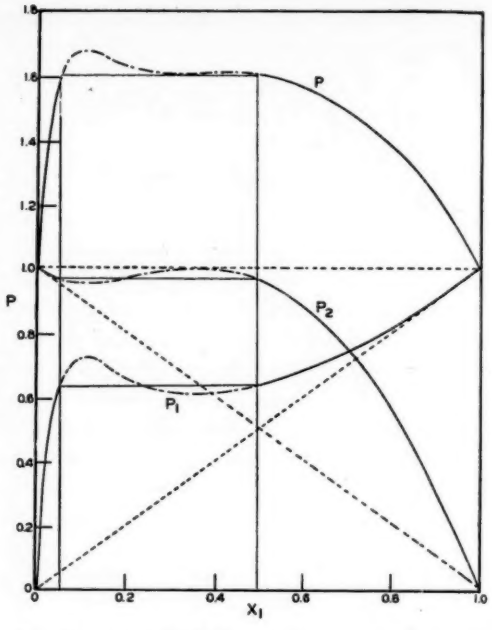

FIG. 5. System exhibiting partial miscibility because of large departure from Eq. (22).

expedient to expand (28) as

$$b\frac{da}{dx_1}-a\left\{1-\frac{bRT}{a}-\left(\frac{bRT}{a}\right)^2-\left(\frac{bRT}{a}\right)^3\cdots\right\}\frac{db}{dx_1}=0, \quad (29)$$

which reduces to a quadratic equation in the composition if one makes use of the fact that bRT/a is small compared to unity and neglects all terms in bRT/a with exponent greater than unity. This approximation is numerically excellent and has the further advantage that two of the physically meaningless roots are simultaneously eliminated.

PARTIAL MISCIBILITY[6]

If positive deviations from Raoult's law are sufficiently great, then the partial vapor pressure curves will exhibit maxima and minima, implying the existence of thermodynamically metastable solutions which would tend to separate into two liquid phases. This gives rise to the phenomenon of partial miscibility, which occurs whenever ϵ (of Eq. (21a)) is a sufficiently large negative number or when departures from (22) are great enough.

The present theory of vapor pressures permits the calculation of critical solution temperatures, but the mathematical expressions are quite involved. At the critical solution temperature, the partial vapor pressure curves will each exhibit horizontal points of inflection, so that $\partial p_1/\partial x_1$ and $\partial^2 p_1/\partial x_1^2$ are simultaneously zero. Using Eq. (7), the conditions for the critical solution point become

$$\frac{1}{x_1}+(1-x_1)\frac{\partial^2 \ln f}{\partial x_1^2}=0, \quad (30)$$

and

$$\frac{1}{x_1^2}+\frac{\partial^2 \ln f}{\partial x_1^2}-(1-x_1)\frac{\partial^3 \ln f}{\partial x_1^3}=0. \quad (31)$$

Since the critical solution point also corresponds to a constant boiling mixture, Eq. (30) can be replaced by (26) without loss of generality. Simultaneous solution of (30) and (31) can be done by numerical methods but is algebraically very complicated for all except some simple special examples.

ILLUSTRATIVE EXAMPLES

To illustrate some of the concepts discussed, calculations have been made for several hypothetical systems all exhibiting departures from Raoult's law. A description of the conditions assumed is given in Table I, and the corresponding graphs are shown in Figs. 1–5. The calculated compositions of the constant boiling mixtures are indicated in the column labeled x_1^*. In every instance, p_1^0 was taken as unity, and a_1/b_1RT equal to 10.

Figure 1 illustrates negative deviations from Raoult's law due to a positive ϵ. Figures 2 and 3 show positive deviations due to negative ϵ in one instance and to departure from Eq. (22) in the other. Figures 4 and 5 exhibit sufficiently large positive deviations so that partial miscibility occurs. The compositions of the two phases are determined by requiring that the partial pressure of each component be the same in both phases. The compositions of the constant boiling mixtures calculated by means of the approximate Eq. (29) agree well with those observed graphically. For the cases involving partial miscibility, the constant boiling mixtures are, of course, hypothetical.

Diffusion in Binary Liquid Hydrocarbon Mixtures

D. J. TREVOY AND H. G. DRICKAMER
Department of Chemistry, University of Illinois, Urbana, Illinois

(Received April 1, 1949)

Diffusion coefficients have been obtained for binary mixtures of paraffin hydrocarbons and for mixtures of paraffin hydrocarbons with benzene using a diaphragm cell. The results have been tested by the equations of Arnold, of Stokes and Einstein, and of Stearn, Irish, and Eyring. Of these only the semi-empirical relationship of Arnold gives satisfactory agreement with experiment.

WHILE there have been a great many measurements of diffusion coefficients in liquid systems, there is little organized information concerning concentrated organic systems. With this in mind measurements have been made in a series of binary mixtures of paraffin hydrocarbons and of paraffin hydrocarbons with benzene.

KINETIC THEORY

In an attempt to correlate diffusivities in liquid systems Arnold[1] gives an equation the form of which was derived from the kinetic theory of gases.

$$D=\frac{0.0010(1/M_1+1/M_2)^{\frac{1}{2}}}{A_1A_2\eta_2^{\frac{1}{3}}S^2}. \tag{1}$$

The constant was determined for 20°C, A_1 and A_2 are abnormality factors to take account of "association," M_1 and M_2 are the molecular weights and S is defined by the relation

$$S=V_1^{\frac{1}{3}}+V_2^{\frac{1}{3}}, \tag{2}$$

where V_1 and V_2 are molecular volumes calculated by the Kopp-Le Bas system. The constants were calculated for dilute solutions and consequently the viscosity of the pure solvent appears in the equation.

For the variation of D with T over short ranges of temperature Arnold suggests the Nernst equation

$$D=D_0[1+b(T-293)], \tag{3}$$

where b is given by the equation

$$b=0.20\eta^{\frac{1}{3}}\rho^{-\frac{1}{3}}. \tag{4}$$

The Stokes-Einstein equation has often been used in the interpretation of diffusivities.

$$D=(kT/6\pi r\eta). \tag{5}$$

It was derived by Einstein[2] by equating the osmotic pressure on a particle, given by van't Hoff's equation, to the resistance given by Stokes' law. The assumptions that osmotic pressure is the driving force in diffusion and that van't Hoff's equation holds are valid only in dilute solution. Stokes' law assumes a continuum and therefore requires that the diffusing molecules are very large compared to those of the medium. Because of these assumptions the Stokes-Einstein equation has limited applicability to diffusion in liquids.

For absolute values of diffusion rates Stearn, Irish, and Eyring[3] derived the relation

$$D=\frac{\mu^2}{(f^{\frac{1}{3}})^{\frac{3}{2}}}\left(\frac{kT}{2\pi m}\right)^{\frac{1}{2}}\exp\left(-\frac{\Delta E_{\text{vap}}}{\nu RT}\right), \tag{6}$$

where μ is the distance between successive equilibrium positions of a molecule and may be taken as $(V/N)^{\frac{1}{3}}$; $(f)^{\frac{1}{3}}$ is the free volume estimated by the equation

$$(f^{\frac{1}{3}})^{\frac{3}{2}}=\frac{sRTV^{\frac{1}{3}}}{N^{\frac{1}{3}}\Delta E_{\text{vap}}}. \tag{7}$$

The quantity s is a packing number and equals 2 for cubical packing, while ν is taken as 3 assuming that the activation energy for diffusion is one-third the energy of vaporization. Mean values for use in Eq. (6) are obtained as follows

$$\mu=\mu_1c_1+\mu_2c_2, \tag{8}$$

$$(f^{\frac{1}{3}})^{\frac{1}{2}}=c_1(f_1^{\frac{1}{3}})^{\frac{1}{2}}+c_2(f_2^{\frac{1}{3}})^{\frac{1}{2}}, \tag{9}$$

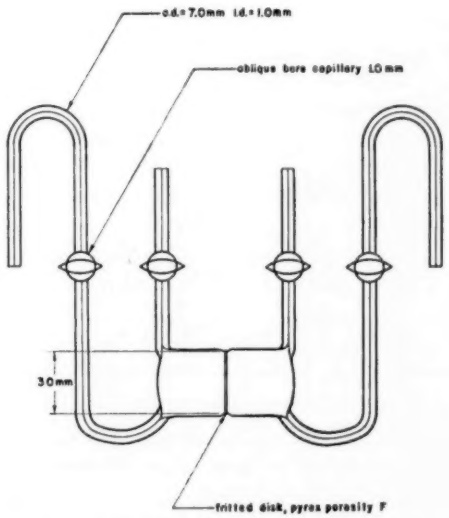

FIG. 1. Diaphragm cell for measurement of diffusion coefficients in liquids.

[1] J. H. Arnold, J. Am. Chem. Soc. **52**, 3937 (1930).
[2] A. Einstein, Ann. d. Physik **17**, 549 (1905).
[3] Stearn, Irish, and Eyring, J. Phys. Chem. **44**, 981 (1940).

$$(\Delta E)_{\text{vap}}^{\frac{1}{2}} = c_1(\Delta E_1)^{\frac{1}{2}} + c_2(\Delta E_2)^{\frac{1}{2}}, \quad (10)$$

$$M = (M_1 M_2 / M_1 + M_2), \quad (11)$$

where M_1 and M_2 are molecular masses and C_1 and C_2 are mole fractions.

PHENOMENOLOGICAL THEORY

The diffusion coefficient has been defined by Fick[4] who stated that for unidimensional diffusion in the x direction the mass diffusing in time dt is

$$-Da(dn/dx)dt, \quad (12)$$

where n is expressed in units of mass per unit volume for either component.

If D is assumed constant, this integrates to

$$\Delta n_i / \Delta n_f = \exp[\gamma D l], \quad (13)$$

where $\gamma = a/l(1/V' + 1/V'')$, a = area for diffusion, V', V'' = cell volumes, l = path length, and $\Delta n = n' - n''$.

This result gives the integral diffusion coefficient over the concentration range. It has been shown[5] that where the cell volumes are equal the integral coefficient equals the differential coefficient at the average concentration.

EXPERIMENTAL METHODS AND RESULTS

1. Purification of Chemicals

Benzene* used in the experiments was thiophene-free, meeting A.C.S. specifications; n-heptane, 2,4-dimethyl pentane† and cyclohexane were Phillips pure grade chemicals having a minimum purity of 99 mole percent.‡ These chemicals were used without purification.

The normal hydrocarbons from decane through octadecane had a minimum purity of 95 mole percent** as purchased. These chemicals were purified by shaking five times in a separatory funnel with concentrated sulfuric acid, water washing three times, alkali washing once, and finally water washing five times. After drying for 24 hours over anhydrous calcium chloride the liquid was decanted and distilled through a short glass column under reduced pressure and at a temperature of about 100°C. The first 10 percent and the last 10 percent of the distillate were discarded, and the middle portion was dried over sodium wire.

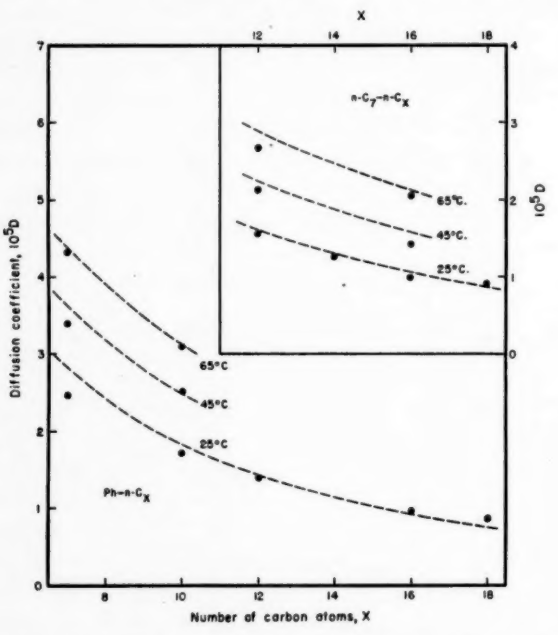

FIG. 2. A comparison of observed diffusion coefficients with values calculated by Arnold's equation. Observed values are indicated by dots.

TABLE I. Diffusion coefficients for 50 mole percent liquid mixtures.

Mixture	c_i'	c_i''	T	$10^5 D$
Ph—n-C_7	0.47	0.53	298	2.47±0.05
			318	3.40±0.04
			338	4.31±0.05
Ph—n-C_{10}	0.47	0.53	298	1.71±0.05
			318	2.51±0.03
			338	3.10±0.03
Ph—n-C_{12}	0.47	0.53	298	1.40±0.04
Ph—n-C_{16}	0.48	0.52	298	
	0.45	0.55	298	
Ph—n-C_{18}	0.45	0.55	298	0.86±0.01
n-C_7—n-C_{12}	0.45	0.55	298	1.57±0.01
			318	2.14±0.07
			338	2.68±0.03
n-C_7—n-C_{14}	0.45	0.55	298	1.28±0.01
n-C_7—n-C_{16}	0.45	0.55	298	1.00±0.01
			318	1.44±0.06
			338	2.04±0.03
n-C_7—n-C_{18}	0.45	0.55	298	0.92±0.02
i-C_7—n-C_{12}	0.45	0.55	298	0.88±0.04
Ph—i-C_7	0.47	0.53	298	2.48±0.06

2. Analysis of Solutions

Samples from the two reservoirs of column or cell were compared in a Zeiss water interferometer using a 0.5-cm cuvette. The glass windows of the cuvette were sealed to the metal part with copper oxide-phosphoric acid cement. The cuvette was placed in the water bath of the interferometer, the bath was agitated by a motor-driven stirrer, and readings were taken as soon as a satisfactory setting could be obtained. In all cases a zero correction to the reading was measured by filling both sides of the cuvette with the same solution and setting the instrument. Analyses were carried out in duplicate or triplicate.

By calibration with mixtures of n-heptane and cyclohexane of known concentration the reading on the interferometer scale was found to vary linearly with the difference in concentration expressed in units of mole percent over the range from 40 to 60 mole percent. From this calibration the mean change in refractive

[4] A. Fick, Pogg. Ann. **94**, 59 (1855).
[5] A. F. Cole and A. R. Gordon, J. Phys. Chem. **40**, 733 (1936).
* A. Daigger and Company, Chicago, Illinois.
† Throughout this work 2,4-dimethyl pentane will be referred to as i-C_7.
‡ Phillips Petroleum Company, Bartlesville, Oklahoma.
** Humphrey-Wilkinson, Incorporated, New Haven, Connecticut.

index per interferometer division was 0.00000405. Refractive indices for pure compounds were taken from a paper by Ward and Kurtz.[6]

3. Diaphragm Cell and Measurement of Diffusion Coefficients

For the measurement of diffusion coefficients the diaphragm cell shown in Fig. 1 was used. It was different in design from the cells previously described in that the contents of either reservoir could be drained or replaced without removing the cell from the water bath or disturbing the contents of the other reservoir. The diaphragm used in this cell was a fine Pyrex fritted disk having a diameter of 30 mm. The volume of each reservoir was measured by weighing the water contained therein. The measured volumes were surprisingly reproducible and mean values were 23.16 23.08 cm³ for V' and V''. Liquid contained by the capillary tubes was insufficient in amount to contribute a significant error in this work. Silicone lubricant was used for the stopcocks.

The method of operation was as follows. One reservoir was filled from a 50 ml Erlenmeyer flask by applying suction to the reservoir on the same side. A considerable quantity of fluid was forced through the disk from one side to the other to insure that all the pores were completely filled with liquid. Finally both reservoirs were filled completely and the cell suspended in a water thermostat with the stopcocks and filling tubes above the water level. The temperature of the water bath was regulated to within 0.02°C. The reservoirs were filled with solutions having slightly different concentrations and after a few hours, when a concentration gradient had been established in the liquid in the disk, the contents of one reservoir were removed and replaced by more of the original solution for that side. Then the contents of the other reservoir were removed and replaced by fresh solution. This technique of first establishing approximately the correct concentration gradient in the disk before beginning an experiment was followed throughout the work.

The diaphragm cell was calibrated with pure water vs. 0.1N HCL using the value 2.90×10^{-5} cm²/sec. for the integral diffusivity at 25°C.[7,8] Samples were analyzed in duplicate by titration with 0.1N KOH in a 5 ml buret graduated in 0.01 ml, and phenolphtalein was used as indicator. The mean value of the cell constant 0.1798 was used throughout the work.

In all cases it was desired to determine the differential diffusion coefficient for a 50 mole percent solution. The concentrations of initial solutions varied between 45–55 and 48–52 mole percent depending on the difference in refractive indices of the components. After diffusing for 12 to 36 hours the concentration difference had reached

[6] A. L. Ward and S. S. Kurtz, Ind. Eng. Chem. Anal. Ed. **10**, 560 (1938).
[7] J. C. Gage, Trans. Faraday Soc. **44**, 253 (1948).
[8] James, Hollingshead, and Gordon, J. Chem. Phys. **7**, 89 (1939).

TABLE II. A comparison of the diffusion coefficient calculated by the equations of Stearn, Irish, and Eyring with observed values, the latter appearing in parentheses.

Mixtures	Diffusion coefficient, 10^5D 25°C	45°C	65°C
Ph—n-C_7	6.73 (2.47)	8.38 (3.40)	10.23 (4.32)
Ph—n-C_{10}	5.04 (1.72)	6.43 (2.51)	8.01 (3.10)
Ph—n-C_{12}	4.63 (1.40)	—	—
Ph—n-C_{16}	4.45 (0.96)	—	—
Ph—n-C_{18}	4.52 (0.86)	—	—
n-C_7—n-C_{12}	4.31 (1.58)	5.56 (2.14)	7.06 (2.69)
n-C_7—n-C_{14}	4.09 (1.29)	—	—
n-C_7—n-C_{16}	4.18 (1.00)	5.41 (1.44)	6.89 (2.05)
n-C_7—n-C_{18}	4.37 (0.92)	—	—
i-C_7—n-C_{12}	4.80 (1.44)	—	—
i-C_7—n-C_{16}	4.69 (0.88)	—	—
Ph—i-C_7	7.41 (2.49)	—	—

¾ to ½ its original value and solutions were removed for analysis. The initial and final differences in concentration were measured directly using the Zeiss water interferometer. Duplicate determinations of the diffusion coefficient were carried out at three temperatures and data are recorded in Table I.

In calculating diffusivities by (13) the ratio $\Delta n_i/\Delta n_f$ was equated to the corresponding ratio of interferometer readings. While interferometer readings have been shown to be directly proportional to differences in concentration expressed in units of mole percent the latter are not directly proportional to the units of Δn, namely g/cm³. However, it can be demonstrated that in this work the error involved in equating a ratio in units of mole percent to the corresponding ratio in units of g/cm³ is extremely small in all cases and is much less than experimental error.

CORRELATION OF RESULTS

For the correlation of diffusivities by Arnold's Eq. (1) (see Fig. 2) the constant was altered from 0.0010 to 0.00161. Values used for the abnormality factors were $A_{CX}=1.00$ and $A_{Ph}=1.33$, and for the molecular volumes $V_C=14.8$ and $V_H=3.7$, subtracting 15 for the benzene ring. The viscosity of the mixture[9] was used. Values of D calculated by Eqs. (1–4) are indicated by dots. It appears that the equations correlate the data fairly well.

As was anticipated earlier the Stokes-Einstein equation is inapplicable for correlating diffusivities of liquid mixtures. One finds that r must decrease as the molecular weight increases, a phenomena which is inconceivable to the authors.

Values of the diffusion coefficient calculated by the equations of Stearn, Irish, and Eyring (5–11) appear in Table II together with observed values in parentheses. The calculated values are too high in all cases and no simple relation exists between observed and calculated values. For mixtures involving iso-paraffins, the calcu-

[9] D. J. Trevoy and H. G. Drickamer, J. Chem. Phys. **17**, 1120 (1949).

lated value of D is in all cases higher than for the corresponding mixture involving a n-paraffin, which is contrary to experiment. Furthermore the calculated diffusivity for n-C_7—n-C_{18} is larger than that for n-C_7—n-C_{12}, whereas experiment shows the former to be much smaller. In general it must be stated that this relationship does not appear to be in any way consistent with the data for hydrocarbon mixtures. At present the only really useful relationship is the semi-empirical one of Arnold.

THE JOURNAL OF CHEMICAL PHYSICS VOLUME 17, NUMBER 11 NOVEMBER, 1949

Thermal Diffusion in Binary Liquid Hydrocarbon Mixtures

D. J. TREVOY AND H. G. DRICKAMER
Department of Chemistry, University of Illinois, Urbana, Illinois

(Received April 1, 1949)

Thermal diffusion coefficients have been measured for a series of binary mixtures of paraffin hydrocarbons and of paraffin hydrocarbons with benzene. The temperature dependence of the thermal diffusion coefficient is shown to be small. The results are correlated quite satisfactorily by assuming that the mobility of a molecule is inversely proportional to the product of the molecular mass and molecular cross section in the direction of flow.

NOMENCLATURE

B = mean circumference of the column, cm.
C_1, C_2 = mole fractions of components 1, 2.
D = coefficient of diffusion cm²/sec.
D_T = coefficient of thermal diffusion cm²/sec.
g = acceleration of gravity cm²/sec.
L = length of column cm.
m = molecular mass.
$\mathbf{v}$ = convection velocity of entire fluid, cm/sec.
$\mathbf{v}_1$ = convection velocity of molecules of Type 1, cm/sec.
V_+ = volume of one reservoir cm³.
ω = one-half the annular spacing—cm.
$\bar{T}$ = average temperature.
ΔT = temperature difference between hot and cold wall.
α = thermal diffusion ratio.
$\beta = -\partial\rho/\partial T$.
ρ = density g/cm³.
η = viscosity, poises.
σ = molecular cross section.
χ = probability of finding a molecule in the hot region.

THERMAL diffusion in the liquid phase was first observed by Ludwig[1] in 1856. When a temperature gradient was maintained in a uniform aqueous solution of sodium sulfate he found that a concentration gradient was established. Later Soret[2] discovered the effect independently, and as a result thermal diffusion in the liquid phase is now termed the Ludwig-Soret effect or the Soret effect.

If a temperature gradient is impressed on a mixture of gases a partial separation of the gases will generally occur, but it was early shown that no simple picture of molecular interaction would predict such an effect. When the other transport properties, viscosity, thermal conductivity and diffusion, can be predicted satisfactorily by assuming simple molecular interaction laws it becomes apparent that thermal diffusion is a second-order effect which is very sensitive to slight differences in interaction between molecules. It is therefore possible to obtain more specific information about how molecules behave in the gas phase by studying thermal diffusion rather than one of the other transport properties.

In liquids and liquid mixtures a simple theory of binary collisions is not sufficient to describe the molecular behavior because the molecules are closely packed and are probably influenced by several neighbors simultaneously. Accordingly, it is considered that binary collisions as conceived in gases are of minor importance compared to the complex force field about each molecule in a liquid. Due to the complexity of the problem a complete mathematical theory of the liquid state has not yet been realized. It is possible, however, that thermal diffusion data for liquids may yield more specific information about the liquid state than the other transport properties as is the case for gases. On this premise thermal diffusion has been adopted as the tool in a study of liquid mixtures.

Scanty data on the Soret effect are available for aqueous solutions of electrolytes but few experiments have involved solutions of organic compounds. The present work is confined to a study of the Soret effect in binary mixtures of unreactive hydrocarbons which form almost ideal solutions. It is desired to discover what fundamental properties of the pure compounds determine the magnitude and direction of the thermal diffusion constant.

KINETIC THEORY

There is at present no kinetic theory of liquids adequate to explain thermal diffusion, but the following argument is consistent with the modern theory of liquids and with the experimental results.

Let us consider a liquid as a network of equilibrium

[1] C. Ludwig, Akad. Wiss. Wien. **20**, 539 (1856).
[2] Ch. Soret, Auh. Sci. Phys. Nat., Geneve (3) **2**, 48 (1879).

TABLE I. Thermal diffusion data obtained with a concentric tube column for 50 mole percent liquid mixtures.

Mixtures	t/3600	T_H	T_C	$100\Delta c$*	α**
Ph—n-C_7	4.50	298.8	293.4	−0.500	−1.19
	10.50	298.8	293.4	−0.579	
	0.02	—	—	−0.072	
	0.06	—	—	−0.128	
	0.12	308.9	303.4	−0.250	
	0.25	309.0	303.5	−0.364	
	1.00	309.0	303.6	−0.486	
	4.00	308.9	303.7	−0.571	
	4.30	308.9	303.5	−0.543	−1.20
	10.00	308.9	303.3	−0.557	
	11.00	308.8	303.5	−0.550	
	4.00	324.0	318.7	−0.443	−1.06
	10.00	323.9	318.7	−0.536	
	3.00	339.0	334.1	−0.510	−1.14
	10.80	340.4	334.3	−0.525	
	4.00	311.7	300.9	−0.585	
	6.00	311.7	300.9	−0.560	−1.24
	13.00	311.8	301.0	−0.568	
	4.30	314.8	298.3	−0.607	
	5.30	314.7	298.4	−0.603	−1.28
	12.00	314.7	298.4	−0.553	
Ph—n-C_{10}	4.00	299.0	293.3	−0.118	−0.22
	8.00	298.9	293.3	−0.145	
	4.00	308.8	303.4	−0.245	−0.41
	9.50	308.9	303.4	−0.231	
	4.00	323.9	318.5	−0.318	−0.44
	8.00	323.8	318.4	−0.190	
	4.00	338.7	333.4	−0.281	−0.47
	7.30	338.8	333.2	−0.213	
	3.50	353.4	348.2	−0.454	−0.68
	7.50	353.6	348.1	−0.268	
Ph—n-C_{12}	4.30	308.9	303.6	−0.230	
	8.00	308.9	303.5	−0.189	−0.31
	11.50	308.9	303.6	−0.189	
Ph—n-C_{14}	4.00	308.9	303.5	−0.164	
	4.50	308.9	303.6	−0.164	−0.41
	11.00	308.9	303.6	−0.124	
Ph—n-C_{16}	4.00	308.9	303.4	+0.025	
	4.00	308.9	303.6	−0.007	−0.001
	12.00	309.0	303.6	−0.043	

* In this table a positive Δc indicates that the first-named component concentrated at the hot wall.

** Mean values of α are given at each temperature. Only points where the steady state was reached were used in calculating.

TABLE I.—*Continued.*

Mixtures	t/3600	T_H	T_C	$100\Delta c$*	α**
Ph—n-C_{18}	4.00	308.9	303.6	+0.105	+0.07
	4.00	308.9	303.6	+0.059	
	14.00	308.7	303.4	+0.053	
n-C_7—n-C_{12}	4.30	298.9	293.5	0.370	+0.57
	10.20	298.9	293.5	0.394	
	4.00	308.8	303.5	0.430	+0.61
	7.80	308.9	303.4	0.370	
	4.00	323.8	318.4	0.287	+0.54
	7.50	323.8	318.4	0.382	
	4.00	338.9	333.6	0.323	+0.56
	8.40	338.8	333.5	0.335	
	4.30	353.7	348.8	0.215	+0.44
	7.60	353.9	348.6	0.263	
n-C_7—n-C_{14}	4 00	308.5	303.6	0.552	+0.90
	10.00	309.2	303.6	0.717	
	4.00	325.1	318.5	0.601	+0.93
	10.00	324.2	318.3	0.679	
	4.00	340.2	333.3	0.881	+1.05
	10.00	339.3	333.3	0.553	
	4.00	313.2	303.1	0.727	+0.88
	10.30	314.4	304.2	0.514	
n-C_7—n-C_{15}	4.50	308.9	303.6	0.735	+1.03
	5.50	308.9	303.6	0.778	
	12.00	308.9	303.6	0.778	
n-C_7—n-C_{18}	4.00	308.9	303.6	0.752	+0.95
	4.30	309.0	303.7	0.838	
	11.00	308.8	303.6	0.900	
i-C_7—n-C_{12}	4.00	308.9	303.6	0.308	+0.43
	4.00	308.9	303.6	0.237	
	10.50	308.8	303.4	0.216	
i-C_7—n-C_{16}	4.00	308.9	303.6	0.107	+0.22
	4.00	308.8	303.4	0.161	
	12.00	308.7	303.4	0.199	
Ph—i-C_7	4.50	308.9	303.5	−0.256	−0.59
	5.00	308.9	303.5	−0.262	
	12.00	308.8	303.6	−0.246	

positions, in which a molecule is held as in a "cage" by the potential energy field of the surrounding molecules. The liquid differs from the solid in that the kinetic energy of the molecules is larger and the surrounding potential barrier is lower and subject to much greater fluctuations. Thus the "retention time" of a molecule in any equilibrium position is relatively short. Higher temperatures correspond to greater kinetic energy, and larger cages with more flexible and penetrable walls, i.e., to shorter retention times. To describe the motion we must consider the tendency to escape from an equilibrium position, the direction in which, on the average, it will move, the possibility of location in a new position, and the probability of moving back toward the old position.

In general, the higher the temperature the greater the mobility, so that all molecules have a tendency to move toward the lower temperature which accounts for the density gradient. If all molecules at the same temperature level have the same kinetic energy, the heavier molecules have the higher momentum and thus the greater tendency to move in the direction of the temperature gradient.

In addition, one must consider a steric effect. The greater the cross section in the direction of the motion the more difficult the motion. This would seem to inhibit the tendency of the large molecules to move in the direction of the temperature gradient, but this effect is overshadowed by the fact that the relative difficulty of movement against the temperature gradient is even greater for large molecules. When moving from hot to cold region the molecules have the advantage of the higher kinetic energy consistent with their higher "temperature" and are able to force themselves into relatively small holes. By the end of a retention time it may be assumed that the molecules have come to thermal equilibrium with the surroundings and have less kinetic energy and a smaller chance of escaping. This "trapping" effect is much more efficient on large molecules more nearly the size of the cage.

The probability of finding a high concentration of a given species in the hot region can be written

$$\chi = k'/m\sigma, \tag{1}$$

where m is the mass and σ the cross section in the direction of flow. The thermal diffusion ratio is proportional to the difference in these probabilities for the two species.

$$\alpha = K[(k_1'/m_1\sigma_1) - (k_2'/m_2\sigma_2)], \tag{2}$$

or

$$\alpha = (k_1/m_1\sigma_1) - (k_2/m_2\sigma_2). \tag{2'}$$

In accord with the above discussion regarding the effect of molecular mass on the direction of thermal diffusion we shall consider that a positive α corresponds to a movement of the heavy molecule to the cold wall and a negative α corresponds to a movement of the heavy molecule to the hot wall.

THEORY OF THE THERMAL DIFFUSION COLUMN

The coefficient of thermal diffusion D_T is defined by the equation of diffusion

$$c_1(\mathbf{v}_1 - \mathbf{v}) = -D \operatorname{grad} c_1 - (D_T/T) \operatorname{grad} T. \tag{3}$$

In the case of gases it has been shown that the coefficient of thermal diffusion is proportional to the product c_1c_2, and therefore a thermal diffusion ratio α is introduced and defined by the relation

$$D_T = Dc_1c_2\alpha. \tag{4}$$

In terms of α Eq. (3) becomes

$$c_1(\mathbf{v}_1 - \mathbf{v}) = D(-\operatorname{grad} c_1 - \alpha(c_1c_2/T) \operatorname{grad} T). \tag{5}$$

From this equation and the Navier-Stokes equation, Furry, Jones, and Onsager[3] have developed a theory of the thermal diffusion column which results in the following equation for the steady state separation factor.

$$\ln q_e = \left[\frac{63\alpha D\eta L}{2\bar{T}\omega^4\beta g}\right]\left[\frac{1}{1+5670(\eta D/g\omega^3\beta\Delta T)^2}\right], \tag{6}$$

where

$$q_e = (c_1/c_2)_{\text{top}}(c_2/c_1)_{\text{btm}}. \tag{7}$$

The development of the transport equation is based on the assumption of laminar flow. Furry, Jones, and Onsager define the Reynolds number

$$R_e = \frac{\omega^3 g\rho^2\Delta T}{4\gamma\eta^2\bar{T}}, \tag{8}$$

employing an average value for the convection velocity and considering the annular space as the characteristic length. For flow between plane surfaces Onsager and Watson[4] have shown experimentally that the critical Re is about 25.

An approximate equation for the rate of approach to the stationary state has been developed by Jones and Furry[5] by assuming that the volume of each reservoir is large compared to the volume between the walls of the column. For the special case in which $c_1c_2 \cong$ constant they have derived a simple exponential approach to the steady state

$$(\Delta c/\Delta c_e) = 1 - \exp(-t/t_r), \tag{9}$$

for which the relaxation time is

$$t_r = \frac{V_+L}{(2\omega^7 g^2\beta^2 B(\Delta T)^2/2835\eta^2 D) + 4\omega DB}. \tag{10}$$

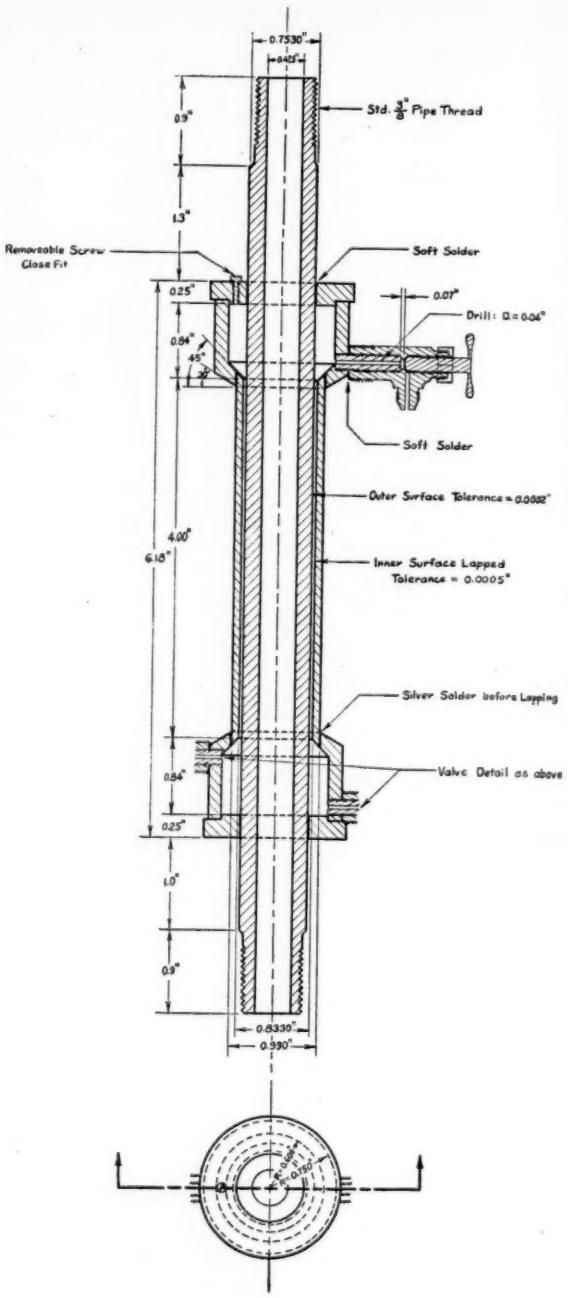

FIG. 1. Thermal diffusion column.

[3] Furry, Jones, Clark, and Onsager, Phys. Rev. **55**, 1083 (1939).
[4] L. Onsager and W. W. Watson, Phys. Rev. **56**, 474 (1939).
[5] Jones, Clark, and Furry, Rev. Mod. Phys. **18**, 151 (1946).

EXPERIMENTAL METHODS AND RESULTS

The systems studied and the analytical methods used were the same as those discussed in the previous paper on diffusion.[6]

The thermal diffusion column was designed with a calculated relaxation time of less than an hour to obtain the stationary state in a reasonable time. A small value for ΔT was chosen to make possible a study of the temperature dependence of α. As a result of this limitation it was necessary to use a relatively large annular space with correspondingly small equilibrium separations. This situation arises from the fact that $\ln q$ is inversely proportional to the fourth power of the gap and t_r is inversely proportional to approximately the seventh power of the gap. The column is shown in the accompanying drawing.

From (8) it is readily shown that these dimensions will give rise to laminar flow in the column.

The column was mounted in a water thermostat, and water from a second thermostat was circulated through the inner tube at a velocity of about 5 feet per second by a positive displacement pump. Water temperatures were regulated to better than 0.1°C, and wall temperatures of the column were measured by copper-constantan thermocouples clamped against the walls. A Leeds and Northrup portable precision potentiometer was used for temperature measurements. No attempt was made to calculate temperature drops through the walls because the term involving ΔT in (6) seldom makes a significant contribution to α for our choice of column and operating variables and consequently accurate values of ΔT are not required.

The method of column operation was as follows. Having drained the water from the bath the column was filled with liquid from a brass reservoir attached by a copper tube and screwed fitting to the lowest valve. The filling reservoir and tube were then removed and a screwed fitting with a closed end was connected to each valve to prevent water entering the valve. After filling the bath with water and adjusting its temperature, circulation from the second bath was begun. At the end of a run, which usually lasted 4 to 10 hours, half the water was drained from the bath and the upper sampling cock was dried with filter paper. The protecting fitting was removed from the cock and the contents of the upper reservoir were drained. The remaining water was siphoned from the bath, cocks were dried with filter paper and the contents of the column and lower reservoir were drained. It was considered important that sampling be done as rapidly as possible and for this reason a rubber blow-tube was connected to the top of the column. The bath could be drained in about 30 seconds and the entire sampling procedure completed in $2\frac{1}{2}$ to 3 minutes.

The concentration of all mixtures was initially 50 mole percent and in most runs the ΔT was about 5°C. All runs were carried out in duplicate or triplicate, and data are recorded in Table I. In calculating Δc the assumption was made that refractive index varies linearly with mole fraction, an excellent approximation over the small range of concentrations involved.

In calculating values of α from Eq. (6) values are

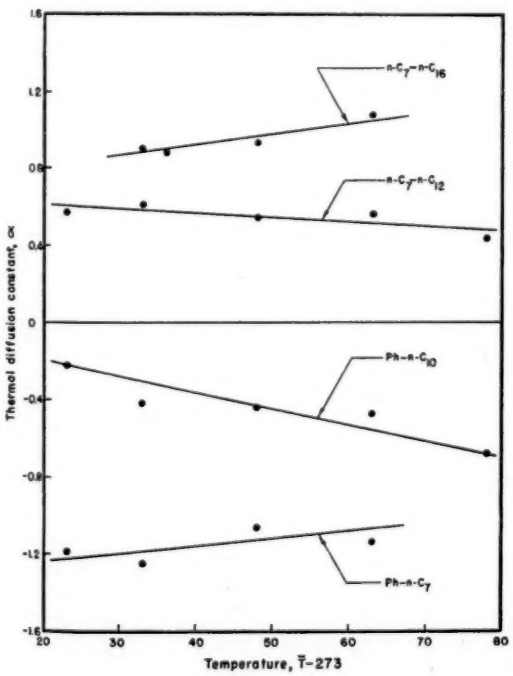

FIG. 2. Variation of thermal diffusion constants with temperature for mixtures of liquid hydrocarbons.

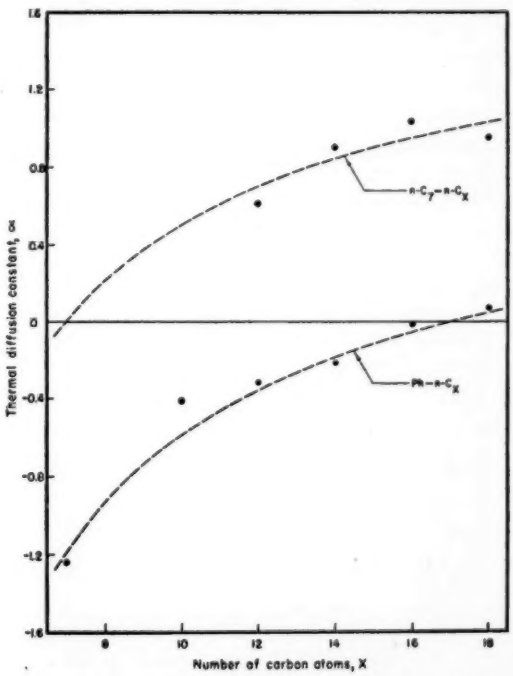

FIG. 3. Comparison of thermal diffusion constants obtained experimentally with those calculated by Eq. (2).

[6] D. J. Trevoy and H. G. Drickamer, J. Chem. Phys. **17**, 1117 (1949).

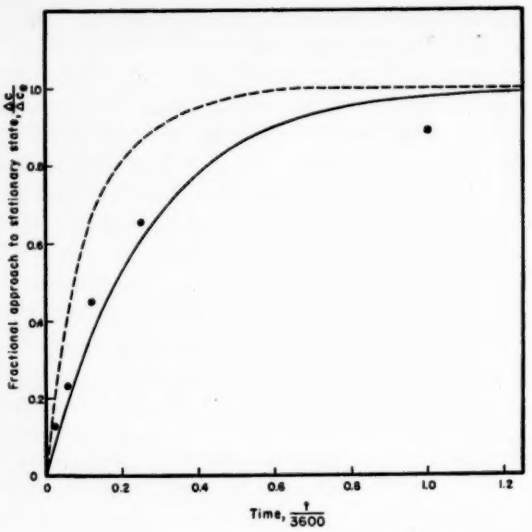

FIG. 4. A comparison of the rate of approach to the stationary state with that predicted theoretically in a thermal diffusion column. Values calculated by (10) are joined with a broken line.

needed for the diffusion coefficient, the coefficient of viscosity, and the temperature coefficient of density. The measured diffusion coefficients are discussed in the previous article.[6] The viscosities of the mixtures have been published earlier.[7] Density data were taken from standard sources[8,9] and the temperature coefficient calculated on an additive basis. The data are shown in Table I.

DISCUSSION OF RESULTS

As predicted by (4) for our choice of column and operating variables α is substantially independent of ΔT. A study of Table I shows this to be true for benzene —*n*-heptane mixtures over a threefold range of ΔT, and for *n*-heptane—*n*-tetradecane over a twofold range.

To illustrate the temperature dependence of α, data taken from Table I for four systems are plotted in Fig. 2. While the data for each system are consistent, within experimental error, α increases slightly with increasing temperature in some cases and decreases slightly in others. For this reason one cannot generalize regarding the dependence of α on temperature although it appears that it does not vary rapidly with temperature over a range of 55°C.

The upper curve in Fig. 3 compares experimental values of α at 303°K with those calculated from Eq. (2′) on the assumption that k is independent of chain length. The agreement shown implies that the normal paraffins up to C_{18} move in the liquid state in the same zigzag chain in which they occur in the solid state.

Using $k=2.75\times10^{-22}$ for the normal paraffins, as obtained from the paraffin-paraffin series, we obtain a value of $k=9.04\times10^{-22}$ for benzene. The lower curve in Fig. 3 indicates that this value is a constant for the entire benzene-paraffin series. From the above data one can see that (k/σ) for benzene is about three times that for the paraffins. It is interesting to note that cross section of a benzene molecule taken edgewise is about twice that of a zigzag paraffin chain, while the cross section flatwise is about four times that of the paraffin chain. This is an indication that k is substantially constant from compound to compound. This low mobility for benzene is consistent with its high viscosity and relatively low diffusivity in many mixtures.

From what is known of the structure of iso-paraffins one would predict a larger cross sestion and therefore a lower mobility for *i*-C_7 relative to nC_7. On this basis α for *i*-C_7—nC_x series should be less than α for the corresponding nC_7—nC_x series. Also $|\alpha|$ for iC_7—Ph should be less than that for nC_7—Ph. This is confirmed by experiment as indicated in Table I.

APPROACH TO STATIONARY STATE IN DIFFUSION COLUMN

From data given in Table I for the system Ph—*n*-C_7 the rate of approach to the stationary state may be compared with that predicted theoretically. The broken line in Fig. 4 represents the rate of approach calculated by (10) while the solid line is that obtained using the mean relaxation time determined by experiment. From (10) $t_r=379$ seconds and from experiment the mean of five values is $t_r=936$ seconds. The derivation of (10) involves several assumptions one of which is that the volume between hot and cold walls is small compared to the volume of the reservoirs. For the present column this assumption is not valid and one would expect the calculated relaxation time to be too small. For this reason agreement between theory and experiment is considered very satisfactory.

[7] D. J. Trevoy and H. G. Drickamer (to be published).
[8] G. Egloff, *Physical Constants of Hydrocarbons* (Reinhold Publishing Corporation, New York, 1941).
[9] *International Critical Tables* (McGraw-Hill Book Company, Inc., New York).

Diffusion in Photo-Chemical Experiments: The Photo-Chemical Decomposition of Acetone

TERRELL L. HILL*
Department of Chemistry, University of Rochester, Rochester, New York
(Received April 13, 1949)

A theoretical analysis is made of the effects of diffusion on the reactions following the photo-chemical decomposition of acetone in a cylindrical cell. It is found that some of the results are quite sensitive to the fate of the free radicals on the walls of the cell. The root-mean-square distance a radical diffuses in its mean lifetime is shown to be a useful qualitative guide in predicting the importance of diffusion in experiments of this type.

I. INTRODUCTION

IN some photo-chemical experiments the shape of the light beam sent through the cell containing gas is such that there is a "light space" (the region through which the light beam passes) and a "dark space" (the remainder of the interior of the cell). Photo-chemical products are formed in the light space and may react with each other or with the original gas in either the light space or the dark space. It has been customary in treating such a system to assume for simplicity that the rate of diffusion of the photo-chemical products in the cell is either (a) infinitely fast or (b) infinitely slow compared to the rate of the chemical reactions of interest.

In this paper we present some calculations in which the actual finite rate of diffusion is taken into account, using the photo-chemical decomposition of acetone as a model. We use standard diffusion equations here; the same general procedure will obviously be applicable to any system in which there is true diffusion (mean free paths of diffusing molecules of interest small compared to the dimensions of the cell). However, the details of any such calculation will depend of course on the geometry of the cell, the geometry of the light beam, the variation in light intensity within the light beam, and on the particular homogeneous and wall reactions taking place.

Actually, only a certain special case of the general problem is particularly tractable: the partial pressure of the original gas is very large compared to the partial pressures of the other gases produced in the cell, and hence the diffusion coefficients of these other gases are independent of time and spatial coordinates. Fortunately, most photo-chemical decomposition experiments are in this class. Also, we consider the steady-state problem only; the time-dependent problem is much more difficult and not very important.

A detailed discussion of the implications of these calculations in the analysis of photo-chemical data is deferred to a later time.

II. DIFFUSION EQUATIONS FOR ACETONE DECOMPOSITION

We now turn to the acetone problem as an example; the generalization to other problems will be obvious.

We consider a cylindrical cell of radius ρ_1 and length z_0 filled with acetone, through which passes a (parallel) concentric, cylindrical, radially uniform light beam of radius ρ_0. Owing to absorption, the light beam will not be of uniform intensity along the length of the cell.

We take into account the following processes at 122°C:[1,2]

$$CH_3COCH_3+h\nu=2\,CH_3+CO \tag{1}$$

$$2CH_3=C_2H_6;\quad k_3c_1^2 \tag{2}$$

$$CH_3+CH_3COCH_3=CH_4+CH_3COCH_2;\quad k_5c_1n_{Ac} \tag{3}$$

$$2CH_2COCH_3=(CH_2COCH_3)_2;\quad k_6c_2^2 \tag{4}$$

$$CH_3+CH_2COCH_3=CH_3COCH_2CH_3;\quad k_7c_1c_2. \tag{5}$$

In these equations, c_1, c_2, and n_{Ac} are the concentrations of methyl radicals, acetonyl radicals and acetone molecules, respectively, expressed in number of molecules per cc. The rate expressions refer to the rate of formation of products in each case.

Let the z axis be the axis of the cell (cylinder) with the beam entering at $z=0$ and leaving at $z=z_0$; let ρ be the radial distance from the z axis; and let $Q(z)$ be the number of methyl radicals produced per cc of light space per second at z, according to Eq. (1). Then we have the following steady-state diffusion equations:[3]
Light space:

$$\begin{gathered}D_1\nabla^2c_1+Q(z)-k_5c_1n_{Ac}-k_7c_1c_2-2k_3c_1^2=0\\(0\leqslant\rho\leqslant\rho_0)\\D_2\nabla^2c_2+k_5c_1n_{Ac}-k_7c_1c_2-2k_6c_2^2=0.\end{gathered} \tag{6}$$

Dark space: Same as above except omit $Q(z)$.

$$(\rho_0\leqslant\rho\leqslant\rho_1),$$

where D_1 and D_2 are the diffusion coefficients of methyl and acetonyl radicals, respectively. We require that c_1, c_2, $\partial c_1/\partial\rho$ and $\partial c_2/\partial\rho$ be continuous at $\rho=\rho_0$. There are further boundary conditions at the walls which can be

* Present address: Naval Medical Research Institute, Bethesda, Maryland.

[1] L. M. Dorfman and W. A. Noyes, Jr., J. Chem. Phys. **16**, 557 (1948).
[2] W. A. Noyes, Jr. and L. M. Dorfman, J. Chem. Phys. **16**, 788 (1948).
[3] N. Rashevsky discusses a number of simple diffusion problems of this type, but with spherical symmetry (for biological cells), in his book *Mathematical Biophysics* (University of Chicago Press, Chicago, 1938).

discussed adequately and more simply in Sections III and IV.

Equations (6) constitute a system of two non-linear second-order partial differential equations in the independent variables z and ρ. Instead of attempting to solve the complete and very formidable problem presented by Eqs. (6), we make the simplification of treating the radial and longitudinal (z) problems independently. As will be clear from Section IV, this should not be a particularly serious approximation in the present case because diffusion has relatively little influence on the longitudinal steady state concentration curves (this in turn is due essentially to the fact that the cell is very long compared to the root-mean-square distance a radical diffuses in its mean lifetime—see Section V).

III. RADIAL DIFFUSION

We now assume that we have an infinitely long cell with a light beam uniform in z as well as in ρ. One could carry out the radial calculation for various values of $Q(z)$, of course. Actually, we have made only two numerical calculations for the radial case with all reactions (1)–(5) included, using the average $\bar{Q}$ in both cases. From Beer's law,

$$Q(z)=Q_0\exp(-\delta z), \tag{7}$$

so that

$$\bar{Q}=Q_0[1-\exp(-\delta z_0)]/\delta z_0 \tag{8}$$

where δ is a constant.

Equations (6) become:

Light space:

$$(0\leqslant\rho\leqslant\rho_0),$$

$$D_1\left(\frac{d^2c_1}{d\rho^2}+\frac{1}{\rho}\frac{dc_1}{d\rho}\right)+\bar{Q}-k_5c_1n_{Ac}-k_7c_1c_2-2k_3c_1^2=0, \tag{9}$$

$$D_2\left(\frac{d^2c_2}{d\rho^2}+\frac{1}{\rho}\frac{dc_2}{d\rho}\right)+k_5c_1n_{Ac}-k_7c_1c_2-2k_6c_2^2=0.$$

Dark space: Same as above except omit $\bar{Q}$.

$$(\rho_0\leqslant\rho\leqslant\rho_1).$$

This is a system of two ordinary second-order non-linear differential equations. An accurate series solution can be obtained by a method of successive approximations.[4] We write

$$\begin{aligned} c_1&=a_0+a_1\rho+a_2\rho^2+\cdots \quad 0\leqslant\rho\leqslant\rho_0\\ &=b_0+b_1x+b_2x^2+\cdots \quad \rho_0\leqslant\rho\leqslant\rho_1\\ c_2&=g_0+g_1\rho+g_2\rho^2+\cdots \quad 0\leqslant\rho\leqslant\rho_0\\ &=f_0+f_1x+f_2x^2+\cdots \quad \rho_0\leqslant\rho\leqslant\rho_1 \end{aligned} \tag{10}$$

where $x=\rho_1-\rho$. Equations (10) are substituted into Eqs. (9) to obtain recurrence relations between the constants of Eqs. (10).

[4] As stated above, only two numerical cases of Eqs. (9) have been computed. These two calculations required about three weeks.

As a first approximation one can set $k_7=0$ and solve the differential equation in c_1 only. There are of course two arbitrary constants [e.g., a_0 and b_0 in the case of reflection of radicals from the walls (see below)—the recurrence relations give the remaining a_i and b_i in terms of a_0 and b_0, respectively] in the general solution of this differential equation. By successive guesses, these constants must be chosen so that c_1 and $dc_1/d\rho$ are continuous at $\rho=\rho_0$.

This first approximation for c_1, once obtained, is then substituted for c_1 in the differential equation in c_2 (no longer taking $k_7=0$). Two constants (e.g., f_0 and g_0) are again adjusted to give eventually in this case a first approximation to c_2. This approximation to c_2 is then put into the differential equation in c_1 (no longer taking $k_7=0$) and a second approximation to c_1 obtained. Thus one can obtain alternately higher approximations to c_1 and c_2. Fortunately, the convergence in this procedure is quite rapid (the fourth approximation gives solutions accurate to about one part in ten thousand).

The two calculations we have carried out correspond to extreme choices for boundary conditions at the wall ($\rho=\rho_1$).

(1) Complete Reflection of Radicals at the Wall

In this case there is no loss of radicals to the wall so that material balance requires for c_1, for example, that

$$\int_0^{\rho_0}\bar{Q}\rho d\rho=\int_0^{\rho_1}(k_5c_1n_{Ac}+k_7c_1c_2+2k_3c_1^2)\rho d\rho. \tag{11}$$

On integrating in the same fashion the differential equation for c_1 in Eq. (9) it therefore follows that

$$\int_0^{\rho_1}d\left(\rho\frac{dc_1}{d\rho}\right)=0, \tag{12}$$

or

$$(dc_1/d\rho)_{\rho=\rho_1}=0. \tag{13}$$

Similarly,

$$(dc_2/d\rho)_{\rho=\rho_1}=0. \tag{14}$$

(2) Appreciable Capture of Radicals at the Wall

Suppose that α_1 is the probability of a methyl radical not returning to the gas *as a methyl radical* on making a collision with the wall. Let $\bar{v}_1$ be the mean velocity of methyl radicals in the gas. Then the number of methyl radicals colliding with one cm² of wall per second is $c_1(\rho_1)\bar{v}_1/4$. Equation (11) should therefore be replaced by

$$\int_0^{\rho_0}\bar{Q}\rho d\rho=\int_0^{\rho_1}(k_5c_1n_{Ac}+k_7c_1c_2+2k_3c_1^2)\rho d\rho$$

$$+\tfrac{1}{4}c_1(\rho_1)\bar{v}_1\rho_1\alpha_1, \tag{15}$$

with a similar expression for acetonyl radicals. This includes reflection as a special case ($\alpha_1=0$). As will be seen below, it actually turns out in the present example

that so long as α_1, $\alpha_2 \geqslant 0.01$, $c_1(\rho_1)$ and $c_2(\rho_1)$ are very small compared to, say, $c_1(0)$ and $c_2(0)$, respectively. In other words, for $0.01 \leqslant \alpha_1$, $\alpha_2 \leqslant 1$ we can use to a very good approximation the boundary conditions $c_1(\rho_1) = c_2(\rho_1) = 0$ instead of the more exact conditions, Eq. (15) and a similar equation for acetonyl radicals.

We have chosen numerical values to correspond as closely as possible to run 9 of reference 1. It has been necessary to estimate several rate constants[1,2] and kinetic theory collision diameters.[5] The various parameters used are summarized in Table I.

TABLE I.

$T = 121.9°C$	$k_6 = 4.169 \times 10^{-12}$ cc sec.$^{-1}$
p (acetone) $= 117.4$ mm	$k_7 = 9.412 \times 10^{-12}$ cc sec.$^{-1}$
$n_{Ac} = 2.871 \times 10^{18}$ cc^{-1}	$\sigma_1 = 3.50$A
$\rho_0 = 0.833$ cm	$\sigma_2 = 4.95$A
$\rho_1 = 1.1$ cm	σ (acetone) $= 4.95$A
$z_0 = 20$ cm	l_1 (mean free path) $= 1/\sqrt{2} n_{Ac} \pi \sigma^2$
$\bar{Q} = 5.72 \times 10^{12}$ cc^{-1} sec.$^{-1}$	$= 4.392 \times 10^{-6}$ cm
$k_3 = 4.064 \times 10^{-12}$ cc sec.$^{-1}$	$l_2 = 3.20 \times 10^{-5}$ cm
$k_5 = 6.44 \times 10^{-19}$ cc sec.$^{-1}$	$D_1 = l_1 \bar{v}_1/3 = 1.093$ cm^2 sec.$^{-1}$
	$D_2 = 0.4086$ cm^2 sec.$^{-1}$

The solutions of Eqs. (9), using the data in Table I, are given in Fig. 1.[6] The computed c_1 reflection curve may be considered as intermediate between $D=0$ ($ABCD$) and $D=\infty$ (EF), the latter two curves corresponding to the two extreme choices possible using the ordinary steady-state rate equations without diffusion terms. The computed c_1 capture curve is intermediate between $D=0$ ($ABCD$) and $D=\infty$ (virtually the abscissa with this ordinate scale). We omit the $D=0$ and $D=\infty$ (reflection) c_2 curves in Fig. 1 for the sake of clarity. They fall at $c_2 = 0.161 \times 10^{12}$ cc^{-1} and $c_2 = 0.152 \times 10^{12}$ cc^{-1}, respectively.

From the point of view of the concentration distribution of radicals in the present example it is clear that $D=0$ is not a very realistic assumption. On the other hand, if there is *reflection* from the walls, $D=\infty$ gives a useful "average" concentration. In Section V we say something about the conditions under which $D=0$ is a fairly good approximation.

By performing numerical integrations using $c_1(\rho)$, $c_2(\rho)$, Eqs. (11) and (15), and similar equations for the acetonyl radicals, one can calculate the over-all material balance in the cell (for, say, a part of the infinite cylinder of height 1 cm). These results are shown in Table II, together with the analogous results for $D=0$ and $D=\infty$ (reflection). The (finite D) reflection calculation can be used as a check (Eq. (11)). It is seen that disappearance checks production as it should. The amount of disappearance at the walls in the capture case is obtained by subtraction (Eq. (15)). These capture figures hold for any value of α large enough (see below) to give essentially $c_1(\rho_1) = c_2(\rho_1) = 0$. From these data it is of course simple to derive the predicted relative amounts of CO, CH_4, C_2H_6, etc. (Eqs. (1)–(5)) produced in the gas. If wall reactions take place (capture), they must of course also be taken into account in predicting relative amounts of products. We shall not discuss this problem in detail in the present paper, but merely state as an illustration that the (finite D) reflection data above lead to 1.000, 0.516, and 0.542 as the relative numbers of molecules of CO, CH_4, and C_2H_6 formed, respectively. The experimental results for this run are 1.000, 0.408, and 0.594, respectively.[1]

It will be noticed in Table II that, in the present case, if there is reflection from the walls, the assumption of $D=\infty$ leads to data on material balance which differ only slightly from the results in the more refined reflection case.

We have for the capture case from Table II and Eq. (15),

$$5.75 \times 10^{12} = \tfrac{1}{4} c_1(\rho_1) \bar{v}_1 \alpha_1 \cdot 2\pi\rho_1,$$

or

$$c_1(\rho_1) = 4.46 \times 10^7/\alpha_1 \text{ cc}^{-1}. \tag{16}$$

Now $c_1(0)$ is in this case 5.68×10^{11} cc^{-1}. Hence if $\alpha_1 \geqslant .01$, $c_1(\rho_1)/c_1(0) \leqslant 0.0079$. Therefore, so long as $\alpha_1 \geqslant 0.01$ (α_2 also—see below), the concentration curve $c_1(\rho)$ will be effectively independent of α_1. Thus the amount of loss to the walls in this event is independent of α_1: the small concentration at the wall, $c_1(\rho_1)$, adjusts so that the product $c_1(\rho_1)\alpha_1$, is constant.

Similarly, for acetonyl radicals, one obtains

$$c_2(\rho_1) = 1.08 \times 10^7/\alpha_2 \text{ cc}^{-1}. \tag{17}$$

From $c_2(0) = 1.43 \times 10^{11}$ cc^{-1}, if $\alpha_2 \geqslant 0.01$, $c_2(\rho_1)/c_2(0) \leqslant 0.0076$. It will be noticed that, for the two cases calculated, we are assuming both radicals to have the same behavior (both reflected, or both captured appreciably).

The curves presented in Fig. 1 thus apply to the cases $\alpha=0$ (reflection) and $0.01 \leqslant \alpha \leqslant 1.00$ (appreciable capture). In the range $0 < \alpha < 0.01$, an analogous calculation can of course be carried out using Eq. (15). To save labor, we have done this only for a simpler case (below) which however, preserves the same relative importance of the wall process.

In view of the time necessary to make the complete calculation for the system of Eqs. (1)–(5), it is of considerable value to obtain solutions in simpler cases, neglecting certain reactions. We have in fact already obtained solutions for $c_1(\rho)$ when acetonyl effects are ignored ($k_7=0$), as a first approximation to the more general problem.[7] This still involves a series solution of a non-linear differential equation. If we put $k_3=0$ also

[5] Using the methods in T. L. Hill, J. Chem. Phys. **16**, 399 (1948) to obtain ϵ and r^* (in the notation of this reference). The collision diameter σ was then taken as that intermolecular distance which gives an intermolecular interaction energy of $+(1/2)kT$ (J. G. Kirkwood and E. M. Boggs, J. Chem. Phys. **10**, 394 (1942)), using a Lennard-Jones potential function.

[6] Since this is a very special case, we do not tabulate a_i, b_i, g_i, f_i, $c_1(\rho)$, and $c_2(\rho)$. These can, however, be obtained from the author if desired. For adequate convergence it was necessary to compute as far as a_{12}, b_7, g_{12}, and f_7 ($a_i = g_i = 0$ for i odd; $b_1 = f_1 = 0$ for reflection; $b_0 = f_0 = 0$ for capture).

[7] The computation of $c_1(\rho)$ when $k_7=0$ takes about 3 hours.

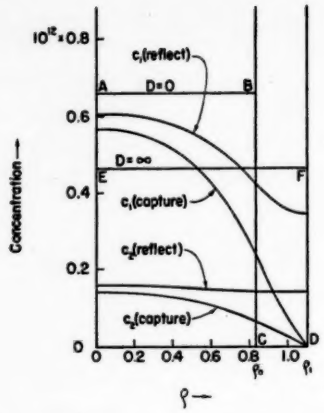

FIG. 1. Radical concentration in radial diffusion.

(neglect CH_3+CH_3), the differential equation in c_1 is now linear; in fact, it is a Bessel equation and explicit solutions can be written. We have

$$D_1\left(\frac{d^2c_1}{d\rho^2}+\frac{1}{\rho}\frac{dc_1}{d\rho}\right)+\bar{Q}-k_5c_1n_{Ac}=0, \quad 0\leqslant\rho\leqslant\rho_0,$$
$$D_1\left(\frac{d^2c_1}{d\rho^2}+\frac{1}{\rho}\frac{dc_1}{d\rho}\right)-k_5c_1n_{Ac}=0, \quad \rho_0\leqslant\rho\leqslant\rho_1. \tag{18}$$

One finds in a straightforward manner,[8] in the *absence of a wall* (this is really a special case of Eq. (21)),

$$c_e=\frac{\bar{Q}L_3K_0(\xi)}{k_5n_{Ac}L},$$
$$c_i=\frac{\bar{Q}}{k_5n_{Ac}}\left[1-\frac{L_4I_0(\xi)}{L}\right], \tag{19}$$

where c_i = concentration of methyl radicals for $0\leqslant\rho\leqslant\rho_0$, and c_e = concentration for $\rho_0\leqslant\rho\leqslant\rho_1$, $I_0(\xi)$ and $K_0(\xi)$ are modified Bessel functions of the first and second kind, respectively, and

$$\begin{aligned}
&\xi=(k_5n_{Ac}/D_1)^{\frac{1}{2}}\rho, && L_4=K_1(\xi_0),\\
&L=L_1L_4+L_2L_3, && L_5=I_0(\xi_1),\\
&L_1=I_0(\xi_0), && L_6=K_0(\xi_1),\\
&L_2=K_0(\xi_0), && L_8=I_1(\xi_1),\\
&L_3=I_1(\xi_0), && L_9=K_1(\xi_1).
\end{aligned} \tag{20}$$

When a wall is present, one can give a single discussion here for the entire range in α, $0\leqslant\alpha\leqslant1$. We choose as the boundary condition at the wall $c_e=c_1(\rho_1)$, where $c_1(\rho_1)$ is arbitrary for the time being. Using this condition and the usual ones at $\rho=\rho_0$, one finds as the solution to Eqs. (18)

$$\begin{aligned}
c_i&=AI_0(\xi)+(\bar{Q}/k_5n_{Ac}),\\
c_e&=BI_0(\xi)+EK_0(\xi),
\end{aligned} \tag{21}$$

where

$$A=\frac{c_1(\rho_1)}{L_5}-\frac{\bar{Q}(L_3L_6+L_4L_5)}{k_5n_{Ac}LL_5}, \tag{22}$$

$$B=\frac{c_1(\rho_1)}{L_5}-\frac{\bar{Q}L_3L_6}{k_5n_{Ac}LL_5}, \tag{23}$$

$$E=\frac{\bar{Q}L_3}{k_5n_{Ac}L}. \tag{24}$$

If we now substitute Eqs. (21) into Eq. (15), putting $k_3=k_7=0$, we obtain a relation between α and $c_1(\rho_1)$:

$$c_1(\rho_1)=\frac{\bar{Q}L_3(L_6L_8+L_5L_9)\xi_1}{k_5n_{Ac}LL_5\left(\frac{\xi_1L_8}{L_5}+\frac{\rho_1\bar{v}_1\alpha_1}{4D_1}\right)}. \tag{25}$$

Using numerical values (Table I), Eq. (25) becomes here

$$c_1(\rho_1)=\frac{1.326\times10^{12}}{0.828+1.878\times10^4\alpha_1}\text{cc}^{-1}. \tag{26}$$

For $\alpha_1\geqslant0.01$, this is approximately

$$c_1(\rho_1)=\frac{7.06\times10^7}{\alpha_1}\text{cc}^{-1}. \tag{27}$$

For $\alpha_1\geqslant0.01$, $c_1(0)=1.028\times10^{12}$ cc^{-1}, and hence $c_1(\rho_1)/c_1(0)\leqslant0.0069$.

Figure 2 gives $c_1(\rho_1,\alpha_1)/c_1(\rho_1,0)$ plotted against α_1 from Eq. (26). That is, this curve gives the *wall* concentration of methyl radicals relative to the wall concentration when $\alpha_1=0$ (complete reflection), plotted against the capture probability α_1. It is seen that for $\alpha_1<10^{-6}$ the wall concentration, and hence the whole concentration curve, is essentially independent of α_1.

TABLE II. Number of radicals $\times10^{-12}$ produced and disappearing in one cm of cylinder per second.

	Reflection		Capture		Reflection $D=\infty$		$D=0$	
	CH_3	CH_2COCH_3	CH_3	CH_2COCH_3	CH_3	CH_2COCH_3	CH_3	CH_2COCH_3
Production	12.47	3.22	12.47	2.04	12.47	3.27	12.47	2.65
Disappearance owing to								
$CH_3+CH_3COCH_3$	3.22		2.04		3.27		2.65	
$2CH_3$	6.76		3.60		6.67		7.64	
$CH_3+CH_2COCH_3$	2.50	2.50	1.08	1.08	2.53	2.53	2.18	2.18
$2CH_2COCH_3$		0.73		0.25		0.74		0.47
Walls			5.75	0.71				

[8] Gray, Mathews, and MacRobert, *Treatise on Bessel Functions* (MacMillan Company, Ltd., London, 1931), especially pp. 160–161.

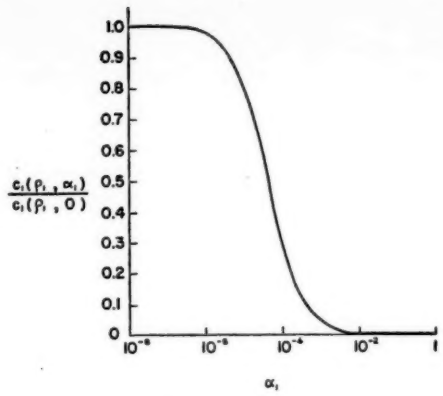

FIG. 2. Relative wall concentration as a function of capture probability.

So "complete reflection" here actually means in practice $\alpha_1<10^{-6}$. Similarly, for any $\alpha_1>10^{-2}$, the relative wall concentration is essentially zero, and the "appreciable capture" concentration curve applies. The important transition between reflection and capture therefore comes in the range $10^{-6}<\alpha_1<10^{-2}$.

The above discussion applies strictly only to the case $k_3=k_7=0$. However, the fact that the ratios 0.0079, 0.0076, and 0.0069 following Eqs. (16), (17), and (27) are all of the same order of magnitude suggests that *relative* effects of α_1 on concentration curves should be at least qualitatively the same when k_3 and k_7 are included as when $k_3=k_7=0$. Also, the consideration that the rate of the collision process on the walls (number of collisions per second per cm of cylinder for unit radical concentration) is very fast compared to the rate of any of the chemical processes under discussion (number of products formed per second per cm of cylinder for unit radical concentration) leads one to the same expectation.

In Fig. 3 we present a few further concentration curves of interest. The curve for $k_3=k_7=0$ with no wall is also the curve for a wall with $\alpha_1=1.00\times10^{-4}$. Also, it will be noticed from the two bottom curves that the inclusion of acetonyl radicals has little effect on the methyl radical concentration curve.

IV. LONGITUDINAL DIFFUSION

Diffusion turns out to be rather unimportant in the longitudinal direction (because the cell is relatively long) so we give a less complete discussion of this problem. We assume that the light beam is radially uniform, filling the entire cell from $\rho=0$ to $\rho=\rho_1$, and that there is complete reflection from the wall.[9] This then eliminates the radial problem. We are left with the z problem.

We start by considering the $k_3=k_7=0$ case. We have

$$D_1\frac{d^2c_1}{dz^2}+Q_0\exp(-\delta z)-k_5n_{Ac}c_1=0. \tag{28}$$

[9] Alternatively we can make the equivalent assumption that the light beam is confined to $0\leqslant\rho\leqslant\rho_0$, $D=\infty$ in the radial direction, and there is reflection from the wall.

There are walls at $z=0$ and $z=z_0$. For reflection, $dc_1/dz=0$ at $z=0$ and $z=z_0$ (normal derivative of concentration is zero is the general boundary condition for reflection). For capture, $c_1\cong0$ at $z=0$ and $z=z_0$ as before. Equation (28) can be solved by elementary methods. We find, for reflection,

$$c_1=\frac{\gamma_0\delta}{\alpha^{\frac{1}{2}}(\alpha-\delta^2)(b_2-b_1)}\Big[(b_3-b_2)\exp(-\alpha^{\frac{1}{2}}z)+(b_3-b_1)\exp(\alpha^{\frac{1}{2}}z)+\frac{\alpha^{\frac{1}{2}}(b_2-b_1)}{\delta}\exp(-\delta z)\Big], \tag{29}$$

and, for capture,

$$c_1=\frac{\gamma_0}{(\alpha-\delta^2)(b_2-b_1)}\Big[(b_3-b_2)\exp(-\alpha^{\frac{1}{2}}z)+(b_1-b_3)\exp(\alpha^{\frac{1}{2}}z)+(b_2-b_1)\exp(-\delta z)\Big], \tag{30}$$

where

$$\gamma_0=Q_0/D_1,\qquad b_2=\exp(\alpha^{\frac{1}{2}}z_0),$$
$$\alpha=k_5n_{Ac}/D_1,\qquad b_3=\exp(-\delta z_0). \tag{31}$$
$$b_1=\exp(-\alpha^{\frac{1}{2}}z_0),$$

Also, from Eq. (28),

$$c_1=\frac{\gamma_0\exp(-\delta z)}{\alpha}\quad\text{for}\quad D_1=0. \tag{32}$$

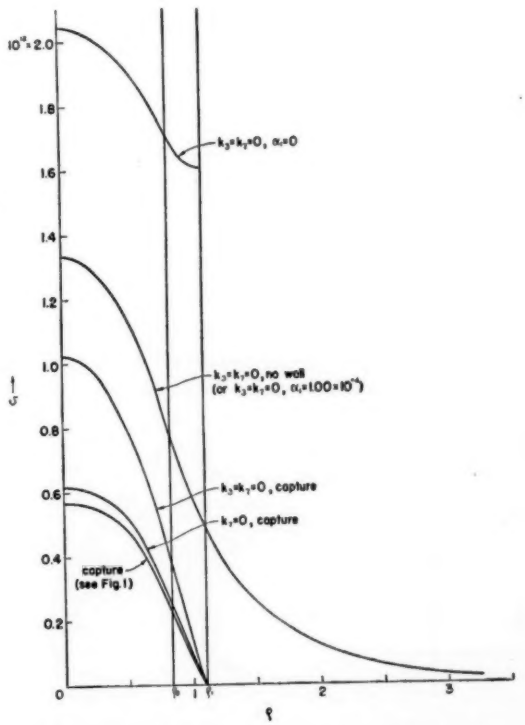

FIG. 3. Methyl radical concentration in radial diffusion.

In Fig. 4 we give curves calculated from Eqs. (29), (30), and (32), using Table I. However, in order to obtain an average production of methyl radicals comparable with that in Section III, we have taken

$$\bar{Q}=5.72\times10^{12}(\rho_0/\rho_1)^2. \tag{33}$$

Using $\exp(-\delta z_0)=0.465$[1] and Eq. (8), this gives $\delta=0.03828$ cm^{-1} and $Q_0=4.694\times10^{12}$ cc^{-1} sec.$^{-1}$. Figure 4 shows that diffusion has a negligible effect here when there is reflection. Even when there is capture, the effect of diffusion is confined to about 4 cm near each end of the cell. With the other chemical reactions introduced, the influence of diffusion is still smaller (see below). The amount of loss to the walls in the capture case of Fig. 4 is relatively small compared to that in the radial problem. This is of course to be expected since most of the gas is not near a (capturing) wall. The difference between the area under the reflection curve and the area under the capture curve relative to the area under the reflection curve gives the fraction of methyl radicals produced which are lost to the walls in this case.

It is seen in Fig. 4 that the capture curve (A), starting at $z=0$, approaches the $D_1=0$ curve (B) very closely at about $z=4$ cm. In this region, say $0\leqslant z\leqslant 5$, if we put $\delta=0$, the $D_1=0$ curve becomes $c_1=\gamma_0/\alpha$ (C) while the finite D_1 curve becomes (D)

$$c_1=(\gamma_0/\alpha)[1-\exp(-\alpha^{\frac{1}{2}}z)]. \tag{34}$$

Now it is easy to show that the above-mentioned curves are related by $(C)-(D)=(B)-(A)$. A similar relation holds near $z=z_0$.

The next step is to solve the equation ($k_7=0$)

$$D_1\frac{d^2c_1}{dz^2}+Q_0\exp(-\delta z)-k_5n_{Ac}c_1-2k_3c_1^2=0. \tag{35}$$

One can set up a series solution as in the radial problem but convergence is slow. We therefore content ourselves with an approximate treatment. If we put $\delta=0$ in Eq. (35) we can solve the resulting equation using numerical integration. This gives a curve analogous to (D) above. Further, the analogs of (B) and (C) are easily obtained, so that (A) can be estimated by assuming that $(C)-(D)=(B)-(A)$ holds here also. This should be a quite accurate assumption. This process has to be carried out for each end of the cell (use γ_0 in one case and $\gamma_0\exp(-\delta z_0)$ in the other).

Equation (35) with $\delta=0$ is solved as follows: Consider the equation

$$\frac{d^2c_1}{dz^2}-\alpha c_1-\beta c_1^2+\gamma_0=0 \tag{36}$$

where $\beta=2k_3/D_1$. The boundary conditions are $c_1=0$ at $z=0$ and

$$c_1=c_0=\frac{(\alpha^2+4\beta\gamma_0)^{\frac{1}{2}}-\alpha}{2\beta},$$
$$dc_1/dz=0, \tag{37}$$

at $z=\infty$. Let us make the standard substitutions (for an equation of this type)

$$u=\frac{dc_1}{dz},\quad u\frac{du}{dc_1}=\frac{d^2c_1}{dz^2}. \tag{38}$$

A first integration can then be carried out. The second integration gives the final result

$$z=\frac{1}{\sqrt{2}}\int_0^{c_1}\frac{dc_1}{[(\beta c_1^3/3)+(\alpha c_1^2/2)-\gamma_0c_1+A]^{\frac{1}{2}}}, \tag{39}$$
$$A=\gamma_0c_0-(\alpha c_0^2/2)-(\beta c_0^3/3),$$

which can be integrated numerically.

The calculated curve is given in Fig. 5. With the additional chemical reaction (CH_3+CH_3), the range of the diffusion effect on the capture curve is thus reduced to about 2 cm on each end. The acetonyl reaction would reduce this a little further (compare the two bottom curves of Fig. 3).

Although we have given an incomplete treatment in this section, it is sufficiently clear that in the present case longitudinal diffusion is unimportant if there is reflection from the walls, and if there is appreciable capture, the diffusion effects are confined to a relatively small region at the ends of the cell.

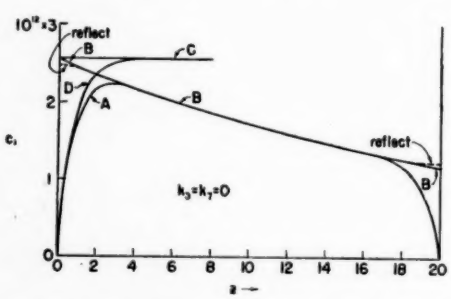

FIG. 4. Methyl radical concentration in longitudinal diffusion.

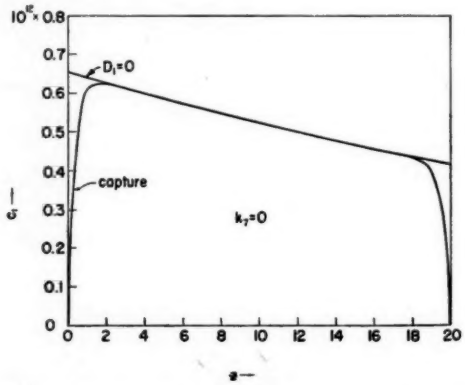

FIG. 5. Methyl radical concentration in longitudinal diffusion.

V. MEAN LIFETIME DIFFUSION DISTANCE

Useful qualitative information concerning the importance of diffusion in a given experiment can be obtained by calculating the root-mean-square distance a radical (or molecule) diffuses in a mean radical lifetime (determined by the rate of the chemical reactions the radical can undergo). This mean lifetime diffusion distance gives the order of distance over which diffusion effects will be important. In the present example (Eqs. (1)–(5)) this distance is about 0.5 cm.[10] This confirms the observation in the preceding sections that diffusion is important radially ($\rho_1=1.1$ cm) but not longitudinally ($z_0=20$ cm) except near the ends of the cell.

Let $\langle r^2\rangle_{Av}$ be the mean square radial displacement of a radical from an initial point owing to diffusion in a time $\bar{t}$. Let $\langle\lambda^2\rangle_{Av}$ be the same distance along some specified axis or direction. Then several well-known relations in diffusion theory are[11] (see Table I also):

$$\langle\lambda^2\rangle_{Av}=\frac{\langle r^2\rangle_{Av}}{3}=\frac{2l\bar{v}\bar{t}}{3}=2D\bar{t}. \tag{40}$$

We are interested primarily in $\langle\lambda^2\rangle_{Av}$ rather than $\langle r^2\rangle_{Av}$. If we have a particle of mass m diffusing through a gas of density n, Eq. (40) becomes

$$\langle\lambda^2\rangle_{Av}=\frac{4}{3\pi^{\frac{1}{2}}\sigma^2 n}\left(\frac{kT}{m}\right)^{\frac{1}{2}}\bar{t}, \tag{41}$$

where σ is the mean collision diameter.

Now it is easy to see that the mean lifetime of a particular methyl radical, in the present case, is given by

$$\bar{t}_1=1/(k_5 n_{Ac}+k_7c_2+2k_3c_1). \tag{42}$$

Only the concentration of acetone molecules has an appreciable effect on the diffusion rate (Eq. (41)), but all reactions are significant in Eq. (42). We are assuming for simplicity in Eq. (42) that the methyl radical of interest is diffusing through a *uniform* medium of acetone (n_{Ac}), methyl radicals (c_1) and acetonyl radicals (c_2). For acetonyl radicals,

$$\bar{t}_2=1/(k_7c_1+2k_6c_2). \tag{43}$$

[10] Of course an appreciable number of radicals have a lifetime diffusion distance considerably greater than the mean value. Thus, in Fig. 4, diffusion effects are noticeable over a 4 cm range while $(\langle\lambda^2\rangle_{Av})^{\frac{1}{2}}=1.09$ cm (see notation below). In Fig. 5, this range is about 2 cm, and one finds $(\langle\lambda^2\rangle_{Av})^{\frac{1}{2}}=0.55$ cm ($z=0$ end) and $(\langle\lambda^2\rangle_{Av})^{\frac{1}{2}}=0.65$ cm ($z=z_0$ end).

[11] E. H. Kennard, *Kinetic Theory of Gases* (McGraw-Hill Book Company, Inc., New York, 1938).

TABLE III.

$\bar{Q}\times10^{-12}$	$c_1\times10^{-12}$	$c_2\times10^{-12}$	$(\langle\lambda^2\rangle_{Av})^{\frac{1}{2}}$	$(\langle\lambda^2\rangle_{Av})^{\frac{1}{2}}(\bar{Q})^{\frac{1}{4}}$
5.72	0.657	0.161	0.501 cm	0.78
10	0.917	0.169	0.448	0.80
30	1.715	0.180	0.354	0.83
100	3.29	0.186	0.268	0.85
1000	10.87	0.192	0.154	0.865
10000	34.85	0.195	0.087	0.87

As an example, let us use average values for c_1 and c_2 from the $D=\infty$ radial (reflection) case discussed in Section III. These are $c_1=0.465\times10^{12}$ and $c_2=0.152\times10^{12}$. One finds $\bar{t}_1=0.142$ sec., $\bar{t}_2=0.177$ sec., $(\langle\lambda_1^2\rangle_{Av})^{\frac{1}{2}}=0.556$ cm, and $(\langle\lambda_2^2\rangle_{Av})^{\frac{1}{2}}=0.381$ cm.

As a further example, we compute[12] the effect of light intensity (essentially $\bar{Q}$) on $(\langle\lambda_1^2\rangle_{Av})^{\frac{1}{2}}$. For this purpose we assume a uniform concentration of methyl and acetonyl radicals over the light space only (in effect assuming $D_1=D_2=0$) and we then try to find how large $\bar{Q}$ must be to produce radical concentrations large enough to make diffusion a slow process compared to the chemical processes. That is, for sufficiently large values of c_1 and c_2, $\bar{t}_1$ and $\bar{t}_2$ will be so small that the assumption $D_1=D_2=0$ can be made:[13] the radicals are in effect confined to the light space.

We use

$$\begin{aligned}\bar{Q}-k_5n_{Ac}c_1-2k_3c_1^2-k_7c_1c_2&=0,\\ k_5n_{Ac}c_1-k_7c_1c_2-2k_6c_2^2&=0,\end{aligned} \tag{44}$$

and the data of Table I, except that $\bar{Q}$ is varied. Equations (41) and (42) then give $(\langle\lambda_1^2\rangle_{Av})^{\frac{1}{2}}$. The results are presented in Table III. It is seen that even with $\bar{Q}\times10^{-12}=10{,}000$, $(\langle\lambda^2\rangle_{Av})^{\frac{1}{2}}$ is not quite sufficiently small[10] compared to the radial dimensions of the cell to make diffusion negligible.

Table III shows that for large enough $\bar{Q}$, $(\langle\lambda^2\rangle_{Av})^{\frac{1}{2}}\propto(\bar{Q})^{-\frac{1}{4}}$. This follows from

$$\begin{aligned}c_1&\cong(\bar{Q}/2k_3)^{\frac{1}{2}},\\ \bar{t}_1&\cong1/2k_3c_1,\end{aligned} \tag{45}$$

and

$$(\langle\lambda^2\rangle_{Av})^{\frac{1}{2}}=(2D_1\bar{t}_1)^{\frac{1}{2}}.$$

The author is indebted to Professor W. A. Noyes, Jr. for suggesting this problem, and to Professor Noyes and Dr. L. M. Dorfman for a number of helpful discussions.

[12] This calculation suggested itself as a result of a personal communication from Professor O. K. Rice to Professor W. A. Noyes, Jr.

[13] Another approach would be to increase the acetone pressure. Increasing $\bar{Q}$ decreases $\bar{t}$; increasing n_{Ac} decreases D (see also Eq. (42)). Both decrease $\langle\lambda^2\rangle_{Av}$.

On the Photographic Reciprocity Law Failure and Related Effects. I. The Low Intensity Failure

E. KATZ
Physics Department, University of Michigan, Ann Arbor, Michigan
(Received April 29, 1949)

(1) The order principle (o.p.) states: "The grains of an emulsion become developable in the course of an exposure in a given sequence independent of the exposure and development variables." This hypothesis appears to have a wide range of applicability. It forms an ideally simple link for correlating experimental isodense exposures and theoretical single grain response predictions. Moreover, in many cases where the o.p. is not strictly applicable, corrections can be derived (Section 12) which again make quantitative comparison of theory and experimental data possible.

(2) Extending ideas of Gurney, Mott, and Webb, a quantitative theory of the low intensity reciprocity law failure (l.i.f.) is developed, by analyzing the statistics of light absorption and the survival function of the electrons. Confrontation of various theoretical possibilities with experimental data selects the following basic assumptions: (a) A monoatomic Ag speck of sub-latent image is unstable against thermal agitation, but a diatomic speck is stable for most practical purposes; finally a triatomic speck is completely stable. (b) The energy required to set free an electron from a monoatomic speck (electron trap depth) is not the same for all traps. There must be a quasi-continuous distribution of depths (e.g. as given by formula (10)).

With these assumptions the theory describes satisfactorily the principal features in the shape of experimental l.i.f. curves. It is found that the l.i.f. slope varies systematically with grain size and the theory checks qualitatively with this result. The experimental temperature dependence of l.i.f. curves agrees satisfactorily with the theory.

1. INTRODUCTION

THE photographic density D does not depend only on the product E of the intensity I and the time t of exposure. Its dependence on I and t is shown schematically in Fig. 1, using the customary variables D; $e={}_{10}\log E$; $i={}_{10}\log I$. Figs. 1a and 1b show the optimal intensity where E is a minimum for given D or D is a maximum for given E. To the left and to the right of the optimum lie the regions of "low" and "high intensity reciprocity law failure" (r.l.f.). For the present we shall concentrate on the low intensity failure (l.i.f.). Its existence means that longtime intervals between successive absorptions of quanta in one grain (interquantic times) reduce the efficiency of latent image formation. Optimal interquantic times are usually $\sim$0.01 sec. at room temperature.

The present paper aims at a semi-theoretical description of the l.i.f. as a basis for the quantitative treatment of such related effects as the sequence effect (II), the intermittence effect (III) and the addition effect (IV).

2. ELEMENTARY RELATIONS

The identity:

$$(\delta D/\delta i)_E \equiv -(\delta D/\delta e)_I \cdot (\delta e/\delta i)_D \qquad (1)$$

holds at any point of the $D(e, i)$ surface.

The quantity:

$$\gamma \equiv (\delta D/\delta e)_I \qquad (2)$$

is practically constant for a large range of intermediate D values (see Fig. 1c). For given D, moreover, γ is only very weakly dependent on I. Consequently, in Fig. 1a curves with parameter values D and $D+\Delta D$ are practically parallel, their spacing $\Delta e = \Delta D/\gamma$. Similarly, in Fig. 1b curves for e and $e+\Delta e$ are parallel only for intermediate densities where the curves of Fig. 1c are straight.

3. THE RELATION BETWEEN DENSITOMETRIC AND SINGLE GRAIN DATA

Experiment generally yields densitometric data whereas theory usually discusses the single grain. How do relations in one field show up in the other one?

The density-exposure curve for a single grain is a step function. Below a certain exposure the grain is not developable but above this it develops completely. The density-exposure curve (Fig. 1c) of the whole emulsion is the sum of a great many of such step functions with different step points and step heights. These curves are sensitive to all spreading effects, such as, e.g., a spread in grain size. Hence they are not well suited to a study of single grain properties.

Do isodense exposures—like those of Fig. 1a—truly represent single grain properties? A. van Kreveld[1] gave a first answer: If isodensity has an intrinsic physical meaning, the following "transformation law" should hold: "exposures which are isodense on a given emulsion under one set of conditions of development and densitometry should again be isodense on the same emulsion under any other set of such conditions." Experiments proved this to be only very approximately true.

As a new approach to the same problem we propose the following hypothesis (to be called "order principle," o.p.): "The *order* in which the grains of a given plate become developable in the course of any exposure is independent of the conditions of exposure and development." An equivalent way of stating the o.p. is: "Exposures that would be isodense on one plate by one particular method of development would render the same grains developable." Hence isodense exposures produce exactly equal effects in the last grain(s) rendered developable. Thus the o.p. links in a very simple way experimental isodense exposures and theoretical

[1] A. van Kreveld, thesis, Utrecht (1933).

single grain data. We shall assume its validity whenever we have no reason to the contrary.

4. LIMITATIONS OF THE ORDER PRINCIPLE

There are a number of obvious restrictions to the validity of the o.p.:

(a) Isodense exposures on a panchromatic plate, produced either by blue or red light will not render all the same grains developable. The red light will favor more grains in deeper layers than the blue light. The o.p. cannot obtain then. Unless otherwise stated we will compare only isodense exposures either in thin emulsions or with the same wave-lengths.

(b) If not all grains of an emulsion are sensitized, blue light will affect all grains but red light only the sensitized ones. Isodensity would then refer to different grains and the o.p. does not hold. Unless otherwise stated we shall assume equal absorption spectra for all grains for all wave-lengths concerned.

(c) One may argue that the o.p. can only hold if either the grain size is rather homogeneous or the sensitivity is a monotonous function of grain size and does not spread very much within each grain size group. We shall assume that at least one of these requirements is satisfied.

(d) Suppose the plate contains a mixture of two or more kinds (groups) of grains and the o.p. holds in each group. In general it will not hold for their sum. Some situations where the o.p. does not apply can be resolved into fractions where it does, and in this way can be handled relatively simply (see Section 12).

(e) Because of the statistical nature of light absorption, even for two experimentally identical exposures on identical plates, the interquantic times for similar grains will fluctuate. Consequently the place of each grain in the order series may fluctuate. Also other links in the chain of processes of latent image formation may be subject to statistical fluctuations, causing corresponding order fluctuations of the grains. We wish to include this sort of statistical flexibility in the o.p. Such fluctuations will never violate any conclusions based on the o.p. in the stricter sense because most grains will fluctuate only a few places of order and the grains taking their places are on the average very similar in all respects.

Other examples may be constructed, restricting the applicability of the o.p. In practice the error arising from disregarding these restrictions will usually be very small and sometimes can be corrected (see Section 12).

It is not easy to verify the o.p. experimentally. The difficulty in a direct test arises from the fact that any experiment to establish the order in which grains become developable as a result of one type of exposure destroys the possibility of performing a second similar experiment with another type of exposure on the same grains. The o.p. can at present only be tested from its consequences. The present study aims at deriving such consequences and comparing them quantitatively with experiment. The l.i.f. and associated phenomena will appear to be particularly amenable to discussion from the standpoint of the o.p.

5. THE DIFFERENCE BETWEEN THE ORDER PRINCIPLE AND THE TRANSFORMATION LAW

The o.p. may hold without the transformation law and the transformation law may hold without the o.p. One example of each kind will be described:

(a) The o.p. is assumed to hold. Consider two different developers. The first one develops all grains that have surface silver specks of n or more atoms, but ignores grains with smaller specks. The second developer acts on silver specks of $(n-1)$ or more atoms. There is no reason why two different exposures that produce the same number of grains with n-atomic specks (i.e., that are isodense with the first developer) should also produce the same number of grains with $(n-1)$-atomic specks (i.e., be isodense with the second developer). In general, therefore, even with the o.p., the isodensity of two different exposures will not be invariant to changes in developer, hence the transformation law is not valid.

(b) The transformation law is assumed to hold. For two isodense exposures, one to red light and one to blue light on a pan plate without r.l.f., the o.p. will not hold because the red light penetrates deeper into the emulsion, consequently involving different grains. The resulting densities, however, are equal for any kind of development.

6. THE MECHANISM OF THE LOW INTENSITY FAILURE AND ITS CONSEQUENCES

In order to explain the l.i.f. Gurney and Mott[2] assumed temporarily that a sulfide sensitivity speck in the silver bromide grain has a tendency to dissociate into an electron and a positive speck owing to thermal agitation. Webb,[3] on the other hand, explains the l.i.f. by assuming that a silver speck is unstable against thermal agitation, dissociating into a conduction electron and expelling a Ag^+ ion into an interstitial lattice position, as long as the speck has not yet surpassed a critical size. From a study of what we shall briefly call the "sequence effect" (see Paper II), Webb derived evidence that this critical size is about half the size required for developability. Webb's hypothesis is in line with known facts about the Herschel effect, where upon absorption of infra-red radiation large (developable) silver specks are known to disintegrate in the same way. Gurney and Mott have apparently accepted Webb's ideas in 1940.[4]

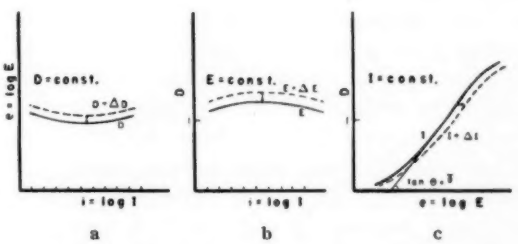

FIG. 1. The three customary ways of mapping the density (D)-log exposure (e)-log intensity (i) surface. Fig. a: lines of constant D (r.l.f. curves); Fig. b: lines of constant e; Fig. c: lines of constant i ("characteristic" curves).

[2] R. W. Gurney and N. F. Mott, Proc. Roy. Soc. A **164**, 151 (1938).
[3] J. H. Webb and C. H. Evans, J. Opt. Soc. Am. **28**, 431 (1938).
[4] R. W. Gurney and N. F. Mott, *Electronic Processes in Ionic Crystals* (Oxford University Press, New York, 1940), p. 247.

We define an n-quantic process as one, the efficiency of which is determined by the time spacings of n quanta. Suppose, for example, that a monoatomic speck of Ag is unstable against thermal agitation, a diatomic speck is stable and a speck of about 4 atoms is developable. The efficiency of forming a developable speck is determined by the time interval between the quanta that build up the first diatomic speck. The time intervals between later quanta are irrelevant for the efficiency. Hence, this is an example of a two-quantic process in the above sense, although the action of four quanta is required to yield a developable speck. *We shall assume that latent image formation is a two-quantic process* on the following grounds. It is the simplest assumption consistent with the existence of the l.i.f. The assumption of a triquantic process leads to results that are not supported by experiment (see section 10). The well-known work of Reinders (recently rediscussed by Berg[5]) shows that a developable silver speck contains about 3–4 atoms. The theoretical work of Silberstein[6] on the shape of characteristic curves also supports the two-quantic assumption.

Now consider one grain absorbing a quantum at $t=0$. Let the survival function $F(t)$ be the chance that at time t there is still, as a result of this absorption, somewhere in the grain an electron "alive." This electron may wander around, being trapped and released at intervals, until it finally "dies" either by being captured in its hole or by being trapped stably at a silver speck. Let $P(t)dt$ be the probability that an interquantic time lies between t and $t+dt$. Then the probability W of liberating a second electron while the first one is still alive is:

$$W=\int_0^\infty F(t)\cdot P(t)dt. \tag{3}$$

If two electrons are present simultaneously, there is a chance c of building a stable speck. Consequently the probability of building a stable speck per interquantic time is cW. The probability of forming a stable speck during an exposure with E' interquantic times becomes then $\sim(1-\exp(-cWE'))$. If E_0 quanta are needed in addition to render the speck developable, the probability of forming a developable speck during an exposure with $E=E'+E_0$ interquantic times is $(1-\exp(-cW(E-E_0)))$. Assuming the validity of the o.p., isodense exposures must correspond to the same probability for a developable speck for the type of grains that became developable last. Consequently isodense exposures should satisfy the relation:

$$W(E-E_0)=\text{const.} \tag{4}$$

This, then, is also the general expression for the l.i.f. Its explicit form depends on that of $F(t)$ and $P(t)$.

[5] W. F. Berg, Phil. Mag. **36**, 337 (1948).
[6] L. Silberstein, J. Opt. Soc. Am. **29**, 67 (1939).

7. THE STATISTICS OF LIGHT ABSORPTION $P(t)$ AND THE SURVIVAL FUNCTION $F(t)$

If a grain with effective receptive area α is illuminated with intensity I, it absorbs $I\alpha$ quanta per unit time. The average interquantic time $\bar{t}=1/I\alpha$. It is easily shown (see e.g.[7]) that the probability of finding among the fluctuating interquantic times values between t and $t+dt$ is:

$$P(t)dt=\exp(-t/\bar{t})d(t/\bar{t}). \tag{5}$$

With (5), (3) becomes:

$$W=\alpha I\int_0^\infty F(t)\exp(-\alpha It)dt. \tag{6}$$

For any given $F(t)$ the integral, hence W, is a function of αI only.

The present state of knowledge of the interior of the grain does not permit an exact theoretical prediction of the survival chance $F(t)$. If all electron traps had the same potential depth, one would have:

$$F(t)=\exp(-t/\theta). \tag{7}$$

This gives with (4) and (6), after a slight rearrangement, for the l.i.f.:

$$I(E-E_0')=\text{const.} \tag{7a}$$

For very low intensities (7*a*) approaches:

$$IE=\text{const.} \tag{7b}$$

A l.i.f. slope as high as 1 is rarely observed. Mostly the straight part at low intensities satisfies:

$$I^xE=\text{const. with } 0.1<x<0.7 \tag{8}$$

and this corresponds with (4) and (6) to:

$$I^x(E-E_0)=\text{const.} \tag{9}$$

and:

$$F(t)\sim t^{-x}. \tag{9a}$$

The number of electrons dying per unit time is then:

$$-dF/dt\sim t^{-x-1}.$$

This has to be interpreted in terms of a certain trap depth distribution (see Section 8). The situation in photographic grains may be closely comparable to that in small ZnS-phosphor grains. Antonow-Romanowsky (quoted from Gurney and Mott[4] p. 216) studied phosphors of grain sizes only slightly larger than photographic grains. Their decay time constants were roughly of the same order of magnitude as the interquantic times for the l.i.f. The phosphorescent intensity, which is a direct measure of the number of electrons dying per unit time, was found to be proportional to t^{-y-1} with $0<y<1$. Smaller grains had the smaller y values. Apparently, in small ZnS grains trap depth distributions do occur which give experimental decay functions such as required to explain the photographic effect.

[7] E. Katz, thesis, Utrecht (1941).

This analogy suggests that the slope x of the l.i.f. should be greater for coarser photographic grains. Table I presents data from literature. Recalling that high speed emulsions have coarser grains than low speed ones we see that the table confirms the expected trend. In addition there seems to be a slight tendency for panchromatic plates to score higher slopes than blue sensitive ones with the same grain size, but more data are needed to ascertain this point.

For the present, then, the form of $F(t)$ has been indicated experimentally.

8. THE SURVIVAL FUNCTION $F(t)$ AND THE TRAP DISTRIBUTION

In this section it will be shown that if the grain is assumed to have many traps of various depths for conduction electrons, then by a plausible choice of the depth distribution a survival function $F(t)\sim t^{-x}$, as required by experiment, results. In other words the experimental results can be explained on the basis of a certain trap distribution.

We consider an ensemble of N copies of one grain. Suppose at $t=0$ they all absorb one quantum of light lifting an electron into the conduction band. Let the fraction $m(U)dU$ of all traps in each grain have an energy depth between U and $U+dU$. The form of $m(U)$ is suggested by the following argument. The sensitivity of a grain is mainly due to minute concentrations of Ag_2S traps in the AgBr lattice. Under ideal conditions each Ag_2S speck might have the same trap depth. In a real crystal strains, dislocations, cracks in the neighborhood of a speck may vary its trap depth U over a continuous range. Since these physical imperfections themselves constitute (shallow) traps for conduction electrons, their combination with a Ag_2S speck will increase the trap depth of the latter. Because the grains have been built and ripened for some time at a temperature T^* well above room temperature, the imperfections may have reached equilibrium. Imperfections, the production of which required an energy V, will represent a fraction $\exp(-V/kT^*)$ of all the imperfections. The simplest assumption is that the energy depth of a Ag_2S trap is increased by an amount proportional to V owing to a neighboring imperfection. This assumption leads immediately to a distribution:

$$\left.\begin{aligned} m(U)&=0 && \text{for } U<U_0 \\ m(U)&=1/\epsilon\cdot\exp\{(U_0-U)/\epsilon\} && \text{for } U\geqslant U_0 \end{aligned}\right\}, \tag{10}$$

where U_0 is the ideal trap depth of a Ag_2S speck and ϵ is the average depth increase due to imperfections. It will be shown that the l.i.f. can be described satisfactorily with (10).

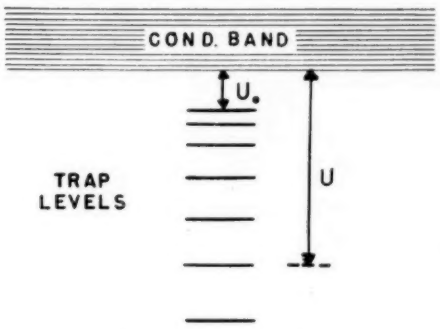

FIG. 2. Schematic distribution of trap depths U.

Thermal motion tends to liberate a trapped electron. The liberation probability per unit time will be:

$$\lambda(U)=C\cdot\exp(-U/kT). \tag{11}$$

C and an effective depth U_e can be estimated by picturing the trapped electron as moving with kinetic energy $\sim kT$ in a potential hole of dimensions $\sim 3.10^{-8}$ cm, the lattice constant. The exponential in (11) represents the escape chance per reflection against the trap wall and C the frequency of hitting the wall. Hence $C=3.10^{14}$. The average time needed for escape must be of the order of the optimal interquantic time t_0($\sim$0.01 sec. at room temperature). Only if electrons arrive at larger intervals, will previous ones have had a reasonable chance of escaping, dying and thus yielding a l.i.f. Hence:

$$\lambda_e\cdot t_0\sim 1 \tag{11a}$$

or $\lambda_e\sim 100$ and $U_e\approx 0.7$ ev. This value, although derived in a crude way, should be close to all relevant trap depths of the whole distribution since λ is very sensitive to changes in U, 0.1 ev corresponding to a change by factor 60. For another independent estimate of U_e see section 9.

When an electron escapes from a trap into the conduction band it may recombine with its hole (probability γ) or it may be caught in another trap (probability $\sigma=1-\gamma$). Since, in our ensemble, there is at most one electron and one hole per grain, γ is a constant. After a time t the fraction $n(U, t, \gamma)dU$ of the ensemble grains will have an electron in traps between U and $U+dU$. The survival function is then:

$$F(t,\gamma)=\int_0^\infty n(U,t,\gamma)dU. \tag{12}$$

TABLE I. Dependence of l.i.f. slope on grain size (experimental).

Ref.	Emulsion	Sensit.	Speed	Average grain size in μ^2	l.i.f. slope x	Radiation
[1]	*I*	pan	high	0.57	0.65	4360Å
[1]	*II*	blue	high	?	0.5	4360Å
[1]	*III*	blue	med.	?	0.23	4360Å
[2]	*I*	blue	high	0.7	0.32	4360Å
[2]	*II*	blue	high	0.7	0.25	4360Å
[2]	*III*	pan	high	0.5	1.0	4360Å
[2]	*IV*	blue	low	0.1	0.15	4360Å

[1] J. H. Webb, J. Opt. Soc. Am. **25**, 4 (1935).
[2] J. H. Webb, J. Opt. Soc. Am. **23**, 159 (1933).

We have the initial condition:

$$n(U, 0, \gamma) = m(U). \tag{13}$$

Traps of depth U may loose electrons by ejection or may gain some that were ejected from other traps. This is expressed by:

$$\frac{dn(U, t, \gamma)}{dt} = -\lambda(U)n(U, t, \gamma) + \sigma m(U)\int_0^\infty n(U', t, \gamma)\lambda(U')dU'. \tag{14}$$

A general solution for n, hence F, in terms of the trap distribution m is not available. We will discuss five cases.

Case A: All traps have the same depth U_0; γ arbitrary.

The rigorous solution is:

$$F(t, \gamma) = \exp(-\lambda_0 \gamma t). \tag{15a}$$

Case B: U has a finite number of values U_i. The deepest traps U_m differ from the rest by more than kT or 0.025 ev; γ arbitrary.

The rigorous solution for F is a sum of exponential terms. A short time after the start only one term with $\lambda(U_m) = \Lambda$ in the exponent is of importance:

$$F(t, \gamma) = c' \exp(-\Lambda \gamma c t) \tag{15b}$$

where c and c' are of the order of magnitude 1.

Case C: Arbitrary trap distribution $m(U)$; $\gamma = 1$; $(\sigma = 0)$.

The rigorous solution is:

$$F(t, 1) = \int_0^\infty m(U) \exp(-\lambda(U) \cdot t) dU. \tag{15c}$$

If (10) is used for m this becomes for $\lambda_0 t > 1$:

$$\text{For } \lambda_0 t \leqslant 1: \quad \left.\begin{aligned} F(t, 1) &\approx (\lambda_0 t)^{-x}\Gamma(1+x) \approx (\lambda_0 t)^{-x} \\ F(t, 1) &= 1 - (\lambda_0 t)/(1+x) + \cdots \end{aligned}\right\} \tag{16c}$$

where λ_0 refers to U_0 (see Fig. 2) and $x = kT/\epsilon$. Note that $F(t)$ has here the form (9a).

Case D: Arbitrary $m(U)$; $\gamma = 1 - \sigma$.

No rigorous solution is available, but we can develop n, hence F, in a power series in σ:

$$F(t, 1-\sigma) = F(t, 1) + G(t) \cdot \sigma + H(t) \cdot \sigma^2 + \cdots \tag{15d}$$

Here the p^{th} coefficient can be related through (14) to the $(p-1)^{st}$ one. The series appears to converge reasonably rapidly. For the distribution (10), excluding very small t, one may show:

$$G(t) \approx g \cdot F(t, 1) \quad (g \lesssim 3) \tag{16d}$$

and $H(t) \ll G(t)$. The principal feature of F, its proportionality to t^{-x}, remains practically undisturbed for a large range of γ-values. However, if $\gamma \to 0$ (case E) the present approximation ceases to be a good one.

Case E: Arbitrary $m(U)$; $\gamma \to 0$.

For $\gamma \to 0$ the following reasoning indicates the form of the solution. After a short time during which practically no electrons died, an equilibrium distribution will be reached over the traps. This distribution decays adiabatically, remaining in equilibrium all the time. Under these conditions (14) yields for F in first approximation:

$$F(t, \gamma \to 0) = \exp(-\bar{\lambda}\gamma t) \tag{15e}$$

with:

$$1/\bar{\lambda} = \int_0^\infty m(U)/\lambda(U) dU. \tag{16e}$$

For a closer approximation we tried:

$$F(t, \gamma) = \exp(-\bar{\lambda}\gamma t) + \gamma F_1(t) + \gamma^2 F_2(t) \cdots$$

in (14). One finds $F_1 \equiv 0$. For the distribution (10) it can be shown that for large t the leading term in F_2 is $\sim t^{-kT/\epsilon}$.

From the analysis of these cases the following conclusions can be drawn for the l.i.f. curve. A small number of trap depths leads invariably to a slope 1 for low intensities according to section 7. This is not in agreement with experiment so that we are driven to the acceptance of a quasi continuous distribution of trap depths. Also in that case extremely small γ values still lead to a slope 1. However, for intermediate and high γ values and the distribution (10) the analysis proves that a survival function (9a) as required by experiment results. The slope is then kT/ϵ, according to (16c, d). The fact that this slope does not depend on the value of γ within a wide range lends credence to the theory. We have no way of measuring γ accurately and no theoretical means of estimating it. The theory in this form agrees with experiment. In the next sections further consequences will support this conclusion.

We terminate this section with a few remarks about the value of kT/ϵ. Formula (10) has a high energy tail that is certainly incorrect. No levels can be expected for energies $U > U_m$, defined by:

$$\int_{U_m}^\infty m(U) dU = 1/M$$

or:

$$U_m - U_0 = \epsilon \ln M \tag{17}$$

where M is the total number of traps per grain. Now the most relevant traps for the l.i.f. are the deepest ones which keep the electrons trapped during the longest times. This may formally be seen from (16e). If the upper limit of integration would be ∞, $\bar{\lambda}$ would diverge. With U_m as an upper limit we obtain:

$$\bar{\lambda} \approx (\epsilon/kT - 1)C \exp(-U_m/kT) \approx \lambda(U_m). \tag{18}$$

The ripening and manufacture of a plate apparently is conducted in such a manner that the maximum trap

depth is not too great, which would cause fog. This limit seems to correspond to $\bar{\lambda}\sim 100$ at room temperature. Using this with (17), (18), $C=3.10^{14}$ and $U_0 \ll U_m$ (see Fig. 2) we obtain for the l.i.f. slope:

$$kT/\epsilon = (\ln M)/29 \qquad (19)$$

General solid state evidence suggests that the relative number of imperfections in a photographic grain may be $\sim 10^{-5}$. For an average grain with 10^{10} ion pairs this means $M\sim 10^5$. Hence, with (19): $kT/\epsilon = 0.40$, which agrees well with average slopes observed. Moreover, (19) indicates why larger grains have steeper slopes (see Table II). The relative amount of imperfection is seen to be not a critical parameter. The qualitative agreement between this table and the experimental data of Table I is as good as may be expected.

9. THE TEMPERATURE DEPENDENCE

The influence of the temperature on the l.i.f. consists of a change of the slope and a shift of the line as a whole:

(a) The change of slope. For $\gamma \to 0$ the slope should be=1, independent of temperature. For intermediate and high γ-values and the distribution (10) the slope was kT/ϵ, according to (16c, d), so that a weak dependence on temperature is expected. The author is not aware of sufficiently accurate data, extending to low enough intensities, permitting a check of this temperature dependence. Such experiments would involve extremely long exposure times because the r.l.f. curves shift as a whole to the low intensity side for lower temperatures. The best data available are those by Webb.[8] Taking their accuracy into account, they are not in disagreement with any weak slope dependence.

(b) The shift of the curve as a whole. Two isodense points with equal values of $E-E_0$ but different T must have the same $W(I)$ according to (4). A pair of such points on neighboring r.l.f. curves will have a difference $\Delta \ln I$ such that:

$$\Delta \ln W = \partial \ln W/\partial \ln I \cdot \Delta \ln I + \partial \ln W/\partial \ln(1/kT)\cdot \Delta(1/kT) = 0.$$

Using (6), (9), (9a), (11) and (16c) we obtain:

$$-\Delta \ln I/\Delta(1/kT) = U_e + kT(\ln \lambda_e i_0 + \ln I_0/I). \qquad (20)$$

If we compare data at an intensity $I=I_0/100$ and use (11a) the right hand side of (20) becomes $=U_e+0.1$ ev. This result is accurate to the extent to which $\lambda_e i_0 = 1$. This is only an order of magnitude relation, so the product may be off by a factor of say 10, but this affects the result only by 0.05 ev. So we see that the temperature shift of the r.l.f. yields a reasonably accurate measure of the effective trap depth U_e. For $\gamma \to 0$ the result turns out to be very similar. In comparing (20) with experiment one precaution must be observed. The optimal exposures are also slightly temperature dependent. This means that only a temperature dependent fraction of the intensity is photo effective.* In order to correct for this effect the r.l.f. curves should be moved as a whole in the direction of lines of constant exposure times, that is in the usual representation towards north-east, until all optimal exposures are equal. If this is done the proportionality between $\Delta \log I$ and ΔT appears satisfactorily. Table III shows results derived from Webb's quoted paper.[8] Comparing Table III with formula (20) we conclude that $U_e = 0.74 - 0.1 = 0.64$ ev. This value is less than the energy of the Herschel effect (1–1.4 ev.) as it should be and is in reasonable agreement with the value of 0.7 ev. estimated in section 8. It suggests that low intensity latent image formation should be greatly slowed down by simultaneous infra-red radiation of wave-length $\sim 2\mu$.

10. TRIQUANTIC AND HIGHER ORDER PROCESSES

In section 6 we postulated that a monoatomic speck is unstable but a diatomic one is stable. Let us investigate briefly the consequences of a theory in which diatomic specks are also unstable but triatomic specks are stable. By arguments similar to those traced out for two quantic processes the equation for the r.l.f. curve

TABLE II. Dependence of l.i.f. slope on grain size (theoretical).

Grains	Ion pairs per grain	l.i.f. slope according to (19) assuming a rel. concentration of imperfections of: 10^{-5}	10^{-6}
small	$10^{7.5}$	0.20	0.12
medium	10^{9}	0.31	0.24
large	$10^{10.5}$	0.43	0.34

TABLE III. The shift of l.i.f. curves with temperature.

Emulsion	Radiation Å	Temperatures °C	Observed $-\Delta \ln I/\Delta(1/kT)$ in ev.
I	4360	0–50	0.72
II	4360	0–50	0.71
III	4360	0–50	0.77
I	3650	0–50	0.78
I	5460	0–50	0.73
			0.74 = average
I	4360	−10–00	0.82
I	4360	0–20	0.77
I	4360	20–50	0.62

[8] J. H. Webb, J. Opt. Soc. Am. **25**, 4 (1935).

* The cause of this dependence may be as follows: An absorbed quantum first excites an electron and this exciton has a certain probability of dissociating into a free conduction electron and a hole. The probability of dissociation is slightly dependent on temperature, as is known from measurements on photo-conductivity.

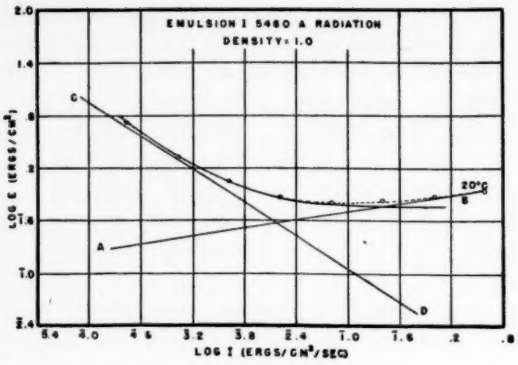

FIG. 3. Theoretical l.i.f. curve (full drawn) adapted to Webb's data (dashed curve and points) and straight line components proposed by Webb.

is again of the form $W\cdot(E-E_0)=$constant, where now:

$$W=C/(\bar{i})^2\cdot\int_0^\infty F_1(t)\exp(-t/\bar{i})dt \cdot\int_0^\infty F_2(t)\exp(-t/\bar{i})dt. \quad (21)$$

The result then depends again on the assumptions regarding the functions F, which now have the meaning: $F_1=$the survival chance of one electron till the second one arrives, $F_2=$the survival chance of two electrons till the third one arrives. If exponentials are taken for these functions, the l.i.f. slope becomes 2. If we assume that one silver atom is very unstable, two silver atoms are metastable and three atoms are practically completely stable, F_2 has a greater time constant than F_1. If the activation energy of a monoatomic speck is about 0.7 ev. as before, the activation energy of a diatomic speck must lie somewhere between 0.7 and 1–1.4 ev., the latter being the energy of the Herschel quanta, needed for the dissociation of completely stable latent image specks. A value of 0.9 ev. seems appropriate for the potential depth of a diatomic speck. The dissociation of a diatomic speck would then be slower by a factor of the order 10^4 than for a monoatomic speck. This simple reasoning suggests, that for intensities, corresponding to interquantic times $t_0<\bar{t}<10^4t_0$ the r.l.f. curve is still determined only by the two-quantic process of the instability of monoatomic specks. Slopes greater than 1 are not to be expected in this intensity region. For intensities $\sim10^4$ times lower than the optimum one might observe a kink in the r.l.f. curve towards a steeper slope. This slope should be less than 2 if it corresponds to stable triatomic silver specks. For still lower intensities again a kink may occur, toward a still higher slope corresponding to tetratomic specks, the triatomic ones now being unstable for such tremendouly long interquantic times.

The exposure times required to observe the first mentioned kink may be of the order of 10^6 seconds or several days, which is feasible. For the second kink they would be of the order of at least 10^9 seconds which is beyond the experimental range. In trying to verify the predicted behaviour at intensities near and below the first kink the present theory encounters some difficulty. A few experimental data are available down to very low intensities, for instance those of Arens and Eggert[9] and a kink is then observed. However, the slope of the r.l.f. curve there becomes infinite. The present author is inclined to interpret this too steep upturn as a spurious effect, masking the true kink that would lie at a slightly lower intensity. Namely, no survival function F of the time only exists, which, when used in (6) will cause the observed upturn towards a vertical asymptote, neither is there a pair for (21). Since (6) was based only on very general features of the picture of Webb, Gurney, and Mott, this discrepancy means that either the explanation of the l.i.f. is basically wrong or that spurious effects veil the true situation in this particular case.** In view of the agreement of the theory with experiment in so many details it seems reasonable to ascribe the too steep upturn to an unaccounted complication and to withhold conclusions in this region of extremely low intensities until more data are available. With this restriction we may conclude from the evidence presented that the l.i.f. can be described by one survival function and stable diatomic Ag specks.

11. THE TRANSITION TO THE REGION OF OPTIMAL INTENSITIES

According to the present theory the r.l.f. curve as it comes down from the region of low intensities, should bend towards horizontal in the region of optimal intensities. This should be so even if the high intensity failure would be absent, because there must be a minimum number of quanta to produce a developable speck. Most experimental curves soon bend upward owing to the high intensity r.l.f. It is not yet possible to predict how much the high intensity effect makes itself felt at intensities slightly below the optimum, but the following estimate shows that its influence vanishes rapidly with decreasing intensities. Suppose the first electron needs on the average a neutralization time τ before a second electron can be admitted to the same speck. If the average interquantic time used is $\bar{i}$ then, according to (5), the chance that another electron will be produced before τ is $\sim\tau/\bar{i}$ for low intensities (high values of $\bar{i}$).

The number of rejections is thus $\sim1/\bar{i}$ or $\sim I$, so we may expect that the loss in efficiency is also $\sim I$ and

[9] H. Arens and J. Eggert, Zeits. f. Wiss. Phot. **27**, 79 (1929-30).

** Possibly such a spurious effect may be caused by a back reaction of the following kind. The experiments were done with non-monochromatic light. As the efficiency of the active light decreases with lower intensity, the destruction of the Ag specks by radiation of 2μ, whose efficiency is not reduced, might have become predominant. Destruction of the sub-latent image by a radiation component would make $F(t)$ in (6) dependent on the intensity I. Functions $F(t, I)$ causing the observed vertical upturn do exist.

hence the number of extra electrons needed to reach the same probability of developability is also $\sim I$. This approximation is only valid if we may neglect the chance that more than one electron will arrive in τ. Therefore, the fact that for intensities above optimal the effect appears to go more slowly than $\sim I$ is not in contradiction with the proportionality to I at lower intensities. From this estimate we may conclude that the high intensity component vanishes rapidly below the optimum which justifies neglecting it there.

The bending towards the horizontal will then be assumed to follow formula (9), i.e., $W(I) \sim I^x$. This implies that for $E-E_0$ the approach to the horizontal in the conventional $e(i)$ plots is exponentially.

Previous empirical formulas describe the r.l.f. curve in the neighborhood of the optimum by a sum of two exponentials.[8] Hence the present theoretical formula will do well anywhere below the optimum. Checks have been carried out in a number of arbitrary examples and proved to be completely satisfactory. A typical example is given, Fig. 3, representing observations by Webb.[8] The points are the same ones that were used by Webb for his analysis of the curve into two straight components (p. 17, Fig. 12).*** The fully drawn curve represents formula (9) with $x=0.800$; $E_0=0.552$ and the constant $=6.91 \cdot 10^{-3}$, chosen in order to give the best fit. It is evident from this and similar examples that the factor $E-E_0$ in (9) gives a very good description of the course of the l.i.f. right up to the optimum.

In addition the following factors may be of slight influence on the form of the curves:

(a) In the derivation of formula (6) E was assumed to be a constant for a given exposure time and intensity. However, E will also fluctuate, although much less than the individual interquantic times. A certain average is represented by the experimental curve, which, in general, will not be exactly the same as a curve belonging to a non-fluctuating average value of E. However, because of the weak curvature of the r.l.f. curve this approximation causes only a negligible error.

(b) Non-uniform light intensity throughout the emulsion and a spread in grain size will cause systematic deviations from the order principle and minute distortions of the r.l.f. curve. They will be treated in Section 12.

(c) It might seem as if the adoption of (9) for the region near the optimum implies the arbitrary assumption that $W(I)$ remains proportional to I.*** This may seem too simple. However, the good agreement between theory and experiment regarding the approach to the optimal point comes essentially from the factor $E-E_0$ and is very insensitive to the particular choice of $W(I)$. For this reason it seems justified to choose a mathematically simple form for $W(I)$, like (9). For very low intensities where $E-E_0$ is a large fraction of E, this approximation approaches a straight line that can be given the correct slope and the correct first-order deviation from a straight line. For high intensities it can be given a horizontal asymptote at the correct height. In this manner, by adapting x, E_0 and the constant an excellent fit to experimental data can always be obtained. For higher intensities $E-E_0$ is only a small fraction of E so that the experimental error in E corresponds to a large uncertainty in $E-E_0$. Hence any reasonable approximation for $W(I)$ is satisfactory in this region.

*** A purely empirical method of analysis for the entire r.l.f. curve, assuming it to be equal to the sum of two straight lines, was suggested by Webb in 1935 (see reference 8). This method, besides lacking theoretical background, is open to the following fundamental criticism. The two processes represented by the two straight lines could either operate in parallel or in series. In parallel this would mean that a small fraction of the developable grains is produced at very low intensities with an abnormally high efficiency. If they are in series, it would mean that the partial process of either one occurs at abnormal efficiencies, either at very low or at very high intensities. It is true that the Gurney-Mott picture was not yet available when the straight line analysis was proposed.

12. THE INFLUENCE OF DEVIATIONS FROM THE ORDER PRINCIPLE

Let us see what corrections must be applied to our previous statements because of deviations from the o.p. in normal r.l.f. experiments. These corrections will also be useful in subsequent papers.

In order to discuss the matter from a general standpoint we assume that the grains can be divided into groups, indicated by a parameter α (if necessary α may stand for several parameters), such that in each group the o.p. holds. The validity of the o.p. in each group does not imply its validity for the whole plate (see section 4.d). The main corrections arise from the variation of light intensity throughout the emulsion-depth, and the spread in grain size. In both cases the grains can be divided into such groups. If the plate receives an exposure E with intensity I, each group will give rise to a partial density $D(\alpha, e, i)d\alpha$ and since densities are known to be additive, the total density is:

$$D=\int D(\alpha, e, i)d\alpha.$$

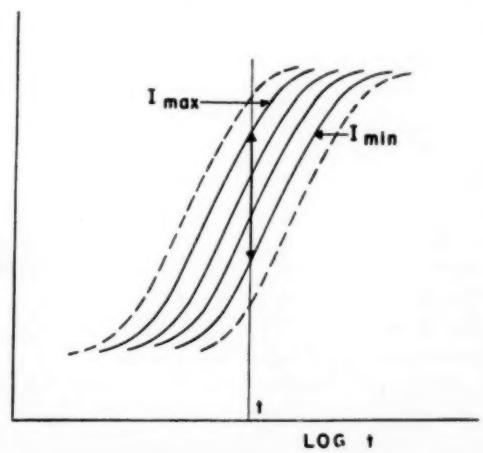

FIG. 4. Illustrating the conditions that γ_α be constant.

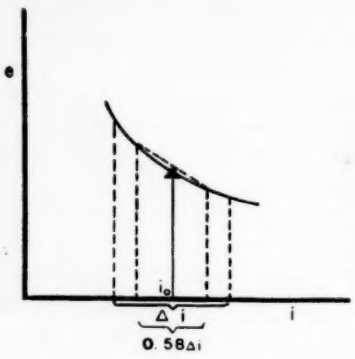

FIG. 5. The influence of non-homogeneous light intensity on the shape of the l.i.f. curve. According to formula (23) the ordinate at i_0 is displaced to the center of the chord subtending $0.58\ \Delta i = \Delta i/\sqrt{3}$.

We wish to find how the shape of total isodense r.l.f. curves compares with the shapes of isodense r.l.f. curves of the various α groups. For this purpose we vary e and i, keeping D constant. We abbreviate as in (2):

$$\partial D(\alpha, e, i)/\partial e = \gamma_\alpha$$

and observe:

$$\int \gamma_\alpha d\alpha = \gamma.$$

Setting $\delta D = 0$, we have with (1):

$$(\delta e/\delta i)_D = 1/\gamma \cdot \int \gamma_\alpha (\delta e/\delta i)_{D(\alpha)} d\alpha. \qquad (22)$$

In words: The observed r.l.f. slope is a certain average of the slopes of the groups. In particular, if all groups have the same slope for a certain value of i, the total r.l.f. has there the same slope.

We shall apply this first to the variation of light intensity with depth. Let α stand for the depth in the emulsion. The following assumptions are made:

(a) All grains are of equal size and the undeveloped grains are homogeneously distributed throughout the depth of the emulsion.
(b) γ_α is independent of α.
(c) The light intensity falls exponentially with the depth α, hence i is linear with α.

Assumption (b) is illustrated in Fig. 4, representing schematically a set of characteristic curves for a single layer with slope γ_α. For an exposure on a thick emulsion the densities to be added lie on a straight vertical segment, corresponding to the exposure time used, and to the intensity range that is present in the plate from front to back. γ_α will be constant through out the emulsion provided the partial density $D(\alpha)$ lies for the whole plate in the straight range of the corresponding curves and the intensity range through the plate does not cover too large an interval, which is usually true for curves referring to a total density of the order 1.

With these assumptions (22) yields by straightforward calculation the following results:

In first approximation the r.l.f. curve for the real (inhomogeneous) exposure is the same as that for an ideal (homogeneous) exposure on the same plate, provided the coordinates e and i are interpreted as the values at the center (half-depth) of the plate. Since usually the plots are made with those variables referring to incident values the curve should be shifted horizontally and vertically over a distance $\log I(\text{center})/I(\text{incident})$.

In second and third approximations the form of the real curve is slightly changed as compared to the ideal one. Straight parts remain straight with the same slope, but curved parts are smoothed out a little. To find the point on the experimental curve with abscissa i, one has to take the average of the ordinates of the two points on the ideal curve with abscissae $i \pm \Delta i/2\sqrt{3} = i \pm 0.29\ \Delta i$, where Δi is the log light range from the front to the back of the plate. With i and e again referring to the half-depth we have:

$$e(i)_{\text{real}} = \tfrac{1}{2}(e(i+0.29\Delta i) + e(i-0.29\Delta i))_{\text{ideal}}, \qquad (23)$$

if differences of the order $(\Delta i)^4$ and higher are neglected.

For a light range of a factor 10 from front to back, or $\Delta i = 1$, as is often the case in practice, the curve for the actual plate should be obtained from the curve for homogeneous light intensity by averaging the values at $i \pm 0.3$. Inspection of actual r.l.f. curves (see e.g. Fig. 3) shows that this correction of the shape is negligible.

We shall next apply (22) to the case of inhomogeneous grain size. Let α represent the effective projective area of the grain. The following assumptions are made:

(a) All grains are exposed to the same intensity.
(b) $\gamma_\alpha d\alpha$ is proportional to the saturation density of the size group α, hence to the number of grains $N(\alpha)d\alpha$ in this group times the area of the grains α: $\gamma_\alpha = cN(\alpha)\alpha$.
(c) The plot of $0.43N(\alpha)\cdot\alpha^2$ (that is the total area of grains between $\log\alpha$ and $\log\alpha + d\log\alpha$) *versus* $\log\alpha$ has a maximum for a certain grain size $\alpha = \alpha_0$ and is symmetrical about this maximum. This is the case in most actual emulsions.
(d) $(\partial\epsilon/\partial i)_{\log\alpha} = (\partial e/\partial i)_{\log\alpha_0} + f(i)\cdot(\log\alpha - \log\alpha_0)$, where $f(i)$ is a small coefficient dependent on i, which is justified by the weak dependence on α discussed in section 7.

With these assumptions (22) yields by straightforward calculations the following results:

In first approximation the r.l.f. curve for the real emulsion is the same as that for an ideal plate containing only grains of class α_0, with the same total projective area.

In second and third approximations the r.l.f. curve differs slightly in form from that for the ideal α_0 plate. Straight parts remain straight with the same slope, but curves are smoothed out a little. To find the point with abscissa i for the real plate one has to take the average of the ordinates of the two points on the α_0-curve with abscissae $i \pm \{\langle(\Delta\log\alpha)^2\rangle_{Av}\}^{\frac{1}{2}}$:

$$e(i)_{\text{real}} = \tfrac{1}{2}[e(i+\langle(\Delta\log\alpha)^2\rangle_{Av}^{\frac{1}{2}}) + e(i-\langle(\Delta\log\alpha)^2\rangle_{Av}^{\frac{1}{2}})]_{\alpha_0} \qquad (24)$$

with:

$$\langle(\Delta\log\alpha)^2\rangle_{Av} \equiv \int (\Delta\log\alpha)^2 N(\alpha)\alpha d\alpha \Big/ \int N(\alpha)\alpha d\alpha.$$

Differences of the order $\langle(\Delta \log a)^4\rangle_{Av}$ or higher are neglected.

For many emulsions the function $N(a)$ is known and permits the calculation of $\langle(\Delta \log a)^2\rangle_{Av}$. For most commercial emulsions this quantity turns out to be ~ 0.4. Inspection of r.l.f. curves shows that the error caused by neglecting this second order correction is negligible. In the worst cases at the most curved parts of the r.l.f. curve it amounts to less than 5 percent of exposure. Although the correction is insignificant for the shape of the r.l.f. curve it becomes important for the intermittency effect (see paper III) when small differences in r.l.f. are the object of the theory.

Summarizing we have found that the two main causes for deviations from the o.p., namely inhomogeneous light intensity and grain size, cause the real r.l.f. curve to be practically identical with the ideal r.l.f. curve that would be obtained if the light intensity would be homogeneous and equal to the value at the center of the plate, and if the plate contained only grains of size a_0, defined above.

Finally we wish to point out that it is not consistent with the observed behaviour of characteristic curves for various intensities, to explain the slope $0<x<1$ of the r.l.f. curves as the result of two groups of grains, the first group having a slope 0 (no r.l.f.) and the second group having a slope $=1$ (one trap depth only), in the intensity region studied. If the o.p. would hold within each one of these two groups the resulting slope would lie indeed between 0 and 1 according to (22), but the characteristic curves for low intensities behave experimentally in a way that contradicts such an assumption. For this reason the scheme with many trap depths had to be introduced.

Note added in proof: The author is greatly indebted to Dr. J. H. Webb for bringing to his attention a series of recent studies by P. C. Burton and W. F. Berg (Phot. J. **86B**, 2, 62 (1946) and **88B**, 13, 84, 123 (1948)) which provide strong support for the assumptions made in Sections 6 and 11.

THE JOURNAL OF CHEMICAL PHYSICS VOLUME 17, NUMBER 11 NOVEMBER, 1949

Dielectric Behavior of Solutions of Electrolytes in Solvents of Low Dielectric Constant. V. The Influence of Temperature and Concentration on Dielectric Properties*

H. A. STROBEL** AND R. H. COLE
Metcalf Research Laboratory, Brown University, Providence, Rhode Island
(Received April 22, 1949)

Dielectric loss and conductance data for octadecyltributylammonium thiocyanate in benzene show large changes in the significant frequency region of absorption and in the magnitude of conductance when the temperature is lowered from 25° to 6°C, but their variation with concentration is very similar at the two temperatures. The broad frequency range of absorption observed at concentrations in the range 0.008–0.02 molal and the failure of the change in macroscopic viscosity to account for the temperature effect suggest that a better understanding of similar systems requires more detailed examination of the interaction of the ionic and dipolar aggregates with the solvent.

OF the several approaches employed in this laboratory in the investigation of the behavior of electrolytes in solvents of low dielectric constant, the measurement of dielectric absorption by a calorimetric method has been among the most revealing. In the earlier papers of this series the information obtained from such measurements has been used, in conjunction with conductance, cryoscopic, and polarization data, to demonstrate the strong dependence of the nature and extent of ion association on the constitution and type of electrolyte.[1,2]

An investigation of the temperature dependence of the dielectric absorption of such systems in the 5–25°C range has formed the basis of the present work. The study was prompted principally by the continued need for new approaches to the complex picture presented by the known results. The available data have been used as well, insofar as seemed justified, in examining the role of concentration as an influence on association. A further result of the work has been the possibility of direct intercomparison of cryoscopic and absorption data.

For the study, octadecyltributylammonium thiocyanate, a fairly strong electrolyte representative of the quaternary ammonium salts already examined[3] was selected. Benzene solutions of that salt have now been investigated at several concentrations both at 25° and at about 6°. Audiofrequency conductance determina-

* This work was supported by a grant from the Research Corporation.

** Present address: Dept. of Chemistry, Duke University, Durham, North Carolina.

[1] (a) Sharbaugh, Schmelzer, Eckstrom, and Kraus, J. Chem. Phys. **15**, 47 (1947); (b) Sharbaugh, Eckstrom, and Kraus, J. Chem. Phys. **15**, 54 (1947).

[2] H. A. Strobel and H. C. Eckstrom, J. Chem. Phys. **16**, 817 (1948).

[3] With the exception of the picrates, all of the strong quaternary ammonium electrolyte already examined at 25° have behaved similarly.

TABLE I. Data measured and calculated for all the solutions investigated.*

Molality $m\times10^2$	Dielectric constant ϵ_0	Loss factor maximum $\Delta\epsilon''_{max}$	α_{expt}	Critical frequency ν_c(Mc)	"Average particle radius" $a(A)$	Dipole moment $\mu(D)$
Data for Octadecyltributylammonium thiocyanate						
0.850	2.300	0.0053	0.40	120	9	3.8
	*2.325***	*0.0039*	*0.32*	*45*	*11*	*2.8*
1.261	2.326	0.0094	0.45	27	15	4.4
	*2.342***	*0.0081*	*0.32*	*10.7*	*18*	*3.3*
1.59	2.370	0.0162	0.45	12.0	19	5.0
	2.386	*0.0144*	*0.40*	*5.2*	*22*	*4.6*
1.73	2.376	0.0204	0.41	9.6	20	5.1
2.04	2.454	0.0368	0.39	4.8	25	6.2
	2.473	*0.0345*	*0.40*	*2.0*	*30*	*5.8*
Data for Tri-*iso*amylammonium picrate						
11.08	3.93	—	0.0	490	4.8	10.4
10.85	*4.03*	—	*0.0*	*275*	*5.3*	*8.9*

* All data taken at 25° *except those in italics* which were taken at 6°.
** Estimated quantities.

tion at 5.3° have provided further information. In addition a 0.1 molal solution of a weak electrolyte, tri-*iso*amylammonium picrate, was studied at low temperatures.

EXPERIMENTAL

Materials

The benzene used was obtained thiophene-free and purified as described in previous papers of this series.[1] Some of the tri*iso*amylammonium picrate prepared by Copenhafer[4] was still on hand and was used after a further recrystallization from ethyl alcohol; M.P., 127.5–128.5° (corr.). Octadecyltri-*n*-butylammonium thiocyanate was made and recrystallized according to the method outlined in an earlier paper.[2]

Method and Equipment

The calorimetric dielectric absorption apparatus used in these determinations has already been described. As indicated in Part III of this series, RCA 9005 diodes now serve in place of the original custom-made voltmeter tubes.[5]

In order to work at temperatures as low as 6° several changes were made in the temperature-controlling system. As before, the temperature of the air bath, containing the calorimetric cell bulb and associated components, was maintained by a flow of constant temperature water supplied by a large reservoir. The flow was increased for this and succeeding work, and the lines between the air-bath jacket and reservoir were reinsulated and shortened. To maintain the water reservoir at temperatures below 15°, ice water was forced from an auxiliary, well-insulated bath through the cooling coils of the thermostating system; no difficulty was experienced in holding the water reservoir constant to within 0.002° for 10–15 hours at a time. With this arrangement the air bath could be held as low as 6° with a variation of no more than 0.02° during a period of several hours, depending on changes in room temperature, etc.

For work below 25° the air bath was always flushed with dry air for a few minutes before and during the cooling process to avoid any condensation of moisture. The possible introduction of moist air during a run was minimized by the tight fit of the air bath and cover. In order to have the upper solution level visible within the capillary of the calorimetric cell during low temperature determinations, small amounts of solution were added to the cell during the cooling period to offset the normal contraction. Additional solution was introduced into the flared open end of the capillary by means of a transfer pipet of small diameter. While the meniscus remained in the capillary stem, the "vapor" bulb attached to the open end of the stem kept evaporation to a minimum.[1a] On low temperature runs re-

TABLE II. Conductance of octadecyltributylammonium thiocyanate in benzene at 25.00±0.01°C.*

Molality $m\times10^2$	χ_0 ohm^{-1} cm^{-1}	Molarity $c\times10^2$	$\Lambda\times10^3$
40.18	2.498×10^{-5}	29.41	84.9
25.03	1.258×10^{-5}	19.51	64.5
13.04	5.219×10^{-6}	10.72	48.7
9.57	3.352×10^{-6}	7.99	41.97
6.21	1.591×10^{-6}	5.27	30.21
3.800	4.89×10^{-7}	3.259	15.01
2.249	9.28×10^{-8}	1.943	4.78
2.045**	7.00×10^{-8}	1.769	3.953
1.733**	4.103×10^{-8}	1.500	2.738
1.604	3.462×10^{-8}	1.390	2.491
1.259**	1.865×10^{-8}	1.093	1.706
0.934	9.74×10^{-9}	0.812	1.200
0.853**	8.12×10^{-9}	0.742	1.094
0.726	5.90×10^{-9}	0.631	0.934
0.442	2.437×10^{-9}	0.3848	0.633
0.2033	7.17×10^{-10}	0.1772	0.4046

* The data for this table are taken from H. S. Young, thesis, Brown University (1948) with the exception of those for the asterisked (**) concentrations, which are from the work of the present authors. χ_0 and Λ are the specific conductance and the equivalent conductance respectively.

TABLE III. Conductance of octadecyltributylammonium thiocyanate in benzene at 5.25±0.07°C.

Molality $m\times10^2$	χ_0 ohm^{-1} cm^{-1}	Molarity $c\times10^2$	$\Lambda\times10^3$
13.48	2.88×10^{-6}	11.32	25.5
8.39	1.475×10^{-6}	7.21	20.46
5.77	7.62×10^{-7}	5.02	15.18
3.63	1.837×10^{-7}	2.96	6.21
2.50	6.51×10^{-8}	2.210	2.95
1.171	6.94×10^{-9}	1.040	0.667
0.769	2.77×10^{-9}	0.685	0.405
0.339	6.32×10^{-10}	0.303	0.2098
0.1065	1.100×10^{-10}	0.0951	0.1156
0.0468	3.84×10^{-11}	0.0418	0.0918
0.0223	1.12×10^{-11}	0.0199	0.0561

[4] D. T. Copenhafer, thesis, Brown University (1942).

[5] It was not mentioned in that paper, but the change in tubes made possible a considerable shortening of the leads between the electrodes of the calorimetric cell and the diode plates. The inductance of the measuring circuit was thus decreased and the accuracy of the determination of the voltage across the cell at high frequencies increased.

quiring two days, however, a little solvent was lost overnight as the bath warmed. The resulting change in concentration (estimated to be ≤ 1.0 percent) was found to have a negligible effect on the results as long as the change in conductance was taken into account. It was possible to find the new conductance by restandardization of the cell for that solution by calorimetric measurements at 60 cycles per second.[1,2]

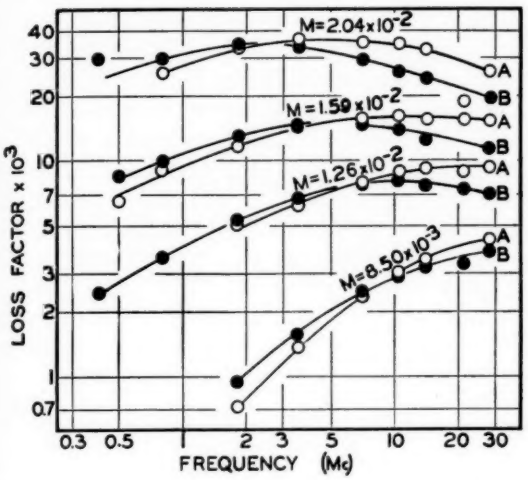

FIG. 1. Loss factor as a function of concentration, frequency, and temperature. Curves: A, $t=25°$; B, $t=6°$ (at molalities given above).

In practice, a given solution was run first at 25° and then at the lower temperature to avoid unnecessary handling. In the calorimetric method of loss measurement, the rate of rise of fluid in the cell capillary is compared at radio frequency and at an audio frequency for which the solution conductance is known. Ideally this comparison should be made under otherwise identical conditions, but in the present work it was found most convenient to make all of the audiofrequency calibrations at 25°. The principal error in this procedure should be proportional to the variation in the product cd/γ (where c is the specific heat, d the density, and γ the thermal expansion coefficient of the solutions[1a]) and is estimated to be of negligible importance in the present work. With the approximation, the specific conductivity χ_ω at any radian frequency ω can be computed from the relation $\chi_\omega=\chi_0(V_0^2t_0/V_\omega^2t_\omega)=A/V_\omega^2t_\omega$. In this expression, V is the voltage across the cell, t the time of rise through a standard capillary interval, and the subscripts 0 and ω refer to audio and radio frequency, respectively. The heating constant A and its determination have been discussed elsewhere,[2] as have calculations based on Debye's relaxation theory and empirical modifications of it.

The audiofrequency conductances reported were measured by the substitution method on a special bridge built around the Campbell-Shackelton shielded ratio box by Leeds and Northrup. The conductance cells used were periodically cleaned with fuming nitric acid, baked at 140° overnight, and cooled while being flushed with dry air. Both conductance series were initiated with the most concentrated solution, and successively less concentrated solutions were obtained by a dilution method.[6] For the measurements at 25° the conductance cells were placed in an air bath, and observations were made when temperature equilibrium was established.

For the work at about 5° the regular conductance cell cap was replaced by one that was open to the atmosphere through a stopcock and a drying tube. A fairly constant (±0.07°) temperature was secured for those measurements by immersing the cell directly in a benzene-benzene ice bath that was stirred vigorously. Before each dilution and the accompanying weighings, the cell was removed and allowed to come to room temperature.

RESULTS

In Table I are collected the results determined experimentally and the constants calculated for these solutions at 25° and at 6°. For convenience the dielectric constants previously determined at 25° for two of these solutions have been included with the new measurements. Benzene was the solvent in all cases.

The frequency dependence of the dielectric loss factors $\Delta\epsilon''$ has, in this work as before, been found in disagreement with the assumption of a single relaxation process. The results are fitted quite accurately however, by the relation of Cole and Cole[7]

$$\Delta\epsilon''=\tfrac{1}{2}(\epsilon_0-\epsilon_\infty)\cos\tfrac{1}{2}\alpha\pi/[\cosh(1-\alpha)x+\sin\tfrac{1}{2}\alpha\pi] \quad (1)$$

based on an empirical relaxation function. In this equation α is an additional parameter to which suitable values must be given, $\Delta\epsilon''$ is the imaginary part of the complex dielectric constant, ϵ_0 and ϵ_∞ are the limiting

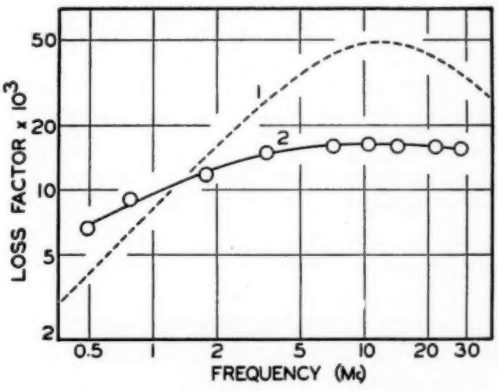

FIG. 2. Loss factor as a function of frequency for $1.6/10^{-2}$ molal benzene solution at 25°. Curves: 1. Loss factor calculated for this system if a single relaxation time assumed. 2. Experimental loss factor.

[6] The method used is essentially that outlined in Mead, Fuoss, and Kraus, Trans. Faraday Soc. **32**, 594 (1936).

[7] K. S. and R. H. Cole, J. Chem. Phys. **9**, 341 (1941).

dielectric constants at low and high frequency, and $x=\ln(\nu/\nu_c)$ where ν is the frequency of measurement and ν_c the critical frequency for which $\Delta\epsilon''$ has a maximum value $\Delta\epsilon''_{max}$. The values of α quoted in Table I are based on the best fit of Eq. (1) to the data. It should be observed that the values of α calculated from the observed values of $\Delta\epsilon''_{max}$ alone are somewhat greater. Work in progress should reveal the reason for this lack of agreement.

There are also included in Table I values of apparent average dipole moments and molecular radii a. These

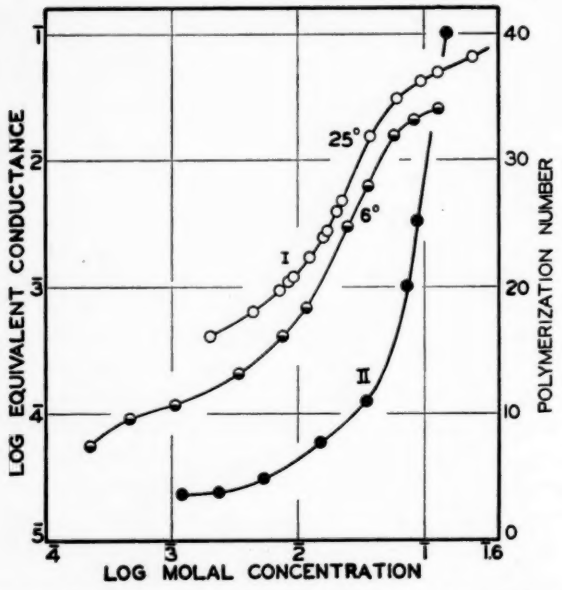

FIG. 3. Equivalent conductance and polymerization number as a function of concentration. Curves I: Equivalent conductance at 25° and at 6°; curve II: Polymerization number.

were calculated by the method previously described[2] and are subject to the same criticism that they have a simple significance only for the case of a single relaxation process. The physical constants necessary for the calculations at 25° and at 6°C are based on previous data;[2] those at 6° were obtained with sufficient accuracy by adding to the solvent values at 6°C (from the *International Critical Tables*) the solution-solvent difference found at 25°.

In Tables II and III are presented conductance data for octadecyltributylammonium thiocyanate in benzene at 25±0.01° and 5.25±0.070°. The specific conductance of the solvent was of the order of 10^{-13} ohm^{-1} cm^{-1} for both runs so that the solvent correction was never greater than one percent.

DISCUSSION

The major factors in selecting lower, rather than higher, temperatures in extending the dielectric absorption and conductance studies on quaternary ammonium salts in benzene were the more convenient ranges of concentration and frequency usable and the possibility of comparing the results with the data available from freezing point measurements. Octadecyltributylammonium thiocyanate was chosen for the study because it is relatively soluble, and both cryoscopic and 25° conductance data have been obtained in other work.

The dielectric properties and conductance were found to change smoothly with temperature over the range 6°–25° and only a comparison of the results at the two extreme temperatures will be made here. The measured loss factors $\Delta\epsilon''$ are plotted in Fig. 1 as a function of frequency for concentrations in the range 0.0085–0.020 molal at both 25° and 6°. From these curves it is evident that the general form is similar at both temperatures for a given concentration, and that the frequency range of absorption changes greatly with both temperature and concentration.

At no concentration in the range is the frequency dependence at all similar to that required for a system having a single characteristic relaxation time. This is shown by the comparison in Fig. 2 of the observed data at 0.016 molal and 25° with the Debye-type curve required to give the same critical frequency of maximum absorption and total dispersion of the dielectric constant. The difference can be expressed by the value of the empirical parameter α necessary to fit the data, and values so obtained are given in Table I. The values at 6° are a little smaller at all but the highest concentration, but show no remarkable behavior apart from the fact that, as in other systems, they represent such great departures from simple behavior.

The effect of temperature on the frequency ν_c of maximum absorption is seen from Table I to be a large one, as the decrease of 20° in temperature reduces ν_c by a factor of about 2.5. This is comparable with the decrease by a factor of roughly two in equivalent conductance at a given molality as shown in Fig. 3.

Neither factor varies appreciably with concentration, and both represent changes very much greater than the 35 percent increase of solution viscosity for the same temperature drop. If the picture of a mixture of ionic and polar aggregates with mobilities determined by hydrodynamic viscous flow is assumed, it is clear that a considerable change in constitution of these aggregates with temperature must be postulated. Further, the remarkable similarity in the effect of concentration on absorption and conductance at the two temperatures, except for the scale factors, also makes this viscous flow model seem less plausible than for data at a single temperature and suggests rather that the mechanism of solute-solvent interaction must be examined more explicitly in these systems.

The very broad range of frequencies in which absorption is significant makes highly uncertain the calculation of dipole moments μ or molecular radii a from the Debye viscosity model of the relaxation process or the extension of it represented by Eq. (1). The calculated values of a in Table I do, to the extent that they mean anything, indicate very large increases in apparent

size of polar aggregates, for the calculated radii increase by a factor of almost three, from 10A at 0.0085 *m* to nearly 30A at 0.020 *m*.

The calculated dipole moments are consistently smaller at the lower temperature and increase with formal concentration. The values are of reasonable magnitude for ionic association, but more quantitative inferences seem unjustified in view of the difficulties already mentioned.

From the plot of the cryoscopically determined polymerization number in Fig. 3, it may be seen that the apparent molecular weights increase from about five to fifteen times the formal weight over the range of the absorption measurements. This increase is proportionately smaller than the changes in conductance and in magnitude and frequency of absorption.

Some correlation can be made between the conductance and dielectric absorption data with regard to concentration effects. At concentrations below 10^{-4} molal in low dielectric constant solvents, the departures of the conductance from its limiting behavior have been attributed by Fuoss and Kraus[10] to ion association, first into neutral dipoles and at somewhat higher concentrations into charged, linear triple ions. These postulates permitted a quantitative analysis of the minimum and subsequent rise characteristic of the equivalent conductance of such systems. At the higher concentrations—above 0.001 molal—for which cryoscopic and dielectric loss information are available, the situation is from any point of view much more complicated. The equivalent conductance, though small, rises rapidly, often with multiple inflections, and the apparent molecular weight increases markedly. These effects in the present system are well shown in Fig. 3.

It is interesting to note that at about 10^{-3} molal a fairly stable situation has developed both in the conductance and apparent molecular weight, the latter not quite four times the formal weight. This suggests that neutral octupoles may be a dominant type of stable aggregations. Absorption data were not taken at this low a concentration in the present work, but results for the closely similar salts with the same ammonium ion but nitrate and iodide cations gave simple absorption curves fitted by Debye equations ($\alpha=0.0$) to within experimental error at about 0.002 *m*. The accuracy of these data was not high,[11] but the simple frequency dependence and the high calculated critical frequencies (500 and 300 Mc) do support the presumption that a single species of small polar aggregates is predominant at concentrations of about 10^{-3} *m*.

At higher concentrations the rapidly increasing conductance and molecular weight indicate a greater complexity of polar clusters, and the absorption curves at concentrations in this range are spread over a much broader frequency band. Any literal correspondence between this breadth and a distribution of aggregate sizes and shapes is too much to expect in view of the difficulties in accounting for the form of the absorption curves by such a picture.

The decreased rate of rise of conductance at greater concentrations (above 0.02 *m* in this case) is apparently accompanied by an increasingly less broad absorption curve. This effect, as measured by decreasing values of the parameter α, just begins to appear in the data of Table I. Measurements on the closely similar octadecyltributylammonium chloride[12] indicate that α drops from a maximum of 0.5 at 0.013 *m*. to 0.03 in the range 0.05–0.07 *m*. Cryoscopic data on sufficiently soluble quaternary salts[4] show maxima in the apparent molecular weight at about 0.1 *m*, followed by quite rapid drops. No adequate absorption data have been obtained in this range because the present apparatus does not give results of sufficient accuracy in the frequency range below 1 Mc, which is of significance at these concentrations, but it would be of great interest to explore the higher concentration region more extensively in suitable systems.

As an example of a salt for which the absorption behavior is much simpler, data are also given in Table I for tri-*iso*amylammonium picrate at 0.11 *m* in benzene. The loss factor $\Delta\epsilon''$ was found to increase linearly with frequency at both 25° and 6° over the range 0.5–30 Mc, and the data are consistent with a single Debye-type dispersion region with critical frequency much greater than 30 Mc. Here the Debye viscosity picture would seem more reasonable. Again, however, the change in the calculated critical frequency from 490 to 275 Mc accompanying the temperature drop is considerably more than can be attributed to increased viscosity alone and the need for a more detailed picture of salt-solvent interaction is once more suggested.

Although the discussion here has been primarily in terms of a particular ammonium salt, the available conductance, cryoscopic and loss data indicate similar behavior for benzene solutions of all quaternary ammonium salts which have three or four short chain alkyl groups (e.g., butyl) and any not too large anion (e.g., the very large picrate ion is excluded). The presence of two or more long chains can from conductance data be expected to give very complex behavior.

[10] R. M. Fuoss and C. A. Kraus, J. Am. Chem. Soc. **55**, 476, 1019, 2387, 3614 (1933).

[11] The uncertainty arises principally from the large corrections necessary to account for losses in the cell walls, and to a lesser extent from residual errors in the calibration method (see reference 2).

[12] Unpublished data in this laboratory.

Molecular Rotation in Sodium Cyanide and Sodium Nitrate*

L. A. SIEGEL
Massachusetts Institute of Technology, Cambridge, Massachusetts
(Received May 9, 1949)

An attempt has been made to decide between the Pauling and Frenkel hypotheses for group disorder in crystals on the basis of x-ray diffraction data.

Measurements of the line intensities of sodium cyanide showed that no decision could be reached between two models involving complete spherical rotation and a tetrahedral distribution of equilibrium positions. The 220 line was found to possess an anomalously large variation of intensity with temperature. A new rhombohedral form of sodium cyanide was found which can be produced only by quenching the cubic form from the vicinity of 300°C. The cubic and rhombohedral forms coexist from 20°C to 80°C. An ordered structure has been proposed for the rhombohedral phase.

The diffuse scattering from a single crystal of sodium nitrate has been studied, and a diffuse maximum has been found which is believed to be a result of group disorder. This maximum shows a strong angular dependence which is incompatible with the predictions of the rotation theory. The data fit a twofold disorder model for the nitrate groups, provided that the positions have an aragonite-type of coordination with the surrounding sodium atoms, rather than the calcite coordination found in the ordered structure.

INTRODUCTION

IT has been found that certain crystals containing atomic groups as structural units show an anomalous behavior of their physical properties with temperature, this behavior generally being associated with a critical temperature. The qualitative explanation of this phenomenon assumes that above the critical temperature the atomic groups are no longer restricted to fixed positions.

Two viewpoints have been evolved concerning the nature of the group behavior. The first, advanced by Pauling,[1] allows the groups to rotate freely. In the alternate hypothesis—that of Frenkel,[2] the groups still behave as torsional oscillators, but may take any of several equivalent equilibrium positions. Although many x-ray diffraction studies of these crystals have been made, and have apparently succeeded in checking the Pauling picture, most of the work has not considered the possibility of the second hypothesis. Furthermore, the diffuse background, a consequence of the crystalline disorder, has been left largely unstudied.

A further diffraction study, both of line and background intensities, has been undertaken in an attempt to choose between the two theoretical models for the cases of sodium nitrate and sodium cyanide. In the case of the cyanide, calculation showed that the disorder diffuse background would be considerably weaker than the Compton background, and thus difficult to detect. Therefore, only the line intensities were investigated for this substance. For the nitrate, only the diffuse background was studied.

TABLE I. Experimental results for NaCN at room temperature.

Ratio of planes	Theoretical intensity value: Rotation	Disorder	Experimental value
$\frac{220}{200}$	0.466	0.469	0.422±2%
$\frac{311+222}{220}$	0.393	0.398	0.308±5%
$\frac{400}{311+222}$	0.175	0.154	0.180±2%
$\frac{331+420}{400}$	2.84	3.00	2.91 ±3%
$\frac{422+333+511}{331+420}$	0.562	0.640	0.676±5%
$\frac{531+442+600}{422+333+511}$	0.521	0.479	0.414±15%

EQUIPMENT

The experiments were carried out with a high temperature vacuum camera. Complete sample rotation was provided to insure smooth powder pattern lines, and in the design of the camera, attention was paid to the elimination of scattering from the collimator pinholes and furnace. The latter precaution is necessary when studying the very weak disorder backgrounds. Crystal monochromated copper K_α radiation was used in all the background studies and in most of the line intensity work. When checked by blank runs, exposures were obtained which were completely free from extraneous scattering. The line intensities were evaluated by numerically integrating the intensity plots obtained from microphotometer records.

EXPERIMENTS WITH SODIUM CYANIDE

The specific heat variation of sodium cyanide[3] shows anomalies at 172°K and 288°K. X-ray investigation[4] shows that the structure is of the rock salt type above

* Submitted in partial fulfillment of the requirements for the degree of Doctor of Philosophy.

[1] L. Pauling, Phys. Rev. **36**, 430 (1930).

[2] J. Frenkel, Acta Physicochimica **3**, 23 (1935).

[3] C. E. Messer and W. T. Ziegler, J. Am. Chem. Soc. **63**, 2703 (1941).

[4] H. J. Verweel and J. M. Bijvoet, Zeits. f. Krist. **100**, 201 (1938).

288°K. Below this temperature the structure has orthorhombic symmetry, there being no apparent change in structure at 172°K. This latter transition, however, may involve a type of disorder in which carbon and nitrogen atoms interchange positions at will. Since these atoms are very similar in scattering power, the resultant changes in the diffraction pattern would be very small.

The previously mentioned cubic phase must involve some kind of disorder of the cyanide group, since fixed units could not simulate the rock salt structure. Using only a spherical rotation model, Verweel and Bijvoet found good agreement between theory and experiment. On the other hand, Ziegler and Messer concluded from specific heat measurements that free rotation could not exist at room temperature, although the restriction on rotation grew weaker at higher temperatures.

Two models were chosen for comparison with the experimental results. The first, involving complete spherical rotation of the CN group, has for its average structure factor

$$\bar{F}=4\left[f_{\mathrm{Na}}+f_{\mathrm{CN}}\left(\frac{\sin 2\pi HR}{2\pi HR}\right)\right].$$

The second, which allows the cyanide group to take, with equal probability, positions along the four cube diagonals, gives

$$\bar{F}=4\left[f_{\mathrm{Na}}+f_{\mathrm{CN}}\left\{\cos\left(\frac{2\pi R}{\sqrt{3}a}h\right)\times\cos\left(\frac{2\pi R}{\sqrt{3}a}k\right)\cos\left(\frac{2\pi R}{\sqrt{3}a}l\right)\right\}\right].$$

In these expressions, f_{Na} and $f_{\mathrm{CN}}=f_{\mathrm{C}}+f_{\mathrm{N}}$, are the atomic form factors.

$H=(2\sin\theta)/\lambda$.
$2R$ is the interatomic separation of the cyanide molecule.
a is the cube edge.
h, k, l are the Miller indices.

The expressions for the structure factors have been derived under the assumption that each group is independent of its neighbors. In the numerical computations $2R$ was taken as 1.05A[5] and a as 5.87A. Since the cyanide group is negatively ionized, an extrapolated value of f_{CN^-} was used.

It was impossible to measure accurately, by photometric means, all the lines in a given pattern, since the line intensities varied very strongly with angle. The procedure finally adopted consisted of measuring the intensity ratios of neighboring lines, thus avoiding the need for an absolute reference scale between various exposures.

The averaged results of twelve powder patterns are presented in Table I and are compared with the theoretical values, the latter being corrected for lattice vibration. In this correction, the usual Debye-Waller expression has been used with a Debye temperature of 218°K.

It is seen that neither model is consistently favored by the experimental results. Particularly surprising is the behavior of the first two intensity ratios. Here, both models are nearly identical in theory, but the experimental results deviated markedly from theory.

It was at first suspected that the discrepancy might be due to an additional temperature effect caused by oscillation of the cyanide molecules. To test this hypothesis, a measurement of the 220/200 intensity ratio as a function of temperature was undertaken.

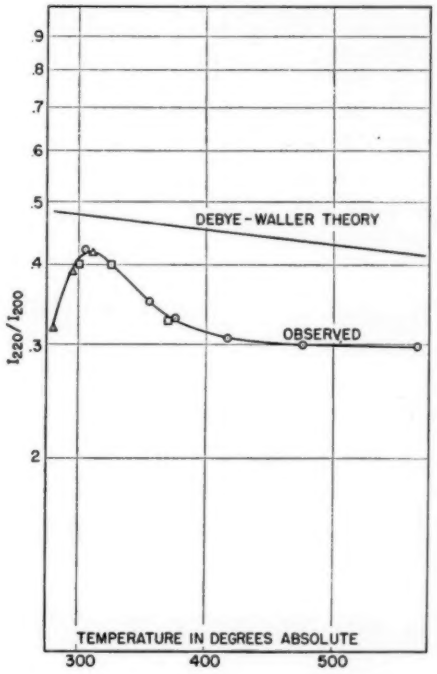

FIG. 1. Temperature dependence of 220/200 intensity ratio for sodium cyanide.

The results are shown in Fig. 1, together with the temperature variation to be expected for the usual lattice vibrations. The additional temperature dependence is quite pronounced, but an extension of Schaeffer's[6] theory for the oscillation effect shows that the observed variation for the 220/200 ratio is much too large to be explained on that basis. In addition, the sharp decrease of the ratio below 30°C would seem more related to the phase transition at 15°C than to the oscillation effect.

Using a sample containing a calibrating substance, it was found that the anomalous behavior of the 220/200 ratio is due solely to the 220 line, the 200 line behaving normally.

In these temperature studies, the position of the lines had remained normal. It was found, however,

[5] J. A. Lely and J. M. Bijvoet, Rec. Trav. Chim. **61**, 249 (1942).

[6] P. A. Schaeffer, Jr., J. Am. Chem. Soc. **69**, 1557 (1947).

that if a sample that had been held at about 300°C was rapidly cooled to room temperature, the appearance of the pattern changed. The 200 line remained normal, but the 220 line had split into three components. The original line was much weaker and was surrounded by two strong satellites. The lines of higher indices had also split into a number of components. By cooling the sample slightly below room temperature, these changes became even more pronounced. The lines of the original cubic pattern almost completely disappeared, and were replaced by a new set which gave a pattern of lower symmetry. When the sample was cooled with dry ice, it was found that the new pattern was superimposed on the previously known orthorhombic pattern.

To study the relationship between the ordinary cubic phase, and the new phase, a sample initially cooled from 300°C to room temperature was slowly heated. Patterns taken at successively higher temperatures showed that the extra lines tended both to weaken and to approach the cubic lines. The pattern finally merged into the normal cubic form at about 80°C and remained this way at higher temperatures. Figure 2 illustrates the gradual disappearance of the extra lines. A pattern of the cubic phase is included for reference.

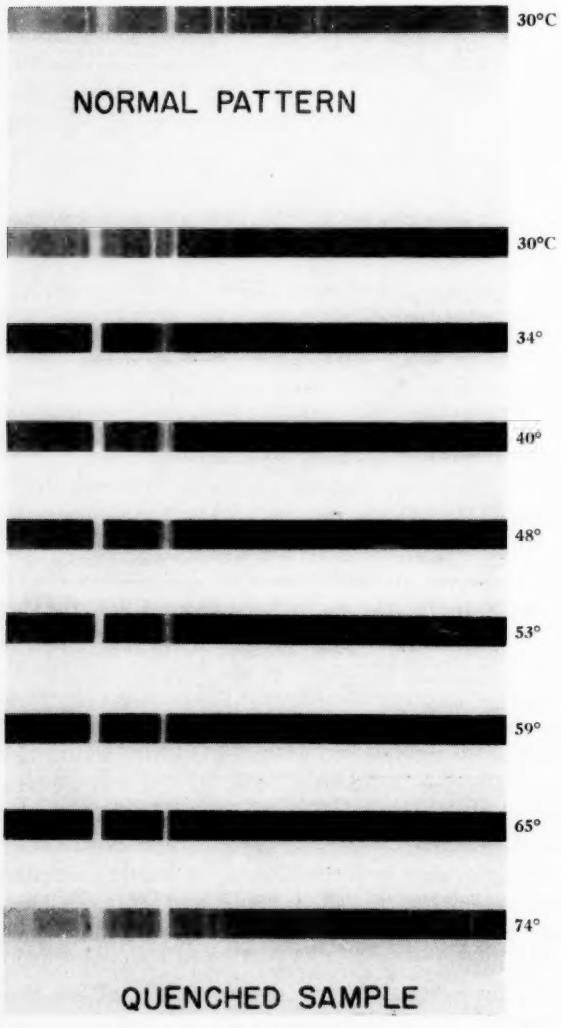

FIG. 2. Patterns of the rhombohedral phase of sodium cyanide.

At any time during the above process, the sample could be recooled and the positions and intensities of the extra lines returned to their previous values. This was true even if the sample was cooled from above 80°C. This reversible behavior, however, was observed only in the case of samples in which the extra phase had previously been introduced by cooling from 300°C. In all cases it was necessary to cool past the 80°C limit before the phase appeared, thus indicating that there is an upper temperature limit to its existence.

In the initial production of the extra phase, it was found that the rate of cooling affected the intensity of the extra lines at room temperature. The slower the cooling the weaker would be the extra lines, although their position was not affected. The new phase thus behaves as if it were retained by quenching, even though it does not exist at the temperature from which the quench is started.

An attempt has been made to find the structure of the new phase. This task was aided by the following considerations. First, it was observed that the 200 line remained unchanged. This indicated that the symmetry could be no lower than rhombohedral or hexagonal. Second, it seemed reasonable to assume that the new structure was a slight deformation of the cubic one.

Using the experimental d spacings, a satisfactory fit corresponding to an axial ratio of 2.86 was found on a rhombohedral Hull chart. This corresponds to a rhombohedral cell edge of 4.37A and an interaxial angle of 53.2°. These values agree well with the concept of a slight deformation of the cubic cell, since for the equivalent rhombohedral cell of the cubic structure an axial ratio of 2.45 and a cell edge of 4.15A would be expected. In analogy with this latter cell, the new rhombohedral cell would be expected to contain one sodium atom and one cyanide group. In order to preserve the rhombohedral symmetry the sodium atom and the center of mass of the cyanide group must lie on the trigonal axis, and, furthermore, the axis of the cyanide group must lie along this symmetry axis or must be disordered in such a way as to obey the symmetry. Such a disorder would be represented by rotation of the cyanide group in a plane perpendicular to the trigonal axis. The former model, however, seems more likely since the cell elongates along the axis.

Accordingly, a structure was proposed in which there was a sodium atom at the origin and a cyanide group lying along the trigonal axis, its center of mass at the center of the cell. In the actual calculations the rhombohedral cell was converted to the equivalent hexagonal cell.

The computed intensities, uncorrected for temperature effects, are given in Table II, where they are compared with the observed values. The agreement is good

TABLE II.

"Parent" cubic line	Hexagonal indices	Sinθ/λ observed	Intensity Theory	Intensity Observed
200	012	0.172	36800	Very strong
220	104	0.232	8190	Strong
220	110	0.256	10820	Strong
311	105	0.268	2340	Medium
222	006		628	
311	113	0.289	1032	Medium
311	201	...	96	...
222	202	0.309	4680	Medium
331	107	0.345	1838	Weak
400	024		2010	
331	205	0.371	654	Very weak
420	116		1090	
333	018	0.386	114	Weak
331	211	...	48	...
440	122	0.400	3350	Weak
420	009		587	

for the first few lines but becomes less satisfactory at higher angles, especially in the case of the 018 line. This may be due in part to the lack of a correction for the molecular oscillation.

The behavior of the composite pattern may be interpreted in the following manner. At the lower temperature the sample is completely, or very nearly so, composed of the rhombohedral phase. As the temperature is raised a portion of the sample undergoes a transition to the cubic phase. The axial ratio of the remaining rhombohedral portion changes in such a manner as to approach the value for its cubic counterpart. This dimensional change of the rhombohedral cell is relatively rapid and is apparently a result of increased oscillational activity of the cyanide group. The conversion of the sample to the cubic phase becomes complete at about 80°C.

The experiments on sodium cyanide can now be summarized. The main results are the anomalously large temperature dependence of the intensity of the 220 line and the existence and properties of the rhombohedral phase. There is no quantitative agreement between the observed line intensities and either a rotation model or a simple disorder model.

At present, no explanation can be given for the intensity variation of the 220 line. The unusual conditions accompanying the production of the rhombohedral phase suggest the possibility of different disorder symmetries at different temperatures. Thus, at room temperature a group would take one of several positions which resembled the orthorhombic phase. In the region of 300°C, the positions would be more reminiscent of the rhombohedral phase.

EXPERIMENTS WITH SODIUM NITRATE

At room temperature sodium nitrate crystallizes with the calcite structure. The specific heat curve shows a very broad maximum with a critical temperature at 275°C. On the diffraction pattern, this behavior has its counterpart in a marked weakening of the reflections to which only oxygen atoms contribute. Above the critical temperature these reflections disappear.

In early investigations of this problem,[7,8] it was shown that good agreement with experiment was obtained by assuming that the nitrate group rotated about the *C*-axis. In a more recent paper, Ketelaar and Strijk[9] have described a careful reinvestigation of the problem, and their work shows conclusively that the disorder must take place in the plane of the nitrate group. Within this limitation it was found that two models agreed with the experimental results, one of them being the previous rotation model. The second was a disorder model in which the group took with equal probability its original position and one rotated by 180° from the latter. From a study of the reflections at large angle, it was concluded that the rotation model was to be preferred. This result, however, is subject to some doubt, since no correction has been made in the disorder model for the oscillatory motion of the group. Since the melting point of the crystal is only thirty degrees above the transition point, this motion would be strongly excited, with a corresponding lessening of the difference between the disorder and rotation models. An actual numerical correction for this effect would, of course, be very difficult to make.

In the case of sodium nitrate, calculations showed that the diffuse background due to disorder would be several times stronger than the Compton background. This indicated that an experimental study of the background was feasible.

The two models initially chosen for comparison were those of Ketelaar and Strijk. Throughout the work, both computation and observation were restricted to the case of the incident and scattered beams perpen-

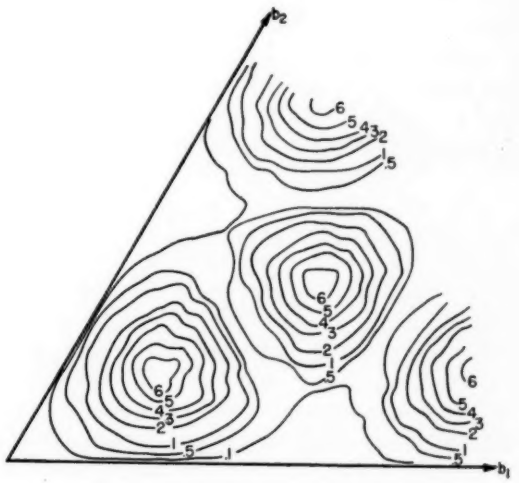

FIG. 3. Disorder scattering function for sodium nitrate.

[7] Kracek, Posjnak, and Hendricks, J. Chem. Soc. **53**, 3339 (1932).

[8] J. M. Bijvoet and J. A. A. Ketelaar, J. Am. Chem. Soc. **54**, 625 (1932).

[9] J. A. A. Ketelaar and B. Strijk, Rec. Trav. Chim. **64**, 174 (1945).

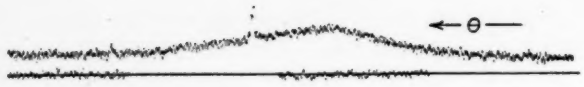

FIG. 4. Diffuse background from sodium nitrate.

dicular to the trigonal axis of a single crystal, this being an orientation particularly convenient for analysis.

For the rotation background, the scattered intensity in electron units is

$$I_D = 3f_0^2[1+2J_0(2\pi\sqrt{3}RH)-3J_0^2(2\pi RH)]$$

where J_0 is the zero order Bessel function and R is the distance of an oxygen atom from the center of the nitrate group. It is to be noted that the background is independent of the orientation of the crystal about the C-axis.

The diffuse background in the disorder case is given by the expression

$$I_D = f_0^2\left[\sin\left(\frac{2\pi R}{a}h\right)+\sin\left(\frac{2\pi R}{a}k\right)+\sin\left(\frac{2\pi R}{a}[h+k]\right)\right]^2.$$

This formula, unlike that for rotation, contains an orientation dependence, which is illustrated in Fig. 3. The scattering function I_D/f_0^2 is shown as a contour map for the b_1b_2 plane in reciprocal space.

The most complete background study would attempt a direct comparison of the observed intensities with those predicted above. This requires that the background due to lattice vibration and group oscillation be known accurately, in order that it can be subtracted, together with the Compton background, from the total experimental background. These additional computations cannot be made in the case of sodium nitrate.

The experimental program was, therefore, based on observing the orientation dependence of the diffuse background, rather than its absolute value. As has been stated, the rotation background should not exhibit such variation, while the disorder background has a maximum for the incident beam along a bond direction.

The sample used was a rod of 0.5 millimeter diameter, its axis along the C direction, formed from a large artificial crystal. The exposures, usually of twenty hours' duration, were made exclusively with a crystal monochromated copper K_α radiation. Maintaining it above the critical temperature, background exposures were taken of the stationary crystal, the exposures being repeated every four degrees through a total angular range of thirty degrees. Many diffuse maxima were observed, but most of these could be identified as due to lattice vibrations since they existed only near a crystalline reflection. There still remained, however, one diffuse maximum which could not be so assigned, and its position on the pattern corresponded to that expected for the disorder background. A microphotometer trace of this pattern is shown in Fig. 4.

The intensity of the diffuse peak varied as the crystal was moved through the angular range, and the peak disappeared thirty degrees from the position of its maximum. While this kind of behavior had been predicted by the disorder model, it was found that the experimental maximum came at the theoretical minimum. However, excellent agreement with experiment could be obtained if the equilibrium positions of the disordered groups were shifted by thirty degrees. This shift would rotate the contours of Fig. 3 by the same angle. The physical meaning of the change in equilibrium positions may be seen as follows.

The ordered form of sodium nitrate is isomorphous with calcite. The latter substance, however, also exists in the orthorhombic aragonite form. This structure differs from calcite in that the carbonate groups have rotated by thirty degrees about the C-axis, and the packing scheme has changed from cubic to hexagonal. In addition, carbonate groups which formerly were in one layer in the calcite structure are now found in positions slightly displaced from the plane of the layer.

It is thus suggested that, above the critical temperature, each disordered nitrate group has an aragonite, rather than calcite, type of coordination with the neighboring sodium atoms. However, there can be no change in the packing scheme, since the resultant change in the position of the sodium atoms would be expected to produce additional strong diffraction lines, and such lines have never been observed. The effect of the displacement of the groups from the layers of the calcite structure would be expected to be small, since as a group shifts from one equilibrium position to another, it oscillates about its position in the calcite structure, as far as displacements along the C-axis are concerned. Such motion does not affect the backgrounds, observed perpendicularly to the C-axis, and will appear as an additional anisotropic temperature factor in the line intensities. The motion would, however, be expected to contribute to a relatively large coefficient of thermal expansion along the C-axis, an expectation which is borne out by experiment. The existence of group oscillation, while affecting the line and background intensities, would not be expected to influence the angular distribution of the backgrounds as strongly, and it is the angular dependence upon which the previous conclusions have been based.

To summarize, the present experiments indicate that above the critical temperature the nitrate group is disordered rather than rotating. Furthermore, any group is related to the neighboring sodium atoms by an aragonite-type of coordination. The position of the sodium atoms, of course, remains unchanged.

In conclusion, the author wishes to express his indebtedness to Professor B. E. Warren for his aid and advice.

Vapor Pressure and Other Thermodynamic Data for *n*-Hexadecane and *n*-Dodecylcyclohexane near Room Temperature

GEORGE S. PARKS AND GEORGE E. MOORE
Department of Chemistry, Stanford University, Stanford, California

(Received May 2, 1949)

Vapor pressure measurements, by the Knudsen effusion method, have been obtained for *n*-hexadecane and *n*-dodecylcyclohexane within the temperature range 299–324°K. From these the following vapor pressure equations have been derived:

$C_{16}H_{34}$; $\log_{10}p$ (in mm) $= 11.2822 - 4212/T$,
$C_{18}H_{36}$; $\log_{10}p$ (in mm) $= 12.4190 - 4880/T$.

Thence, values at 298.16°K have been calculated for (a) the changes in enthalpy and free energy in the standard-state vaporization of these hydrocarbons and (b) the corresponding enthalpies and free energies of formation in the gaseous state.

INTRODUCTION

THIS investigation was carried out in 1940 in order to provide some vapor pressure data for *n*-hexadecane and *n*-dodecylcyclohexane in the neighborhood of room temperature. Since these two substances are rather typical hydrocarbons of high molecular weight, the results are naturally of considerable interest in themselves. Moreover, the vapor pressure values also provide a basis for computing important enthalpy and free energy data pertaining to the hydrocarbons in the gaseous state.

In the present study the effusion method, used previously by Knudsen[1] and others, was employed. It consists essentially in measuring the rate of flow of the gaseous substance through a hole in a thin plate, the diameter of which is small compared with the mean free path of the gas molecules. When the pressure on one side of such a plate is that of the gas saturated by contact with the liquid phase and a high vacuum is maintained on the other side, the vapor pressure of the liquid is given by the relation

$$p = (w/at)(2\pi RT/M)^{\frac{1}{2}}, \qquad (1)$$

where w is the mass of gas effused in the time t, a is the cross section of the hole in the plate, R is the gas constant per mole, T is the absolute temperature, and M is the molecular weight of the substance under study.

TABLE I. Vapor pressure data.

n-hexadecane			*n*-dodecylcyclohexane		
Hole No.	Temp., °K	$p \times 10^3$ mm of Hg	Hole No.	Temp., °K	$p \times 10^3$ mm of Hg
1	309.3	4.92	3	304.4	0.245
1	323.1	17.6	3	309.2	0.457
2	299.8	2.30	3	323.4	2.14
2	310.1	6.34	4	301.9	0.180
2	323.3	22.9	4	309.6	0.458
3	299.1	1.65	Calc.	298.16	0.113
3	300.4	1.72			
3	304.2	2.66			
3	309.4	4.41			
Calc.	298.16	1.43			

[1] M. Knudsen, Ann. d. Physik **28**, 999 and **29**, 179 (1909); T. H. Swan and E. Mack, Jr., J. Am. Chem. Soc. **47**, 2112 (1925); W. H. Rodebush and T. DeVries, J. Am. Chem. Soc. **47**, 2488 (1925); A. R. Ubbelohde, Trans. Faraday Soc. **34**, 282 (1938).

APPARATUS

The apparatus, which we devised for the application of Eq. (1), consisted essentially of a small vaporizer suspended on a sensitive silica spring within an evacuated, thermostatic space.

This vaporizer was a thin-walled, glass bulb, weighing about 0.07 g and with a volume of about 1.5 cc. Its top was closed by a disk, made out of platinum foil 0.07 mm thick, which was fused tightly onto the glass surface. Prior to installation, a small hole, ranging in diameter from 0.15 to about 1.0 mm in different sets of measurements, was drilled through such a disk and the platinum was then carefully thinned around the hole by hammering, so that the edge of the orifice would be sharp. After each set of measurements, the cross-sectional area of the hole was determined by taking photo-micrographs beside a Zeiss standard scale. Enlargements were then made and the areas of the hole could thus be evaluated by a planimeter with an absolute error of less than 2 percent. Prior to measurements, the glass vaporizer bulbs were filled with a suitable amount of hydrocarbon by means of a small hypodermic needle inserted through a capillary side tube, which was subsequently sealed off in a minute flame.

In the course of the measurements the vaporizer rested in a light basket of copper wire, with the platinum disk uppermost, and the basket in turn was suspended

TABLE II. Enthalpy and free energy data at 298.16°K (in calories per mole of hydrocarbon).

	$C_{16}H_{34}$	$C_{18}H_{36}$
$\Delta H°$ of vaporization	19,270 (±360)	22,330 (±300)
$\Delta F°$ of vaporization	7810 (±30)	9320 (±30)
$\Delta H_f°$ of liquid	−108,720 (±600)	−112,010 (±800)
$\Delta F_f°$ of liquid	11,300 (±800)	18,940 (±1000)
$\Delta H_f°$ of gas	−89,450 (±700)	−89,680 (±850)
$\Delta F_f°$ of gas	19,110 (±800)	28,260 (±1000)

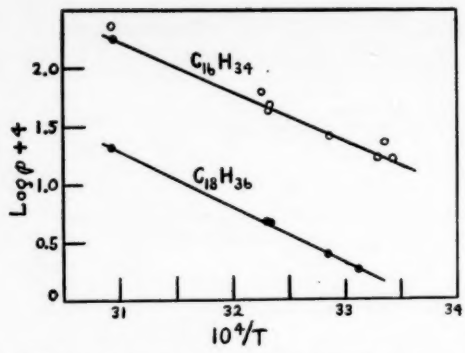

FIG. 1. Plot of $\log_{10}$ of the measured vapor pressures against the reciprocals of the absolute temperatures and the lines representing Eqs. (2) and (3).

on a fused silica, spring balance of the McBain-Bakr[2] type. Extensions of this spring were measured from time to time by a reading telescope and interpreted through a previous calibration with known weights. The vaporizer and balance were contained within a glass chamber, which for the vapor pressure measurements was evacuated to about 10^{-6} mm of mercury by means of a pumping arrangement, consisting consecutively of a Megavac oil pump, a mercury vapor diffusion pump, and finally a tube of activated charcoal immersed in liquid air. Pressures for this system were measured by a suitable McLeod gauge.

This entire vapor pressure apparatus was maintained in a specially constructed air thermostat, the temperatures of which were measured by a two-element, copper-constantan thermocouple in conjunction with a White potentiometer. Computations based on the characteristics of our apparatus indicated that the hydrocarbon sample might require as much as twenty-five minutes to attain thermal equilibrium after a change of setting of this thermostat temperature but that subsequently to such a period it would never differ significantly in temperature from the thermostat.

In the actual determinations, decreases in the weight of the liquid hydrocarbon varied from 0.00257 to 0.02330 g and the time intervals for such evaporations ranged from 17,000 to 138,000 seconds.

MATERIALS

The *n*-hexadecane employed in this study was a part of Sample 2, used and described previously by Richardson and Parks[3] in their measurements of heats of combustion. Likewise, the *n*-dodecylcyclohexane was from the same material used by Moore, Renquist, and Parks.[4]

The main impurities in these hydrocarbon samples were undoubtedly closely related isomers and should not produce more than one percent error in the vapor pressure values as experimentally measured.

[2] J. W. McBain and A. M. Bakr, J. Am. Chem. Soc. **48**, 690 (1926).
[3] J. W. Richardson and G. S. Parks, J. Am. Chem. Soc. **61**, 3543 (1939).
[4] Moore, Renquist, and Parks, J. Am. Chem. Soc. **62**, 1505 (1940).

EXPERIMENTAL RESULTS AND DERIVED DATA

Three sets of measurements, with holes of different sizes, were carried out on the *n*-hexadecane and two sets on the *n*-dodecylcyclohexane. The results are summarized in Table I and are also represented graphically in Fig. 1, where the $\log_{10}p$ values have been plotted against the reciprocals of the absolute temperatures. Over the limited temperature range involved, the numerical data (except for Hole 2 with the hexadecane) are represented quite satisfactorily by the straight lines

$$C_{16}H_{34};\quad \log_{10}p\ (\text{in mm}) = 11.2822 - 4212/T, \quad (2)$$

$$C_{18}H_{36};\quad \log_{10}p\ (\text{in mm}) = 12.4190 - 4880/T. \quad (3)$$

From the character of the experimental measurements we estimate that vapor pressures computed by such equations may involve uncertainties of about 5 percent in absolute values, although they are probably reliable to within 2 percent for relative purposes.

The three determinations on *n*-hexadecane with Hole 2 yielded values about 30 percent above those of Eq. (2) and corresponded to a straight line with an almost identical slope. As it was found after these particular measurements that the platinum disk was not completely sealed to its glass bulb, such higher results can be readily explained on the basis that some molecules of the hydrocarbon vapor were also escaping through a crack in the glass-to-platinum seal.

By Eqs. (2) and (3) values for the vapor pressure of these two hydrocarbons were calculated for the standard temperature of 298.16°K (i.e., 25°C) and these are also recorded in Table I.

The vapor pressure results have been used in turn as a basis for deriving the enthalpy and free energy data pertaining to the gaseous state, which are recorded in Table II. Here the molal heats of vaporization were obtained from the slopes of the vapor pressure equations by the Clausius-Clapeyron relationship. The corresponding values for the free energy change for the hypothetical vaporization of liquid hydrocarbon to yield a vapor at 1 atmos. fugacity were computed from the respective vapor pressures by the equation

$$\Delta F^\circ = RT \ln(760/p). \quad (4)$$

In a paper presenting extensive thermal data for hydrocarbons, which is to be published in the near future, Parks and his collaborators have calculated values for the ΔH°_{298} and ΔF°_{298} of formation of *n*-hexadecane and *n*-dodecylcyclohexane in the liquid state. These are here reproduced in the third and fourth lines of this table. Combination of such values with the present ones for the standard-state vaporization process thus yields our tabulated data for the enthalpy and free energy of formation from the elements (H_2 and β-graphite) of these two hydrocarbons as hypothetical gases at 298.16°K and 1 atmos. fugacity.

In this connection it is interesting to note that the

work of American Petroleum Institute Research Project 44,[5] largely dependent on statistical calculations and extrapolations from the lower members of the respective homologous series, has yielded $\Delta F_f^\circ = 20{,}520$ cal. for *n*-hexadecane and $\Delta F_f^0 = 29{,}930$ cal. for *n*-dodecylcyclohexane as hypothetical gases under these same conditions, with estimated uncertainties of the order of 1000 cal. The agreement with our present results is reasonably good.

[5] F. D. Rossini and co-workers, *Selected Values of Properties of Hydrocarbons* (United States Government Printing Office, Washington, D. C., 1947), pp. 362 and 365.

THE JOURNAL OF CHEMICAL PHYSICS VOLUME 17, NUMBER 11 NOVEMBER, 1949

The Structure and Growth of Evaporation LiF and NaCl Films on Amorphous Substrates

L. G. SCHULZ*
Institute for the Study of Metals, University of Chicago, Chicago, Illinois
(Received February 28, 1949)

Thin films of LiF and NaCl were prepared by evaporation in a vacuum and studied by means of electron diffraction, electron microscopy, x-ray diffraction, and optical methods. It was found that on amorphous substrates the films possessed a crystal orientation which varied with the film thickness. For both LiF and NaCl deposits thinner than a hundred angstroms showed almost completely random structure but with a small amount of [100] preferred orientation. As the thickness was increased there was a change, first to completely random, and then to a very definite and strong preferred orientation which was [111] for LiF and [110] for NaCl. The extent of these orientations both on the surface and in the interior of the film was studied in relation to crystal growth. The films are composed of loosely packed crystals set together so as to give the characteristic orientation and with appreciable spaces where the crystals do not make contact. A less extensive study of five other substances showed the following orientations: CaF_2, [111]; KCl, [110]; MgF_2, [302]; NaBr and KBr, random or a vague [211]. MgF_2 was amorphous for deposits under 1000A but became crystalline for greater thicknesses. Detailed consideration is given to the comparison and interpretation of results obtained by different experimental methods.

INTRODUCTION

THIN films formed by evaporation and deposition of solids in a vacuum have been of scientific interest for some time. More recently they have become of commercial importance, in particular in the optics and vacuum tube industries. These films are in general too thin to be examined by standard x-ray methods and are best studied by electron diffraction. The study of metals using this technique has been extensive and summaries of the work are available.[1–3] Little attention, however, has been given to films of non-metals. The present work was therefore undertaken to examine films of a few well-known alkali halides giving special emphasis to those currently used for optical purposes.

In the formation of thin films three relations are of interest: (1) that of the substrate to the structure of the initial deposit; (2) the changes in orientation with increasing thickness, and (3) the changes in structure produced by variations in the evaporating conditions. All three relations were studied, most effort being given to (1) and (2). Concurrent with this investigation of evaporated films a study of electron diffraction itself was also made. It is unfortunate that the application of electron diffraction is often seriously limited by the lack of trustworthy interpretations for many of even the most typical patterns. In the experiments to be described[4] an effort was made to eliminate some of the uncertainty by comparing data secured by different methods. In addition, attempts were made to correlate various types of diffraction data with those given by optical methods.

For small thicknesses the results are naturally divided into two groups, one group for amorphous substrates, and the other for polycrystalline substrates. In this paper only the first group will be considered.[4]

EXPERIMENTAL PROCEDURE FOR ELECTRON DIFFRACTION

The electron diffraction experiments were done with a modified electron microscope which has been described in detail elsewhere.[5] To secure approximately uniform radial exposure a sector disk was inserted immediately above the plane of the photographic plate.[6] This disk was run at 1000 r.p.m. and had an opening proportional to the square of the radius. Nearly all the samples were prepared within the vacuum of the diffraction apparatus, evaporation taking place from a small source

* The experiments described in this paper were begun in 1947 at the Electrical Engineering Department of Ohio State University and were completed at the University of Chicago during 1948.

[1] F. Kirchner, Ergeb. d. exskt. Naturwiss. **11**, 64 (1932).

[2] G. I. Finch and H. Wilman, Ergeb. d. exskt. Naturwiss. **16**, 353 (1937).

[3] G. P. Thomson and W. Cochrane, *Theory and Practice of Electron Diffraction* (MacMillan Company, Ltd., London, 1939).

[4] Some of the results have been reported earlier: L. G. Schulz, Phys. Rev. **75**, 345 (1949); Phys. Rev. **75**, 1284 (1949); J. Opt. Soc. Am. **38**, 440 (1948).

[5] A. F. Prebus, *Colloid Chemistry*, (Reinhold Publishing Corporation, New York, 1944) edited by Alexander, Vol. 5, p. 152.

[6] The author wishes to thank Professor Bauer of Cornell University for pointing out the advantages of using a sector disk, and also for suggesting some of the mechanical details.

mounted on a mechanism which made it possible to move the source out of the path of the diffracted electrons. A fifty-kilovolt beam was used of such intensity that exposures of from one to three seconds were required.

A rather extensive survey of possible reflection substrates showed that microscope slide glass gave no pattern of its own and was smooth to magnifications of one hundred thousand diameters. The glass was cut into one-eighth inch strips and cleaned by the procedure used in preparing mirrors for silvering. Transmission sample supports were made of collodion held on a sixty-mesh screen rolled flat and then cleaned in hydrochloric acid. A glass strip and screen could be mounted adjacent and co-planar to the sample control mechanism. When first inserted into the diffraction instrument the substrates were kept in a position at which they were shielded from the evaporation source.

The experimental procedure was as follows: The beam was first focused to a five-mil spot and the source heated almost to the evaporation temperature. Then one-half inch of the sample substrates was moved out of the shielding with the collodion transmission substrate in the beam. Evaporation was then begun and the changes in the diffraction pattern followed on the fluorescent screen. The source gave so little light that it was easy to see the diffraction pattern as it developed. In general a sequence of changes was observed several times before any part was photographed. For each trial a clean area of the sample holder could be moved into position. A procedure such as this was not only time-saving but made it possible to detect changes likely to be missed when observations are not continuous. The plate chamber had a capacity of twelve plates each 3 by 4 inches. With three exposures per plate it was possible to record all changes in a sequence without admitting air into the apparatus to change plates.

During evaporation a pressure of 10^{-5} mm of mercury or lower was maintained with an eight-inch diffusion pump. At this pressure the mean free path of the diatomic molecules was well above the source to sample distance. For dielectrics there was a detectable deposit on the shadow side of the substrates indicating an accommodation coefficient of less than one. A film so formed will be referred to as an "indirect deposit." The extent of the indirect deposit was determined by the geometry of the vacuum system and usually never exceeded more than a fraction of a percent of the direct deposit. There was no evidence for migration over the edge of the substrate, this conclusion being checked by extensive experiments in a bell jar evaporation set-up.

The film thicknesses given in this paper are only approximations; on the average the probable error was about thirty percent. The radiation characteristics of a source containing a weighted charge were determined both by weighing the deposit and by counting the interference fringes. For the type of source employed the film thickness was five to six times that given by radiation from a point. In addition to the direct method of determining thickness by weighing the material evaporated from a calibrated source, it was possible after some practice to very roughly judge film thicknesses during evaporation by the extent of the incoherent scattering, the color of the source, and the pattern given by the indirect deposit.

Experimental methods other than electron diffraction were used in studying the films, but the details of the procedures are either well known or are described with the presentation of the results.

SAMPLE CONTAMINATION IN RELATION TO FILM GROWTH

A factor in the consideration of film growth which is difficult to evaluate is the effect of sample contamination. This contamination is principally that of the substrate in handling before it is inserted into the vacuum, or after insertion due to foreign vapors in the residual gas. To insure that contaminations were not determining the results various auxiliary experiments were performed.

FIG. 1. Drawings illustrating the electron diffraction patterns given by common types of preferred orientation. In all four cases the crystal structure is fcc and the fiber axis is normal to the substrate. The orientations are as follows: A, [100]; B, [111]; C, [110]. D shows a transmission pattern given by crystals having a [100] orientation relative to a substrate which is at an angle of 45° to the electron beam. Drawings A, B, and C each contain two patterns. The lower pattern in each case shows one-half of the reflection pattern, the heavy horizontal line indicating the shadow edge and the dots giving the positions of possible reflections. To show the relative position of the spots the fcc rings have been drawn in but these rings do not appear in the diffraction pattern. Likewise the more lightly drawn horizontal layer lines are for clarity only. Points lying on the vertical lines in A locate the reflections given from the more complete [100] orientation in which the crystals have a [100] direction parallel as well as perpendicular to the beam. The upper parts of A, B, and C are the patterns given by transmission when the fiber axis is parallel to the beam. The short arcs are sections of the rings to be expected. These arcs can be readily indexed from the fcc rings immediately below in the reflection patterns.

One such experiment was to vary the rate of evaporation from one layer of atoms per second to 500 layers. This extreme variation produced no change in the character of the films produced. The number of atoms per square centimeter in the (100) face of LiF is 25×10^{14}. At the working pressure of 10^{-5} mm of mercury the number of gas molecules striking the same area per second is 3.5×10^{15}. Since this is equivalent to about three atom layers per second the bombardment of the residual gas could be a factor in crystal growth but the experimental results showed it was not a dominant one.

In addition to residual gas molecules there are also some oil molecules from the diffusion pump. Condensation of such molecules on the substrate was found to be negligibly small. Single crystals of LiF and NaCl were kept in the vacuum for several days during which time the diffusion pump was in operation. The accumulation of oil on the crystal surfaces was insufficient to make a perceptible change in the Kikuchi lines. Inasmuch as an average deposit of only about 10A was sufficient to change appreciably the Kikuchi pattern, the oil condensed during the course of an experiment was of no consequence.

Experiments were also performed which showed that films formed in the electron beam were no different from those formed outside it. The maximum current density was about one ampere per square centimeter which was the limit the transmission samples could withstand before rupture.

In the experiments to be described the approach was to determine experimentally the nature of the films formed at some definitely known condition which was reasonably easy to realize in practice rather than at unattainable ideal conditions. Conceivably extremely minute contaminations such as one foreign atom per crystal formed may determine the film structure. The methods were totally inadequate for detecting such effects. Indirect evidence, as well as direct, seemed to indicate, however, that contaminations had no important effect. Additional remarks concerning this matter will be made in conjunction with particular results.

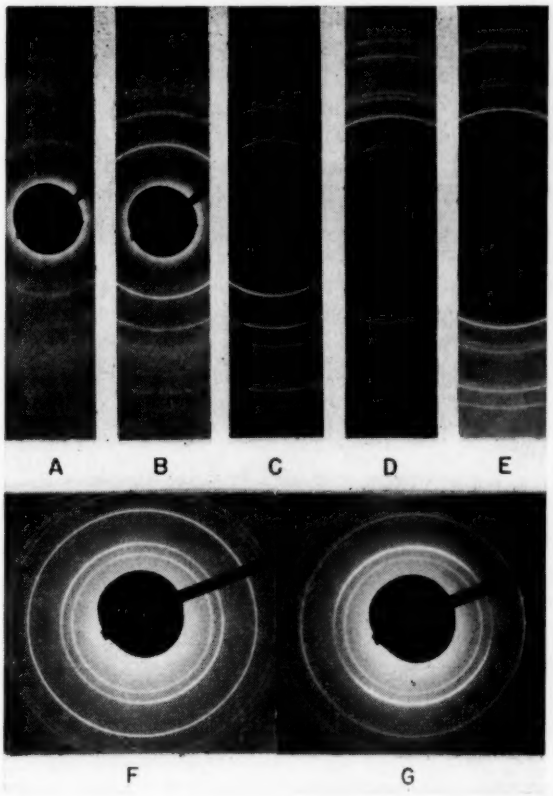

FIG. 2. Transmission patterns through thin films of LiF showing the change in relative ring intensity as the thickness is increased. The approximate thicknesses are: A, 30A; B, 60A; C, 300A; D, 600A; and E, 1000A. Patterns F and G are complete transmission patterns through a film of LiF which is 1500A thick. To emphasize the inner rings these patterns were taken without the sector disk. Pattern F shows the film normal to the beam, and G the same sample tipped at an angle of thirty-five degrees.

DIFFRACTION PATTERNS GIVEN BY CRYSTALS WITH PREFERRED ORIENTATIONS

Since nearly all the films examined showed a type of preferred orientation known as "fiber structure" special consideration was given to the interpretation of the resulting diffraction patterns. In this type of orientation individual crystals tend to be aligned with one principal axis in a preferred, or common, direction. The orientation about the preferred direction, however, is random. For thin films prepared by evaporation this direction was normal, or nearly normal, to the plane of the film. Thus in a film said to have a [111] orientation a (111) plane of all crystals lies in the plane of the film. It follows that the associated [111] direction in the crystals is normal to the film plane. The diffraction patterns to be expected can be obtained by following the pro-

TABLE I.

Substance	Density	Molecular weight	Melting temperature	Boiling temperature	Crystal type	Unit cell dimensions	Atomic separation in the vapor state*	Preferred orientation
NaCl	2.163	58.45	809°C	1413°C	NaCl	5.628	2.51	110
KCl	1.984	74.57	776°	1500°	NaCl	6.28	2.79	110
NaBr	3.205	102.91	755°	1390°	NaCl	5.94	2.64	211
KBr	2.752	119.01	730°	1380°	NaCl	6.57	2.94	211
LiF	2.295	25.94	870°	1676°	NaCl	4.01	Unknown	111
CaF_2	3.180	78.08	1360°	—	CaF_2	5.46	Unknown	111
MgF_2	3.00	62.32	1396°	2239°	SnO_2	4.66/3.08	Unknown	302

*Maxwell, Hendricks, and Mosley, Phys. Rev. 52, 968 (1937).

cedure commonly used in x-rays. The theory has been repeated by Kirchner with special emphasis on its application to electron diffraction.[7] No evidence was found for preferred orientation other than fiber structure.

The drawings of Fig. 1 show the transmission and reflection patterns for the most commonly occurring orientations assumed by fcc crystals. When the beam is parallel to the preferred direction the rings are complete and uniform but may show anomalous intensities. In particular this is true for [111] as shown in Fig. 1 upper B. On the other hand, for [110] in upper C only two rings, the (420), (431), are absent in the range shown. Changing the angle between the beam and the sample breaks the rings into arcs. For example, upper A is changed to pattern D by rotating the sample 45 degrees. With the help of the drawings of Fig. 1 one can determine directly the amount of rotation required to bring any particular reflection to the maximum intensity. It is possible to judge roughly the perfection of the orientation from the arc lengths.

Although most of the experiments were devoted to a study of films of two alkali halides, LiF and NaCl, several other similar compounds were also examined. A list of all these substances, together with relevant physical data, is given in Table I.

EXPERIMENTAL RESULTS FROM LiF FILMS

A. Results Given by Electron Diffraction

Films of various thicknesses were first examined by transmission. Typical results given in Fig. 2 show a definite change in relative ring intensity as the thickness was increased. In pattern A the reflections from the (200) and (220) planes are dominant indicating a [100] orientation (see Fig. 1, upper A). When the film was inclined at forty-five degrees to the beam there was a slight arcing of the rings in the positions shown in Fig. 1, D. In pattern B there is still a trace of [100] orientation but the strength of the other rings shows a trend toward the completely random orientation which is reached in pattern C. The sample producing C gave no arcing when inclined to the beam. Furthermore, the pattern was found to be identical with that given by a sample prepared by catching on a screen the "smoke" from LiF evaporated in air (see Fig. 4, C). For additional increases in thickness patterns D and E show the beginning of a [111] orientation (compare with Fig. 1, upper B). The most pronounced changes are: (1) the increase in intensity of the (220) ring, and (2) the great diminution and almost complete disappearance of the (200) and (400) rings. There was only a very slight

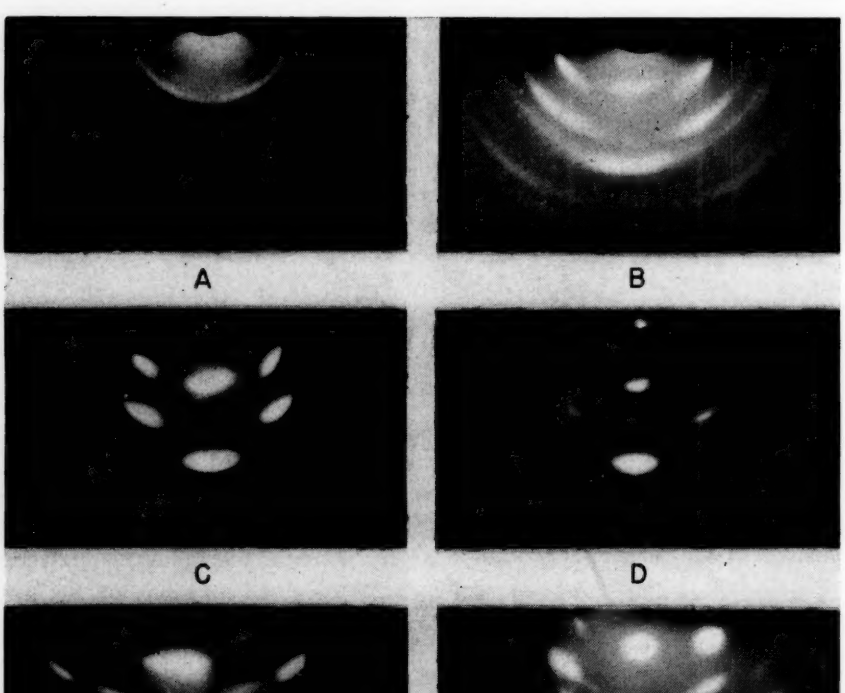

FIG. 3. Reflection patterns from LiF showing the change in surface orientation with increasing thickness. The approximate thicknesses are: A, 100A; B, 500A; C, 1000A; and D, 50,000A. E is the same sample as D but has been turned to a greater angle with the beam. Pattern F is for a film formed when the vapor strikes the substrate at an oblique angle.

[7] F. Kirchner, Zeits. f. Physik **76**, 593 (1932).

amount of arcing when thick samples were inclined to the beam. In pattern F is shown a sample normal to the beam, and in G the same sample at an angle of thirty-five degrees.

Electron diffraction by reflection failed to give distinct patterns for deposits thinner than about 75A. Beginning at 100A a random orientation was detected which changed to [111] for greater thicknesses as shown in Fig. 3. Whereas the transmission samples were limited to films below about 2000A, films of almost unlimited thickness could be examined by reflection. Patterns D and E of Fig. 3 for a film of 50,000A show that as the thickness increases the orientation becomes more pronounced. Another effect associated with increased thickness is the change in the direction of the fiber axis with variations in the angle of incidence of the vapor; for LiF the axis tips away from the direction of deposition as shown in F of Fig. 3. When the films were formed by indirect deposition the structure still passed through the transition from random to [111] orientation with the fiber axis always normal to the substrate. When the thickness of LiF exceeded about 70,000A the crystal grains in the surface reached a size sufficient to scatter light, and as a result the film had a characteristic white color known as "bloom." Electron diffraction by reflection showed nothing new at this thickness, but rather that the [111] surface orientation persisted from thin deposits of a few hundred angstroms to those of several hundred thousand.

A comparison of the volume structure revealed in Fig. 2A with the surface structure shown in Fig. 3A makes possible a description of the nature of the initial film growth. The thinnest film of LiF on collodion which was sufficient to give a significant transmission pattern was about 10A. Although the rings for such a thin deposit were faint because of substrate scattering there was no evidence of pronounced broadening of the kind found for thin metal films.[1] Germer has shown that the initial deposit of gold and similar metals collects into crystals which are at first so small they fail to give a typical crystal lattice diffraction pattern.[8] This is evident from the anomalous ring intensities as well as their breath. As the thickness of the metal deposits is increased the average size of the crystals increases until eventually the normal diffraction pattern is obtained. The structure of very thin films of dielectrics like LiF is much different from that of metals. Apparently there is sufficient mobility to permit the formation of crystals at least 50A on an edge. Since evidence to be given later indicates that these crystals have a tendency to be cubic in shape, the [100] orientation observed in Fig. 2A would result from cube faces resting on the smooth collodion substrate. Because the angular orientation of these first crystals is random about the normal to the film surface, and because of variations in their size, the instantaneous substrate on which succeeding crystals must form is not smooth but is rough relative to the originally clean collodion surface. As a result the [100] orientation cannot persist. At 100A the reflection pattern of Fig. 3A already shows a random structure and after a few more hundred angstroms have been added the characteristic [111] orientation of freely growing LiF becomes prominent.

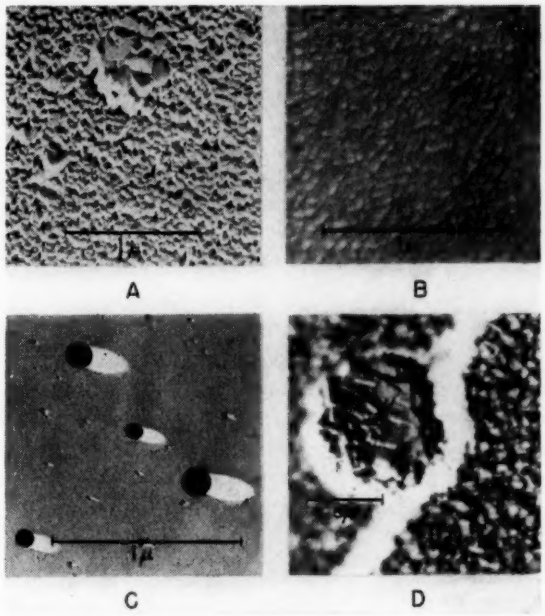

FIG. 4. Micrographs of the surfaces of LiF films. Patterns A, B, and C were taken with an electron microscope and D with a light microscope. Pattern A is a collodion replica of a film just approaching the blooming stage; B, a replica of a similar film covered with aluminum; C, a direct photograph of LiF evaporated in air; and C, a photograph of a film 300,000A thick. Pattern A was obtained by shadowing with uranium, patterns B, C, and D by shadowing with chromium.

Qualitative information concerning the structure of films near the transmission limit in thickness is given in pattern F and G of Fig. 2. The great change in relative ring intensity in C to E of this figure tends to overemphasize the extent of the [111] orientation. Accordingly patterns of the type E and F are most useful for identification purposes, and the arcing pattern shown in G is a more reliable measure of the magnitude of the volume orientation. Moreover, such arcing occurs for all types of orientation whereas the change in ring intensity with normal incidence may be small or practically zero as is the case for [110] structure. In general a transmission pattern with the fiber axis normal to the substrate will show less definite arcing than a reflection pattern from the same sample. In an effort to obtain at least a semiquantitative guide for evaluating arced patterns the following experiment was done: A sample was found which showed almost complete orientation (see Fig. 9B). To this was added measured quantities of random material and the changes in the diffraction pattern observed. It was found that a small but well-oriented component tended to have an exaggerated in-

[8] L. H. Germer and A. H. White, Phys. Rev. **60**, 447 (1941).

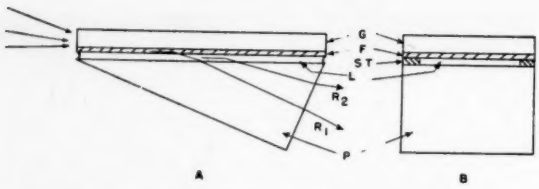

FIG. 5. Experimental arrangement for measuring the index of refraction of LiF films. P is the prism of the refractometer; F is the sample film on the glass substrate G; ST is Scotch Tape, and L is the contact liquid.

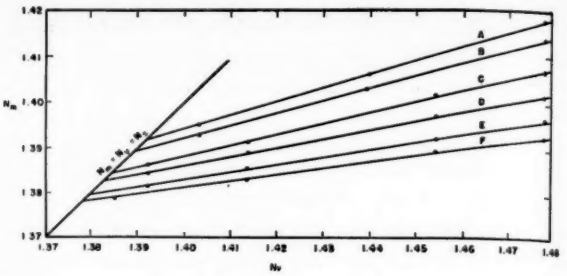

FIG. 6. Experimental results on the measurement of the index of refraction of LiF films. (The symbols are defined in the text.)

fluence on the pattern. A rough estimate indicated that approximately 10 percent of the crystals in a film 1000A thick had a [111] direction within 10 degrees of the surface normal. The initial deposit of Fig. 2A had a somewhat higher [100] orientation which tended to increase for samples of decreasing thickness.

If only reflection data were available one might conclude from the arcs of Fig. 3 that a film of LiF about one thousand angstroms thick is rather highly oriented. It has just been shown, however, from transmission data that this is not the case. The seeming conflict can be removed by assuming that the surface projections which produce the reflection patterns do possess the high orientation revealed by Fig. 3, but that the main bulk of the volume which grows into the space between the projections is less completely oriented. As the film grows these projections are continuously being submerged into the volume to give some orientation to the bulk. It is this structure which is revealed by transmission patterns. A more complete quantitative measure of volume orientation in thick films will be given by x-ray data.

B. Results Given by Electron Microscopy

The results given in Fig. 3 show that the projections from a film have nearly perfect crystallographic orientation but diffraction data can give only very indirect information concerning the actual surface contour. The existing theories of crystal growth, however, predict a cubic shape for individual crystals,[9] and in addition, it is known that NaCl crystals grown from the vapor are cubic in form.[10] Accordingly, a [111] fiber structure with a tendency for the formation of cubes requires that the surface of a film be composed of three-sided pyramids, each side being a face of a cube.

Experimental evidence consistent with this prediction was found by electron microscopy. In Fig. 4A is shown a collodion replica pattern of the surface of a film just at the blooming stage.[11] All the larger crystals, as well as some of the small ones, show the three-sided pyramids as expected, but most of the particles are not sufficiently well resolved to give with distinctness the crystal faces. Great difficulty was experienced in obtaining electron micrographs because replica material tended to penetrate into the interior of the films and when removed, brought some of the surface with it. The photograph of Fig. 4A was obtained using a very viscous replica material but still there was some penetration as revealed by the tail-like structures. These results give information on the film texture suggesting that the interior is not solid but is composed of very loosely fitting and relatively independent individual particles. Most likely the particles are rather irregular in shape although most of those protruding through the surface possessed definite plane faces. Examination of films of various thicknesses showed that the size of particles in the film surface was roughly proportional to the film thickness. A film of thickness near 500A contains crystals about 50A on an edge.

Included in Fig. 4 are several variations from the pyramid patterns. Pattern B is the result of depositing a just-opaque layer of aluminum on a film similar to A. Aluminum shows no structure of its own, but migrates sufficiently to cover the deep recesses in the LiF. Pattern C shows LiF which was evaporated in air at atmospheric pressure. The units are spherical in form but it is not known whether or not each is a single crystal. These units are formed before the material strikes the substrate. Pattern D shows the surface contour of a very thick film (order of 300,000A) evaporated in a vacuum. No explanation was found for the unusual formations but additional experiments are being tried to investigate ideas suggested by these variations.

C. Results from Optical Methods

Neither electron diffraction nor electron microscopy gave information on the texture of films formed by evaporation. Electron microscope photographs did, however, suggest that the interior of the films is porous, and direct visual inspection seemed to indicate that bloom is a volume property. Measurements of the index of refraction using polarized light have given values below that of the bulk material, a result which can be explained by assuming that films are diluted with voids.[12] To examine further this explanation the index

[9] Adolph Smekal, *Handbuch der Physik* (Verlag, Julius Springer, Berlin, 1933), Vol. 24, p. 795.

[10] Peter Groth, *Chemische Krystallographie* (W. Engelman, Leipzig, 1906), p. 176.

[11] The author is indebted to Professor Robley C. Williams of the University of Michigan for Fig. 4A and Fig. 4D.

[12] K. Blodgett, Phys. Rev. **57**, 921 (1940).

TABLE II.

Curve	Thickness in angstroms	N_s	Inaccessible voids in percent	Accessible voids in percent	Solid LiF in percent	Effective index (N)
A	20,000	1.3915	0.0	30.0	70.0	1.275
B	35,000	1.3890	0.7	28.5	70.8	1.279
C	100,000	1.3842	1.3	24.2	74.5	1.295
D	135,000	1.3825	1.9	20.2	77.9	1.305
E	165,000	1.3795	2.7	16.4	80.9	1.317
F	180,000	1.3780	3.1	14.4	82.5	1.323

of refraction of LiF films was measured with great accuracy.

Films were formed on sheets of glass in an 18-inch bell jar at a pressure of about 5×10^{-5} mm of Hg. Following the deposition the glass was removed, cut into samples approximately one inch square, and then examined with an Abbe refractometer using the arrangement shown in Fig. 5. Narrow strips of Scotch Tape were put over the two long edges of the prism, and on this tape was placed the glass sample, film downward. Optical union was produced by running a liquid into the narrow opening defined by the tape thickness. Sufficient illumination entered the system through the broken edge of the glass. If the liquid had an index higher than that of the film, two critical angles existed with this arrangement. The first, associated with the film and defined by the ray, R_1, in Fig. 5 arises because the film has the lowest index of the various materials in contact. The second critical angle is associated with the liquid and is possible because the LiF film is slightly rough and for this reason permits the passage of some light beyond the usual critical angle. For films thinner than 15,000A the first (the normal) critical angle is poorly defined whereas the second is sharp and prominent. For thick films—above 40,000A—the film angle becomes well defined but the liquid angle, although still sharp, shows but faintly. The procedure was to measure both critical angles for a range of liquid indices and film thicknesses. The results of a series of such measurements are shown in Fig. 6 where each curve is for a given film thickness. N_m is the index of the film when immersed in a liquid with an index N_v. A suitable range of N_v was obtained by mixing benzine and alcohol in various proportions.

A description of the film texture consistent with the data of Fig. 6 is as follows: The film is made up of three phases: (1) solid LiF crystals having the same index, 1.3919, as the bulk material; (2) accessible voids which become filled with the contact liquid, and (3) inaccessible voids between the solid LiF crystals. This second type of void will have an index of unity, or at most 1.0002 which is the value for air. During the course of an experiment phases (1) and (3) remain unchanged, and will be treated as a single combination phase. The optical path through this solid-inaccessible void combination will be designated by N_sl_s where N_s is its effective index and l_s the path length. Similarly N_vl_v is the optical path through the accessible void phase. The effective index, N_m, of the mixture of all three phases will then be found from

$$N_sl_s+N_vl_v=N_ml, \tag{1}$$

where l is the actual film thickness.

The general validity of Eq. (1) is shown by the linear relationship of N_m and N_v in Fig. 6. The relation $N_v=N_m=N_s$ is shown in the graph as the terminus of the experimental curves. Along this line the two critical angles become equal. For the thinnest deposits examined N_s became equal to 1.3919 but for thicker films it was less. This was interpreted to indicate that inaccessible voids did not exist in thin deposits. With this description of the film structure it is possible to calculate exactly the magnitude of each quantity. For purposes of calculation Eq. (1) is rewritten,

$$N_sf_s+N_v(1-f_s)=N_m, \tag{2}$$

where f_s is the fractional part of the optical path which is composed of the combination of phases (1) and (3). The value of f_s can be calculated since N_s, N_v, and N_m are given directly from the graph. (N_s is constant along any one curve.) An equation similar to (2) useful for finding the inaccessible voids is

$$1.3191f_{1s}+1.0002(1-f_{1s})=N_s. \tag{3}$$

Here f_{1s} is the fractional part of LiF in the combination phase and $(1-f_{1s})$ is that of the inaccessible voids. In Table II is given a set of values from the curves in Fig. 6. Of practical interest is the effective index of the film in air which is given by

$$1.3919(1-f_v)+1.0002f_v=N, \tag{4}$$

where f_v is the total fractional void content of the film.

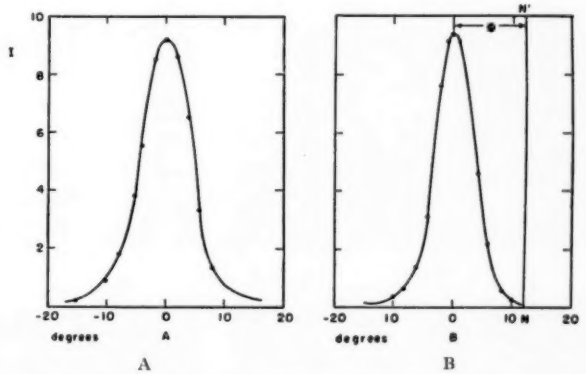

FIG. 7. Graphical representation of the extent of volume orientation as revealed by x-rays. The abscissa is the angle made with the fiber-axis, and the ordinate the density of the 111 crystal axes.

These values could be obtained graphically from Fig. 6 if the curves were extended to the left to intercept the vertical axis at $N_v=1.0002$. Because of the extent of this extrapolation relative to the experimental range of N_v, N has one less significant figure than N_s.

An interesting empirical relationship was found from the curves of Fig. 6: When extended to the left they were found to have a common intersection at $N_v=1.320$ and $N_m=1.370$. Substituting these values in Eq. (2) gives,

$$f_s=[0.050/(N_s-1.320)]. \quad (5)$$

If the nature of the film remains the same as the thickness is increased, then the following predictions can be made for very thick films: (1) N_s will approach 1.370 as a limit; (2) the extent of the accessible voids will tend to disappear; (3) the inaccessible voids will reach a maximum of about 6 percent of the volume, and (4) the effective index, N, in air will become 1.370.

E. Results Given by X-Ray Diffraction

As already indicated, the range of application of electron diffraction has certain restrictions: The reflection method yields information only on the surface projections and the transmission method is limited to films thinner than about 2000A. Moreover, the transmission results do not give a quantitative measure of the volume orientation. Because of these limitations, x-ray diffraction was used to supplement the electron diffraction data.[13] In Fig. 7 are given representative results obtained with a Phillips x-ray spectrometer. Here I is a measure of the density per unit solid angle of the [111] crystal axes as a function of their angle with the fiber-axis. A horizontal line would represent the result for random orientation and complete [111] orientation would give a single narrow spur. The resolving power of the experimental arrangement was such that a single crystal gave a curve having a width of one degree at half-maximum. Curve A of Fig. 7 for a sample 70,000A thick shows the fiber axis normal to the substrate; curve B for a film of the same thickness but prepared by oblique deposition has the fiber-axis at an angle of 11 degrees with the surface normal. For both cases the distribution was symmetrical about the fiber-axis. These curves indicate that virtually all of the crystals in the interior of a film have a tendency to be oriented. It is, therefore, not a case of a mixture of partly oriented and completely random crystals as was true for films near 1500A in thickness.

Examination of over fifty samples of various thicknesses and conditions of preparation showed certain tendencies in film growth. The angle of tilt had no simple relation to the angle of deposition. In general the tilt increased to a maximum of 9° to 12° as the angle of deposition was increased to about 45°. For more oblique deposition the fiber-axis angle with the normal decreased and when the LiF was deposited at grazing angle the fiber-axis tipped toward the source. These tendencies seemed to be independent of the film thick-

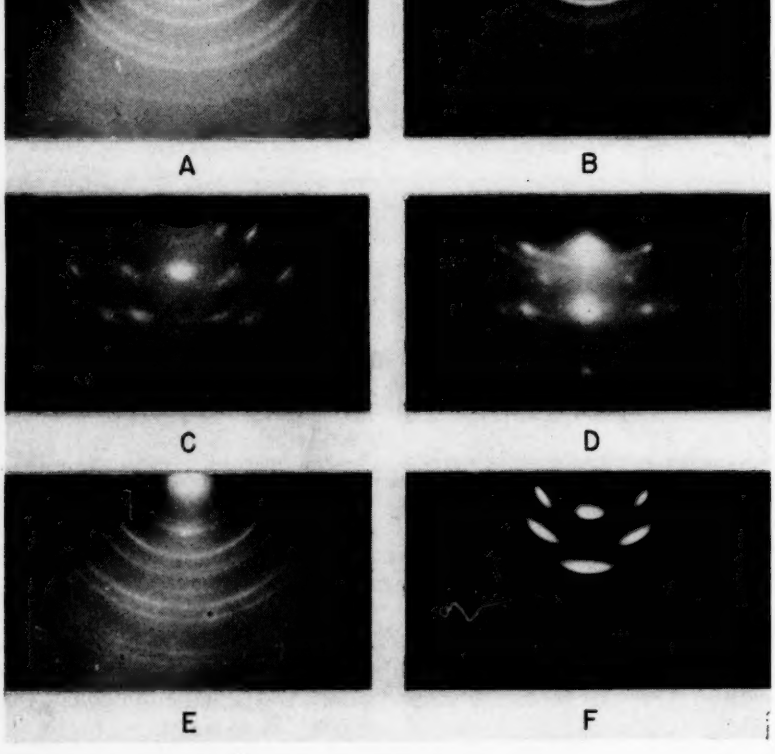

FIG. 8. Reflection patterns from thin films of NaCl. The thicknesses of the samples are as follows: A, 150A; B, 500A; and C, 5000A. Pattern D is the pattern given by a sample 20A thick after exposure to air and E shows the change produced by subsequent additional evaporation. Pattern F is a film showing [111] structure formed by indirect deposition.

[13] The experimental details will be described elsewhere.

ness except that the width of the curves, such as those given in Fig. 7, decreased with increasing thickness.

EXPERIMENTAL RESULTS FROM NaCl FILMS

Electron diffraction experiments similar to those just described for LiF were also performed on films of NaCl. Transmission showed some [100] orientation for deposits less than 100A. Beyond that thickness up to 1000A the diffraction patterns were those to be expected for a random structure. The reflection patterns of Fig. 8 A, B, and C, however, indicate a definite change from random structure to a decided [110] orientation as the thickness was increased above 700A. For very great thicknesses of the order of 25,000A the orientation either returned to random or to a vague [210]. When the film of NaCl was formed completely by indirect deposition the orientation was [111] as in Fig. 8F. A sample formed at grazing incidence had no orientation or a confused [210].

The details of NaCl films can be conveniently described by comparing them with those for LiF. The films of these two materials are similar in that both begin with some [100] structure, then pass through a random to a preferred orientation as the film thickness is increased. The orientation is the same, [111], for indirect deposition, but different if the deposition is direct being [111] for LiF and [110] for NaCl. When the direct deposition was not normal to the substrate there was a tipping of the fiber-axis, for NaCl toward the source and for LiF away from it. Electron diffraction showed further that there was a difference in the uniformity of crystal size for these two substances. Whereas LiF transmission patterns always contained very narrow rings resulting from the uniform size of large crystals, NaCl rings were broader suggesting a component of very small crystals as did also the larger general background. In addition, for NaCl there was evidence for a component of very large crystals. Great changes in thickness, 500 to 1000A, were required to produce the transition from random to [110] orientation. Also the appearance of bloom at about 10,000A for NaCl is caused by the development of large crystals.

Because NaCl is very soluble in water thin films could not be exposed to undried air without being essentially altered. When a sample 30A thick was exposed to laboratory air the pattern changed to that of D which indicates a [100] orientation. The larger size of the new crystals together with a cubic shape would account for the new orientation. When more NaCl was subsequently evaporated on to the sample giving the pattern of D complete rings grew in as shown in pattern E. These results were also observed in transmission experiments.

Electron microscopy was used in a direct examination of the products of the recrystallization process. The initial step was to prepare a film with an average thickness of about 10A on a collodion substrate. This thickness was just sufficient to show the beginning of a transmission pattern. The size and shape of the crystals

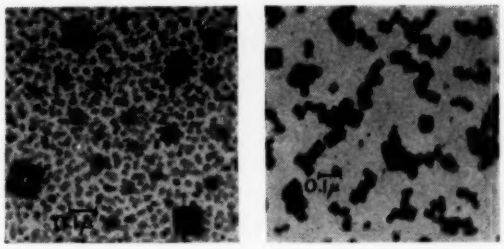

A B

FIG. 9. Electron micrographs of thin NaCl films which have been exposed to air.

produced were then entirely dependent on the type of atmosphere to which the film was exposed. The three sizes shown in Fig. 9A were produced as follows: (1) A deposit of 20A was exposed to very moist air for a few minutes. This gave the large particles about one-thousand angstroms on an edge. (2) An additional deposit of 10A was exposed to laboratory air for one minute giving particles of intermediate size. (3) Another deposit of 5A was formed and air admitted to the microscope almost to atmospheric pressure and then immediately pumped out. This step was repeated until most of the free area had been covered with small crystals a few hundred angstroms on an edge. Those small crystals which appear dark are in a favorable position for reflection, light ones for transmission. In pattern B is shown the result of a very slow recrystallization which required several hours in rather dry air. There was an obvious tendency for crystals to grow in groups.

No serious attempt was made to determine the mechanism of recrystallization but several observations were made. Results from slow recrystallization such as that given in Fig. 9B suggested that the rate of the process may be an important factor. Since the sample was handled several times during the operation, contaminations could effect the results. No definite statement, however, can be made in this case, but as stated earlier, results with single crystals indicated that no contamination effects were controlling the process.

EXPERIMENTAL RESULTS FROM OTHER HALIDES

Although the object of this research was to study intensely the films of a few related substances, a digression was made from this original plan during the examination of films of CaF_2 and MgF_2. These two dielectrics, together with LiF, are widely used in optics, so that the results have more than academic interest. Films of CaF_2 easily prepared both for transmission and reflection followed the usual behavior during growth of showing a random structure for the first few hundred angstroms followed by preferred orientation, in this case [111], for thicker deposits.[14] The growth of MgF_2, however, did not follow the usual sequence. Thin evaporated films tended to be amorphous making them much

[14] For more extensive experiments on CaF_2 see W. G. Burgers, Physica **1**, 549 (1934). Also more recently, J. Bannon and C. E. Curnow, Nature **161**, 137 (1948); **163**, 62 (1949).

more difficult to study than those of LiF or NaCl. To obtain a reference pattern MgF_2 was heated in air and some of the "smoke" caught on a glass substrate. The reflection pattern was the same as that given by x-rays. Up to thicknesses of 1000A no reflection pattern could be obtained from films produced in a vacuum but at 2000A faint broad rings emerged with the (301) reflection very evident. This reflection continued to dominate the pattern as the film thickness was increased until at 10,000A, and beyond, a crystalline pattern showing a [302] orientation became pronounced. A consideration of the unit cell dimensions shows that such an orientation makes the diagonal of a large face perpendicular to the substrate. The data obtained from transmission patterns of MgF_2 was insufficient to support any argument concerning orientation. Several samples were examined of each of three other dielectrics. KCl showed a [110] orientation and in other respects resembled NaCl. NaBr and KBr tended to remain random or grew into an ill-defined [211]. These results are included in the last column of Table II and photographs were given previously.[4]

GENERAL REMARKS ON THE GROWTH OF THIN FILMS OF AMORPHOUS SUBSTRATES

In the previous sections when describing the individual experimental results a detailed interpretation was included wherever possible. At this point several general factors will be considered.

It was clear that amorphous substrates such as glass and collodion had no influence on the initial growth of dielectric films. Moreover when these substrates were first covered with a few thousand angstroms of aluminum there was no change in the film growth of dielectrics. These results indicate that the factors controlling the size and orientation of the crystals reside in the dielectrics themselves and in the evaporation conditions. As has been mentioned, the existence of some [100] orientation below 100A is attributed not to the influence of the substrate but is a natural consequence of small cubes resting on the plane surface of the substrate. This is also the explanation for the [100] orientation of NaCl which has been recrystallized in moist air (see Fig. 8A and Fig. 9).

When a comparison is made of the various results it is clear that the popular idea of molecular mobility over the film surface must be used with caution. Obviously there must be some migration or crystals would not grow at all. On the other hand, the range must be extremely limited because of the tendency of all crystals to be of uniform size. Even the surface projections which are practically free from the interfering effect of neighbors never exceeded a few hundred angstroms in size. Another result in favor of very limited mobility was the tipping of the fiber axis away from or toward the direction of the incident vapor. This would indicate that immediately after striking the surface the molecules are already appreciably bound. If the mobility were high the surface might be in a semiliquid state and then the direction of deposition would be of no consequence.

Some mention of the uniformity of results would be of significance. In nearly a hundred repetitions LiF showed the behavior given in Figs. 2 and 3; there were no exceptions. There was a limitation in the maximum thickness studied in that beyond about 300,000A the film flaked off the glass. Moreover excessive surface roughness did not permit good reflection patterns. The same limitation existed for NaCl. The results of Fig. 8 were obtained repeatedly below 20,000A but above that thickness the results were erratic.

The value of these experiments, in addition to giving detailed information on a number of particular substances, is in pointing out the problems involved in the study of the process of transition from the vapor to the solid phase. It appears that for a complete understanding of the nature of film growth it is necessary to have a quantitative measure of the relative importance of forces and tendencies involved. All that can be done with the data now available is to ascertain what these tendencies are. If the experiments were done over a wide range of pressure and temperature, then perhaps the nature of the material and type of orientation might be used to evaluate the forces. Furthermore, to be valuable a theory must be equally valid for all similar substances, consequently experimental data are required for additional materials. For completeness these data should include results from many experimental approaches.[15]

ACKNOWLEDGMENTS

The experiments in electron diffraction were done in the Electrical Engineering Department of Ohio State University. The author wishes to thank the following: The Westinghouse Electric Corporation for supporting the Post-Doctorate Fellowship in Electron Optics which made the experiments possible; Professor A. F. Prebus for suggestions and encouragement; Mr. John Dankworth for preparing the photographs, and Dr. Schwartz and Dr. Austin of Battelle Memorial Institute for help in replica technique.

The experiments in x-ray diffraction and index of refraction were done at the Institute for the Study of Metals. Mr. Clifton and Mr. Hess assisted in the diffraction experiments and Professor Barrett made helpful suggestions during discussions of the results.

Experiments on electron and light microscopy were done at the University of Michigan with the help of Professor Robley C. Williams.

[15] It was mentioned at the beginning that experiments have been done with single crystal substrates. Although the initial deposit was decidedly different from that for amorphous substrates, the conclusions here presented are in no way changed by, or dependent on the single crystal experiments. These experiments will be described later.

Letters to the Editor

THIS section will accept reports of new work, provided these are terse and contain few figures, and especially few halftone cuts. The Editorial Board will not hold itself responsible for opinions expressed by the correspondents. Contributions to this section should not exceed 600 words in length and must reach the office of the Managing Editor not later than the 15th of the month preceding that of the issue in which the letter is to appear. No proof will be sent to the authors. The usual publication charge ($4.00 per page) will not be made and no reprints will be furnished free.

The Infra-Red Spectrum of Solid Hydrogen Cyanide*

ROBERT E. HOFFMAN** AND D. F. HORNIG
Metcalf Research Laboratory, Brown University, Providence, Rhode Island

September 8, 1949

THE C—N stretching frequency, ν_1, of HCN has not been definitely observed in the gas. However, Choi and Barker[1] observed a band at a frequency, 2100 cm^{-1}, which is very close to the expected value for this fundamental. Because of the unusual structure of the band which they observed, they assigned the three peaks to $3\nu_2$, $4\nu_2(\Sigma^+)-\nu_2$, and $4\nu_2(\Delta)-\nu_2$. (ν_2 is the degenerate bending vibration at 712 cm^{-1}.) The difficulty with this assignment is that the Boltzmann factor for the last two transitions is only 0.06 while the three peaks are of approximately equal intensity. Another explanation for the complicated structure lies in a Coriolis interaction between $3\nu_2$ and ν_1 although this explanation is untenable unless the absorption region actually covers more than the 25 cm^{-1} observed by Choi and Barker.

One may expect the fundamental frequency, ν_2, to be considerably shifted in crystalline HCN so that any coincidence between $3\nu_2$ and ν_1 should be eliminated. We have, therefore, studied the infra-red spectrum of thin non-scattering films of HCN at −180°C. The frequencies and relative intensities in the crystal and the gas frequencies are compared in Table I.

All three fundamentals were observed, as well as the first overtone of the bending mode. The degeneracy in the bending vibration is split and the two components appear at 828 and 838 cm^{-1}. This behavior is illustrated in Fig. 1 where the component at 828 cm^{-1} is almost completely absent in the non-scattering film, indicating a highly oriented film, but both components appear in the more highly scattering film. The relative intensities of the two vary from film to film, apparently as a consequence of partial orientation. This frequency is more than 100 cm^{-1} higher than the corresponding frequency in the gas. There can therefore be no doubt that the very sharp line observed at 2097 cm^{-1} is the fundamental ν_1. This is confirmed by the appearance of the corresponding frequency of the isotopic molecule HC^{13}N with the proper frequency shift. This fundamental and the isotopic line are shown in Fig. 2.[2] On the other hand, the second overtone of ν_2, $3\nu_2$, was not observed at all.

TABLE I. Frequencies and relative intensities of the bands observed in solid HCN.

Frequency Gas*	Frequency Solid	Relative intensity	Assignment
3312	3132	5.7	ν_3
2800	—	—	$\nu_2+\nu_1$
2089	2097	1.0	ν_1
—	2063	0.03	$\nu_1(HC^{13}N)$
1412	1632	0.49	$2\nu_2$
712	838 / 828	1.4	ν_2

* See G. Herzberg, *Infrared and Raman Spectra of Polyatomic Molecules* (D. Van Nostrand Company, Inc., New York, 1945), p. 279.

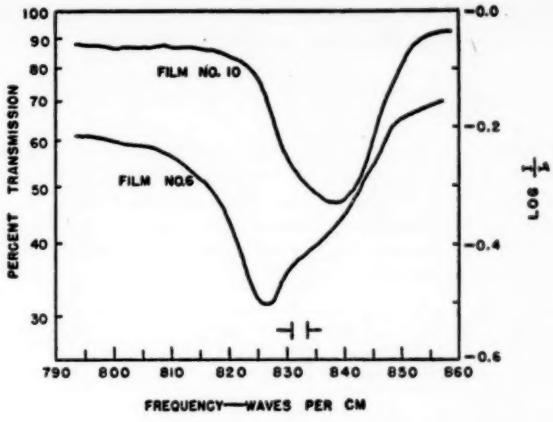

FIG. 1. The infra-red absorption due to the bending fundamental, ν_2, of HCN in the crystal at −180°C.

These observations suggest that the intensity in the vicinity of 2100 cm^{-1} in the gas originates primarily from ν_1 rather than $3\nu_2$. However, they do not necessarily negate the conclusions of Choi and Barker because of the remarkable intensity changes which take place upon crystallization. In the gas the bending vibration, ν_2, is approximately 250 times as intense as the C—H stretch and the C—N stretch is certainly extremely weak. In the crystal, on the other hand, the bending vibration is only ¼ as intense as the C—H stretch and only slightly more intense than the C—N stretch. These relative intensity changes of the order of 1000 times indicate very considerable structural changes accompanying the formation of the hydrogen bonds in the crystal.

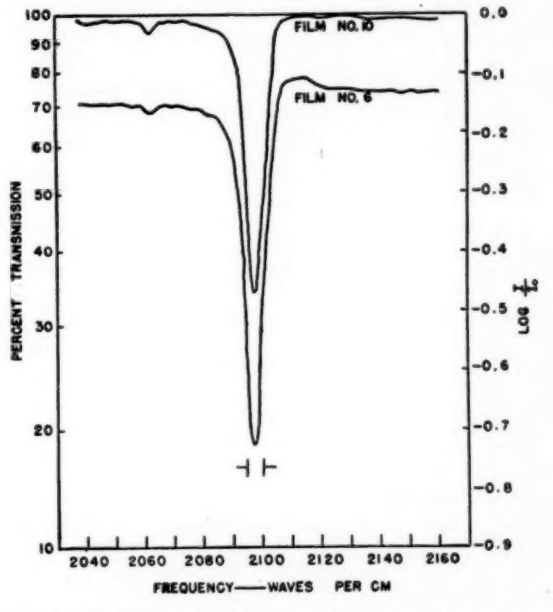

FIG. 2. The infra-red absorption due to the C—N stretching fundamental, ν_1, of HCN and HC^{13}N in the crystal at −180°C.

* This work was supported in part by the ONR under Contract N6ori-88, Task Order 1.

** Stanolind Oil and Gas Company Fellow, 1947–48. Present address: Research Laboratory, General Electric Company, Schenectady, New York.

[1] K. N. Choi and E. F. Barker, Phys. Rev. **42**, 777 (1932).

[2] The distortion introduced by scattering, even when small, is quite evident in the thicker film in Fig. 2. It is usually characterized by a transmission maximum on one side of the peak and a tail on the other.

Temperature Coefficients for the Mass Spectra of a Number of Hydrocarbons

CLIFFORD E. BERRY
Consolidated Engineering Corporation, Pasadena, California
September 2, 1949

TWO recent communications[1,2] in this Journal have discussed the effects of ion source temperature on mass spectra. Fox and Hipple[1] gave experimental results for four ions from isobutane. Stevenson[2] gave results for Ne, A, CO_2, N_2, and Kr, and discussed the theoretical reasons for the existence of temperature effects. These may be summarized as follows:

(a) An increase in temperature increases the kinetic energy of the gas molecules in the ion source and thus increases the rate of effusion from the source. Therefore, the density of the gas in the source is reduced, reducing the rate of formation of ions.
(b) Increased kinetic energy increases the discrimination losses in the source and collector system.[3,4]
(c) An increase in temperature increases the vibrational energies of the molecules, and thus alters the ionization probabilities for the various ions formed.

In the present work, no attempt was made to separate these effects; rather, the over-all temperature coefficients for a number of hydrocarbons were determined. The mass spectrometer used was a laboratory version of the Consolidated Model 21-102 with the ion source modified so that the power supplied to the filament raised the source temperature to only 80°C instead of to approximately 220°C, as in a standard source. Higher temperatures were obtained by using an auxiliary heater.*

Figure 1 shows the results obtained for the principal ions formed in *n*-butane. All curves except the dotted one show the variation with temperature of the relative abundances of the various ions referred to the intensity of the mass 58 (parent) ion. The dotted curve gives the temperature variation of the actual ion current of the parent ion, i.e., the temperature variation of the *sensitivity*. The curves are plotted on a semilogarithmic scale; the only justification for this is that over the range of temperatures used, the curves are very nearly linear, so that a single number can be used to express each slope. In general, all substances studied gave similar straight lines.

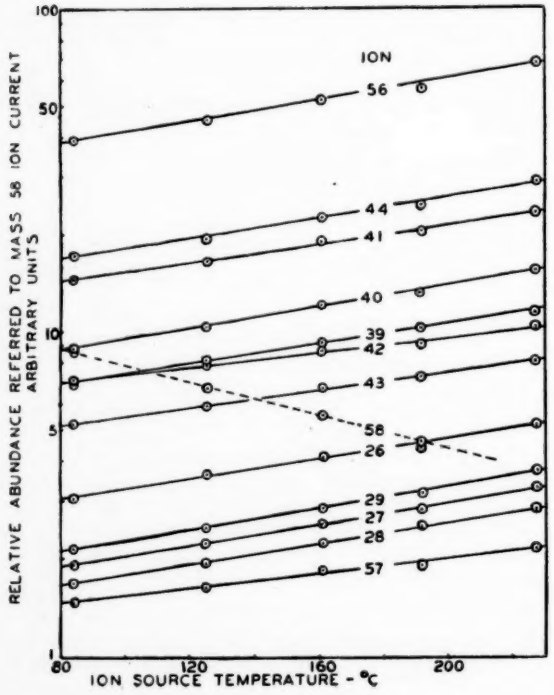

FIG. 1.

TABLE I. Temperature coefficients in percent/°C for relative abundances and sensitivity.

Mass of ion	Paraffins: Ethane	Propane	*n*-butane	Isobutane	*n*-pentane	Isopentane	2-4-dimethylhexane	2,2,4-trimethylpentane	2,2,3-tetramethylbutane
25	0.07								
26	0.06	0.3	0.4	0.4					
27	0.07	0.2	0.1	0.4	0.5	0.7	0.0	0.03	0.2
28	0.04	0.09	0.4	0.5	0.5	0.5	0.3	0.08	0.2
29	0.09	0.2	0.4	0.4	0.5	0.7	0.0	0.1	0.04
38		0.04		0.5					
39		0.2	0.3	0.4	0.5	0.6	0.2	0.03	0.03
40		0.2	0.4	0.5	0.4	0.6	−0.1	0.1	0.06
41		0.1	0.3	0.4	0.5	0.7	0.04	0.03	0.07
42		0.05	0.3	0.3	0.5	0.6	0.07	0.03	0.0
43			0.3	0.4	0.5	0.7	0.0	0.06	0.2
44							0.08		
53							0.1	0.0	0.0
54							−0.09	0.0	0.01
55					0.7	0.6	−0.02	0.0	0.05
56			0.4	0.5	0.5	0.4	−0.08	−0.2	−0.2
57			0.3	0.3	0.4	0.6			
58								−0.05	0.02
69							−0.01	0.0	0.0
70							−0.3		
71					0.3	0.3	−0.1	0.06	
83							−0.3	−0.1	0.03
84							−0.1	0.01	
85							−0.01		
99								−0.3	−0.2
114							−1.0		
Sensitivity	−0.03	−0.3	−0.6	−0.9	−0.7	−0.5	−1.0	−0.1	−0.3

Tables I and II give the results on all compounds studied. Where the curves were not linear the slopes were measured at the temperature of 160°C. The values given are in percent per degree C. As with the *n*-butane curve, these are the temperature coefficients of the relative abundances referred to a base ion. For the three C_3 compounds, the parent ion was too weak to use as the base; for these three materials the mass 57 ion was used as reference. If the parent peaks had been used, the temperature coefficients would have been much greater.

Table III compares the results obtained here for isobutane with values determined from the curves obtained with a Westinghouse instrument by Fox and Hipple. The differences are most probably accounted for by assuming greater discrimination effects against ions having initial kinetic energies in their apparatus. D. P.

TABLE II. Temperature coefficients in percent/°C for relative abundances and sensitivity.

Mass of ion	Olefins and diolefins: Ethene	Propene	Butene-1	Butene-2	Isobutene	Butadiene-1,2	Butadiene-1,3
25	0.05						
26	0.07	−0.1	0.2	0.2	0.1		0.1
27	0.03	−0.05	0.1	0.08	0.07	0.1	0.1
28			0.06		0.1		0.06
29			0.07	0.1	0.1		
37		0.3		0.2	0.2	0.2	0.04
38		−0.09	0.3	0.05	0.0	0.09	0.02
39		0.0	0.1	0.08	0.03	0.05	0.1
40		−0.08	−0.05	0.05	0.07		
41		−0.05	0.1	0.3			
49							0.1
50						0.07	0.03
51					−0.1	0.05	0.05
52						−0.05	0.06
53			−0.05	0.0	−0.06	−0.06	0.0
54			−0.2	−0.2	−0.07		
55			−0.06	−0.1	−0.2		
Sensitivity	−0.2	0.0	−0.3	−0.2	−0.2	−0.4	−0.05

TABLE III. Comparison with data given by Fox and Hipple for isobutane.

Mass of ion	Slope in percent/°C	
		F-H
41	+0.4	+0.75
43	+0.4	+0.6
57	+0.3	+0.5

Stevenson, in a private communication, reports a closer correspondence between data taken on another Westinghouse instrument and these data.

Several general conclusions may be drawn from the data.

(1) The heavier the molecule, the greater the dependence of both relative abundances and sensitivity on temperature.
(2) Branched molecules show greater coefficients than their corresponding straight chain isomers.
(3) Olefins and diolefins show smaller temperature coefficients than their corresponding saturated compounds.

A final conclusion is that in view of the considerable magnitudes of many of the temperature coefficients, accurate analytical work requires some form of temperature control of the ion source.

* In a separate experiment, it was demonstrated that the gas entering the ion source came into thermal equilibrium with the walls of the source before ionization.

[1] R. E. Fox and J. A. Hipple, J. Chem. Phys. **15**, 208 (1947).
[2] D. P. Stevenson, J. Chem. Phys. **17**, 101 (1949).
[3] N. D. Coggeshall, J. Chem. Phys. **12**, 19 (1944).
[4] H. W. Washburn and C. E. Berry, Phys. Rev. **70**, 559 (1946).

The Effect of Pressure on the Thermal Diffusion Ratio

H. G. DRICKAMER AND J. R. HOFTO
Department of Chemistry, University of Illinois, Urbana, Illinois
September 6, 1949

ACCORDING to the theory of Enskog and Chapman[1] the thermal diffusion ratio should be independent of pressure at ordinary pressures. Experimental evidence is scanty and somewhat contradictory. Grew[2] shows data at two pressures for CO_2-H_2 which indicate the α is independent of pressure. Data obtained for the system $CO_2-C_3H_8$ in a column at pressures from 0.3 to 1.8 atmos.[3] indicate that either α varies with pressure for this system or that the theory of the column must be modified. This situation is being investigated exhaustively in this laboratory. As a preliminary step, runs were made over a series of pressures from 0.5 to 2.0 atmos. in the system argon-neon. The two-bulb set-up previously described[4] was used. The gases were analyzed in a thermal conductivity apparatus.[5]

The system was chosen because the molecules were spherically symmetrical and the system would be far above the critical temperature, offering the simplest possible place to start. The results are shown in Table I and Fig. 1. Some difficulty was experienced

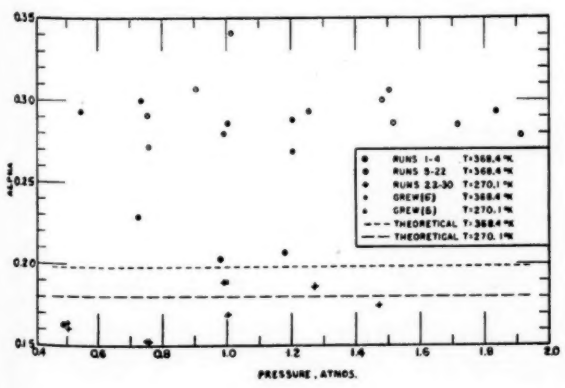

FIG. 1.

TABLE I. Thermal diffusion data.

Run No.	Pressure atmos.	Time hr.	T_H°K	T_C°K	%Ne_H	%Ne_C	Alpha
1	1.179	21.5	474	293	49.5	47.0	0.207
2	0.981	5.5	466	290	49.9	47.5	0.203
3	0.725	10.0	466	291	50.1	47.4	0.229
4	0.489	7.2	473	290	49.6	47.6	0.163
5	0.547	16.8	476	291	50.7	47.1	0.293
6	0.757	15.0	468	288	53.2	49.9	0.272
7	1.012	8.3	476	291	54.0	49.8	0.341
8	1.202	10.4	478	292	54.2	50.9	0.269
9	1.518	10.3	476	292	53.4	49.9	0.286
10	1.717	11.1	468	290	53.6	50.2	0.285
11	1.912	10.3	481	287	53.2	49.6	0.279
12	1.503	11.3	478	291	53.4	49.6	0.306
13	0.990	10.4	479	291	53.0	49.5	0.280
14	0.752	11.2	471	287	52.7	49.1	0.291
15	1.839	22.0	476	291	52.1	48.5	0.293
16	1.462	10.3	477	292	51.7	48.0	0.300
17	1.201	11.2	473	291	51.7	48.2	0.288
18	0.904	10.6	484	291	50.3	46.4	0.307
19	0.698	12.6	474	291	51.8	46.3	0.452
20	1.256	20.8	479	293	51.7	48.1	0.293
21	1.005	9.3	483	292	52.1	48.5	0.286
22	0.733	12.7	479	293	51.7	48.0	0.300
23	0.990	5.8	382	198	50.6	47.5	0.189
24	0.751	5.8	379	197	50.7	48.2	0.153
25	0.504	5.5	378	196	50.4	47.7	0.164
26	1.471	6.0	377	198	50.5	47.7	0.175
27	1.272	6.2	375	209	50.7	48.1	0.186
28	1.002	4.8	374	202	50.3	47.7	0.169
29	0.758	4.9	378	197	50.7	48.2	0.153
30	0.503	6.9	386	197	50.4	47.7	0.161

with the analyses at low densities. The theoretical lines were calculated using the Lennard-Jones model as previously described.[4] It can be seen that runs 1–4 and 22–30 agree well with the theory and with the data of Grew.[6] It is believed that a slight amount of air was present in the system for runs 5–22. It can be said that at low pressures and at temperatures well above the critical there is no effect of pressure on α. At lower temperatures some increase of α with pressure is possible. Measurements are now being made in a column at pressures up to 100 atmos. and in the neighborhood of the critical point.

[1] S. Chapman and T. G. Cowling, *The Mathematical Theory of Non-Uniform Gases* (Cambridge University Press, London, 1939).
[2] K. E. Grew, Nature **156**, 267 (1945).
[3] Drickamer, O'Brien, Brese, and Ockert, J. Chem. Phys. **16**, 122 (1948).
[4] Drickamer, Downey, and Pierce, J. Chem. Phys. **17**, 408 (1949).
[5] P. E. Palmer and E. R. Weaver, Tech. Pap. Bur. Stand. **18**, No. 29, 35–100 (1924).
[6] K. E. Grew, Proc. Roy. Soc. (London) **189**, 402 (1947).

The Near Ultraviolet Absorption Spectra of the Diazines

FREDERICK HALVERSON AND ROBERT C. HIRT
Stamford Research Laboratories, American Cyanamid Company, Stamford, Connecticut
September 12, 1949

ULTRAVIOLET absorption spectra of pyridazine[1] and pyrazine[1] vapors have been obtained for use in a "semi-empirical" evaluation of the C—N and N—N bond integrals and for additional data on nitrogen-containing compounds isoelectronic with benzene. Replacement of CH groups in benzene by the more electronegative N atoms causes marked changes in the near ultraviolet spectrum. Pyridazine, pyrazine, and pyrimidine[2] have two medium to strong absorption transitions in the near ultraviolet—a diffuse system near 2500A and a sharp system at longer wavelengths. The diffuse system is composed of a series of broad bands with rather wide spacings, while the sharp system is built up of line-like bands. These sharp bands form short progressions with spacings (332–398, 474–485, 532–585, 936–968, 957–1014 cm^{-1})

TABLE I. Near ultraviolet absorption by diazine solutions.

System		Pyridazine* Hexane	Pyridazine* Water	Pyrazine** Cyclohexane	Pyrazine** Water	Pyrimidine† Water
Sharp	λ_0	~3700A	~3400A	~3330A	~3230A	~2950A
	λ_{max}	3400A	2990A	3270A	3000A	~2700A
	ϵ_{max}	~400	~355	1018	780	~400
Diffuse	λ_0	~2680A	~2600A	~2800A	~2800A	~2580A
	λ_{max}	2480A	2450A	2600A	2600A	2405A
	ϵ_{max}	~690	~1200	6350	6580	~2350

* R. C. Evans and F. Y. Wiselogle, J. Am. Chem. Soc. **67**, 60 (1945).
** This investigation.
† F. M. Uber and R. Winters, J. Am. Chem. Soc. **63**, 137 (1941).

similar to those of pyridine[3] and the monosubstituted benzenes.[4] The O—O transitions are the strongest lines in the sharp systems and occur at 26,656 cm^{-1} (3750A) for pyridazine, at 30,879 cm^{-1} (3238A) for pyrazine, and at 31,079 (3217A) for pyrimidine.

Both the band systems apparently correspond to "allowed" transitions by virtue of their intensities. The transition involved for the sharp system must be to a state with dimensions similar to those of the ground state because of the line-like character of the bands and the lack of long progressions. Yet the vibrational frequencies in this excited state seem comparable to those in the $^1B_{2u}$ benzene state (considering substituted benzenes). Assuming sp^2 hybridization for the valence electrons of both carbon and nitrogen atoms in the molecular plane, and considering only the π-electrons being mobile, as in benzene, transitions from the ground state to the lowest two excited singlet states are allowed for the diazines. This picture of the electronic levels is being investigated by a semi-empirical molecular orbital treatment.

Spectra of these compounds in solution are functions of the solvent and are displaced slightly from the vapor phase values. Values for λ_0 (long wave-length edge of the band), λ_{max}, and ϵ_{max} are given in Table I.

A detailed account of the observed bands and their assignments, and the results of investigations of possible electronic states involved, will be published in future papers.

[1] The authors wish to thank Dr. R. C. Evans for the sample of pyridazine and Mr. J. F. Bruesch for the sample of pyrazine.
[2] F. M. Uber, J. Chem. Phys. **9**, 777 (1941).
[3] H. Sponer and H. Stücklen, J. Chem. Phys. **14**, 101 (1946).
[4] R. C. Hirt and J. P. Howe, J. Chem. Phys. **16**, 480 (1948).

Raman Spectra of Certain Phosphoric Acids and Their Salts

T. J. HANWICK AND P. HOFFMANN
Department of Physics, New York University, New York, New York
September 6, 1949

IN continuing the work indicated in a recent Letter to the Editor,[1] the following lines in Table I were found and their depolarization factors determined.

TABLE I.

HPO_3		$NaPO_3$		KH_2PO_2		NaH_2PO_2	
$\Delta\nu$	ρ	$\Delta\nu$	ρ	$\Delta\nu$	ρ	$\Delta\nu$	ρ
373	0.76	303	0.62	470	0.96	465	0.85
513	0.96	387	0.73	589	0.36	592	0.37
723	---*	662	0.15	784	0.56	784	0.52
897	0.07	1100	0.28	928	0.86	930	0.82
1073	0.14	1155	0.13	1046	0.20	1047	0.28
1179	0.33	1249	1.00	1087	0.97	1090	0.70
				1162	0.73	1157	0.78
				2356	0.37	2359	0.37

$K_4P_2O_7$		$K_2H_2P_2O_7$		$Na_2H_2P_2O_7$		$K_2Na_2P_2O_7$	
$\Delta\nu$	ρ	$\Delta\nu$	ρ	$\Delta\nu$	ρ	$\Delta\nu$	ρ
339	0.70	314	0.63	318	0.51	344	0.55
532	0.88	469	0.72	475	0.69	511	0.81
722	0.25	711	0.35	728	0.27	709	0.27
1027	0.15	952	0.34	956	0.18	1027	0.16
1118	0.67	1087	0.21	1103	0.22	1112	0.48
		1175	0.68				

H_3PO_4		KH_2PO_4		K_2HPO_4		K_3PO_4**		NaH_2PO_4	
$\Delta\nu$	ρ	$\Delta\nu$	ρ	$\Delta\nu$	ρ	$\Delta\nu$	ρ	$\Delta\nu$	ρ
366	0.64	379	0.39	394	0.79	420	0.58	383	0.87
508	0.74	514	0.52	537	0.89	573	0.71	511	0.87
918	0.18	753	---*	865	0.08	704	---*	886	0.08
1058	0.40	880	0.07	976	0.09	936	0.19	1062	0.14
		1069	0.10						
		1196	---*	1081	0.62	1014	0.58		

* The symbol --- indicates the lines were too faint for depolarization measurements.
** Repeated investigations do not show the very faint line 2385 which was reported earlier.

It is to be noted that some discrepancies between the values of the depolarization factors for similar salts are present. These are being investigated more closely and will be reported in a later paper.

[1] P. Hoffmann and T. J. Hanwick, "Raman spectra of certain phosphoric acids and their salts," J. Chem. Phys. **16**, 1163 (1948).